Advanced Thermally Stable Jet Fuels

Final Report

Principal Investigator

Harold H. Schobert

Faculty Associates

André L.Boehman
Michael M. Coleman
Semih Eser
Patrick G. Hatcher
Chunshan Song
Peter M. Walsh

Natalie Nodianos and Richard M. Neumann
Editors

Contract Number
DE-FG22-92PC92104

Table of Contents

Executive Summary ES-1

Task 1: Investigation of the Quantitative Degradation Chemistry of Fuels..... 1-1

1.1 Effects of Hydrogen Donors on the Pyrolysis of Tetradecane at 450°C Under N_2 Pressure..... 1-2
1.2 Pyrolysis of Tetradecane at Elevated Pressure for Long Duration: Product Distribution and Reaction Mechanisms..... 1-12
1.3 Product Distribution of the Pyrolysis of n-Tetradecane at 400°C and 425°C..... 1-15
1.4 Effects of Initial Phase Behavior on the Thermal Degradation of n-Tetradecane..... 1-26
1.5 Kinetics of n-Tetradecane Pyrolysis at Near-Critical Region..... 1-33
1.6 Effects of Sample Volume and Inert Nitrogen Pressure on the Pyrolysis of n-Tetradecane in Both Gas and Supercritical Phase..... 1-37
1.7 Product Distributions from Pyrolysis on n-Tetradecane in Near-Critical Region..... 1-47
1.8 Thermal Decomposition of N-Tetradecane in Near-Critical Region..... 1-63
1.9 Re-examining the Effects of Reactant and Inert Gas Pressure on Tetradecane Pyrolysis. Effect of Cold Volume in Batch Reactor..... 1-71
1.10 Effects of Reactant and Inert Gas Pressure on the Solid Formation in Both Supercritical- and Gas-Phase Pyrolysis of n-Tetradecane at 450°C..... 1-75
1.11 Exploratory Studies on the Pyrolysis of Binary Mixtures of n-Tetradecane and Hydrogen Donors at 450°C in a Batch Reactor..... 1-78
1.12 Studies on the Pyrolysis of Binary Mixtures of n-Tetradecane and Hydrogen Donors at 450°C in a Batch Reactor..... 1-81
1.13 Studies on the Effects of the Concentration of Hydrogen Donors on the Pyrolysis of n-Tetradecane at 450°C in a Batch Reactor..... 1-84
1.14 Surface Effects on Carbon Deposit Formation from Jet Fuel and n-Dodecane..... 1-86
1.15 Surface Effects on the Formation of Carbon Deposits from Thermal Stressing of Jet A Fuel and n-Dodecane..... 1-89
1.16 Thermal Degradation Studies of ^{13}C-labeled Dodecane Mixed with a Petroleum Derived Jet Fuel, JP-8P, Using Gas Chromatography-Select Ion Monitoring..... 1-90
1.17 Condensed-Phase Pyrolysis of Long-Chain Paraffins. Unusual Effects of Sample Volume and Inert Gas Pressure..... 1-96
1.18 Thermal Decomposition of n-Alkanes in Near- and Supercritical Regions..... 1-100
1.19 Thermal Decomposition of n-Alkanes in Near Critical and Supercritical Regions: Product Distributions and Reaction Mechanisms..... 1-103
1.20 High Temperature Cracking and Deposition Behavior of an n-Alkane Mixture..... 1-110
1.21 Thermal Decomposition of Norpar-13 Under Supercritical Conditions..... 1-112
1.22 Pyrolysis of Alkylcyclohexanes at 450°C and Elevated Pressure. Product Distribution and Reaction Mechanisms..... 1-114
1.23 Pyrolytic and Catalytic Reactions of Potential Endothermic Fuels: Cis- and Trans-Decalin..... 1-132
1.24 Thermal Decomposition of n-Butylcyclohexane in Near-Critical and Supercritical Regions: Product Distributions and Reaction Mechanisms..... 1-134
1.25 Thermal Decomposition of Decalin in Near-Critical and Supercritical Regions: Product Distributions and Reaction Mechanisms..... 1-137
1.26 Chemistry for Thermal Degradation of Bicyclic Hydrocarbon Components of Jet Fuels in Pyrolytic Regime..... 1-140
1.27 Reactive Structure Index for Correlation of High Temperature Thermal Stability of Saturated Hydrocarbons..... 1-142
1.28 Pyrolysis of Butylbenzenes: Effects of Structure of Alkyl Side Chain on the Pyrolysis of Alkylbenzenes..... 1-146
1.29 Exploratory Study of Gas Phase Pyrolysis of n-Butylbenzene at Atmospheric Pressure in Flow Reactor..... 1-153
1.30 Thermal Decomposition of n-Butylbenzene in Near-Critical and Supercritical Regions: Product Distributions and Reaction Mechanisms..... 1-164
1.31 Supercritical Phase Thermal Decomposition of a Mixture of n-Dodecane and n-Butylbenzene..... 1-167

1.32 Supercritical-Phase Thermal Decomposition of a Mixture of n-Butylbenzene and n-Buytylcyclohexane 1-170
1.33 Detailed Characterization of Minor Liquid Products from Thermal Stressing of Amylbenzene and n-Hexylbenzene 1-173
1.34 Use of Site-Specific ^{13}C-Labeling to Examine the Thermall Stressing of 1-Phenylhexane: A Case Study for the Determination of Reaction Kinetics in Complex Fuel Mixtures Versus Model Compound Studies.....1-184
1.35 Pyrolysis of Octylbenzene: Effects of Structure of Alkyl Side Chain on the Pyrolysis of Alkylbenzenes 1-187
1.36 Pyrolysis of n-Alkylbenzenes.....1-193
1.37 Thermal Stability Testing of Napthenic Liquids 1-204
1.38 Determination of Critical Properties of Jet Fuels 1-206
1.39 Detection of Polycyclic Aromatic Hydrocarbons Present in Highly Stressed Jet Fuel by High Performance Liquid Chromatography (HPLC) Using Normal-Phase Separation with Diode Array Detection 1-210
1.40 Temperature-Programmed Retention Indices for GC and GC-MS Analysis of Coal- and Petroleum-Derived Jet Fuels.....1-217
1.41 Literature Review on Thermal Stability of Jet Fuels 1-229
1.42 Estimation of Critical Temperatures of Jet Fuels.....1-235
1.43 Surface Effects on Deposit Formation in a Flow Reactor System 1-238
1.44 The Study of Quantitative Structure-Thermal Stability Relationships in the Pyrolysis of Hydrocarbons.....1-242
1.45 The Study of Hydrocarbon Degradation Using the Quantitative Structure-Property Relationship Method.....1-244
1.46 Characterization and Degradation Studies of Coal- and Petroleum-Derived Aviation Jet Fuels and Middle Distillates 1-248
1.47 The Use of Site-Specific ^{13}C Labeling to Examine the Thermal Degradation of Jet Fuel Components 1-250
1.48 Effect of Carbon Surfaces on Thermal Decomposition of Hydrocarbons.....1-252
1.49 The Study of Quantitative Structure-Thermal Stability Relationships in the Pyrolysis of Hydrocarbons.....1-255
1.50 Clarification of Key Interactions Among Fuel Components.....1-258
1.51 Phase Effects on Fuel Degradation and Solid Deposition 1-259

Task 2 — Investigation of Incipient Deposition..... 2-1

2.1 Growth and Deposition of Particles During Heating of Coal-Derived Aviation Gas Turbine Fuels.....2-2
2.2 Deposit Growth During Heating of Coal Derived Aviation Gas Turbine Fuels 2-18
2.3 Modeling Heat Transfer to Flowing Jet Fuels 2-27
2.4 Investigation of Incipient Depositon 2-29
2.5 Study of Hydrocarbon Fuel Degradation in the Presence of Hydrogen Donors as Stabilizers.....2-32
2.6 Kinetics of Deposit Formation from Jet Fuel.....2-37

Task 3 — Characterization of Solid Gums, Sediments, and Carbonaceous Deposits..... 3-1

3.1 SEM Study of the Deposits on Stainless Steel Flow Reactor Tube Surface.....3-2
3.2 Surface Effects on the Formation of Carbon Deposits A Literature Review 3-4
3.3 Carbonaceous Deposit Formation on Metal Foils from Thermal Stressing of Coal Derived Jet Fuels (JP-8C) 3-7
3.4 Surface Effects on Deposit Formation in a Flow Reactor System 3-9
3.5 Surface Effects on the Formation of Carbonaceous Solid from Thermally Stressed Jet Fuels and Model Compounds.....3-13
3.6 Surface Effects on Fuel Decomposition.....3-15
3.7 Effects of Pretreatment with High Surface Area Activated Carbon PX-21 on Thermal Stressing of JPTS Jet Fuel.....3-17
3.8 Effects of High Surface Area Activated Carbon as a Catalyst during Thermal Stressing of n-Octane and n-Dodecane.....3-19
3.9 Effects of High Surface Area Activated Carbon and Decalin on Thermal Degradation of Jet A-1 Fuel and n-Dodecane.....3-24
3.10 Studies of Surface Chemistry of PX-21 Activated Carbon During Thermal Degradation of Jet A-1 Fuel and n-Dodecane 3-26

3.11 Effects of Surface Changes and Toluene Extraction of PX-21 Carbon on Thermal Stressing of Model Compounds 3-28
3.12 Catalytic Effects of Carbon Surfaces in Organic Reactions A Literature Review 3-30
3.13 Effects of High Surface Area Activated Carbons on Thermal Stressing of Model Compounds 3-33
3.14 Effects of Solid Carbon Surfaces on Thermal Decomposition of n-Dodecane 3-35
3.15 Effect of Carbon Surfaces on Thermal Decomposition of Hydrocarbons 3-37
3.16 Effects of Adding Solid Carbons on Thermal Degradation of Jet Fuel 3-40
3.17 Carbonaceous Deposit Characterization 3-46
3.18 Characterization of Actual Engine Deposits 3-50
3.19 Nature of High Temperature Deposits from n-Alkanes in a Flow Reactor 3-51
3.20 Thermal Decomposition of Tetralin in Near-Critical and Supercritical Regions: Product Distributions and Reaction Mechanisms 3-53

Task 4 — Coal-Based Fuel Stabilization Studies 4-1

4.1 Use of ^{13}C Labels to Trace Reactions of Potential Antioxidants for Jet Fuels 4-2
4.2 The Mechanism of Hydrogen Transfer from Hydroaromatic Compounds a Literature Review 4-6
4.3 Thermal Stability Studies Using the Model Compound Dodecane 4-8
4.4 Hydrogen-Transferring Pyrolysis of Tetradecane Enhancing High-Temperature Stability of Jet Fuels by H-Donors 4-22
4.5 Screening Potential Jet Fuel Stabilizers Using the Model Compound Dodecane 4-24
4.6 Theoretical Models to Study the Phase Behavior of Jet Fuel 4-29
4.7 Study of the Phase Behavior of Jet Fuels Using the Lattice Fluid Model 4-31
4.8 In Situ Regeneration of the Thermal Stabilizer Benzyl Alcohol 4-37
4.9 Exploratory Screening and Development of Potential Jet Fuel Thermal Stabilizers Over 400°C 4-41
4.10 Kinetic Studies on Potential Jet Fuel Stabilizers 4-44
4.11 Further Studies on Potential Jet Fuel Stabilizers 4-47
4.12 Toward the Design of Thermally Stable Jet Fuels at Both Moderate (<250°C) and High (>400°C) Temperatures 4-49
4.13 Design and Synthesis of Second Generation Jet Fuel Stabilizers 4-58
4.14 Fundamentals of High-Temperature Stability 4-60
4.15 Design of Superior Stabilizers 4-62
4.16 Low-Temperature Oxidation Resistance of Thermal Stabilizers 4-65

Task 5 — Exploratory Studies on the Direct Conversion of Coal to High Quality Jet Fuels 5-1

5.1 Production of Jet Fuels from Coal 5-2
5.2 Characterization of Isolated Resinite Maceral 5-4
5.3 Statistical Models for Bituminous Coal: A Three-Dimensional Evaluation of Structural and Physical Properties Based on Computer-Generated Structures 5-6
5.4 Direct Coal Liquefaction: A Potential Route to Thermally Stable Jet Fuel 5-14
5.5 Structural Correlation of Coal Liquefaction Oils with Flash Pyrolysis Products 5-20
5.6 A Study of the Molecular Structure of Polycadinene from Dammar Resin: The First Phase of a Comparative Study to Understand the Chemistry and Structure of Resin from Blind Coal Samples 5-23
5.7 Preliminary Investigation into Producing Cycloalkanes from Dammar Resin 5-26
5.8 Design of Batch Mode and a Continuous Mode Three-Phase Reactor Systems for the Liquefaction of Coal and Upgrading of Coal Liquids 5-31
5.9 Design, Assembly, and Operation of a Batch Mode and a Continuous Mode Three-Phase Reactor System for the Liquefaction of Coal and Upgrading of Coal Liquids 5-35
5.10 Contribution of Mineral Matter to Low Temperature Liquefaction Mechanisms 5-40
5.11 Hydrogenation/Dehydrogenation Reactions of Rosin 5-42
5.12 Hydrotreatment of Multicyclic Compounds to Produce Cycloalkanes 5-46
5.13 Hydrogenation/Dehydrogenation of Polycyclic Compounds Using MoS_2 as Catalyst 5-50
5.14 Exploratory Studies on the Possibility of Non-Radical Hydrogen Transfer Under Low Temperature Liquefaction Conditions 5-53

5.15 Low Temperature Routes to Hydrogenation of Pittsburgh No. 8 Coal 5-58
5.16 The Study of Coal Using Low-Temperature Hydrogenation in the Presence of Hydrogen-Donor Solvents 5-60
5.17 Hydrogenation/Dehydrogenation of Polycyclic Aromatic Hydrocarbons Using Ammonium Tetrathiomolybdate as Catalyst Precursor 5-62
5.18 Hydrogenation of Coal at Mild Conditions 5-66
5.19 Hydroboration of Coal as a New Method of Coal Hydrogenation and a Possible Method of Liquid Product Upgrading 5-75
5.20 Shape-Selective Isopropylation of Naphthalene Over Zeolite Catalysts 5-78
5.21 Shape-Selective Naphthalene Hydrogenation for Production of Thermally Stable Jet Fuels 5-81
5.22 Noble Metal Catalysts for Low-Temperature Naphthalene Hydrogenation in the Presence of Benzothiophene 5-86
5.23 Conformational Isomerization of cis-Decahydronaphthalene over Zeolite Catalysts 5-93
5.24 Zeolite Supported Pd and Pt Catalysts for Low-Temperature Hydrogenation of Naphthalene in the Absence and Presence of Benzothiophene 5-95
5.25 A Structural Study of Blind Canyon Coals Using Solid State ^{13}C NMR Spectroscopy 5-97
5.26 The Thermal Decomposition of ^{13}C-Labeled Bibenzyl in the Presence of Additive Free Jet A-1 5-99
5.27 A Structural Study of the Blind Canyon Coals Using Solid State ^{13}C NMR Spectroscopy 5-103
5.28 Temperature-Programmed Liquefaction of Coals Using Bimetallic Dispersed Catalysts from Organometallic Complexes 5-105
5.29 Bimetallic Dispersed Sulfide Catalysts from Organometallic Clusters for Coal Liquefaction 5-107
5.30 Novel Bimetallic Dispersed Catalysts from Heteronuclear Organometallic Clusters for Promoting Coal Liquefaction 5-111
5.31 Exploratory Studies on Coal Liquid Upgrading Using Mesoporous Molecular Sieve Catalysts 5-113
5.32 Conformational Isomerization of Cycloalkanes 5-124
5.33 Carbon Skeletal Isomerization 5-125
5.34 Hydrodeoxygenation Under Coal Liquefaction Conditions Using Novel Organometallic Catalyst Precursors 5-127
5.35 Hydrodeoxygenation in Coal Liquefaction Systems Using Novel Organometallic Precursors 5-130
5.36 Novel Approaches to Low-Severity Coal Liquefaction and Coal Resid Co-processing Using Water and Dispersed Catalysts 5-131
5.37 Development of Coal-Based Jet Fuels Via Coprocessing of Coal and Resid 5-135
5.38 Coal/Resid Coprocessing 5-141
5.39 Coprocessing of Coal/Petroleum 5-143
5.40 Co-Coking of Petroleum Residua and Coals 5-144

EXECUTIVE SUMMARY

The Pennsylvania State University program in advanced thermally stable coal-based jet fuels has five broad objectives:

1. Development of mechanisms of degradation and solids formation
2. Quantitative measurement of growth of sub-micrometer and micrometer-sized particles suspended in fuels during thermal stressing
3. Characterization of carbonaceous deposits by various instrumental and microscopic methods
4. Elucidation of the role of additives in retarding the formation of carbonaceous solids
5. Assessment of the potential of production of high yields of cycloalkanes by direct liquefaction of coal.

Future high-Mach aircraft will place severe thermal demands on jet fuels, requiring the development of novel, hybrid fuel mixtures capable of withstanding temperatures in the range of 400°-500°C. In the new aircraft, jet fuel will serve as both an energy source and a heat sink for cooling the airframe, engine, and system components.

The ultimate development of such advanced fuels requires a thorough understanding of the thermal decomposition behavior of jet fuels under supercritical conditions. Considering that jet fuels consist of hundreds of compounds, this task must begin with a study of the thermal degradation behavior of select model compounds under supercritical conditions.

The research performed by The Pennsylvania State University was focused on five major tasks that reflect the objectives stated above:

Task 1: Investigation of the Quantitative Degradation of Fuels

Task 2: Investigation of Incipient Deposition

Task 3: Characterization of Solid Gums, Sediments, and Carbonaceous Deposits

Task 4: Coal-Based Fuel Stabilization Studies

Task 5: Exploratory Studies on the Direct Conversion of Coal to High Quality Jet Fuels

The major findings of each of these tasks are presented in this executive summary. A description of the sub-tasks performed under each of these tasks and the findings of those studies are provided in the remainder of this volume (Sections 1 through 5).

TASK 1: INVESTIGATION OF THE QUANTITATIVE DEGRADATION OF FUELS

A. Pyrolysis of *n*-Alkanes

^{13}C-Labeled Dodecane. Gas chromatography-selection monitoring in combination with carbon-13 labeling proved to be an excellent technique for monitoring the thermal degradation of 6-^{13}C-dodecane in JP-8P. Using this technique, we were able to distinguish between naturally occurring unlabeled dodecane in the system and added carbon-13 by differences in their molecular weights.

Pyrolysis of Tetradecane. The major products in the initial stage of reaction were C_1-C_{11} *n*-alkanes and C_2-C_{12} 1-alkenes. There were very few paraffinic products with 12 or 13 carbon atoms; however, 1-dodecene was as abundant as the C_1-C_{11} 1-alkenes. Compared to gas-phase pyrolysis, the alkene/alkane molar ratios were much smaller, except for the C_{12} group, where the ratio of 1-dodecene/dodecane can be as high as 9 in the initial stage. 1-Hexene and 1-pentene appeared to be formed preferentially among the alkenes after a 12-minute period, perhaps as a result of 1,4- and 1,5-shift isomerization of primary radicals. The peak of carbon number distribution shifted toward 2 for paraffinic products and towards 3 for olefinic products, and the ratios of alkenes to alkanes decreased with increasing residence time up to 60 minutes. Alkane molecules are the source for hydrogen abstraction in the initial periods, but in the later stages the olefinic products also underwent H-abstraction reactions, leading to the formation of cyclohexanes, cyclopentanes, and alkylaromatics. The alkylaromatics include mainly alkylbenzenes, with smaller amounts of alkyl-substituted indanes and naphthalenes.

Unusual Effects of Sample Volume and Inert Gas Pressure on Condensed-Phase Pyrolysis of Long-Chain Paraffins. A significant pressure dependence was observed for the pyrolysis of *n*-tetradecane at 450¡C for 30 minutes. At least two processes were affected by the reactant pressure, but in opposite directions. The influence of inert gas pressure is dependent on both the initial sample volume and the pressure range. However, when the inert gas pressure is within a certain range, the changes in the sample volume have no impact on *n*-tetradecane conversion. Below or above this range, increasing inert gas pressure can either decrease or increase conversion, depending on the sample volume.

Pyrolysis of *n*-Tetradecane. Modeling studies demonstrated that the product distribution from pyrolysis of *n*-tetradecane at 400° and 425°C could not be predicted by known reaction mechanisms reported in the literature, such as the Kossiakoff-Rice mechanism or the Fabuss-Smith-Satterfield mechanism. We proposed new mechanisms and performed modeling to determine their validity. The study was also extended to examine the effects of initial phase behavior on the thermal degradation of *n*-tetradecane. Supercritical phenomena near the critical point, such as large partial molar volume, local anisotropy, and high compressibility, have significant effects on the thermal reactions.

Apparent kinetic parameters for the thermal decomposition of *n*-tetradecane were calculated using the Arrhenius expression for six different sample loadings in the microreactor. However, first-order kinetics with an Arrhenius relationship can only be considered an

approximation over a certain range of temperature, pressure, and extent of conversion near the critical point.

In the pyrolysis of *n*-tetradecane, nitrogen serves as an inert reaction medium that can influence reactions through mechanical pressure effects, phase behavior, and/or diffusional limitations. A large number of elementary reactions contribute to the global reaction. At least two radical reaction processes (unimolecular and bimolecular) are affected by the reactor pressure in opposite directions. The activation volumes of some of the reactions involved in the pyrolysis are very sensitive to pressure changes near the critical point.

The induction period observed in the measurements of deposit mass/area can be accounted for by two types of intermediates one formed directly on decomposition of tetradecane, but slow in reacting with deposits, and a second produced from the first by further reactions. These are the reactive species directly responsible for deposit growth.

Thermal Decomposition of *n*-Alkanes. Thermal decomposition studies, using glass tube reactors, were extended to two additional model compounds: *n*-decane and *n*-dodecane. We also compared the results obtained from stressing *n*-tetracane in a stainless steel microautoclave (using both nitrogen and air atmospheres) versus a glass tube reactor.

Effect of Cold Volume in Batch Reactor. Temperature measurements in the reactor system showed that the connecting line (i.e., the stem that attaches the body of the microautoclave to the pressure gauge and valve) could have a considerably lower temperature (200°C) than the sandbath (450°C) in which the remainder of the reactor is immersed. This temperature differential seems to induce circulation of reactants inside the reactor, leading to fluctuations in the reaction rates and mechanisms (particularly for experiments in the near-critical region) and underestimated rate constants. A modification of the standard microautoclave reactor design led to the discovery that the relatively cool connecting line may have significant effects on the decomposition of *n*-tetradecane. Subsequently, we suggest that purposefully adding a cooler portion to the fuel system would help to reduce reactant (i.e., fuel) decomposition by serving as a venting place for some reactive radicals.

B. Pyrolysis of Alkylbenzenes

Pyrolysis of *n*-Alkylbenzenes. The effect of chain length on the pyrolytic behavior of various *n*-alkylbenzenes has been evaluated. The formation of various products depends on the initiation of the reaction, which can begin with abstraction of hydrogen from α- or y-positions on the alkyl chain. α-Hydrogen abstraction is preferred by increasing reaction temperature (i.e., α-hydrogen abstraction has a higher activation energy than y-hydrogen abstraction.). y-Hydrogen abstraction is relatively easier as the length of the alkyl chain increases.

Pyrolysis of Butylbenzenes. We examined the pyrolysis of four isomers of butylbenzene and determined that the rates of disappearance of substrates depend on the bonding energy of the C_α-C_β bond in the side chain in the initial period of pyrolysis reactions. Bimolecular and secondary reactions become dominant after a short period of reaction time. The rates of substrate conversion depend largely on the secondary reactions, such as H-abstraction, β-bond scission and isomerization. Rapid conversion of a starting material did not necessarily result in a high

yield of solid products. *n*-Butylbenzene was quickly transformed, yet produced the least amount of solid products perhaps a result of the large amount of cracking products (such as toluene and ethylbenzene) formed in its pyrolysis and the concurrent formation of more stable compounds (such as naphthalene). Styrene-series compounds might act as major free radical chain carriers in the sequence to form polycyclic aromatic compounds and solid products.

Gas Phase Pyrolysis of *n*-Butylbenzene. This study, conducted in a flow reactor at atmospheric pressure, identified a number of similarities to trends previously observed in high-pressure static reactions. In both cases, ethylene and propylene appeared to go through a maximum and then decline and the same major compounds were formed primarily benzene, toluene, ethylbenzene, styrene, methylstyrene, naphthalene, biphenyl, C_3-benzenes, and C_4-benzenes. However, there were also differences between the two reaction systems. For example, styrene was the most abundant product in the flow reactions, whereas toluene and ethylbenzene dominated among the microautoclave products.

Thermal Decomposition of *n*-Butylbenzene. Thermal decomposition of *n*-butylbenzene was studied in the near-critical and supercritical regions as a function of pressure, temperature, and conversion. Thermal stressing experiments were carried out in a Pyrex glass tube reactor that eliminated the concerns for temperature variations and possible catalytic effects of metallic surfaces often encountered with the standard microautoclave reactors.

Supercritical Phase Thermal Decomposition of a Binary Mixture of *n*-Dodecane and *n*-Butylbenzene. Pyrolysis showed a strong interaction between the components, which affected the conversion of individual compounds and produced hybrid species that were not found in the products from pyrolysis of pure compounds. In the binary mixture, the conversion of dodecane was inhibited, while the conversion of butylbenzene was accelerated relative to the results of pyrolysis of the individual compounds under the same conditions.

Supercritical Phase Thermal Decomposition of a Binary Mixture of *n*-Butylbenzene and *n*-Butylcyclohexane. Interaction occurred between the individual components, as evidenced by the changes in the decomposition rates of these compounds relative to those obtained from neat pyrolysis experiments. In addition, the pyrolysis products from the binary mixture contained hybrid compounds, which were produced by cross-reactions between *n*-butylbenzene and *n*-butylcyclohexane species. These results suggest that the solid deposition from the binary mixture can have different characteristics with possible non-additive effects that cannot be predicted from the behavior of the individual compounds.

Substantial differences were observed between the composition of the pyrolysis products obtained from the binary mixtures under a starting supercritical or gas phase. Starting supercritical conditions favor the formation of toluene, C_6-diphenyls, and cyclohexyl-C_6-benzenes, and suppress the formation of styrene, cyclohexylbenzene, and other light products. Depending on the effective solid formation or deposition mechanisms, these differences in pyrolysis product composition as a function of pressure can also influence the deposit formation.

Pyrolysis of Amylbenzene and *n*-Hexylbenzene. Our analysis of the liquid products included variations in gas chromatographic methodology and open column liquid

chromatographic separation of the product prior to analysis of selected fractions. These procedures allowed improved detection of aromatic high molecular weight compounds.

Thermal Stressing of 1-Phenylhexane. The reaction kinetics for 1-phenylhexane and 1-phenyl-1-^{13}C-hexane were not the same; therefore the mechanism for the thermal degradation of neat 1-phenylhexane versus that of JP-8C are not equivalent. As radicals are formed by the degradation of 1-phenylhexane in the jet fuel mixture, they are quickly quenched by hydrogen-donor molecules present in the fuel. In the neat compound, there are no hydrogen-donor molecules available to retard the thermal breakdown of the 1-phenylhexane.

Pyrolysis of Octylbenzene. The pyrolysis of octylbenzene was studied at 400°, 425°, and 450°C. There were some similarities with the reactions of butylbenzenes. For example, both produce a large amount of smaller alkylbenzenes during pyrolysis. Reaction kinetics of octylbenzene were calculated, and the major chemical pathways in its thermal reactions were determined.

C. Pyrolysis of Cycloalkanes, Alkylcyclohexanes, and Hydroaromatics

Thermal Decomposition of Decalin. The thermal decomposition of decalin was investigated under near-critical and supercritical conditions. The reactivities of the two isomers, *cis*- and *trans*-decalin, differed significantly, but the yields of major products of thermal decomposition showed no significant differences. The thermal decomposition of the two isomers proceeded by the same mechanism.

Pyrolytic and Catalytic Reactions of Potential Endothermic Fuels. Decalin seems an ideal candidate for a future jet fuel. *trans*-Decalin is much more stable than *cis*-decalin; their stabilities are similar to those of methylcyclohexane and *n*-butylcyclohexane, respectively. Conformational isomerization is the dominant reaction for *cis*- and *trans*-decalin at 450°C.

Pyrolysis of Alkylcyclohexanes at 450°C and Elevated Pressure. We investigated the product distribution and reaction mechanisms for pyrolysis of cyclohexane and a variety of alkylcyclohexanes in nitrogen atmospheres, along with pseudo-first order rate constants, and possible reaction mechanisms for the origin of major pyrolysis products.

Thermal Decomposition of Tetralin. The thermal decomposition of tetralin was studied in glass reactors at 425-474°C, in near-critical and supercritical conditions. The most abundant product was 1-methylindan. Yields of products change with pressure, temperature, and reaction time. We developed reaction mechanisms to explain these changes.

D. Critical-Region Phenomena

Critical Temperatures. The critical temperatures of a suite of petroleum- and coal-derived jet fuels were measured using a rapidly heating sealed tube method. The measured results were satisfactory and exhibited good reproducibility.

Critical temperature calculations using six different methods showed that while most of the methods give satisfactory critical temperature predictions for petroleum-derived jet fuels,

they are less reliable for coal-derived fuels because of the differences in the composition of these fuels. A new correlation was developed on the basis of the boiling points and specific gravities of the compounds found in the coal-derived jet fuels. The new correlation provides satisfactory critical temperature predictions for coal-derived jet fuel samples.

E. Analytical Methodology

Polycyclic Aromatic Hydrocarbons. Significant progress was made in the detection of polycyclic aromatic hydrocarbons present in highly stressed fuels using high-performance liquid chromatography (HPLC) with diode-array detection. These compounds, which are not detectable by gas chromatography, are low in concentration but could play a significant role in the formation of solid deposits.

Temperature-Programmed Retention Indices. These indices have proven very useful for gas chromatographic and gas chromatography/mass spectrometric analysis of coal- and petroleum-derived jet fuels. To demonstrate, we identified more than 100 components in two JP-8 fuels and their liquid chromatographic fractions.

F. Surface Effects

Effect of Activated Carbon Surfaces. The role of activated carbon surfaces as catalysts in the thermal stressing of jet fuel was investigated using *n*-dodecane and *n*-octane as model compounds. In some cases, 5% decalin was added to test the ability of the carbon to catalyze the transformation of decalin to naphthalene.

Later, we generated additional evidence on the activity of carbon surfaces in stabilizing the free radicals generated during the thermal stressing of *n*-dodecane. Various solid carbons were used, including an interesting carbon-coated ceramic monolith. The activity of a carbon surface can be closely related to the concentration and nature of surface oxygen functional groups. These groups decompose at the temperatures of fuel stressing to create active sites that readily interact with radicals from the fuel.

G. Modeling

Relative Stability of Hydrocarbon Components. The relative stability of alkanes and cycloalkanes increases with increasing chain or side-chain length. Cycloalkanes are desirable components of advanced jet fuels, in terms of having higher thermal stability and density than *n*-alkanes of the same carbon number. The *cis*-isomer is typically more reactive than the *trans*-isomer, with the exception of *cis*-1,3-dimethylcyclohexane, which is more stable than its *trans*-isomer. The presence of a branch or branches appears to decrease the decomposition rate compared to alkanes.

Reactive Structure Index. We developed a reactive structure index to correlate the molecular structures of saturated hydrocarbons with their reactivities using a linear group method. The index is composed of several sub-indices determined from the structure, including carbon group indices, ring index and conformation index. We examined the effects on

decomposition of ring structure, side-chain length, steric isomers, and branching. Good correlations were obtained for two sets of saturated hydrocarbons.

Quantitative Structure-Thermal Stability Relationships. Quantitative structure-property relationships (QSPR) were applied to study the thermal stability of pure hydrocarbons typical of jet fuel components. A simple method of chemical structure description in terms of Benson groups was tested in searching for structure-property relationships for the hydrocarbons we tested experimentally. We also tested molecular connectivity as a structure-based approach to chemical structure-property relationship analysis.

The quantitative structure-property relationship method proved to be a better predictor of degradation behavior for 13 compounds stressed for 4 hours at 450¡C than other approaches based only on topological descriptors. In addition, correlations based on comprehensive descriptors require a smaller number of parameters to achieve the same accuracy of prediction.

H. Thermal Stressing of Authentic or Surrogate Fuels

Key Interactions Among Fuel Components. This study focused on alkylated cycloalkanes and hydrogen donors, such as tetrahydronaphthalene. Both components are predominant in coal-derived jet fuels. We performed model-compound studies of their thermal behavior and interactions with *n*-alkanes, focusing primarily on temperature dependence. We also addressed the possibility of enhancing *n*-alkane stability using specific amounts of cycloalkanes at various temperatures.

Pyrolysis of Binary Mixtures of *n*-Tetradecane and Hydrogen Donors. Model compound reactions were carried out at 450°C in batch reactors. Tetralin appeared to be more effective than benzyl alcohol or *n*-butylcyclohexane in providing lower conversion of the *n*-tetradecane and leaving higher amounts of unconverted hydrogen donor.

Thermal Decomposition of Norpar-13. Norpar-13, a mixture of *n*-alkanes, was found to be a useful model for observing the effects of high-temperature stressing of jet fuels. Norpar was stable in the oxidative regime and increased the amount of pyrolytic deposition detected. The increased pyrolytic deposits made observing the mitigating effects of the additives easier than in an authentic jet fuel. Tetrahydroquinoline (THQ), benzyl alcohol, and tetralin all increased the thermal stability of Norpar-13 in a flow reactor. THQ was the most effective, consistent with batch reactor results, although an oxidative deposit formed with THQ addition.

Norpar-13 was studied under supercritical conditions, both at 425°C in a glass tube reactor and at 450°C in conventional microautoclave batch reactors. Homogenous processes occurring in the bulk fuel formed reactive species, but nucleation of coke particles did not occur at 723K under supercritical conditions. Cycloalkanes, xylene, toluene, and benzene were stable and did not contribute to the formation of solid deposits. Indan and C_2 and C_2-indans were very stable. Radicals formed from tetradecane and other alkanes can abstract hydrogen from these stable compounds to form reactive radicals. Deposit formation in jet fuel/tetradecane mixtures was proportional to the initial concentration of tetradecane, but the direct correlation between deposit mass and tetradecane conversion was poor.

Characterization and Degradation Studies. The oxidative and thermal stabilities of seven fuels were studied by differential scanning calorimetry and in microautoclave reactors. The order of oxidative stability for the fuels was found to be: Jet A > JP-8P > Jet A-1 > JP-7 = JPTS > FR-MD > JP-8C. There was an inverse relationship between oxidative stability and thermal stability. The fuels with higher contents of 1- to 3-ring cycloalkanes and/or hydroaromatics were more stable (in terms of less gas formation) than those with higher contents of long-chain alkanes. Among the paraffinic fuels, higher stability was observed for those fuels having narrower distribution of alkanes with relatively shorter chains. Those fuels with lower aromatic content and more hydrogen-donor compounds exhibited less solid formation. Overall, coal-derived JP-8C and HRI-MD had the best thermal stability among the ten fuels studied, in terms of less gas and solids formation.

TASK 2: INVESTIGATION OF INCIPIENT DEPOSITION

Growth and Deposition of Particles during Heating. We studied the catalytic effects of metal surfaces on thermal degradation and deposit formation at temperatures above 400¡C. Carbon deposition depends on the composition of the metal surfaces and the chemical compositions of the reactants. For Jet-A and *n*-dodecane the same type of metal surfaces have different effects on the formation of carbon deposit. Carbon deposition is also related to the transfer properties of the reaction system. The structure of the deposit provides clues to the competition of different reaction mechanisms (i.e., surface carbon vs. gas-phase carbon deposition).

We placed transmission electron microscope grids at the top and bottom of reactors before thermally stressing Jet A and dodecane to study the deposition processes. Our goal was to obtain information about the phases that existed during thermal stressing by observing the microstructures of the carbonaceous solid. Optical textures and morphologies of carbonaceous deposits generated on reactor walls and on metal grid surfaces were examined and the effect of surface roughness on deposit formation was studied.

Deposit formation from coal-derived JP8C fuel occurred by addition of reactive species at the wall of the reactor, as well as by gravitational settling of particles formed in the bulk phase. Stabilization of reactive species by hydrogen donors present in the fuel occurred simultaneously. Solid formation was determined by the competition among addition of active species to already formed particles, direct addition to the wall, and stabilization by hydrogen donors. The diameter of particles present in suspension at steady state is a function of the concentrations of the intermediates, their diffusion coefficient, the densities of particles and fluid, and the fluid viscosity.

In investigating the gravitational settling (to the reactor bottom) of particles formed in suspension, we calculated the settling velocities by equating the difference between gravitational and buoyant forces to Stokes' Law for viscous drag. The calculated particle settling rate at 8 hours closely agreed with experimental measurements, but at the longest measurement times the calculated rates were nearly 100 times higher. This discrepancy could have been caused by resuspension of large particles during opening and emptying of the reactor.

In studying the initial stages of fuel decomposition and the onset of deposition, we proposed a simple model to describe deposit formation and provide a quantitative framework for calculating rate coefficients. The model involves a first-order decomposition step leading to reactive intermediates, followed by reaction of the intermediates to produce particles, which ultimately settle.

Pretreatment of JPTS fuel with PX-21 activated carbon (50 mg of PX-21 in 15 mL IPTS) delayed degradation and prevented carbon deposition during thermal stressing at 425°C for 5 hours in nitrogen and air atmospheres. The carbonaceous solid formed during stressing was deposited on the activated carbon surface.

Dodecane was thermally stressed with different metal surfaces to determine the effect of metal on deposit formation. Nickel surface catalyzed deposition by forming filamentous carbon. Copper surface formed fibrous carbon. Stainless steel surface had no apparent catalytic effect on the deposit formation process. Eventually the metal surfaces were covered by carbon layers with circular or oval rings on the carbon layers. The ring-formation process is likely related to steady-state growth of the deposit on all available surfaces.

Emphasis of studies of incipient deposition included the formation of deposits on the vertical walls of the reactor by direct deposition of reactive species. Comparison of the particle formation rate per unit of particle surface area for suspended particles and particles on reactor walls showed that these rates were approximately the same, suggesting that similar species and reactions might be involved in both processes. The measured particle size distribution of suspended carbon particles formed in thermal stressing was extremely sensitive to the refractive index of the particles.

The study of carbonaceous deposits on metal surfaces was enhanced by extending previous work to new experimental techniques, including micro-Raman spectroscopy, static secondary ion mass spectroscopy, and environmental scanning electron microscopy. Variations in molecular ordering may be associated with differences in chemical constitution of the deposit, particularly in hydrogen content. The base carbon substrate is more disordered structurally than the unusual ring-shaped structures that form on the deposit. The preferential gasification of the edges of deposit cracks, carried out in the environmental electron microscope, could lead to microstructural surgery that will provide new information on the layered structure of the deposits and on the nature of the metal surfaces under different features of the deposits.

Efforts on refining the deposit growth measurement and characterization of suspended matter in stressed fuels have lead to improvements in the analysis of stressed fuels. The refinements have included detailed quantification of sources of experimental uncertainty in the analytical equipment, elimination of specific sources of measurement error, and development of more accurate procedures for characterizing suspended matter in the stressed liquid fuel.

Deposit Growth. High-surface area activated carbons PX-21 and Maxsorb 92-11A, 94-06, and 94-20 had significant effects on decomposition reactions during thermal stressing of *n*-alkanes at 425¡ and 450¡C. The surface area and surface functionalities were the two most important parameters influencing carbon activity. The higher the surface area, the more prominent the effect of activated carbon; however, carbons with very high surface area (>2000 m^2/g) did not differ in their performance during thermal stressing.

The carbonaceous solids deposited on the carbon surfaces during thermal stressing also played a catalytic role, which is attributed to specific oxygen functionality on the carbon surface and adsorbed species. Carbonaceous solid deposited on the carbon surfaces led to a sharp decrease in nitrogen BET surface area.

Modeling Heat Transfer to Flowing Jet Fuels. We developed a means of modeling heat transfer for flowing jet fuels, using an entry-length heat and mass transfer model for flow in tubes.

Hydrocarbon Fuel Degradation in the Presence of Hydrogen Donors as Stabilizers. We attempted to establish the minimum volumetric concentrations of hydrogen donors (i.e., tetralin, benzyl alcohol, and THQ) needed to significantly inhibit the degradation of *n*-tetradecane at 450°C for a residence time of 30 minutes. We also compared the efficacy of each donor under identical conditions and investigated the stability of THQ in the binary mixture at low temperature (250°C) and long residence time (up to 6 hours).

TASK 3: CHARACTERIZATION OF SOLID GUMS, SEDIMENTS, AND CARBONACEOUS DEPOSITS

Effects of Adding Solid Carbons on Thermal Degradation. Thermal stressing of JP-8 was conducted in the presence of alumina, carbonaceous deposits recovered from earlier stressing experiments, activated carbon, carbon black, and graphite. The addition of different solid carbons during thermal stressing led to different reaction mechanisms. Activated carbon, carbon black, and graphite prevented solid deposition during thermal stressing of JP-8 at 450¡C for five hours. Alumina and the deposit obtained from previous thermal stressing resulted in a considerable increase in the amount of carbonaceous solid. The only obvious difference in the appearance of liquid products occurred with addition of 1 g of activated carbon to 10 mL of JP-8, which produced a much lighter colored liquid than the JP-8 stressed without an additive.

Deposition mechanisms were also affected by the presence of different carbon surfaces during thermal stressing. The solid carbons with the most disordered structure and highest surface reactivity (i.e., activated carbons) produced the most significant effect on thermal degradation. These surfaces appeared to be effective in stabilizing free radicals or enhancing recombination reactions. It is not yet clear whether the surface area or the pore size distribution of the activated carbons is responsible for preventing solid deposition and stabilizing the fuel.

Addition of PX-21 activated carbon effectively stops the formation of carbonaceous solids on reactor walls during thermal stressing of JPTS. We found that 50 mg of PX-21 per 10 mL of fuel was sufficient to prevent carbon deposition and stabilize JPTS at 425¡C. At least 100 mg of PX-21 was necessary to prevent solid deposition at 450¡C for 5 hours. The reactions during thermal stressing of JPTS with high surface area activated carbon were quite different from those that occurred in the absence of added carbon.

Carbonaceous Deposit Formation on Metal Foils. Filamentous carbon and fibrous carbon were detected on nickel and copper surfaces respectively, possibly as a result of the catalytic effects of the metal surfaces. A common feature of carbon deposit on all metal surfaces studied was the circular or oval ring structure, which is probably related to the further growth of deposit on previously formed carbon deposit surfaces. For nickel alone, the deposit produced from JP-8C was covered by another glassy layer of material, suggesting that nickel is involved in the thermal degradation chemistry.

Effects of High-Surface-Area Activated Carbon and Decalin on Thermal Degradation of Jet A-1 Fuel. Adding decalin as a hydrogen donor reduced the extent of decomposition of both dodecane and the jet fuel. The activated carbon addition appears to promote H-transfer reactions during thermal stressing. In addition, primary radicals were stabilized on the carbon surfaces. The degree of thermal degradation of both the fuel and the dodecane depends on the amounts of activated carbon and decalin added.

Effects of Surface Chemistry on PX-21 Activated Carbon during Thermal Degradation of Jet A-1 Fuel and *n*-Dodecane. The nature and activity of the activated carbon surface during thermal stressing was an important parameter in deposit formation. The surface oxygen concentration was reduced by outgassing at 900°C in nitrogen. The activity of PX-21 in

preventing carbon deposition increased considerably with the pretreatment. The outgassed carbon showed lower catalytic activity in promoting hydrogen-transfer reactions and converting decalin to naphthalene. Surface complexes on the carbon surface apparently act as active sites for hydrogen-transfer reactions.

A carbonaceous overlayer that formed on the surface of PX-21 after thermal stressing of model compounds inhibits further deposition more effectively than the original PX-21. Surface oxygen complexes on the carbonaceous overlayer appeared to be the active species during thermal stressing. Unusual carbon filaments or fibers appear to originate from a carbonaceous overlayer formed during the first stressing. The formation of carbon filaments on activated carbon surfaces at the relatively low temperature of 425°C had not been reported in previous literature. Extraction of PX-21 with toluene showed the presence of aromatic hydrocarbons that may diminish its activity during thermal stressing.

High-Surface-Area Activated Carbons. High-surface-area activated carbons suppress carbon deposition and help retard the degradation of dodecane. Surface area higher than 2000 m^2/g did not increase the catalytic effect and the ability of the carbon to suppress deposition during thermal stressing. Toluene extraction of activated carbons before thermal stressing resulted in an increase in the effectiveness of the activated carbon added. The concentration of naphthalene in the stressed liquids depended on both the H-transfer reactions and degradation processes that took place during thermal stressing.

Characterization of Actual Engine Deposits. Different reaction and deposition mechanisms prevailed in different sections of the fuel system. Temperature and concentrations of oxygen were important factors governing deposition on different parts of an engine fuel system. Metal surface also seemed to affect the formation of deposits inside the main tip. The deposits obtained with model compounds heated in the presence of metal foils beared resemblance to those from actual engines in that a two-layer deposit structure was observed on an active metal substrate, such as nickel.

Surface Effects on Deposit Formation in a Flow Reactor System. Further flow reactor experiments were conducted with Norpar-13 to study metal surface effects on deposit formation. Large amounts of carbon deposit formed at 500 psig, 550°C for 5 hours. Filamentous and platelet carbon form under these conditions, neither of which is normally expected to form under these flow reactor conditions. We surmised that a narrow temperature window must exist for the formation of large amounts of filamentous carbon and thick carbon platelets, because no collectable carbon deposits were formed at 525°C or 575°C.

Effect of Carbon Surfaces on Thermal Decomposition of Hydrocarbons. We stressed cyclohexane and ethylbenzene at 450°C for 2 to 23 hours. The addition of PX-21 high-surface-area activated carbon inhibited thermal decomposition of cyclohexane, but accelerated decomposition of ethylbenzene.

TASK 4: COAL-BASED FUEL STABILIZATION STUDIES

Use of ^{13}C Labels to Trace Reactions of Potential Antioxidants. ^{13}C NMR spectroscopy, along with ^{13}C-labeling techniques, were used to examine the thermal stability of a jet fuel sample mixed with 5% benzyl alcohol. A Jet A-1 fuel laced with α-^{13}C -labeled benzyl alcohol was thermally stressed. ^{13}C labeling at the α position of the benzyl alcohol enabled us to clearly follow the reaction pathway of the labeled α carbon in the presence of complex mixtures of hydrocarbons whose carbons were at natural abundance levels (1%). Toluene and benzene were the major reaction products with the production of benzoic acid and benzaldehyde as intermediates.

Thermal Stability Studies Using the Model Compound Dodecane. We chose to simplify the experimental methodology of fuel stabilization studies to elucidate the underlying mechanisms involved. Understanding the reasons why benzyl alcohol and similar molecules retard the formation of carbonaceous solids in hydrocarbon mixtures at high temperature is an important precursor to the development of superior additives. Dodecane was chosen as a model compound for additive studies because it is the most abundant hydrocarbon in jet fuels and numerous other studies have been performed on dodecane.

Infrared studies indicated that during the thermal degradation of dodecane, the formation of alkenes occurs, followed by subsequent cyclization, aromatization, and condensation. In dodecane, aromatic species are directly derived from the parent hydrocarbon upon thermal stressing. Infrared studies were supplemented by proton nuclear magnetic resonance and gas chromatography/mass spectrometry to help determine mechanistic ramifications.

Screening Potential Jet Fuel Stabilizers Using Dodecane. Seven additives were tested for their ability to retard decomposition of dodecane at 450°C under nitrogen. Of these seven compounds, 9,10-dihydrophenanthrene and 1,2,3,4-tetrahydroquinoline gave superior results. The 9,10-dihydrophenanthrene has excellent thermal stability at 450°C and good resonance stabilization of the radical scavenger.

Parameters have been developed to predict the effectiveness of organic additives in stabilizing fuels (i.e., inhibiting thermal degradation) and preventing the formation of carbonaceous solids. The additives must be thermally stable above 400°C and must have hydrogen atoms that can be transferred or abstracted by hydrocarbon radicals. The greater the number of these available hydrogen atoms, the better. The radicals generated from hydrogen atom abstraction should be stabilized by resonance.

Tetrahydroquinoline appeared to be a superior additive for inhibiting the thermal degradation of dodecane. It has four transferable hydrogens and is relatively stable at 425°C. Its N-H bond is weaker than the C-H bond and the radicals formed are stabilized by delocalization through the aromatic ring.

Tetrahydroquinoline. Tetrahydroquinoline (THQ) was also studied for its ability to inhibit degradation of *n*-tetradecane at 450°C for various sample volumes. THQ was shown to

be a very effective hydrogen donor, in terms of both its radical scavenging abilities and its own thermal stability at this temperature.

Hydrogen-Transferring Pyrolysis of Tetradecane. Hydrogen transferring pyrolysis-thermal decomposition of hydrocarbons in the presence of hydrogen donors was investigated as a means for enhancing high-temperature stability. Compared to pyrolysis of pure tetradecane at 450°C, adding 10 vol% of the hydrogen donor tetralin suppressed decomposition by about 68% after 11 minutes, 66% after 21 minutes, and 37% after 30 minutes. Tetralin also altered the product distribution. Decomposition and isomerization of primary radicals were strongly suppressed. The overall reaction mechanism for the initial pyrolysis stage was characterized by one-step β-scission of a secondary radical followed by H-abstraction of the resulting primary radical. Adding 10 vol% tetralin to JP-8, tetradecane, and *n*-butylbenzene reduced the formation of deposits by 90%, 77%, and 54%, respectively.

Phase Behavior of Jet Fuels Using the Lattice Fluid Model. Spinoidal lines for phase diagrams of dodecane with benzene, toluene, ethylbenzene, and phenol were calculated. In all cases, a 95:5 mixture was assumed for the calculation. The benzene, toluene, and ethylbenzene systems were reasonably similar, but the dodecane/phenol mixture was significantly different.

In Situ Regeneration of Benzyl Alcohol. Benzyl alcohol and 1,4-benzenedimethanol are effective stabilizers at temperatures above 400°C for jet fuels and the model compound dodecane. The addition of ethanol to hydrocarbon/benzyl alcohol mixtures had a significant effect on the thermal stabilization of jet fuels above 400°C. Ethanol appears to reduce the benzaldehyde formed during the degradation of benzyl alcohol, effectively regenerating the benzyl alcohol. Thus, in the presence of ethanol, less benzyl alcohol is required for thermal stabilization of jet fuel.

Kinetic Studies on Potential Jet Fuel Stabilizers. Kinetic studies were performed on dodecane, dodecane/tetrahydroquinoline mixtures, and dodecane/benzyl alcohol mixtures in the temperature range 400-500¡C. Rate constants and Arrhenius parameters were calculated.

Design of Thermally Stable Jet Fuels at Moderate and High Temperatures. We examined the prospects of stabilizing fuels at both moderate temperatures (<250°C) and high temperatures (>400°C), performing systematic experiments to investigate the reactions of dodecane with a tetrahydroquinoline additive and of Jet A-1 with tetrahydroquinoline and benzyl alcohol additives.

Design and Synthesis of Second Generation Jet Fuel Stabilizers. We identified several novel additives as important leads in the development of practical high-temperature thermal stabilizers. Their susceptibility to autoxidation at lower temperatures limited their application. Consequently, we undertook a series of studies to develop novel hybrid stabilizers, based on the combination of two or more existing additives which have complementary antioxidant abilities for the full temperature range of stabilization.

TASK 5: EXPLORATORY STUDIES ON THE DIRECT CONVERSION OF COAL TO HIGH QUALITY JET FUELS

Production of Jet Fuels from Coal. Work was undertaken to develop novel bimetallic dispersed catalysts and determine optimum conditions for coal conversion. Several heterometallic complexes consisting of two transition metals and sulfur in a single molecule were synthesized and tested as precursors of bimetallic dispersed catalysts for liquefaction of Montana subbituminous and Pittsburgh #8 bituminous coals. We found that both the ligands to the metal species and the type of bonding between the two metals significantly affected the activity of the resulting catalyst. Among the M-M type precursors tested, Co-Mo thiocubane, $Mo_2Co_2S_4(Cp)_2(CO)_2$ [Cp = cyclopentadiene], produced the best catalyst. The performance of the Co-Mo bimetallic sulfide catalyst was further enhanced in temperature programmed liquefaction.

Hydrogenation/Dehydrogenation. Coals rich in resinite are potential feedstocks for jet fuel production, because resins consist predominantly of two-ring cycloalkane structures. These cycloalkanes are linked to the side chains of the coal networks and can be liberated in the liquefaction process. To improve our understanding of the structures of potential coal feedstocks, we collected various NMR parameters of two samples of Blind Canyon (Utah) bituminous coal using solid state ^{13}C NMR. The experiments included cross-polarization and magic-angle spinning, Bloch decay, dipolar dephasing and various relaxation time experiments. Because resinite is a complex mixture of polymerized products, we chose to study the model compounds rosin, which makes analysis of products easier and evaluation of reaction pathways less complicated. In a sense, rosin is a simplified analog of resinite and its hydrogenation and dehydrogenation behavior provides insight into resinite liquefaction.

Structural Correlation by Coal Liquefaction Oils. We found that with careful selection of the feedstock, we could achieve 85—95% conversion of coal to liquids, with 40—50% of the dichloromethane-soluble products being naphthalenes. (Further hydrogenation of the naphthalenes likely would produce the highly stable decalins.) Pyrolysis-gas chormatography/mass spectrometry has proven to be a useful predictive tool in relating the composition of lighter liquefaction products to the structural features of the feedstock coals.

Molecular Structure of Polycadinene from Dammar Resin. Nuclear magnetic resonance data for Dammar resin indicated that structures proposed in previous literature were not entirely correct. A new structural composition must be proposed for polycadinene-like resin polymers such as Dammar resin. Considering Dammar resin s similarity to the resinite from the Blind Canyon bituminous coal, we made significant progress toward developing a working structural model for this component of a potential feedstock for jet fuel production.

Thermal Decomposition of ^{13}C-Labeled Bibenzyl in the Presence of Additive-Free Jet A-1. Carbon-13 nuclear magnetic resonance was used to follow the decomposition of bibenzyl and benzyl alcohol and the formation of toluene in thermal stressing. No other ^{13}C- labeled reaction products were detected within 24 hours. Had any high-molecular-weight aromatics formed from bibenzyl, they would have implicated the reactive benzylic radical as a precursor to the

formation of carbonaceous solid deposits. We determined that the benzylic radicals instead acted as hydrogen scavengers and were capped to form toluene as the only significant product.

Producing Cycloalkanes from Dammar Resin. In the hydrogenation of Dammar resin, the low-molecular-weight dimers and trimers of cadinene began to crack into naphthalenes and benzenes. At long reaction times, undesirable recombination reactions occurred, but the low-molecular-weight fraction was almost totally converted to compounds that can be upgraded to cycloalkanes. The polymeric fraction of the resin was converted to dimethylnaphthalene and cadinane.

Blind Canyon Coals Study. Elemental analyses and ^{13}C NMR data of Blind Canyon vitrinite show that the average carbon structure consists of approximately four aromatic rings per cluster with a crosslink density of five attachments per cluster. Aliphatic side chains with terminal methyl groups are the primary functional groups forming these attachments. The low aliphatic ether and carboxyl and carbonyl fractions suggest that the majority of the oxygen occurs in phenol or phenolic ether groups. The NMR data also predict that there are approximately 2 protonated carbons, 2 bridgehead carbons, 1.3 substituted carbons, and 0.7 phenolic carbons per cluster.

Hydrotreatment of Multicyclic Compounds to Produce Cycloalkanes. We clearly demonstrated that cycloalkanes and hydroaromatics are desirable components of advanced jet fuels because of their high thermal stabilities. Therefore, materials that are predominantly cycloparaffinic could be ideal potential feedstocks for advanced fuels. We examined the hydrogenation, dehydrogenation, and cracking of rosin, and the hydrocracking reactions of Dammar.

Shape-Selective Naphthalene Hydrogenation. The ability to convert naphthalene selectively to *trans*-decalin could result in a fuel of exceptional stability. Decalin is a useful additive for suppressing degradation. The propensity of a fuel to form carbons can be reduced by limiting its aromatic content (e.g., converting naphthalene to decalin). We found that *trans*-decalin is more stable than *cis*-decalin. We prepared and tested eight catalysts to determine their ability to selectively convert naphthalene to *trans*-decalin.

Hydrogenation experiments with naphthalene showed that *cis*-decalin rapidly formed and isomerized to *trans*-decalin. A unique catalyst, platinum on HY zeolite, produced *cis*-decalin with high selectivity and did not promote isomerization.

Coal Liquids Upgrading Using Mesoporous Sieve Catalysts. This work involved the synthesis of mesoporous molecular sieves, characterization of these materials, and their catalytic evaluation for the conversion of polycyclic aromatic model compounds and coal-derived oils. We characterized the mesoporous molecular sieve catalysts using chemical analysis, surface area measurement, thermal analysis, and solid state nuclear magnetic resonance spectroscopy. We also catalytically evaluated these materials for hydrogenation of naphthalene and phenanthrene and alkylation of naphthalene.

In the preparation of mesoporous molecular sieve catalysts for upgrading coal liquids, sodium aluminate proved to be a good source of aluminum for synthesis of the mesoporous

aluminosilicates. Differential scanning calorimetry can be used to determine the relative acidities of the molecular sieves. Platinum loading on samples of a mesoporous molecular sieve, Al-MCM-41, by wet impregnation yielded large crystallites with good uniformity. The sieves are also capable of converting large molecules, such as 1,3,5-triisopropylbenzene.

Reactor Systems. We designed and constructed two new reactor systems for performing studies in coal liquefaction a 300 mL batch autoclave reactor system and a continuous flow mini-pilot plant reactor system.

Hydrogenation/Dehydrogenation of Polycyclic Compounds using MoS_2 as Catalyst. We examined the catalytic hydrogenation and dehydrogenation behavior of naphthalene, tetralin, pyrene, and hydropyrenes, using molybdenum disulfide as a catalyst. We confirmed that both decalin isomers can be produced in parallel during naphthalene hydrogenation over metal-loaded zeolites. The hydrogenation of A9,10-octalin and A1,9-octalin may play an important role in determining the decalin *cis*-/*trans*- configuration.

There were strong synergistic effects between water and dispersed molybdenum sulfide catalyst for promoting liquefaction of Wyodak subbituminous coal and Pittsburgh #8 bituminous coal at temperatures below 375°C. The promoting effects of water were more pronounced for the lower rank subbituminous coal. At temperatures below 400°C, water had a negative impact on the catalytic liquefaction of both coals. This effect was more dramatic for Wyodak coal than for Pittsburgh #8.

Low Temperature Routes to Hydrogenation. We conducted preliminary studies of Wyodak coal to determine whether non-radical pathways are responsible for hydrogen incorporation at mild conditions (350°C, 1000 psi H_2, and 30 minutes reaction). We found that conversions of Wyodak at 350°C were not catalyzed by mineral matter present in the coal. Pittsburgh #8 was reacted in hydrogen without solvent or catalyst at 300°C. No evidence of hydrogenation was observed.

Hydrogenation/Dehydrogenation of Polycyclic Aromatic Hydrocarbons. The hydrogenation and dehydrogenation behaviors of naphthalene, phenanthrene, and pyrene were investigated via their product distributions and kinetic and thermodynamic parameters. Hydrogenations were carried out at 350°, 400°, and 450¡C for various times up to equilibrium conditions. We calculated the forward and reverse rate constants and Arrhenius parameters. We also obtained enthalpy data and compared the values to published values. We found that the temperature at which dehydrogenation became favorable relative to hydrogenation reactions decreased with increasing ring size.

Noble Metal Catalysts for Low-Temperature Naphthalene Hydrogenation. Low-temperature catalytic hydrogenation of naphthalene was investigated as a model reaction for low-temperature hydrotreating of coal-derived liquids to produce thermally stable jet fuels. We found supported noble metal catalysts to be significantly more active than a commercial NiMo hydrotreating catalyst. At 473 K, naphthalene hydrogenation over these noble metal catalysts proceeded, even in the presence of 4200 ppm benzothiophene. Sulfur addition decreased the activity of all noble metal catalysts. Palladium catalysts had higher sulfur resistance than

platinum. A Pd/TiO_2 catalyst was the most active and the least affected by sulfur among the three noble metal catalysts studied.

Conformational Isomerization of *cis*-Decahydronaphthalene over Zeolite Catalysts. Platinum- and palladium-loaded mordenites proved to be very effective catalysts for conformational isomerization of *cis*-decalin to *trans*-decalin at 473K under hydrogen. The selectivity to *trans*-decalin is nearly 100%, with a *trans*-/*cis*- ratio of nearly 13.

For hydrogenation of naphthalene in *n*-tridecane at 200°C, both platinum and palladium catalysts supported on MCM-41 zeolite were substantially more active than the corresponding catalysts supported on alumina or titania. Both Pt/MCM-41 and Pd/MCM-41 catalysts promoted hydrogenation to completion, so that the dominant products were *trans*- and *cis*-decalin. Palladium catalysts showed higher selectivity to *trans*-decalin, whereas higher selectivity to *cis*-decalin was afforded by platinum catalysts. The selectivity to decalin isomers also depended on the support and metal type. Among the three supports, MCM-41 produced the highest *trans*-/*cis*- ratio. Palladium has the higher *trans*-/*cis*- ratio.

Contribution of Mineral Matter to Low Temperature Liquefaction Mechanisms. Based on experiments with Wyodak subbituminous coal, we found that there was no mineral matter catalysis of hydrogen donation.

Zeolite-Supported Pd and Pt Catalysts for Low-Temperature Hydrogenation of Naphthalene. In our effort to develop a kinetic model for deposit formation from jet fuel, we performed parameter estimation from multi-response data. Zeolite-supported Pt and Pd catalysts were prepared using a mordenite (HM38) and a Y-zeolite (HY) as support materials, and were applied for hydrogenation of naphthtalene in *n*-tridecane at 200°C in the absence and presence of added benzothiophene. The results were compared to those with Al_2O_3- and TiO_2-supported Pt and Pd catalysts. Both Pd/HM38 and Pd/HY catalysts were substantially more active than the Pd/Al_2O_3 and Pd/TiO_2 catalysts, even when the former was used with less catalyst loading under H_2 pressure. The same trend was observed when comparing the Pt catalysts. The sulfur-resistance and the activity of the catalysts depended strongly on the type of support and metal. Addition of sulfur to form benzothiophene decreased the activity of all catalysts tested. The noble metals demonstrated significantly improved sulfur tolerance when supported on zeolites, rather than Al_2O_3 or TiO_2. The Pd catalysts supported on both Y-zeolite and mordenite showed higher sulfur tolerance than all other catalysts. Overall, Pd/HM38 showed the best activity and the highest resistance to sulfur poisoning.

Development of Coal-Based Jet Fuels Via Coprocessing of Coal and Resid. An investigation of co- coking of coals with petroleum resids was undertaken to investigate the feasibility of adding coal to delayed cokers as an economical alternative to putting coal into oil refineries. This would enable us to take advantage of some of the desirable, highly thermally stable coal-derived components.

A series of coals and petroleum resids were reacted under conditions simulating delayed coking to investigate retrogressive reactions and soluble product composition. Preliminary results suggest that there are systems which can produce substantial two- and three-ring aromatics in the liquid products.

Hydrogenation of Coal at Mild Conditions. We determined that petrological composition, coal rank, and mineral matter composition must be taken into account in coal hydrogenation. The comparison of hydrogenation behavior can be made only for coal with similar petrological composition. The most common types of catalysts are the metal precursor catalysts (e.g., Mo, Fe, and Sn) and acid catalysts (e.g., metal halides). Several new methods of coal hydrogenation are available, including hydroboration-protonolysis and plasma hydrogenation. Plasma hydrogenation is a good candidate method; it could potentially allow us to decrease the temperature below 200°C and replace the high pressure with a vacuum.

Hydroboration as a Method of Coal Hydrogenation and Liquid Product Upgrading. We found that hydroborane reacted with the coal structure, causing some interesting changes. It could also react with the condensed structure of the liquefaction residue. If further experimentation confirms these assumptions, hydroboration could be a very effective method of coal hydrogenation. In addition, it could allow us to hydrogenate condensed aromatic blocks.

Hydrodeoxygenation Under Coal Liquefaction Conditions Using Novel Organometallic Catalyst Precursors. The combination of either a CoMo or a NiMo catalyst and a liquefaction stage could potentially increase the quality of liquefaction distillates by facilitating oxygen removal. This hypothesis must first be tested on a wide range of coals with varying rank and oxygen content. The catalysts precursors must be comparable (e.g., similar surface area, dispersion, active forms, and conversion to those active forms) and the organometallic precursors must show a marked improvement to prove the viability of this approach.

Coal/Resid Coprocessing. We found that water can aid the conversion during coal/resid coprocessing with an ATTM catalyst at 375°C and suppress the conversion at 475°C. In addition, water removal before the second stage reaction at 425°C can significantly improve coal conversion. Further increasing either the first- or second-stage temperature can be detrimental to the conversion under the conditions used.

Carbon Skeletal Isomerization. When the initial hydrogen pressure of 1000 psig and temperature of 330°C for two metal mordenite catalysts is increased to 350°C for two Y-zeolite catalytic systems, the isomers of cyclohexane include methylcyclopentane and other by-products. Selectivities over two mordenite catalysts are more strongly influenced by and more sensitive to temperature changes. The amount and number of by-products are also dependent on temperature change. Among the by-products were cyclo-isomers. More research will be required to determine the mechanics of these reactions.

TASK 1. INVESTIGATION OF THE QUANTITATIVE DEGRADATION CHEMISTRY OF FUELS

1.1 EFFECTS OF HYDROGEN DONORS ON THE PYROLYSIS OF TETRADECANE AT 450¡C UNDER N_2 PRESSURE

This study is explained in detail in *Advanced Thermally Stable Jet Fuels Technical Progress Report, August—October 1992.*

Introduction

The hydrogen-transferring pyrolysis described here refers to the thermal decomposition of hydrocarbons in the presence of H-donors. This work was a continuation of a fundamental study of condensed-phase pyrolysis of saturated hydrocarbons including the straight-chain paraffins, alkylcyclohexanes, trans- and cis-steric isomers of decalin, as well as hydroaromatics such as tetralin. One of the critical problems in developing thermally stable jet fuels for high-Mach aircraft is the formation of solids from hydrocarbon fuels in pyrolytic regime.[1, 2, 3] In studying the pyrolytic degradation of jet fuels, we concluded that hydrogen-transfer from H-donors, such as those present in coal-derived JP-8C jet fuel, could play an important role in suppressing thermal decomposition of hydrocarbon components and solid formation[3, 4, 5, 6].

The experimental conditions used in this work closely approximated the severity of the anticipated high-temperature thermal environment of jet fuel in the future high-Mach aircraft under consideration.[3] These conditions were characterized by condensed or supercritical phases, relatively high pressure, a static reactor, and a long residence time. Such conditions distinctly differ from those used in most previous paraffin pyrolysis work (which were characterized by vapor phase, low-pressure, flow reactor, and short residence time). We performed a detailed analysis of products from pyrolytic degradation of tetradecane; examined the inhibiting effects of H-donors on the decomposition of *n*-tetradecane (n-C_{14}); and determined the mechanisms of the pyrolysis and H-transferring pyrolysis of *n*-C_{14}.

Experimental

We used reagent-grade normal tetradecane, *n*-C_{14}, tetralin, trans-decalin (trans-D) and cis-decalin (cis-D), and decalin (mixture) from Aldrich and a petroleum-derived JP-8P jet fuel [Song et al., 1992a, 1992b]. The hydrogen-donor compounds examined in this work included tetralin, decalin, cis-D and trans-D. In a typical run, 5 mL of *n*-tetradecane (about 3.8 g, 19 mmoL) was charged into the reactor. For hydrogen-transferring pyrolysis, the mixture of *n*-tetradecane and a H-donor agent, usually 10% by volume, was transferred into the reactor. The pyrolysis was conducted at 450¡C for 0-8 hours under 0.69 MPa UHP-N2 (cold) in 25 mL tubing bombs using a 5 mL sample [Song et al., 1993a]. A fluidized sandbath preheated to 450¡C was used as heater. The products were identified by capillary GC-MS and quantified by GC. More analytical details may be found in an earlier paper [Lai et al., 1992].

Results and Discussion

1. *n*-Tetradecane pyrolysis. Pyrolysis of *n*-tetradecane at 450¡C for 0-8 hours produced nearly 175 compounds, and the products ranged from lightest molecules, such as hydrogen and methane, to heavy polyaromatics, such as pyrene and solid deposits. **Table 1.1-1** shows the yields of products expressed as molar percentage based on *n*-tetradecane.

Several trends can be seen from the data in Table 1.1-1:

1. In the liquid products, there are no particular products that have high selectivity from C_4 to C_{11}.

2. In the early periods of the pyrolysis, 1-tridecene and *n*-C_{13} products are scarce and there is very little *n*-C_{12}. After 30 minutes at 450¡C, 1-dodecene is still more abundant than *n*-C_{12}.

3. The conversion of *n*-tetradecane (*n*-C_{14}) increases, but the ratio of 1-alkene to the corresponding *n*-alkane in the products decreases with increasing residence time. The yields of some 1-alkenes increase and reach a maximum after 1 to 2.5 hours at 450¡C, then start to decrease. After 30 minutes at 450¡C, 53 percent of the *n*-C_{14} has been decomposed, and the main products are C_1-C_{13} alkanes and C_2-C_{13} 1-alkenes.

4. Finally, in the liquid products, cyclohexanes appear before alkylbenzenes, and alkylbenzenes appear before alkylnaphthalenes. This observation supports the proposed mechanisms for solid formation from jet fuels under pyrolytic conditions.[6] By analyzing the product distribution and its variation with time in a quantitative fashion, we have developed a general and fundamental understanding of the reaction mechanisms for thermal cracking of long-chain *n*-alkanes, such as *n*-tetradecane, under high-pressure pyrolytic conditions.

Scheme I shows the proposed, generalized reaction mechanisms for thermal cracking of long-chain alkanes, such as tetradecane, under the conditions employed.[6] Under these conditions, the pyrolysis of *n*-tetradecane proceeds by radical reaction pathways. The initiation reaction is the homolytic cleavage of a carbon-carbon bond, producing two radicals. These radicals then abstract hydrogen from a molecule, primarily the reactant substrate itself, in the initial period. The first substrate radicals from *n*-C_{14} include both *sec*-$C_{14}H_{29}$¥ (eq.2) and *pri*-$C_{14}H_{29}$¥ (eq. 3). Formation of the primary radical requires slightly higher activation energy (e.g., the activation energies required for H-abstraction by a radical from *n*-butane to form 2-C_4H_9¥ and 1-C_4H_9¥ at 700 K are 10.4 and 12.3 kcal/mol, respectively).

The data in Table 1.1-1 indicates that the carbon number distribution of the products from *n*-tetradecane is broad and there is little selectivity. There are two possible explanations for the largely non-selective product distribution. First, the energy required to abstract any secondary hydrogen in long-chain paraffins such as *n*-tetradecane is about the same. Second, the homolytic cleavage of long-chain alkanes is not very selective, because both the activation energy and the A-factor values are similar for the formation of different pairs of two radicals with ≥ 2 carbon atoms. Supporting evidence can be found from the Arrhenius parameters for three different initiation reactions of *n*-hexane at 700 K, as shown in **Table 1.1-2**.

Thermal decomposition of long-chain paraffins is still the subject of pyrolysis research. Several papers within the last decade reported the preferential formation of 1-alkenes from vapor-phase pyrolysis of long-chain paraffins.[7, 8] In this work, significant amounts of olefins, mainly 1-alkenes, were also detected, both in liquid and gaseous products. However, unlike the literature results for high temperature and short-residence time pyrolysis, our work indicated that the olefins were not dominant species for most product groups with the same carbon number, with the exception of C_{12}, for which 1-dodecene yield was substantially higher than dodecane for 6-21 minute runs.

In the initial stage of *n*-C_{14} pyrolysis (6 minutes, Table 1.1-1), there was very little *n*-dodecane, but 1-dodecene was dominant among the C_{12} products. This results from the different reaction pathways involved in the formation of these two compounds. In the initial reaction stage, the m-2 paraffinic product $C_{m-2}H_{2(m-2)+2}$ of the reactant C_mH_{2m+2} can probably only be formed from β-scission **(Scheme II)** of a primary C_mH_{2m+1}¥ followed by hydrogen abstraction, whereas the secondary CmH_{2m+1}¥ radical of the substrate affords the m-2 olefinic product $C_{m-2}H_{2(m-2)}$. Therefore, among reactions 2 and 3 in **Scheme 1**, reaction 2 is dominant.

Another general trend involved the decrease in yields of 1-alkenes including 1-dodecene, and an increase in the corresponding *n*-alkanes including *n*-dodecane as time increased up to certain residence time, as shown in Table 1.1-1. This can probably be attributed to two kinds of reactions in later stage: 1)Formation of diene from 1-alkene followed by cyclization and dehydrogenation and 2) Hydrogenation of the alkenes by the hydrogen generated in situ.

The possible mechanism for olefin hydrogenation is shown in **Scheme IV**. GC analysis indicated the presence of molecular H_2 in the gas products, and its yield increased with residence time from 3.2% (mol%) in 1 hour to 8.4% in 8 hours, as shown in Table 1.1-1. Apparently, H2 was produced through dehydrogenation, cyclization, and condensation reactions. The free hydrogen atom for reaction 9 could be formed by the H-abstraction reaction **(Scheme III)** of a radical from molecular H2. Such radical H-abstraction reactions require relatively low activation energy (e.g., 11.3, 15.2, and 16.0 kcal/mol for CH_3¥, C_2H_5¥ and 1-C_3H_7¥ respectively). When the free hydrogen becomes available, the olefin hydrogenation can proceed easily, because such reactions require very low activation energies. The activation energies for hydrogen-atom addition to C_2 to C_5 1-alkenes to form 2-alkylradical at 700 K are as low as 1.2-1.5 kcal/mol.

In regard to other reactions of olefins, other research has found that alkylation of the olefin by the radicals can produce C_{18} to C_{30} branched alkanes during liquid-phase pyrolysis of *n*-hexadecane. Such reactions, if any, could also compete with the reactions 9 and 10. The activation energies for the addition of CH_3¥ and C_2H_5¥ radicals to propylene at 700 K are approximately 7.4 and 7.5 kcal/mol, respectively. However, our detailed GC-MS and GC analyses of products indicate that essentially all of the C_4-C_{13} alkanes and C_4-C_{13} alkenes produced from *n*-C_{14} under the present conditions are straight-chain products. These results suggest that the C_{15} to C_{18} *n*-alkanes we detected resulted from the combination of two 1-alkyl radicals.

Higher alkanes such as pentadecane, hexadecane, heptadecane, and octadecane were also detected in very small amounts from *n*-C_{14} after 6-150 minutes at 450¡C. These products have 1-9 more carbon atoms in their chain than *n*-C_{14}, indicating the occurrence of radical recombination between two primary radicals, C_mH_{2m+1}¥ and CnH_{2n+1}¥, generated from *n*-C_{14} (See equation 8, Scheme I). These higher alkanes begin to diminish after 1 hour at 450¡C.

2. Hydrogen-transferring pyrolysis of *n*-tetradecane. **Table 1.1-3** presents the results for hydrogen-transferring pyrolysis of *n*-tetradecane in the presence of the hydrogen donor, tetralin. For H-transferring pyrolysis at 450¡C for 30 minutes, adding tetralin significantly suppressed the decomposition of *n*-C14. Upon addition of 10 vol% tetralin, the conversion of *n*-C_{14} decreased from 32 to 11 mol% after 21 minutes, and from 53 to 37 mol% after 30 minutes Pyrolysis of *n*-C_{14} in the presence of tetralin at 450¡C for 12-30 minutes gave decreased yields of both alkanes

and alkenes. Surprisingly, the yields of lower alkanes decreased more than those of corresponding 1-alkenes upon tetralin addition. For example, for *n*-C_{14} pyrolysis at 450¡C for 30 minutes, the ratio of 1-dodecene to *n*-dodecane increased from 1.6 to 2.6, and that of 1-undecene to undecane increased from 0.5 to 0.6 upon addition of 10 vol% tetralin.

Table 1.1-3 also indicates that methane formation from *n*-C_{14} was suppressed greatly by adding tetralin. The extent of the decrease in CH4 yields, relative to pure *n*-C_{14} pyrolysis, increased with increasing amount of tetralin added from 5 to 50%. At 450¡C for 12-30 minutes with 10% tetralin, the yields of 1-alkenes from *n*-C_{14} also decreased with increasing carbon-number from 4 to 13.

The effects of tetralin appear to be dependent on the residence time. Within the first 6 minutes, the effects of tetralin on *n*-C_{14} pyrolysis are small. This is primarily because the first 6 minutes involves mainly the heat-up period, and the extent of decomposition of *n*-C_{14} is very small, only 4%. When the residence time is extended to 12 minutes, the presence of 10 vol% tetralin had a remarkable effect: 12% more *n*-C_{14} remained unconverted i.e., the decomposition of *n*-C_{14} was inhibited by about 14% [(94.6-83.1)/83.1 = 13.8%]. The presence of 10 vol% tetralin suppressed the decomposition of *n*-C_{14} by about 31% [(89.2-68.3)/68.3 = 30.6%] after 21 minutes, and by about 42% [(66.2-46.7)/46.7 = 41.8%] after 30 minutes.

Adding tetralin or decalin can significantly suppress solid formation[9, 10]. The enhanced stability of hydrocarbons in H-transferring pyrolysis can be attributed to the stabilization of the reactive radicals via hydrogen-abstraction from tetralin or decalin type compounds, which contributes mainly to inhibiting the secondary radical reactions and suppressing solid formation, as shown in **Scheme V**.

Based on the compositional differences of the products and the mechanisms shown in Schemes I and V, tetralin seems to be more effective in stabilizing the *pri*-radicals than the *sec*-radicals, the latter being more stable than the former. In other words, the *pri*-radical appears to be more active than *sec*-radical in abstracting hydrogen from tetralin, leading to decreased yields of alkanes and alkenes, but an increased ratio of alkene/alkanes for short duration runs. In long duration pyrolysis, the effect of tetralin in suppressing *n*-C_{14} decomposition is lessened because H-donors inhibit the radical-induced reactions, but do not suppress the homolytic C-C bond cleavage. After 4 hours, the major effects of H-donor contribute appear to be the elimination or reduction of solid formation[10] and inhibition of the formation of C_1-C_4 hydrocarbon gases, as can be seen from Table 1.1-3.

$C_mH2_{m+2} \rightarrow R¥ + R¥$ 1)

$R¥ + C_mH_{2m+2} \rightarrow$ *sec*-$C_mH_{2m+1}¥ + RH$ 2)

$R¥ + C_mH_{2m+2} \rightarrow$ *pri*-$C_mH_{2m+1}¥ + RH$ 3)

sec-$C_mH_{2m+1}¥ \rightarrow 1\text{-}C_nH_{2n} +$ *pri*-$C_{m-n}H_{2(m-n)+1}¥$ 4)

pri-$C_mH_{2m+1}¥ \rightarrow C_2H_4 +$ *pri*-$C_{m-2}H_{2(m-2)+1}¥$ 5)

pri-$C_{m-n}H_{2(m-n)+1}¥ + C_mH_{2m+2} \rightarrow n\text{-}C_{m-n}H_{2(m-n)+2} +$ *sec*-$C_mH_{2m+1}¥$ 6)

pri-$C_{m-2}H_{2(m-2)+1}¥ + C_mH_{2m+2} \rightarrow n\text{-}C_{m-2}H_{2(m-2)+2} +$ *sec*-$C_mH_{2m+1}¥$ 7)

$C_mH_{2m+1}¥ + C_nH_{2n+1}¥ \rightarrow C_{m+n}H2(m+n)+2$ 8)

Scheme I. Mechanisms of Pyrolysis of *n*-Alkanes CmH_{2m+2}
(Modified from C. Song, W.-C. Lai, and H.H. Schobert, ***Am. Chem. Soc. Div. Fuel Chem. Prepr.***, 1992, 37 (4), 1655-1663)

sec-$C_{14}H_{29}¥ \rightarrow 1\text{-}C_nH_{2n} +$ *pri*-$C_{14-n}H_{2(14-n)+1}¥$ 4)

n≠1

n≠2

n=3 1-C_3H_6 + *pri*-$C_{11}H_{23}¥$ 4A)

n=4 1-C_4H_8 + *pri*-$C_{10}H_{21}¥$ 4B)

n=5 1-C_5H_{10} + *pri*-$C_9H_{19}¥$ 4C)

n=6 1-C_6H_12 + *pri*-$C_8H_{17}¥$ 4D)

n=7 1-C_7H_{14} + *pri*-$C_7H_{15}¥$ 4E)

n=8 1-C_8H_{16} + *pri*-$C_6H_{13}¥$ 4F)

n=9 1-C_9H_{18} + *pri*-$C_5H_{11}¥$ 4G)

n=10 1-$C_{10}H_{20}$ + *pri*-$C_4H_9¥$ 4H)

n=11 1-$C_{11}H_{22}$ + *pri*-$C_3H_7¥$ 4I)

n=12 1-$C_{12}H_{24}$ + $C_2H_5¥$ 4J)

n=13 1-$C_{13}H_{26}$ + $CH_3¥$ 4K)

Scheme II. Radical Decomposition (β-scission) Reactions of Secondary-Radical (sec-R¥) During *n*-Tetradecane Pyrolysis

pri-$C_{14-n}H_{2(14-n)+1}$¥ + $C_{14}H_{30}$ → $C_{14-n}H_{2(14-n)+2}$ + sec-$C_{14}H_{29}$¥ 6)

n≠1

n≠2

n=3 n-$C_{11}H_{24}$ + sec-$C_{14}H_{29}$¥

n=4 n-$C_{10}H_{22}$ + sec-$C_{14}H_{29}$¥

n=5 n-C_9H_{20} + sec- $C_{14}H_{29}$¥

n=6 n-C_8H_{18} + sec- $C_{14}H_{29}$¥

n=7 n-C_7H_{16} + sec- $C_{14}H_{29}$¥

n=8 n-C_6H_{14} + sec- $C_{14}H_{29}$¥

n=9 n-C_5H_{12} + sec- $C_{14}H_{29}$¥

n=10 n-C_4H_{10} + sec-$C_{14}H_{29}$¥

n=11 C_3H_8 + sec-$C_{14}H_{29}$¥

n=12 C_2H_6 + sec-$C_{14}H_{29}$¥

n=13 CH_4 + sec-$C_{14}H_{29}$¥

Scheme III. Possible Radical Hydrogen-Abstraction Reactions of Primary-Radical (Pri-R¥) During *n*-Tetradecane Pyrolysis

R—CH =CH_2 + H¥ → R—CH—CH_3 9)

R—CH—C_3H_7 + H_2 → R—CH_2—CH_3 + H¥ 10)

Scheme IV. Hydrogenation of 1-alkene Products During *n*-alkane Pyrolysis

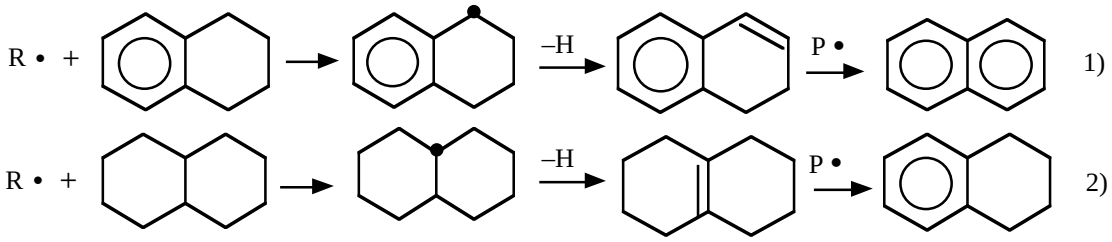

Scheme V. Radical Stabilization via H-Transfer from Tetralin and Decalin

Table 1.1-1. Products from Pyrolysis of 5 mL of *n*-C_{14} at 450°C under 0.69 MPa N_2

	Reactor Residence Time in Sandbath Preheated to 450°C[a]							
Residence time	6 min	12 min	21 min	30 min	60 min	150 min	240 min	480 min
Expt No.	TS84	TS83	TS82	TS85/86	TS45	TS62	TS67**	TS75
Yields (mol %)[b]								
Hydrogen (H_2)	0	0	0	1.17	3.21	4.67	8.09	8.43
Methane (C_1)	0.45	1.73	3.90	8.33	21.63	34.93	70.31	73.48
Ethane (C_2)	1.04	3.53	6.78	13.76	29.01	49.44	74.48	84.05
Ethylene	0.37	1.06	1.62	2.21	4.37	2.36	2.38	2.69
Propane (C_3)	0.83	1.95	3.58	7.08	18.94	37.25	46.93	57.54
Propylene	0.49	1.57	2.70	5.20	10.01	12.69	10.52	11.23
iso-Butane	0	0	0	0.03	0.26	0.88	1.45	1.97
n-Butane^S	0.15	0.46	0.84	1.75	5.49	12.71	15.10	17.66
n-Butane^L	0.20	1.56	3.47	6.66	2.00	3.47	2.52	3.42
1-Butene^S	0.12	0.38	0.63	1.02	2.41	3.55	2.43	2.06
1-Butene^L	0.27	1.35	3.00	5.72	1.22	1.04	0.40	0.34
n-Butane (n-C_4)$^{sum\#\#}$	0.35	2.02	4.31	8.41	7.49	16.18	17.62	21.08
1-Butene$^{sum\#\#}$	0.39	1.73	3.63	6.74	3.63	4.59	2.83	2.40
Pentane (n-C_5)	0.16	1.17	3.15	7.00	10.00	16.45	14.71	13.76
1-Pentene	0.41	2.13	3.36	5.71	5.08	6.32	2.45	1.25
n-Hexane (n-C_6)	0.23	1.21	2.75	5.67	10.38	12.23	12.65	11.75
1-Hexene	0.40	2.10	3.20	4.96	3.99	3.16	2.70	1.17
n-Heptane (n-C_7)	0.24	1.28	2.70	5.15	9.63	9.60	9.21	7.38
1-Heptene	0.35	1.61	2.50	3.35	3.74	3.83	2.36	2.95
n-Octane (n-C_8)	0.21	1.13	2.36	4.44	7.59	7.62	6.99	4.35
1-Octene	0.31	1.36	1.95	2.61	2.02	0.24	0.06	0
n-Nonane (n-C_9)	0.21	1.04	2.11	3.66	6.34	5.82	4.93	2.53
1-Nonene	0.31	1.23	1.77	2.31	0.59	0.22	0.09	0
n-Decane (n-C_{10})	0.19	0.92	1.82	2.94	4.85	4.50	3.25	1.64
1-Decene	0.29	1.13	1.53	1.47	1.05	0.27	0.03	0
n-Undecane (n-C_{11})	0.20	0.93	1.76	2.69	4.04	3.54	2.30	1.05
1-Undecene	0.27	1.00	1.32	1.27	0.67	0	0	0
n-Dodecane (n-C_{12})	0.03	0.19	0.45	0.82	1.37	1.04	0.81	0.36
1-Dodecene	0.27	0.97	1.28	1.17	0.31	0.05	0	0
n-Tridecane (n-C_{13})	0.02	0.09	0.26	0.51	0.78	0.58	0.40	0.20
1-Tridecene	0.06	0.22	0.32	0.25	0.06	0	0	0
n-Tetradecane (n-C_{14})	**96.02**	**83.08**	**68.32**	**46.67**	**29.73**	**9.37**	**2.92**	**0.84**
1-Tetradecene	0	0.02	0.14	0.21	0	0	0	0
n-Pentadecane (n-C_{15})	0.08	0.14	0.24	0.36	0.42	0.23	0	0
n-Hexadecane (n-C_{16})	0	0.06	0.16	0.26	0.29	0.12	0.06	0
n-Heptadecane (n-C_{17})	0	0.04	0.11	0.17	0.16	0.04	0	0
n-Octadecane (n-C_{18})	0.13	0.13	0.15	0.18	0.13	0.01	0	0
n-Nonadecane (n-C_{19})	0	0.02	0.07	0.09	0	0	0	0
n-Eicosane (n-C_{20})	0	0.02	0.06	0.07	0	0	0	0
n-Henicosane (n-C_{21})	0	0.02	0.04	0.05	0	0	0	0
n-Docosane (n-C_{22})	0	0.01	0.03	0.04	0	0	0	0
n-Tricosane (n-C_{23})	0	0.01	0.02	0.03	0	0	0	0
Alkylcyclopentanes	0	0.06	0.20	0.69	3.40	3.43	3.52	5.01
Alkylcyclohexanes	0	0.13	0.57	1.71	5.68	6.80	5.62	5.53
Alkylbenzenes	0	0	0	0.44	4.50	14.48	21.39	23.35
Tetralins	0	0	0	0	0	0	0.04	0.13
Indanes						1.45	2.64	2.94
Alkylnaphthalenes	0	0	0	0	0	1.57	2.95	4.16
Other Polyaromatics	0	0	0	0	0	0.03	0.24	0.47
Solids (wt% of C14)	0	0	0	0	0	1.0	3.0	4.7

a) The reactors reach 450°C in about 3 minutes after plunge into the sandbath.
b) The molar yield based on n-tetradecane substrate.

Table 1.1-2. Arrhenius Parameters and Rate Constants at 700 K for Radical Initiation Reactions

Reactant	Products		log[A/S^{-1}]	E kcal/mol	log[k/S^{-1}]
n-C_5H_{12}	CH_3¥	1-C_4H_9¥	17.5	85.5	-9.2
n-C_5H_{12}	C_2H_5¥	1-C_3H_7¥	17.1	81.6	-8.4
n-C_6H_{14}	CH_3¥	1-C_5H_{11}¥	16.8	85.4	-9.9
n-C_6H_{14}	C_2H_5¥	1-C_4H_9¥	16.8	81.9	-8.8
n-C_6H_{14}	1-C_3H_7¥	1-C_3H7¥	16.5	81.9	-9.1

Table 1.1-3. Hydrogen-transferring Pyrolysis of n-Tetradecane in the Presence of Tetralin

	Reactor Residence Time in Sandbath Preheated to 450°C[a]										
Residence time	6 min	12 min	21 min	30 min	30 min	240 min	240 min	240 min	240 min	240 min	240 min
vol% of Tetralin	10%-THN	10%-THN	10%-THN	10%-THN	100%THN	5 % THN	10%-THN	15 % THN	25 % THN	50 % THN	100 % THN
Expt No.	MTS32	MTS31	MTS30	MTS26	TS79	MTS14	MTS20	MTS24	MTS21	MTS7	TS6
Yields (mol %)[b]											
Hydrogen (H_2)					0.73						
Methane (C_1)	0.38	0.59	0.98	2.39	0.01	87.29	45.85	40.43	28.06	23.77	0.41
Ethane (C_2)	1.01	1.43	2.21	4.55	0.07	84.18	56.05	50.74	37.40	29.93	0.21
Ethylene	0.22	0.40	0.55	0.76	0	1.75	1.41	0.60	1.11	0.50	0.01
Propane (C_3)	0.60	0.78	1.22	2.51	0.02	44.10	38.24	37.01	26.86	19.14	0.27
Propylene	0.41	0.64	1.07	2.08	0.04	10.11	6.40	9.03	8.21	5.73	0.06
iso-Butane	0.02				0.01	0.66	0.92	0.96	0.42	0.20	0.09
n-Butene[g]	0.14	0.19	0.30	0.60	0.02	11.20	13.46	12.72	9.01	6.16	0.23
n-Butene[L]	0.17	0.30	1.01	4.66			10.76		11.49		
1-Butene[g]	0.08	0.14	0.23	0.38	0	2.23	1.77	2.24	2.10	1.56	0.03
1-Butene[L]	0.17	0.49	1.04	3.17			1.20		1.27		
n-Butane ($n\text{-}C_4$)[sum##]	0.31	0.49	1.31	5.26			24.22		20.5		
1-Butene[sum##]	0.34	0.63	1.27	3.55			2.97		3.37		
Pentane ($n\text{-}C_5$)	0.13	0.35	0.73	5.48			17.70		20.06		
1-Pentene	0.28	0.69	1.28	4.99			1.27		5.02		
n-Hexane ($n\text{-}C_6$)	0.18	0.43	0.84	4.82			14.36		18.09		
1-Hexene	0.25	0.60	1.16	3.76			1.36		1.59		
n-Heptane ($n\text{-}C_7$)	0.20	0.44	0.93	2.27			10.62		9.51		
1-Heptene	0.22	0.50	1.01	3.34			2.03		3.00		
n-Octane ($n\text{-}C_8$)	0.18	0.39	0.83	2.66			7.95		7.05		
1-Octene	0.22	0.47	0.90	2.24			?		?		
n-Nonane ($n\text{-}C_9$)	0.16	0.37	0.80	2.40			5.21		5.28		
1-Nonene	0.21	0.44	0.85	1.73			0.14		0.17		
n-Decane ($n\text{-}C_{10}$)	0.15	0.34	0.73	2.05			3.70		3.90		
1-Decene	0.21	0.43	0.80	1.46			0		0		
n-Undecane ($n\text{-}C_{11}$)	0.16	0.35	0.75	1.96			2.72		3.05		
1-Undecene	0.19	0.39	0.72	1.23			0		0		
n-Dodecane ($n\text{-}C_{12}$)	0.03	0.04	0.13	0.44			0.85		0.89		
1-Dodecene	0.18	0.37	0.70	1.15			0		0		
n-Tridecane ($n\text{-}C_{13}$)	0	0.01	0.05	0.21			0.40		0.38		
1-Tridecene	0.05	0.10	0.17	0.26			0		0		
n-Tetradecane ($n\text{-}C_{14}$)	**97.36**	**94.61**	**89.16**	**66.24**			**4.52**		**8.02**		
1-Tetradecene	0	0	0	0							
n-Pentadecane ($n\text{-}C_{15}$)	0.09	0.09	0.10	0.18			0.05		0.15		
n-Hexadecane ($n\text{-}C_{16}$)	0	0	0.02	0.09			0.22		0.02		
n-Heptadecane ($n\text{-}C_{17}$)	0	0	0	0.08			0.02		0.04		
n-Octadecane ($n\text{-}C_{18}$)	0.13	0.13	0.13	0.13			0.03		0		
n-Nonadecane ($n\text{-}C_{19}$)				0.05			0		0		
n-Eicosane ($n\text{-}C_{20}$)				0.06			0		0		
n-Henicosane ($n\text{-}C_{21}$)				0.03			0		0		
n-Docosane ($n\text{-}C_{22}$)				0.02			0		0		
n-Tricosane ($n\text{-}C_{23}$)				0.02			0		0		
Alkylcyclopentanes				0.24							
Alkylcyclohexanes				0.49							
Alkylbenzenes	0	0	0	0.29							
Tetralins				83.03							
Indanes				5.06							
Alkylnaphthalenes	0.68	0.83	1.36	8.41							
Other Polyaromatics											

a) The reactors reach 450°C in about 3 minutes after plunge into the sandbath.
b) The molar yield based on n-tetradecane substrate.

[1] Roquemore, W.M. et al. Prepr. Pap. — Am. Chem. Soc. Div. PetrolChem. 1989. 34(4) 841-849.

[2] Hazlett, R.N. Thermal Oxidation Stability of Aviation Turbine Fuels. ASTM Mongraph 1. Philadelphia: ASTM, 1991. 163.

[3] Song, C. et al. Energy & Fuels. 1993.

[4] Song, C. et al. Compositional Factors Affecting Thermal Degradation of Jet Fuels, Technical Progress Report for Period October 1990-January 1991. Air Force Aero Propulsion Laboratory, 42-3462-TPR-2. 1991. 96.

[5] Song, C. et al. Advanced Thermally Stable Jet Fuel Development Program Annual Report, Vol. 2, Final Report for Period July 1990-July 1991. Air Force Aero Propulsion Laboratory, WL-TR-91-2117, Vol. II. 1991. 180.

[6] Song, C. et al. Am. Chem. Soc. Div. Petrol. Chem. Prepr. 1992. 37 (2).

[7] Zhou, P. et al. Ind. Eng. Chem. Res. 1987. 26. 846-852.

[8] Fairburn, J. F. et al. Fuel. 1990. 69(12). 1537-1545.

[9] Song, C. et al. Am. Chem Soc. Div. Petrol. Chem. Prepr. 1992. 37 (2). 540-547.

[10] Song, C. W.C. Lai, and H.H.Schobert. Am. Chem Soc. Div. Petrol. Chem. Prepr. 1992. 37 (4). 1655-1663.

1.2 PYROLYSIS OF TETRADECANE AT ELEVATED PRESSURE FOR LONG DURATION: PRODUCT DISTRIBUTION AND REACTION MECHANISMS

This study is explained in detail in *Advanced Thermally Stable Jet Fuels Technical Progress Report, November—January 1993*.

This study was undertaken to clarify the product distribution and the reaction mechanisms of pyrolysis of *n*-tetradecane (*n*-C_{14}) in relation to high-temperature thermal degradation of jet fuels. We know that the content of long-chain alkanes in all commercial and millitary aviation jet fuels (usually within the carbon number range of C_7-C_{17}) is over 70 vol%[1]. Understanding the pyrolysis of long-chain alkanes at elevated pressures for long duration is important for developing advanced thermally stable jet fuels for future high-Mach aircraft, which use fuel both as an energy source and a primary heat sink to cool the airframe, engine, and system components. The heat-sink function can lead to high bulk-fuel temperatures of 400-500¡C. The development of advanced jet fuels requires testing at long residence times in fuel systems where fuel is subjected to moderate to high heat loads, and under conditions of very high heat flux at short residence times (which fuels encounter in their passage through fuel struts and injectors).[2, 3] Hazlett et al[4] studied the effects of temperature on oxidation and pyrolysis of *n*-dodecane using a flow reactor; their results apply to short-residence time (28 seconds) degradation. This study focused on the medium- (the order of minutes) and long-duration (the order of hours) pyrolytic degradation characteristics of paraffinic jet fuels at high temperatures.

We conducted the pyrolysis of *n*-C_{14}, a typical component of both commercial and military jet fuels, under high-severity thermal conditions, using a main test temperature of 450¡C considered a close approximation to the anticipated high bulk fuel temperature for future high-Mach aircraft. The experimental conditions used in this work are characterized by a closed reactor, relatively high and continuously increasing pressure, condensed-phase (higher density gas phase or supercritical phases), and long residence time. Such conditions are distinctly different from those used in most previous alkane pyrolysis work (vapor phase, low pressure, flow reactor, short residence time). The reaction temperature of 450¡C (also 400-425¡C for selected runs) used in this work, though relatively high for the thermal stressing of jet fuels, was near the low end compared to temperatures cited in most literature on hydrocarbon pyrolysis.

This work differed from earlier studies[5, 6] of pyrolysis of long-chain alkanes at 450¡C in a number of ways. It detailed:

- Distribution of products ranging from C_1 to C_{23} and their changes with residence time
- The general reaction mechanisms for condensed-phase long-duration pyrolysis of long-chain alkanes
- The competitive reaction pathways based on Arrhenius parameters of elementary reactions
- The observed characteristic product distribution patterns, such as the lack in C_{m-2} paraffinic product from C_mH_{2m+2} (m = 14) in early stage and the preferrential formation of C_5 and C_6 olefinic products from alkyl radical isomerization
- The formation of cyclic compounds and the corresponding pathways

- The apparent kinetic parameters including activation energy, frequency factor, and rate constants
- The theoretical prediction of conversion based on the kinetic parameters for *n*-tetradecane pyrolysis.

Our work provided detailed information on the characteristic distribution of products from condensed-phase pyrolysis of *n*-tetradecane, the shift of carbon number distribution for both paraffinic and olefinic products with increase in residence time, and the pathways for radical reactions at 450¡C under elevated pressures for long durations. Such information is important in considering the pyrolytic degradation of long-chain alkanes during high-temperature thermal stressing of jet fuels. Such stressing will be encountered both during high-Mach flight of advanced jet aircraft and after landing, where some fuel is confined in very hot fuel lines for a period of time.

Results and Conclusions

For pyrolysis of a long chain alkane, C_mH2_{m+2} (m = 14 for tetradecane) at 450¡C under elevated pressures (~ 2-9 MPa) for 6 to 480 minutes, the major products in the early stage were *n*-alkanes in the carbon number range of C_{1-} to C_{m-3} and terminal 1-alkenes in the carbon number range of C_{2-} to C_{m-2}. Among the paraffinic products within first 12 minutes, there were very few compounds with m-2 and m-1 carbon atoms. Among the olefinic products, formation of the compound with m-1 carbon atoms was very limited in the initial stage. As compared to the well-known gas-phase pyrolysis, the molar ratios of alkenes to alkanes were much smaller (≤1), except the ratio for the group with m-2 carbon atoms, where the ratio of 1-alkene to *n*-alkane can be as high as 9 in the initial stage. This results because terminal alkene 1-$C_{m-2}H_{2(m-2)}$ is produced from β-scission of secondary radical 4-C_mH_{2m+1}¥, whereas *n*-$C_{m-2}H_{2(m-2)+2}$ is formed from a primary radical, 1-C_mH_{2m+1}¥, whose population is much less than the secondary radicals due to both higher activation energy and the competing isomerization reaction.

There appeared to be a preferential formation of 1-hexene and 1-pentene among the 1-alkenes formed after 12 minutes. This was attributed to the 1,5-shift and 1,4-shift isomerization of primary radicals formed during tetradecane pyrolysis. The peak of carbon number distribution shifts towards 2 for paraffinic products and towards 3 for olefinic products, and the ratios of alkenes to alkanes decrease with increasing residence time up to 150 minutes.

We proposed a general reaction mechanism (see Scheme I, Section 1.1) for tetradecane pyrolysis under these conditions, which is characterized by the one-step decomposition of secondary radicals and the 1,5- and 1,4-shift isomerization of primary radicals to secondary radicals. Compared to the two known extremes of pyrolysis[7], the proposed mechanism is significantly different from the Rice and Kossiakoff mechanism but is relatively closer to the mechanism of Fabuss-Smith-Satterfield.[8]

The fate of olefinic products and generation of cyclic compounds are also characteristic of long-duration pyrolysis. The substrate alkane molecules are the source for hydrogen abstraction in the early periods, but in the later stages the olefinic products also undergo the H-abstraction reactions, which lead to the formation of cyclic compounds such as cyclohexenes, cyclohexanes, cyclopentanes and alkylaromatics. Aromatics include mainly alkylbenzenes, together with smaller amounts of alkyl-substituted indanes and naphthalenes. The possible

pathways leading to cyclic alkanes and alkenes may involve Diels-Alder type reaction and intramolecular addition of olefinic radicals leading to ring closure. Considerable deposit formation was observed when aromatics formation became significant after long residence time (150 minutes) at 450¡C.

---

[1] Lai, W.C., C. Song, and H.H. Schobert. Pyrolytic Degradation of Coal-and Petroleum-Derived Jet Fuels and Middle Distillates. *Am. Chem. Soc. Div. Petrol. Chem. Prepr.* 1992. 37(4). 1671-1680.

[2] Roquemore, W.M. et al. Fouling in Jet Fuels: A New Approach. *Am Chem Soci. Div. Petrol Chem. Prepr.* 1989. 34(4). 841-849.

[3] Lee, C.M. and R.W. Niedzwiecki. High Speed Commercial Transport Fuels Considerations and Research Needs. *Am. Chem. Soc. Div. Petrol Chem. Prepr.* 1989. 34(4). 911-919.

[4] Hazlett, R.N., J.M. Hall, and M. Matson. Reactions of Aerated n-Dodecane Liquid Flowing Over Heated Metal Tubes. *Ind. Eng. Chem. Prod. Res. Dev.* 1977. 16. 171-177.

[5] Mushrush, G.W. and R.N. Hazlett. Pyrolysis of Organic Compunds Containing Long Unbranched Alkyl Groups. *Ind. Eng. Chem. Fundam.* 1984. 23. 288-294.

[6] Hazlett, R.N., J.M. Hall, and M. Matson. Reactions of Aerated n-Dodecane Liquid Flowing Over Heated Metal Tubes. *Ind. Eng. Chem. Prod. Res. Dev.* 1977. 16. 171-177.

[7] Poutsma, M.L. *Energy & Fuels.* 1990. 4(2). 113-131.

[8] Fabuss, B.M., J.O. Smith, and C.N. Satterfield. Thermal Cracking of Pure Saturated Hydrocarbons. *Adv. Petrol. Chem. Refin.* 1964. 9. 158-201.

1.3 PRODUCT DISTRIBUTION OF THE PYROLYSIS OF *N*-TETRADECANE AT 400¡C AND 425¡C

This study is explained in detail in *Advanced Thermally Stable Jet Fuels Technical Progress Report, July—September 1993.*

Introduction

This study complemented our previous study of the pyrolysis of *n*-tetradecane (n-C_{14}) at 450¡C for 6—480 minutes, which has led to: 1) the proposed reaction mechanisms of the condensed-phase pyrolysis of *n*-C_{14} at elevated pressures; 2) the mechanisms accounting for the characteristic product distribution patterns and their changes with residence time; and 3) the observations of the fate of olefinic products and formation of cyclic compounds during the long-duration pyrolysis.[1, 2] The reaction temperatures in this work were 400¡C and 425¡C. This study focused on the detailed product distribution of the pyrolysis of *n*-C_{14} at 400¡C and 425¡C, and the global kinetic parameters of *n*-C_{14} pyrolysis. The modeling work was based on the mechanism of Fabuss-Smith-Satterfield.[3] We found that the product distribution observed under the conditions used in our work could not be predicted by the known reaction mechanisms proposed in previous literature by Kossiakoff and Rice[4] and Fabuss-Smith-Satterfield.[3] Future work will focus on modeling new proposed reaction mechanisms.

Experimental

Aldrich reagent-grade normal tetradecane, $CH_3(CH_2)_{12}CH_3$, with purity of 99+% (MW: 198.4; d: 0.763 g/mL) was used as received for all the pyrolysis experiments. The pyrolyses were performed in 25 mL tubing bomb reactors at 400¡C or 425¡C for a heating period of 21—240 minutes under an initial pressure of 0.69 MPa UHP N_2 (cold). After being loaded with a 5 mL sample, the reactor was first leak-tested and then purged repetitively (6 times) with 6.9 MPa UHP N_2 to remove oxygen or air in the reactor or dissolved in the sample. The reactor pressure and temperature were monitored immediately after the reactor was plunged into the sandbath. The sample reached within 4¡C of the desired pyrolysis temperature in 4—6 minutes. The reactor was removed from the fluidized sand bath after the desired stressing time, and immediately quenched in a cool water bath. The products were collected and separated into gas, liquid, and solid deposits immediately after the reactor had cooled sufficiently. The fresh gaseous and liquid products were analyzed by GC and GC-MS.

The gaseous products were analyzed using a Perkin-Elmer Autosystem GC equipped with two detectors, a thermal conductivity detector, and a flame ionization detector. The liquid products were analyzed on an HP 5890 Series II GC coupled with an HP 5971A Mass Selective Detector and quantified by a Perkin-Elmer GC 8500. More analytical details are provided by Lai[5] and Song.[6]

Results and Discussion

1. Decomposition Kinetic Parameters. The detailed products of the pyrolysis of *n*-C_{14} at 400¡C and 425¡C are reported in **Table 1.3-1**, where only major individual reaction products are presented. The hydrocarbon products are expressed as molar percentage of the initial amounts of reactants (*n*-C_{14}).

The major products include C_1—C_4 gaseous yields and liquid yields such as alkanes, alkenes, and cycloalkanes. We approximated the thermal decomposition by a first-order relation as shown in Equation (1).

$$-\frac{dC}{dt} = kC \qquad (1)$$

where C is the reactant concentration, t is the reaction time, and k is the first-order rate constant. The rate constant can then be expressed as a function of the reactant conversion (α, the fraction of reactant reacted) as shown in Equation (2).

$$k = \frac{1}{t} \ln \frac{1}{1-\alpha} \qquad (2)$$

As mentioned earlier, the preheat or heat-up (from room temperature to the desired reaction temperature) time is about 4—6 minutes, and has to be accounted for in calculating an adjusted (effective) reaction time. From least-squares regression, the calculated pseudo-first-order rate constants at 400¡C, 425¡C, and 450¡C, are 0.000734, 0.00580, 0.02405 min^{-1}, respectively. The relation between activation energy (E_a) and the rate constant (k) is given by the Arrhenius equation:

$$k = A\, e^{-E_a / RT} \qquad (3)$$

where A is the Arrhenius frequency factor (often called the pre-exponential factor), R is the gas constant, and T is the absolute temperature in K. **Figure 1.3-1** presents the Arrhenius plot (ln k vs 1/T). Determined from the Arrhenius plot, the activation energy (E_a) and the Arrhenius frequency factor (A) are 67.6 kcal/mol and 7.17×10^{18} min^{-1}, respectively. The overall reaction kinetics (E_a = 67.6 kcal/mol and A = 7.17×10^{18} min^{-1}) are comparable with available literature values. The observed activation energies for first-order reactions of long-chain alkanes (e.g., *n*-dodecane and *n*-hexadecane) are generally in the range of 60−5 kcal/mol. Ford[7] reported that the kinetics for both liquid-phase and gas-phase pyrolysis of *n*-hexadecane are similar, and the activation energy for both is about 60 kcal/mol.

Figure 1.3-2 compares the experimental *n*-C_{14} conversions (over the range from 0.02 to 0.70) to the values predicted from the kinetic parameters. The line corresponding to exact agreement is drawn as a diagonal. The predicted and experimental conversions are generally in good agreement; however, significant deviations exist at high conversions.

Fabuss[8] observed the phenomena of so-called self-acceleration and self-inhibition, reporting that self-inhibition generally occurs in the decomposition of alkanes as a result of the formation of free radical inhibitors such as alkenes. On the other hand, self-acceleration can also occur. Our system pressure displayed a monotonic increase with increasing residence time as a result of the continuous decomposition of *n*-C_{14} to form smaller compounds and the secondary decomposition reactions of the primary products.[9] Fabuss et al reported that an increase in pressure can result in self-acceleration.[8] Our earlier study on the pyrolysis of *n*-C_{14} at 450¡C for 30 minutes also indicated that there was significant pressure dependence of *n*-C_{14} conversion, although a few fundamental questions remain to be answered.[9] All existing data suggests that hydrocarbon pyrolysis at elevated pressure is very complex kinetically. A simple first-order

relation, as shown in Equation (1), might not suffice to represent the thermal decomposition over the whole conversion range. However, the simple first-order relation seemed to give good approximation for the thermal decomposition up to about 50% conversion.

2. Pyrolysis Products. **Figure 1.3-3** presents the ratio of *n*-alkane to the corresponding 1-alkene for C_2—C_{13} products from the pyrolysis of *n*-tetradecane at 400¡C. In the early stage of the pyrolysis (up to 60 minutes, conversion 4.5%), except for C_2, the ratios were less than 1.0. In other words, the yield of an *n*-alkane in the C_3—C_{13} range was lower than the corresponding 1-alkene. However, all C_2—C_{13} ratios increase progressively with time, and the C_3—C_{11} *n*-alkanes begin to exceed the corresponding 1-alkenes at the conversion level of about 6—7% (approximated by interpolation). The products in the C_{12} and C_{13} groups were quite different from the others; the yields of *n*-C_{12} and *n*-C_{13} are very low compared with other *n*-alkane products.

Similarly, **Figure 1.3-4** presents the ratio of *n*-alkane to the corresponding 1-alkene for C_2—C_{13} products from the pyrolysis of *n*-tetradecane at 425¡C. Figure 1.3-4 also shows that, in the early stage of the pyrolysis, the yield of an *n*-alkane in the C_5—C_{13} range was lower than the corresponding 1-alkene. Note that the C_5—C_{11} *n*-alkanes began to exceed the corresponding 1-alkenes at a higher conversion level of 10% at 425¡C than that at 400¡C. At 450¡C, the C_5—C_{11} *n*-alkanes did not exceed the corresponding 1-alkenes until at a much higher conversion level, greater than 20%. These observations imply that the lower temperature favors bimolecular reaction (H-abstraction) to form alkanes, while higher temperature facilitates unimolecular reaction (β-scission) to form alkenes. This may be explained by the fact that the activation energy required for a bimolecular H-abstraction is lower than that for an unimolecular β-scission.

Figure 1.3-5 presents the *n*-C_{14} selectivity at 400¡C to *n*-alkanes (C_1—C_{13}) and 1-alkenes (C_2—C_{13}). The reactant selectivity was defined as the ratio of a product's molar yield to the conversion of reactant. Several trends are obvious:

a) At low conversion (2.1 mol%), ethane and propylene are the most abundant alkane and alkene, respectively, and there are no particular alkanes in the liquid products (C_5 to C_{11}) that have high selectivity.

b) The yield of *n*-C_{12} is very low compared with any of the C_1—C_{11} alkanes, and the amounts of *n*-C_{13} products are even smaller. The formation of *n*-tridecane becomes apparent long after 60 minutes, but it is still much less than C_1—C_{11} alkanes.

c) The selectivities of most of the 1-alkenes increase and reach a maximum after a certain period of time, then start to decrease.

d) Earlier we reported that at 450¡C there appeared a selectively enhanced formation of 1-hexene and 1-pentene from *n*-C_{14} when the *n*-C_{14} conversion reached 17 mol %. This kind of product distribution was also observed at lower temperatures (400¡C), as shown in Figure 1.3-5. We propose a facile isomerization of primary radicals to account for such selectivity (*i.e.*, the preferential formation of 1-hexene and 1-pentene was attributed to a 1,5-shift and 1,4-shift, respectively, coiling-type isomerization of a primary radical generated from substrate molecule followed by a β-scission).

e) With further increases in residence time or conversion, the peak of carbon number distribution for alkane products shifted toward four. This is also true for the pyrolysis at 425¡C, as shown in **Figure 1.3-6**, which displays the *n*-C_{14} selectivity at 425¡C to *n*-alkanes (C_1—C_{13}) and 1-alkenes (C_2—C_{13}). Note that for the pyrolysis at 450¡C, ethane is always the most abundant alkane through the studied conversion range (from 4% to 99%) in spite of the fact that there appeared a slightly enhanced formation of *n*-C_4. The much-enhanced formation of *n*-C_4 at 400¡C and 425¡C was attributed to the preferential formation of certain types of radicals from isomerization of primary radicals, followed by a β-scission. The following types of radicals are the sources of *n*-C_4: C_{12}^6 and C_m^{m-5}, where $6 \le m \le 11$ and C_{12}^6 represents a 6-dodecyl radical.

3. Modeling Results Based on Fabuss-Smith-Satterfield Mechanism. The Fabuss-Smith-Satterfield mechanism[10] was based on the modified Kossiakoff-Rice radical theory.[4] The modeling results based on the Fabuss-Smith-Satterfield mechanism are discussed below. The two-step decomposition is represented by Equations 4 — 7:

$M \rightarrow R_1$	radical formation	(4)
$R_1 \rightarrow R_1' \rightarrow Ol_1 + R_2$	first-step isomerization and fission	(5)
$R_2 \rightarrow R_2' \rightarrow Ol_2 + R_3$	second-step isomerization and fission	(6)
$R_3 + M \rightarrow R_3H + R_1$	hydrogen transfer	(7)

Where: M is the decomposing reactant

R_1 is a first-generation free radical

R_1' is a free radical isomerized from R_1

Ol_1 and R_2 are respectively a first-generation olefin and a second-generation free radical produced from scission of R_1'

R_2' is a free radical isomerized from R_2

Ol_2 and R_3 are respectively a second-generation olefin and a third-generation free radical produced from scission of R_2'

R_3H is an alkane converted from R_3 by hydrogen transfer

The basic assumptions are as follows. For radical formation, the activation energy difference is 2 kcal for removing a second and primary hydrogen and 4 kcal for removing a tertiary and primary hydrogen. For radical isomerization, the activation energy difference for internal hydrogen transfer between a primary and a secondary position is 4 kcal, and the different secondary radicals are formed in equal amounts. For the scission reaction, the scission occurs at a β C-C bond from the radical position, and they are assumed to have equal probability when there are two β positions available except when one of the scission results in a methyl radical, whose probability is assumed to be 0.25 instead of 0.5.

Figure 1.3-7 presents the predicted versus measured *n*-C_{14} selectivity to *n*-alkanes and 1-alkenes at 400¡C. Results from both 2-step and 1-step (without second-step isomerization and fission i.e, Equation 6 decomposition) are shown for comparison. For the 1-step decomposition

mechanism, the experimental 1-alkene yields were in fair agreement with the prediction, although the yields of propylene, 1-undecene, 1-dodecene, and 1-tridecene were overpredicted and 1-pentene and 1-hexene were underpredicted. The 1-step decomposition mechanism, however, did not adequately predict the experimental *n*-alkane yields; smaller alkanes were underpredicted and predicted decane and undecane yields were much higher than the experimental data. Figure 1.3-7 also shows that the *n*-alkanes were better predicted by the 2-step decomposition mechanism. However, the model tends to underpredict longer alkanes and exaggerate the 1-alkenes yields.

In summary, the overall product distribution, including alkanes and alkenes, could not be accurately predicted by either a 1-step or 2-step F-S-S decomposition mechanism. The F-S-S mechanism tends to result in the significantly preferential formation of 1-alkenes, which is not true for our data, particularly when the conversion level is high. The failure of the F-S-S model in predicting our experimental data can be attributed to the following:

a) The higher pressure (>24 atmospheres) in our pyrolysis experiments favors the bimolecular H-transfer, which leads to more alkanes; whereas lower pressure favors β-scission, producing more alkenes.

b) Too few initial primary radicals were produced based on their assumption. More alkanes can be produced from H-abstraction reactions between more abundant primary radicals and reactant.

c) The lack of an alkene consumption step resulted in the monotonic increase of alkenes.

d) The omission of possible 1,5-shift and 1,4-shift isomerization led to the unsuccessful prediction of 1-hexene and 1-pentene.

These circumstances were taken into consideration in our subsequent development of proposed reaction mechanisms and modeling work.

Table 1.3-1. Products from *n*-Tetradecane Pyrolysis at 425°C and 400°C under 0.69 MPa N_2 (Cold)

	Reactor Residence Time in Sand Bath Preheated to 425°C or 400°C								
Temperature °C	425°C	425°C	425°C	425°C	400°C	400°C	400°C	400°C	400°C
Residence time (min)	21	30	60	150	21	30	60	150	240
Experiment No.	AS42	AS43	AS44	AS61	AS53	AS54	AS55	AS56	AS65
Conversion (mol %)	6.85	8.33	21.44	59.21	2.11	2.53	4.49	12.48	15.14
YIELDS (mol %)[b]:									
Hydrogen (H_2)				0.73	0.68		0.43	0.21	0.19
Methane (C_1)	0.45	0.62	1.29	3.81	0.19	0.26	0.32	0.62	0.75
Ethane (C_2)	1.08	1.46	2.64	7.01	0.52	0.72	0.86	1.59	1.82
Ethylene	0.27	0.34	0.46	0.64	0.12	0.16	0.18	0.23	0.22
Propane (C_3)	1.06	1.48	3.68	17.14	0.34	0.45	0.78	2.16	2.20
Propylene	1.08	1.51	3.29	11.13	0.37	0.49	0.81	1.96	1.87
Isobutane				0.02					
n-Butane (n-C_4)	0.95	1.28	3.74	18.62	0.18	0.24	0.53	2.00	2.58
1-Butene	0.84	1.04	2.31	8.28	0.26	0.32	0.65	1.62	1.49
n-Pentane (n-C_5)	0.68	0.85	3.46	14.96	0.11	0.18	0.42	1.95	2.35
1-Pentene	1.05	1.12	2.00	6.64	0.22	0.24	0.59	1.46	1.54
n-Hexane (n-C_6)	0.67	0.85	2.47	11.43	0.12	0.16	0.40	1.51	1.99
1-Hexene	0.95	1.11	2.34	5.28	0.21	0.23	0.51	1.38	1.48
n-Heptane (n-C_7)	0.64	0.79	2.25	9.00	0.14	0.15	0.38	1.38	1.90
1-Heptene	0.74	0.86	1.79	3.75	0.14	0.17	0.40	1.11	1.29
n-Octane (N-C_8)	0.54	0.68	1.84	6.70	0.11	0.14	0.32	1.16	1.64
1-Octene	0.61	0.73	1.47	2.95	0.12	0.16	0.34	0.88	0.99
n-Nonane (n-C_9)	0.46	0.60	1.65	5.01	0.10	0.11	0.29	1.04	1.44
1-Nonene	0.54	0.64	1.20	1.67	.011	0.14	0.30	0.73	0.80
n-Decane (n-C_{10})	0.39	0.50	1.33	3.35	0.08	0.10	0.24	0.83	1.20
1-Decene	0.48	0.57	1.00	1.10	0.10	0.13	0.28	0.62	0.66
n-Undecane (n-C_{11})	0.38	0.47	1.29	2.67	0.07	0.13	0.24	0.78	1.17
1-Undecene	0.39	0.45	0.80	0.67	0.08	0.11	0.23	0.52	0.55
n-Dodecane (n-C_{12})	0.04	0.06	0.26	0.69			0.02	0.13	0.22
1-Dodecene	0.37	0.43	0.80	0.55	0.07	0.10	0.21	0.48	0.49
n-Tridecane (n-C_{13})			0.14	0.31				0.05	0.11
1-Tridecene	0.07	0.09	0.17	0.04	0.02	0.02	0.04	0.10	0.10
n-Tetradecane (n-C_{14})	93.15	91.67	78.56	40.79	97.89	97.47	95.51	87.52	84.86
1-Tetradecene			0.24					0.04	0.06
n-Pentadecane (n-C_{15})			0.11	0.15				0.05	0.08
n-Hexadecane (n-C_{16})			0.05	0.12				0.04	0.05
n-Heptadecane (n-C_{17})			0.08	0.16				0.04	0.06
n-Octadecane (n-C_{18})			0.04	0.10				0.03	0.03
n-Nonadecane (n-C_{19})			0.04	0.07				0.03	0.02
n-Eicosane (n-C_{20})			0.03	0.03				0.02	
n-Henicosane (n-C_{21})			0.03	0.03				0.02	
n-Docosane (n-C_{22})			0.01					0.01	
n-Tricosane (n-C_{23})								0.01	
Methylcyclopentane		0.02	0.12	1.11				0.04	0.10
Methylcyclohexane			0.11	0.88				0.04	0.18
Ethylcyclohexane			0.02	0.06					
Toluene				0.04					

[a] Pyrolysis of 5 ml of *n*-tetradecane in 25 ml reacotrs plunged into the sand bath preheated to 425°C or 400°C

[b] Molar percentage based on the initial molar number of *n*-tetradecane feed.

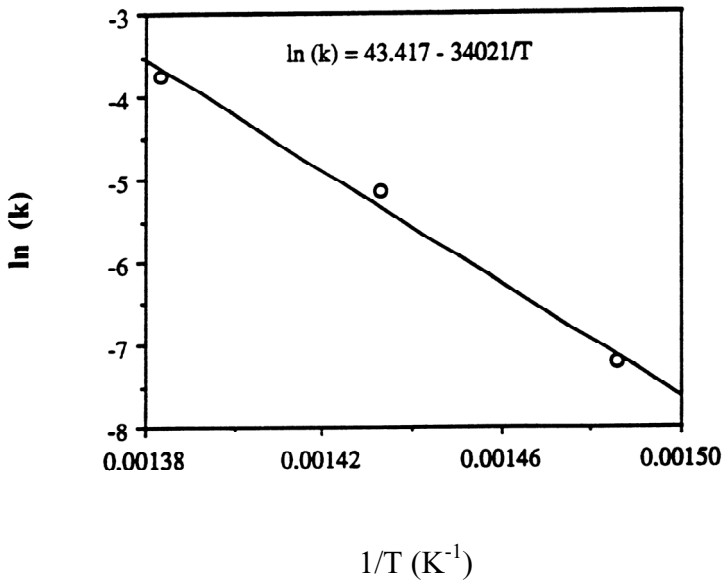

Figure 1.3-1. Arrhenius Plot for the Pyrolysis of *n*-Tetradecane

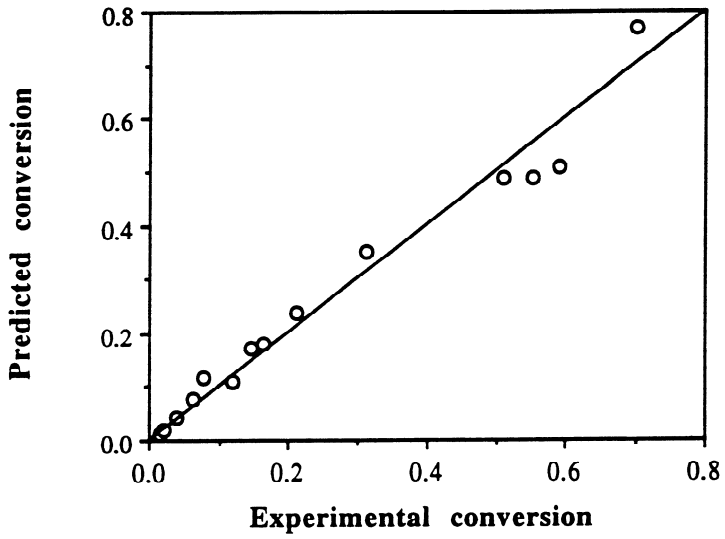

Figure 1.3-2. Predicted versus Measured Values of *n*-Tetradecane Conversion Between 400 and 450°C

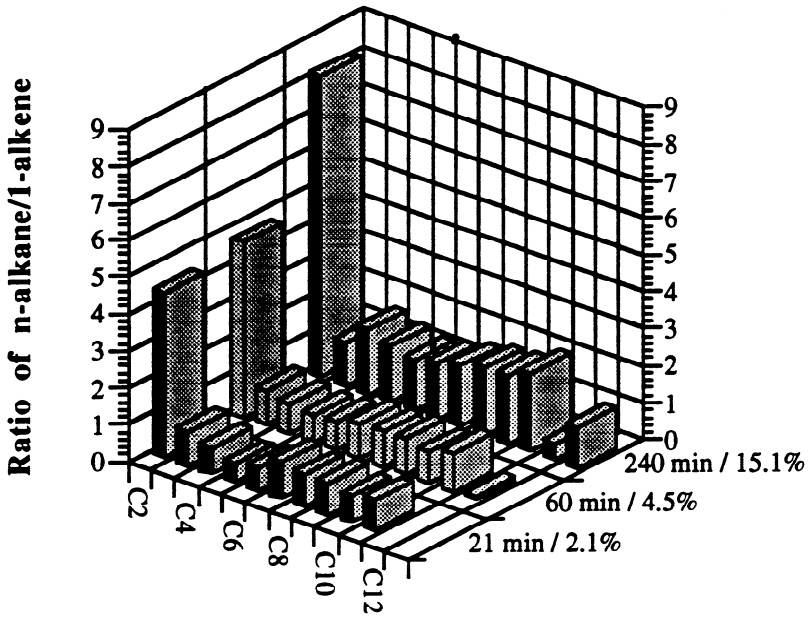

Figure 1.3-3. Ratio of n-Alkane to the Corresponding 1-Alkene for C_2-C_{13} Products from the Pyrolysis of n-Tetradecane at 400°C.

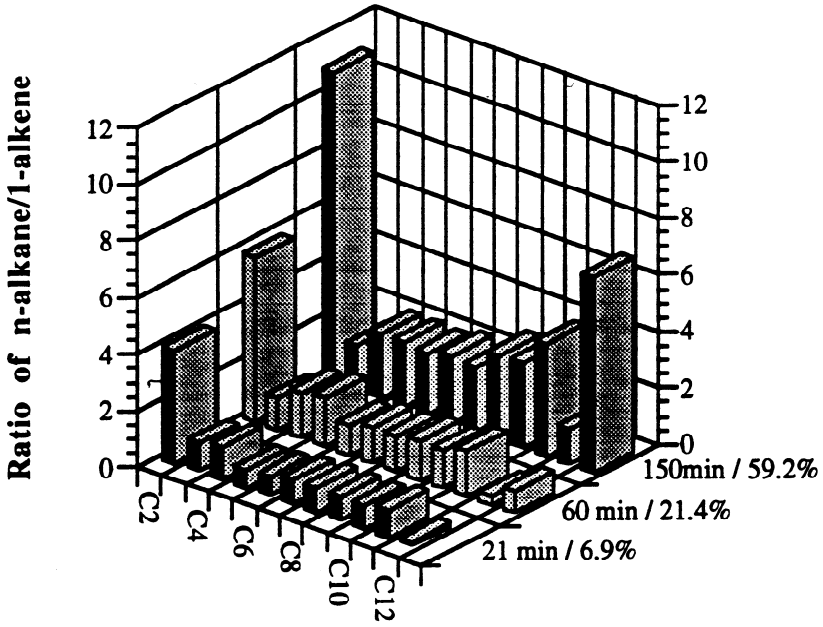

Figure 1.3-4. Ratio of n-Alkane to the Corresponding 1-Alkene for C_2-C_{13} Products from the Pyrolysis of n-Tetradecane at 425°C

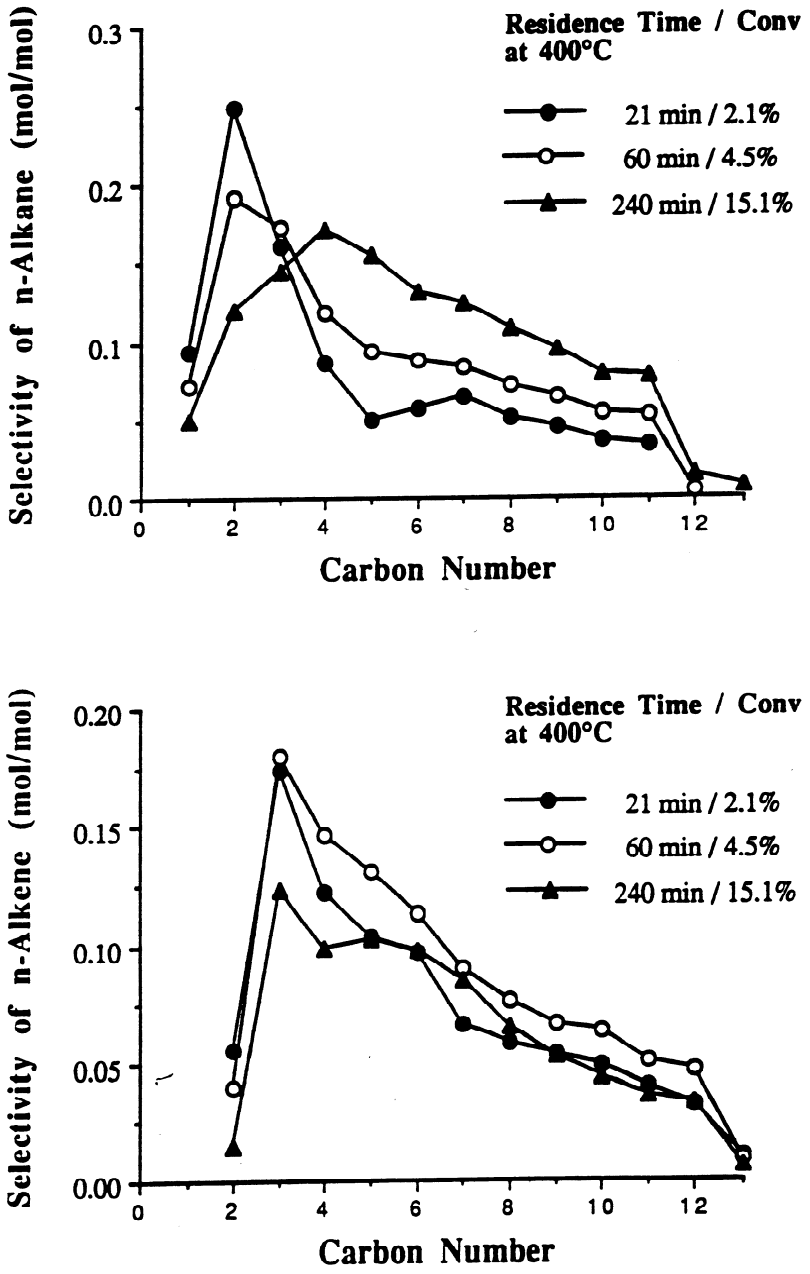

Figure 1.3-5. The n-C_{14} Selectivity to n-Alkanes (top) and 1-Alkenes (bottom) at 400°C under Initial N_2 Pressure of 0.69 MPa (Cold)

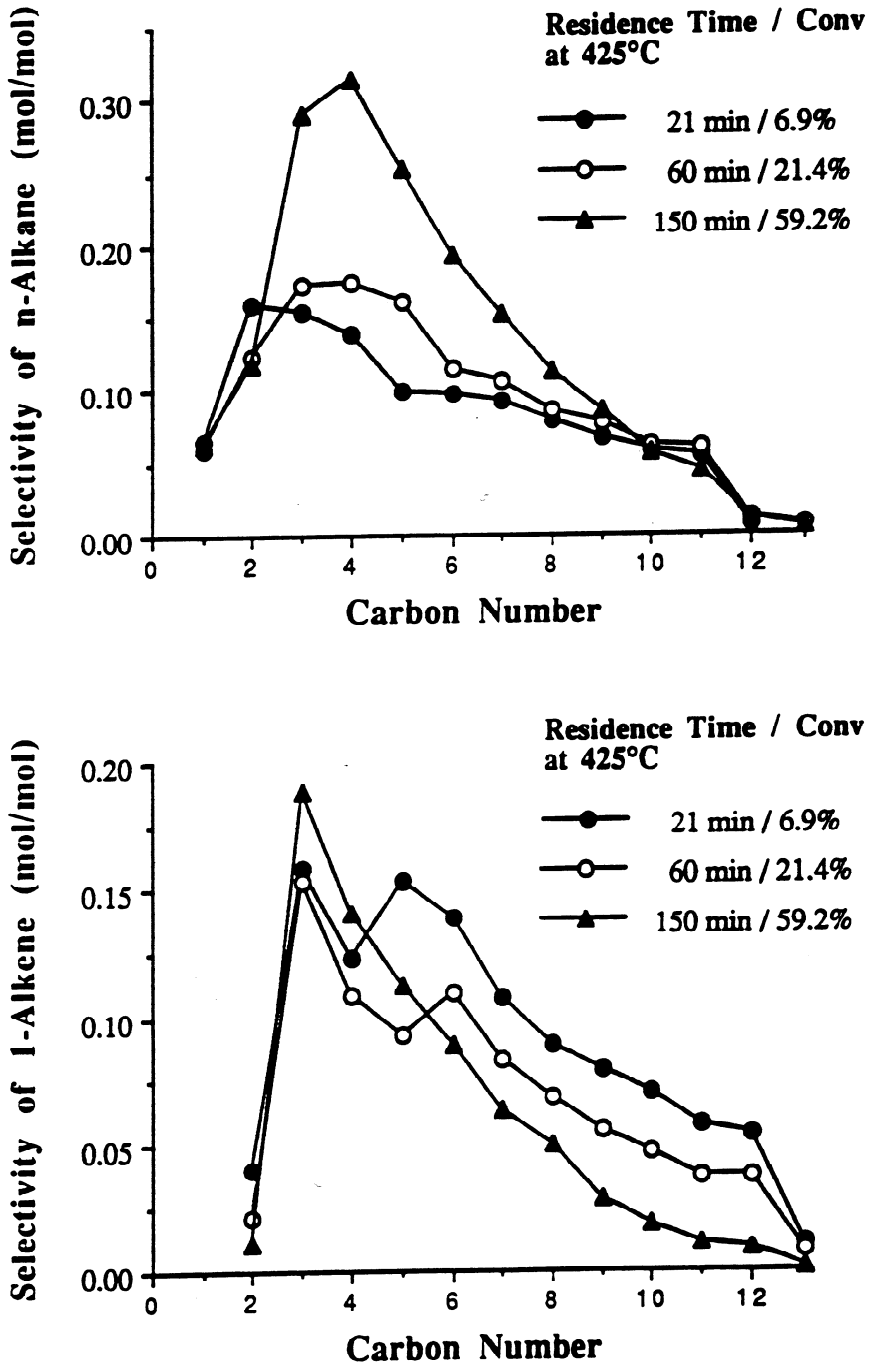

Figure 1.3-6. The n-C_{14} Selectivity to n-Alkanes (Top) and 1-Alkenes (Bottom) at 425°C under Initial N_2 Pressure of 0.69 MPa (Cold)

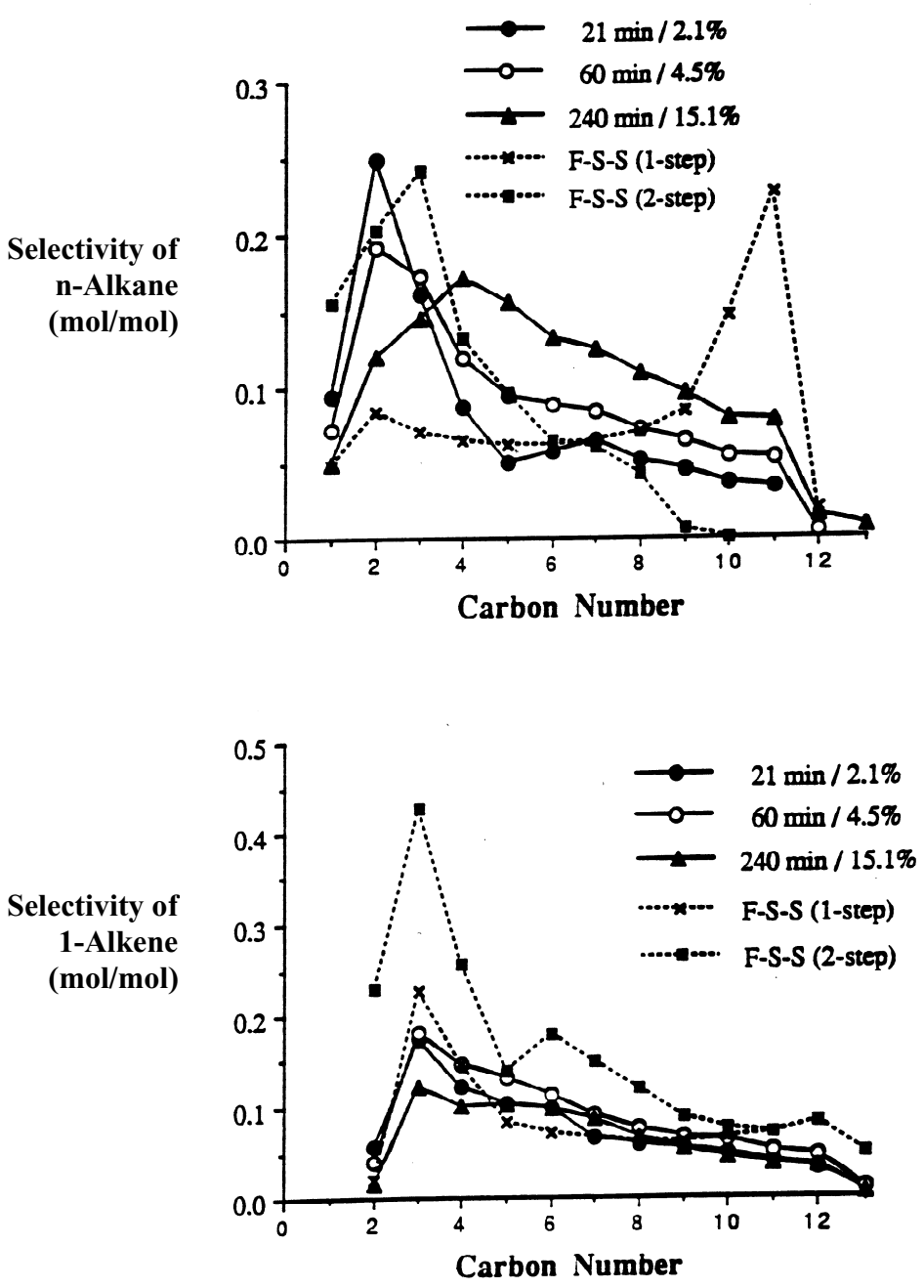

Figure 1.3-7. The Predicted versus Measured n-C_{14} Selectivity to n-Alkanes (top) and 1-Alkenes (bottom) at 400°C under Initial N_2 Pressure of 0.69 MPa (Cold)

[1] Song, C.; W.C. Lai, and H.H. Schobert. *Ind. Eng. Chem. Res.* 1993.

[2] Schobert, H.H. et al. *Advanced Thermally Stable Jet Fuels Technical Progress Report, November 1992 — January 1993.* The Pennsylvania State University. 1993.

[3] Fabuss, B. M., J.O. Smith, and C.N. Satterfield. *Advances in Petroleum Chemistry and Refining*. Interscience Publishers: New York. Volume 9. 1964. 156-201.

[4] Kossiakoff, A. and F.O. Rice. *J. Am. Chem. Soc.* 1943. *65.* 590-595.

[5] Lai, W.C. and C. Song. *Fuel.* 1993.

[6] Song, C.; W.C. Lai, and H.H. Schobert. *Ind. Eng. Chem. Res.* 1993.

[7] Ford, T.J. *Ind. Eng. Chem. Fundam.* 1986. *25.* 240-243.

[8] Fabuss, B. M. et al. *Ind. Eng. Chem. Proc. Des. Dev.* 1964. 3(3). 248-254.

[9] Schobert, H. H. et al. *Advanced Thermally Stable Jet Fuels Technical Progress Report, February 1993 - March 1993*. The Pennsylvania State University. 1993.

[10] Fabuss, B. M., J.O. Smith, and C.N. Satterfield. *Advances in Petroleum Chemistry and Refining*. Interscience Publishers: New York. Volume 9. 1964. 156-201.

1.4 Effects of Initial Phase Behavior on the Thermal Degradation of *n*-Tetradecane

This study is explained in detail in *Advanced Thermally Stable Jet Fuels Technical Progress Report, October–December 1993.*

Introduction

In our continuing study of the thermal decomposition behavior of jet fuels under supercritical conditions, we examined the effect of initial phase behavior on the thermal degradation of *n*-tetradecane. We selected n-tetradecane as a model compound based on the fact that it is one of the major paraffins present in petroleum-derived jet fuels and its critical properties (419.15°C, 15.73 bar[1]) are comparable with those of jet fuels (*e.g.*, 405°C, 21 bar for JP-7[2]).

Results and Discussion

1. Phase Behavior Calculations. Phase behavior has important effects on thermal decomposition reactions. As soon as the thermal reactions begin, the original reactant is converted into a complex mixture. It is, therefore, difficult to calculate the phase behavior of the reaction mixture. In this work, the initial phase behavior was estimated by calculating the initial pressure at any given temperature and sample loading using the Soave-Redlich-Kwong equation of state (SRK EOS).[3] SRK EOS has a high accuracy for predicting phase behavior of hydrocarbons and works well at high pressures, such as those under supercritical conditions. For pure compounds, SRK EOS can be expressed as follows:

$$P = RT / (V - b) - a / [V(V+b)] \quad (1)$$

where

$$b = 0.08664\ RT_c / P_c \quad (2)$$

$$a = a_c\alpha \quad (3)$$

$$ac = 0.42748\ (RT_c)^2 / P_c \quad (4)$$

$$\alpha^{0.5} = 1 + m\ (1 - T_r^{0.5}) \quad (5)$$

$$m = 0.48 + 1.574\ \omega - 0.176\ \omega^2 \quad (6)$$

where T_c is the critical temperature, P_c is the critical pressure, T_r is the reduced temperature (T / T_c), and ω is the acentric factor.

Figures 1.4-1, **1.4-2**, and **1.4-3** show the relationships between calculated reduced pressure P_r (P / P_c) and loading ratio, r, at three different temperatures (r = sample volume/reactor volume). Because 400°C is lower than the critical temperature of *n*-tetradecane, saturated vapor pressure was first calculated and Equation 1 was expressed in cubic form with respect to molar volume, V. The resulting equation was solved using a FORTRAN subroutine, CUBIC, to get three roots for the Vs. The largest root corresponds to the molar volume of the saturated vapor, V_v^{sa}, and the smallest root corresponds to the molar volume of the saturated

liquid, V_l^{sat}. At r, between the value corresponding to V_v^{sat} and the value corresponding to V_l^{sat}, P_r is equal to P_r^{sat}.

2. Effects of Initial Phase Behavior on Conversions. **Figures 1.4-4**, **1.4-5**, and **1.4-6** show the effect of initial phase behavior on the conversion of n-tetradecane stressed at three different temperatures for 5 hours. At 400°C, the n-tetradecane conversion first increases, reaches a maximum, and then decreases with r. The initial phase of the reactant changes from a vapor phase through a vapor-liquid phase and to a liquid phase as the loading ratio increases. The effect of pressure on the n-tetradecane differs depending on the phase in which the initial reactions take place.

At 425°C (Tr = 1.008) the relationships between the n-tetradecane conversion and the loading ratio are more complicated. Because the initial phase changes from a gas phase to a supercritical phase, the conversion was plotted against Pr. The conversion curve is much more complicated at the near-critical region than in the gas phase and far-supercritical region. At 450°C (Tr=1.045) the conversion curve shows an unusual behavior at the near-critical region, which will require additional investigation to explain.

3. Effects of Initial Phase Behavior on Product Distribution. **Figures 1.4-7**, **1.4-8**, and **1.4-9** show the effect of initial phase behavior on the overall mole ratio of C_5–C_{13} *n*-alkanes to the corresponding 1-alkenes. In all three cases, products contain more *n*-paraffins than 1-alkenes. At 400°C, the mole ratio increases from 1 to around 3 as the loading ratio increases. At 425°C, the higher *n*-alkane selectivity is reached with a maximum in *n*-alkane selectivity at the near-critical region. The *n*-alkane selectivity at 450°C is even higher and also exhibits a maximum at near-critical region. The higher *n*-alkane selectivity can be attributed to the relatively high pressure used in this study. At high pressures, bimolecular reactions such as hydrogen abstraction, radical addition, and radical recombination are favored over the unimolecular radical decomposition. These bimolecular reactions produce higher paraffins as primary reaction products.

Comparing the *n*-alkanes/1-alkenes mole ratio curves at 425°C and at 450°C with the corresponding *n*-tetradecane conversion curves reveals that the mole ratio curve and conversion curve have similar shapes, although the tendency of change with Pr is contrary. It is not clear whether these phenomena are typical. Because critical conditions change with chemical reactions, and the critical properties of the reaction products after five hours of reaction can be much different from those of the original reactant, the ability to correlate both the *n*-alkanes/1-alkenes mole ratio and *n*-tetradecane conversion to the initial critical point was surprising. Future work will focus on initial reactions to avoid large changes in the critical properties.

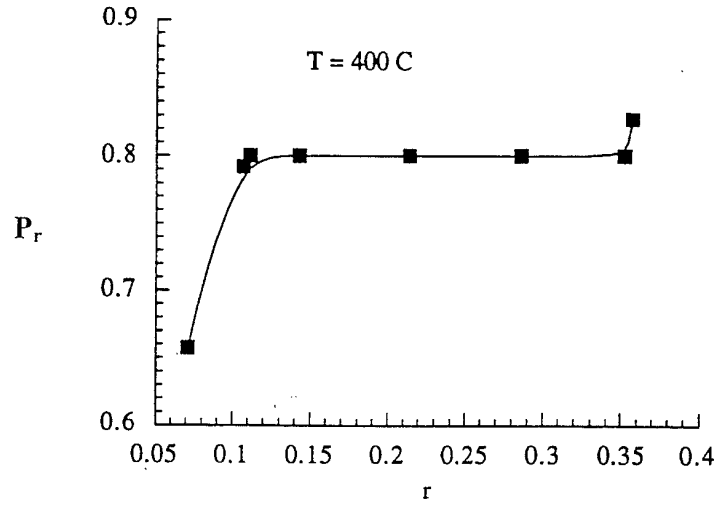

Figure 1.4-1. Calculated Reduced Pressure vs Loading Ratio for *n*-Tetradecane at 400°C

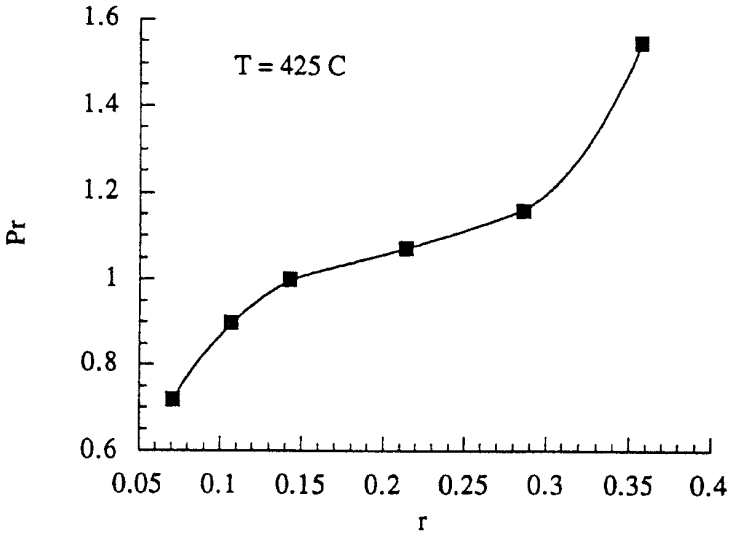

Figure 1.4-2. Calcualted Reduced Pressure vs Loading Ratio for n-Tetradecane at 425°C

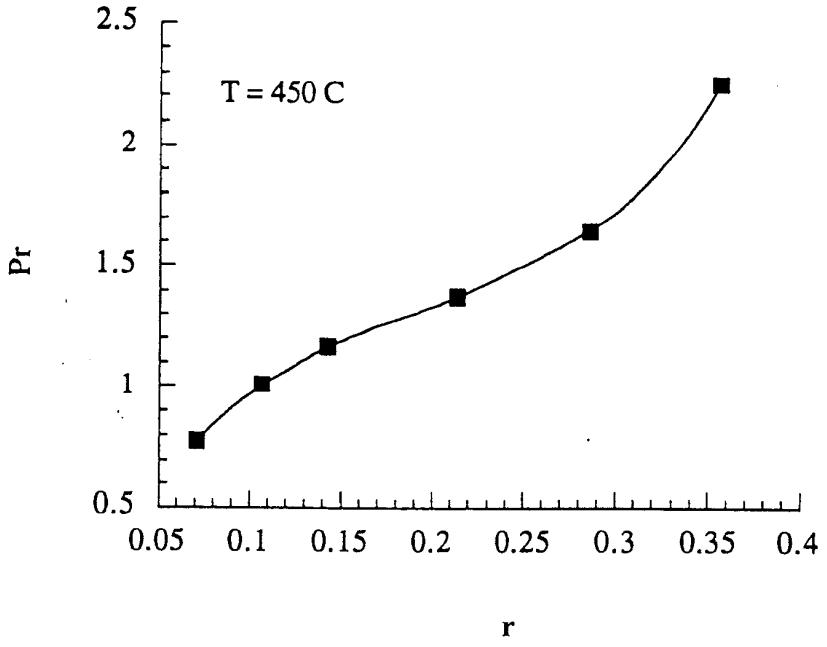

Figure 1.4-3. Calculated Reduced Pressure vs. Loading Ratio for n-Tetradecane at 450°C

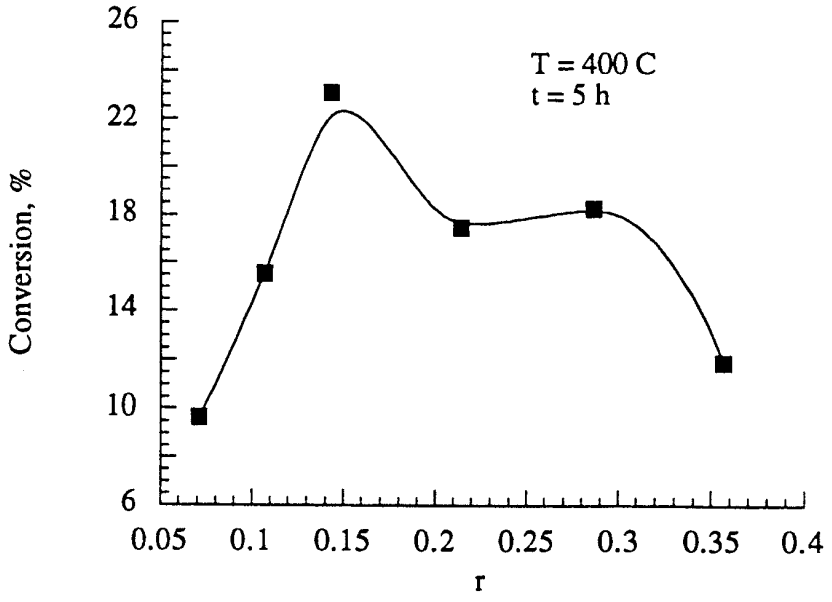

Figure 1.4-4. The *n*-Tetradecane Conversion (%) vs Loading Ratio Stressed at 400°C for 5 Hours

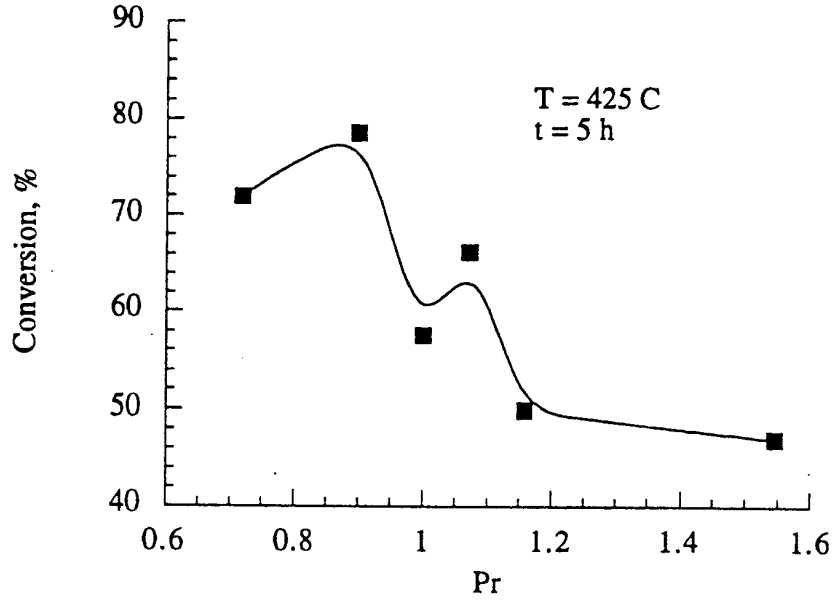

Figure 1.4-5. *n*-Tetradecane Conversion (%) vs. Reduced Pressure Stressed at 425°C for 5 Hours

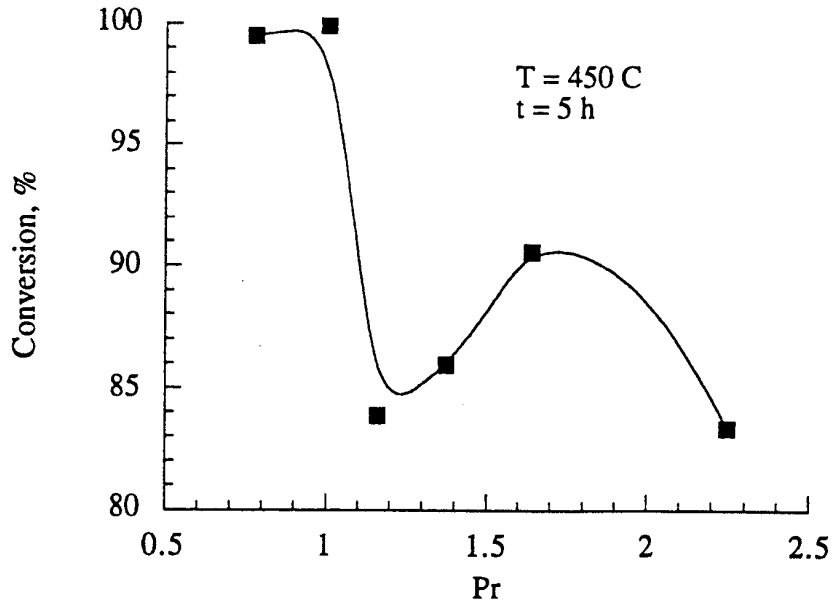

Figure 1.4-6. The n-Tetradecne Conversion (%) vs. Reduced Pressure Stressed at 450°C for 5 Hours

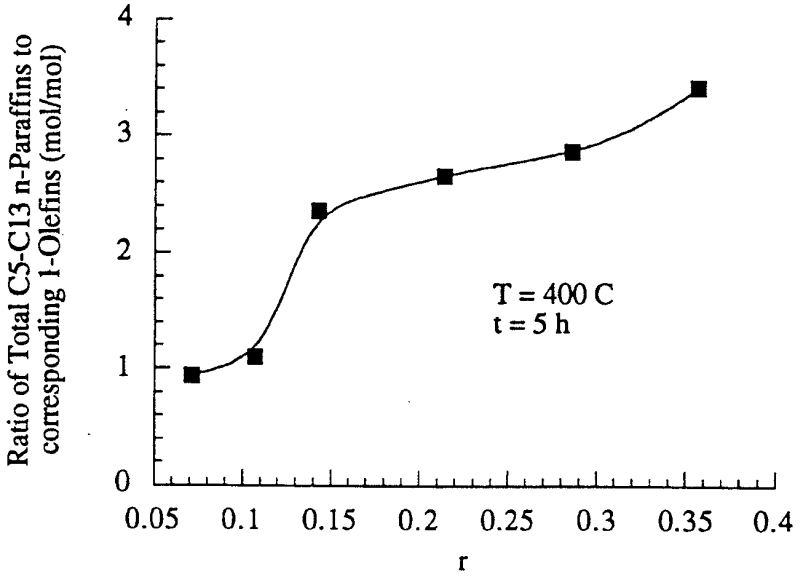

Figure 1.4-7. Overall Mole ratio of C_5-C_{13} *n*-Alkanes to Corresponding 1-Alkenes vs. Loading Ratio from n-Tetradecane Thermal Decomposition at 400°C for 5 Hours

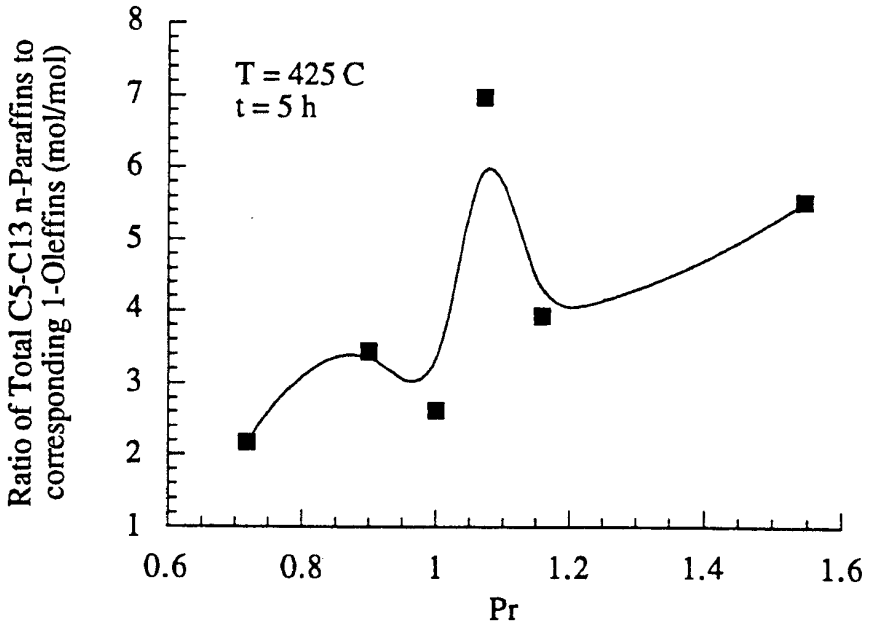

Figure 1.4-8. Overall Mole Ratio of C_5-C_{13} n-Alkanes to Corresponding 1-Alkenes vs. Reduced Pressure from *n*-Tetradecane Thermal Decomposition at 425°C for 5 Hours

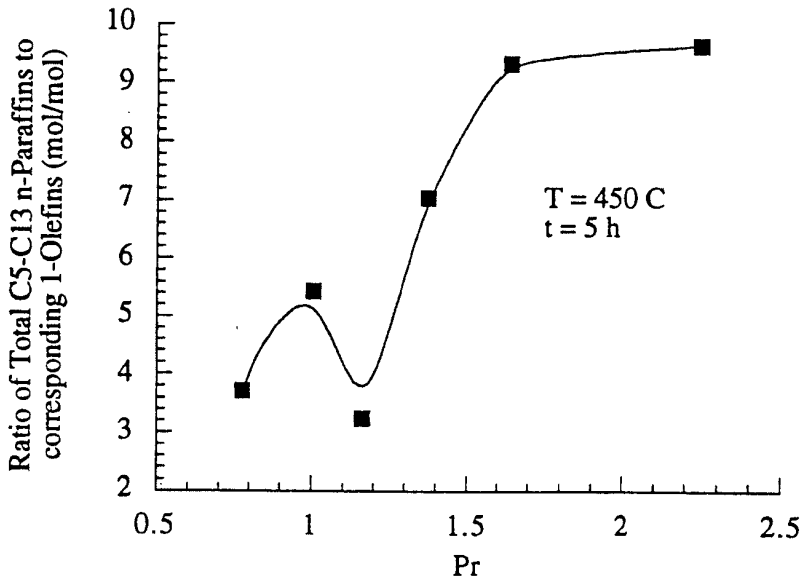

Figure 1.4-9. Overall Mole Ratio of C_5-C_{13} *n*-Alkanes to Corresponding 1-Alkenes vs Reduced Pressure from *n*-Tetradecane Thermal Decomposition at 450°C for 5 Hours

[1] Teja, A. S. et al. *Fluid Phase Equili.* 1990. 56, 153.

[2] Schobert, H. H. et al. *Advanced Thermally Stable Jet Fuels, Technical Progress Report, July 1993 - September 1993.* The Pennsylvania State University: University Park, PA. 1993.

[3] Soave, G. *Chem. Eng. Sci.* 1972. 27, 1197.

1.5 KINETICS OF N-TETRADECANE PYROLYSIS AT NEAR-CRITICAL REGION

This study is explained in detail in *Advanced Thermally Stable Jet Fuels Technical Progress Report, January–March 1994.*

A preliminary study showed that initial phase behavior has a significant effect on the thermal decomposition of *n*-tetradecane (*n*-C_{14}).[1] The purpose of this study was to extend our work to include short reaction times, performing kinetic studies of *n*-C_{14} pyrolysis with an emphasis at the near critical region.

Thermal decomposition reactions of *n*-C_{14} were carried out in the tubing bomb reactors for 0.5 to 5.0 hours. The experimental procedures were similar to those used in preceding works. Three temperatures (400°C, 425°C, and 450°C) and six to nine loading ratios (defined as the ratio of initial sample volume to reactor volume) were used to include different initial phase conditions (liquid, gaseous, and supercritical). The temperature and pressure regions fell in the range of reduced temperature, $T_r = T/T_c = 0.97\text{-}1.05$, and reduced pressure, $P_r = P/P_c = 0.4\text{-}5.2$, where T_c and P_c are the critical temperature and pressure of *n*-C_{14}. Their values were 419.5°C and 1.573 MPa, respectively.[2] Using the data obtained from thermal stressing experiments, we performed a kinteic analysis. Previous studies indicated that simple first-order kinetics were reasonably effective for thermal decomposition of straight-chain alkanes.[3,4] Therefore, the rate constants were determined by this first-order expression:

$$\ln[(1/(1-x)] = kt \qquad (1)$$

where x is the fraction of the reactant converted, k is the rate constant (h^{-1}), and t is the reaction time (h). We found the rate constant (k) at various loading ratios for each of the three different temperatures (400°C, 425°C, and 450°C) using the least-squares regression by plotting ln[(1/(1-x)] as the function of t.

Figures 1.5-1, **1.5-2**, and **1.5-3** show the change in the rate constant with loading ratio. At 425°C and 450°C, the rate constants were plotted as the function of initial reduced pressure P_r, which was calculated at the given temperature and loading ratio using the Soave-Redlich-Kwong equation of state.[5,6] At 400°C, the calculations showed that initial phase condition changes from a vapor phase (first two data points) through a vapor-liquid phase (following three data points) to a liquid phase as the loading ratio increases.

Figure 1.5-3 indicates that there is no significant difference between the rate constants at different sample loadings except at the first data point, which has a higher value. This deviant observation can probably be attributed to the narrow pressure range ($P_r = 0.79\text{-}0.83$ for the last five data points). On the other hand, at temperatures above Tc, large changes in the rate constants were observed at near-critical regions. At 450°C (T_r=1.045) the rate constants decrease significantly as pressure increases in the pressure region near P_c. In the supercritical region, however, pressure changes do not influence the rate constants significantly.

A similar relationship between the rate constant and pressure was observed at 425°C (T_r = 1.008) except that the rate constants present a more complex pressure dependence at the near-critical region. Note that the actual pressure in the reactor is lower than the calculated value, as a result of the effect created by the lower temperature at the top stem of the reactor. Subsequently,

the curves in Figures 1.5-2 and 1.5-3 should shift toward the left, indicating that significant changes in the rate constants fall in the sub- and near-critical regions and do not extend into the supercritical region.

Few kinetic data have been reported in the literature for the reactions of long-chain alkanes under near-critical conditions. Fabuss et al[7] found that the first-order rate constants for the thermal decomposition of *n*-Hexadecane (*n*-C_{16}) are independent of pressure in the range of T_r = 1.20-1.35 and P_r = 0.99-4.9, in agreement with the present results, as shown in Figure 1.5-2. The complex relationships between the rate constant and pressure at 425°C and the near-critical region may result from the unique properties of the fluid near the critical point (e.g., large activation volume, local anisotropy, and high compressibility).

The apparent kinetic parameters for the thermal decomposition of *n*-C_{14} were calculated using the Arrhenius law for six different sample loadings. **Table 1.5-1** lists the results. The calculated apparent activation energies are lower than the reported value of about 60 kcal/mol for long-chain alkanes.[7, 8] This difference is probably due to different experimental conditions. The unusual physicochemical properties of the fluid near its critical point, as stated above, may contribute to this inconsistency. The change in the rate constant with pressure is also a factor. In this work, the activation energy was calculated at certain sample loading from three different temperatures that result in three different pressures. This approach for determining activation energy assumes that the rate constants are independent of pressure. This is not the case for the reactions conducted at near-critical region.

Existing literature confirms this disagreement between the values of activation energy for long-chain alkane thermal decomposition. Zhou et al[9, 10] found that the activation energy for *n*-dodecane (*n*-C_{12}) pyrolysis under atmospheric pressure is considerably lower than that obtained from high-pressure thermal decomposition of *n*-C_{12} (≈39 kcal/mol at atmospheric pressure; ≈65 kcal/mol at 9.2 MPa nitrogen pressure). Moler and Steward[11] reported a value of 46.4 kcal/mol for *n*-C_{12} pyrolysis under atmospheric pressure.

Note that the value of the activation energy is largely dependent on how it is measured. Activation energy measured at constant reaction time for thermal decomposition of propane was 30 kcal/mol lower than that obtained at constant conversion.[12]

The preceding discussion suggests that the first-order kinetics with an Arrhenious relationship for long-chain alkane pyrolysis may only hold over a certain range of temperature, pressure, and extent of conversion. Evidently, phase behavior may also influence the kinetic parameters. For example, in this work, the activation energies obtained under gas-phase conditions (2-3 mL loading) are 10 kcal/mol greater than those determined under liquid and supercritical conditions (4-10 mL loading).

The values of activation energies and pre-exponential factors given in Table 1.5-1 display a compensation effect which is common to heterogeneous reaction systems, involving absorption on catalyst surfaces. It is not clear why our data displays an apparent compensation effect, since thermal decomposition of *n*-tetradecane is presumably a noncatalytic process that takes place in a fluid phase. Further study may be required to resolve this issue.

Table 1.5-1. Kinetic Parameters for n-C_{14} Pyrolysis at Different Sample Loading

Sample Volume (ml)	Rate Constant (h^{-1})			E_a (kcal/mol)	A (h^{-1})
	400°C	425°C	450°C		
2	0.0686	0.2638	1.1954	55.2	5.61×10^{16}
3	0.0502	0.323	0.7750	53.2	1.05×10^{16}
4	0.0604	0.1806	0.5766	43.6	8.53×10^{12}
6	0.0513	0.2162	0.5529	46.1	5.06×10^{13}
8	0.0565	0.1385	0.5530	44.0	9.95×10^{12}
10	0.0507	0.2026	0.5349	45.7	3.57×10^{13}

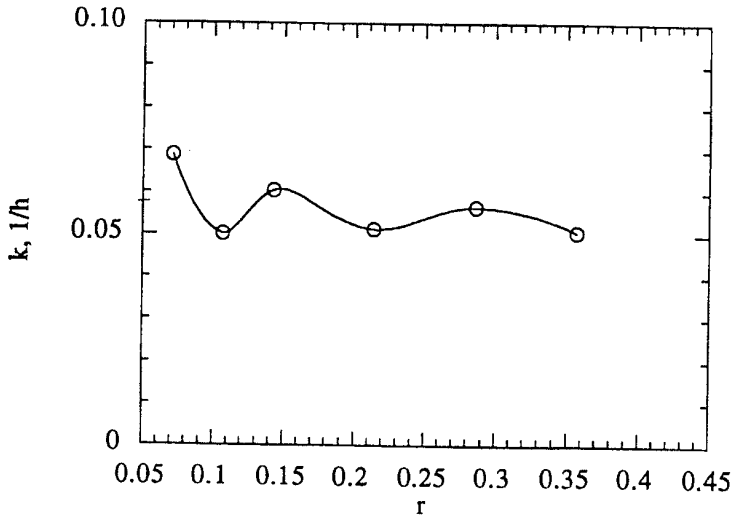

Figure 1.5-1. Change in Rate Constant with Loading Ratio at 400°C

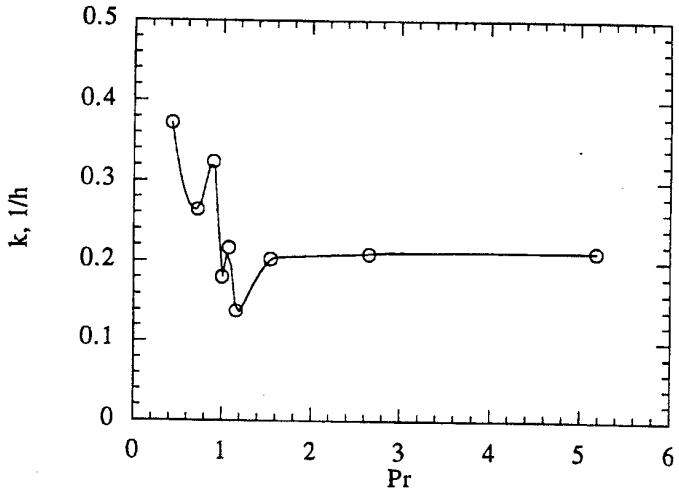

Figure 1.5-2. Change in Rate Constant with Initial Reduced Pressure at 425°C

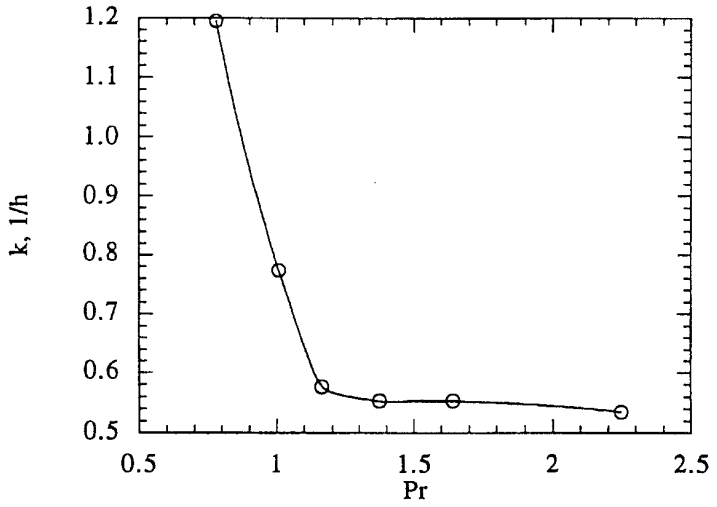

Figure 1.5-3. Change in Rate Constant with Initial Reduced Pressure at 450°C

---

[1] Schobert, H.H. et al. *Advanced Thermally Stable Jet Fuels, Technical Progress Report, October 1993-December 1993*. 1994.

[2] Teja, A. S. et al. *Fluid Phase Equili.* 1990. 56. 153.

[3] Fabuss, B. M., J. O. Smith, and C. N. Satterfield. *Adv. Pet. Chem. Refin.* 9, 157. 1964.

[4] Voge, H. H. and G. M. Good. *J. Am. Chem. Soc.* 71, 593. 1949.

[5] Schobert, H.H. et al. *Advanced Thermally Stable Jet Fuels, Technical Progress Report, October 1993-December 1993*. 1994.

[6] Soave, G. *Chem. Eng. Sci.* 27, 1197. 1972.

[7] Fabuss, B. M., J. O. Smith, and C. N. Satterfield. *Adv. Pet. Chem. Refin.* 9, 157. 1964.

[8] Voge, H. H. and G. M. Good. *J. Am. Chem. Soc.* 71, 593. 1949.

[9] Zhou, P. and B. L. Crynes. Ind. Eng. Chem. Process. Des. Dev. 25, 508. 1986.

[10] Zhou, P., O. L. Hollis, and B. L. Crynes. *Ind. Eng. Chem. Res.* 26, 852. 1987.

[11] Moler, J. L. and E. M. Steward. *Prepr. Pap, Am. Chem. Soc., Div. Pet. Chem.* 34, 837. 1989.

[12] Davis, H. G. and K. D. Williamson. *Adv. Chem. Ser.* 183, 41. 1979.

1.6 Effects of Sample Volume and Inert Nitrogen Pressure on the Pyrolysis of *n*-Tetradecane in both Gas and Supercritical Phase

This study is explained in detail in Advanced Thermally Stable Jet Fuels Technical Progress Report, January–March 1994.

Introduction

This work further explores our previous discovery of significant pressure dependence in *n*-tetradecane (*n*-C_{14}) conversion during pyrolysis at 450°C for 30 min. This work covered the thermal decomposition of *n*-C_{14} in both gas phase and supercritical phase (i.e., under temperatures higher than the critical temperature and various pressure conditions—from low to elevated pressures).

No literature existed that addressed the thermal stability of long-chain paraffins and jet fuels under supercritical conditions. Little was known about the role of inert gas in supercritical fluids at high temperatures. Literature on the pressure effects of free radical reactions during hydrocarbon pyrolysis was quite limited. The studies that had been conducted could not fully explain the pressure dependence of the alkane pyrolysis; therefore, we undertook this study.[1, 2, 3, 4, 5, 6, 7, 8, 9, 10, 11] This work involved pyrolyzing *n*-tetradecane using 1-11 mL samples at 450°C for 30 min under initial (cold) N_2 pressures of 0.17-2.03 MPa (10-280 psig) in 28-mL microreactors. The experimental conditions were characterized by a closed reactor, relatively high and continuously increasing pressure, low to high density gas phase or supercritical phases, and medium residence time. We chose to use 450°C—a lower temperature than most previous alkane pyrolysis studies had used.

Results and Discussion

1. Phase Behavior Calculation. **Figure 1.6-1** shows that the system pressure quickly increased to 2 and 4 MPa, respectively, for the two differing initial N_2 pressures in 6 minutes, due to vaporization of initial *n*-C_{14} liquid. The system pressure then increased steadily with increasing residence time with different rates, depending on the initially charged N_2 pressure. This monotonic pressure increase was indicative of the continuous hydrocarbon decomposition to smaller compounds, implying that the pressure or amount of initially charged N_2 seems to have a significant impact on the decomposition behavior of *n*-C_{14}. The originally simple reaction system quickly becomes a very complex mixture—pyrolysis of *n*-tetradecane at 450°C for 30 min produced more than 50 compounds, ranging from hydrogen to long-chain alkanes such as *n*-tricosane (*n*-C_{23}).

The thermodynamic properties of *n*-tetradecane and nitrogen are shown in **Table 1.6-1**, which presents the boiling point (T_b), critical temperature (T_c), critical pressure (P_c), critical volume (V_c), and accentric factor (ω).[12, 13, 14] These properties were needed to estimate critical properties using empirical correlations and to determine the phase behavior of the mixture of *n*-C_{14} and N_2.

The mixture critical temperature was calculated from the Li equation[15] and was usually bounded by the maximum and minimum critical temperatures among the components. This implies that in our reaction system, *n*-C_{14} could exist in either gas or supercritical state, since the

reaction temperature of 450°C is well above the T_c. On the other hand, the estimation of mixture critical pressure is often less reliable when the estimation methods are applied to mixtures containing methane and nonhydrocarbon gases. Therefore, we limited our study to phase behavior at the initial or early stage (low conversion).

Figure 1.6-2 presents the estimated reduced pressure (P_r) as a function of the charged volumes of *n*-C_{14} under vacuum condition (i.e., without the addition of N_2). Although no reaction was run without N_2, Figure 1.6-2 is still useful in helping determine the mixture phase at low N_2 mole fraction. It shows that for a pure *n*-C_{14} system, it is likely that at 450°C, the reactant exists in supercritical phase when the initial sample volume is greater than 3 mL, and in the gas phase otherwise. The system pressure was estimated from Soave's modification of the Redlich Kwong equation of state;[16] the mixture critical pressure was approximated by an expression using conformal solution theory.[17] On the basis of the estimated reduced properties, **Table 1.6-2** summarizes the estimated initial system phase at 450°C as a function of both the charged *n*-C_{14} sample volume and intial N_2 pressure (cold). The table indicates that for *n*-C_{14} and N_2 mixture systems at 450°C, the reactant likely exists in supercritical phase when the initial sample volume is greater than 7.8 mL under the studied N_2 pressure ranges, and in gas phase when the initial sample volume is less than 3 mL. With a 5 or 7 mL sample, the phase of the reactant at 450°C could either be gas or supercritical, depending on the initial N_2 pressure.

2. Effect of Sample Volume and Inert N_2 Pressure. The effects of initial sample volume of *n*-C_{14} on pyrolysis rate constant under different N_2 pressures are presented in **Figure 1.6-3** for experiments in or near supercritical phase. The figure indicates that in the supercritical phase, the initial sample volume, or the pressure of the reactant, affects the *n*-C_{14} in two ways:

a) When pyrolysis experiments were carried out under a low initial (cold) N_2 pressure of 0.17 MPa (10 psig), the change in the initial sample volume from 5 mL to 11 mL had little impact on *n*-C_{14} conversion or decomposition rate constants.

b) When the initial N_2 pressure was increased to 0.79-2.03 MPa, the decomposition rate decreased as sample volume increased. On average, a 2mL increase of *n*-C_{14} volume decreased the rate constant by approximately 0.2 hr^{-1}, which corresponds to about a 7 mol% decrease in conversion.

In short, in or near the supercritical phase, increasing the pressure of inert N_2 enhanced *n*-C_{14} conversion; on the other hand, the *n*-C_{14} decomposition may be retarded by the increase in the pressure of the *n*-C_{14} sample. The results can be summarized in terms of initial mole fraction of *n*-C_{14} as shown in **Figure 1.6-4.** The figure shows that in the supercritical phase region, the *n*-C_{14} decreased almost linearly with the increasing mole fraction of *n*-C_{14}, and in the gas phase region, the conversion varied to a lesser extent—with an average value of 41 mol% ± 7.8 mol%. Compared with supercritical pyrolysis, there is less significant pressure dependence of *n*-C_{14} conversion during gas-phase pyrolysis. However, in gas-phase pyrolysis, the influence of inert gas pressure and sample volume is interdependent (i.e., increasing inert gas pressure can either decrease or increase *n*-C_{14} conversion, depending on the sample volume, and vice versa). The fact that the influence of sample volume and initial pressure of inert gas (N_2) depends on the phase behavior of the reaction system, illustrates the complexity of the mechanisms governing the pressure effects of inert gas and reactant.

The product distributions and reaction extent were controlled by isothermally adjusting the inert gas pressure and sample volume. The ratios of 1-alkene to the corresponding *n*-alkane for C_2 and C_{10} products from the pyrolysis of *n*-C_{14} are shown in **Figure 1.6-5** as a function of the initially charged *n*-C_{14} volume and N_2 pressure. Although only the results of C_2 and C_{10} are shown in Figure 1.6-5, they display representative trends for C_2-C_{13}. The figure shows that respective 1-alkene/*n*-alkane ratios increased with both decreases in initial pressure of N_2 and decreases in sample volume. These observations imply that lower pressure facilitates unimolecular reaction (β-scission) to form alkenes, while higher pressure favors bimolecular reaction (H-abstraction) to form alkanes.

The *n*-C_{14} pyrolysis exhibited similar reaction rates with different molar selectivities when reaction occurred in a supercritical region rather than a gas region. Comparing results at the two different phases shows that, at a similar conversion level, 1-alkene/*n*-alkane is larger in the gas phase than in the supercritical phase, as indicated by **Figure 1.6-6**. This reveals that the proportion of bimolecular H-abstraction reactions increases with increasing sample volume. In short, the results showed that supercritical phase pyrolysis of long-chain alkanes is characterized by a higher proportion of bimolecular reactions, whereas unimolecular β-scission is common in conventional vapor-phase processes reported in the literature.

3. Mechanistic Considerations. N_2 acts as an inert reaction medium in the pyrolysis system. In this study, N_2 could influence reactions in several ways—via mechanical pressure effect, phase behavior, and diffusional limitations. A large number of elementary reactions contributed to the global reaction. At least two radical reaction processes (unimolecular and bimolecular) are affected by the pressure in opposite directions, giving rise to the unusual reversed volcano-shaped and linear relationships, as shown in **Figure 1.6-7**. These findings also provide experimental evidence that activation volumes ($\Delta V^{\neq}$) of some reactions involved in *n*-C_{14} pyrolysis are very sensitive to pressure changes near the critical point.

Table 1.6-1. Thermodynamic Properties of *n*-Tetradecane and Nitrogen

Compound Name	T_b (K)	T_c (K)	P_c (MPa)	V_c (cm^3/mol)	ω
n-Tetradecane	526.7	692.3	1.57	830	0.662
Nitrogen (N_2)	77.4	126.2	3.39	89.8	0.039

Table 1.6-2. The Estimated Initial System Phase of *n*-C14 and N2 Mixtures

	Initial N_2 Pressure					
	0.17 MPa	0.79 MPa	1.41 MPa	2.03 MPa	0.35 MPa	1.23 MPa
n-C_{14}	Estimated Initial System Phase					
1 mL	LDG	LDG	LDG	LDG		
3 mL	MDG	LDG	LDG	LDG		
5 mL	NSC	MDG	MDG	MDG		
7 mL	NSC	NSD	MDG	MDG		
9 mL	SC	NSC	NSC	NSC		
11 mL	SC	SC	SC	SC		
2.2 mL					LDG	LDG
7.8 mL					NSC	NSC

Key:
LDG = low density gas phase
MDG = medium-density gas phase
NSC = near supercritical phase (high-density gas phase or supercritical phase)
SC = supercritical phase

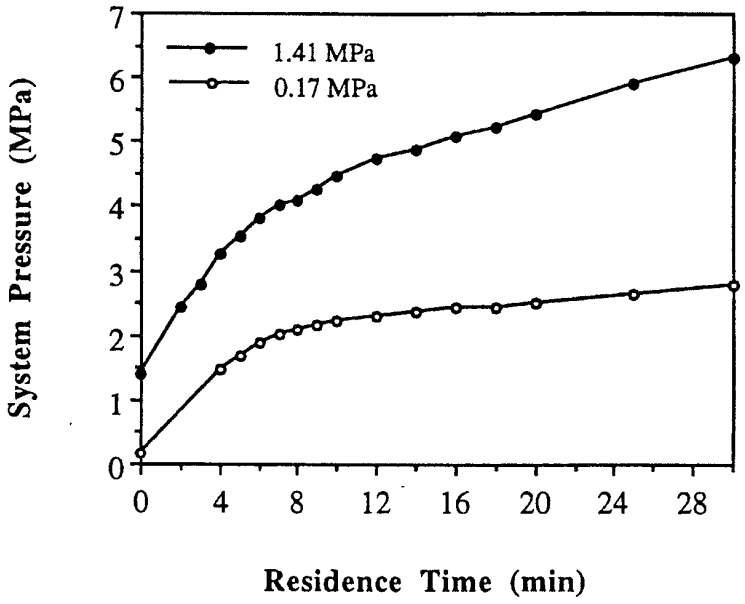

Figure 1.6-1. System Time-Pressure Profiles During Pyrolysis of 9 ml of n-Tetradecane at 450°C under Initial N_2 Pressure (Cold) of 0.17 and 1.41 MPa

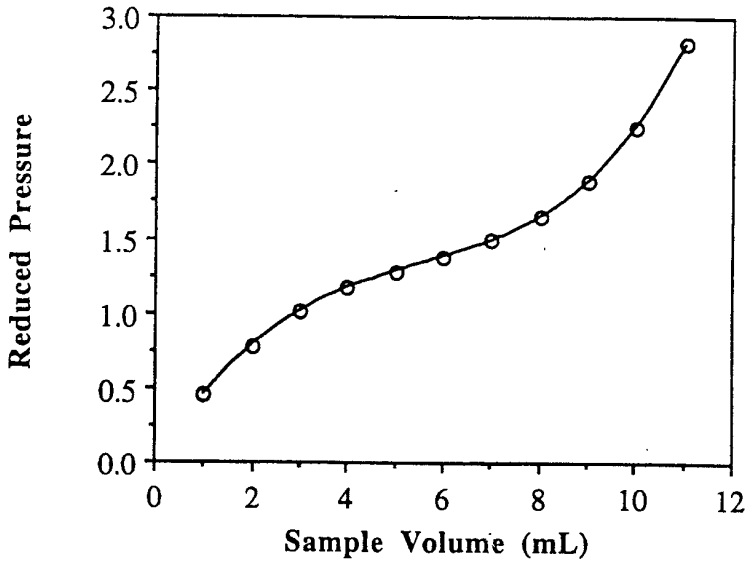

Figure 1.6-2. Estimated Reduced Pressure (P_r) as a Function of the Initially Charged Volumes of *n*-C_{14} under Vacuum Condition (without the Addition of N_2).

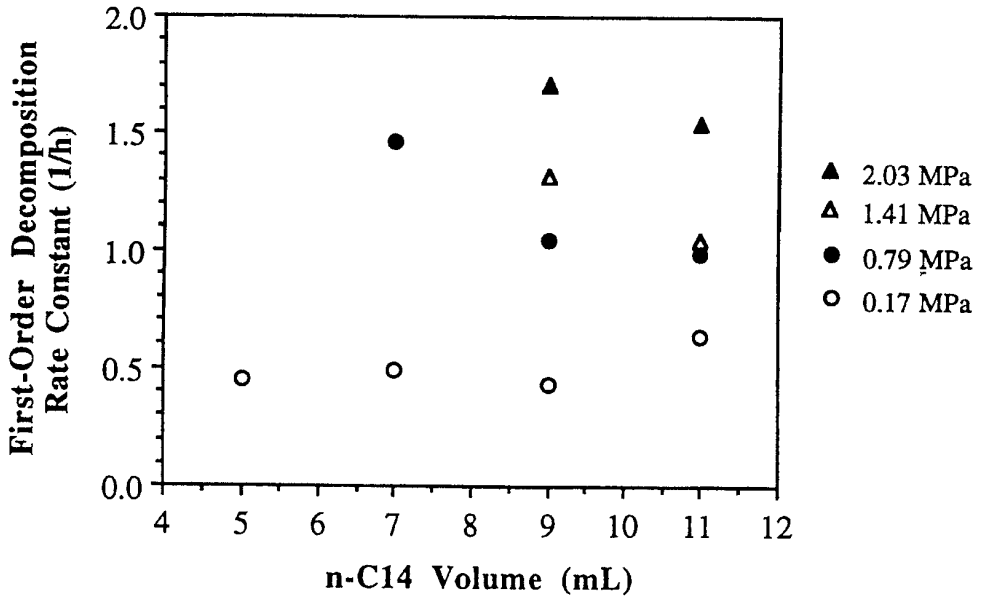

Figure 1.6-3. Effects of Initial Volume of *n*-C_{14} on Pyrolysis Rate Constant at 450°C for 30 Minutes under Different Pressures of UHP N_2 in 28-mL Microreactors (All Experiments were in or near Supercritical Phase)

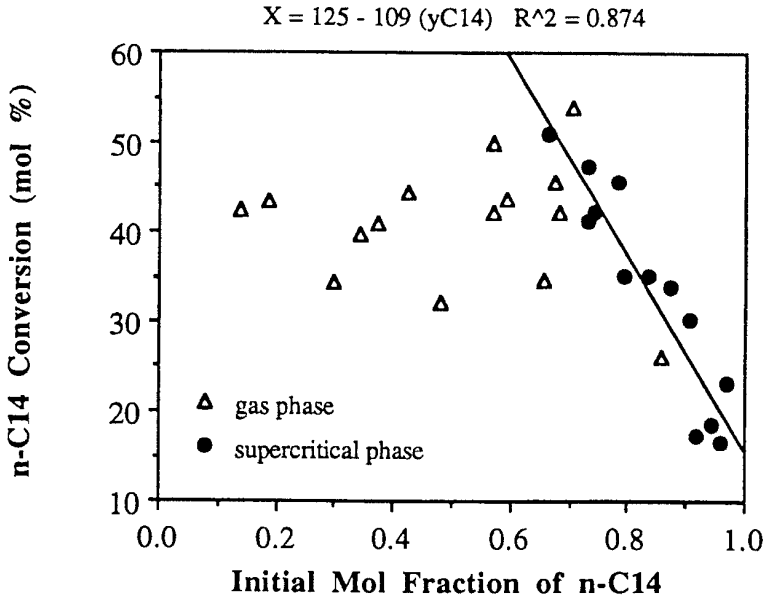

Figure 1.6-4. Conversion of *n*-C_{14} Pyrolysis at 450°C for 30 Minutes as a Function of Initial Mole Fraction of *n*-C_{14} in a Mixture of *n*-C_{14} and N_2

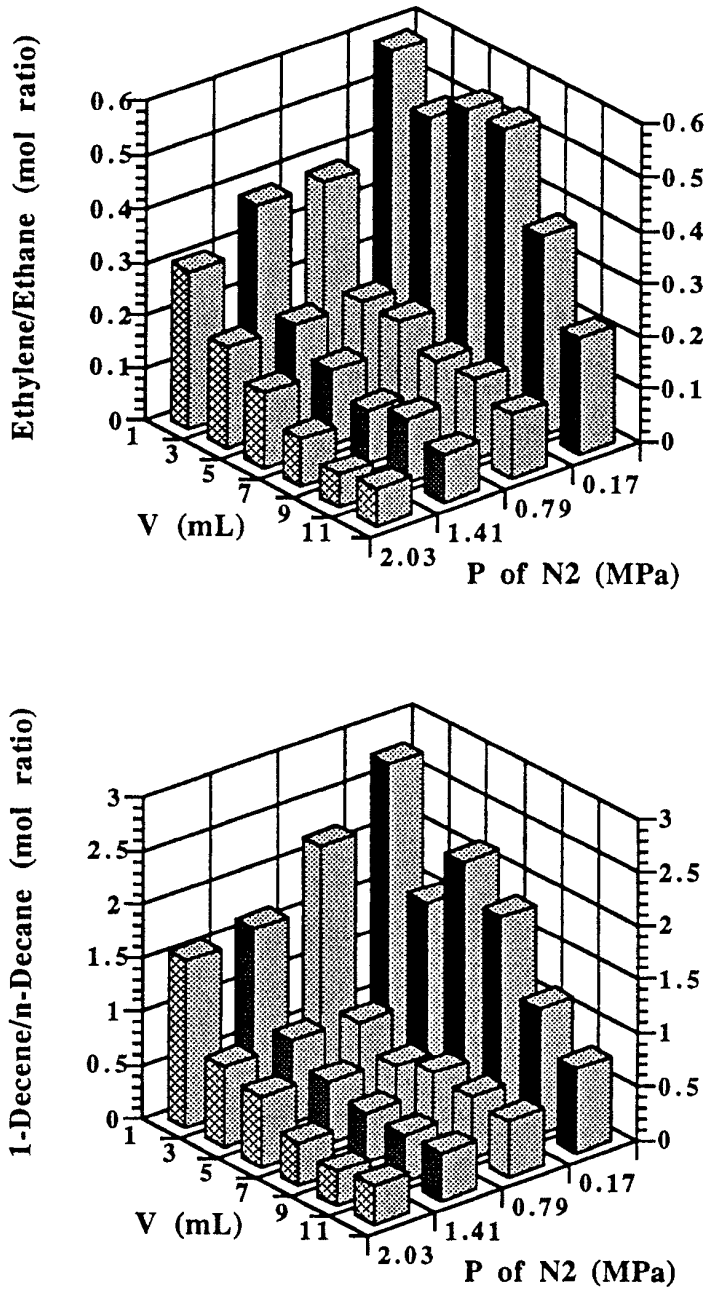

Figure 1.6-5. The Ratios of 1-Alkene to the Corresponding n-Alkane for C_2 and C_{10} Products from the Pyrolysis of n-C_{14} as a Function of the Initially Charged n-C_{14} Volume and N_2 Pressure

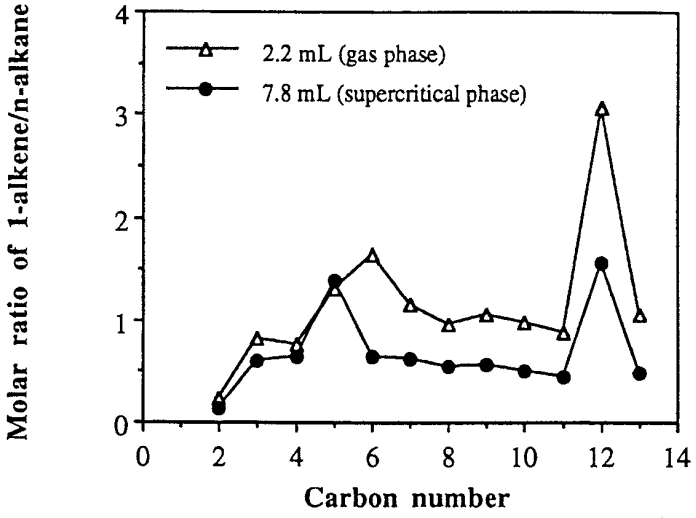

Figure 1.6-6. Ratios of 1-Alkene to the Corresponding n-Alkane for C_2-C_{13} Products from the Pyrolysis of n-C_{14} at 450°C for 30 Minutes under Initial N_2 Pressure of 1.23 Mpa for Two Sample Volumes of 2.2 and 7.8 mL

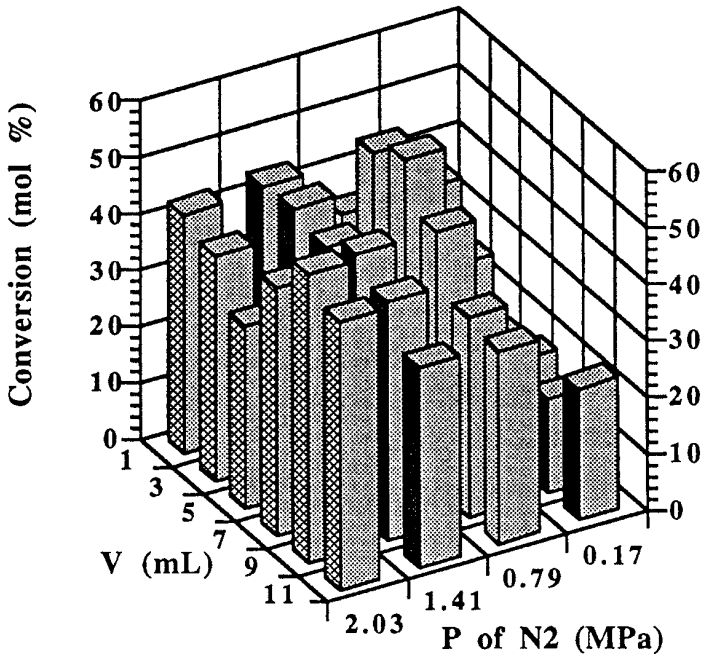

Figure 1.6-7. Conversion of *n*-C_{14} as a Function of the Initially Charged *n*-C_{14} Volume and N_2 Pressure

[1] Voge, H. H. and G. M. Good. *J. Am. Chem. Soc.* 71, 593. 1949.

[2] Fabuss, B. M. et al. "Thermal Decomposition Rates of Saturated Cyclic Hydrocarbons." Ind. Eng. Chem. Proc. Des. Dev. 1963. 3(3). 248-254.

[3] Fabuss, B. M., J. O. Smith, and C. N. Satterfield. "Thermal Cracking of Pure Saturated Hydrocarbons." *Advances in Petroleum Chemistry and Refining.* New York: Interscience Publishers, 1964. 156-201.

[4] Doue, F. and G. Guiochon. "The Formation of Alkanes in the Pyrolysis of *n*-Hexadecane: Effect of an Inert Gas on the Decomposition of Alkyl Radical." *Can. J. Chem.* 1969. 47. 3477-80.

[5] Jackson, K. J. et al. "Measurement of Pressure Effects on *n*-Hexadecane Cracking Rates." *Prep. – Am. Chem. Soc. Div. Fuel Chem.* 1992. 37 (4). 1614-20.

[6] Domine, F. "High Pressure Pyrolysis of *n*-Hexane, 2,4 Dimethylpentane and 1-Phenylbutane. Is Pressure and Important Geochemical Parameter?" *Org. Geochem.* 1991. 17(5). 619-634.

[7] Domine, F. "Kinetics of Hexane Pyrolysis at Very High Pressures. 1. Experimental Study." *Energy & Fuels.* 1989. 3. 89-96.

[8] Domine, F. et al. "Kinetics of Hexane Pyrolysis at Very High Pressures. 2. Computer Modeling." *Energy & Fuels.* 1990. 4. 2-10.

[9] Mallison, R. G. et al. "Detailed Chemical Kinetics Study of the Role of Pressure in Butane Pyrolysis." *Nd. Eng. Chem. Res.* 1992. 31. 37-45.

[10] Zhou, P. and B. L. Crynes. "Thermolytic Reaction s of Dodecane." *Ind. Eng. Chem. Res.* 1986. 25(2). 508-14.

[11] Zhou, P. et al. "Thermolysis of Higher Molecular Weight Straight-Chain Alkanes (C9-C22)." *Ind. Eng. Chem. Res.* 1987. 26. 856-52.

[12] Reid, R. C., J. M. Prausnitz, and B. E. Poling. *The Properties of Gases & Liquids.* Fourth Edition. New York: McGraw-Hill. 1987.

[13] Daubert, T. E. and R. P. Danner. "Critical Properties." *Technical Data Book – Petroleum Refining.* American Petroleum Institute. 5th Edition. 1987.

[14] Teja, A. S. et al. "Correlation of the Critical Properties of Alkanes and Alkanols. *Fluid Phase Equili.* 1990. 56. 153-169.

[15] Li, C. C. *Can. J. Chem. Eng.* 1971. 49. 709.

[16] Soave, Giorgio. Equilibrium Constants from a Modified Redlich-Kwong Equation of State. Chem. Eng. Sci. 1972. 27. 1197-1203.

[17] Kreglewski, A. and W. B. Kay. *J. Phys. Chem.* 1969. 73. 3359.

1.7 PRODUCT DISTRIBUTIONS FROM PYROLYSIS OF N-TETRADECANE IN NEAR-CRITICAL REGION

This study is explained in detail in *Advanced Thermally Stable Jet Fuels Technical Progress Report, April–June 1994.*

Previous studies have shown that initial phase behavior has a significant effect on the thermal decomposition of n-tetradecane (n-C_{14}).[1, 2] These studies found that at temperatures above the critical temperature (T_c), the first-order rate constants for n-C_{14} decomposition exhibited a large pressure dependence in the near-critical region. Significant changes in the rate constants fell in the sub- and near-critical regions and did not extend to farther supercritical region. Following up this previous work, we examined product distributions from n-C_{14} pyrolysis in the near-critical region.

We studied the change in the yield of individual paraffinic and olefinic products with loading ratio (the ratio of initial sample volume to reactor volume) at 400°C and with reduced pressure, P_r ($P_r = P/P_c$), at 425°C and 450°C. P_r was calculated at a given temperature and loading ratio using the Soave-Redlich-Kwong equation of state.[3] Under the conditions used in this study, the major pyrolytic products were n-alkanes with carbon numbers from C_1 to C_{11} and 1-alkenes with carbon numbers from C_2 to C_{12}. Also present in very small amounts were n-C_{12}, n-C_{13}, 1-C_{13} and minor reaction products such as branched-chain alkanes, internal alkenes, cycloalkanes, and aromatics. Hydrogen was detected only at 450°C. In total, 50 to 100 liquid components were eluted from the GC column. Because this study was concerned with product distributions from n-C_{14} pyrolysis at near critical conditions, minor product distributions were excluded.

Figures 1.7-1 through 1.7-9 present the changes in yields of the major paraffinic and olefinic products with loading ratio or reduced pressure. C_4 products were dissolved in liquid product, but significant losses occurred before the liquid sample could be analyzed; therefore, the yields of both butane and butene were not included. 1-C_{12} was removed to improve the clarity of the figures. Our findings are summarized below:

Changes of Product Components with Loading Ratio (r) at 400°C and Reaction Times of 3 and 5 Hours

Yields of Gas Components	• Propane and propylene increased with r • Ethane and ethylene decreased with r • Methane remained in a very narrow range • Yields of gas components decreased in this order: propane>propylene>ethane>methane>ethylene
Yields of Liquid Components	• Components with longer chains in the same homologous series tended to have low yields (Figure 1.7-2 and 1.7-3) • Paraffinic component increased with r • Olefinic component decreased with r

Changes of Product Components with Loading Ratio (r) at 425°C with Reaction Times of 0.5 and 1 Hour	
Yields of Gas Components	• Followed similar order as in 400°C trial • Changes in yields under reduced pressure (P_r) exhibited unusual features in near-critical region (Figure 1.7-4)
Yields of Liquid Components	• Paraffinic and olefinic decreased with increasing carbon number • In the near-critical region, paraffinic component increased rapidly with P_r; in the farther supercritical region, the yield did not change significantly with P_r • In the near-critical region, olefinic component exhibited complex pressure dependence for an 0.5 hour run; for a 1 hour run, it decreased with P_r, exhibiting significant change in the near-critical region.
Changes of Product Components with Loading Ratio (r) at 450°C with Reaction Time of 0.5 and 1 Hour	
Yields of Gas Components	• Exhibited similar order and pressure dependence as in 400°C and 425°C trials at 0.5 hours (Figure 1.7-7) • For 1.0 hour run, complex pressure dependence was apparent, although the ethylene yield remained the lowest among gas products and decreased with P_r.
Yields of Liquid Components	• The longer the chain of a specific component, the smaller the yield for that component (Figures 1.7-8 and 1.7-9) • Paraffinic component increased with P_r; olefinic component decreased with pressure • No large pressure dependence of the yield in the region near P_r=1

Figures 1.7-10 through 1.7-12 show the changes in the molar ratios of *n*-alkane to 1-alkene with r or P_r for selected carbon numbers of 7, 9, 11 under different conditions. The selectivity for paraffinic component relative to olefinic component with the same carbon number increases with pressure. At 425°C, significant changes in *n*-alkane/1-alkene ratios were observed in the near-critical region. At all three temperatures, the product selectivities for *n*-alkanes are very high, exceeding the selectivities for corresponding 1-alkenes at higher pressures. These results differ from those obtained under typical *n*-alkane pyrolysis conditions (~atmospheric pressure, >600°C) which usually cite methane and ethane as the only paraffinic products.

These findings can be explained by free radical theory and transition state theory. For *n*-C_{14} the homolytic initiation reaction produces two primary radicals. These primary radicals then abstract hydrogen from surrounding reactant molecules to form various parent radicals. Most are secondary radicals, because the formation of a primary radical by hydrogen abstraction requires higher energy activation. The parent radicals undergo β-scission to form a 1-alkene and a primary radical. The subsequent reactions of these primary radicals include hydrogen abstraction, β-scission, isomerization, and addition at higher conversions. The competitions between these reactions determine the final product distribution. At high temperatures and low pressures, unimolecular radical decomposition reactions are favored because of higher activation energies than bimolecular reactions. At high pressures and lower temperatures, bimolecular reactions, such as hydrogen abstraction and radical addition reactions, are favored.

Using the Arrhenius rate parameters,[4] we estimated the relative rates of hydrogen abstraction and radical decomposition. At 425°C, the rate ratio of hydrogen abstraction and radical decomposition was approximately 2,500, indicating that hydrogen abstraction was

favored under those conditions. This means that the larger free radical formed from β-scission of the parent radical would tend to be stabilized by hydrogen abstraction from a surrounding molecule, rather than undergoing further decomposition. This would result in equimolar distributions between *n*-alkanes and 1-alkenes in the products. In addition, the radical addition reaction between a free radical and an olefinic molecule would also be favored at high pressures and higher conversion (e.g., larger than 10 percent). Both hydrogen abstraction and radical addition reactions increase the ratio of *n*-alkanes to 1-alkenes in the products. This explains the observed results: high ratios of *n*-alkanes to 1-alkenes, low ethylene yields, increasing *n*-alkane yields and decreasing 1-alkene yields with increasing pressure.

The large changes in the rations of *n*-alkanes to 1-alkenes in the near-critical region probably resulted from unusual properties of the fluid in this region. In the near-critical region, the fluid exhibited very high compressibility and many physicochemical properties change significantly with pressure. When the reaction is carried out in the near-critical region, pressure may influence the rate constant significantly. This can be explained by means of transition state theory.[5 6]

The results of this study indicated that the magnitudes of the activation volumes ($\Delta V^{\neq}$) for elementary bimolecular reactions (e.g., hydrogen abstraction and radical addition) or for elementary radical decomposition, could attain rather large values when the reaction is carried out in the near-critical region of *n*-C_{14} (425°C and initial P_r near 1). The large negative values of the $\Delta V^{\neq}$ for bimolecular reactions or the large positive values for the $\Delta V^{\neq}$ for the unimolecular radical decomposition reaction results in the large increases in the ratios of *n*-alkane to 1-alkene with pressure in the near-critical region of *n*-C_{14}. We cannot infer which reactions have large $\Delta V^{\neq}$ values, because hydrogen abstraction, radical addition, and radical decomposition are competitive reactions; therefore, the existence of a large $\Delta V^{\neq}$ value for any reaction can result in large changes in the ratios of *n*-alkane to 1-alkene. Such information can be obtained only by studying elementary reactions. While the detailed mechanism governing this unique product distribution in the near-critical region is not yet clear, we can infer that unusual properties of the fluid in the near-critical region may have significant effects on thermal reactions.

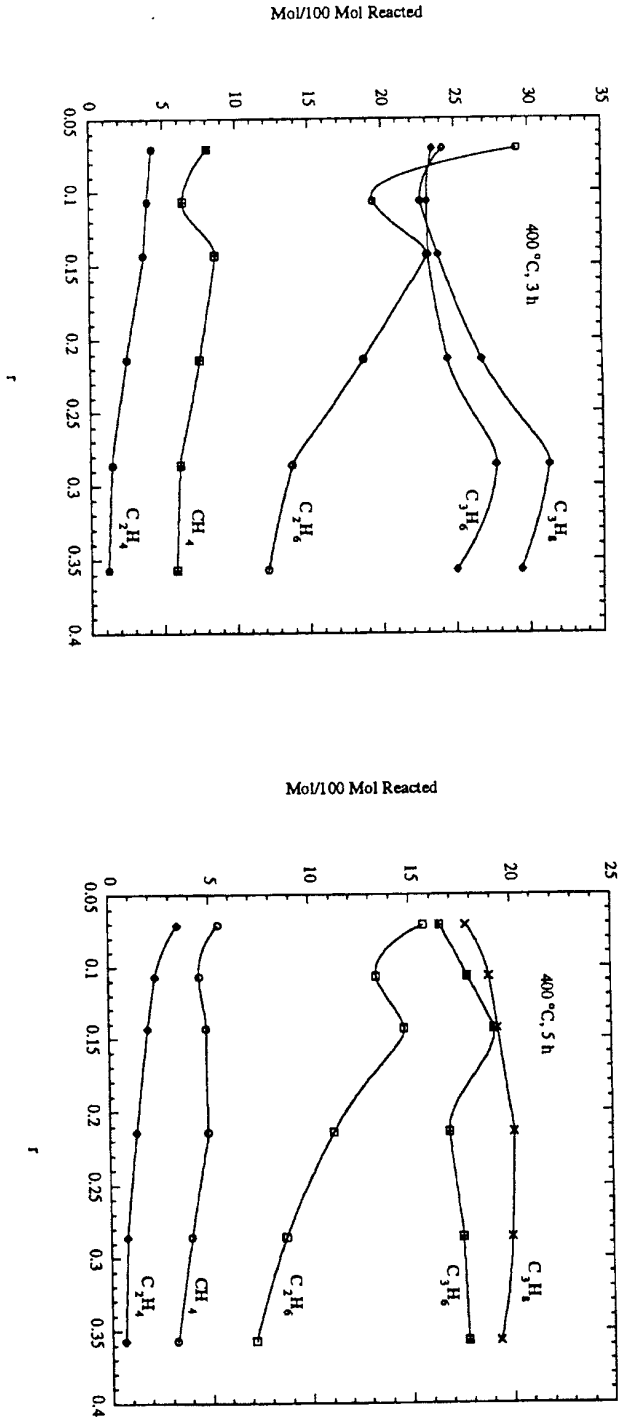

Figure 1.7-1. Effects of Loading Ratio (r) on Gas Product Distributions from n-C_{14} Pyrolysis at 400°C for 3 and 5 Hours

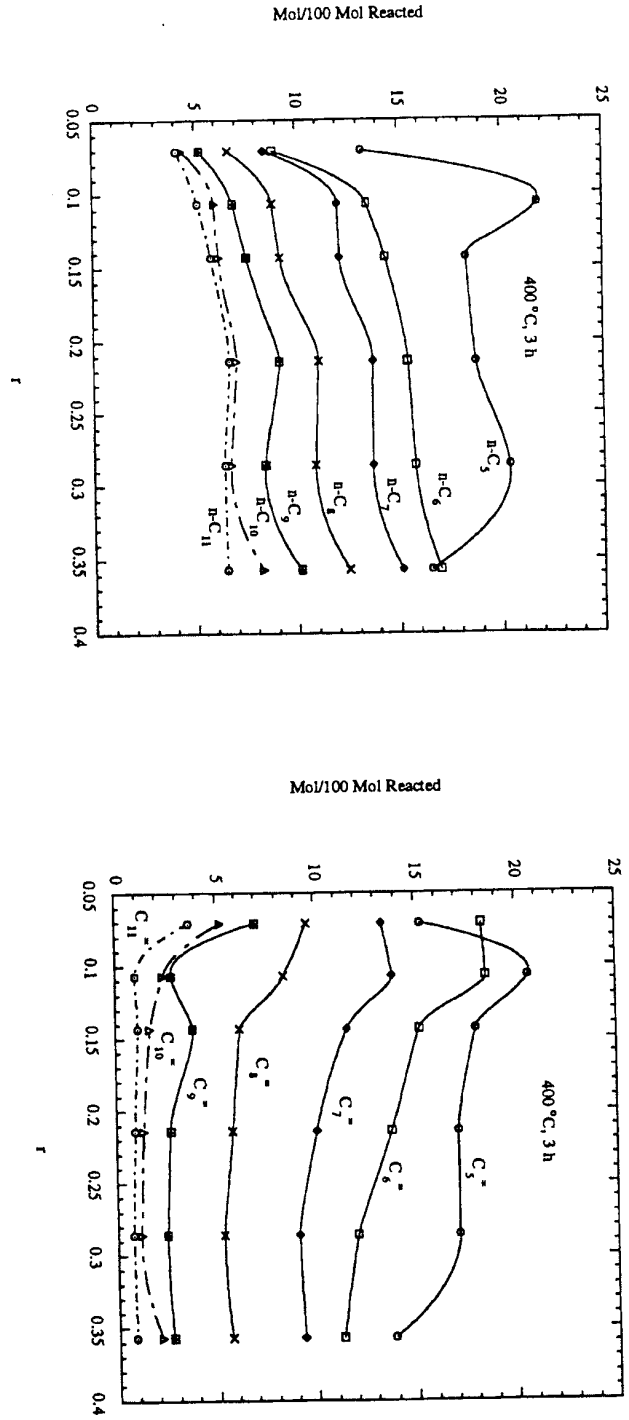

Figure 1.7-2. Effects of Loading Ratio (r) on Liquid Product Distributions from n-C_{14} Pyrolysis at 400°C for 3 Hours

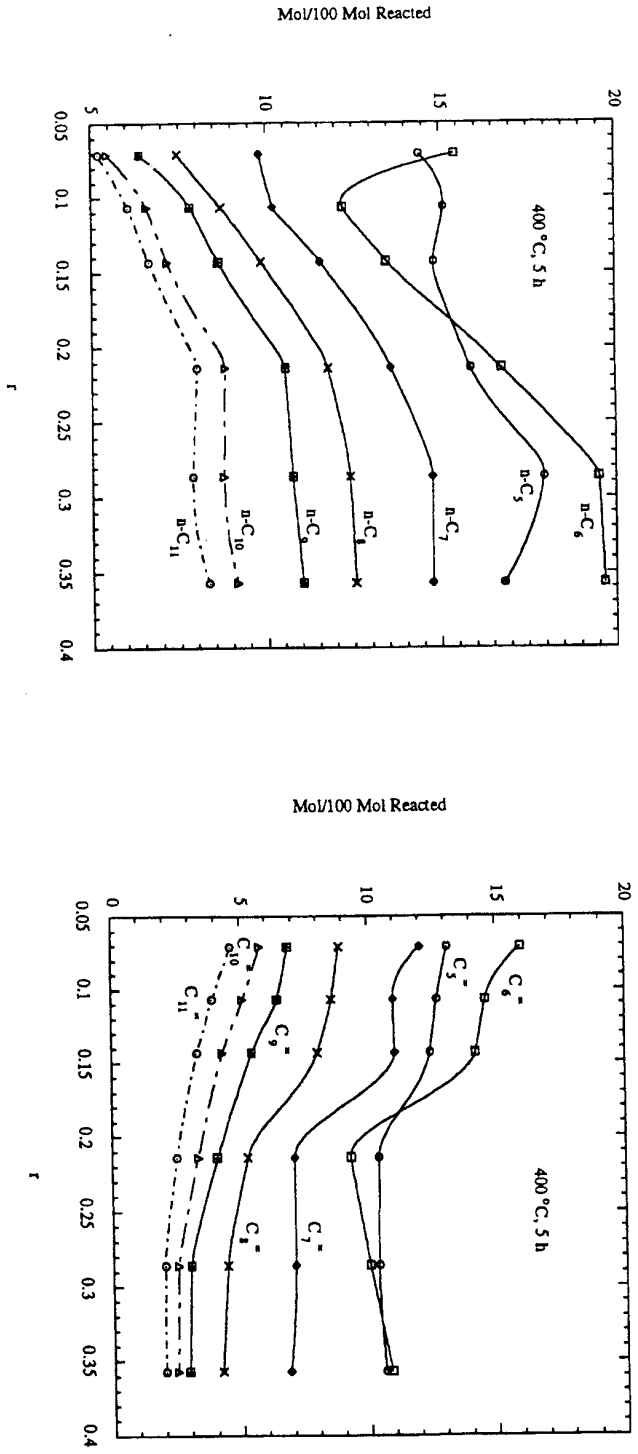

Figure 1.7-3. Effects of Loading Ratio (r) on Liquid Product Distributions from n-C_{14} Pyrolysis at 400°C for 5 Hours

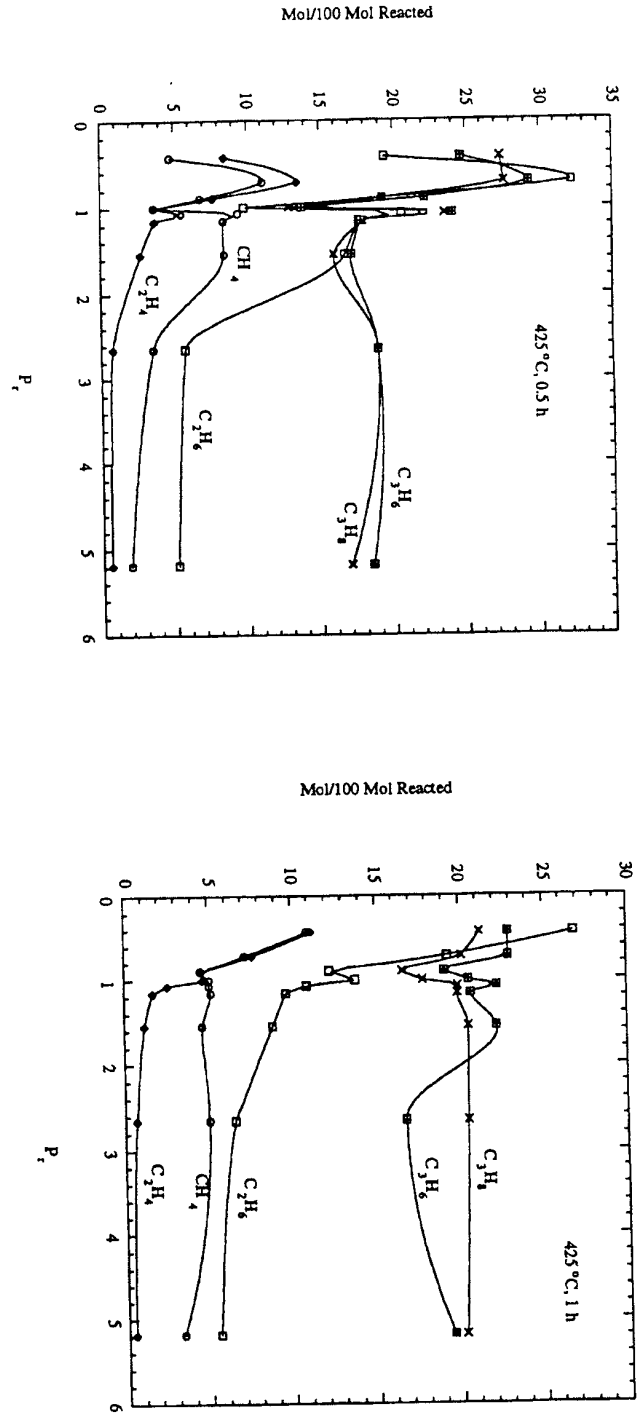

Figure 1.7-4. Effects of Initial Reduced Pressure (P_r) on Gas Product Distributions from n-C_{14} Pyrolysis at 425°C for 0.5 and 1 Hour

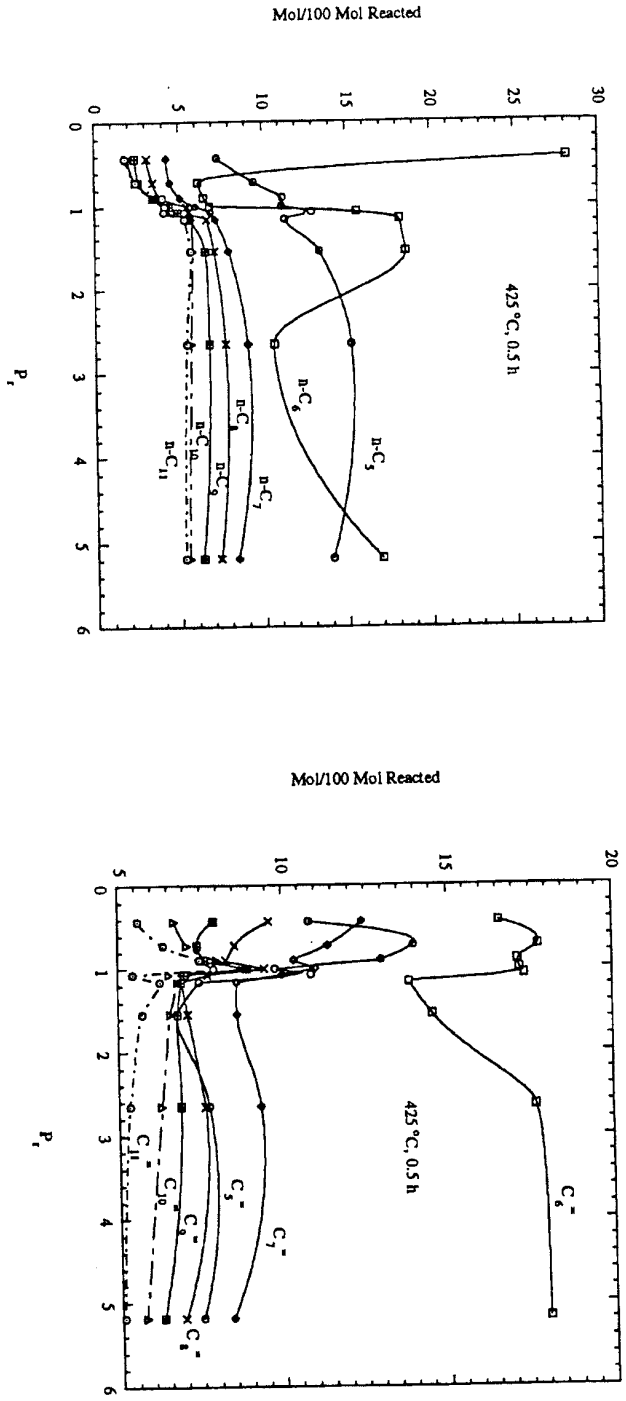

Figure 1.7-5. Effects of Initial Reduced Pressure (P_r) on Liquid Product Distributions from n-C_{14} Pyrolysis at 425°C for 0.5 Hour

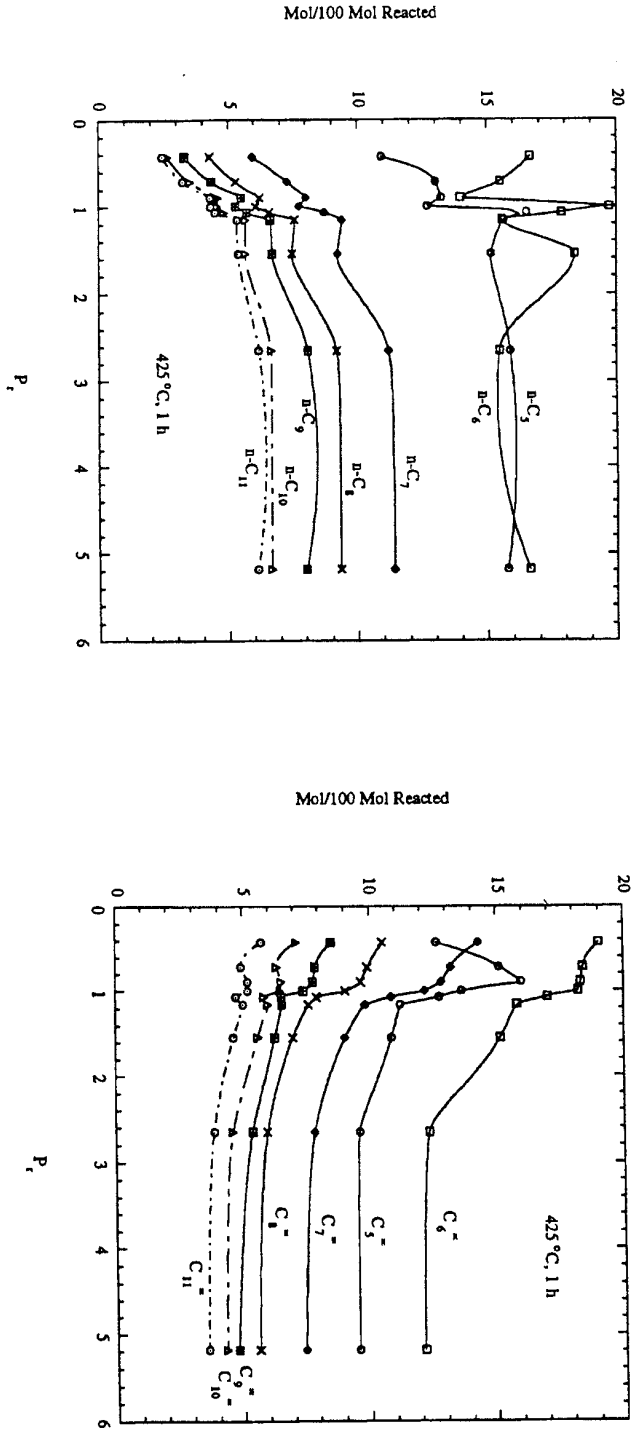

Figure 1.7-6. Effects of Initial Reduced Pressure (P_r) on Liquid Product Distributions from n-C_{14} Pyrolysis at 425°C for 1 Hour

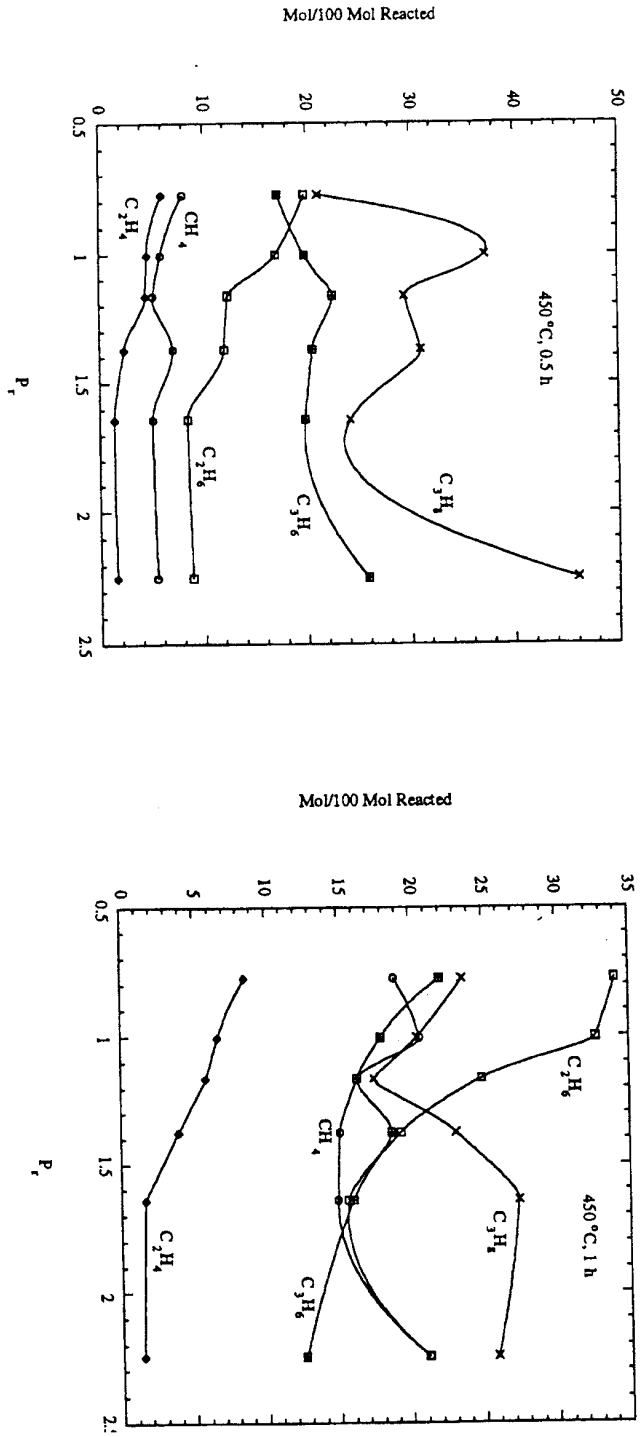

Figure 1.7-7. Effects of Initial Reduced Pressure (P_r) on Gas Product Distributions from n-C_{14} Pyrolysis at 450°C for 0.5 and 1 Hour

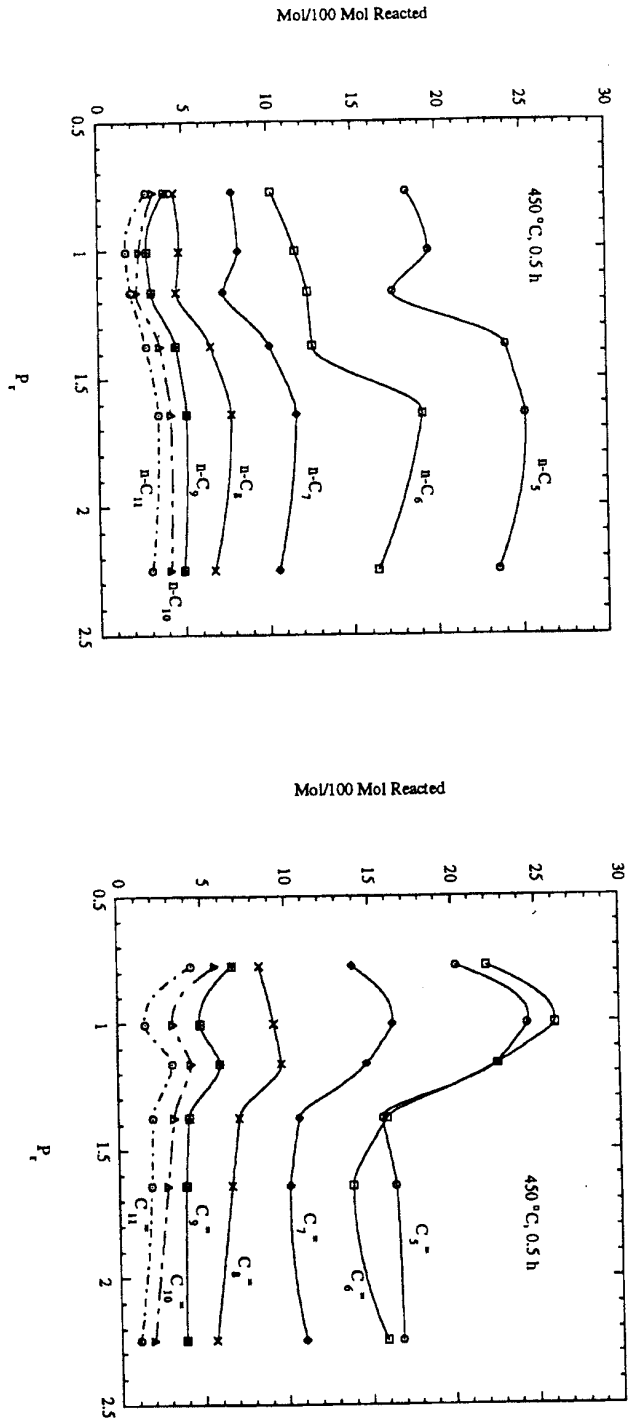

Figure 1.7-8. Effects of Initial Reduced Pressure (P_r) on Liquid Product Distributions from n-C_{14} Pyrolysis at 450°C for 0.5 Hour

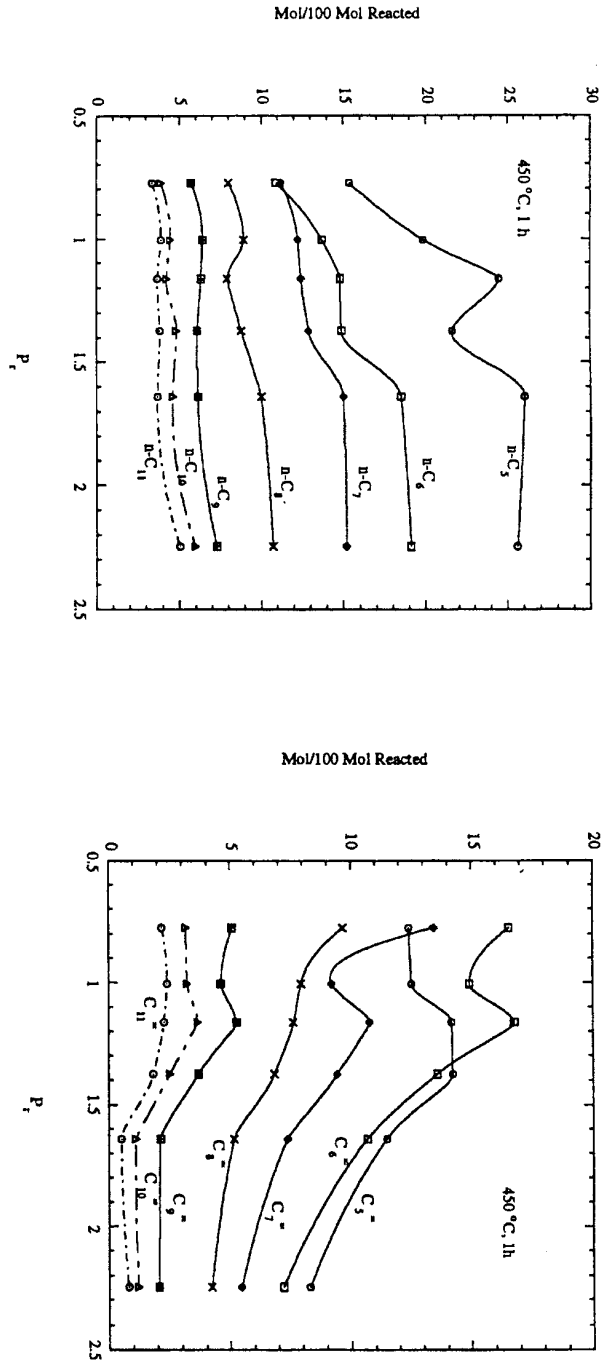

Figure 1.7-9. Effects of Initial Reduced Pressure (P_r) on Gas Product Distributions from n-C_{14} Pyrolysis at 450°C for 1 Hour

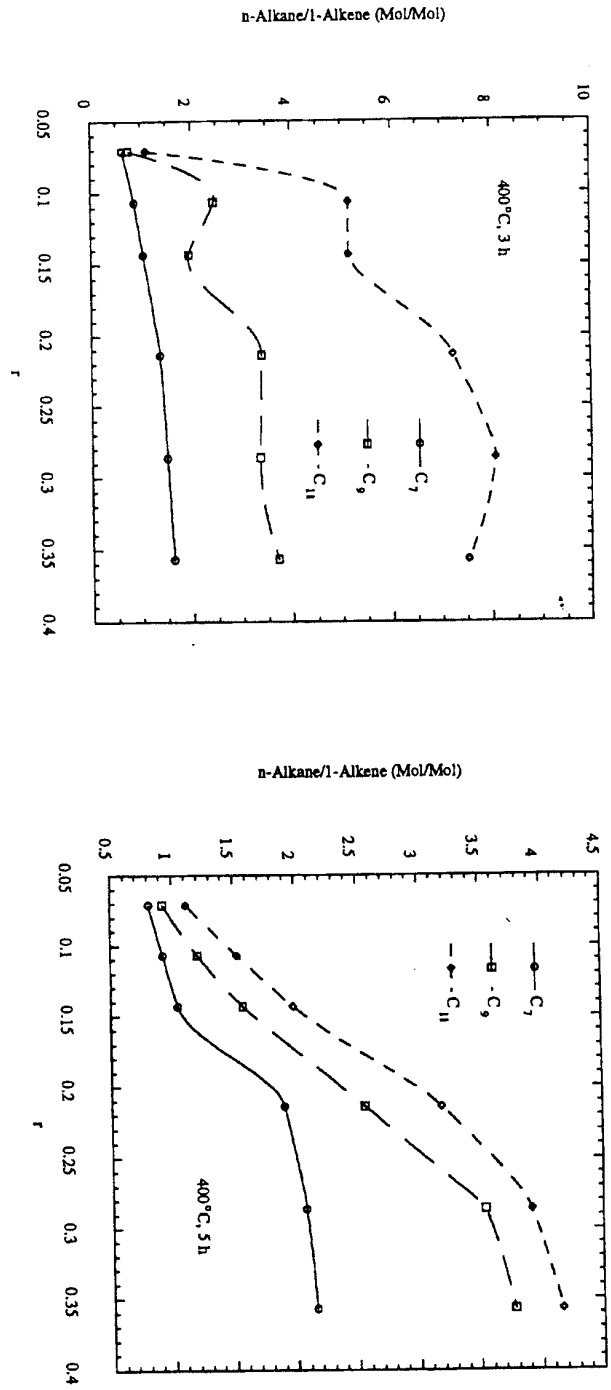

Figure 1.7-10. Effects of Loading Ratio (r) on n-Alkane/1-Alkene Ratio (for C_7, C_9, and C_{11}) from n-C_{14} Pyrolysis at 400°C for 3 and 5 Hours

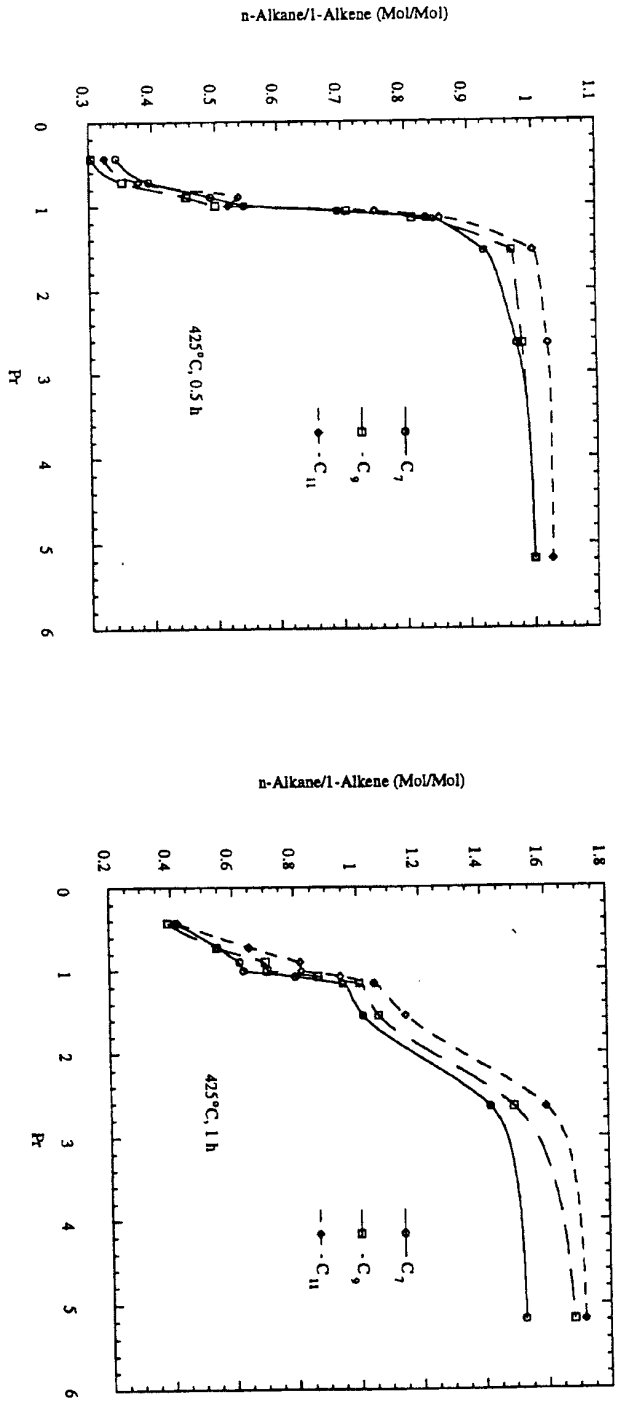

Figure 1.7-11. Effects of Initial Reduced Pressure (P_r) on n-Alkane/1-Alkene Ratio (for C_7, C_9, and C_{11}) from n-C_{14} Pyrolysis at 425°C for 0.5 and 1 Hour

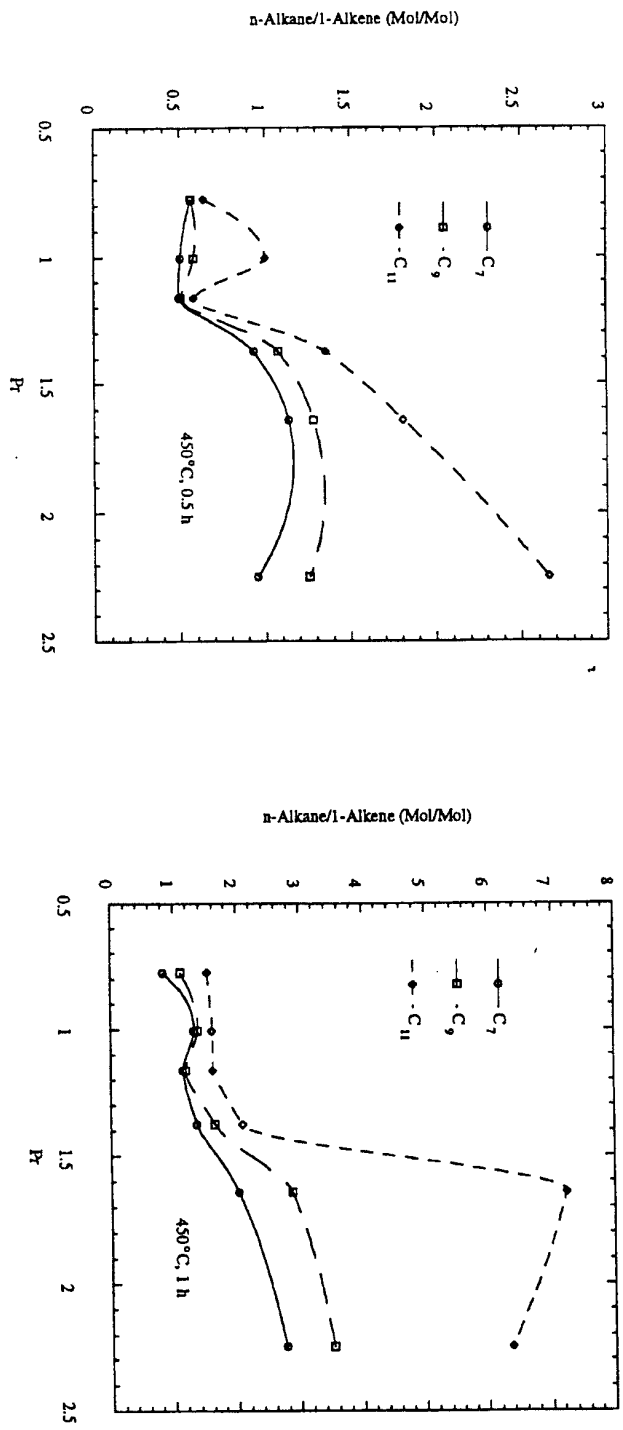

Figure 1.7-12. Effects of Initial Reduced Pressure (P_r) on n-Alkane/1-Alkene Ratio (for C_7, C_9, and C_{11}) from n-C_{14} Pyrolysis at 450°C for 0.5 and 1 Hour

[1] Schobert, H. H. et al. *Advanced Thermally Stable Jet Fuels, Technical Progress Report, January 1994-March 1994.* The Pennsylvania State University. 1994.

[2] Schobert, H. H. et al. *Advanced Thermally Stable Jet Fuels, Technical Progress Report, October 1993-December 1993.* The Pennsylvania State University. 1994.

[3] Soave, G. "Equilibrium Constants from a Modified Redlich-Kwong Equation of State." *Chem. Eng. Sci.* 1972. 27. 1197.

[4] Song, C., W.C. Lai, and H. H. Schobert. "Condensed Phase Pyrolysis of *n*-Tetradecane at Elevated Pressures for Long Duration: Product Distribution and Reaction Mechanisms." *Ind. Eng. Chem. Res.* 1994. 33. 534.

[5] Laidler, K. J. *Chemical Kinetics.* McGraw-Hill: New York. 1965. Chapter 5.

[6] Eckert, C. A. "High Pressure Kinetics in Solution." *Annual Rev. Phys. Chem.* 1972. 23. 239.

1.8 THERMAL DECOMPOSITION OF N-TETRADECANE IN NEAR-CRITICAL REGION

This study is explained in detail in *Advanced Thermally Stable Jet Fuels Technical Progress Report, July–September 1994.*

Introduction

Thermal stressing experiments in tubing bomb reactors showed that pressure has a significant effect on the thermal decomposition of *n*-tetradecane (*n*-C_{14}) in the near-critical region.[1,2] We found that at 425°C, a few degrees above the critical temperature (Tc) of *n*-C_{14} (419.15°C), both the first-order rate constants and the product distributions exhibited larger pressure dependence in the near-critical region. While unusual, the pressure dependence of the first-order rate constants and product distributions may result from unusual properties of a fluid near its critical point, such as large partial molar volume, local anisotropy, and high compressibility. The complex pressure dependence of the rate constants and the yield of olefinic components cannot be readily explained. For example, the first-order rate constants for *n*-C_{14} decomposition neither increased nor decreased monotonously, but fluctuated with pressure, in the range near the critical pressure (P_c, 1.573 MPa for *n*-C_{14}).[1] When the reactions were carried out at 425°C for 30 minutes, the yield of olefinic components also fluctuated with pressure in the near critical region.[2]

The observed complex relationships may result from uncontrolled mixing problems in the tubing bomb reactor, which includes a top stem with a lower temperature. Measurements showed that the temperature in the stem just above the surface of the fluidized sand bath was as low as 200°C when the temperature of the sand bath was 450°C.[3] We can reasonably expect that a circulation of reactants occurs within the entire reactor (i.e., the reactants with lower density at higher temperature at the reactor body rise to the top stem, condense at a certain position as a result of the lower temperature, and return to the bottom of the reactor). Such a circulation leads to fluctuations in the reaction rates and mechanisms, particularly during the experiments that are carried out in the near-critical region of the compound studied. Also, the average temperature of the sample stressed will be lower than the sand bath temperature, resulting in underestimated rate constants from thermal reactions carried out in tubing reactors with long stems. Because correcting for the effect of the top stem would be difficult, if not prohibitive, the resulting kinetic parameters may be misleading. Therefore, either a modified tubing bomb reactor or a new reactor should be used to obtain more reliable kinetic data. In this study, we used glass tubes as reactors for the thermal decomposition experiments of *n*-C_{14}.

Results and Discussion

1. Effects of Pressure on Conversion and Product Distributions. The effects of pressure on the conversion and product distributions were studied in the near- and super-critical regions. The different loading ratios were used to obtain different initial pressures.

Figure 1.8-1 shows the change in conversion with initial reduced pressure from thermal decomposition of *n*-C_{14} at 425°C for 15 minutes. The reduced pressure (P_r=P/P_c) was calculated at a given temperature and loading ratio using the Soave-Redlich-Kwong equation of state.[4] The pressure has a significant effect on conversion in the near-critical region. For example, when P_r increases from 1 to 1.5, the conversion at 15 minutes decreases from ≈12% to ≈9% and the

conversion at 30 minutes decreases from ≈19% to 16%. The significant changes in the conversions seem to fall in the near-critical region and do not extend to the far supercritical region.

The experiment at 425°C for 30 minutes showed that conversion with a P_r of 7.7 was not significantly different from that with P_r of 1.5. When these results were compared to previous data,[1] we found that the conversions from the tubing bomb reactor experiments were lower than those from glass tube experiments. The lower reaction rates in the tubing reactor experiments resulted from the lower average temperature caused by the effects of the top stem of the reactor, which has a lower temperature and accounts for almost 20 percent of the total volume of the reactor. The uncontrolled low-temperature region in the top stem of the tubing bomb reactor likely resulted in underestimated reaction rates.

Figures 1.8-1 through 1.8-4 show the changes in product composition with initial reduced pressure from the thermal decomposition of *n*-C_{14} at 425°C for 15 minutes. The yields of *n*-alkanes increased with pressure and the yields of 1-alkenes decreased with pressure. The largest changes in both yields occurred in the near-critical region. Small amounts of minor reaction products exist—such as internal alkenes and straight-chain and branched chain alkanes with carbon numbers from 15 to 26. While the amounts of C_{14}+ alkanes were low at lower pressure, their amounts were significant at higher pressure. The yield of C_{14}+ alkanes also exhibited larger increases with pressure in the near-critical region than in the far supercritical region. The relationships between the molar yield of individual paraffinic components and olefinic components and pressure were consistent with Figure 1.8-1. Figures 1.8-1, 1.8-3, and 1.8-4 reveal that under the conditions used in this study, the major pyrolytic products are *n*-alkanes with carbon numbers up to 11 and 1-alkenes with carbon numbers up to 12.

Figures 1.8-5 and **1.8-6** show the change in molar ratio of overall C_6-C_{13} *n*-alkanes to 1-alkenes with pressure, and the changes in corresponding ratios with pressure for selected C_7, C_8, and C_9 components from the thermal decomposition of *n*-C_{14} at 425°C for 15 minutes. The selectivity for paraffinic components relative to olefinic components with the same carbon number increased with pressure. Large changes in *n*-alkane/1-alkene ratios with pressure occurred in the near-critical region. Under supercritical conditions, the product selectivitites for *n*-alkanes were very high, exceeding even those for corresponding 1-alkenes. These results were largely different from those obtained under typical *n*-alkane pyrolysis conditions (≈atmospheric pressure, >600°C) which usually list methane and ethane as the only paraffinic products. The results obtained from this study can be explained by free radical and transition state theories.[3]

2. Kinetics of Supercritical Phase Thermal Decomposition. The lower temperature of the top stem of the tubing bomb reactor caused the rate constants to be underestimated; therefore, the kinetic parameters from previous experiments may not be reliable and must be reexamined.

Kinetic data were obtained from the thermal decomposition of *n*-C_{14} at 400°, 425°, and 450°C for different times. Previous studies showed that simple first-order kinetics hold reasonably well for the thermal decomposition of straight-chain alkanes. Therefore, in this work the rate constants were determined by the following first-order expression:

$$\ln [1 / (1-x)] = kt \qquad (1)$$

where x is the fraction of the reactant converted, k is the rate constant (h^{-1}), and t is the reaction time (h). Since pressure affects conversion considerably in the near-critical region, a suitable loading ratio must be selected to avoid larger pressure effect in kinetic analysis. Also, the loading ratio must remain fixed to obtain reproducible results. Previously, when the loading ratio was larger than 0.35, which corresponds to a P_r of about 1.5, the conversion did not change significantly with pressure. In this work, a loading ratio of 0.36 was used.

For three different temperatures (400°, 425°, and 450°C), the first-order rate constants, k, were obtained from the method of least squares by plotting ln [1 / (1-x)] as the function of t. **Figure 1.8-7** shows the relationship between ln [1 / (1-x)] and t. The straight lines at three different temperatures indicate that *n*-C_{14} thermal decomposition under supercritical condition can be represented quite well by the first-order kinetics. From the slopes of the three lines in Figure 1.8-7, these first-order rate constants were obtained: 0.0620, 0.3477, and 1.7081 h-1 for 400°, 425°, and 450°C, respectively. According to these data, the apparent kinetic parameters for the thermal decomposition of *n*-C_{14} were calculated using the Arrhenius law. **Figure 1.8-8** shows the relationship between rate constant and temperature. The estimated activation energy is 64.2 kcal/mol, in good agreement with the value of 60-65 kcal/mol usually observed for the first-order reactions of long-chain alkane pyrolysis.[5]

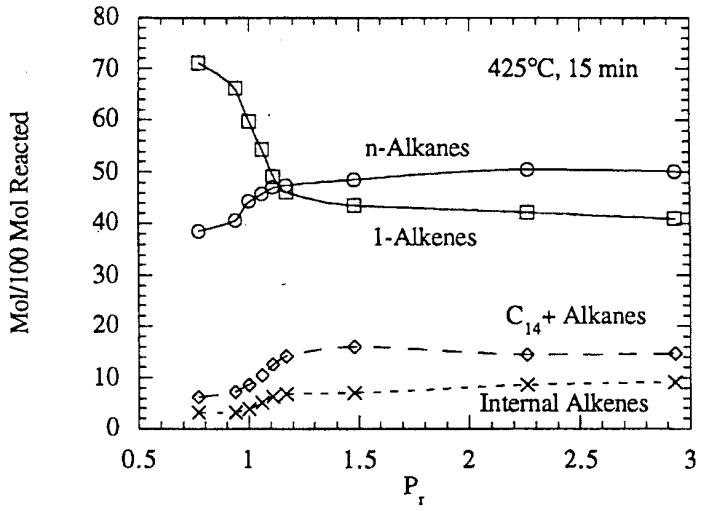

Figure 1.8-1. Changes in Molar Yields of C_6-C_{13} n-Alkanes, 1-Alkenes, Internal Alkenes , and C_{14}+ Alkanes with Initial Reduced Pressure at 425°C for 15 Minutes from *n*-Tetradecane

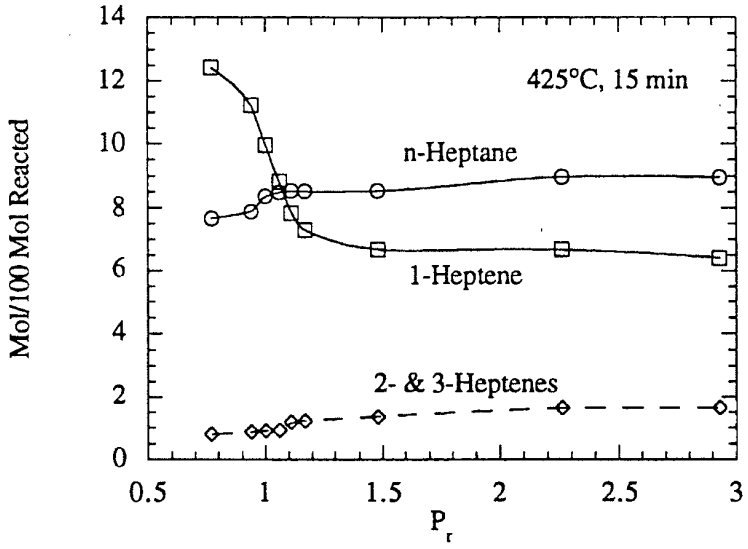

Figure 1.8-2. Changes in Molar Yields of C_7 Fractions with P_r at 425°C for 15 Minutes from n-Tetradecane.

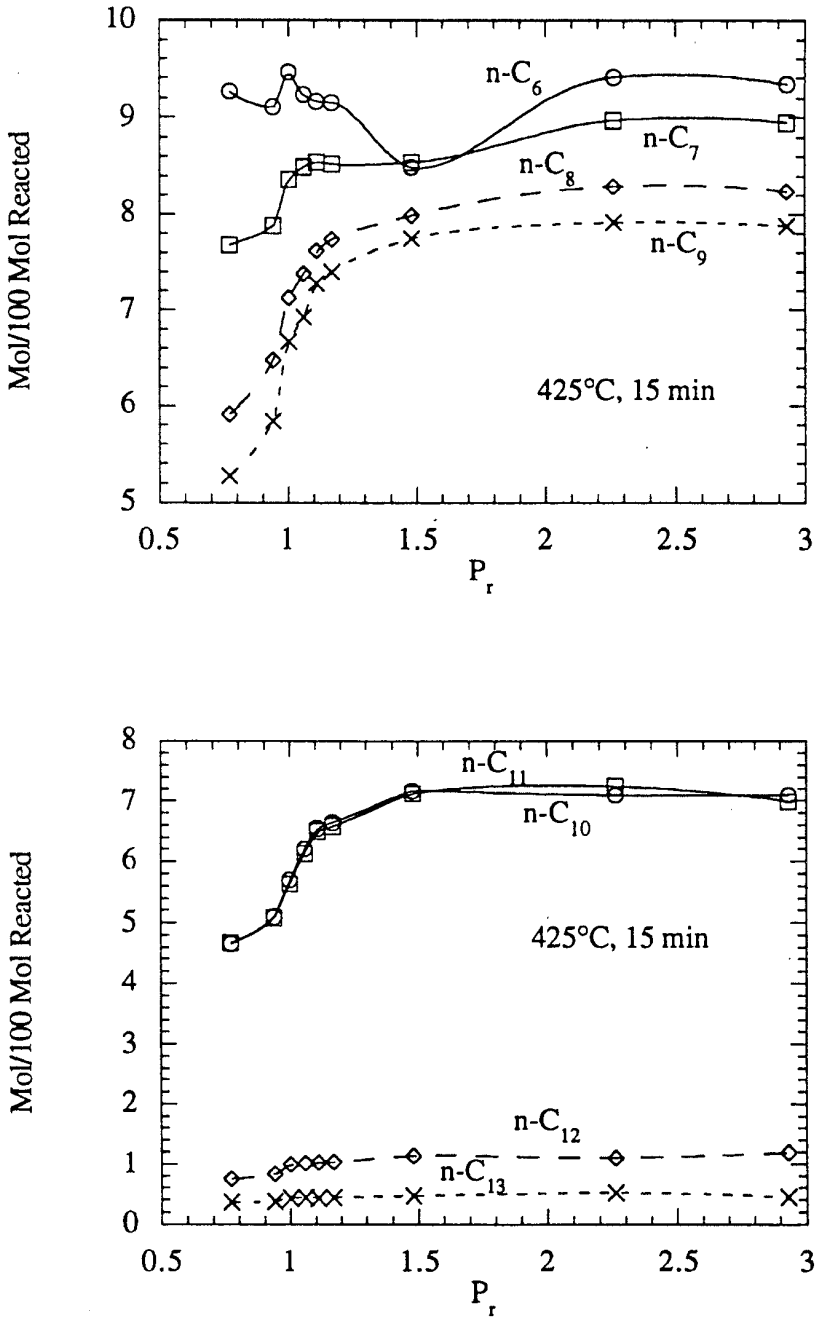

Figure 1.8-3. Changes in Molar Yields of n-Alkanes with P_r at 425°C for 15 Minutes from *n*-Tetradecane

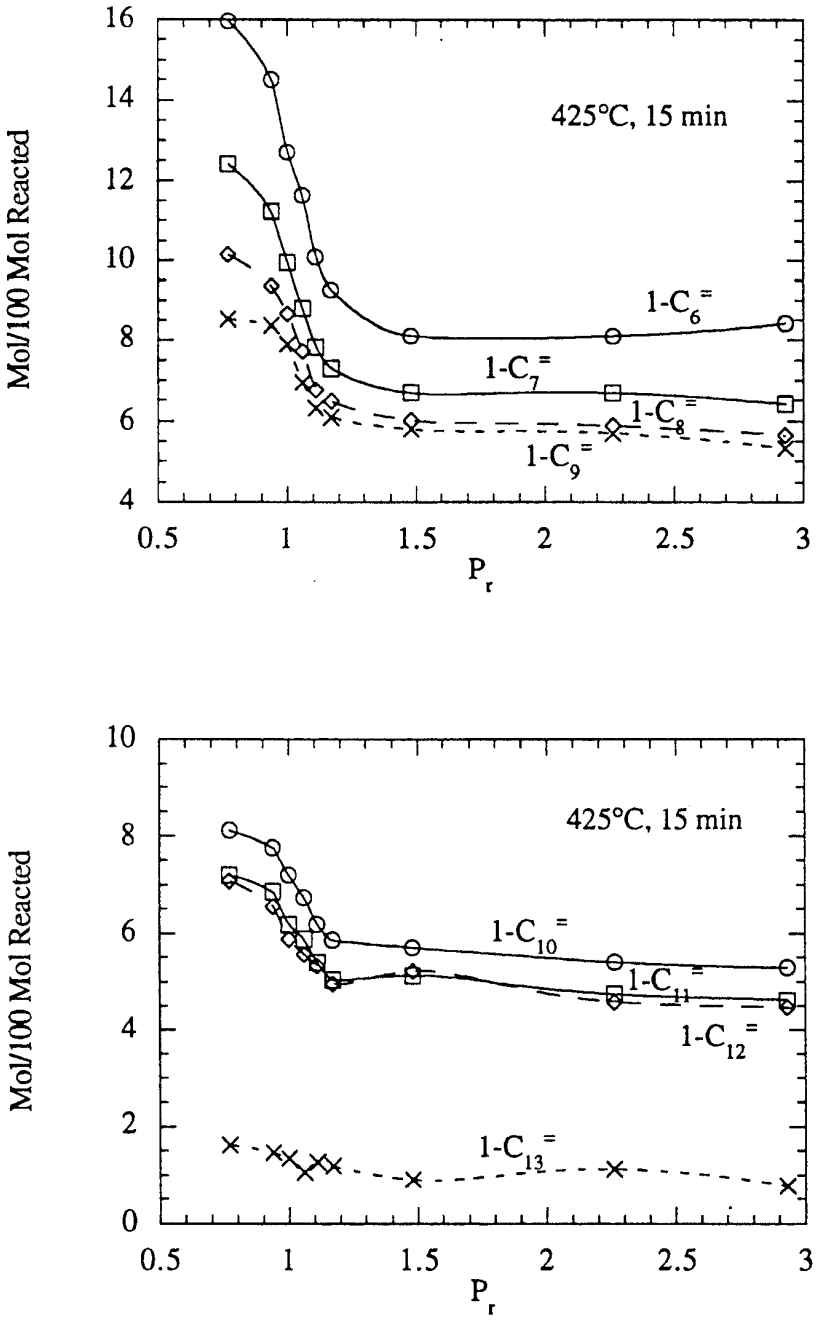

1.8-4. Changes in Molar Yields of 1-Alkenes with P_r at 425°C for 15 Minutes from *n*-Tetradecane

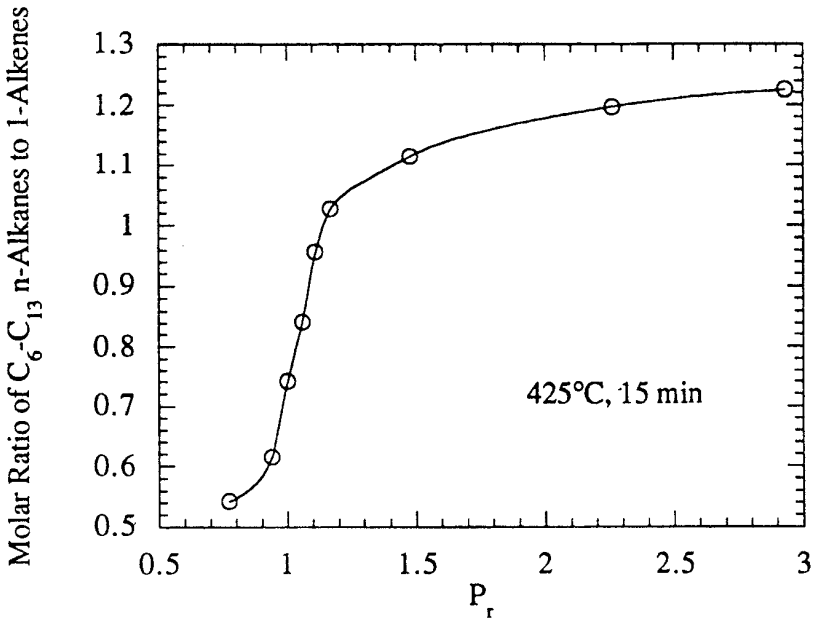

Figure 1.8-5. Change in Molar Ratio of C_6-C_{13} Alkanes to 1-Alkenes with P_r at 425°C for 15 Minutes from n-Tetradecane

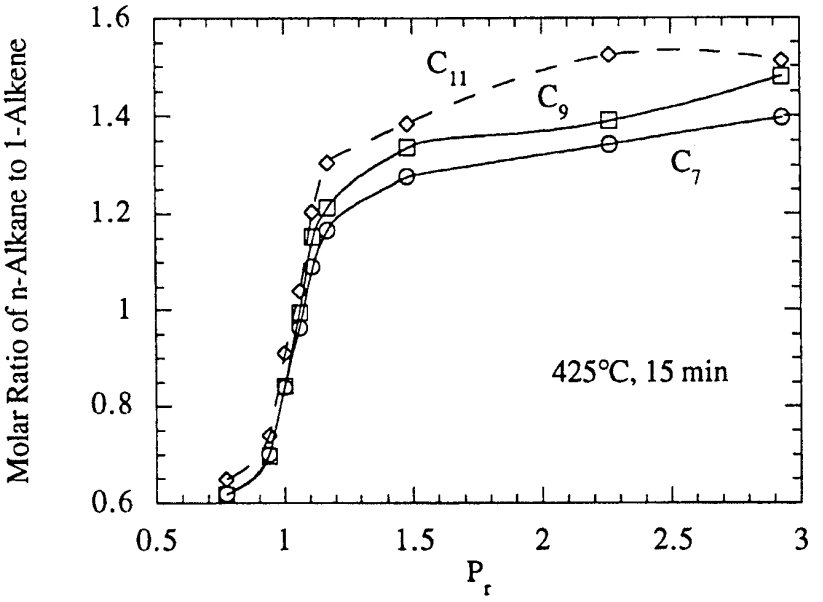

Figure 1.8-6. Change in Molar Ratio of C_7, C_9, and C_{11} n-Alkane to 1-Alkene with P_r at 425°C for 15 Minutes from n-Tetradecane

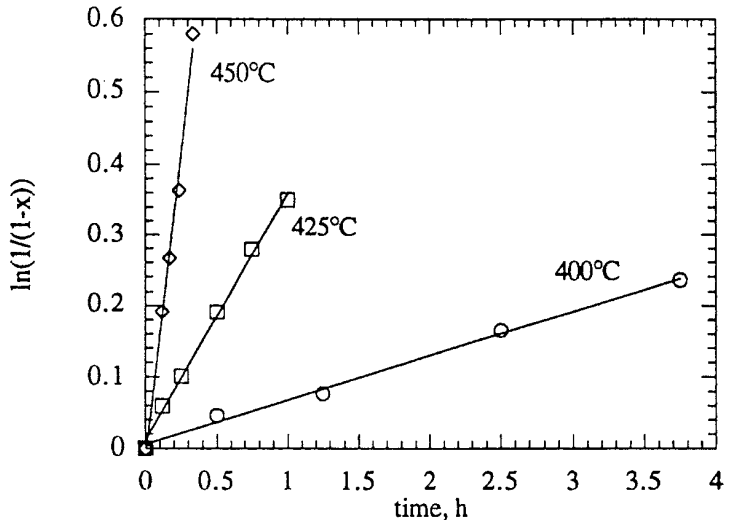

Figure 1.8-7. Relationship Between ln[1/(1-x)] and Time for Conversion of n-Tetradecane

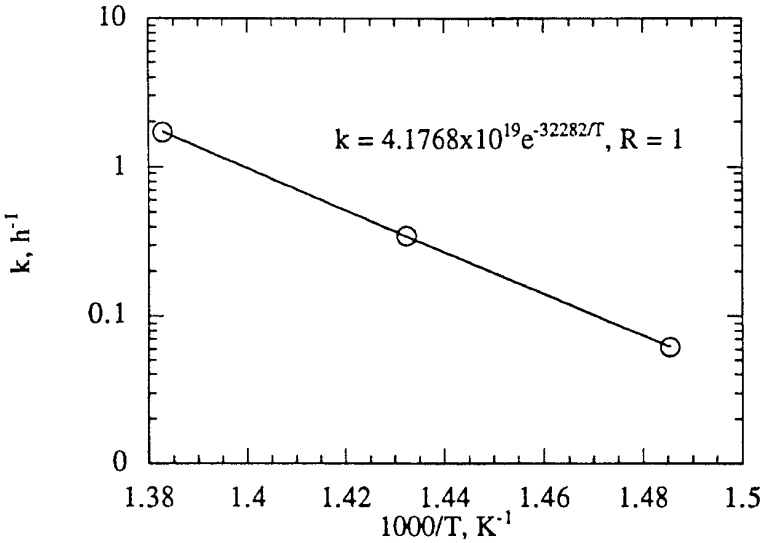

Figure 1.8-8. Relationship Between Rate Constant and Temperature for *n*-Tetradecane Conversion

---

[1] Schobert, H. H. et al. *Advanced Thermally Stable Jet Fuels, Technical Progress Report, January 1994-March 1994.* The Pennsylvania State University. 1994.

[2] Schobert, H. H. et al. *Advanced Thermally Stable Jet Fuels, Technical Progress Report, April 1994-June 1994.* The Pennsylvania State University. 1994.

[3] Lai, W. C. *Private Communications.* 1994.

[4] Soave, G. *Chem. Eng. Sci.* 1972. 27. 1197.

[5] Fabuss, B. M., J. O. Smith, and C. N. Satterfield. Adv. Pet. Chem. Refin. 1964. 9. 157.

1.9 RE-EXAMINING THE EFFECTS OF REACTANT AND INERT GAS PRESSURE ON TETRADECANE PYROLYSIS: EFFECT OF COLD VOLUME IN BATCH REACTOR

This study is explained in detail in *Advanced Thermally Stable Jet Fuels Technical Progress Report, July—September 1994*

Introduction

With regard to batch reactors, little is known about the effect of the volume of the tube connecting the reactor and the pressure gauge, which is a common part of most batch reactors. The tube is much cooler than the reactor tube, and its volume is considered cold volume. In a prior study observing pyrolysis of *n*-tetradecane (n-C_{14}) at 450°C, we found that the cool connecting line had significant effects on the *n*-C_{14} decomposition behavior. The volume of the connecting line comprises 20 percent of the total reactor volume.

To obtain a better defined reactor system, we modified the microreactors by minimizing the volume of the connecting lines, replacing the _ (6.35 mm o.d.) connecting tubings with 1/8 ones and filling the interior with inert glass beads or rods. The volume of the connecting line was reduced to 3 percent of the total reactor volume (23.2 mL). This study examines *n*-tetradecane pyrolysis at 450°C for 30 minutes under initial (cold) N_2 pressure of 0.17-1.41 MPa using 1-11 mL of samples in the modified 23.2 mL microreactors.

Results and Discussion

1. Pressure Effects Observed in the Modified 23.2 mL Microreactors. The uniformity of concentration and temperature inside the tubing reactor was obtained by agitating the reactor vertically at the speed of about 240 cycles/minute. The temperature uniformity inside the reactor, which is about 10 cm in length, was confirmed by the temperature measurements near the centerline at several different positions. The major temperature difference occurred within the first 4 minutes of the heating-up period. The conversion in that period (below 425°C) is less than 1 mol% and can be considered to have a small effect on the overall conversion results.

Figure 1.9-1 shows the *n*-C_{14} conversion as a function of the initially charged *n*-C_{14} volume at three different initial N_2 pressures in the 23.2 mL microreactors. This study found that there are considerable changes in *n*-C_{14} conversions with changes in sample volume (concentration), especially when the *n*-C_{14} loading increases from 1 mL to 2 and 3 mL. For example, at a low initial N_2 pressure (0.17 MPa), increasing sample volume from 1 to 2 mL significantly increased *n*-C_{14} conversion from 39 to 48 mol%. Further increasing sample volume from 2 to 3 mL increased the conversion by an additional 2%. Changes in sample volume between 3 and 7 mL had little impact on *n*-C_{14} conversion, but a decrease in conversion did occur with further increases in sample volume up to 11 mL. In contrast to the effect of reactant pressure (concentration or sample volume), the pressure of the inert gas (N_2) had less impact on the decomposition rate of *n*-C_{14} under the studied N_2 pressure ranges.

The *n*-C_{14} conversion displayed a concave downward behavior with the reactant volume (concentration); a maximum conversion occurred near 0.66 mole/L (or 4 mL of *n*-C_{14}). The 3 mL conversion data were fitted to a three-parameter model:

$$X = \frac{A_1C(1+a_3C)}{(1+a_1C)(1+a_2C+a_3C)} \quad (1)$$

where X is the *n*-C14 conversion (the fraction of *n*-C_{14} reacted), C is the *n*-C_{14} concentration (mol/L), and a_1, a_2, and a_3 are the three parameters with the values of 5.61, 1.33, and 0.90, respectively.

Equation (1) was represented by the solid curve in Figure 1.9-1, which shows that the influence of the reactant volume (concentration) appears to also depend on the system phases. Earlier, we found that the mixture critical temperature was usually bounded by the maximum and minimum critical temperatures among the components.[1] This implies that, in the current reactor system, *n*-C_{14} could exist in either gas or supercritical state, because the reaction temperature of 450°C is well above the critical temperature.

We examined the estimated reduced pressure (the ratio of system pressure to the critical pressure) as a function of the charged volumes of *n*-C_{14} under vacuum condition (i.e., without the addition of N_2 for two tubing bombs with different capacities). We found that, for a pure *n*-C_{14} system, at 450°C, the reactant likely exists in the supercritical phase when the initial sample volume is greater than 3 mL, and in gas phase otherwise. We found that, near the critical condition, the *n*-C_{14} decomposition rate was enhanced when the system phase was changed from gas to supercritical phase. However, at conditions far above the critical point (e.g., $P_r>2$), the *n*-C_{14} conversion decreased with further increases in pressure (density). The decrease could be attributed to cage effects or diffusion limitations, which can be expected at extremely high density.

2. Results Comparison Between Modified 23.2 mL and Unmodified 28 mL Microreactors. **Figure 1.9-2** presents the *n*-C_{14} conversion as a function of the initial sample volume of *n*-C_{14} in these two tubing bombs with different capacities (23.2 mL and 28 mL). The significant effect of initial N_2 pressure on the conversion was observed in unmodified reactors by not in the modified reactors. In general, the pyrolysis experiments carried out in the modified reactors exhibited higher conversion. The differences could be explained as follows:

- The cooler upper portion of the reactor system (i.e., the connecting line) introduced non-uniform distributions of radical concentration and temperature inside the system. The lower (shorter) alkyl radicals tended to escape to the cooler upper portion and stay there longer than the higher radicals; this phenomenon was similar to removing a great deal of reactive radicals from the reaction system, thus retarding the decomposition process. The lack of lower alkyl radicals also resulted in much lower yields of higher alkanes (C_{15}-C_{26}), which was observed in the reaction products from the unmodified reactor.
- With the additional cool parts and larger total reactor volume, the reactant concentration of the system pressure in the unmodified reactor was lower than its counterpart when the same amount of *n*-C_{14} was added initially. The lower concentration could have resulted in lower decomposition rates under the studied conditions.

- N_2 competes with the lower radicals for the cooler space in the upper part of the unmodified reactor system, reducing the chance of the lower radicals to escape to there from the tubing bomb body where the reactions occur. This was consistent with the observation that the decomposition rate with the unmodified reactor decreased with increasing initial N_2 pressure in or near supercritical phase.

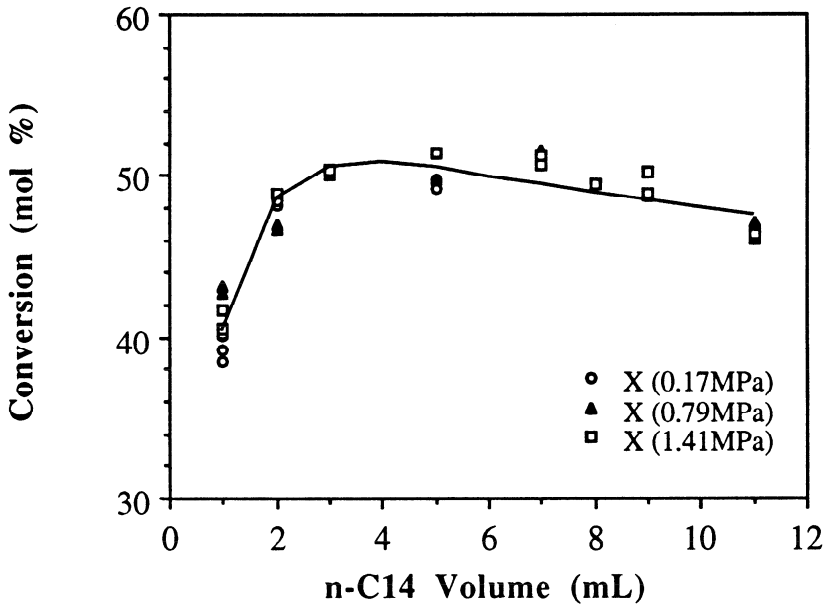

Figure 1.9-1. Effects of Initial Sample Volume of n-C_{14} (at Room Temperature) on Pyrolic Conversion at 450°C for 30 Minutes under Different Initial Pressure of N_2 in 23.2-mL Microreactors

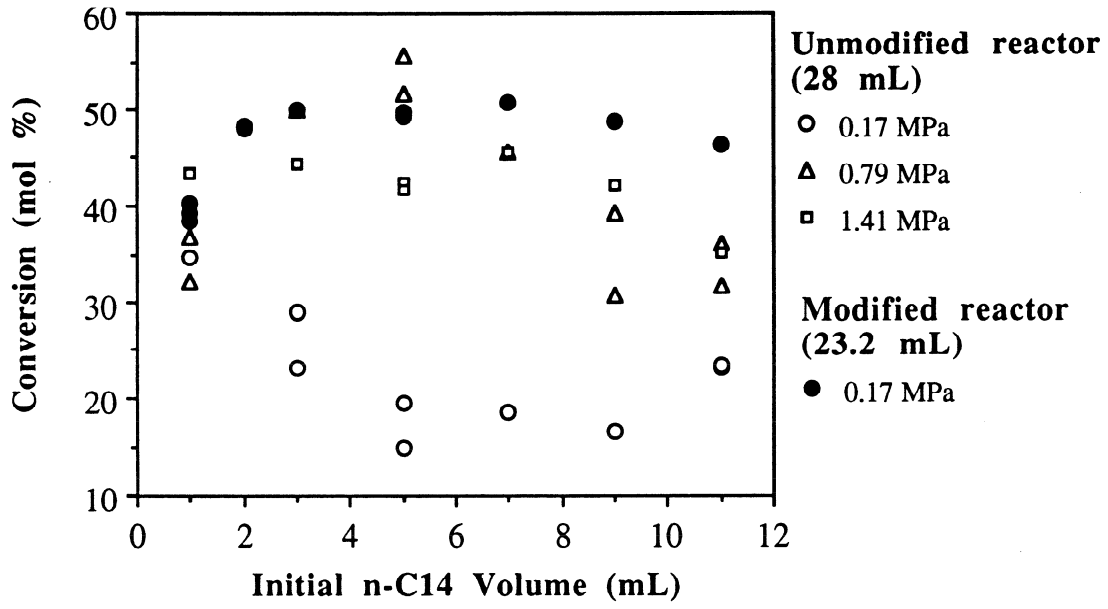

Figure 1.9-2. Effects of Initial Sample Volume of n-C_{14} (at Room Temperature) on Pyrolic Conversion at 450°C for 30 Minutes under Different Initial Pressure of N_2 in Two Tubing Bombs with Different Capacity (23.2 mL and 28 mL)

[1] Schobert, H. H. et al. *Advanced Thermally Stable Jet Fuels, Technical Progress Report, January-March 1994*. The Pennsylvania State University. 1995.

1.10 EFFECTS OF REACTANT AND INERT GAS PRESSURE ON THE SOLID FORMATION IN BOTH SUPERCRITICAL AND GAS-PHASE PYROLYSIS OF *N*-TETRADECANE AT 450°C

This study is explained in detail in *Advanced Thermally Stable Jet Fuels Technical Progress Report, July—September 1995.*

Introduction

We have previously reported the significant pressure dependence in pyrolysis of *n*-tetradecane (*n*-C_{14}). Our experiments were carried out at 450¡C for 30 minutes under initial (cold) N_2 pressures of 0.17-2.03 MPa using 1-11 mL samples in two types of microreactors (28 mL and 23.2 mL).[1, 2] Little is known about the role of reactant and inert gas pressure in supercritical fluids at high temperatures for long-duration pyrolysis. To better understand the effects of reactant and inert gas (N_2) pressure on the *n*-C_{14} decomposition, as well as solid deposit formation and product distribution, we pyrolyzed *n*-tetradecane using 1-9 mL samples at 450¡C for 4 hours under initial (cold) N_2 pressures of 0.17-2.03 MPa (10-280 psig) in 28-mL microreactors. The present work covers the long-duration thermal decomposition of *n*-C_{14} in both supercritical phase and gas phase.

Experimental

Aldrich reagent-grade *n*-tetradecane, *n*-C_{14} (purity: 99+ %) was used. A given amount of *n*-C_{14} (1, 5, or 9 mL) was charged into a 28-mL microreactor (unmodified reactor with cold volume [2]). After the reactor was sealed and purged six times with 6.9 MPa ultra-high purity (UHP) N_2, it was pressurized with UHP N_2 to a specific pressure ranging from 0.17 MPa to 2.03 MPa. The pyrolysis was conducted at 450¡C for 4 hours in a fluidized sand bath. The products were separated into gases, liquids, and solid deposits.[3] The gaseous and liquid products were analyzed by GC and GC-MS with packed or capillary columns.

Results and Discussion

Because the pyrolysis temperature is above the critical temperature of *n*-C_{14} (419 ¡C), we will address the initial system pressure and phase behavior of the *n*-C_{14}-N_2 mixtures. Since the effect of sample volume reflects the influence of reactant pressure, we have calculated the initial total pressure of the *n*-C_{14}-N_2 mixtures (at 450¡C) and their critical pressures and temperatures using the equations of state recommended by Reid et al.[4] The reduced pressure (ratio of total pressure to the critical pressure) of the mixtures at 450¡C indicated that the reactant likely exists in supercritical phase when the initial sample volume is 9 mL under all of the N_2 pressures examined, and in low-density gas phase when the initial sample volume is 1 mL. With a 5 mL sample, the phase of the reactant at 450¡C could be either medium-density gas phase or near supercritical phase, depending on the initial N_2 pressure. In general, pressure affects the density, viscosity, and diffusivity. Pressure change near critical point can change the system from gas-like to liquid-like phases or vice versa, and may affect the chemical reaction behaviors.

We examined the *n*-C_{14} conversion as a function of the initially charged *n*-C_{14} volume at four different initial N_2 pressures in the 28 mL microreactors. The experimental error was 0.83%, determined from three replicates using 5 mL samples under 0.79 MPa N_2. One mL of *n*-C_{14} corresponds to a *n*-C_{14} concentration of 0.138 mol/L. The *n*-C_{14} conversion displayed a concave downward (volcano-like) behavior with the reactant volume (concentration); a

maximum conversion occurred at 0.69 mol/L (or 5 mL of *n*-C_{14}). These results indicate that there are moderate changes in *n*-C_{14} conversions with changes in sample volume (concentration), especially when the *n*-C_{14} loading increases from 5 mL to 9 mL. For example, at a low initial N_2 pressure (0.17 MPa), increasing sample volume from 5 to 9 mL decreased *n*-C_{14} conversion from 98.6 to 91.2 mol%. Changes in sample volume from 1 to 5 mL had less impact on *n*-C_{14} conversion, causing only a small increase in conversion.

The pressure of the inert gas (N_2) had little impact on the decomposition rate of *n*-C_{14} when a small sample (1 or 5 mL) was used; however, at a higher initial *n*-C_{14} concentration (9 mL sample), increasing N_2 pressure increased *n*-C_{14} conversion. In short, the influence of the reactant volume (concentration) appears to also depend on the system phases. We found that the *n*-C_{14} decomposition rate was retarded when the system phase was changed from gas to supercritical phase. The decrease could likely be attributed to cage effects or diffusion limitations, which may be expected at high density due to the more restricted mobility of molecules.

Solid formation was inhibited when either reactant or inert gas pressure was changed. The curve representing solid yields as a function of the initially charged *n*-C_{14} volume and N_2 pressure displayed a volcano-like behavior similar to the *n*-C_{14} conversion. Maximum solid formation occurred at 0.69 mol/L (or 5 mL of *n*-C_{14}). In general, the solid formation was retarded when the system phase was changed from medium-density gas phase to supercritical phase. For example, at an initial N_2 pressure of 0.79 MPa, increasing the reactant concentration from 0.69 mol/L (or 5 mL of *n*-C_{14}) to 1.24 mol/L (or 9 mL of *n*-C_{14}) reduced the formation of deposits by 77 % (from 3.1 wt% to 0.7 wt %). The decrease of solid deposition might be attributed to the enhanced solid solubility of the fuel under supercritical condition (a physical process)[5], or it might be caused by a chemical process as suggested by Edwards and Zabarnick.[6] The pressure of N_2 also had significant impact on the formation of deposits when a small sample (1 mL) was used. For example, the solid yields ranged from 0.6 wt% to 2.8 wt% when the pyrolysis was started with 1 mL *n*-C_{14}. In short, the influences of sample volume and inert gas pressure on solid formation are interdependent increasing sample volume can either decrease or increase solid formation, depending on the inert gas pressure, and vice versa. This illustrates the complexity of the mechanisms governing the pressure effects of reactant and inert gas.

The total gas yields (C_1-C_4) as a function of the initially charged *n*-C_{14} volume and N_2 pressure decreased with increasing reactant volume (concentration) under constant initial N_2 pressure. In contrast to the effect of reactant pressure, the pressure of the inert gas (N_2) had less impact on the total gas yield under the studied N_2 pressure ranges, and the effect of N_2 pressure also depended on the reactant pressure. These observations imply that lower reactant pressure facilitates unimolecular reaction (β-scission) to form low molecular-weight gases while higher reactant pressure favors bimolecular reaction (H-abstraction). It is possible to control the product distributions as well as the reaction extent by isothermally adjusting the system pressure in terms of sample volume or inert gas pressure.

---

[1] Schobert, H. H. et al. *Advanced Thermally Stable Jet Fuels, Technical Progress Report, January - March 1994.* The Pennsylvania State University. 1994.

[2] Schobert, H. H. et al. *Advanced Thermally Stable Jet Fuels, Technical Progress Report, July - September 1994.* The Pennsylvania State University. 1994.

[3] Lai, W.-C. et al. *Prep. - Am. Chem. Soc. Div. Pet. Chem.* 1992. 37(4). 1671-1680.

[4] Reid, R. C., J. M. Prausnitz, and B. E. Poling. *The Properties of Gases & Liquids*. Fourth Edition., McGraw-Hill Book Company: New York. 1987.

[5] Taylor, W. F. *Ind. Eng. Chem. Prod. Res. Dev.* 1974. 13(2). 133-138.

[6] Edwards, T. and S. Zabarnick. *Ind. Eng. Chem. Res.* 1993. 32. 3117-3122

1.11 EXPLORATORY STUDIES ON THE PYROLYSIS OF BINARY MIXTURES OF *N*-TETRADECANE AND HYDROGEN DONORS AT 450°C IN A BATCH REACTOR

This study is explained in detail in *Advanced Thermally Stable Jet Fuels Technical Progress Report, July—September 1996.*

Introduction

This study investigated the interactive chemistry among the components of jet fuel during their pyrolytic degradation. We considered recent experimental work aimed at determining the product distribution and the extent of degradation of reactants in binary mixtures comprising a model compound, *n*-tetradecane, and a hydrogen donor such as tetralin (1,2,3,4-tetrahydronaphthalene), benzyl alcohol, or *n*-butylcyclohexane at 450° C in a batch reactor. Tests were also conducted on neat *n*-tetradecane.[1, 2] Although previous studies were carried out on *n*-tetradecane at 450°C in a batch reactor, we soon realized that there is a significant cold volume effect in those reactors. Consequently, there is a need to reanalyze the product distribution and evaluate the extent of pyrolytic decomposition of such reactant mixtures in a modified batch reactor that has a minimal cold volume. [3]

This work involved the pyrolysis of 5 ml samples of binary mixtures, comprising 10% by volume of the hydrogen donor and 90% by volume of *n*-tetradecane, at 450°C for residence times of 12, 20, and 30 minutes under an initial (cold) nitrogen pressure of 280 psig in a 23 mL batch reactor. The results have also been compared with those obtained with neat tetradecane under identical conditions.

Experimental

Aldrich reagent-grade normal tetradecane, 1,2,3,4-tetrahydronaphthalene, benzyl alcohol, and *n*-butylcyclohexane (all of 99%+ purity) were employed in the pyrolytic experiments. Experimental details are provided in the corresponding Technical Progress Review.[4]

The product gases were analyzed by a gas chromatograph equipped with two different columns and detectors (FIID and TCD) for various hydrocarbons and gases. The retention time and the relative area (expressed as a fraction of the total) of the eluted peak for each component in the product gas were determined through computer-aided measurements and compared to those obtained from analyzing standard gas mixtures from Supelco. The volume response factor (VRF_i) for each gas was subsequently calculated from the ratio of its known volumetric fraction in the standard and that measured by the GC, and expressed relative to the VRF obtained for propane, thereby generating its relative volume response factor ($RVRF_i$) for quantification purposes. The molar yield of each component in the product gas, Y_i, was calculated as follows:

$$Y_i\,(\%) = \frac{[A_i \bullet RVRF_i]}{\sum_{i=1}^{N} (A_i \bullet RVRF_i)} \bullet \frac{(W_G \bullet MW_r)}{(MW_G \bullet W_r)} \bullet 100 \qquad (1)$$

where A_i is the area of the eluted peak for a component, i; W_G and W_r, the total weight of the product gas and *n*-tetradecane, respectively; MW_r, the molecular weight of the reactant (*n*-tetradecane), and MW_G, the average molecular weight of the product gas, which was calculated as:

$$MW_G = \sum_{j=1}^{N} \frac{[A_j \bullet RVRF_j]}{\sum_{i=1}^{N} (A_i \bullet RVRF_i)} \bullet MW_j \qquad (2)$$

where MW_j is the molecular weight of component j.

The components in the product liquid were analyzed by GC, as described in the original Technical Progress Report.[4] The weight response factor, WRF_i, for each pure component, i, was first retrieved from the analysis of standard liquid mixtures prepared from over 35 pure compounds. Typical pure compounds utilized were the *n*-alkanes, 1-alkenes, alkyl cyclohexanes, benzene, toulene, alkyl aromatics, and various hydrogen donors. The relative weight response factor, $RWRF_i$, for a component i in the product liquid was subsequently calculated relative to that for the major component in the liquid product, *n*-tetradecane. The molar yield of each component in the liquid product, X_i, was determined using this equation:

$$X_i\,(\%) = \frac{[A_i \bullet RWRF_i]}{\sum_{i=1}^{N} (A_i \bullet RWRF_i)} \bullet \frac{(W_L \bullet MW_r)}{(MW_i \bullet W_r)} \bullet 100 \qquad (3)$$

where W_L is the total weight of the product liquid. Note the difference between Equation (1) and (3); Eq. (3) involves the weight fraction of each component in the product liquid, while Eq. (1) deals with the volume or mole fraction of each component in the product gas.

Results and Discussion

The values of the $RVRF_i$ for each gas and vapor for both the FID and TCD detectors indicated that there is a substantial variation in the RVRF for the *n*-alkanes and 1-alkenes; in general, the response factors decrease with an increase in the number of carbon atoms in each gas. The values obtained from FID and TCD closely agreed with those reported elsewhere.[5]

The RWRFs for the pure liquids, unlike the RVRFs for the gases, displayed only a slight variation with changes in carbon number. The standard deviation was ≈10% and the mean is approximately unity. These values reasonably agree with those reported by other researchers.[5] The RWRFs for pure liquid components were close to unity.

The analytical results obtained during the pyrolysis of neat *n*-tetradecane showed that the conversion of tetradecane increased from 20.8 to 52% as the residence time was increased from 12 to 30 minutes. On comparing these values for the 23 mL microreactor with those obtained under identical conditions for a 28 mL reactor,[2] we observed that the conversions in the former are higher than those for the latter this is expected, given the smaller cold volume in the former.[3] We can also infer from this data that the molar ratio of *n*-alkane to alkene for the paraffinic and olefinic products with carbon numbers ranging from 5 to 13 increases with an increase in residence time from 12 to 30 minutes.

The yield of lighter hydrocarbons is lowest for the binary mixture of *n*-tetradecane and tetralin at all residence times. Yields of *n*-alkanes and alkenes from the addition of hydrogen donors are significantly lower than those obtained during the pyrolysis of neat tetradecane at all the residence times. The degree of conversion of *n*-tetradecane is the lowest for the aforementioned binary mixture at all the residence times. Moreover, it can be observed that the fraction of hydrogen donor remaining (unconverted) in the product mixture is also the highest for tetralin at all retention times. Thus, tetralin appears to be more effective then either benzyl alcohol or *n*-butylcyclohexane in terms of lower conversion of *n*-tetradecane, and higher amount of remaining (unconverted) hydrogen donor under the conditions employed for this study. These results are consistent with earlier work[6] in the sense that hydrogen donors, such as tetralin and benzyl alcohol, have been found to be effective in inhibiting the decomposition of *n*-alkanes. However, the relative order of effectiveness observed in these tests carried out at 450°C is somewhat different from the results of earlier work performed at 425°C.

---

[1] Song, C., W. C. Lai, and H. H. Schobert. *Prepr.-Am. Chem. Soc. Div. Pet. Chem.* 1992. 37(4).

[2] Song, C., W. C. Lai, and H. H. Schobert. *I&EC Research.* 1994. 33.

[3] Lai , W.C. and C. Song. *Advanced Thermally Stable Jet Fuel*s, Technical Progress Report, July - September 1994. #92PC92104-TPR-9. The Pennsylvania State University. 1994. 17-20.

[4] Schobert, H. H. et al. *Advanced Thermally Stable Jet Fuels, Technical Progress Report, July - September 1996.* The Pennsylvania State University. 1997.

[5] Yu, Jian. *Ph.D. Dissertation,* Department of Materials Science and Engineering, Pennsylvania State University. 1996. p. 175.

[6] Yoon, E. M. et al. *Energy and Fuels.* 1996. 10(3). 806-811.

1.12 STUDIES ON THE PYROLYSIS OF BINARY MIXTURES OF *N*-TETRADECANE AND HYDROGEN DONORS AT 450°C IN A BATCH REACTOR

This study is explained in detail in *Advanced Thermally Stable Jet Fuels, Technical Progress Report, October—December 1996.*

Introduction

Previously we discussed the results of our exploratory work aimed at evaluating the efficacy of hydrogen donors in inhibiting the pyrolytic degradation of *n*-tetradecane at 450°C in the sub- and supercritical regimes of pyrolysis in a batch reactor.[1] Specifically, the hydrogen donors that we employed were tetralin (1, 2, 3, 4-tetrahydronaphthalene), benzyl alcohol, and *n*-butylcyclohexane. We determined the product distributions and extent of degradation of *n*-tetradecane in 5 mL binary mixtures comprising 10% by volume of the hydrogen donor and 90% by volume of *n*-tetradecane, and compared the results with those obtained from the pyrolysis of neat *n*-tetradecane.

In this report, we present the results of our investigation aimed at evaluating the role of a specific hydrogen donor, 1, 2, 3, 4-tetrahydroquinoline (THQ), in inhibiting the degradation of *n*-tetradecane at 450°C for various sample (reactant) volumes in a 23.2 mL batch reactor under an initial nitrogen (UHP) pressure of approximately one atmosphere. Our decision to use THQ was based on the results of an earlier study,[2] which determined THQ to be the most efficacious compound for inhibiting the pyrolytic degradation of *n*-dodecane at 425°C in a batch reactor. We also compare the THQ results with those obtained for tetralin and neat *n*-tetradecane under identical conditions for various sample (reactant) volumes.

Experimental

A detailed description of the experimental setup, analytical procedure for determining the product distributions and extent of degradation of reactants, and methodology for the analyses are reported elsewhere.[3] The sample volumes employed were varied from 1 mL to 11 mL in increments of 2 mL, for the runs involving THQ, tetralin, and neat tetradecane. In these runs, the volume ratio of the hydrogen donor to that of the neat tetradecane fuel was kept constant at 10% for both THQ and tetralin. The purity of THQ and tetralin from GC and GC/MS analyses were determined to be approximately 98% and 97%, respectively.

Results and Discussion

Examining the product distributions obtained from the pyrolysis of a binary mixture of 10 vol% THQ and 90 vol% tetradecane at 450°C for a reactant volume of 11 mL at various residence times in the 23.2 mL batch reactor, we determined that the extent of degradation of *n*-tetradecane does not change appreciably as the residence time is increased from 12 to 30 minutes, especially after taking into account the experimental uncertainties in the measured concentration of *n*-tetradecane. The same is true for the molar concentrations of alkanes and alkenes with carbon numbers ranging from 2 to 13. This observed inhibition in the decomposition of *n*-tetradecane is attributable to the highly efficient radical scavenging ability of THQ, its excellent resonance stabilization properties, and the donation of four hydrogen atoms for every THQ molecule converted to the stable final product, quinoline.[2] Note that the

concentration of quinoline increases as the residence time is increased from 12 to 20 minutes, and finally to 30 minutes.

The effect of THQ in inhibiting *n*-tetradecane decomposition is discernable for both sub- and supercritical regimes of pyrolysis. For the 11 mL sample, pyrolysis likely occurred under a near-critical or supercritical regime for all of the residence times. We reasonably assumed that the system attained the near-critical or supercritical state for a residence time of 12 minutes, due to the large reactant volume of 11 mL. This rationale was substantiated by comparing the data on the product distributions for a residence time of 12 minutes; the molar concentrations of alkenes, alkanes, and quinoline are similar and undergo a noticeable change as the residence time is increased to 20 minutes likely the result of a transition from the sub-critical gas phase to the near-critical or supercritical regime. This change, however, was not discernable for the tests done with reactant volume of 11 mL. A similar phenomenon occurred with for the 1 mL sample for all the residence times, especially for hydrocarbons with carbon numbers ranging from 4 to 14. In these cases, pyrolysis could have occurred in the sub-critical gas phase for all of the residence times, as a result of the low system pressure measured.

Conclusion

The overall implication of these results is that the interactions between THQ and *n*-tetradecane are not affected significantly by the phase conditions. In other words, the two types of molecular species, radicals and molecules, that ultimately determine the extent of overall reaction, seem to exist in the same phase during pyrolysis, regardless of whether the phase is likely to be gas phase as in the case of the 1 mL sample or the supercritical phase as in the case of the 11 mL sample. Furthermore, we concluded, from a comparison of the results on the extent of decomposition of *n*-tetradecane at identical residence times for various reactant volumes, that the sample or reactant volume does not exert a significant influence on the pyrolysis of the binary mixture.

The product distributions and the product gas and liquid weights obtained from the pyrolysis of a binary mixture comprising 10 vol% tetralin and 90 vol% tetradecane under identical conditions indicate that the efficacy of tetralin is not as pronounced as that of THQ in inhibiting the decomposition of *n*-tetradecane for all sample volumes. Moreover, it is possible to compare the relative stabilities of THQ and tetralin under identical conditions (i.e., same residence time and sample volume) by contrasting the data on the amount of hydrogen donor left unconverted. This exercise indicated that the relative stability of THQ is only marginally higher than that of tetralin, if not similar, if cognizance is taken of the experimental uncertainties in the measured values. This is to be expected as both THQ and tetralin can transfer four hydrogen atoms for every donor molecule, and the terminal products, quinoline and napthalene, from these donors are both very stable. A rationale to account for the greater radical scavenging ability of THQ relative to tetralin is yet to be established.

The effects of the sample volume on the conversion of *n*-tetradecane in the presence of tetralin can be investigated by comparing the data for identical residence times. This shows that the effect of sample volume is only marginal within the levels of experimental uncertainty in the measured values, similar to that observed for THQ. There are some exceptions, however; for example, the amount of *n*-tetradecane remaining unconverted in the 11 mL sample was relatively low (i.e., 78% at a residence time of 30 minutes). This could be attributed to the highly probable

supercritical regime of pyrolysis that results in enhanced degradation of *n*-tetradecane.[4] We noticed a possible trend in the variation of the unconverted molar concentration of both THQ and tetralin with the sample volume for identical residence times. For certain ranges of sample volumes (3, 5, and 9 mL, and 1, 3, and 5 mL, for THQ and tetralin, respectively), the lower the sample volume, the greater the amount of the hydrogen donor remaining unconverted at identical residence times. This theory remains speculation pending further experimentation.

The product distributions and the amount (mol%) of unconverted *n*-tetradecane obtained from the pyrolysis of neat *n*-tetradecane at 450°C demonstrate that the decomposition of *n*-tetradecane is much greater in the neat fuel than in the binary mixtures for all sample volumes at identical residence times.

Based on these studies, we concluded that THQ is by far the most effective hydrogen donor both in terms of its radical scavenging abilities and its own stability at 450 °C.

---

[1] Venkatraman, A., C. Song, and A. Coleman, A. *Advanced Thermally Stable Jet Fuels, Technical Progress Report, July - September 1996.* 92PC92104-TPR-9. The Pennsylvania State University. 1996

[2] Yoon, E. M. et al. *Energy and Fuels.* 1996. 10(3). 806-811.

[3] Song, C. S., W. C. Lai, and H. H. Schobert. *I & EC Research.* 1994a. 33. 534-547.

[4] Lai, W. C. and Song, C., *Prepr. -Am. Chem. Soc. Div. Pet. Chem.* 1996. 41(2). 502-507.

1.13 STUDIES ON THE EFFECTS OF THE CONCENTRATION OF HYDROGEN DONORS ON THE PYROLYSIS OF *N*-TETRADECANE AT 450°C IN A BATCH REACTOR

This study is explained in detail in *Advanced Thermally Stable Jet Fuels, Technical Progress Report, April—June 1997*.

Introduction

This work was aimed at establishing the minimum necessary volumetric concentration of each hydrogen donor tetrahydroquinoline, tetralin , and benzyl alcohol for significantly inhibiting the degradation of *n*-tetradecane at 450°C for 30 minutes and a sample volume of 5 mL in a 23.2 mL batch reactor under initial nitrogen (UHP) pressure of approximately one atmosphere. We compared the efficacy of each donor under identical conditions and investigated the stability of 1,2,3,4-tetrahydroquinoline (THQ) in the binary mixture at a low temperature (250°C) and long residence times (up to 6 hours) in a batch reactor under UHP nitrogen atmosphere.

Experimental

A detailed description of the experimental setup, analytical procedure for determining product distributions and extent of degradation of reactants, and methodology for analysis was reported by Song and Lai.[1] The volumetric concentration of the three hydrogen donors was varied and included 0.5, 1, 3, 5, and 10 vol% runs at 450°C. Residence time was kept constant at 30 minutes for a sample volume of 5 mL and an initial nitrogen pressure of one atmosphere. The low temperature runs involving THQ were carried out at residence times of 2, 4, and 6 hours. The purity of THQ, tetralin, and benzyl alcohol as determined from GC and GC/MS analyses were approximately 98%, 97%, and 99%, respectively.

Results

In examining the results of pyrolysis of binary mixtures of THQ and tetradecane at 450°C, we noted that the extent of degradation of *n*-tetradecane is small and does not change appreciably as the volumetric concentration of THQ is decreased from 10 to 3%. The same was true for the molar concentrations of paraffins and olefins with carbon numbers in the range from 8 to 13. The inhibition in the decomposition of *n*-tetradecane is attributable to the highly efficient radical scavenging ability and excellent resonance stabilization properties of THQ, in addition to its donation of 4 hydrogen atoms for every THQ molecule converted to the stable final product, quinoline.

However, when the THQ volumetric concentration was decreased from 3 to 1%, and then to 0.5%, the molar percent of *n*-tetradecane that decomposed into products (paraffins and olefins) increased sharply. We anticipate that further decreases in THQ concentrations would cause the mole percent of *n*-tetradecane remaining unconverted to rapidly approach that for infinite dilution (i.e., pyrolysis of neat *n*-tetradecane). We, therefore, concluded that the minimum necessary volumetric concentration of THQ that results in a significant (acceptable) inhibition of *n*-tetradecane decomposition is approximately 1 vol%.

Product distributions for the binary mixtures exhibited behavior similar to THQ as the volumetric concentration of each hydrogen donor was decreased from 10 to 3%, and then to

0.5%. When the volumetric concentration of the donor is less than approximately 1%, the decomposition of *n*-tetradecane increases significantly and the scavenging power of each donor is greatly diminished.

Plotting the molar concentration of *n*-tetradecane remaining unconverted in the reactor against the volumetric concentration of the hydrogen donor in the binary mixture, we confirmed that THQ is clearly the best and most effective stabilizer at all of the concentrations investigated. A 1 vol% strength of THQ is more effective in inhibiting *n*-tetradecane decomposition than 10 vol% strengths of either tetralin or benzyl alcohol. The efficacy of 0.5 vol% THQ is comparable to that of 10 vol% of benzylalcohol, although the molar amount of the latter donor that remained unconverted was higher. The remarkable scavenging power of THQ is not yet fully understood, given the fact that tetralin also donates four hydrogen atoms per parent molecule and its product, naphthalene, is equally or more stable than quinoline.

The low-temperature (250°C) stressing of a binary mixture composed of 10 vol% THQ and 90 vol% *n*-tetradecane did not generate any measurable quantities of gas or C_3 to C_{13} alkanes/alkenes in the liquid product. No measurable quantities of THQ reaction products could be detected in the liquid product, even after 6 hours of stressing. Additional research will investigate the behavior of tetralin and benzyl alcohol under these same low-temperature conditions.

---

[1] Song, C. S., W. C. Lai, and H. H. Schobert. *I&EC Research*. 1994. 33. 534-557.

1.14 SURFACE EFFECTS ON CARBON DEPOSIT FORMATION FROM JET FUEL AND *N*-DODECANE

This study is explained in detail in *Advanced Thermally Stable Jet Fuels Technical Progress Report, August — October 1992.*

Introduction

Possible catalytic effects of metal surfaces on thermal degradation of jet fuels and deposit formation at high temperatures (>400¡C) had not been studied prior to this work. It is generally believed that copper is the most deleterious material at relatively low temperatures because it can significantly increase the amount of deposit formed on a metal surface.[1] Over a wider temperature range, stainless steel (type 316) tubes were found to give more deposit than aluminum tubes, approximately by a factor of 2.[2, 3] Taylor[1] suggested that the observation of a copper tube producing more deposit may be due to the catalysis of oxidation reactions by oxides of copper. In the low-temperature regime, according to Hazlett[4] (1977), autoxidation is the dominant reaction in fuel degradation. Since thermal degradation processes at high temperatures involve principally pyrolysis reactions, rather than autoxidation reactions, one should expect different catalytic effects, if any, at high temperatures.

This project involved a systematic study of the effects of metal surface on deposit formation at high temperatures (> 400¡C). Metals such as copper (Cu), nickel (Ni), iron (Fe), titanium (Ti), stainless steel (SS), and gold (Au), among others, were used in the form of transmission electron microscope (TEM) grids, wires, powders, and foils to study surface effects on the thermal stability of *n*-dodecane and Jet A fuel. We also developed a scanning electron microscopy (SEM) characterization of the carbon deposit on a stainless steel tube.

Deposits Collected from the Reactor Walls

The experimental conditions of all three scenarios involved 5 ml *n*-dodecane with an initial N_2 pressure of 100 psi at a contant temperature of 450¡C throughout a 5-hour test period.

1. Thermal stressing of *n*-dodecane with metal grids. TEM metal grids (200 mesh) made of Cu, Ni, Ti, SS, and Au were used to study the deposits collected on different metal surfaces. The experiment involved placing five pieces of grid at the bottom of the tubing bomb reactor. In general, the presence of SS, Au, and Ni grids increased the amount of deposit slightly, while the addition of Ti and Cu grids decreased the amount of deposit significantly.

2. Thermal stressing of Jet A with metal grids. The Jet A fuel was added to the tubing bomb reactor which contained 8 pieces of grid. The presence of any type of metal grid increased the amount of deposit relative to neat Jet A. In addition, the amount of deposit collected from Jet A was higher than that from *n*-dodecane. In contrast to *n*-dodecane stressing, the differences between grids were not significant and were within the experimental error.

3. Thermal stressing of *n*-dodecane and jet A with different wires. Three kinds of metal wires, Cu, Ni, and Fe, all with a diameter of 1 mm, were tested in thermal stressing experiments. Two segments of wire were put inside the reactor: one of 1 cm lying at the bottom of the reactor, the other of 6 cm standing against the reactor wall. The amount of deposit collected is shown in **Figures 1.14-1** and **1.14-2**.

Morphology of Carbonaceous Solids on Metal Grids

The morphology of the carbonaceous deposits on the grids can provide useful information for elucidating the mechanisms of the solid deposition process. The morphology of the carbonaceous deposit on metal grids has been studied mainly by SEM.

1. Deposit on metal grids from thermal stressing of *n*-dodecane. In summary, two types of globular carbon deposits and three distinct growth patterns were observed with the metal grid tests. The globular carbon deposit consisted of spheres either of 5—17 μm in diameter or of 0.5 μm in diameter. The larger spheres are not likely to be agglomerates of the smaller spheres. These two types of carbon may result from different reaction or growth history (e.g., surface pyrolytic carbon/liquid mesophase carbon vs. gas phase carbon).

The three growth patterns include lateral, perpendicular, and combined lateral-perpendicular growth. Lateral growth was mainly found with Ni and Ti grids, perpendicular growth was found with SS and Au grids, and a combined growth pattern was observed with Cu grids.

We attempted to correlate the amount of deposit collected with the types of the deposit and the growth pattern. In general, perpendicular growth produced more deposit and lateral growth created less deposit, with the exception of Ni grids. As far as the types of deposit are concerned, more deposit is produced when there are large spheres (SS, Au, and Ni) and less deposit is produced when there are smaller spheres (Cu and Ti).

2. Deposit on grids from thermal stressing of Jet A. No distinct growth patterns could be found in Jet A tests. Carbon morphologies on different grids indicated more severe reactions in Jet A than their counterparts in *n*-dodecane. This finding is consistent with the actual amount of deposit collected on reactor walls in both sets of tests.

Conclusions

The analyses of carbon deposits and morphologies on metal grids concluded the following:

- Carbon deposition depends on the composition of the metal surfaces. It could be surface sensitive (lateral growth as on Ni and Ti grids), or surface insensitive (perpendicular growth as on Au and SS grids), or intermediate (lateral-perpendicular combined). In terms of the amount of solid, the limitations of our tests prevented us from detecting any consistent correlation between the amount of deposit and the kind of metal grids.
- Carbon deposition depends on the chemical compositions of the reactants. For Jet A and *n*-dodecane, the effects of the same kind of metal grids on the formation of carbon deposit are found to be different.

Lower reaction temperatures and different metal geometries will be used in the future studies to elucidate the effects of metal surfaces on thermal degradation reactions and solid deposition.

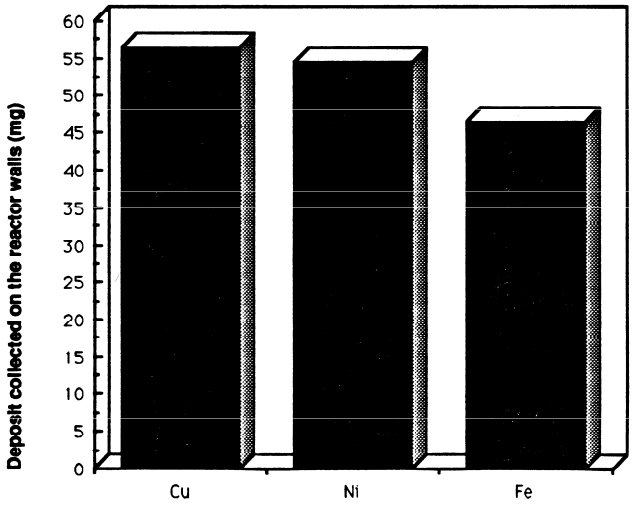

Figure 1.14-1. Carbon Deposit Collected on the Reactor Walls in the Presence of Metal Wires (450°C, 5 hours, 5 ml dodecane)

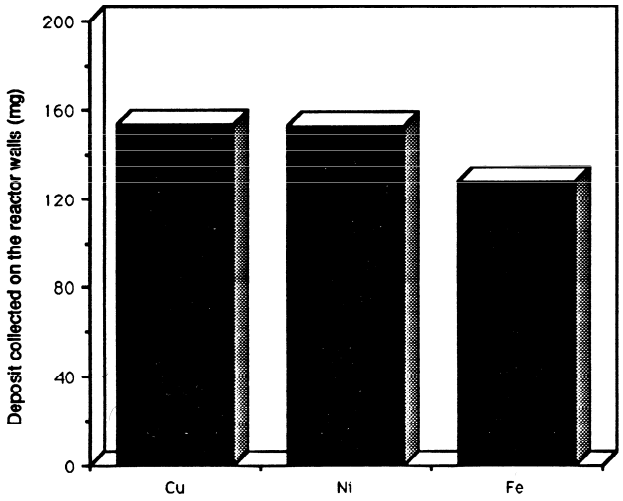

Figure 1.14-2. Carbon Deposit Collected on the Reactor Walls in the Presence of Metal Wires (450°C, 5 hours, 5 ml Jet A fuel)

---

[1] Taylor, W.F. Kinetics of Deposit Formation from Hydrocarbons, III. Heterogeneous and Homogeneous Metal Effects. *J. Appl. Chem.* Vol. 18: 1968. 251.

[2] Wong, E.L. and D.A. Bittiker. Effects of Hydrocarbon Fuel Type on Fuel Thermal Stability. *NASA-TM 82916*. 1982.

[3] Kendall, D.R. and J.S. Mills. The Influence of JFTOT Operating Parameters on the Assessment of Fuel Thermal Stability. *Proceedings of the Aerospace Technology Conference and Exposition, Long Beach, CA*. 1985. 143.

[4] Hazlett, R. W., J.M. Hall, and M. Matson. Reactions of Aerated n-Dodecane Liquid Flowing Over Heated Metal Surface. *I & EC Prod. Res. Dev.* 1977. 16(2). 171.

1.15 SURFACE EFFECTS ON THE FORMATION OF CARBON DEPOSITS FROM THERMAL STRESSING OF JET A FUEL AND *N*-DODECANE

This study is explained in detail in *Advanced Thermally Stable Jet Fuels Technical Progress Report, November 1992 — January 1993*

This work involved placing TEM grids at the top and bottom of reactors before thermal stressing with Jet A and *n*-dodecane, to study the deposition processes at the existing phases during thermal stressing within a microautoclave, based on the observed microstructures of the carbonaceous solid. Optical textures and morphologies of carbonaceous deposits generated on reactor walls and on metal grid surfaces from Jet A and *n*-dodecane at 450¡C for 1, 3, and 5 hours were examined using polarized-light optical microscopy (PLM) and scanning electron microscopy (SEM). The metal grid-deposit interface was also examined by PLM. In addition, the effect of surface roughness on deposition formation was studied, since the grids inherently contain both smooth and rough surfaces.

Nickel (Ni), copper (Cu) and stainless steel (SS) grids were used. The Ni and Cu grids had both a polished smooth side, and a dull, rough side. The SS grids had no specific finishing, but were cut in a way to introduce rough edges.

The microscopic examination of carbonaceous deposits collected on different metal grids indicates a layer-by-layer growth of solid deposits on surfaces primarily by incorporation of liquid-like spherules nucleated in a vapor phase and diffused onto the substrates. Ni grids appear to have a strong catalytic effect on incipient deposit formation from Jet A fuel. Ni, among other group VIII metals, has been well identified as a catalyst for carbon formation.[1] Cu grids also caused some catalysis with incipient deposition, whereas stainless steel grids did not show any catalytic effect. The deposits produced from Jet A appear to be more heterogeneous in structure than those from *n*-dodecane, presumably due to a greater variety of deposit precursors generated during Jet A reactions.

[1] Alstrup, I.J. *Catalysis*. 1988. 109. 241-251.

1.16 THERMAL DEGRADATION STUDIES OF ^{13}C-LABELED DODECANE MIXED WITH A PETROLEUM-DERIVED JET FUEL, JP-8P, USING GAS CHROMATOGRAPHY-SELECT ION MONITORING

This study is explained in detail in *Advanced Thermally Stable Jet Fuels Technical Progress Report, January—March 1996.*

Introduction

Long chain *n*-alkanes in the carbon number range of C_7-C_{17} comprise approximately 70 vol.% of commercial and military aviation jet fuels.[1] Therefore, understanding the thermal degradation mechanisms and kinetics of these saturated hydrocarbons is critical to developing thermally stable fuels for future high-Mach aircraft. In addition to using the fuel for propulsion systems, these aircraft will also use it for heat-sinking purposes. Under these circumstances, the fuel may reach temperatures of 400°-500°C.[2] Therefore, a thorough understanding of the pyrolysis mechanisms and rate of *n*-alkane degradation at these temperatures is important.

Site-specific ^{13}C-labeling of hydrocarbons is an excellent technique for following the rate of thermal degradation of specific target molecules in complex fossil fuel systems.[3, 4, 5] This technique rivals that of model compound studies, because the calculated kinetic parameters and reaction mechanisms are based on experiments in which a target fuel component is thermally stressed in the presence of a complex fuel system. Burnham et al[4] developed an isotopic method in which a double-^{13}C label is detected by gas chromatography-mass spectrometry. In this method, *n*-alkanes derived from the thermal degradation of 1,2-^{13}C-hexadecane are monitored by plotting the ion chromatogram corresponding to m/z=31, which corresponds to the mass of the di-^{13}C-labeled fragment ion. However, caution must be exercised when applying this method to avoid errors in the quantitation of the ion chromatograms.

McKinney et al[3, 5] have used primarily ^{13}C NMR techniques to follow the decomposition of singly ^{13}C-labeled hydrocarbons. In this methodology, reactions involving the ^{13}C-labeled carbon lead to significant changes in the chemical shift of this carbon in ^{13}C NMR spectra. By enriching the reactive compound with 100% ^{13}C at one reactive site, an enhancement in the ^{13}C NMR sensitivity is realized for the labeled carbon. Optimal results are only obtained with this method when the signals resulting from the ^{13}C-labeled carbons of the starting material and the products do not overlap with regions of the spectrum containing a large number of carbon signals.

In an effort to obtain quantitative data with a higher degree of certainty over a large dynamic range, we used gas chromatography-select ion monitoring (GC-SIMS) and ^{13}C-labeling techniques in model studies examining the thermal degradation of ^{13}C-labeled dodecane mixed with a petroleum-derived jet fuel, JP-8P. GC-SIMS is a GC-MS technique that is most often used to precisely quantify trace-level components. When combined, ^{13}C-labeling and GC-SIMs provide a quantitative method for monitoring the thermal degradation rates of specific molecules in fossil fuel systems.

We stressed a petroleum-derived jet fuel, laced with 6-^{13}C-dodecane, at varying time and temperature regimes, and analyzed the product mixtures by gas chromatography (GC) and GC-SIMs to determine the kinetic parameters for its thermal degradation.

Experimental

6-^{13}C-dodecane was synthesized using a similar reaction scheme to that described by McKinney et al.[5] The jet fuel sample used in this work is a petroleum derived JP-8 fuel with similar properties to those of commercial jet fuel Jet A-1.[1]

Details of the pyrolysis experiment and product collection and analysis are provided in the corresponding Technical Progress Report.[6] Following pyrolysis, we performed quantitative gas chromatography and quantitative gas chromatography-select ion monitoring.

Quantitation of the GC-SIMs data for the 6-^{13}C-dodecane-JP-8P mixture was carried out using an internal standard method. First, unlabeled dodecane and d_{26}-dodecane were mixed in pentane at four varying concentration levels for the dodecane (25, 50, 75, and 150 ng/μL) while the d_{26}-dodecane concentration (50 ng/μL) remained constant in each of the four standards. Each of these samples was then analyzed using GC-SIMs analysis using the same acquisition parameters as were used for the thermally stressed jet fuel mixtures with one exception: the M+1 parent ion monitored for the unlabeled dodecane will be one mass unit less, *m/z* = 171.2035, than that monitored for the 6-^{13}C-dodecane. A plot of Area *n*-C_{12}/ Area d_{26}-C_{12} versus Wt. *n*-C_{12}/Wt. d_{26}-C_{12} produces a linear curve that can be described by the general formula y = mx + b, where m is the slope and b is the y-intercept:

$$\frac{\text{Area n-}C_{12}}{\text{Area } d_{26}\text{-}C_{12}} = 1.4623 \times 10^{-2} + 1.3671\left(\frac{\text{Wt. n-}C_{12}}{\text{Wt. } d_{26}\text{-}C_{12}}\right)$$

Rearranging this equation, we determined the weight of *n*-C_{12} in the mixture, as determined by GC-SIMS, by knowing the area of *n*-C_{12}, the area of d_{26}-C_{12}, and the weight of d_{26}-C_{12}:

$$\text{Wt. n-}C_{12} = \frac{\left(\frac{\text{Area n-}C_{12}}{\text{Area } d_{26}\text{-}C_{12}} - 1.4623 \times 10^{-2}\right)}{1.3671} * \text{Wt. } d_{26}\text{-}C_{12}$$

We assumed that the response of the M+l parent ion detected for unlabeled dodecane, used to construct the calibration curve, was the same as the M+1 parent ion detected for the carbon-13 labeled dodecane.

Results and Discussion

In considering the thermal degradation of long chain *n*-alkanes, the rate is generally first-order in the reactant. Studies confirming this assumption were all performed using model compounds in which the concentration of the starting *n*-alkane was relatively large at the beginning of the reaction in comparison to the products.[7, 8, 9, 10] Thus, at low conversions, the rate of formation of products from the starting material is much larger in comparison to the reverse reaction in which the starting material is being formed by either recombination mechanisms of smaller chain *n*-alkanes or homolytic cleavage of C-C bonds in higher carbon chain *n*-alkanes. In general, in a model compound system at low conversions, the rate of formation of the model compound is not a critical factor. This is not the case in complex fossil fuel systems; however,

because the concentrations of larger and smaller molecules, with respect to the target molecule, are significant. Thus, we must take into account the rate of formation as well as the rate of degradation of the target molecule.

Figure 1.16-1 displays a typical GC and GC-SIMs plot for the thermal degradation of 6-^{13}C-dodecane in JP-8P. Gas chromatography allows us to quantifyall hydrocarbons in a complex fuel mixture. However, how does one differentiate between carbon-13 labeled dodecane and unlabeled dodecane present naturally in the fuel? As shown in Figure 1.16-1, GC-SIMs differentiates between hydrocarbons containing carbon-13s and those at natural abundance. This is done by monitoring the M+1 peak of the parent ion of the labeled compound. Since this ion corresponds to an M+2 peak of the unlabeled species, we do not expect to see any contribution from unlabeled species. Thus, one can discriminate between naturally occurring dodecane in the jet fuel and carbon-13 labeled dodecane added using GC-SIMS.

In considering the rate of degradation of 6-^{13}C-dodecane in JP-8P, we must also consider the formation of dodecane from larger molecular weight *n*-alkanes and recombination of lower molecular weight *n*-alkanes. However, there is a low probability, in a diluted system, that an *n*-alkane having a carbon number greater than C_{12}, in the jet fuel range, will be carbon-13 labeled, and, thus, degrade to form carbon-13 labeled dodecane. The same is true for a recombination mechanism of lower molecular weight *n*-alkanes in that the probability of a carbon-13 labeled dodecane being formed by recombination of a naturally abundant radical and a carbon-13 labeled one is insignificant. In this respect, we can observe the thermal degradation of carbon-13 labeled dodecane in a fossil fuel system without concern for the production of this species.

Figure 1.16-2 shows a stack plot of the gas chromatograms of 6-^{13}C-dodecane mixed in JP-8P at time 0, at 400°C for 6 hours, at 431°C for 3 hours, and at 470°C for 3 hours. Conversion of 6-^{13}C-dodecane in JP-8P is denoted in the upper right corner of each chromatogram as determined by GC-SIMS. At this point, more data points are needed in order to calculate rate constants for the various temperatures used and to establish whether or not the reaction is first order with respect to 6-^{13}C-dodecane. Once this accomplished, the activation energy and preexponential factor can be calculated and compared to values obtained for the stressing of dodecane by itself.

Conclusions

Gas chromatography-select ion monitoring in combination with carbon- 13 labeling has been demonstrated as an excellent technique for monitoring the thermal degradation of 6-^{13}C-dodecane in JP-8P. We demonstrated that, using this technique, one can discriminate between naturally occurring unlabeled dodecane in the system and added carbon-13, based on the differences in their molecular weights. Preliminary data on the conversion of 6-^{13}C-dodecane in JP-8P was presented in this study; future work will determine the rates of thermal degradation, activation energy, and preexponential factor. This future work will also demonstrate the applicability of this technique to other labeled hydrocarbons, such as polycyclic aromatic hydrocarbons and alkylbenzenes.

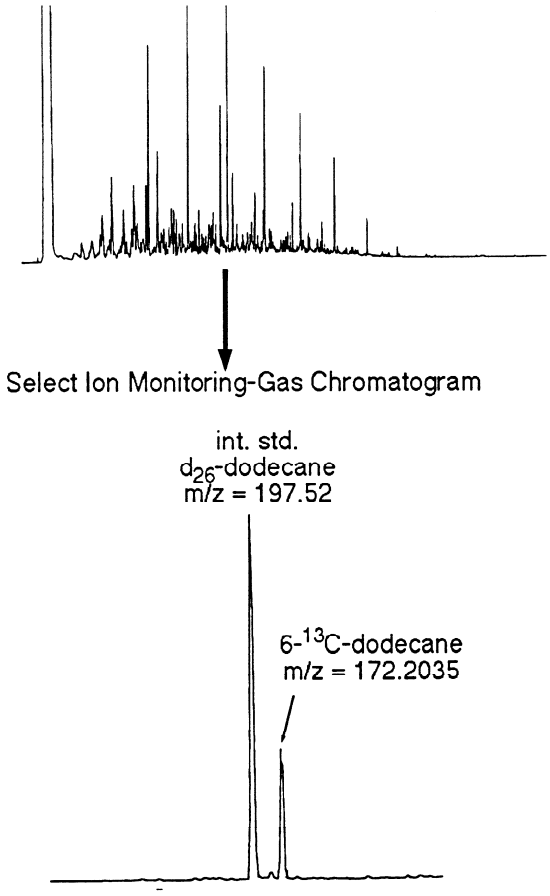

Figure 1.16-1. *(Top)* **Gas Chromatogram of 6-^{13}C-Dodecane Mixed with JP-8P at a Concentration of 0.5% by Weight** *(Bottom)* **Select Ion Monitoring Chromatogram Where the Two Ions of Interest Correspond to M+1 Peak of the Internal Standard, d_{26}-Dodecane, and the M+1 peak of 6-^{13}C-Dodecane**

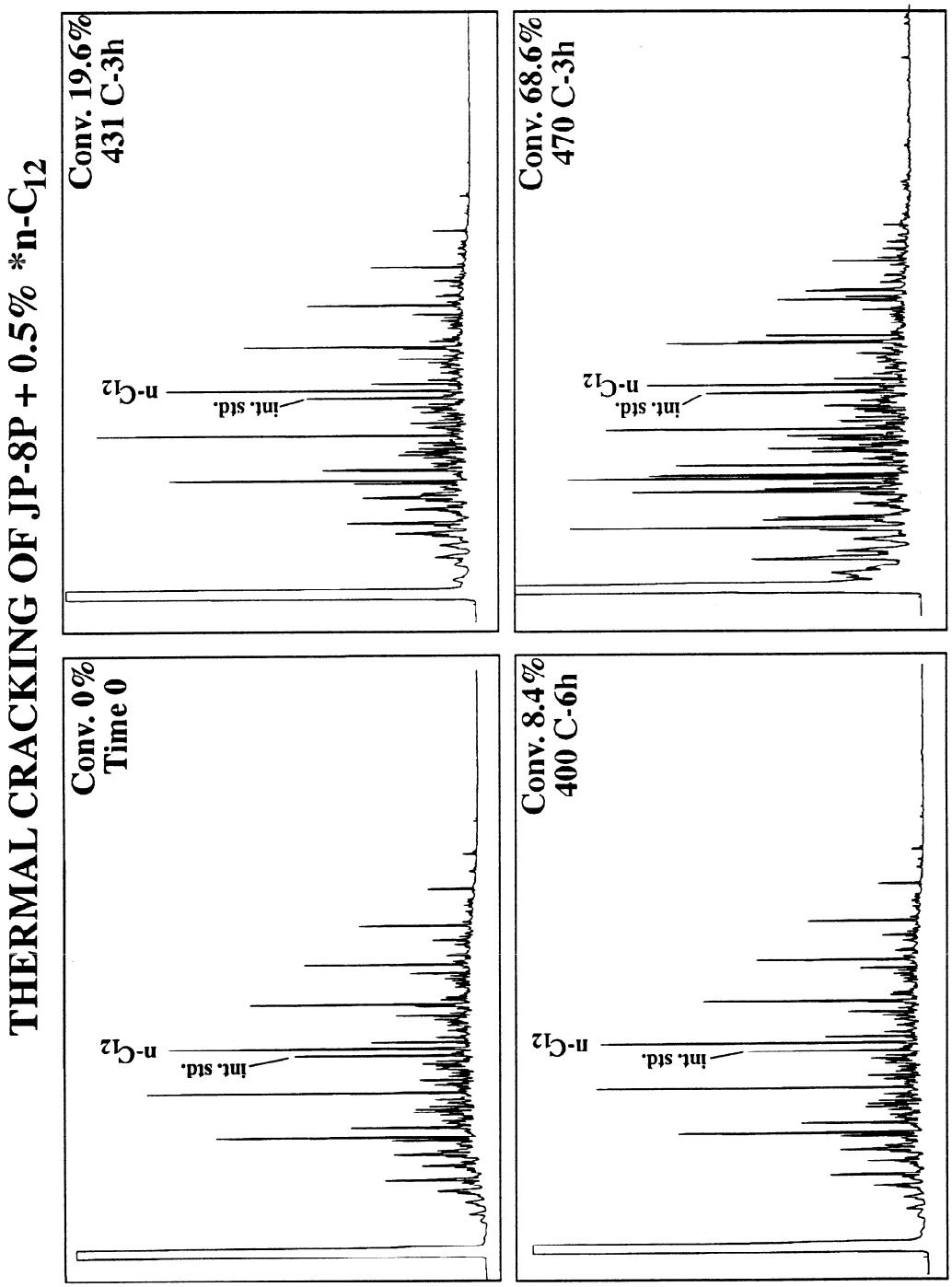

Figure 1.16-2. A Stack Plot of the Gas Chromatograms of 6-^{13}C-Dodecane Mixed In JP-8P at Time 0, at 400°C for 6 Hours, at 431°C for 3 Hours, and at 470°C for 3 Hours

[1] Martel, C. R. *Military Jet Fuels 1944-1987.* Summary Report, U. S. Air Force, AFWAL-TR-97-2062. 1987. 662.

[2] Storch, D. M.; and W. E. Harrison, III. Personal Communication. Fuels and Lubrication Division, U.S. Air Force Wright Laboratory, WPAFB. Nov. 23, 1992.

[3] McKinney, D. E., J. M. Bortiatynski, and P. G. Hatcher. *Energy Fuels.* 1993. (7). 578-581.

[4] Burnham, A. K.; Gregg, H. R.; Braun, R. L. *Energy Fuels.* 1995. (9). 190.

[5] McKinney, D. E., J. M. Bortiatynski, and P. G. Hatcher. *Prepr.-Am. Chem. Soc., Div. Pet. Chem. Prepr.* 1996. 534-538.

[6] Schobert, H. H. et al. *Advanced Thermally Stable Jet Fuels, Technical Progress Report, January - March 1996.* The Pennsylvania State University. 1996.

[7] Voge, H. H. and G. M. Good. *J. Am. Chem. Soc.* 1949. 71. 593-597.

[8] Fabuss, B. M. et al. *N. Ind. Eng. Process Des. Dev.* 1962. 1. 293-299.

[9] Fabuss, B. M., J. O. Smith, and C. N. Satterfield. *Adv. Pet. Chem. Refin.* 1964. 9. 158-201.

[10] Zhou, P. and B. L. Crynes. *Ind. Eng. Che. Process Des. Dev.* 1986. 25. 508-514.

1.17 CONDENSED-PHASE PYROLYSIS OF LONG-CHAIN PARAFFINS. UNUSUAL EFFECTS OF SAMPLE VOLUME AND INERT GAS PRESSURE

This study is explained in detail in *Advanced Thermally Stable Jet Fuels Technical Progress Report, February — March 1993*.

Introduction

With the goal of understanding the pressure dependence of the condensed-phase paraffin pyrolysis, we pyrolyzed *n*-tetradecane using 1—9 mL samples at 450¡C for 30 minutes under initial (cold) N_2 pressure of 0.07—2MPa (10—280 psig) in 25 mLmicroreactors. The experimental conditions were characterized by a closed reactor, relatively high and continuously increasing pressure, higher density gas phase or supercritical phases, and long residence time. The temperature of 450¡C used in this work was at the lower end of temperatures used in previous alkane pyrolysis studies reported in literature.

Results and Discussion

1. Effect of volume of reactant. **Figure 1.17-1** shows the molar conversion of *n*-C_{14} as a function of the volume of the *n*-C_{14} sample initially charged into the reactor. It appears from Figure 1.17-1 that the initial sample volume, or the pressure of the reactant, affects the *n*-C_{14} conversion in four different ways:

a) When the pyrolysis experiments were carried out under a low initial (cold) N_2 pressure of 0.07 MPa (10 psi), increasing sample volume from 1 to 5 mL decreased *n*-C_{14} conversion from 35 to 15 mol%. Further increases in sample volume from 5 to 9 mL had little impact on *n*-C_{14} conversion.

b) Two different regions exhibit entirely opposite effects of sample volume on *n*-C_{14} conversion when the initial N_2 pressure was increased from 0.07 to 0.7 MPa (100 psi). Figure 1.17-1 shows an increase in conversion when sample volume is increased from 1 to 5 mL, but a decrease in conversion when sample volume is further increased from 5 to 9 mL.

c) When the reactor was pressurized to a certain level with N_2, the change in the initial sample volume had little impact on *n*-C_{14} conversion. This was the case when the initial N_2 pressure was 190 psi.

d) The fourth case is qualitatively opposite to (b). When the initial N_2 pressure was 280 psi, the conversion decreased as sample volume increased from 1 to 5 mL, but increased as sample volume increased from 5 to 9 mL.

These findings illustrate the complexity of the mechanisms governing the effects of sample volume, or pressure of the reactant.

2. Effect of pressure of inert N_2 gas. **Figure 1.17-2** shows the influence of the pressure of inert N_2 gas on the *n*-C_{14} conversion. When the sample volume was 9 mL in the 25 mL microreactor, increasing N_2 pressure from 0.07 to 2 MPa led to a monotonic increase in *n*-C_{14} conversion from about 16 to 50 mol%. However, when 5 mL of sample volume was used, a volcano-shaped curve was obtained. Increasing N_2 pressure in the low pressure range (0.07 to

0.7 MPa) increased *n*-C_{14} conversion significantly, from about 15 mol% to about 51 mol%, but further increasing N_2 pressure from 0.7 to 2, MPa resulted in substantially decreased conversion, from 51 to 32 mol%.

Figure 1.17-2 reveals that, for a constant sample volume, the trends of changes brought about by increasing the pressure of inert N_2 gas are dependent on both the sample volume range and the pressure range. These results differ significantly from earlier data that indicated that the rate constant of alkane pyrolysis increases with pressure up to a maximum at about 100-300 atm[1].

3. Gas-phase or supercritical phase pyrolysis? The critical temperature (T_c) and critical pressure (P_c) of *n*-C_{14} are 423.7¡C and 1.5 MPa (218 psi), respectively. Because the reaction temperature of 450¡C is well above the T_c, *n*-C_{14} could exist in either a gas or supercritical state. Based on the critical density of *n*-C_{14} (0.239 g/cm^3) reported in the literature[2] and the volume of the reactor system (25 mL), at 450¡C the reactant likely exists in supercritical phase when the initial sample volume is 9 mL, and in gas phase when the sample volume is 1 mL and the initial N_2 pressure is 0.07 MPa. With a 5 mL sample, the phase of the reactant at 450¡C could be either gas or supercritical, depending on the pressure.

In general, pressure affects the density, viscosity, and diffusivity. Pressure change near the critical temperature can change the system from gas-like to liquid-like phases. However, addressing the effect of pressure on the phase behavior is difficult, because the pressure increases continuously during 30 minutes in the sealed tubing bombs as a result of the continuous formation of lighter compounds from thermal decomposition. Prior to this work, no literature addressed thermal stability of long-chain alkanes and jet fuels under supercritical conditions. Little was known about the role of inert gas in supercritical fluids at high temperatures. Figure 1.17-2 suggests a significant pressure dependence of pyrolysis of long-chain alkanes and paraffinic jet fuels under supercritical conditions.

4. Mechanistic considerations. For alkane pyrolysis, high temperature-low pressure conditions generally favor the unimolecular β-scission, while low temperature-high pressure conditions facilitate the bimolecular H-transfer. This work, however, involves the pyrolysis at the same temperature. Under the isothermal conditions, pressure can affect the rate constants according to the Evans and Polanyi equation:

$$\left[\frac{\partial \ln}{\partial P}\right] - \frac{\overline{\quad}^{\neq} - \overline{\quad}}{T} = \frac{-\Delta V^{\neq}}{R\,T} \qquad (1)$$

where $\Delta V^{\neq}$ is the difference in partial molar volumes between transition state ($V_x^{\neq}$) and initial state (V_I) of reagents, known as the activation volume.[3] The activation volume reflects the response of reaction rate to increasing pressure. The formation of a bond between two molecules is accompanied by a reduction in volume. The bond cleavage, however, involves a volume increase and, consequently, $\Delta V^{\neq}$ ($\Delta V^{\neq} = V_I - V^{\neq}$) is positive for the unimolecular decomposition reactions such as radical initiation and β-scission. In contrast to this, $\Delta V^{\neq}$ is negative for bimolecular reactions such as intermolecular hydrogen transfer, radical addition, and radical recombination reactions. According to the transition state theory,[4] the rate constants of

bimolecular reactions should increase with pressure, while those for unimolecular reactions should decrease with pressure.

Since both inert gas and reactant are present, a fundamental question that arises is how the molecules experience pressure. Literature on the pressure effects of free radical reactions during hydrocarbon pyrolysis is still very limited and contradictory.[5, 6, 7, 8, 9] In this work, the complexity of the response of *n*-C_{14} conversion to the sample volume (Figure 1.17-1) and N_2 pressure (Figure 1.17-2) at the same temperature of 450¡C for the same duration suggests that the *n*-C_{14} pyrolysis is sensitive to the pressures of both the reactant and inert gas at the temperatures near its critical point, and the pressure effects of the reactant and inert gas seem to be interdependent. At least two different radical reaction processes are affected by the pressure in opposite directions, giving rise to the unusual reversed volcano- and volcano-shaped and linear relationships. The present results also provided experimental evidence that activation volumes ($\Delta V^{\neq}$) of some reactions involved in *n*-C_{14} pyrolysis are very sensitive to pressure changes near the critical point of *n*-C_{14}.

Summary

There is significant pressure dependence of *n*-C_{14} conversion during its pyrolysis at 450¡C for 30 minutes. Unusual volcano-shaped and reverse volcano-shaped curves represent the relationship between *n*-C_{14} conversion and the initial sample volume, which is translated into pressure of the reactant upon heat-up. At least two processes appear to be affected by the reactant pressure in opposite directions. The influence of inert gas pressure is dependent on both the initial sample volume and the pressure range. However, when the inert gas pressure is within a certain specific range, the changes in the sample volume have no impact on *n*-C_{14} conversion. Below or above this range, increasing inert gas pressure can either decrease or increase *n*-C_{14} conversion, depending on the sample volume.

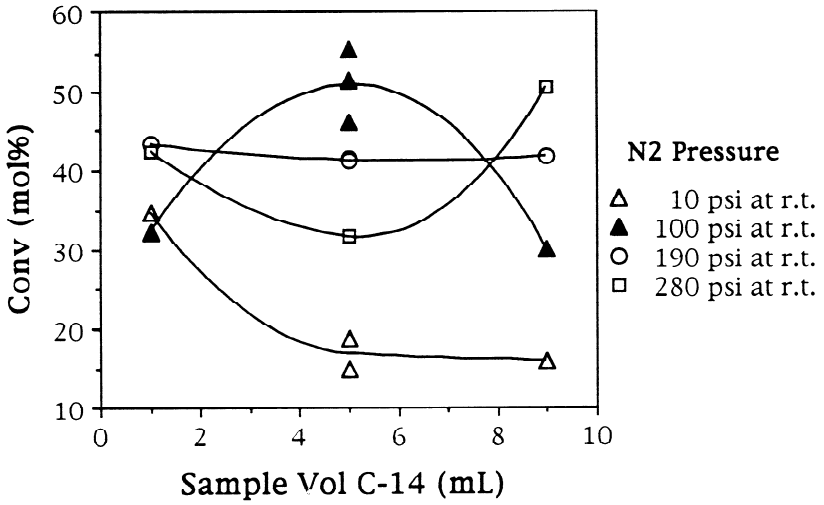

Figure 1.17-1. Effects of Initial Sample Volume of *n*-C_{14} (at Room Temperature) on Pyrolysis at 450°C for 30 Minutes under Varying Pressure of UHP N_2 in 25 mL Microreactor

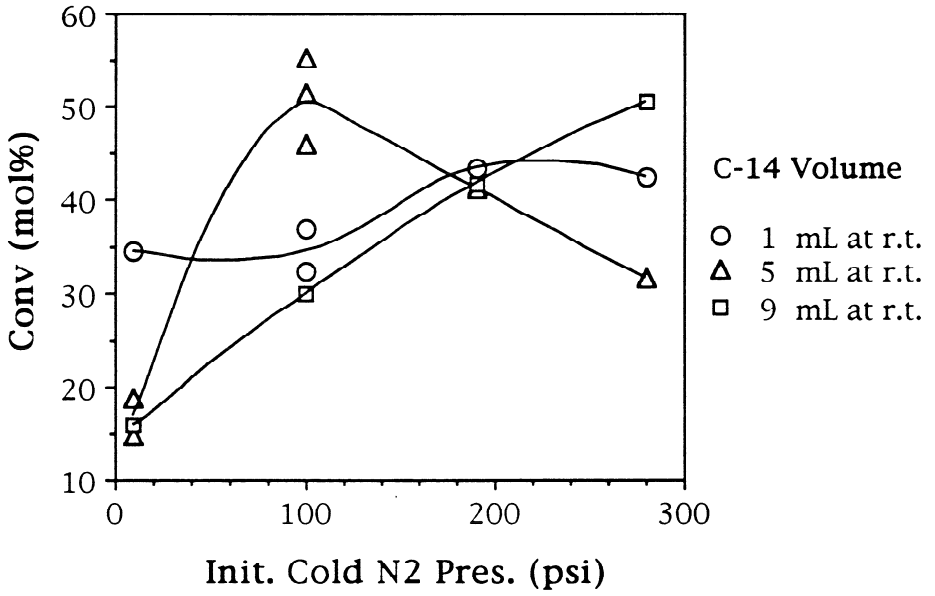

Figure 1.17-2. Effects of Initial N_2 Pressure at Room Temperature on Pyrolysis of *n*-C_{14} with Different Initial Sample Volume at 450°C for 30 Minutes in 25 mL Microreactor

[1] Fabuss, B.M., J.O. Smith, and C.N. Satterfield. *Adv. Petrol. Chem. Refin.* 1964. 9. 158-201.

[2] Yaws, C.L. et al. *Hydrocarbon Processing.* 1989. No.7. 61-64.

[3] Isaacs, N.S. *Liquid Phase High Pressure Chemistry.* Wiley: New York. 1981. 181-353.

[4] Yaws, C.L. et al. *Hydrocarbon Processing.* 1989. No.7. 61-64.

[5] Fabuss, B.M., J.O. Smith, and C.N. Satterfield. *Adv. Petrol. Chem. Refin.* 1964. 9. 158-201.

[6] Doue, F. and G. Guiochon. *Can. J. Chem.* 1969. 47. 3477-3480.

[7] Domine, F. *Energy & Fuels.* 1989. 3. 89-96.

[8] Domine, F. *Org. Geochem.* 1991. 17. 619-634.

[9] Mallinson, R.G. et al. *Ind. Eng. Chem. Res.* 1992. 31. 37-45.

1.18 THERMAL DECOMPOSITION OF *N*-ALKANES IN NEAR- AND SUPERCRITICAL REGIONS

This study is explained in detail in *Advanced Thermally Stable Jet Fuels Technical Progress Report, January – March 1995.*

Introduction

In previous reports, we presented experimental results from thermal decomposition of *n*-tetradecane in the near- and supercritical regions, using both the tubing bomb and glass tube reactors. We found that the experiments using the tubing bomb reactor underestimated rate constants while those with glass tube reactors produced kinetic parameters that closely agreed with the published values for thermal decomposition of long-chain alkanes. We concluded that the erroneous kinetic parameters obtained from tubing bomb reactor data resulted from uncontrolled mixing in the reactor, which includes a top stem with a lower temperature.

Our focus in this work was to extend the thermal decomposition studies using glass tube reactors to two other model compounds of petroleum-derived jet fuels—*n*-decane and *n*-dodecane. We also compared the results from the tubing bomb and glass tube reactors for *n*-tetradecane. The glass tube had not been completely evacuated before sealing, allowing small amounts of oxygen to remain in the sealed tube. We carried out experiments on *n*-tetradecane in tubing bomb reactors under nitrogen and air atmospheres to determine what effects oxygen had on thermal decomposition behavior.

Experimental

The *n*-decane, *n*-dodecane, and *n*-tetradecane, all with 99+% purity, were obtained from Aldrich and were used as received. The thermal reaction experiments of *n*-decane and *n*-dodecane were carried out using the glass tube reactors. The experimental procedures were presented in an earlier Technical Progress Report.[1] The thermal reaction experiments of *n*-tetradecane under both nitrogen and air atmospheres were carried out using the tubing bomb reactors. The experimental[2] and analytical procedures were used earlier and described in previous reports.[1]

Results

1. Kinetics of Thermal Decomposition of *n*-Decane and *n*-Dodecane. We determined that, for three different temperatures—400°, 425°, and 450°C—thermal decomposition can be represented by first-order kinetics. Based on our data, the apparent kinetic parameters for the thermal decomposition of *n*-decane and *n*-dodecane could be calculated using the Arrhenius law:

$$k = A\, e^{-Ea/RT} \qquad (1)$$

where E_a is the apparent activation energy and A is the pre-exponential factor. The estimated activation energies for *n*-decane and *n*-dodecane, as well a *n*-tetradecane, agreed with the value of 60±5 kcal/mol usually observed for the first-order reactions of long-chain alkane pyrolysis.[3]

We calculated the rate constants and used the least-squares method to determine its relationship with the carbon number at each of the three temperatures. At 400°, 425°, and 450°C, our respective rate constants were:

$$k = (0.00685n - 0.0343)\ h^{-1} \quad (2)$$

$$k = (0.04225n - 0.259)\ h^{-1} \quad (3)$$

$$k = (0.23727n - 1.6201)\ h^{-1} \quad (4)$$

We compared these with the findings of Tilicheev[4] and Voge and Good[5]. The differences in the three rate constants could be explained by differences in pressure. The pressures used in our work were in the range of 50-100 atmospheres, which falls between the ranges used by Tilicheev and by Voge and Good. Although first-order rate constants seemed to increase as pressure increased for the pressure range we used, we later found that that is not always the case.

2. Effects of Pressure on Conversion. We studied the effects of pressure in both the near- and supercritical regions, using different loading ratios to obtain different initial pressures. The experiments were carried out at 425°C for 15 minutes. For *n*-dodecane, the experiments were also carried out at 400°C for 60 minutes. Through these experiments, we determined that pressure has a significant effect on conversion in the near-critical region. For example, for thermal decomposition of *n*-dodecane at 400°C ($T_r = T/T_c = 1.022$) for 60 minutes, an increase in Pr from 1 to 1.5 resulted in a decrease in conversion from ≈5% to ≈3.5%. The significant changes in conversion fell in the near-critical region and did not extend to the supercritical region. At pressures greater than 1.5, the rate constants only exhibited a slight decrease with increased pressure. For *n*-decane, we found no large decrease in the rate constant with increased pressure from P_r = 1-1.5, because the reaction temperature was much higher than the critical temperature ($T_r = 1.130$).

After reviewing the literature on the subject, we concluded that the effects of pressure on the first-order rate constant for the thermal decomposition of alkanes are not only related to the structure of the compound, but also depend on the temperature and pressure ranges studied. The different or even inverse pressure dependence of the rate constant may result from different compound and/or different temperature or pressure range. We found that, while the rate constants for thermal decomposition of *n*-tetradecane under supercritical conditions decrease with increased pressure, the contrary may be true under subcritical conditions.

3. Comparison of the Results Obtained from Glass Tube Reactors and Tubing Bomb Reactors. The reaction rates we obtained from the glass tube reactor were much larger than those from the tubing bomb reactor. We believe that the lower rates in the tubing reactor experiments result from uncontrolled mixing in the tubing bomb reactor—the lower temperature at the top stem serves to lower the average temperature and, thus, underestimate rate reactions. Correcting for the effect of the top stem would be difficult; we merely assert that the resulting kinetic parameters may be misleading.

Examining the changes in *n*-alkane and 1-alkene, we note that the changes in product distributions with carbon number are sharper with the tubing bomb reactor than the glass reactor. The mole yields of all 1-alkene components were lower in the glass tube reactor. These results can also be explained by the top stem temperature difference. Because the higher pressure favors bimolecular hydrogen abstraction reactions and radical addition reactions, which enhance the yields of *n*-alkanes and depress the yields of 1-alkenes, the higher long-chain *n*-alkane yields and the lower 1-alkene yields are observed in the glass tube reactor. The sharper product distribution vs. carbon number curves in the tubing bomb reactor can also be attributed to the existence of the

low-temperature region in the top stem, which results in non-uniform distributions of the primary products, and to significant secondary reactions at higher conversions (≈25%). During the reaction, the light primary product stays longer in the low-temperature region in the top stem and, thus, undergoes fewer secondary reactions, while the heavier primary products stay mainly in the high-temperature region and undergo significant secondary reactions. This results in the sharper changes in product distribution vs. carbon number curves.

4. Effect of Oxygen on Thermal Decomposition. When we conducted experiments in tubing bombs under both nitrogen and air, using *n*-tetradecane as the reactant, there were no significant differences in the conversion or main product distributions between the nitrogen and air atmospheres. This did not, however, hold true for the level of deposit formation. The liquid products obtained from the different atmospheres exhibited very different appearances and we concluded that the presence of oxygen enhances deposit formation.[6]

---

[1] Schobert, H. H. et al. *Advanced Thermally Stable Jet Fuels, Technical Progress Report, July – September 1994.* The Pennsylvania State University. #92PC92104-TPR-9. 1994.

[2] Schobert, H. H. et al. *Advanced Thermally Stable Jet Fuels, Technical Progress Report, October – December 1993.* The Pennsylvania State University. #92PC92104-TPR-6. 1994.

[3] Fabuss, B. M., J. O. Smith, and C. N. Satterfield. *Adv. Pet. Chem. Refin.* 1964. 9. 157.

[4] Tilicheev, M. D. *Foreign Petro. Technol.* 1939. 7. 209.

[5] Voge, H. H. and G. M. Good. *J. Am. Chem. Soc.* 1949. 71. 593.

[6] Taylor, W. F. *Ind. Eng. Chem. Prod. Res. Dev.* 1974. 13. 133.

1.19 THERMAL DECOMPOSITION OF *N*-ALKANES IN NEAR CRITICAL AND SUPERCRITICAL REGIONS: PRODUCT DISTRIBUTIONS AND REACTION MECHANISMS

This study is explained in detail in *Advanced Thermally Stable Jet Fuels Technical Progress Report, April–4June 1995.*

Introduction

In Section 1.18, we presented some results from the thermal decomposition of *n*-alkanes in the near-critical and supercritical regions. We discussed the kinetics and the effects of pressure on conversion, compared the results obtained from glass tube reactors and tubing bomb reactors, and discussed the effect of oxygen on thermal decomposition. Here we summarize the product distributions and reaction mechanism for the thermal decomposition of *n*-alkanes.

Results and Discussion

In the following discussion, all the results were obtained from the experiments with the glass tube reactor, unless noted otherwise. The data from the tubing bomb experiments is identified as such.

1. Product Distributions. The product distributions were obtained from the thermal decomposition of *n*-C_{10}, *n*-C_{12}, and *n*-C_{14} under different loading ratios, temperatures, and conversions. All experiments were conducted using a fixed loading ratio of 0.36 except for those dealing with the effect of loading ratio.

The reaction products from thermal decomposition of C_{10}-C_{14} *n*-alkanes under the near-critical and supercritical conditions can be divided into two categories: those from the primary reactions and those from the secondary reactions of the primary products. The primary products included *n*-alkanes from C_1 to C_{m-2} (m = number of carbon atoms in the reactant) and 1-alkenes from C_2 to C_{m-1}. The secondary products included internal alkenes (mainly *cis*- and *trans*-2-alkenes), *n*-C_{m-1}, *n*-C_{m+1}, and C_{m+2} to C_{2m-2} normal and branched alkanes. There were also small amounts of cyclopentanes and cyclohexanes. The yields of branched alkanes that were lighter than the reactant were not significant until high conversion. The relative yields of the primary and secondary products were dependent on reaction conditions (loading ratio, temperature, and residence time or conversion).

The product distributions from the thermal decomposition of *n*-C_{10}, *n*-C_{12}, and *n*-C_{14} were very similar, so the following discussion on the effects of loading ratio, temperature, and conversion will focus only on *n*-C_{14}. The effects of chain length will be discussed at the end of this section.

Change in Overall Molar Yield with Loading Ratio from Thermal Decomposition of *n*-C_{14} at 425°C for 15 Minutes. As loading ratio increased, the overall yield of C_6-C_{13} *n*-alkanes increased and that of C_6-C_{13} 1-alkenes decreased. While the overall yield of C_6-C_{13} *n*-alkanes was lower than that of corresponding 1-alkenes at low loading ratio, their overall yield exceeded that of C_6-C_{13} 1-alkenes at high loading ratio. The overall yields of C_6-C_{12} 2-alkenes and C_{14}+ alkanes were low at low loading ratio, but their yields became significant as loading ratio increased. Because understanding the effects of pressure on the product distributions is beneficial, we plotted the product yields as functions of pressure. The plots showed that the

large changes in product distributions with pressure occurred in the near-critical region. This can be attributed to the large pressure dependence of density or concentration in this region, resulting in a significant change in reaction mechanism. Individual C_6-C_{13} *n*-alkanes and 1-alkenes exhibited similar changes in molar yields with loading ratio/pressure from the thermal decomposition of *n*-C_{14} at 425°C for 15 minutes.

Carbon Number Distributions as Functions of Loading Ratio from Thermal Decomposition of *n*-C_{14} in the Tubing Bomb Reactor at 425°C for 30 Minutes. As loading ratio increased, the yields of C_6-C_{13} *n*-alkanes increased and the yields of methane, ethane, and propane decreased. The yields of all olefinic components decreased as loading ratio increased. Among the gaseous products, the yields of C_2-C_3 gases decreased significantly while the yield of methane remained within a narrow range as loading ratio increased. The yield of methane was always lower than that of ethane and propane and the yield of ethylene was always lower than that of propylene in the range of loading ratio examined. At the lower loading ratio, the yields of ethane, propane, and propylene were high and equivalent, while those of methane and ethylene showed intermediate values. In the supercritical region (loading ratio > 0.15), ethylene was formed in the lowest yield compared to other gaseous products and very low ethylene yield was obtained at high loading ratio. The low ethylene yield indicates that the reaction mechanism under the conditions used in this study was different from that under low-pressure and high-temperature pyrolysis conditions, which give very high ethylene yield.

The major reaction products from *n*-C_{14} thermal cracking were *n*-alkanes with carbon number from C_1 to C_{m-3} and 1-alkenes with carbon number from C_2 to C_{m-2}. While *n*-C_{m-2}, *n*-C_{m-1}, and 1-C_{m-1} were also present in the products, their yields were considerably lower than those of the major products. The same applies for thermal decomposition of *n*-C_{10} and *n*-C_{12}.

Product Distribution as a Function of Carbon Number from the Thermal Decomposition of *n*-C_{14} at Two Temperatures and For Similar Conversions. At similar conversions, the formation of 1-alkenes is favored at the higher temperature, while the production of *n*-alkanes is facilitated at the lower temperature. The selectivity for *n*-alkanes is affected by temperature more significantly at higher conversion.

Effects of Conversion on the Overall Product Distributions from *n*-C_{14} Thermal Cracking at 425°C. The overall yields of C_6-C_{13} *n*-alkanes and C_{14}+ alkanes increased gradually, while the yields of C_6-C_{13} 1-alkenes decreased rapidly with increased conversion. The overall yield of C_6-C_{12} 2-alkenes increased quickly at lower conversion and then remained at a stable level as conversion increases. A similar change occurred in the molar yields of individual C_6-C_{13} *n*-alkanes and 1-alkenes with conversion from the thermal decomposition of *n*-C_{14} at 425°C.

Carbon Number Distributions of *n*-Alkane and 1-Alkene Products as Functions of Conversion from the Thermal Decomposition of *n*-C_{14} in the Tubing Bomb Reactor at 425°C. The relationship between the yield of liquid component and conversion is consistent with that observed in the glass tube reactor experiments—the higher the conversion, the higher the yields of C_6-C_{13} *n*-alkanes and the lower the yields of C_6-C_{13} 1-alkenes. The yields of C_1-C_3 gases decreased with increased conversion. In the conversion range examined, the yields of gaseous products decreased in the order of propane > propylene > ethane > methane > ethylene.

The Effect of Chain Length on the Product Distribution from the Thermal Decomposition of C_{10}-C_{14} *n*-Alkanes at 425°C for Similar Conversions. The yields of *n*-C_{m-1}, *n*-C_{m-2}, and 1-C_{m-1} were significantly lower than those of other *n*-alkane and 1-alkene products. The yields of individual *n*-alkane and 1-alkene with the same carbon number, except for *n*-C_{m-1}, *n*-C_{m-2}, and 1-C_{m-1}, increased as chain length decreased. This occurs because the number of components in the products from the thermal cracking of the lighter reactant is less than that from the heavier reactant. Therefore, at similar conversions the yield of the same component would be higher from the thermal cracking of the lighter reactant than from that of the heavier reactant.

2. Reaction Mechanism for Thermal Decomposition of *n*-Alkanes. The thermal decomposition of *n*-alkanes can be described by the free-radical mechanism. According to the product distributions and the changes in product composition with reaction conditions, the following mechanism has been developed for the thermal decomposition of *n*-alkanes under near-critical and supercritical conditions:

$$n\text{-}C_mH_{2m+2} \rightarrow R_i^{1\bullet} + R_j^{1\bullet} \quad (1)$$

$$R_i^{1\bullet} + n\text{-}C_mH_{2m+2} \rightarrow n\text{-}C_iH_{2i+2} + R_m^{x\bullet} \quad (2)$$

$$R_m^{x\bullet} \rightarrow R_m^{y\bullet} \rightarrow 1\text{-}C_kH_{2k} + R_n^{1\bullet} \quad (y\text{-}x \geq 4;\ 2 \leq k \leq m\text{-}1;\ n \leq m\text{-}2) \quad (3)$$

$$R_n^{1\bullet} + n\text{-}C_mH_{2m+2} \rightarrow n\text{-}C_nH_{2n+2} + R_m^{x\bullet} \quad (4)$$

$$R_n^{1\bullet} \rightarrow C_2H_4 + R_{n-2}^{1\bullet} \quad (3 \leq n \leq 5) \quad (5a)$$

$$R_n^{1\bullet} \rightarrow R_n^{x\bullet} \rightarrow 1\text{-}C_kH_{2k} + R_{n-k}^{1\bullet} \quad (n \geq 6;\ x \geq 5) \quad (5b)$$

$$R_n^{1\bullet} + 1\text{-}C_kH_{2k} \rightarrow R_{n+k}^{x\bullet} \quad (6)$$

$$R_m^{1\bullet} + 1\text{-}C_kH_{2k} \rightarrow R_{m+k}^{x\bullet} \quad (7a)$$

$$R_m^{x\bullet} + 1\text{-}C_kH_{2k} \rightarrow R_{m+k}^{b\bullet} \quad (x \neq 1) \quad (7b)$$

$$1\text{-}C_kH_{2k} \rightarrow 2\text{-}C_kH_{2k} \quad (8)$$

$$R_n^{1\bullet} + R_m^{x\bullet} \rightarrow \text{products} \quad (9)$$

where $R_n^{1\bullet}$ is the primary radical with a carbon number of n, $R_m^{x\bullet}$ is the primary or secondary parent radical with a free electron at site x of carbon skeleton, $R_{m+k}^{x\bullet}$ is the heavy normal alkyl radical, and $R_{m+k}^{b\bullet}$ is the heavy branched alkyl radical.

The initiation reaction occurs by homolytic carbon-carbon bond cleavage to produce two primary radicals (eq 1). These radicals then abstract hydrogen from surrounding reactant molecules to form various parent radicals (eq 2), of which most are secondary radicals, since the formation of a secondary radical by hydrogen abstraction requires a lower activation energy. The parent radical isomerizes and then decomposes by P-scission to form a 1-alkene and a lower primary radical (eq 3). This lower primary radical could undergo one of these reactions: hydrogen abstraction from the reactant molecule (eq 4), decomposition to form an 1-alkene and a smaller primary radical (eqs 5a and 5b), and, except for fairly low conversion, addition to the terminal carbon of a 1-alkene to give a higher radical (eq 6). For the radical with carbon number larger than five, isomerization occurs before decomposition. Under the conditions used, the following reactions also occur: the addition of a primary parent radical or a secondary parent radical to an 1-alkene to produce a heavy *n*-alkyl radical (eq 7a), or a heavy branched alkyl radical (eq 7b), and the double bond isomerization of 1-alkene to 2-alkene (eq 8). The termination reaction occurs mostly by the recombination of a lower primary radical and a parent radical (eq 9). The recombination reactions between lower primary radicals and between parent radicals are less important because of relatively low concentrations of the lower primary radicals and low oriented collision frequencies between the parent radicals.

The isomerization of the lower primary radicals, which are produced by the β-scission of the parent radicals (eq 3), only occurs as an intermediate step during their decomposition (eq 5b). This assumption is reasonable according to the observed product distributions. If the isomerization of these lower primary radicals occurred immediately after their formation, one would expect considerably more lower secondary radicals than lower primary radicals before they underwent further reactions, according to the R-K mechanism.[1] If this were the case, significant amounts of lighter branched alkanes ($< C_m$) would be present, in addition to heavy ones, because the addition reactions between these lower secondary radicals and 1-alkenes could also occur. Our results showed no significant amounts of lighter branched alkanes.

The final product distributions are dependent on the reaction conditions. At high temperatures and low pressures (low loading ratios), unimolecular radical decomposition reactions (eqs 5a and 5b) are favored over bimolecular reactions such as hydrogen abstraction (eq 4) and radical addition (eq 6) because of higher activation energies than bimolecular reactions and low reactant and product concentrations. At low temperatures and high pressures (high loading ratios), bimolecular reactions are favored over radical decomposition reactions. According to the elementary kinetic parameters given by Ranzi et al for the thermal decomposition of long-chain *n*-alkanes, the relative rates of radical decomposition to hydrogen abstraction can be estimated.[2] For a heavier primary radical in the system of *n*-C_{14} as a reactant, for example, the estimated rate parameters for β-scission are $A = 10^{14.0}$ 1/s and $E_a = 30.0$ kcal/mol, while those for hydrogen abstraction are $A = 10^{8.3}$ L/(mol s) and $E_a = 12.0$ kcal/mol. At 425°C and a loading ratio of 0.36, the rate ratio of radical decomposition to hydrogen abstraction would be 0.84:1. This means that about 54% of the larger primary radicals formed from β-scission of the parent radicals would tend to be stabilized by hydrogen abstraction from the surrounding reactant molecules rather than undergoing further decomposition. This would result in the formation of significant amounts of higher *n*-alkanes. Since the hydrogen abstraction would gradually be favored as loading ratio increases, the yields of higher *n*-alkanes would increase and, correspondingly, those of 1-alkenes would decrease with increased loading

ratio. Also, the depressed radical decomposition rate would result in lower yields of C_1-C_3 gases at a higher loading ratio.

The formation of C_{m+2} to C_{2m-2} heavy normal and branched alkanes clearly indicates that significant addition reactions between parental radicals and 1-alkenes occur. Ford found significant amounts of C_{18}-C_{30} branched and normal alkanes in the liquid-phase thermal decomposition of *n*-hexadecane.[3] Khorasheh and Gray observed similar results in a study of high-pressure thermal cracking of *n*-hexadecane.[4] Ford identified all heavy alkanes as alkyl hexadecanes and attributed their formation to the addition reactions between parent *n*-hexadecyls (secondary or primary) and 1-alkenes. The results obtained in this study are consistent with Ford's suggestion. For the thermal decomposition of *n*-C_{14} at 425°C for 15 minutes, the heavy alkanes with the same carbon number were composed of seven different compounds—one normal alkane and six alkyl tetradecanes with branches at sites 2 to 7 of the carbon skeleton. These were identified based on their retention orders by analogy with those reported by Ford. The seven different compounds were produced for each carbon number because there were only seven different C_{14} radicals. The C_{16} to C_{26} normal and branched alkanes are formed, because the addition reactions occur between primary and secondary C_{14} radicals and C_2 to C_{12} 1-alkenes, which are primary products of thermal decomposition. There are negligible amounts of C_{27} alkanes because of low concentration of 1-C_{13}.

In the reaction products from the thermal cracking of *n*-C_{10}, *n*-C_{12} and *n*-C_{14}, we also noted the presence of *n*-C_{m-1} and *n*-C_{m+1}. The same observation was made by Khorasheh and Gray in the high-pressure thermal decomposition of *n*-hexadecane.[4] The formation of *n*-C_{m-1} and *n*-C_{m+1} in the thermal cracking of *n*-C_m can be explained by the addition reactions between low primary radicals and 1-alkenes (eq 6). For example, the addition of 1-pentyl radicals to the terminal carbons of 1-C_{m-6} and 1-C_{m-4} results in the formation of secondary C_{m-1} and C_{m+1} radicals, which then abstract hydrogen atoms from surrounding reactant molecules to produce the corresponding *n*-alkanes.

The addition reactions between alkyl radicals and 1-alkenes have activation energies as low as 7 to 8 kcal/mol[5] and thus are favored at lower temperatures, such as those used in this study. As long as the concentrations of 1-alkenes reach some extent, this secondary reaction could occur significantly. Since the radical addition reactions are enhanced as loading ratio and/or conversion increases, because of increased 1-alkene concentrations, we would expect the yields of heavy normal and branched alkanes to increase with increased loading ratio and/or conversion.

The mole yields of C_6-C_{m-1} *n*-alkanes increase as conversion increases. The mole yields of C_6-C_{m-1} *n*-alkanes should decrease with increased conversion because of increased rates of addition reactions between C_6-C_{m-1} radicals and 1-alkenes (eq 6) (due to increased concentrations of 1-alkenes), and increased rates of addition reactions between parent radicals and 1-alkenes (eqs 7a and 7b). The latter factor would result in decreased formation of primary products (C_1 to C_{m-2} *n*-alkanes and C_2-C_{m-1} 1-alkenes) per 100 mol of reactant converted because the percent of parent radicals that cannot undergo decomposition would increase as conversion increases. One possible explanation for the increased molar yields of C_6-C_{m-1} *n*-alkanes with increased conversion is that addition reactions are heavily weighted toward small radicals and small 1-alkenes because of higher oriented collision frequencies.[6] As conversion increases, the addition rates between small radicals and small 1-alkenes would increase much faster than those between

larger radicals and larger 1-alkenes. As a result, the yields of higher *n*-alkanes (e.g., C_6-C_{13}) increase while those of lighter ones (C_1 to C_4) decrease with increased conversion. The other possible explanation is that the rates of hydrogen abstraction reactions (eq 4) increase as conversion increases. In the closed reactor, pressure would increase with increased conversion because of the increased product concentrations. Because pressure increase would increase the rate constant of bimolecular hydrogen abstraction reaction and suppress that of unimolecular radical decomposition, we would expect the yields of higher *n*-alkanes to increase and those of 1-alkenes and light *n*-alkanes to decrease with increased conversion.

The double bond isomerization, which results in the formation of 2-alkenes, can be explained by the following mechanism suggested by Shabtai et al:[7]

$$R\bullet + R'CH_2CH = CH_2 \rightarrow RH + R'\dot{C}HCH = CH_2 \quad (10)$$

$$R'\dot{C}HCH = CH_2 \leftrightarrow R'CH = CH\dot{C}H_2 \quad (11)$$

$$R'CH = CH\dot{C}H_2 + RH \rightarrow R'CH = CHCH_3 + R\bullet \quad (12)$$

Since the concentrations of C_6-C_{12} 1-alkenes increase as loading ratio or conversion increases, the mole yields of corresponding 2-alkenes would increase with increased loading ratio or conversion. Other internal alkenes can be formed by the similar mechanism. We can expect that after a certain conversion a balance would be reached so that the mole yields of 2-alkenes would no longer increase with further increases in conversion.

Although the mechanism we presented provides feasible explanations for the observed experimental results, we cannot easily estimate whole product distributions quantitatively because we do not know the kinetic parameters for secondary reactions. However, if we focus our attention on low conversions, we could predict primary product distributions because, in that case, we can neglect secondary reactions.

The following calculations were performed for the thermal decomposition of *n*-C_{14} at 425°C and at different loading ratios, on the basis of the method suggested by Fabuss et al.[8] To determine the distributions of initial C_{14} parent radicals, we assume that the activation energy for the formation of a secondary C_{14} parent radical is 2 kcal/mol lower than that for the formation of a primary C_{14} parent radical.[1] The C_{14} parent radicals initially formed are assumed to undergo isomerization in such a way that any radical can only isomerize into a free radical in which the radical position is four or more carbon atoms away from the original position. For example, the 2-tetradecyl radical can only isomerize into one of the radicals in which the radical positions can be found from 6 to 14. For the isomerization of the initial parent radicals, we assume that the secondary radicals are 4 kcal/mol more stable than the primary radicals.[1]

The various C_{14} parent radicals formed after isomerization can decompose by β-scission into a 1-alkene and a lower primary radical. When two positions are available for β-scission, the relative rates for rupture are assumed to be equal if both processes give ethyl or higher primary radicals. We assume that the rupture to yield a methyl radical requires an activation energy of 1.5 kcal/mol higher than the rupture to produce a higher primary radical.[2]

Under the conditions used in this study, some of the lower primary radicals formed from the decomposition of parent radicals would isomerize and then immediately decompose according to the rules used above. The remainder of the radicals would abstract hydrogen from surrounding reactant molecules to produce an *n*-alkane and a parent radical, because secondary reactions are negligible at low conversion. The relative rates of radical decomposition to hydrogen abstraction increase with increased radical size.[6] To account for observed product distributions, we assume that the rate ratio of radical decomposition to hydrogen abstraction doubles as the carbon number of the radical increases by one. For the thermal decomposition of *n*-C_{14} at 425°C and at a loading ratio of 0.357, this ratio is taken as one for C_{10} radicals. The rate ratio for other radicals can be calculated according to the same assumption. For the reactions carried out at other loading ratios, the rate ratio of decomposition to hydrogen abstraction for any radical can be obtained from the corresponding value at 0.357 loading ratio multiplied by a factor that is equal to 0.357 divided by the loading ratio examined. We assume that the small radicals formed from the decomposition of those lower radicals are stabilized by abstracting hydrogen from surrounding reactant molecules and no longer undergo further decomposition.

We compared the predicted product distributions by the method stated above with the experimental results from the thermal decomposition of *n*-C_{14} at 425°C for three different loading ratios and at lower conversions. Taking into account the assumptions made on the decomposition of those lower radicals, the agreement between predicted and experimental product distributions was quite satisfactory. In order to predict the product distributions at higher conversion, a much more sophisticated calculation is required because of significant secondary reactions.

---

[1] Kossiakoff, A. and F. O. Rice. "Thermal Decomposition of Hydrocarbons, Resonance Stabilization and Isomerization of Free Radicals." *Journal of American Chemistry Society.* 1943. 65. 590-595.

[2] Ranzi, E. et al. "Initial Product Distributions from Pyrolysis of Normal and Branched Paraffins." *Ind. Eng. Chem. Fundamentals.* 1983. 22. 132-139.

[3] Ford, T. "Liquid-Phase Thermal Decomposition of Hexadecane: Reaction Mechanisms." *Ind Eng. Chem. Fundam.* 1986. 25. 240-243.

[4] Khorasheh, F., and M. R. Gray. "High-Pressure Thermal Cracking of *n*-Hexadecane." *Ind. Eng. Chem. Res.* 1993. 32. 1853-1863.

[5] Allara, D. L. and R. A. Shaw. "Compilation of Kinetic Parameters for the Thermal Degradation of *n*-Alkane Molecules." *J. Phys. Chem. Ref. Data.* 1980. 9. 523-559.

[6] Dente, M. E. and E. M. Ranzi. "Mathematical Modeling of Hydrocarbon Pyrolysis Reactions." *Pyrolysis: Theory and Industrial Practice.* Albright, L. F., Crynes, B. L., Corcoran, W. H., Eds.; Academic Press: New York. 1983. 133-175.

[7] Shabtai, J., R. Ramakrishnan, and A. G. Oblad. "Hydropyrolysis of Model Compounds." Adv. *Chem. Ser.* 1979. 183. 297-328.

[8] Fabuss, B. M., J. O. Smith, and C. N. Satterfield. "Thermal Cracking of Pure Saturated Hydrocarbons." *Adv. Petro. Chem. Refin. 1964.* 9. 157-201.

1.20 High Temperature Cracking and Deposition Behavior of an *n*-Alkane Mixture

This study is explained in detail in *Advanced Thermally Stable Jet Fuels Technical Progress Report, October–December 1995.*

Introduction

The deposits that form in jet fuel at elevated temperatures can inhibit and degrade the performance of fuel lines, heat exchangers, nozzles and other aircraft systems. Two types of carbon deposits can form. Oxidative deposits form by autoxidation reactions at temperatures from 120° to 200°C. Pyrolytic deposits begin to form from the gas phase when the fuel begins to crack at temperatures above 450°C. The thermal cracking of jet fuel proceeds via a free radical mechanism which can lead to the formation of deposits.

A cost-effective model compound mixture was needed to study the chemical breakup of jet fuel at high temperatures and to enable us to observe the effects of thermal stabilizers on the fuel products. The many complex species found in jet fuel can often mask these effects. An *n*-alkane mixture, consisting of mainly dodecane, tridecane, and tetradecane, called Norpar-13 (from Exxon Corporation) was used in these experiments. Norpar-13 was both cost effective and allowed for comparison to past batch reactor work done with these alkanes.

Several compounds help increase the thermal stability of jet fuel in batch reactor tests at temperatures greater than 400°C. The stabilizers used in this study were tetrahydroquinoline (THQ), benzyl alcohol (BzOH), and tetrahydronapthalene (tetralin). These stabilizers donate hydrogen to react with the fuel radicals that form during thermal stressing. This hydrogen transfer helps to suppress the thermal decomposition of the fuel and inhibit the pyrolytic carbon deposition. We were also interested in the effects of these compounds at lower temperatures on oxidative deposition. In addition, the effects of a dispersant additive, Betz SPEC-AID 8Q405, used to eliminate thermal oxidative deposition, was examined in the Norpar under pyrolytic deposition conditions.

Experimental

Experimental details were provided in the corresponding Technical Progress Report.[1]

Results

Norpar-13 was found to be a useful model solvent in observing the effects of high temperature stressing of jet fuels. Norpar was both stable in the oxidative regime and increased the amount of pyrolytic deposition detected. The increased pyrolytic deposits simplified observation of the mitigation effects of the additives, compared to attempts to observe the same effects in a jet fuel. The effects of stabilizers on the liquid products could be determined and results could be related to prior work done with single model compounds such as dodecane and tetradecane.

Tetrahydroquinoline, benzyl alcohol, and tetralin all increased the thermal stability of Norpar-13 under flow reactor conditions. THQ was observed to increase the pyrolytic stability the most, as was seen in batch reactor tests. However, an adverse oxidative deposit formed from

the addition of THQ. Nitrogen-saturating the Norpar-13 caused increased deposits and eliminated the benefits from THQ and tetralin. Species formed by air in the Norpar, oxygen functionalities formed by the addition of BzOH, and components within jet fuel could all contribute to increasing the pyrolytic stability.

---

[1] Schobert, H. H. et al. *Advanced Thermally Stable Jet Fuels, Technical Progress Report, October – December 1995.* The Pennsylvania State University. #92PC92104-TPR-14. 1996.

1.21 THERMAL DECOMPOSITION OF NORPAR-13 UNDER SUPERCRITICAL CONDITIONS

This study is explained in detail in *Advanced Thermally Stable Jet Fuels Technical Progress Report, October–December 1995.*

Introduction

Our previous studies of the thermal decomposition of pure normal alkanes, namely *n*-C_{10}, *n*-C_{12}, and *n*-C_{14}, under supercritical conditions found that the thermal decomposition can be well-represented by first-order kinetics.[1,2] Pressure has significant effects on the first-order rate constant and product distribution in the near-critical region. The major products are a series of *n*-alkanes and 1-alkenes. The relative yields of *n*-alkanes and 1-alkenes depend on the reaction conditions. The observed product distributions and changes in product composition with reaction conditions were explained by a modified free-radical mechanism.

In this work, the thermal decomposition of a mixture of *n*-alkanes, Norpar-13, was studied under supercritical conditions. The thermal stressing experiments were carried out at 425 °C in a glass tube reactor and at 450 °C in a tubing bomb reactor.

Results and Discussion

Norpar-13 is composed of *n*-C_{11} (0.43 wt%), *n*-C_{12} (12.59%), *n*-C_{13} (50.80%), *n*-C_{14} (35.71%), *n*-C_{15} (0.41%), and a small amount of impurities. We calculated the overall conversion of Norpar-13 as follows:

$$x = (y_{12}^\circ \times x_{12} + y_{13}^\circ \times x_{13} + y_{14}^\circ \times x_{14}) / (y_{12}^\circ + y_{13}^\circ + y_{14}^\circ) \qquad (1)$$

where y_{12}°, y_{13}°, and y_{14}° were molar fractions of *n*-C_{12}, *n*-C_{13}, and *n*-C_{14} in Norpar-13 and x_{12}, x_{13} and x_{14} were apparent individual conversions for *n*-C_{12}, *n*-C_{13}, and *n*-C_{14}, respectively.

Changes in Conversions with Loading Ratio from the Thermal Decomposition of Norpar-13 at 425 °C for 15 Minutes. As loading ratio increased, the conversion of *n*-C_{12} decreased, while the conversion of *n*-C_{14} first increased and then decreased. The conversion of *n*-C_{13} remained almost unchanged before 0.25 loading ratio and then decreased with loading ratio. The compound with a longer chain has a higher conversion in the mixture. Individual compounds seem to interact with each other in the mixture thermal reaction.

The conversions for the thermal decomposition of *n*-C_{12} in Norpar-13 are similar to those for the decomposition of pure *n*-C_{12}. However, the conversions of *n*-C_{14} decrease from 10–12% (depending on loading ratio) in the thermal decomposition of pure compound at 425 °C for 15 minutes to 6–7% in the thermal reaction of Norpar-13 at similar conditions. This indicates significant inhibition of the heavier alkane by the lighter alkane.

Changes in Conversions of *n*-C_{12} and *n*-C_{14} with Reaction Time from the Thermal Decomposition of the Pure Compound and Norpar-13. The conversions for the thermal decomposition of *n*-C_{14} in Norpar-13 were lower than those obtained for the decomposition of pure *n*-C_{14}. We concluded that the real conversions for the decomposition of *n*-C_{12} in Norpar-13 could be larger than those obtained for the decomposition of pure *n*-C_{12}, because some portion of remainder *n*-C_{12} after reaction resulted from decomposition of *n*-C_{13} and *n*-C_{14}. The initial amount of *n*-C_{12} in Norpar-13 was only about 13%, while the total amount of *n*-C_{13} and *n*-C_{14}

was above 86%, indicating that the amount of *n*-C_{12} from the decomposition of *n*-C_{13} and *n*-C_{14} could be significant.

Conversions for the thermal decomposition of *n*-C_{12} and *n*-C_{14} in JP-8P were much lower than those obtained for the decomposition of pure compounds. This results from the fact that JP-8P contains significant amounts of cycloalkanes and aromatics which inhibit the decomposition of *n*-alkanes.

Changes in Molar Yields of C_6-C_{10} *n*-Alkanes and 1-Alkenes with Reaction Time from the Thermal Decomposition of Norpar-13 at 425 °C for Two Different Loading Ratios. The yield decreased as chain length increased. While the yields of *n*-alkanes slightly increased, those of 1-alkenes decreased with increased reaction time. The reaction with the higher loading ratio gave higher *n*-alkane yields and lower 1-alkene yields than that with the lower loading ratio, indicating increased rates of hydrogen abstraction and radical addition reactions with increased loading ratio.

Changes in Product Yields with Reaction Time from the Thermal Decomposition of Norpar-13 at 450 °C in the Tubing Bomb Reactor for Two Different Loading Ratios. The molar yields of both C_7-C_{10} *n*-alkanes and 1-alkenes decreased with increased reaction time, indicating significant secondary reactions at higher temperature and longer reaction time. Among the gaseous products, the yields of hydrogen, methane, ethane, and propane increased while the yields of ethylene and propylene decreased as reaction time increased. The yields of benzene, toluene, *m*-xylene and *o*-xylene (BTX) steadily increased with increased reaction time.

Comparing the product distributions from two different loading ratios revealed that the higher loading ratio gave higher yields of *n*-alkanes and lower yields of 1-alkene, BTX ,and gases. This is caused by bimolecular reactions, such as hydrogen abstraction and radical addition, which are favored over radical decomposition reactions at high loading ratio (high pressure). The increased hydrogen abstraction rate increases the formation of *n*-alkanes and the increased radical addition rate suppresses the production of 1-alkenes. Also, the depressed radical decomposition rate results in lower gaseous yields at higher loading ratio. Because monoaromatics, such as BTX, are produced from the reactions of 1-alkenes, their yields are lower at higher loading ratio because of lower 1-alkene yields. The monoaromatics undergo further reactions to form polyaromatics, which are the precursors for the deposit formation, leading us to conclude that the deposit formed at higher loading ratio would be lower than that formed at lower loading ratio. This was the case. For example, the amounts of the deposits from the thermal decomposition of Norpar-13 at 450 °C for 5 hours were 2.4, 2.0, and 1.4% of the feeds for the three different loading ratios, 0.14, 0.25, and 0.36 respectively.

---

[1] Schobert, H. H. et al. *Advanced Thermally Stable Jet Fuels, Technical Progress Report, January - March 1995*. The Pennsylvania State University. 1995.

[2] Schobert, H. H. et al. *Advanced Thermally Stable Jet Fuels, Technical Progress Report, April - June 1995*. The Pennsylvania State University. 1995.

1.22 PYROLYSIS OF ALKYLCYCLOHEXANES AT 450°C AND ELEVATED PRESSURE: PRODUCT DISTRIBUTION AND REACTION MECHANISMS.

This study is explained in detail in *Advanced Thermally Stable Jet Fuels Technical Progress Report, April–June 1993.*

Introduction

Future jet fuels can derive from hydrocarbon resources such as coal, oil shale, and tar sands, as well as from petroleum. These fuels tend to have very different compositions. Lai and Song[1] characterized two JP-8 jet fuel samples, a coal-derived JP-8C and a petroleum-derived JP-8P. They found that coal-derived JP-8C fuel has a significantly different molecular composition than petroleum-based JP-8P. JP-8P is rich in long-chain alkanes (≈61%) ranging from C_8 to C_{17}, with major components in the range of C_{10} to C_{15}, and contains alkylcyclohexanes that account for about 14% of JP-8P. In contrast, JP-8C, which is derived from hydrotreating coal liquids produced as by-products from coal gasification, is composed mainly of monocyclic and bicyclic alkanes, and hydroaromatic compounds. The dominant compounds in JP-8C are alkyl-substituted cyclohexanes (≈40%) and decalins; long-chain alkanes only account for about 10% of JP-8C. Unlike JP-8P, the low-boiling components are abundant in JP-8C. For example, cyclohexane and C_1- to C_2-substituted cyclohexanes are the dominant components in JP-8C, accounting for about 22% of JP-8C. Most of the cyclohexanes in JP-8P are C_3- to C_6-substituted cyclohexanes.

The study of model compounds helps to clarify the chemistry of pyrolytic degradation and mechanisms of solid formation, enabling the stability of jet fuels to be enhanced through optimized fuel composition. Our work focused on the pyrolytic thermal stability study of alkylcyclohexanes. The results concerning the pyrolysis of model long chain compounds (tetradecane) and the effects of hydrogen-donors on the fuel stability were described by Song et al.[2]

Results and Discussion

1. Decomposition rate constant. **Figure 1.22-1** shows representative system time-pressure profiles during pyrolysis of three model compounds—cyclohexane (CH), ethylcyclohexane (ECH), and *n*-butylcyclohexane (BCH)—at 450°C under initial N_2 pressure (cold) of 0.69 MPa. The pyrolysis was conducted in a static apparatus (25 mL tubing bomb) using a 5 mL sample. The volume ratio of sample to reactor is kept constant (about 1/5), which implies that the initial reactant concentrations in the reactor are different for the hydrocarbon reactants studied.

For example, the initial reactant concentrations are approximately 1.81×10^{-3} mol/mL, 1.41×10^{-3} mol/mL, and 1.15×10^{-3} mol/mL, for CH, ECH, and BCH, respectively. The different initial concentrations are reflected in the early-stage time-pressure profiles. Figure 1.22-1 shows that the system pressure quickly increases to 4.5 MPa, 3.9 MPa, and 3.2 MPa, for CH, ECH, and BCH, respectively, in 5 min when the hydrocarbon liquids reach an equilibrium boiling state. The system pressure then increases with increasing residence time, under different pressure increase rates that are dependent on the sample type. The system pressure for the pyrolysis of CH remained nearly constant after the initial increase; on the other hand, the pressure increased steadily for ECH and BCH. The monotonic pressure increase indicates continuous hydrocarbon decomposition to smaller compounds.

The results of detailed product analysis for the pyrolysis of CH, MCH, and ECH were reported in **Table 1.22-1**, where only major individual reaction products and product groups were presented. The hydrocarbon products were expressed as molar percentage of the initial amounts of reactants (cyclohexane, methylcyclohexane, or ethylcyclohexane). Similarly, **Tables 1.22-2** and **1.22-3** provide the molar yields of products from the pyrolysis of other alkylcyclohexanes (PCH, BCH, HCH, OCH, and DCH). The products include C_1-C_4 gaseous yields and liquid yields such as alkanes, alkenes, cycloalkanes, cycloalkenes, benzenes, and naphthalenes.

Hydrocarbon pyrolysis at elevated pressure is very complex kinetically. The thermal decomposition, in general, can be approximated by a first-order relation, although self-acceleration and self-inhibition are not uncommon[3]. The first-order rate equation can be expressed as shown in Equation (1).

$$-\frac{dC}{dt} = kC \qquad (1)$$

where C is the reactant concentration, t is the reaction time, and k is the first-order rate constant. The rate equation can be solved for the rate constant, and expressed as a function of the reactant conversion (α, the fraction of reactant reacted), as shown in Equation (2).

$$k = \frac{1}{t} \ln \frac{1}{1-\alpha} \qquad (2)$$

The preheat time (from room temperature to the reaction temperature, 450°C) is 4–6 minutes, and has to be accounted for in calculating an adjusted (effective) reaction time. **Table 1.22-4** presents the calculated pseudo-first-order rate constants using least-squares regression[4]. **Figures 1.22-2** and **1.22-3** compare the experimental reactant conversions to the values predicted from the rate constants in Table 1.22-4 for two compounds, PCH and OCH. The line corresponding to exact agreement is drawn as a diagonal. The predicted and experimental conversions closely agree for both PCH and OCH.

Fabuss et al[5, 6] used an empirical group contribution method to develop an empirical equation to correlate molecular structure and the first-order rate constant for cyclic saturated hydrocarbons decomposed at 427°C and elevated pressures. They used a characterization number, n, to represent the molecular structure. The characterization number depends on the basic ring structure and the type of side chains. Their correlation is shown as Equation (3).

$$k = 0.044 - 0.0114\,n + 0.00008\,n^2 \qquad (3)$$

Fabuss et al cautioned that this equation was probably less reliable for alkyl side chains longer than C_4.

We used a similar approach and developed a correlation for alkylcyclohexanes (up to DCH). The characterization numbers of cyclohexanes studied in our work are also shown in Table 1.22-4. **Figure 1.22-4** presents the experimental rate constants of alkylcyclohexanes at 450°C as a function of characterization number (n) of molecular structure. The data were fitted to a second-order polynomial as shown in Equation 4.

$$k = -0.151 + 0.00875\,n + 0.000426\,n^2 \qquad (4)$$

Statistical measures indicate that Equation 4 is adequate and useful for estimating decomposition rate constants for cyclohexane and C_1- to about C_{10}-cyclohexanes stressed at 450°C in a batch reactor with volume ratio of sample to reactor about 1/5.

2. Pyrolysis products and Reaction Mechanisms. The data in Tables 1.22-1 through 1.22-3 reveals several trends regarding the relative product distribution for alkylcyclohexanes with various side-chain length:

a) The yields of isomerization products (cyclopentanes) from cyclohexanes decrease with increasing side-chain length.

b) For the pyrolysis of alkylcyclohexanes with alkyl ≥ C_4-, at early decomposition stage (i.e., at low conversion level), the major six-membered ring products are cyclohexane, methylenecyclohexane, and cyclohexene. The primary reaction pathway seems to result in major product pairs. For example, pyrolysis of OCH results in cyclohexane plus 1-octene, methylenecyclohexane plus *n*-heptane, cyclohexene plus *n*-octane, and methylcyclohexane plus 1-heptene. Other product pairs (e.g., *n*-alkanes plus cyclohexylalkenes and 1-alkenes plus alkylcyclohexanes) were also produced, but in lower yields.

c) The yields of unsaturated compounds such as cyclohexene tend to increase to a maximum, then decrease with time.

d) There is an induction period for the formation of aromatic compounds such as benzenes and naphthalenes.

Figure 1.22-5 presents the cyclohexane selectivity to major products at 450°C for 4 hours, which has a cyclohexane conversion of 5.0%. The product selectivity was defined as the ratio of a product's molar yield to the conversion of reactant. At the conversion level of 5.0 mol%, the major products are methylcyclopentane (4.2 mol%), hydrogen (1.1 mol%), and cyclohexene (0.35 mol%). Apparently, methylcyclopentane, an isomerization product, is the most abundant product and accounts for 83% (selectivity) of the pyrolysis molar yields. The pyrolysis of cyclohexane has been studied extensively under high temperatures (above 600°C). Billaud et al[7] compiled cyclohexane pyrolysis literature after 1960 that demonstrated that the thermal decomposition of cyclohexane under high temperatures led to 1-hexene, cyclohexene, and the lighter cracking products, such as hydrogen; methane; acetylene; ethylene; ethane; propene; 1,3-butadiene; and 1-butene. Few studies since then have shown such a significant selectivity (83%) to methylcyclopentane as our study did. Based on the identified product distribution, the possible reaction mechanisms for major pyrolysis products of cyclohexane were proposed as shown in **Scheme I**.

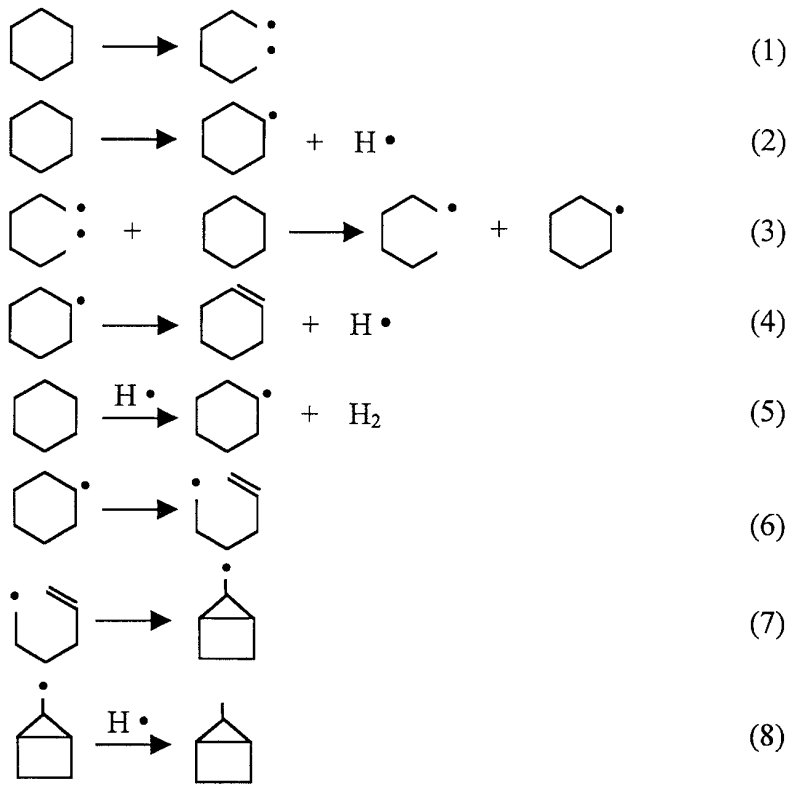

Scheme I. Possible Mechanisms for Major Pyrolysis Products of Cyclohexane

The pyrolysis of cyclohexane proceeds by radical reaction pathways. The reaction mechanisms consist of initiation (paths 1 and 2), propagation (paths 2–7), and termination (path 8). The mechanisms in Scheme I are for major products and, thus, are just a part of more complete mechanisms. The main initiation process is believed to proceed through ring-opening with the formation of *n*-hexyl diradical (path 1), and path 2 is the minor initiation process. This can be reasoned from the bond dissociation energies; the breaking of the C-H bonds require an energy of 95.5 kcal/mole,[8] whereas breaking the C-C bonds only requires 77 kcal/mole.

The *n*-hexyl diradical then abstracts hydrogen from cyclohexane and forms cyclohexyl radical and 1-hexyl radical (path 3). The cyclohexyl radical then proceeds to form cyclohexene through decomposition (path 4). Hydrogen and more cyclohexyl radicals are formed through hydrogen transfer reaction (path 5). The 5-hexenyl radical formed from cyclohexyl radical through path 6; the intramolecular hydrogen transfer (ring closure) of the former results in the formation of methylcyclopentyl radical (path 7). The rate constant for the ring closure process (path 7) is $k = 1.0 \times 10^5\ s^{-1}$ at 25°C with E_a=6.1 kcal/mole.[9] Methylcyclopentane was formed in path 8 through hydrogen transfer. The formation of methylcyclopentane from intermediate 5-hexenyl radical has been reported by Lamb et al,[10] Lal et al,[11] and March.[12] The rules for ring closure were reported by Baldwin and co-workers.[13, 14, 15, 16] It was reported that both five- and six-membered rings may form from radicals containing a 5,6 double bond, but in general the

five-membered rings (exo addition) are more favored, as a result of more favorable entropy and stereoelectronic factors than the larger, six-membered rings (endo addition).

Figure 1.22-6 presents the methylcyclohexane selectivity to major products at 450°C for 4 hr, which has a conversion of 12%. The major products are methane (7.5 mol%), dimethylcyclopentanes (5.1 mol%), hydrogen (3.2 mol%), ethylcyclopentane (1.2 mol%), cyclohexene (0.95 mol%), and methylcyclopentene (0.74 mol%). Similar to the pyrolysis of cyclohexane, isomerization products (now dimethylcyclopentane and ethylcyclopentane) are still the major products; however, methane becomes the most abundant product. The pyrolysis of methylcyclohexane also proceeds by radical reaction pathways, and its mechanisms are similar to those of cyclohexane. However, for methylcyclohexane, the initiation process now proceeds through more paths. Two of them are believed to be the major paths and have comparable rates [i.e., ring-opening with the formation of methylhexyl diradical (path1), and the homolytic cleavage of the C-C bond between the ring and the side-chain to form methyl and cyclohexyl radicals (path 2)]. The formation of methyl radical may partly account for the abundant CH_4 yield. Other initiation processes include abstraction of the single hydrogen atom attached to the cyclohexyl carbon bearing the methyl group (path 3), and abstraction of the hydrogen atom on the methyl side chain (path 4). The former abstraction step produces a relatively more stable tertiary MCH radical and the latter leads to less stable primary MCH radical.

Figure 1.22-7 shows the product distribution from ECH pyrolysis at 450°C as a function of conversion. Methane and ethane are the most abundant products through the entire pyrolysis period; the ECH selectivities to methane and ethane range from about 0.4 to 0.6. The selectivity of ECH to the 5-membered ring isomerization product, C_3-cyclopentane, is about 0.14–0.19 for the first 4 hour and drops to 0.1 at 8 hour stressing. It is clear from Tables 1.22-1 and 1.22-2 that the selectivity of cyclohexanes to the corresponding five-membered ring isomerization product, cyclopentane, decreases with increasing side-chain length.

Another important point regarding alkylcyclohexanes (C_2- to about C_{10}-cyclohexane) is that, in general, alkylcyclohexanes with a longer side-chain seem to have higher molar yields of methylcyclopentane as shown in **Figure 1.22-8**, which presents the temporal methylcyclopentane yield for the pyrolysis of ECH, PCH, BCH, and OCH, at 450°C. The exception is that PCH and BCH have similar methylcyclopentane yields. Figure 1.22-8 also shows that the methylcyclopentane yield increases with time; this implies that methylcyclopentane is mainly a primary product from the ring-closure process of the 5-hexenyl radical as shown in Scheme I.

Figure 1.22-9 shows the *n*-butylcyclohexane selectivity to major products at 450°C for 0.2 hr, which has a conversion of 4.0%. The primary reaction pathway for the pyrolysis of *n*-butylcyclohexane seems to result in five major product pairs at an early decomposition stage; the preference for certain product pairs formation allows proposing the possible reaction mechanisms. The possible reaction mechanisms based on the identified products were presented as shown in **Scheme II**. The mechanisms were based on the discussion of BCH pyrolysis and can be generalized and applied to other alkylcyclohexanes.

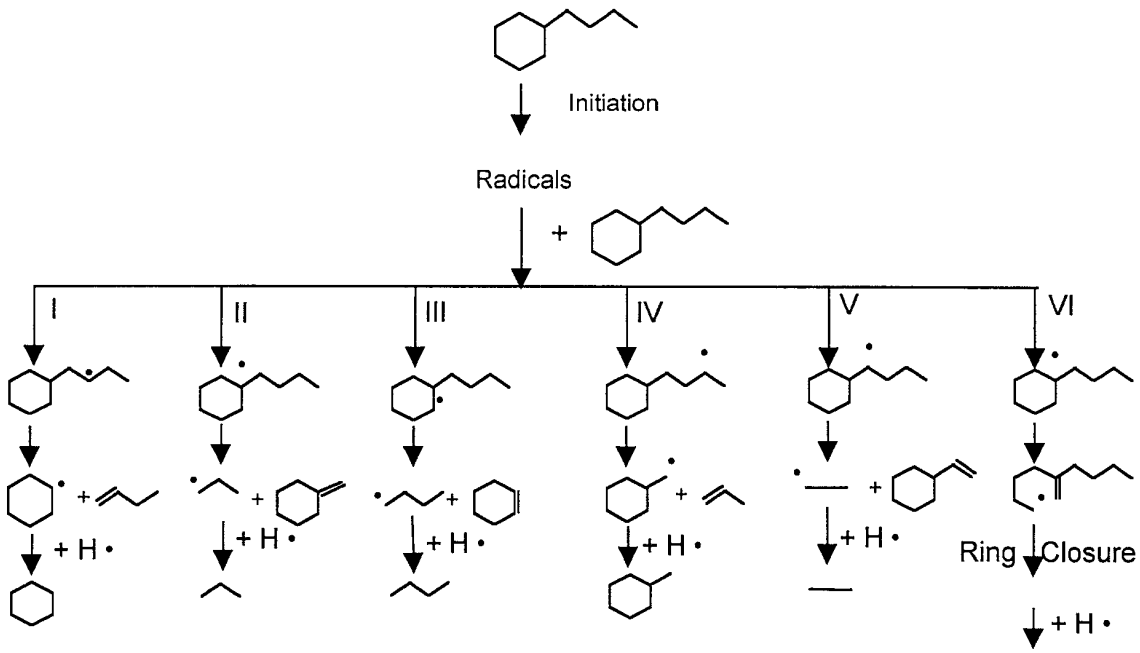

Scheme II. Possible Mechanisms for Major Products of *n*-Butylyclohexane

The pyrolysis of *n*-butylcyclohexane starts with an initiation reaction, followed by propagation and termination pathways. The initiation processes likely include:

2. The cleavage of the C-C bonds on the side chain especially the β and γ bonds (and δ bonds for longer side-chain); however, the homolytic cleavage of the C-C bond between the ring and the side-chain (α bond) to form cyclohexyl and 1-butyl radicals is less favorable because of higher bond energy
3. The cleavage of the C-H bonds on the side chain

The propagation pathways involving β-scission and H-transfer were given in Scheme II.

The formation of the five-pair major initial products can be rationalized by the radical reaction pathways I-V. Note that ring-opening process was also included as pathway VI in Scheme II to account for the formation of 5-membered ring compounds. Pathway VI in Scheme II is similar to paths 6-8 of Scheme I for cyclohexane. We can see from **Figure 1.22-10**, which presents product distribution for BCH pyrolysis, that after 1 hour at 450°C, the yields of methylenecyclohexane and ethenylcyclohexane begin to decrease with increasing residence time, presumably due to hydrogenation to form methylcyclohexane and ethylcyclohexane, respectively. Cyclohexane and methylcyclohexane become the two most predominant liquid products after 2.5 hour stressing. These results suggest that pathways I and IV dominate in long-duration BCH pyrolysis. Cyclohexene is the most abundant liquid yield followed by cyclohexane and methylcyclohexane. Methylenecyclohexane is only a minor product in this case. The preference for cyclohexene formation indicates that the reaction via cyclohexyl radical is a major path, similar to path III in Scheme II, and the low methylenecyclohexane yield indicates that one of the major pathways for *n*-BCH becomes a minor one for ECH.

Figure 1.22-11 presents product distribution for PCH pyrolysis. At a low conversion level (3.4%), PCH has high selectivity to cyclohexane (0.22), methylenecyclohexane (0.14), and cyclohexene (0.12). The molar yields of methylenecyclohexane and cyclohexene reach a maximum at the conversion level of approximately 0.39 (after 2.5 hour stressing). On the other hand, the molar yield and selectivity of cyclohexane and methylcyclohexane increase monotonically with heating time. After 4 hour stressing (PCH conversion = 0.65), the yield and selectivity of cyclohexane are 19.5 mol% and 0.30, respectively.

Examining the results of ECH, PCH, and BCH at a low conversion level, we can make the following observations:

a) For ECH pyrolysis, the pathway to cyclohexene is favored, followed by cyclohexane and MCH, and the yield of methylenecyclohexane is low.

b) For BCH pyrolysis, the pathways to cyclohexane and methylenecyclohexane are favored (selectivity ≈ 0.2), followed by cyclohexene, MCH, and ethenylcyclohexane (selectivity of approximately 0.12, 0.08, and 0.07, respectively).

c) For PCH pyrolysis, the reaction mechanisms are more like those for BCH than those for ECH. For example, at the PCH conversion level of 7.1%, the pathway to cyclohexane is highly favored (selectivity ≈ 0.29), followed by methylenecyclohexane and cyclohexene (selectivity ≈ 0.16). The high selectivity of methylenecyclohexane is a characteristic of alkylcyclohexane with a long side chain such as BCH. The early selectivity to MCH is low (≈ 0.02).

d) The yields of 5-membered ring isomerization products (alkylcyclopentanes) from cyclohexanes decrease significantly with increasing side-chain length (e.g., unlike the pyrolysis of cyclohexane and methylcyclohexane, which has very high selectivity to alkylcyclopentanes, the selectivity to isomerization products from ECH and PCH is low—0.14 and 0.08, respectively).

Figure 1.22-12 presents the OCH selectivity to major products at 450°C for 0.2 hour, which has an OCH conversion of 9%. Like the pyrolysis of BCH, methylenecyclohexane and cyclohexane have the highest selectivity (approximately 0.17 and 0.14, respectively) followed by cyclohexene (selectivity ≈ 0.09) and other minor products such as MCH, ethenylcyclohexane, and 3-butenylcyclohexane (selectivity ≈ 0.04–0.05). The pathways to produce cyclohexylalkenes such as 3-butenylcyclohexane and 4-pentenylcyclohexane are similar to and can be generalized from pathway V in Scheme II. **Figure 1.22-13** presents the DCH selectivity to major products at 450°C for 0.2 hr, which has a DCH conversion of 17%. The product selectivity distribution is quite similar to that of BCH and OCH. For pyrolysis of alkylcyclohexanes with long side-chain such as OCH and DCH, the selectivity to individual products was all reduced. This can be rationalized from the production of more minor products through pathway V in Scheme II.

Table 1.22-1. Molar Yields of Products from the Pyrolysis of Cyclohexane, Methylcyclohexane, and Ethylcyclohexane at 450°C under Initial 0.69 MPa N_2

Reactant Name	CH	MCH	ECH	ECH	ECH	ECH	ECH	ECH	ECH
Reactant (mmole)	45.37	39.06	35.29	35.17	35.21	35.24	35.29	35.57	35.52
Reactant (g)	3.811	3.828	3.952	3.939	3.944	3.947	3.952	3.984	3.978
Experimental No.	TS91	TS92	AS1	AS2	AS3	TS43	TS60	TS65	TS73
Residence time[a]	4 hr	4 hr	0.2 hr	0.5 hr	1 hr	1 hr	2.5 hr	4 hr	8 hr
Product	molar yield (%)[b]								
Hydrogen	1.07	3.20		0.68	1.29	1.08	2.40	3.58	8.89
Methane	0.21	7.46	1.83	2.93	5.05	4.09	8.67	14.16	37.88
Ethylene	0.04	0.14	0.30	0.40	0.54	0.40	0.79	0.67	0.53
Ethane	0.09	0.65	1.20	1.88	3.29	3.57	6.97	11.88	32.97
Propene	0.05	0.32	0.03	0.04	0.10	0.15	0.28	0.48	0.69
Propane	0.03	0.31	0.05	0.08	0.18	0.24	0.62	1.78	5.17
1-Butene	0.08	0.47	0.00	0.01	0.05	0.05	0.17	0.49	0.46
n-Butane	0.00	0.10		0.00	0.07	0.05	0.15	1.05	1.74
Pentenes (mainly 2- and 3-)		0.11	0.03	0.06	0.14	0.15	0.22	0.58	0.77
n-Pentane		0.03				0.00	0.08	0.42	1.08
1-Hexene	0.04	0.03							
n-Hexane	0.01		0.05	0.05	0.05	0.07	0.08	0.18	0.47
Cyclohexene	0.35	0.95	0.56	1.12	2.01	1.83	3.75	4.43	1.53
Cyclohexane	94.97	0.28	0.18	0.39	0.76	0.72	2.04	3.89	8.91
Methylcyclohexene		0.35		0.06	0.12	0.07	0.14	0.60	0.40
Methylenecyclohexane		0.08	0.19	0.17	0.24	0.17	0.27	1.18	1.49
1-Methylcyclohexene		0.59	0.27	0.66	1.21	0.85	1.64	2.81	0.93
Methylcyclohexane		88.12	0.42	0.43	0.46	0.48	1.07	1.89	5.08
C_2-cyclohexene			0.10	0.19	0.31	0.28	0.77	1.01	0.79
Ethylcyclohexane	0.03		97.10	94.81	91.23	92.39	82.64	66.26	37.00
C_3-cyclohexane		0.08	0.05	0.05	0.05	0.03	0.03	0.05	0.06
n-Propylcyclohexane	0.02						0.08	0.10	0.22
C_4-cyclohexane				0.02	0.02	0.02	0.33	0.34	0.62
C_5-cyclohexane							0.04	0.09	0.16
Cyclopentene	0.04	0.11							
Methylcyclopentene		0.74							
Methylcyclopentane	4.18	0.08	0.08	0.13	0.23	0.25	0.57	1.32	4.16
Dimethylcyclopentane		5.05							
Ethylcyclopentane		1.18							
C_3-cyclopentane			0.41	0.93	1.64	1.07	2.46	6.27	6.22
Benzene		0.12			0.04	0.04	0.40	1.11	4.21
Toluene		0.09			0.13	0.13	0.54	2.06	5.73
C_2-benzene							0.19	0.47	3.00
C_3-benzene							0.07	0.28	1.27
C_4-benzene								0.05	0.31
Indan							0.01	0.04	0.29
Methylindan								0.06	0.60
C_2-indan								0.04	0.18
Naphthalene							0.02	0.03	0.37
Methylnaphthalene							0.02	0.05	0.46
C_2-naphthalene								0.02	0.12
(Alkyl-)bicyclohexyl							0.15	0.19	0.15

a) Pyrolysis of 5 ml reactant in 25 ml reactors plunged into the sandbath preheated to 450°C.
b) The molar yield based on initial reactants (cyclohexane, methylcyclohexane, or ethylcyclohexane).

Table 1.22-2. Molar Yields of Products from the Pyrolysis of *n*-Propylcyclohexane and *n*-Butylcyclohexane at 450°C under Initial 0.69 MPa N_2 (Cold)

Reactant Name	PCH	PCH	PCH	PCH	PCH	BCH	BCH	BCH	BCH	BCH	BCH
Reactant (mmole)	31.40	31.47	31.52	31.46	31.13	29.21	28.55	29.21	28.70	28.88	28.54
Reactant (g)	3.957	3.965	3.972	3.964	3.922	4.090	3.997	4.090	4.018	4.043	3.996
Experimental No.	AS4	AS5	AS6	AS7	TS93	AS8	TS81	AS36	TS61	TS66	TS74
Residence time[a]	0.2 hr	0.5 hr	1 hr	2.5 hr	4 hr	0.2 hr	0.5 hr	1 hr	2.5 hr	4 hr	8 hr
Product	molar yield (%)[b]										
Hydrogen		0.54	0.93	3.03	6.07		0.73	1.25	4.23	6.45	12.08
Methane	0.81	1.03	2.49	6.12	14.67	0.24	1.29	3.23	8.28	16.01	49.73
Ethylene	0.13	0.17	0.29	0.39	0.58	0.12	0.23	0.71	0.78	0.92	0.69
Ethane	1.65	2.19	4.97	12.34	25.13	0.42	2.10	2.98	9.73	17.09	36.44
Propene	1.41	2.05	3.67	4.35	5.02	0.34	0.91	1.34	2.67	3.05	2.99
Propane	0.70	1.15	2.90	7.06	14.87	0.74	2.30	5.28	12.14	20.76	31.04
1-Butene		0.01	0.08	0.25	0.60	0.72	1.35	3.29	3.06	2.72	1.81
n-Butane		0.03	0.13	0.63	2.04	0.37	1.10	2.15	7.31	11.40	12.17
1-Pentene		0.02	0.07	0.21	0.30		0.04	0.05	0.41	1.41	0.72
n-Pentane		0.07	0.24	0.83	1.60		0.06	0.09	0.80	2.06	2.80
n-Hexane		0.03	0.11	0.40	0.57		0.07	0.16	0.84	1.46	1.36
Heptene								0.07	0.13	0.23	0.39
Heptane								0.10	0.50	0.80	0.98
Cyclohexene	0.40	1.14	2.62	4.16	3.73	0.49	1.02	2.14	2.33	3.21	0.35
Cyclohexane	0.76	2.04	4.93	10.98	19.51	0.81	2.80	3.67	9.53	20.14	16.91
Methylcyclohexene		0.04	0.14	0.59	1.00			0.08	0.92	1.26	0.31
Methylenecyclohexane	0.47	1.08	1.93	1.98	1.39	0.90	2.23	2.64	2.20	1.90	0.62
1-Methylcyclohexene	0.06	0.31	0.96	2.59	2.56	0.07	0.61	0.98	2.93	3.19	1.09
Methylcyclohexane	0.05	0.13	0.43	1.52	4.40	0.33	1.76	1.55	6.56	12.68	11.77
Ethenylcyclohexane	0.12	0.24	0.35	0.30	0.20	0.30	0.83	0.95	0.46	0.11	
1-Ethylcyclohexene+Ethylidenecyclohexane							0.15	0.16	0.70	0.43	
Ethylcyclohexane	0.26	0.28	0.36	0.72	1.17	0.04	0.13	0.21	1.09	2.27	1.97
2-Propenylcyclohexane				0.09		0.07	0.19	0.20	0.10		
C_3-cyclohexane			0.05	0.12	0.12				0.29	0.62	0.78
n-Propylcyclohexane	96.58	92.86	82.96	61.41	35.22	0.02	0.09	0.10	0.68	0.91	0.90
C_4-cyclohexene			0.03	0.07	0.08	0.41	0.57	0.61	1.16	0.64	0.57
C_4-cyclohexane	0.07	0.09	0.12	0.18	0.38	0.24	0.58	0.81	2.34	1.94	1.15
n-Butylcyclohexane	0.01	0.03	0.08	0.15	0.30	95.95	88.08	81.79	57.47	25.56	6.35
C_5-cyclohexane			0.05	0.17	0.21					0.21	0.11
n-Pentylcyclohexane				0.05	0.07		0.04	0.05	0.32	0.18	0.18
C_6-cyclohexane		0.09	0.27	0.79	0.71		0.02		0.11	0.08	0.05
n-Hexylcyclohexane				0.09	0.10						
Methylcyclopentane	0.13	0.38	0.99	2.45	5.43	0.11	0.48	0.64	2.07	5.71	7.41
Ethylcyclopentane		0.04	0.04	0.12	0.31			0.04	0.13	0.47	0.80
C_3-cyclopentane				0.17	0.26					0.55	1.25
C_4-cyclopentane	0.28	0.62	1.50	2.80	3.24						
Benzene			0.16	0.64	2.43		0.02	0.05	0.71	2.51	4.71
Toluene			0.08	0.76	3.22				1.36	5.20	8.93
C_2-benzene				0.24	1.22				0.60	0.70	4.68
C_3-benzene				0.22	0.77				0.20	0.89	2.18
C_4-benzene				0.03	0.26		0.04		0.09	0.54	1.03
C_5-benzene					0.04				0.09	0.15	0.25
Indan					0.14				0.06	0.18	0.64
Methylindan					0.29					0.44	1.27
C_2-indan					0.17					0.23	0.75
Naphthalene					0.13		0.02		0.13	0.28	1.18
Methylnaphthalene					0.25				0.05	0.34	1.18
C_2-naphthalene					0.06					0.22	0.75
(Alkyl-)bicyclohexyl			0.07	0.37	0.44		0.03	0.04	0.27	0.19	0.17

a) Pyrolysis of 5 ml reactant in 25 ml reactors plunged into the sandbath preheated to 450°C.
b) The molar yield based on initial reactants (n-propylcyclohexane or n-butylcyclohexane).

Table 1.22-3. Molar Yields of Products from the Pyrolysis of *n*-Hexylcyclohexane, *n*-Octylcyclohexane, and *n*-Decylcyclohexane at 450°C under Initial 0.69 MPa N_2 (Cold) (continued)

Reactant Name	HCH	HCH	OCH	OCH	OCH	OCH	DCH	DCH	DCH
Reactant (mmole)	23.74	23.68	20.78	20.77	20.81	20.82	18.12	18.18	18.21
Reactant (g)	3.989	3.978	4.073	4.071	4.079	4.080	4.058	4.072	4.078
Experimental No.	AS9	AS10	AS11	AS32	AS12	AS35	AS13	AS34	AS14
Residence time[a]	0.2 hr	0.5 hr	0.2 hr	0.35 hr	0.5 hr	1.0 hr	0.2 hr	0.35 hr	0.5 hr
Product	molar yield (%)[b]								
Hydrogen	1.01	1.68		0.40	1.41	5.41	2.01	0.88	2.35
Methane	0.62	1.30	0.89	0.94	1.96	10.99	0.77	1.43	2.22
Ethylene	0.39	0.48	0.53	0.47	0.53	1.11	0.42	0.44	0.62
Ethane	1.00	1.84	1.46	1.71	2.57	8.79	1.35	1.63	3.16
Propene	0.89	1.39	1.00	2.02	2.13	3.09	1.48	1.87	2.98
Propane	1.04	1.91	1.22	2.48	3.28	10.72	2.00	3.38	5.19
1-Butene	0.52	0.67	0.62	1.31	1.90	3.07	1.02	1.32	1.82
n-Butane	0.73	1.91	0.81	1.97	3.02	8.20	1.44	2.46	4.71
1-Pentene	0.40	0.67	0.63	1.24	1.32	2.38	1.08	1.35	1.96
Pentenes (2- and 3-)		0.13				0.54		0.21	0.27
n-Pentane	1.92	4.55	0.49	1.40	2.66	6.89	1.03	1.63	3.20
1-Hexene	1.16	2.05	0.55	1.12	1.49	2.00	1.22	1.70	2.25
Hexenes (2- and 3-)	0.13	0.38		0.12	0.22	0.84	0.07	0.22	0.43
n-Hexane (n-C_6)	0.72	1.69	0.46	1.07	1.86	4.63	0.93	1.42	2.60
1-Heptene			0.43	0.84	1.12	1.07	0.81	1.11	1.53
2-Heptene		0.05		0.07	0.14	0.45	0.06	0.08	0.22
n-Heptane (n-C_7)			1.29	2.77	4.64	9.03	0.81	1.22	2.20
1-Octene			1.05	1.82	2.31	2.27	0.64	0.71	1.24
n-Octane (n-C_8)		0.18	0.44	1.09	1.80	4.06	0.64	1.03	1.88
1-Nonene					0.06		0.50	0.60	0.79
n-Nonane (n-C_9)			0.03	0.06	0.18	0.56	1.98	2.97	4.96
1-Decene					0.03		1.18	1.51	1.77
n-Decane (n-C_{10})	0.01	0.03		0.05	0.12	0.35	0.81	1.22	2.14
n-Undecane (n-C_{11})	0.02	0.06	0.02	0.06	0.12	0.39	0.03	0.13	0.23
n-Dodecane (n-C_{12})	0.02	0.05	0.02	0.11	0.09	0.26	0.06	0.11	0.21
n-Tridecane (n-C_{13})						0.08		0.05	0.16
n-Tetradecane (n-C_{14})				0.08		0.04		0.03	0.08
n-Pentadecane (n-C_{15})									0.11
n-Hexadecane (n-C_{16})								0.10	0.11
Cyclohexene	0.88	2.04	0.79	1.85	2.83	4.74	1.36	2.03	3.22
Cyclohexane	1.43	3.43	1.29	3.11	5.07	11.81	2.43	3.84	6.49
Methylcyclohexene	0.13	0.51		0.05	0.20	0.79	0.08	0.18	0.61
Methylenecyclohexane	0.48	0.48	1.52	2.72	3.20	3.23	1.75	2.23	2.17
1-Methylcyclohexene	1.42	3.38	0.23	0.90	2.32	4.18	1.18	2.13	4.41
Methylcyclohexane	0.56	1.41	0.52	1.30	2.27	5.78	0.94	1.52	2.93
Ethenylcyclohexane	0.44	0.66	0.44	0.80	1.00	0.73	0.60	0.96	0.90
1-Ethylcyclohexene+Ethylidenecyclohexane	0.07	0.26	0.05	0.06	0.31	0.76	0.16	0.19	0.47
Ethylcyclohexane	0.43	1.08	0.45	1.06	1.83	4.25	0.79	1.29	2.40
2-Propenylcyclohexane	0.40	0.67	0.41	0.71	0.90	0.69	0.57	0.72	0.95
Cyclohexylpropene	0.03	0.06		0.04	0.10	0.21	0.03	0.08	0.15
C_3-cyclohexene					0.04	0.12			0.13
n-Propylcyclohexane	0.35	0.82	0.34	0.74	1.26	2.73	0.76	1.10	1.96
3-Butenylcyclohexane	0.34	0.51	0.34	0.55	0.65	0.43	0.46	0.60	0.68
Cyclohexylbutene				0.04	0.13	0.39	0.03	0.16	0.24
n-Butylcyclohexane	0.06	0.14	0.24	0.53	0.86	1.71	0.48	0.76	1.35
4-Pentenylcyclohexane	0.08	0.12	0.29	0.48	0.51	0.35	0.41	0.58	0.56
n-Pentylcyclohexane	0.02	0.06	0.27	0.61	0.98	1.82	0.49	0.80	1.39
5-Hexenylcyclohexane			0.29	0.50	0.50	0.37	0.40	0.54	0.55
Cyclohexylhexene						0.14		0.05	0.09
1-Hexylcyclohexene	0.14	0.12				0.08			
C_6-cyclohexane	0.67	0.96				0.07			
n-Hexylcyclohexane	89.21	79.48	0.07	0.17	0.23	0.72	0.44	0.72	1.12

Table 1.22-3. (cont'd) Molar Yields of Products from the Pyrolysis of *n*-Hexylcyclohexane, *n*-Octylcyclohexane, and *n*-Decylcyclohexane at 450°C under Initial 0.69 MPa N_2 (Cold)

6-Heptenylcyclohexane			0.06	0.11	0.11	0.08	0.34	0.41	0.44
Cyclohexylheptene				0.08	0.09	0.15	0.04	0.05	0.07
C_7-cyclohexane	0.14	0.12							
n-Heptylcyclohexane	0.03	0.04	0.03	0.07	0.11	0.32	0.46	0.68	1.10
7-Octenylcyclohexane			0.02	0.02	0.04	0.09	0.37	0.46	0.38
C_8-cyclohexane			0.26	0.65	0.85	1.19			
n-Octylcyclohexane			90.93	79.90	69.35	38.67	0.11	0.19	0.29
8-Nonenylcyclohexane							0.09	0.11	0.10
C_9-cyclohexane			0.08	0.06	0.05	0.03			
n-Nonylcyclohexane	0.01	0.02	0.05	0.09	0.09	0.15	0.06	0.11	0.15
C_{10}-cyclohexane							0.47	0.63	0.88
n-Decylcyclohexane			0.05	0.06	0.07	0.10	83.21	75.13	56.81
C_{11}-cyclohexane			0.13	0.04			0.06	0.06	0.06
n-Undecylcyclohexane				0.04	0.05	0.08	0.07	0.08	0.10
C_{12}-cyclohexane	0.03	0.08		0.04	0.12	0.19		0.05	0.15
n-Dodecylcyclohexane					0.02	0.04	0.06	0.07	0.10
C_{13}-cyclohexane			0.02	0.06	0.06	0.13	0.03	0.07	0.28
n-Tridecylcyclohexane							0.05		0.07
C_{14}-cyclohexane					0.02	0.02		0.06	0.10
n-Tetradecylcyclohexane					0.02	0.03	0.02	0.03	0.04
C_{15}-cyclohexane				0.04	0.08	0.11	0.03	0.03	0.15
n-Pentadecylcyclohexane					0.02	0.04	0.02	0.03	0.03
C_{16}-cyclohexane				0.05	0.07	0.14	0.03	0.06	0.10
n-Hexadecylcyclohexane					0.01		0.02	0.04	0.02
n-Heptadecylcyclohexane							0.02	0.07	0.02
Methylcyclopentane	0.20	0.50	0.12	0.40	0.67	2.17	0.26	0.45	0.91
Dimethylcyclopentene				0.05	0.13	0.38	0.04	0.06	0.20
Ethenylcyclopentane	0.02	0.03		0.04	0.05	0.05			0.04
Ethylcyclopentane		0.03			0.05	0.27			0.12
Benzene	0.02	0.09		0.04	0.11	0.85			0.24
Toluene	0.09	0.41		0.05	0.21	1.26	0.08		0.70
C_2-benzene		0.04				0.27			0.14
C_3-benzene						0.06			0.05
(Alkyl-)bicyclohexyl	0.61	0.60		0.03	0.11	0.40	0.02	0.08	0.12

a) Pyrolysis of 5 ml reactant in 25 ml reactors plunged into the sandbath preheated to 450°C.
b) The molar yield based on initial reactants (n-hexylcyclohexane, n-octylcyclohexane, or n-decylcyclohexane).

Table 1.22-4. Pseudo-First-Order Rate Constants of Alkylcyclohexanes at 450°C

Compound	Conversion Range	Rate Constant (hr^{-1})	Characterization No. (n)
Cyclohexane	0.05	0.013	12
Methylcyclohexane	0.11	0.030	13
Ethylcyclohexane	0.024-0.63	0.12	17
n-Propylcyclohexane	0.032-0.65	0.25	21
n-Butylcyclohexane	0.034-0.94	0.34	25
n-Hexylcyclohexane	0.092-0.19	0.53	33
n-Octylcyclohexane	0.087-0.61	0.99	41
n-Decylcyclohexane	0.163-0.43	1.28	49

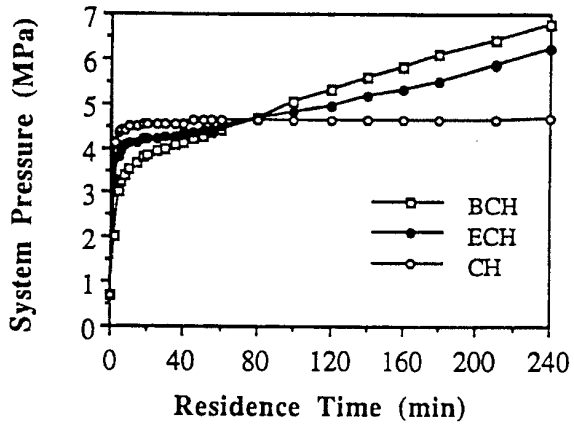

Figure 1.22-1. System Time-Pressure Profiles During Pyrolysis of Cyclohexane, Ethylcyclohexane, and n-Butylcyclohexane at 450°C under 0.69 MPa Initial N_2 Pressure (Cold)

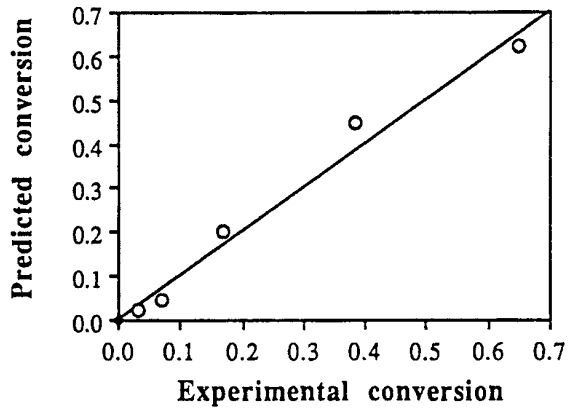

Figure 1.22-2. Predicted versus Measured Values of n-Propylcyclohexane Conversion at 450°C

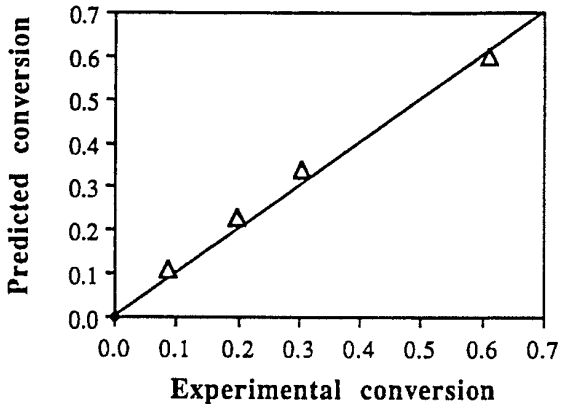

Figure 1.22-3. Predicted Versus Measured Values of n-Octylcyclohexane Conversion at 450°C

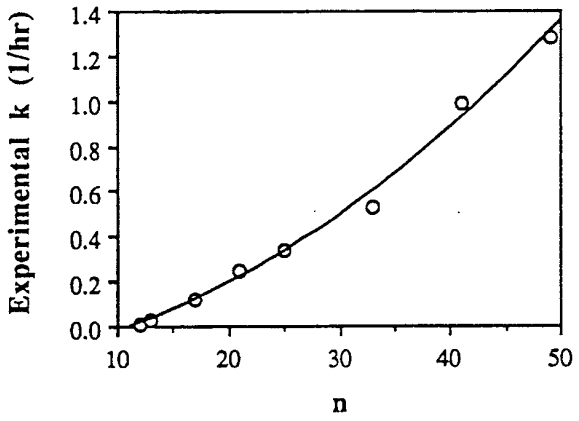

Figure 1.22-4. Experimental Rate Constants of Alkylcyclohexanes at 450°C as a Function of Characterization Number (n) of Molecular Structure

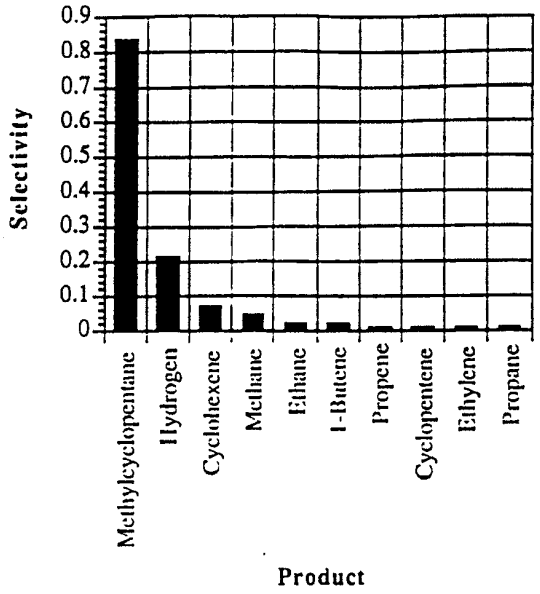

Figure 1.22-5. Cyclohexane Selectivity to Major Products at 450°C for 4 Hours under Initial N_2 Pressure (Cold) of 0.69 MPa (Conversion = 0.05)

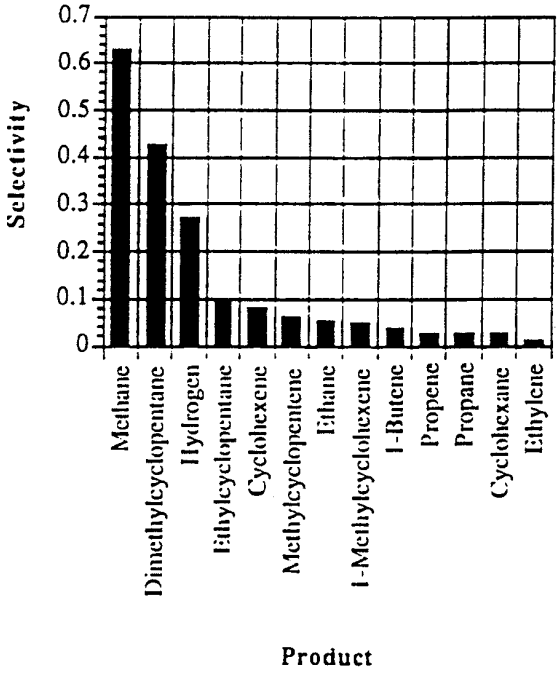

Figure 1.22-6. Methylcyclohexane Selectivity to Major Products at 450°C for 4 Hours under Initial N_2 Pressure (Cold) of 0.69 MPa (Conversion = 0.12)

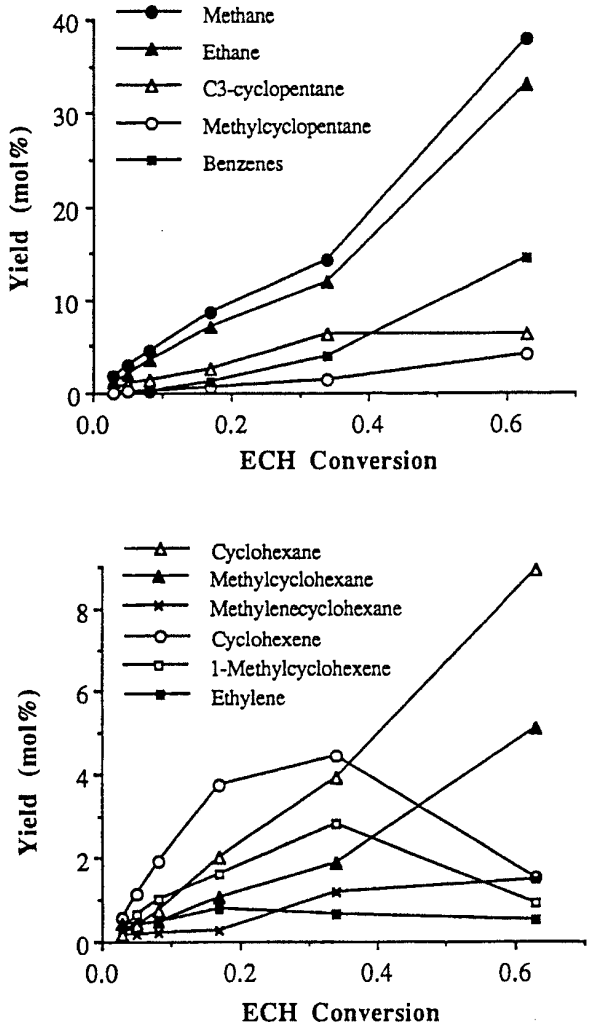

Figure 1.22-7. Product Distribution for Ethylcyclohexane Pyrolysis at 450°C under Initial N_2 Pressure (Cold) of 0.69 MPa

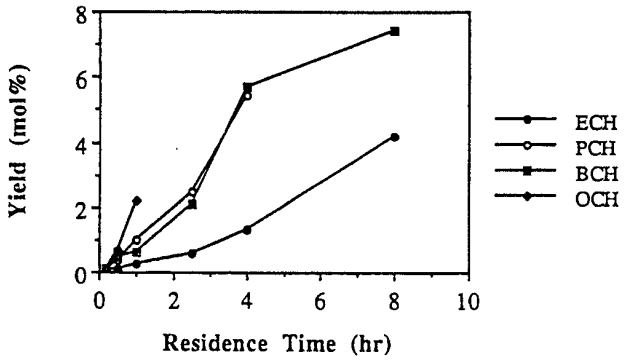

Figure 1.22-8. Temporal Methylcyclopentane Product for Alkylcyclohexane Pyrolysis at 450°C under Initial N_2 Pressure (Cold) of 0.69 MPa

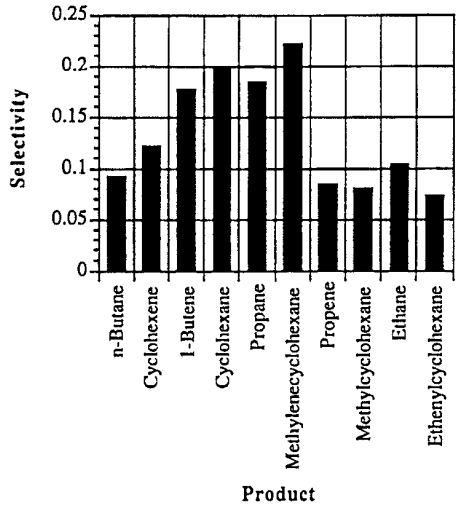

Figure 1.22-9. n-Butylcyclohexane Selectivity to Major Products at 450°C for 0.2 hours under Initial N_2 Pressure (Cold) of 0.69 MPa (Conversion = 0.04)

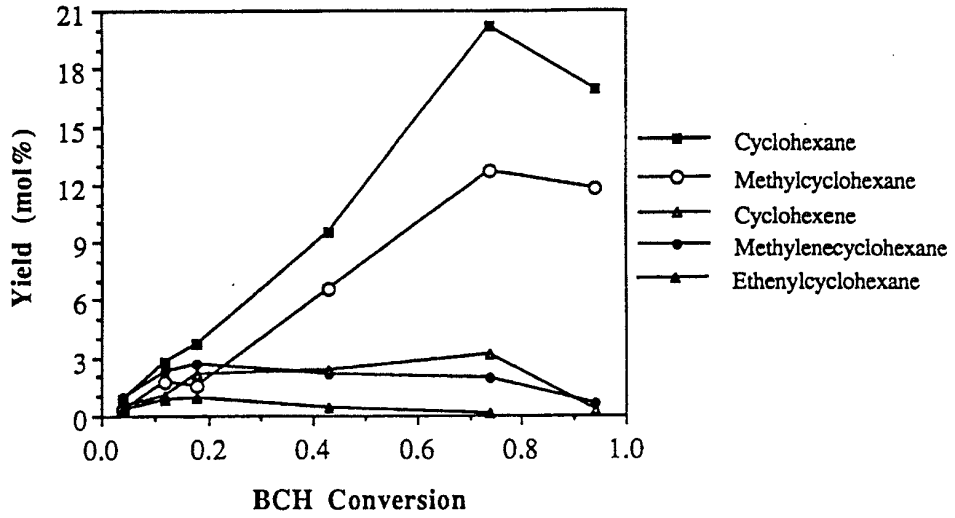

Figure 1.22-10. Product Distribution for n-Butylcyclohexane Pyrolysis at 450°C under Initial N_2 Pressure (Cold) of 0.69 MPa

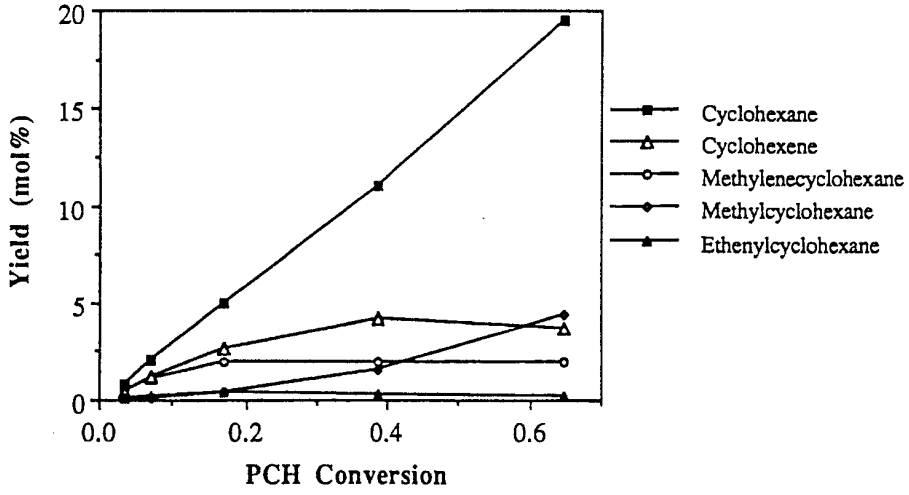

Figure 1.22-11. Product Distribution for n-Propylcyclohexane Pyrolysis at 450°C under Initial N_2 Pressure (Cold) of 0.69 MPa

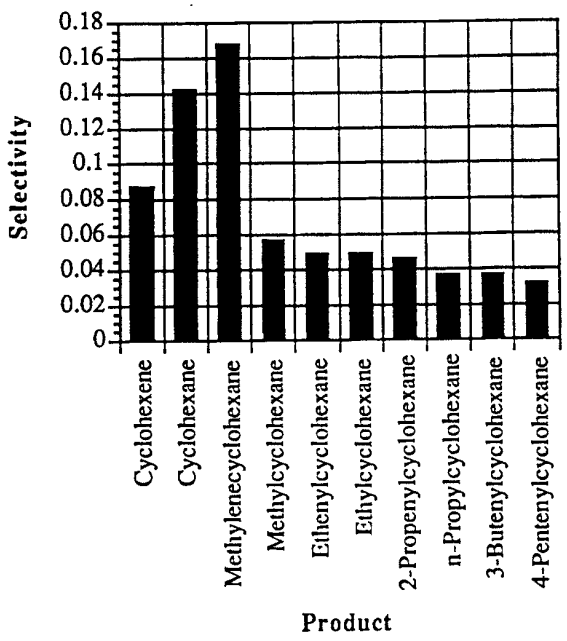

Figure 1.22-12. n-Octylcyclohexane Selectivity to Major Products at 450°C for 0.2 Hours under Initial N_2 Pressure (Cold) of 0.69 MPa (Conversion = 0.09)

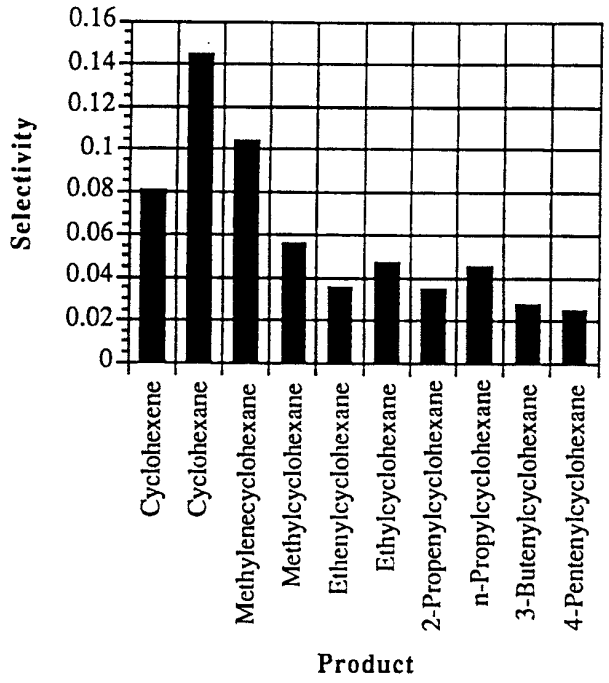

Figure 1.22-13. n-Decyclohexane Selectivity to Major Products at 450°C for 0.2 Hours under Initial N_2 Pressure (Cold) of 0.69 MPa (Conversion = 0.17)

[1] Lai, W.C., and C. Song. *Fuel.* 1993.

[2] Song, C., W.C. Lai, and H.H. Schobert. *Ind. Eng. Chem. Res.* 1993.

[3] Fabuss, B. M., et al. *Ind. Eng. Chem. Proc. Des. Dev.* 1964. *3*(3). 248-254.

[4] Draper, N. R., and H. Smith. *Applied Regression Analysis.* 1981. John Wiley & Sons: New York.

[5] Fabuss, B. M., et al. *Ind. Eng. Chem. Proc. Des. Dev.* 1964. *3*(3). 248-254.

[6] Fabuss, B. M., J.O. Smith, and C.N. Satterfield. *Advances in Petroleum Chemistry and Refining.* 1964. Interscience Publishers: New York. Volume 9. 156-201.

[7] Billaud, F. et al. *Ind. Eng. Chem. Res.* 1991. 30. 1469-1478.

[8] March, J. *Advanced Organic Chemistry.* 3rd Edition. 1985. Wiley: New York.

[9] Franz, J.A., R.D. Barrows, and D.M. Camaioni. *J. Am. Chem. Soc.* 1984. 106. 3964.

[10] Lamb, R.C., P.W. Ayers, M.K. Toney. *J. Am. Chem. Soc.* 1974. 96. 6355-6377.

[11] Lal, D. et al. *J. Am. Chem. Soc.* 1963. 85. 3483-3486.

[12] March, J. *Advanced Organic Chemistry.* 3rd Edition. 1985. Wiley: New York.

[13] Baldwin, J.E. *J. Chem. Soc., Chem. Commun.* 1976. 734-736.

[14] Baldwin, J.E. and L. Kruse. *J. Chem. Soc., Chem. Commun.* 1977. 233-235.

[15] Baldwin, J.E. et al. *J. Org. Chem.* 1977. *42* (24). 3846-3852.

[16] Baldwin, J.E. and M.J. Lusch. *Tetrahedron.* 1982. *38* (19). 2939-2947.

1.23 PYROLYTIC AND CATALYTIC REACTIONS OF POTENTIAL ENDOTHERMIC FUELS: CIS- AND TRANS-DECALIN

This study is explained in detail in *Advanced Thermally Stable Jet Fuels Technical Progress Report, October–December 1994.*

Introduction

We previously demonstrated that *trans*-decalin (*trans*-DHN) can inihibit solid deposit formation from jet fuels and their components.[1] As a result, DHN has potential as an endothermic jet fuel that can serve as the primary heat sink to cool the hot surfaces and system components. In order to better understand potential endothermic fuels such as saturated cyclic hydrocarbons, we undertook this study of *cis*- and *trans*-DHN pyrolysis at 450°C for 0.5 to 8 hours under initial (cold) N_2 pressure of 0.79 MPa. This work demonstrates that *trans*-DHN is much more stable than *cis*-DHN.

Results and Discussion

1. Pyrolytic Reactions. There were several distinct features of the product distribution from pyrolysis of *cis*-DHN, *trans*-DHN, and DHN:

- There was no solid deposit formed after an 8-hour thermal stressing at 450°; indicating that DHN has a much higher thermal stability than a JP-8C fuel (2.6 wt% solid deposit) or a JP-8P fuel (8.9 wt% solid deposit).
- *Trans*-DHS is much more stable than *cis*-DHS. The average first-order rate constants over the stressing range studied are 0.31 ± 0.04 h^{-1} for *cis*-DHN and 0.06 ± 0.02 h^{-1} for *trans*-DHN. The first-order rate constants for *cis*-DHN and *trans*-DHN are similar to those of *n*-butylcyclohexane and methylcyclohexane, respectively. *Cis*-DHN produced significantly higher gas yields than *trans*-DHN. Major gas components are CH_4, C_2H_6, and C_3H_8. These results imply that a higher degree of ring-opening reactions and subsequent dealkylation for *cis*-DHN. The steric isomers of cycloalkanes react at different rates and, in general, *trans*-isomers are more stable than their *cis*- counterparts. As a result, *trans*-isomers could be more desirable compounds for the advanced jet fuels, because most of their product compounds are more stable and have less tendency to form solid deposits.
- Isomerization was the dominant reaction under the conditions employed. For pyrolysis of *cis*-DHN, the dominant products are two types of isomers—*trans*-DHN (from conformational isomerization) with about 55% selectivity (defined as the ratio of molar yield of the product to the conversion) and C_4-cyclohexene or cyclohexylbutene (ring-opening isomerization) with about 10% selectivity. Other major products were: C_0-C_2-benezene alkanes/alkenes, tetralin and naphthalene and alkyldecalins. Isomerization products were also major *trans*-DHN pyrolysis products. The conformational isomerization of *trans*- to *cis*-DHN (30% selectivity) is not as dominant as that of *cis*- to *trans*-DHN (55% selectivity).

2. Catalytic Reactions. We performed catalyzed isomerization of *cis*-DHN using 1-g commercial DHN as starting reactant at 200-250°C for 2 hours with 0.79 MPa of UHP H_2 or N_2.

Pt- and Pd-loaded mordenites were very effective catalysts under H_2 atmosphere for the conformational isomerization of *cis*-DHN to *trans*-DHN event at low temperature (200°C). The conversion selectivity towards *trans*-DHN reaches 100% (i.e., there are no side products). Pt- and Pd-loaded mordenites are less effective catalysts under N_2 atmosphere. The other three catalysts studied—HY, LaHY, and HM38—were much less effective than Pt- and Pd-loaded mordenites, and their performance was not affected by H_2. With further investigation, HY performed slightly better than LaHY, in terms of activity and selectivity and HM38 was the least effective of the catalysts studied. Also, selectivity towards *trans*-DHN seemed to decrease with increasing temperature and decrease with increasing conversion level under isothermal condition.

---

[1] Song, C., W.-C. Lai, and H. H. Schobert. "Hydrogen Transferring Pyrolysis of Long-Cahin Alkanes and Thermal Stability Improvement of Jet Fuels by Hydrogen Donors." Ind. Eng. Chem. Res. 1994. 33. 548-557.

1.24 THERMAL DECOMPOSITION OF *N*-BUTYLCYCLOHEXANE IN NEAR-CRITICAL AND SUPERCRITICAL REGIONS: PRODUCT DISTRIBUTIONS AND REACTION MECHANISMS

This study is explained in detail in *Advanced Thermally Stable Jet Fuels Technical Progress Report, April–June 1996.*

Introduction

Jet fuels contain significant amounts of alkylcyclohexanes. For example, JP-8P, a petroleum-derived jet fuel, and JP-8C, a coal-derived jet fuel, contain about 14 wt% and 40 wt% of C_6 to C_{14} cyclohexanes, respectively.[1] Studying thermal decomposition of alkylcyclohexanes is important for understanding thermal degradation behavior of jet fuels. In this work, we studied thermal decomposition of *n*-butylcyclohexane in near-critical and supercritical regions. Thermal stressing experiments were carried out in a Pyrex glass tube reactor with a total volume of 45–50 mL.

Results and Discussion

1. Product Distributions. The liquid products from thermal decomposition of *n*-butylcyclohexane included cyclohexane, methylenecyclohexane, cyclohexene, methylcyclohexane, vinylcyclohexane, allylcyclohexane, ethylcyclohexane, 1-methylcyclohexene, 3-methylcyclohexene, methylcyclopentane, 1-ethylcyclohexene, *n*-propylcyclohexane, C_4-cyclohexenes, and C_4-cyclohexanes. Among these compounds, the first seven were the primary products. Some high-molecular-weight compounds, although not identified, were also found as the conversion exceeded 10%. At the highest conversion (39%, 475°C, 20 minutes), about 130 peaks were obtained from the chromatogram of the liquid products.

The initial reduced pressure ($P_r = P/P_c$) was calculated at the given temperature and loading ratio, defined as the sample volume at room temperature divided by the reactor volume, using the Soave-Redlich-Kwong equation of state.[2] The conversion steadily decreased from 3.24 to 1.82% as P_r increased from 0.67 to 2.64. The yields of the primary products decreased while those of the secondary products, except methylcyclopentane, increased as pressure increased, indicating the increasing importance of the secondary reactions with the increasing pressure. Under supercritical conditions, the most abundant liquid products are 1-methylcyclohexene and cyclohexane, followed by cyclohexene, methylcyclohexane, and vinylcyclohexane. Other liquid products were present in lower yields (< 5 mol/100 mol reactant converted). The 1-methylcyclohexene and 3-methylcyclohexene seem to be converted from methylenecyclohexane, because the total yield of the three compounds remained almost unchanged within the pressure range examined.

The yields of saturated compounds (cyclohexane, methylcyclohexane, ethylcyclohexane, *n*-propylcyclohexane, and methylcyclopentane) remained unchanged with increasing conversion, indicating the higher stabilities of these compounds. Among the unsaturated compounds, the yields of 1-methylcyclohexene, vinylcyclohexane, and allylcyclohexane decreased while those of methylenecyclohexane and cyclohexene did not change significantly with the increasing conversion. The yield of 3-methylcyclohexene first increased and then remained constant; that of 1-ethylcyclohexene increased and then decreased as the conversion increases.

2. Reaction Mechanisms. The reaction products from thermal decomposition of *n*-butylcyclohexane can be divided into those from primary reactions and those from secondary reactions. Equations for both are provided in the corresponding Technical Progress Report.[3]

The primary products can be produced as follows. The initiation occurs by homolytic cleavage of carbon-carbon bond to produce two radicals. These radicals then abstract hydrogen atoms from the surrounding *n*-butylcyclohexane molecules to form various parent radicals. Each of these parent radicals could decompose by β-scission to form a small radical and an unsaturated product. The formation of methylenecyclohexane, cyclohexane, cyclohexene, methylcyclohexane, vinylcyclohexane, allylcyclohexane, and ethylcyclohexane can be explained by these primary reactions.

The secondary products can be produced by the following reactions. Methylenecyclohexane can be converted to 1-methylcyclohexene. This conversion should occur quickly because the abstraction of a secondary allylic hydrogen on the ring of methylenecyclohexane is a relatively simple process. The 1-methylcyclohexene could be converted to 3-methylcyclohexene by similar reactions. Methylcyclopentane could be formed by β-scission of the cyclohexyl radical, followed by ring closure and subsequent hydrogen abstraction. The 1-ethylcyclohexene could be formed from ethylcyclohexane. The *n*-propylcyclohexane could be produced from the addition of 1-propyl radical to cyclohexene, followed by hydrogen abstraction.

The differences in the yields of individual reaction products can be explained by the differences in the relative formation rates of the parent radicals and differences in the subsequent decomposition rates of these radicals. Among the various parent radicals, the formation of a tertiary butylcyclohexane radical would be favored because of its relatively higher stability as compared with other parent radicals (secondary or primary). Although we might expect the yield of methylenecyclohexane to be highest among the primary products, the results of this work indicate otherwise. This is because methylenecyclohexane is rapidly converted to 1-methylcyclohexene, as discussed before. It seems that high-pressure supercritical conditions favor this conversion.

The rates for the formation of α-, β-, and γ-butylcyclohexane radicals should be equivalent because of the similar dissociation energies of secondary carbon-hydrogen bonds. One would expect the yields of vinylcyclohexane, cyclohexane plus allylcyclohexane, and methylcyclohexane to be roughly equal. Our results revealed that the yield of cyclohexane is much higher than those of vinylcyclohexane and methylcyclohexane. This difference in product yield can be attributed to the difference in the decomposition rate for the three parent radicals. The decomposition of the β-butylcyclohexane radical by β-scission of the C_{ring}–C_{α} bond would be favored because a relatively stable secondary cyclohexyl radical is produced. The decomposition of other two radicals produces less stable primary radicals. Therefore, cyclohexane would be formed in higher yield than vinylcyclohexane and methylcyclohexane. We note that the decomposition of the β-butylcyclohexane radical could also occur by β-scission of the C_{γ}–C_{δ} bond. However, this route for β-scission is much less favorable because the methyl radical is highly unstable. This was confirmed by the low yield of allylcyclohexane.

The yield of vinylcyclohexane is equivalent to that of methylcyclohexane at low pressures, but decreases as pressure increases, indicating the significant addition reaction that

occurs between a radical and this compound. The yield of cyclohexene is higher than those of vinylcyclohexane and methylcyclohexane because the concentration of butylcyclohexyl radical is higher than those of α- and γ-butylcyclohexane radicals. Ethylcyclohexane is formed in a low yield because the formation of a primary butylcyclohexane radical is less favorable.

---

[1] Schobert, H. H. et al. *Advanced Thermally Stable Jet Fuels, Technical Progress Report* (April 1995 – June 1995), The Pennsylvania State University, 1995.

[2] Soave, G. Chem. Eng. Sci. 1972, 27, 1197-1203.

[3] Schobert, H. H. et al. *Advanced Thermally Stable Jet Fuels, Technical Progress Report, April - June 1996.* The Pennsylvania State University. 1996.

1.25 Thermal Decomposition of Decalin in Near-Critical and Supercritical Regions: Product Distributions and Reaction Mechanisms

This study is explained in detail in *Advanced Thermally Stable Jet Fuels Technical Progress Report, July–September 1996.*

Introduction

Decalin is a typical component found in coal-derived jet fuels. As a model compound for naphthenic feedstocks for alkene production, decalin has been pyrolyzed at high temperatures (> 700°C) and low pressures. Ring cracking dominates the pyrolysis of decalin at high temperatures. The major gaseous products from decalin cracking are ethylene, hydrogen, methane, propylene, and 1,3-butadiene. At very high conversions, the major liquid products are C_6 to C_8 benzenes, while at low to moderate conversions the main liquid products are C_6 to C_8 cycloalkenes and cycloalkanes. At moderate temperatures and high pressures, significant dehydrogenation reactions occur. For example, in the thermal cracking of decalin at 550°C and 69 atm, the main liquid product is 1,2,3,4,5,6,7,8-octahydronaphthalene.

In this work, thermal decomposition of decalin was investigated under near-critical and supercritical conditions. Thermal reaction experiments of decalin, which consists of 47.90% of *cis*-decalin and 51.88% of *trans*-decalin, as well as small amounts of tetralin and other impurities, were conducted at 450°C for 15-60 minutes. The effects of pressure were studied at 450°C for 15 minutes.

Results and Discussion

1. Product Distributions. The major liquid products from the thermal decomposition of decalin include spiro[4,5]decane, 1-methylcyclohexene, 1-butylcyclohexene, and 1-methylperhydroindan. Also appearing, but in slightly lower yields, are toluene, some C_4-cyclohexenes, n-butylbenzene, and three unidentified compounds which eluted between *trans*-decalin and tetralin from the GC column. Some minor products include cyclohexane, cyclohexene, methylcyclopentane, methylcyclohexane, 3-methylcyclohexene, methylenecyclohexane, benzene, ethylbenzene, n-butylcyclohexane, tetralin, naphthalene, and some high molecular weight compounds. At 450°C for 60 minutes, approximately 80 compounds were found in the liquid products.

At 450°C for 15 minutes, the conversions of decalin—about 2.9% based on the disappearance of *cis*- and *trans*-decalin—did not change significantly with pressure changes. The yield of spiro[4,5]decane rapidly increased while that of 1-methylcyclohexene rapidly decreased with the increasing pressure. The yield of 1-butylcyclohexene increased while that of 1-methylperhydroindan gradually decreased as pressure increased.

For the thermal decomposition of decalin at 450°C with a loading ratio of 0.36 ($P_r = P/P_c$ = 1.63), the yields of all products decreased with the increasing conversion. In the conversion ranges examined, the yields of $C_{10}H_{18}$ products, including spiro[4,5]decane, 1-

methylperhydroindan, 1-butylcyclohexene, and three other C4-cyclohexenes, were found to be more than 40 mol/100 mol *cis*- and *trans*-decalin converted, indicating that significant isomerization reactions had occurred. This means that the reaction mechanism for the thermal decomposition of decalin under near-critical and supercritical conditions is different from that under low-pressure and high-temperature conditions, which result in dominant cracking reactions and produce light gases, C_6 to C_8 benzenes, and C_6 to C_8 cycloalkenes and cycloalkanes as major products.

One interesting characteristic of decalin thermal decomposition under near-critical and supercritical conditions is interconversion between *cis*- and *trans*-decalins. Decalins are namely a mixture of *cis*- and *trans*-decalin, *cis*-decalin (99+% purity), and *trans*-decalin (99+% purity). For the *cis*- and *trans*-decalin mixture, the weight percent of *cis*-decalin decreases while that of *trans*-decalin increases with the increasing reaction time. For example, as the weight percent of *cis*-decalin decreases from initial 47.90 to 29.25%, that of *trans*-decalin increases from 51.88 to 58.36%. About 35% of disappeared *cis*-decalin was converted to *trans*-decalin. This result is different from those obtained under low-pressure, high-temperature conditions where no significant isomerization of the decalins was found.[1]

The net rate of interconversion between *cis*- and *trans*-decalins depends on the relative concentrations of these two isomers. At 450°C, the equilibrium constant for the reaction of *cis*-decalin ↔ *trans*-decalin is 4.69, calculated using $\Delta G°_T$ = -2.22 kcal/mol,[2] and the corresponding equilibrium composition is 17.6% *cis*-decalin and 82.4% *trans*-decalin. Therefore, if the concentration of either decalin exceeds its equilibrium concentration, it will be converted to the other one. The final relative concentrations of *cis*- and *trans*-decalins from the thermal decomposition of three different decalins at the conditions used are *(cis*-decalin/*trans*-decalin): 33.4/66.6 for decalin, 73.2/26.8 for *cis*-decalin, and 5.1/94.9 for *trans*-decalin. This means that the equilibrium was not attained under the conditions used in this work.

cis-Decalin is less stable, therefore, the reactant with a higher concentration of *cis*-decalin would exhibit higher reactivity. An increase in pressure seems to shift equilibrium toward *trans*-decalin. Although the weight percent of the remainder decalin does not change with pressure, the relative concentrations of *cis*- and *trans*-decalins change slightly, with the weight percent of *cis*-decalin decreasing and that of *trans*-decalin increasing with the increasing pressure.

Although the reactivities of *cis*- and *trans*-decalin differ significantly, the yields (based on 100 moles of the reactant converted) of major products for the thermal decomposition of the three decalins show no significant differences. This means that the thermal decomposition of *cis*- and *trans*-decalins proceeds by the same mechanism.

2. Reaction Mechanisms. The observed product distributions from the thermal decomposition of decalin can be explained by the reaction mechanisms shown in **Figure 1.25-1**. The initiation occurs by homolytic cleavage of the carbon-carbon bond shared by both rings to form a biradical (eq 1). This biradical could undergo further reactions to form two small radicals and one or two unsaturated products, depending on the number of decomposition steps. The radicals can abstract hydrogen atoms from decalin to form three decalyl radicals (eq 2), of which most are 9-decalyl radicals. The 9-decalyl radical could decompose by β-scission to form 1-

cyclohexenylbutyl radical, which could either abstract a hydrogen atom from decalin to form 1-butylcyclohexene (eq 3a) or undergo ring closure and subsequent hydrogen abstraction to form spiro[4,5]decane (eq 3b). The 1-decalyl radical could undergo decomposition, followed by ring closure to form 1-indanylmethyl radical which could then be converted to 1-methylindan upon hydrogen abstraction (eq 4). The 2-decalyl radical could undergo the reactions shown in eq 5 to form methylenecyclohexane, which could then be converted to 1-methylcyclohexene.[3]

Toluene and n-butylbenzene can be formed from 1-methylcyclohexene and 1-butylcyclohexene, respectively, through dehydrogenation reactions. The latter two compounds seem to be unstable because their secondary allylic hydrogen atoms on the ring are easily abstractable. The formation of other compounds can be explained by different decomposition routes of three decalyl radicals and/or by further reactions of the major products.

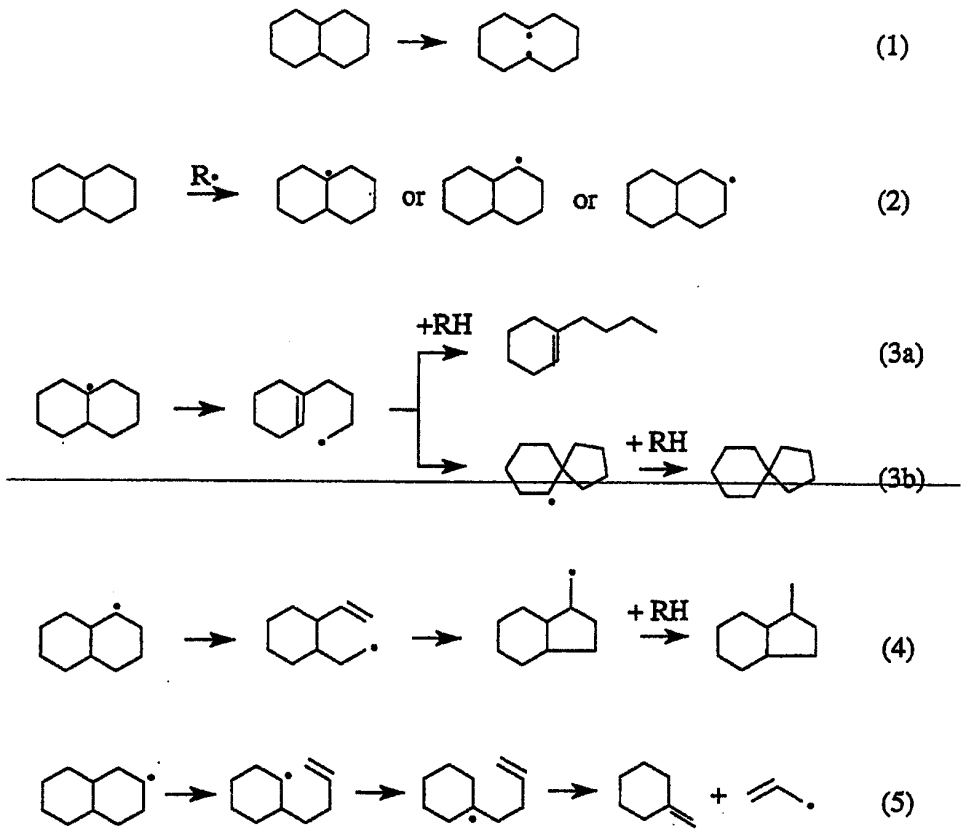

Figure 1.25-1. Reaction Mechanisms for Decalin Thermal Decomposition.

[1] Bredael, P. and D. Rietvelde. *Fuel.* 1979. 58. 215.

[2] *TRC Thermodynamic Tables-Hydrocarbons.* Thermodynamic Research Center, The Texas A & M University System, College Station, Texas, 1995.

[3] Schobert, H. H. et al. *Advanced Thermally Stable Jet Fuels, Technical Progress Report, April - June 1996.* The Pennsylvania State University. 1996.

1.26 Chemistry for Thermal Degradation of Bicyclic Hydrocarbon Components of Jet Fuels in Pyrolitic Regime

This study is explained in detail in *Advanced Thermally Stable Jet Fuels, Technical Progress Report, October–December 1997.*

Introduction

High-temperature thermal stability is an important property of advanced jet fuels for future high-Mach aircraft because they will also be used to cool critical engine components and may be exposed to temperatures above 450°C. We have established, through our previous work, that coal-derived jet fuels are more stable than petroleum-derived jet fuels near that temperature. Thermal degradation of petroleum-derived and coal-derived jet fuels in the pyrolytic regime is chemically complex and involves many parallel and consecutive reactions. We have discussed the reaction mechanisms for pyrolytic decomposition of normal long-chain paraffins,[1] cyclohexane, and alkylcyclohexanes,[2, 3] and the hydrogen-transferring pyrolysis of long-chain paraffins in the presence of hydrogen donors.[1, 4] This study addressed the relative stability of various hydrocarbons and reaction pathways for thermal degradation of cyclic hydrocarbons in the pyrolytic regime.

Relative Stability of Saturate Hydrocarbons

We carried out thermal stressing of about 40 pure hydrocarbons and determined their pseudo-first-order rate constants in the temperature range of 400-475°C, with most tests done at 450°C under nitrogen pressure in a batch microautoclave. Based on the results of such model fuel pyrolysis runs, we can discuss the relative stability of various cyclic and acyclic hydrocarbons and the pyrolytic reaction pathways of bicyclic hydrocarbons.

The relationships between stability of cyclic and acyclic hydrocarbons and their ring-size, side chain length or carbon number are based on the pseudo-first-order rate constants for pyrolysis at 450°C. In general, the cycloalkanes are more stable than the long-chain paraffins with the same or even smaller carbon number. For cycloalkanes, the stability decreases with increasing ring-size or increasing length of side chain. The range of applicable temperatures for these qualitative trends of stability is estimated to be 350-500°C. We could not ascertain whether the relationships would be valid at extremely high fuel temperatures such as 600-850°C where the differences in reactivity become less important.

The mechanisms of pyrolytic decomposition are discussed at length in the corresponding Technical Progress Report.[5]

Summary

We evaluated the relative stability of various types of hydrocarbon components in petroleum- and coal-derived jet fuels and found that the reactivity of alkanes/cycloalkanes increases with increasing chain/side-chain length. Cycloalkanes ($\geq$ 5-membered ring) are more stable than *n*-alkanes with the same carbon number. The *cis*-isomer usually decomposes about 3-5 times faster than the *trans*-isomer, with the exception of *trans*-1,3-dimethylcyclohexane, which decomposes about 2.5 times faster than its *cis*-isomer. The presence of a branch or branches appears to decrease the rate of decomposition as compared to that of the *n*-alkanes.

The reaction pathways for the isomerization, decomposition, and dehydrogenation reactions of decalins were proposed and discussed. The *trans*-decalin isomer is among the most stable hydrocarbons in the jet fuels boiling range. Cycloalkanes in general are more stable and produce substantially less solid in the pyrolytic regime under moderate to high-severity stressing. However, at extremely high temperatures, cycloalkanes may produce more solids as a result of faster dehydro-condensation reactions.

In addition, based on the results of pyrolysis reactions of model compounds at 400-475°C, a reactive structure index (RSI) system for different types of saturate compounds in jet fuels was developed by integrating several sub-indices determined from the structure via a simple group contribution method, including carbon group indices, ring index, and conformation index. Strong correlations between RSI and rate constant were obtained for 38 saturated hydrocarbons.[6]

---

[1] Song, C., W. C. Lai, and H. H. Schobert. *Ind. Eng. Chem. Res.* 1994. 33(3).

[2] Lai, W.-C., and C. Song. *Fuel Processing Technology.* 1996. 48 (1).

[3] Song, C., W.-C. Lai, and H. H. Schobert. Am. Chem. Soc. Div. Fuel Chem. Prepr. 1992. 37 (4). 1655.

[4] Selvaraj, L. et al. *Energy & Fuels.* 1994. 8 (4). 839.

[5] Schobert, H. H. et al. *Advanced Thermally Stable Jet Fuels, Technical Progress Report, October - December 1997.* The Pennsylvania State University. 1998.

[6] Lai, W.-C. and C. Song. *Am. Chem. Soc. Div. Petrol. Chem. Prepr.* 1996. 41(2). 524.

1.27 Reactive Structure Index for Correlation of High Temperature Stability of Saturated Hydrocarbons

This study is explained in detail in *Advanced Thermally Stable Jet Fuels Technical Progress Report, January–March 1996.*

Introduction

We examined how the structure of various (jet fuel range) hydrocarbons affects their thermal stability at temperatures above 400°C under elevated pressures. Our objective was to develop a reactive structure index (RSI) to correlate the molecular structures of saturated hydrocarbons with their decomposition rate constants using a group contribution method. We studied the effects of ring-structure, side-chain length (up to C_{10}), steric isomers, and branching on the decomposition rate of open-chain alkanes and cycloalkanes at 450°C under an initial pressure of 0.79-MPa N_2 in batch reactors. The RSI was derived by integrating several sub-indices determined from the structure via a simple group contribution method, including carbon group indices, ring index, and conformation index.

Although group contribution has been used in other applications, this work is novel in that we developed a reactive structure index (RSI) system that incorporates the effects of ring structure, side-chain length, steric isomers, and length and branching on the reactivity of open-chain alkanes and cycloalkanes. The pyrolysis experiments were carried out in or near the supercritical region, which is relevant to the anticipated environments in future high-Mach jet aircraft.

Experimental

In total, 38 reagent-grade hydrocarbons were used in this study. Classes of compounds studied were

- *n*-alkanes (C_mH_{2m+2}, m = 5-12, 14, 16)
- Branched alkanes including 2,2,4-trimethylpentane, 2,2,5-trimethylhexane, 3-methylundecane, and 2,2,4,6,6-pentamethylheptane
- Cycloalkanes including cyclohexane, seven *n*-alkylcyclohexanes (alkyl side-chain = CmH_{2m+l}, m = 1, 2, 3, 4, 6, 8, 10), isopropylcyclohexane, isobutylcyclohexane, tert-butylcyclohexane, cyclopentane, and methylcyclopentane
- Bicyclics including dicyclohexyl, 1,2-dicyclohexylethane, and dicyclopentyl
- Steric *(trans- and cis-)* isomers including 1,2-dimethylcyclohexane (DMCH), 1,3-DMCH, 1,4-DMCH, and decahydronaphthalene (decalin).

Pyrolytic reactions were performed in 23.2-mL stainless steel tubing bomb reactors at 450°C for a heating period of 21-480 minutes under an initial pressure of 0.79 MPa UHP-N_2. The reactor was loaded with 5-mL samples and leak-tested. To ensure an inert environment and minimize oxidation reactions, the sealed reactor was purged repetitively (six times) with 6.9 MPa UHP-N_2 to remove air and dissolved oxygen in the sample. The reactor was then pressurized to 0.79 MPa with UHP-N_2 before being immersed in a fluidized sand bath preheated to 450°C. The

reactor was quenched in a cold water bath and the gaseous and liquid products were collected and analyzed using a GC and GC-MS, respectively.[1]

Results and Discussion

The pseudo-first-order rate constants of hydrocarbons at elevated pressure were chosen as the measure of their reactivities. Pyrolysis at 450°C was approximated by a first order relation as shown in Equation 1

$$-\frac{dC}{dt} = kC \qquad (1)$$

where C is the reactant concentration (mol/cm^3), t is the reaction time (h), and k is the first-order rate constant (h^{-1}). The first-order rate constant was derived from reactant conversion (X) as shown in Equation 2.

$$k = \frac{1}{t}\ln\frac{1}{1-X} \qquad (2)$$

Based on these calculations, we found that:

- The decomposition rate of n-alkanes/n-alkylcyclohexanes (ACH) increased with increasing chain/side-chain length. The overall decomposition rate for n-alkanes and n-ACH was a linear function of TCN over the entire carbon number range studied except for cyclohexane and methylcyclohexane, indicating that n-ACH with long side chains reacted like n-alkanes.
- The general reaction mechanism of n-alkanes was characterized by radical mechanisms involving initiation, hydrogen abstraction, radical isomerization such as 1,5- and 1,4-shift isomerization, radical decomposition, radical addition, and termination.
- The major reaction pathways of n-ACH strongly depend on the side-chain length.
- Although the compounds differ widely in structure, they can all be constructed from a small number of functional groups, and their decomposition mechanisms display some similarities. Therefore, the linear group contribution may be applicable to the estimation of compound reactivity. n-Alkylcyclohexanes are more stable than n-alkanes with the same total carbon number (TCN).
- The compounds with the 5-membered ring were more stable than those with a 6-membered ring.
- The rate constants of three sets of isomers (normal and branched alkanes) demonstrated that the presence of a branch or branches appears to decrease the rate of decomposition as compared to that of the n-alkanes. This implies that the overall decomposition rate is a function of both TCN and the types of carbons in the alkanes

- The *cis-* isomer usually decomposes about 3-5 times faster than the trans-isomer, with the exception of trans-1,3-DMCH, which decomposes about 2.5 times faster than its *cis*-isomer.

These results indicate that RSI may be derived by integrating several structure sub-groups determined from the structure via a simple group contribution method, including carbon group index, ring index, and conformation index. We found that the RSI can be derived by a simple linear combination of six sub-group indices:

$$RSI = \sum_{j=1}^{6} a_j I_j \qquad (3)$$

where a_j (j=1,...,6) is the number of sub-groups; I_j (j=1,...,4) is the carbon group index including primary, secondary, tertiary, and quaternary, respectively; I_5 is the ring index, and I_6 is the correction index to distinguish the interactions of non-bonded, next-nearest neighbors such as conformational effects and 1,5-H repulsion.[2]

The pseudo-first-order rate constant (k, a measure of reactivity) depending on the overall RSI, was assumed to follow the linear Equation 4.

$$k = a + b\,(RSI) \qquad (4)$$

The constants a and b in Equation 4 and Ij (j=1,...,6) in Equation 3 were determined from the data of 38 model compounds by regression analysis. The values of the sub-indices were empirically determined. A plot of the experimental rate constants as a function of the RSI produced the following linear relationship at 450°C:

$$k_{pred} = 0.54 + 0.0178\ RSI \qquad (5)$$

The sub-group indices and Equation 5 reliably predicted rate constants over a wide range (two orders of magnitude) of decomposition rates. Note that *k* increases with increasing RSI, but the relationship is not strictly linear. In fact, the linear relationship given in Equation 5 is just a special case of a more general quadratic relationship.

To further examine the applicability of the sub-group indices and RSI data in different reaction conditions, we performed additional experiments using 17 hydrocarbons in different reactors with larger capacity (28 mL). The new experiments were carried out at a lower effective reaction temperature than 450°C and with smaller reactant concentrations. The results demonstrated the following quadratic relationship:

$$k_{pred} = -0.144 + 0.00267\ RSI + 6.76 \times 10^{-5}\ (RSI)^2 \qquad (6)$$

These results demonstrate the potential usefulness of RSI in predicting thermal stability and to screen potential thermally stable compounds.

The RSI correlation developed in this work for saturated hydrocarbons should also be applicable to aromatic compounds, such as alkylated benzenes, by introducing a ring index for

the aromatic ring. These compounds all proceed through radical mechanisms involving similar elementary steps such as initiation, hydrogen abstraction, radical isomerization, radical decomposition, radical addition, and termination.

Because of the fundamental nature of the chosen sub-groups, such as carbon types, the indices are expected to be valid for many more hydrocarbons. Another benefit of developing RST based on carbon types is that the primary, secondary, tertiary, and quaternary carbons of saturated hydrocarbons can be easily distinguished through ^{13}C NMR. Finally, the current RSIs are derived based on reactivity of pure compounds at 450°C. The RSI results may only be applicable to reactions near 450°C, and may not be applicable to a mixture system.

Conclusions

A reactive structure index was developed to correlate the molecular structures of saturated hydrocarbons with their reactivities using a simple linear group contribution method. The RSI is composed of several sub-indices determined from the structure, including carbon group indices, ring index, and conformation index. We examined the effects of ring structure, side-chain length (up to C_{10}), steric isomers, and branching on decomposition rate. We achieved good correlations between RSI and pseudo-first-order rate constants for two sets of saturated hydrocarbons (38 and 17 compounds, respectively).

The reactivity of alkanes/cycloalkanes increased with increasing chain/side-chain length. Cycloalkanes ($\geq$ 5-membered ring) are more desirable components for advanced jet fuels, in terms of higher stability and density, than *n*-alkanes of the same carbon number. The *cis*-isomer usually is more reactive than the *trans*-isomer except for *cis-1,3*-dimethylcyclohexane, which is more stable than its *trans*-isomer. The presence of a branch or branches appears to decrease the decomposition rate compared to *n*-alkanes.

---

[1] Song, C., W.-C. Lai, and H. H. Schobert. "Condensed-Phase Pyrolysis of n-Tetradecane at Elevated Pressures for Long Duration. Product Distribution and Reaction Mechanisms." *Ind. Eng. Chem. Res.* 1994. 33. 534-547.

[2] Benson, S. W. *Thermochemical Kinetics, Methods for the Estimation of Therinochemical Data and Rate Parameters*. 2nd ed. Wiley: NewYork. 1976.

1.28 PYROLYSIS OF BUTYLBENZENES: EFFECTS OF STRUCTURE OF ALKYL SIDE CHAIN ON THE PYROLYSIS OF ALKYLBENZENES

This study is explained in detail in *Advanced Thermally Stable Jet Fuels Technical Progress Report, August 1992 – October 1992.*

Introduction

In 1989, Freund and others[1] proposed a reaction mechanism for pyrolysis of *n*-butylbenzene at low conversion, based on detailed kinetic modeling with no involvement of the secondary reaction. Extensive mechanistic and kinetic studies of long chain alkylbenzene conducted by Savage[2,3] and Billaud[4] identified two pairs of major products—toluene plus N-1 carbon atom alkene (where N is the number of carbons in the alkyl side chain) and styrene plus N-2 carbon atom alkane. The work demonstrated the following:

- The most probable reactive sites in an alkylaromatic compound are at the C_α-C_β position in the side chain
- Resonance stabilization of the benzene ring effectively lowers the strength of the C_α-C_β bond
- The pyrolysis behavior of alkyaromatics resembles that of aromatic compounds when the side chain is short. When the side chain is longer, the pyrolysis resembles that of the long chain paraffins.
- The nature of the core aromatic structure is such that as the number of aromatic rings increases, there is a net increase in the reaction rate and, simultaneously, the linkage between the alkyl group and the aromatic rings becomes easier to break as a result of the "autocatalytic effect."[5]

Our study focused on the pyrolysis of four isomeric alkylbenzenes: *n*-butylbenzene (n-BB), isobutylbenzene (i-BB), sec-butylbenzene (s-BB) and tert-butylbenzene (t-BB) at higher pressure (0.69 MPa) and higher substrate conversions. The effects of the structure of the alkyl side chain on the pyrolysis in terms of product (gaseous liquid and solid) formation and distribution were studied in detail. This summary presents the pyrolytic pathways of the four butylbenzenes and their tendencies of solid formation and emphasizes the importance of bimolecular and secondary reactions in pyrolysis at high pressure and high substrate conversions.

Experimental

Thermal stressing tests were conducted in batch tubing bomb reactors using commercially obtained reagent-grade chemicals. The reactors were immersed in a fluidized sand bath at 450°C. The reactor was loaded with 5.00 ml of the model compound. The compound was deoxygenated by repeated pressurizing to 7 MPa ultra high purity (UHP) nitrogen and purging (five times) after the reactor was sealed. A starting pressure of 0.69 MPa was used for each test. The reactor reached the reaction temperature within 6 to 7 minutes after immersion in the sand bath. After the desired reaction duration, the reactor was removed from the sand bath and quenched in cold water to ambient temperature. A detailed description of the experimental methodology—including the measurement and calculation of gas and liquid products—is provided in the corresponding Technical Progress Report.[6]

Results and Discussion

1. Rate of disappearance of substrate compounds. The original report presented the curves of the disappearance of butylbenzenes with reaction time pyrolyzed at 450°C (**Figure 1.28-1**). The reactions of each compound seem to initially proceed through the most thermodynamically favorable bond homolysis path to form resonance stabilized benzyl or benzylic-type radicals:

$C_6H_5CH_2C_3H_7 \rightarrow C_6H_5CH_2\bullet + n\text{-}C_3H_7\bullet$ (a)

$C_6H_5CH(CH_3)C_2H_5 \rightarrow C_6H_5\dot{C}HCH_3 + C_2H_5\bullet$ (b)

$C_6H_5CH(CH_3)C_2H_5 \rightarrow C_6H_5\dot{C}HC_2H_5 + CH_3\bullet$ (c)

$C_6H_5CH_2CH(CH_3)_2 \rightarrow C_6H_5CH_2\bullet + CH_3\dot{C}HCH_3$ (d)

$C_6H_5C(CH_3)_3 \rightarrow C_6H_5\dot{C}(CH_3)_2 + CH_3\bullet$ (e)

This study determined that t-BB decomposes more slowly than the other three isomers, unlike earlier studies which pyrolyzed alkylbenzenes using carrier techniques and very low pressure pyrolysis. Most of the studies measured either heats of formation of radicals or the calculation of C_α-C_β bond dissociation energies (BDE) in the side chain of the alkylbenzenes. An important determinant of the accuracy of the data obtained was the degree to which secondary reactions could be eliminated. As a result of flow techniques using toluene as a radical scavenger, these previous studies concluded that *n*-BB had an activation energy significantly higher than t-BB. Our results indicated just the opposite.

Calculations of bonding energies at 450°C of α (alkyl-aryl) and β (C_α-C_β) bonds in the side chains of butylbenzenes gave the results in **Figure 1.28-2**. Although the BDE value for t-BB is a slightly lower than those of the other three isomers, the difference is not significant compared to the large scattering of the thermodynamic data (usually ±2 kcal/mol).

The differences in the rate of the disappearance of the reactants must be attributed to factors other than bonding energies. In the present study, the reactions were carried out at 450°C under 0.69 MPa N_2 over-pressure. This high pressure enabled secondary reactions to occur after a short period of reactions. There seemed to be little difference in the rate of pyrolysis within the first 15 minutes (see Figure 1.28-1). Because all four compounds have similar bonding energy at the β position, they showed similar rates of reaction. As the reactions proceeded, bimolecular or even secondary reactions become more important. Typical bimolecular reactions included β-bond scission and H-abstraction, with the latter being preferred in a high pressure system[7]. The H-abstraction and β-bond scission reactions that likely occurred in the reactor are listed below.

H-abstraction:

$C_6H_5CH_2C_3H_7 + R\bullet \rightarrow C_6H_5CH\bullet C_3H_7 + RH$ (f)

$C_6H_5CH(CH_3)C_2H_5 + R\bullet \rightarrow C_6H_5C\bullet(CH_3)C_2H_5 + RH$ (g)

$C_6H_5CH_2CH(CH_3)_2 + R\bullet \rightarrow C_6H_5CH\bullet CH(CH_3)_2 + RH$ (h)

$C_6H_5C(CH_3)_3 + R\bullet \rightarrow C_6H_5C(CH_3)_2CH_2\bullet + RH$ (i)

β-bond scission:

$$C_6H_5CH\bullet C_3H_7 \rightarrow C_6H_5CH{=}CH_2 + C_2H_5\bullet \quad (j)$$

$$C_6H_5C\bullet(CH_3)C_2H_5 \rightarrow C_6H_5C(CH_3){=}CH_2 + CH_3\bullet \quad (k)$$

$$C_6H_5CH\bullet CH(CH_3)_2 \rightarrow C_6H_5CH{=}CHCH_3 + CH_3\bullet \quad (l)$$

There are several unique characteristics in the reactions regarding t-BB. The $C_6H_5C(CH_3)_2CH_2\bullet$ radicals formed in reaction (i) are not resonance-stabilized radicals, such as those formed in reactions (f), (g) and (h). Therefore, we can infer that the rate of reaction (i) would either be unfeasible or significantly slower than the others. On the other hand, all of the benzylic or benzylic-type radicals formed after H-abstraction reactions in (f), (g), and (h) can easily undergo β-bond scission to form styrene series compounds according to reactions (j), (k), and (l). Therefore, t-BB cannot react in a similar manner, because of the lack of benzylic-hydrogen or β-hydrogen in $C_6H_5C(CH_3)_2CH_2\bullet$ radicals. This would account for its low reactivity.

The rates of secondary reactions play a dominant role in the pyrolysis of butylbenzenes at later stages. Concurrently, larger differences occur in the rates of substrate conversion in the pyrolysis after 15 minutes .

2. Tendencies of solid deposit formation from butylbenzenes. **Figure 1.28-3** shows the yields of solid products formed between 0 and 8 hours, demonstrating that each compound has a different induction time for the formation of solid products. This induction period reflects the ability of the compound to resist the formation of solid products. As shown in Figure 1.28-1, t-BB has the longest induction time and *n*-BB has the shortest. The order of the induction period for the four compounds is *n*-BB<s-BB<i-BB<t-BB—the same as their rates of disappearance.

The amounts of the solids formed increase with the reaction time for s-BB, i-BB, and t-BB, and their rates of increase are similar. This behavior is similar to that of jet fuels, which also exhibit monotonic increases in the amount of solid products. Although solid products are quickly formed in the pyrolysis of *n*-BB, the rate of their formation is significantly lower than that of the other three isomers, and the amounts almost leveled off to an asymptotic value around 5 hours. As a result, the least amounts of solids are formed from the reactions of *n*-BB after 8 hours at 450°C. These patterns of solid formation are certainly correlated to the reaction kinetics of individual compounds. The differences in the compositions of gaseous and liquid products might be responsible for the different behaviors in their solid formation, as discussed below.

3. Product distribution and lumping of major products. **Table 1.28-1** provides an overall picture of the molar yields of the major gaseous and liquid products from the pyrolysis of butylbenzenes at 450°C for 1 hour. It appears that the complex mixture of hundreds of compounds in the gaseous and liquid products can be lumped into five groups: gaseous products, cracking products, isomerization products, stable high molecular weight products, and intermediate products, according to their phase in the reactor and in situ thermal stabilities during reactions.

Conclusions

The structures of the side chain in alkylbenzenes significantly affect their reactivities and solid formation tendencies. In the initial short period of pyrolysis, the pyrolysis reactions were controlled by rate of the unimolecular dissociation processes of $C\alpha$-$C\beta$ bonds in the side chains. The four compounds studied exhibited similar rates of disappearance initially, because of their similar $C\alpha$-$C\beta$ bonding energies. After the initial period of reaction, the rates of the disappearance of the substrates are determined by the secondary reactions other than the one mentioned above because of the presence of high pressure. The order of reactivity was found to be *n*-BB > s-BB > i-BB > t-BB in terms of their rates of consumption.

Isomerization reactions occur during the pyrolysis of butylbenzenes in competition with the characteristic breakdown of individual compounds. Isomerization plays an important role in the pyrolysis of t-BB. It showed a large extent of isomerization to i-BB, and to s-BB to a lesser extent. It is proposed that the mechanism to form i-BB is through a so-called neophyl rearrangement process caused by the strains in the α-bonds of t-BB. The mechanism helps to explain the low reactivity of t-BB and some similar behavior between the pyrolysis of i-BB and t-BB.

In a whole spectrum of products, cracking products, such as benzene, toluene and ethylbenzene are stable at 450°C. C-3 substituted benzenes are unstable only at very high conversions. High molecular weight products, such as naphthalene, biphenyl, methyl-biphenyls, terphenyls, methylterphenyls and phenylnaphthalenes seem to be "inactive" or "passive" in the pyrolysis. Unless attacked by very reactive radicals, they are probably quite stable. Styrene-series compounds, on the other hand, can easily be involved in chain reactions to form large radicals. These compounds may be unstable intermediate compounds which facilitate the polycondensation reactions and therefore solid product formation.

It appears necessary to differentiate the reactivity (defined in terms of the rate of substrate consumption) of a compound and its solid formation tendency. The properties of the product mixture formed during the ongoing reactions determine the solid formation tendency. Although *n*-BB quickly disappeared during pyrolysis, it does not form the highest amount of solids, because it produces significant amounts of cracking products (such as toluene and ethylbenzene) and stable high molecular weight products (such as naphthalene). It also produces less styrene-series compounds. In contrast, a variety of styrene series compounds are identified in the liquids of t-BB, i-BB and s-BB, which also form higher amounts of solid products.

Table 1.28-1 Molar Yields (%) of Major Products from the Pyrolysis of Butylbenzenes

Compounds	n-BB	s-BB	i-BB	t-BB
CH_4	2.90	35.21	17.89	3.50
C_2H_6	19.89	3.28	1.17	0.02
C_2H_4	0.11	1.27	0.15	0.05
C_3H_8	1.1	0.52	2.04	0.04
C_3H_6	2.15	0.28	5.49	0.02
i-C_4H_{10}				0.11
Benzene	0.36	0.27	0.33	0.35
Toluene	27.25	2.25	9.05	0.37
Ethylbenzene	13.04	8.57	1.21	0.06
Styrene	1.30	0.27	0.38	
Isopropylbenzene	0.93	11.35	0.35	0.50
n-Propylbenzene	1.16	2.28	2.22	0.06
Allylbenzene		0.12	0.40	
t-Butylbenzene		0.03	ND	85.63
i-Butylbenzene	0.39	0.05	66.23	3.11
s-Butylbenzene	1.18	55.13	0.41	0.55
α-Methylstyrene		0.31	0.11	0.36
2-Methylstyrene	0.13		1.89	0.21
Methylpropenylbenzene		0.97	0.32	0.14
n-Butylbenzene	37.10	ND	ND	
Trans-β-methylstyrene		2.20	7.10	0.73
t-Butyl-3-methylbenzene				0.03
C_5-Benzene	0.25	0.37	0.08	
α-Ethylstyrene		1.01		
Dimethylstyrene		1.86	0.16	0.01
Methylindans	0.21	0.08	0.25	0.20
2-Allyltoluene	1.18		0.80	
4-Ethylstyrene		0.12		
C_6-Benzenes	0.13			
Methylindenes		0.24	0.09	
Cyclopentylbenzene	0.24	0.07		
Naphthalene	1.39	0.26	0.61	
C_7-Benzenes	0.47			
2-Methylnaphthalene	0.15	0.09	0.13	0.02
1-Methylnaphthalene	0.29	0.21	0.09	
2-Ethylnaphthalene	0.04	0.06		
Biphenyl	0.14	0.10	0.06	0.02
1-Ethylnaphthalene	0.03	0.05		
Dimethylnaphthalene		0.10	0.05	
Diphenylmethane	0.19	0.07	0.07	
Methylbiphenyls	0.11	0.06	0.07	
Methyl-t-butylbiphenyls				0.05
Di-t-butylbiphenyls				0.06
C_2-Biphenyls		0.13	0.03	
Bibenzyl	0.30	0.11	0.09	
Diphenylpropanes	0.36		0.02	
Fluorene		0.01	0.04	
Diphenylbutanes	0.39			
Diphenylethylenes		0.11		
Diphenylhexanes	0.92			
1-Phenylnaphthealene	0.19			
Terphenyls	0.11	0.31	0.04	
2-Phenylnaphthalene	0.07	0.12	0.04	0.05

ND: not determined because it coelutes with other peaks

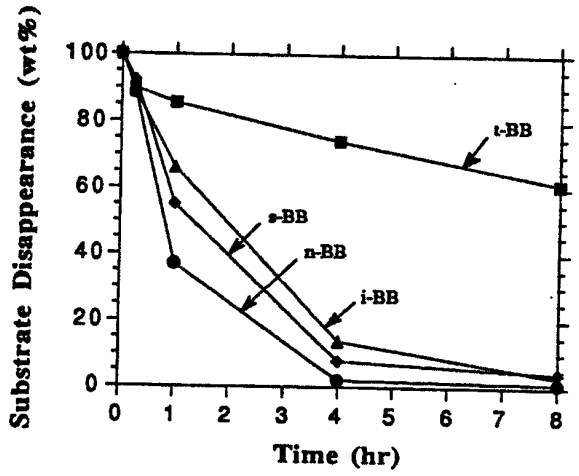

Figure 1.28-1. The Disappearance of the Substrate Compounds with Reaction Time at 450°C

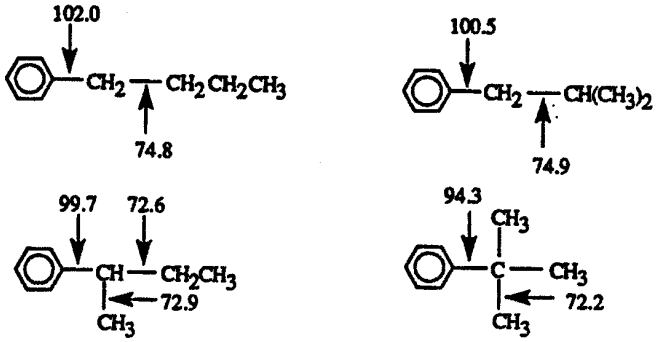

Figure 1.28-2. Bonding Energies of α and β Bonds in Butylbenzenes at 450°C

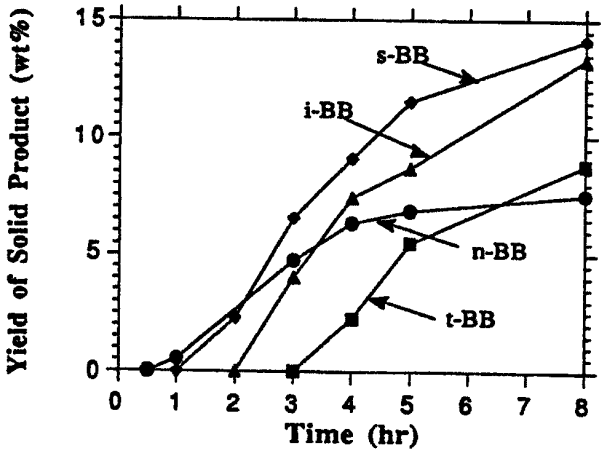

Figure 1.28-3. The Formation of Solid Products Versus Reaction Time at 450°C from the Pyrolysis of Butylbenzenes

[1] Freund, H. and W.N. Olmstead. *Int. J. Chem. Kinetics*. 1989. 21, 561.

[2] Savage, P.E. and D.J. Korotney. *Ind. Eng. Chem Res.* 1990. 29, 499.

[3] Savage, P.E. and M.T. Klein. *Ind. Eng. Chem Res.* 1987. 26,488.

[4] Billaud, F., et al. *Ind. Eng. Chem Res.* 1988. 27, 1529.

[5] Savage, P.E., G.E. Jacobs, and M. Javanmardian. *Ind. Eng. Chem. Res.* 1989. 28, 645.

[6] Schobert, H. H. et al. *Advanced Thermally Stable Jet Fuels, Technical Progress Report, August -October 1992*. The Pennsylvania State University. #92PC92104-TPR-1. 1992.

[7] Poutsma, M.L. *Energy Fuels*. 1990. 4, 113.

1.29 EXPLORATORY STUDY OF GAS PHASE PYROLYSIS OF *N*-BUTYLBENZENE AT ATMOSPHERIC PRESSURE IN FLOW REACTOR

This study is explained in detail in *Advanced Thermally Stable Jet Fuels Technical Progress Report, July—September 1993*

Introduction

Previous studies have been conducted at elevated pressures, with 100 psi ultra-high purity (UHP) N_2 (cold) as the most often used operating condition. This study was conducted to compare the pyrolysis reactions of alkylbenzenes (specifically *n*-butylbenzene) stressed under elevated pressures and at atmospheric pressure.

The reaction mechanisms and kinetics of most short-chain alkylbenzenes have been studied at high temperature, short residence times and in the gas phase.[1] This operating condition enhances the primary reactions of the substrate molecule, minimizing the complex secondary reactions and, therefore, simplifying the reaction mechanism and kinetics. β-bond scission is promoted in an atmospheric pressure reaction relative to H-transfer reactions.

This study was conducted at three different temperatures, 600¡C, 550¡C and 500¡C. By extending the high-temperature gas-phase reaction to the complex supercritical reaction condition (450¡C, 100 psi UHP N_2) typically used for alkylbenzene stressing, taking into account the pressure effect, we hoped to elucidate a more detailed reaction mechanism and establish a model describing the complex reaction kinetics.

Experimental

n-Butylbenzene was pyrolyzed under 600¡C, 550¡C, and 500¡C in a Xytel Automat IV flow reactor (shown in **Figure 1.29-1**) which was constructed of stainless steel and designed with one preheating zone (Zone 1) and three heating zones (Zones 2, 3 and 4). The volume of the reactor is 24.83 mL. There are three gas delivery systems. Two are for N_2 and one is for air. One N_2 line was used in this study; N_2 served as a diluent gas. *n*-Butylbenzene was provided through a 50 mL feed supply syringe and the 5 mL feeding syringe to the reactor. Manual and computer-controlled electronic solenoid valves combined with the mass flow meters to isolate and distribute the required gas flow through the system. The product isolation and analysis network consisted of a liquid product receiver (cooling trap) and a gaseous product receiver. Gaseous products were collected after reaction into gas bags by water displacement. The amount of product gas obtained was calculated by the mass of water displaced and recorded by the balance. All data were collected and stored by the computer. The amount of liquid products were obtained by weighing the liquid receiver before and after the reaction. Solid formation was ignored because of the relatively short residence times of the reactions.

Results and Discussion

1. Experiment Profiles. A total of 23 preliminary experiments, separated into 5 groups, were conducted. Groups 1 and 2 tested the effects of changing the flow rate of N_2 and *n*-butylbenzene. With Groups 3, 4, and 5, we varied the reaction temperatures and residence times of *n*-butylbenzene, while keeping the molar ratio of N_2 and *n*-butylbenzene unchanged. **Table 1.29-1** shows the experimental parameters and raw data obtained from the 23 runs.

2. Residence time calculation. The residence time of each run was determined by the volume of the reactor (V, mL) divided by the total volumetric flow (V',mL/s). Volumetric flow through the reactor depended on the flow rate of *n*-butylbenzene (R_{NB}, ml/min), flow rate of N_2 (R_{N2}) and total molar density of the two feeds. Volumetric flow was calculated from the following equation:

$$V' = (n_1 + n_2) / (\rho_1 + \rho_2) \quad (1)$$

where ρ_1 (mol/mL) is the molar density of *n*-butylbenzene, ρ_2 (mol/mL) is the molar density of N_2, n_1 is the molar flow rate of *n*-butylbenzene (mol/s) and n_2 is the molar flow rate of N_2 (mol/s). From the ideal gas law,

$$\rho_1 = \rho_2 = P / RT \quad (2)$$

The molar flow rate of *n*-butylbenzene (mol/s) can be determined from:

$$n_1 = R_{NB} \times 0.86 / (60 \times 134) \quad (3)$$

The molar flow rate of N_2 (mol/s) can be determined from:

$$n_2 = R_{N2} / (22400 \times 60) \quad (4)$$

Therefore, the residence time, τ, can be calculated as:

$$\tau = V / V' = (\rho_1 + \rho_2) \times V / (n_1 + n_2) \quad (5)$$

3. Product distribution and analysis. Only preliminary data are reported here. Some makeup experiments and data analysis occurred later and appear in later studies within this report. **Figures 1.29-2**, **1.29-3**, and **1.29-4** show the variations of the rates of formation of some major gaseous and liquid products with N_2 flow rate. For most of the product compounds, the amount formed per minute declined as the N_2 flow rate was increased. The amount formed per minute of C_4 gaseous species seemed to increase as the rate of N_2 increased; however, because the concentrations of the C_4 gaseous species were relatively limited compared to other gaseous species, these fluctuations might be in the range of experimental error.

Another noteworthy trend involves ethylene and propylene. Similar to the situations in the tubing bomb reactions where elevated pressures are used, these two substances went through a maximum as the rate of N_2 was increased. Far fewer compounds were detected in the liquid products, as compared with the tubing bomb reactions, although the major compounds identified were the same (e.g., benzene, toluene, ethylbenzene, styrene, C_3-benzene, methylstyrene, C_4-benzene, naphthalene, and biphenyl). Among them, styrene was the most abundant. This is significantly different from pressurized reactions, where toluene and ethylbenzene comprised a high portion of liquid and styrene was always less important. **Figures 1.29-5**, **1.29-6**, and **1.29-7** show the variations of some major gaseous and liquid products with varying *n*-butylbenzene flow rates. Monotonic increases of each product with the concentration of butylbenzene has been observed. Similar to the above, styrene shows highest amount among the products.

The pyrolysis of *n*-butylbenzene was also conducted at 600¡C, 550¡C, and 500¡C. Under a similar molar ratio of 0.8 (*n*-butylbenzene to N_2), different flow rate combinations of the two

feed materials were selected (Table 1.29-1) in order to vary the residence time of each run. The residence time range chosen was from 4.5 seconds to 3.63 minutes. The results are shown in **Figures 1.29-8 through 1.29-14**. These figures demonstrate that the rates of formation of all species (mol/min) decrease after a relatively long reaction time. A similar type of rate inhibition effect was observed in tubing bomb reactions where the rates of decomposition of the substrate compounds decreased with thermal stressing time. At 600¡C, the decreasing trends for most of compounds were monotonic, as shown in Figures 1.29-8, 1.29-9 and 1.29-10. For 550¡C and 500¡C, the rates of most of species go through a maximum before finally declining at long residence times. The reason for this phenomenon cannot be fully understood without additional study.

Table 1.29-1. Operating Parameters and Some Raw Data Collected from Each Run

Sample number	Reaction temp. (¡C)	Rate of NB ml/min	Rate of N_2 ml/min	Volume product gas ml	Duration gas collection min	Receiver before reaction g	Receiver after reaction g	Liquid weight g	Duration liquid collection min
NB4	600	0.1269	7.16	153	9.75	33.434	32.456	0.978	10.25
NB5	600	0.1269	26.60	320	9.58	35.080	34.134	0.946	10.00
NB6	600	0.1269	50.00	523	9..00	33.304	32.472	0.832	10.25
NB7	600	0.1269	100.14	1083	10.42	33.382	32.544	0.838	10.72
NB8	600	0.3399	19.11	142	5.08	35.671	34.143	1.528	5.40
NB9	600	0.1679	19.11	264	10.00	33.747	32.460	1.287	10.17
NB10	600	0.0670	19.11	198	9.63	33.020	32.537	0.483	10.00
NB11	600	0.03343	19.11	352	21.50	34.398	34.145	0.253	21.72
NB12	600	0.1269	20.80	181	9.57	33.363	32.528	0.835	10.00
NB13	600	0.2517	42.75	451	9.70	36.185	34.127	2.058	10.00
NB14	600	0.0670	11.23	110	9.75	32.981	32.536	0.445	10.00
NB15	600	0.0256	4.55	160	21.08	32.670	32.453	0.217	21.33
NB16	600	0.6671	111.71	233	4.67	36.853	32.453	4.400	4.92
NB18	500	0.1269	20.85	178	9.67	33.686	32.471	1.215	10.00
NB19	500	0.6671	111.79	397	3.80	36.522	34.130	2.392	4.00
NB20	500	0.03343	5.64	166	39.70	33.580	32.519	1.061	40.00
NB21	500	0.0129	2.48	42.3	39.58	34.167	34.122	0.045	40.00
NB22	500	0.2517	42.39	436	10.67	34.876	32.453	2.423	11.00
NB24	550	0.2517	42.78	411	9.60	36.283	34.135	2.148	10.00
NB25	550	0.1269	21.15	199	8.716	33.483	32.454	1.029	10.00
NB26	550	0.0129	2.27	232	10.00	34.226	34.124	0.102	10.27
NB27	550	0.0670	11.57	222	9.65	33.509	32.443	1.066	10.00
NB28	550	0.6671	111.11	444	3.78	36.608	34.147	2.461	4.00

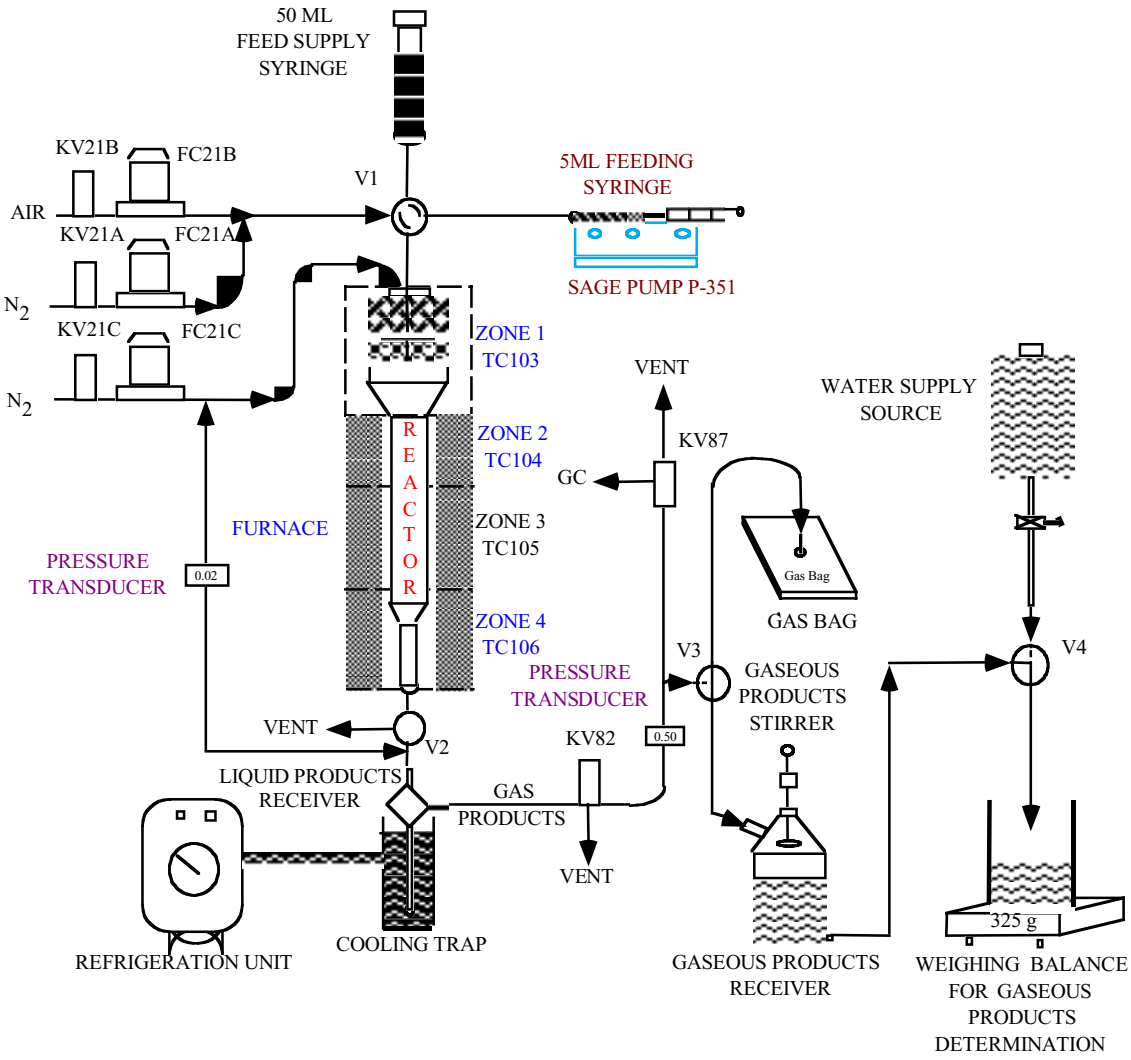

Figure 1.29-1. Schematic Diagram of the Xytel Equipment

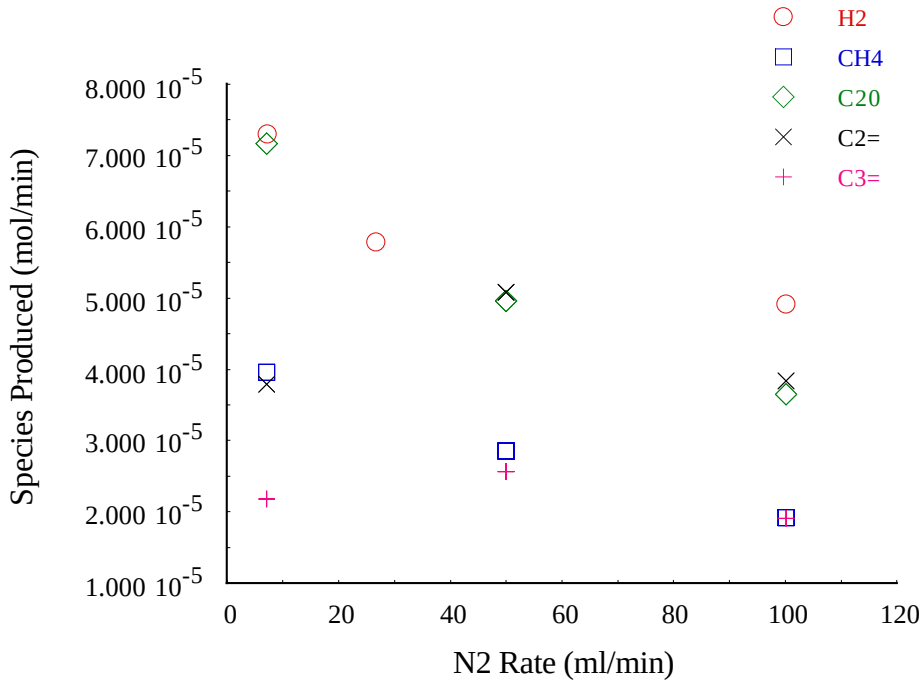

Figure 1.29-2. Variations of Some Gaseous Products with N_2 Flow Rate at 600¡C

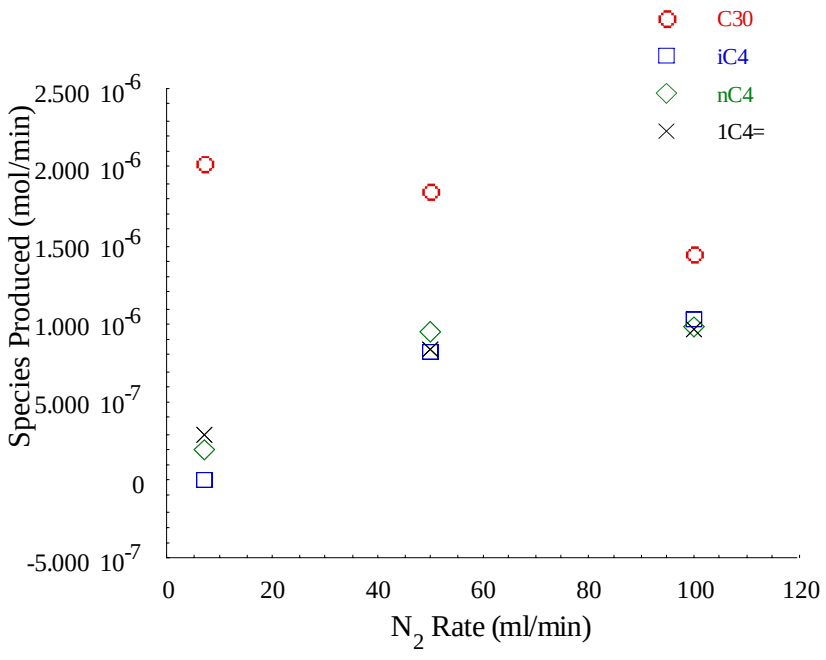

Figure 1.29-3. Variations of Some Gaseous Products with N_2 Flow Rate at 600¡C

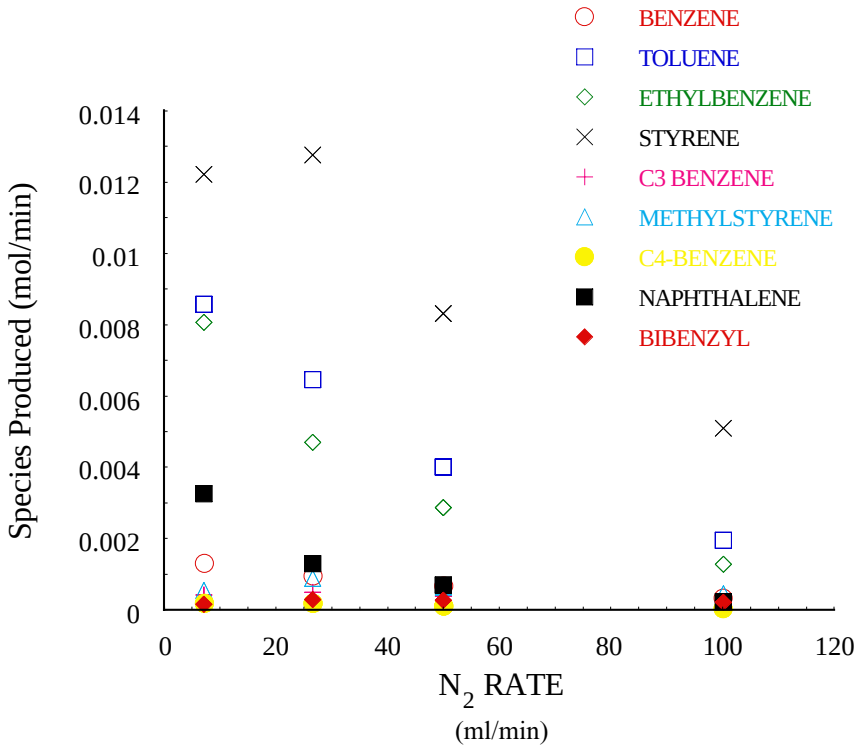

Figure 1.29-4. Variations of Some Major Liquid Products with N_2 Flow Rate at 600¡C

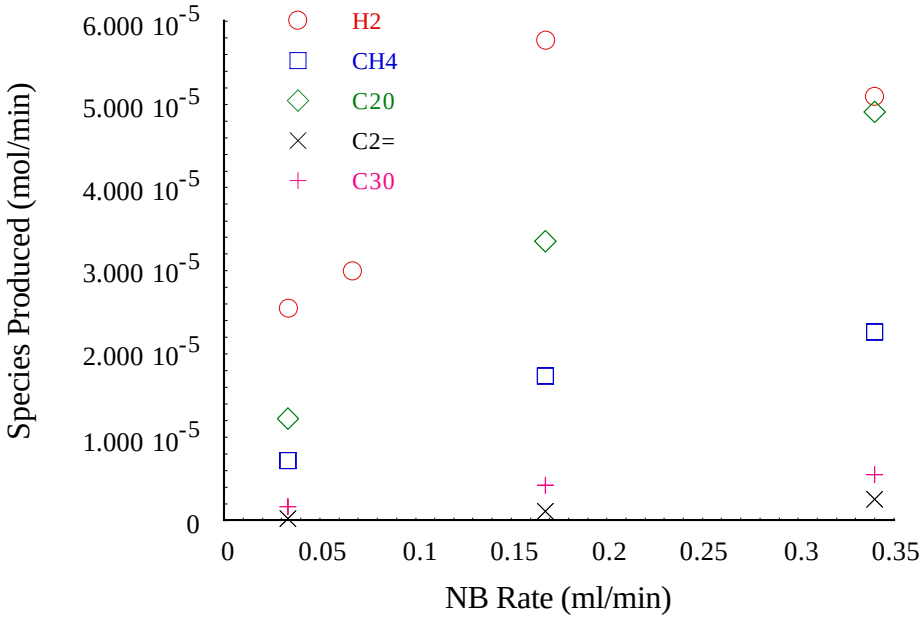

Figure 1.29-5. Variations of Some Gaseous Products with *n*-Butylbenzene Flow Rate at 600¡C

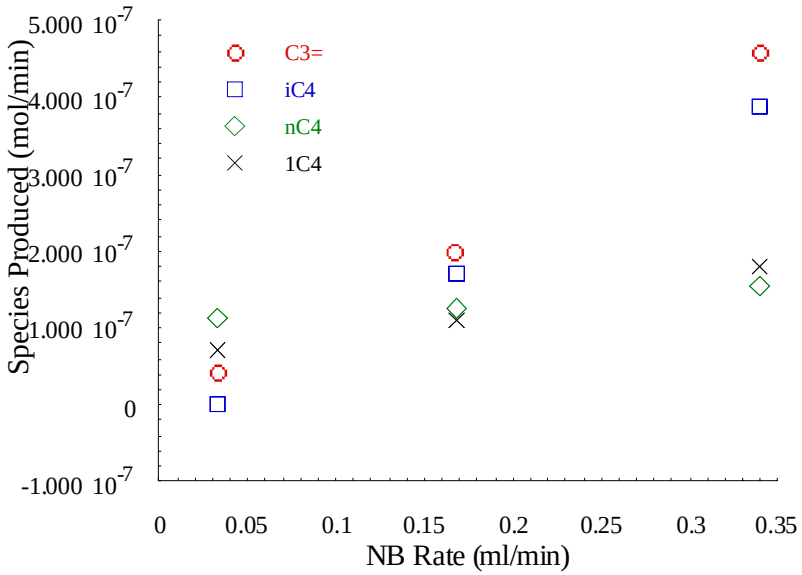

Figure 1.29-6. Variations of Some Gaseous Products with *n*-Butylbenzene Flow Rate at 600¡C.

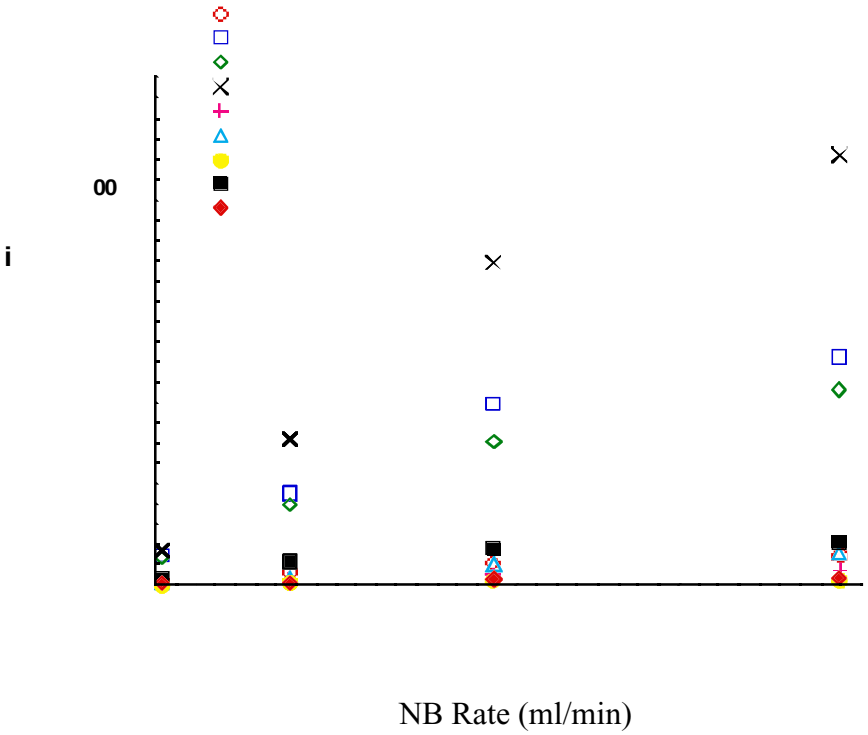

Figure 1.29-7. Variations of Some Major Liquid Products with *n*-Butylbenzene Flow Rate at 600¡C.

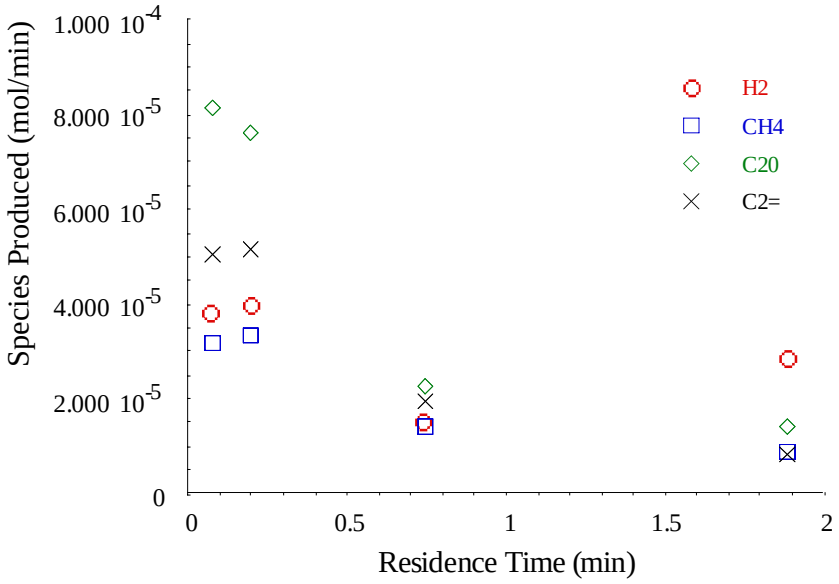

Figure 1.29-8. Variations of Some Gaseous Products with Residence Time at 600¡C

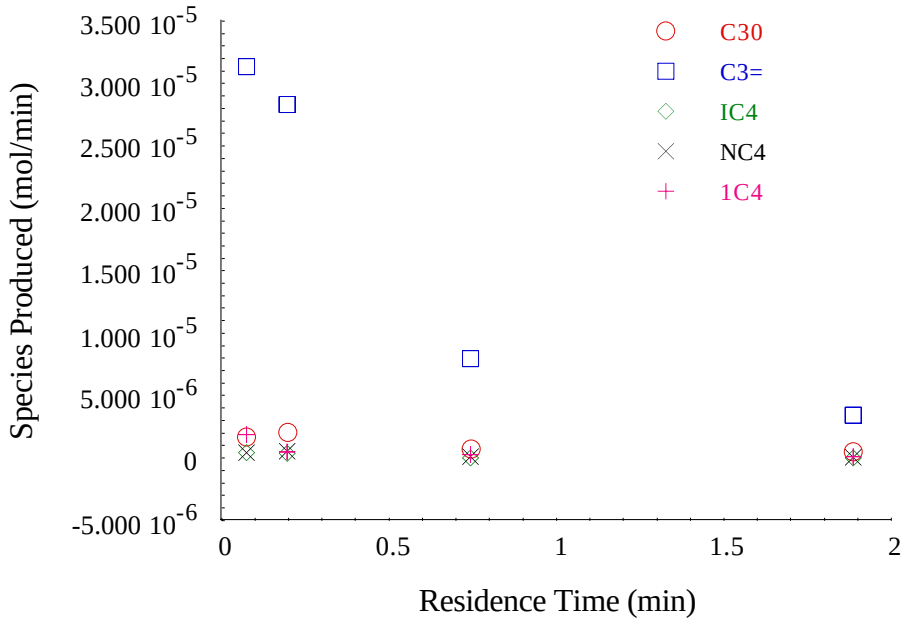

Figure 1.29-9. Variations of Some Gaseous Products with Residence Time at 600¡C

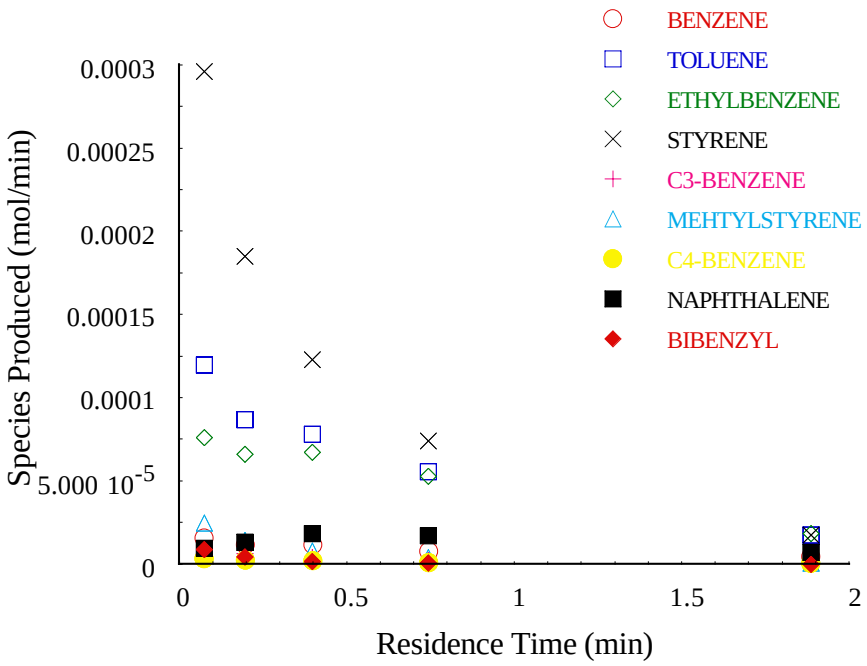

Figure 1.29-10. Variations of Major Liquid Products with Residence Time at 600¡C

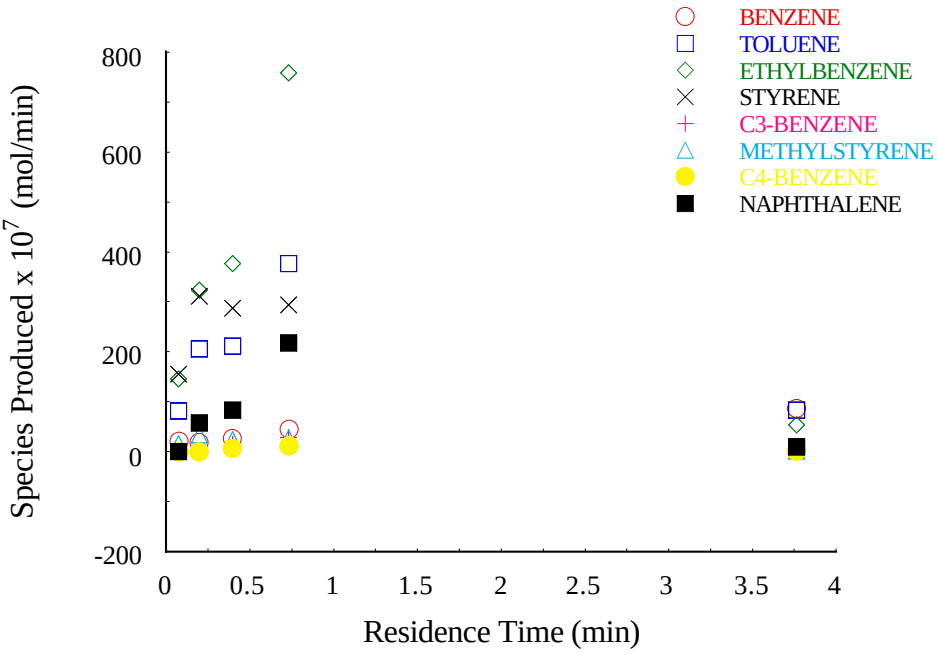

Figure 1.29-11. Variations of Some Major Liquid Products with Residence Time at 550¡C.

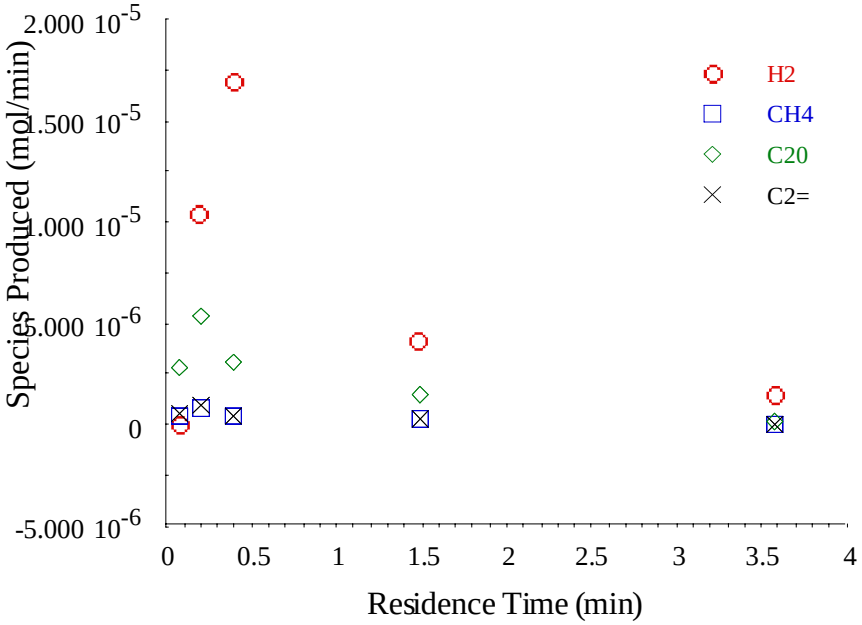

Figure 1.29-12. Variations of Some Gaseous Products with Residence Time at 500¡C

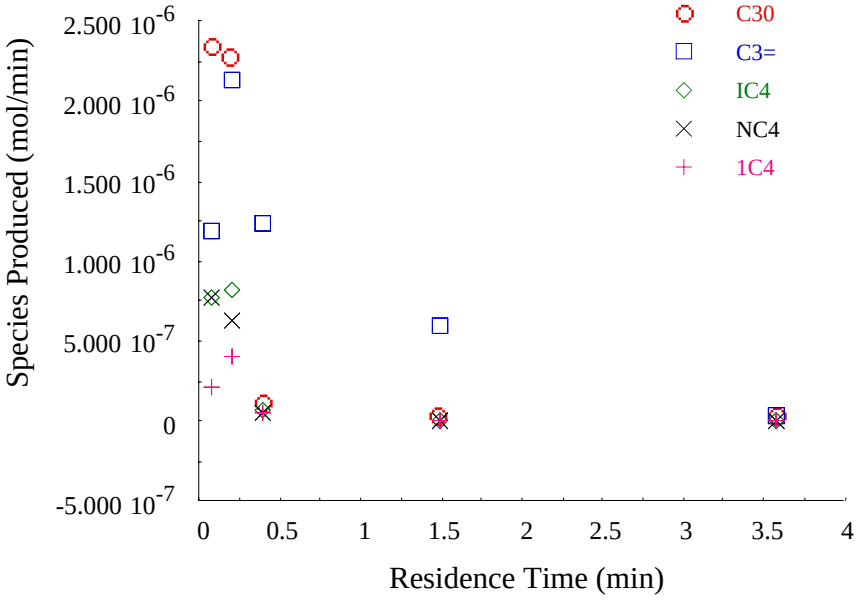

Figure 1.29-13. Variations of Some Gaseous Products with Residence Time at 500¡C

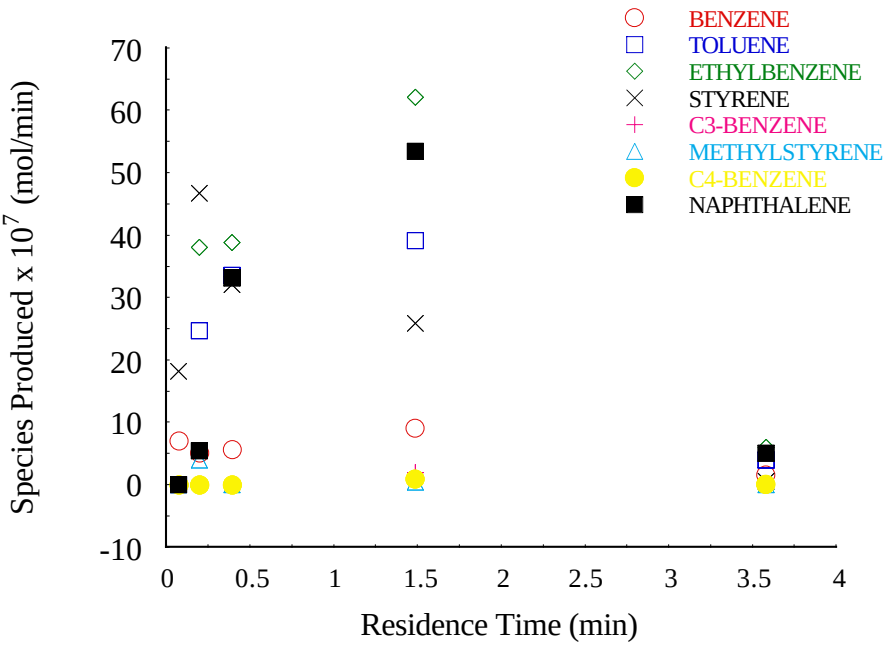

Figure 1.29-14. Variations of Major Liquid Products with Residence Time at 500¡C

[1] Advanced Fuel Composition and Use. *FY93 New Initiative, Joint AFOSR and WPAFB Announcement*. 1991.

1.30 THERMAL DECOMPOSITION OF *N*-BUTYLBENZENE IN NEAR-CRITICAL AND SUPERCRITICAL REGIONS: PRODUCT DISTRIBUTIONS AND REACTION MECHANISMS

This study is explained in detail in *Advanced Thermally Stable Jet Fuels Technical Progress Report, January—March 1996.*

Introduction

A previous study on thermal decomposition of *n*-butylbenzene focused on higher conversions using tubing bomb reactor for thermal stressing experiments carried out at 450°C with a sample loading of 5 mL.[1] In this work, thermal decomposition of *n*-butylbenzene was studied in near-critical and supercritical regions as a function of pressure, temperature, and conversion.

Experimental

Thermal stressing experiments were carried out in a Pyrex glass tube reactor with a total volume of 45-50 mL. A sealed glass tube was used to eliminate concerns regarding temperature variations in the reactor, as encountered in the tubing bomb reactor, and possible catalytic effects of metal surfaces during thermal treatment.

Results and Discussion

1. Product Distributions. The liquid products from thermal decomposition of *n*-butylbenzene include toluene, styrene, ethylbenzene, benzene, alkllbenzene, and tetralin. Also present are some secondary products, including *n*-propylbenzene, isopropylbenzene, sec-butylbenzene, isobutylbenzene, *n*-amylbenzene, 1 -propylbutylbenzene, 1,3-diphenylpropane, 1,4-diphenylbutane, 1,6-diphenylhexane, and three other C_6-diphenyls. At higher conversions (> 30 %), more than 150 liquid compounds were found.

We found that high-pressure supercritical conditions suppressed the formation of styrene. Conversely, the increasing pressure caused the yields of ethylbenzene and benzene to remain unchanged and the yield of allylbenzene to decrease. The yields of all the secondary products, except *n*-propylbenzene, increased with the increasing pressure. Under supercritical conditions, the major secondary products included sec-butylbenzene, 1,3-diphenylhexane, one C_6-diphenyl, and 1,3-diphenylpropane.

As temperature increased, the yields of styrene and allylbenzene increased, while those of toluene, ethylbenzene, and benzene remained almost unchanged. The yields of most secondary products decreased with the increasing temperature.

Conversion also affected product distributions. For 100 moles of reactant converted, the yield of styrene decreased from 26 to 3.5 moles and that of ethylbenzene increased from 4 to 11 moles as conversion increased from 6.9 to 35.5%. The yield of toluene slightly increased and that of benzene did not change significantly with the increasing conversion. The allylbenzene yield decreases with the increasing conversion. Among the secondary products, the yields of sec-butylbenzene and 1,3-diphenylhexane decreased while those of isobutylbenzene, *n*-propylbenzene, and isopropylbenzene increased. The yield of 1,3-diphenylpropane first increased

and then decreased, while that of 1-propylbutylbenzene first increased and then remained constant.

2. Reaction Mechanisms. Thermal decomposition of *n*-butylbenzene proceeds by free radical mechanisms. To account for the observed product distributions and the changes in product composition with reaction conditions, the following mechanisms have been suggested for the thermal decomposition of *n*-butylbenzene in the near-critical and supercritical regions.

The reaction products from the thermal decomposition of *n*-butylbenzene include compounds from primary and secondary reactions. The major primary reactions can be described by:

$$C_6H_5CH_2CH_2CH_2CH_3 \rightarrow C_6H_5CH_2\cdot + CH_3CH_2CH_2\cdot \quad (1)$$

$$R\cdot + C_6H_5CH_2CH_2CH_2CH_3 \rightarrow RH + C_6H_5(C_4H_8)\cdot \quad (2)$$

$$C_6H_5\dot{C}HCH_2CH_2CH_3 \rightarrow C_6H_5CH{=}CH_2 + CH_3CH_2\cdot \quad (3)$$

$$C_6H_5CH_2\dot{C}HCH_2CH_3 \rightarrow C_6H_5CH_2CH{=}CH_2 + CH_3\cdot \quad (4)$$

$$C_6H_5CH_2CH_2\dot{C}HCH_3 \rightarrow C_6H_5CH_2\cdot + CH_2{=}CHCH_3 \quad (5)$$

$$C_6H_5CH_2CH_2CH_2CH_2\cdot \rightarrow C_6H_5CH_2CH_2\cdot + CH_2{=}CH_2 \quad (6)$$

$$R_1\cdot + R_2\cdot \rightarrow \text{products} \quad (7)$$

The significant formation of secondary products reveals that the following addition reactions occur:

$$C_6H_5CH{=}CH_2 + CH_3\cdot \rightarrow C_6H_5\dot{C}HCH_2CH_3 \quad (8)$$

$$C_6H_5CH{=}CH_2 + CH_3\cdot \rightarrow C_6H_5CH(CH_3)CH_2\cdot \quad (9)$$

$$C_6H_5CH{=}CH_2 + CH_3CH_2\cdot \rightarrow C_6H_5CH(CH_2CH_3)CH_2\cdot \quad (10)$$

$$C_6H_5CH_2\cdot + CH_2{=}CHCH_3 \rightarrow C_6H_5CH_2CH(CH_3)CH_2\cdot \quad (11)$$

$$C_6H_5\dot{C}HCH_2CH_2CH_3 + CH_2{=}CHCH_3 \rightarrow C_6H_5CH(C_3H_7)CH_2\dot{C}HCH_3 \quad (12)$$

$$C_6H_5CH{=}CH_2 + C_6H_5CH_2\cdot \rightarrow C_6H_5\dot{C}HCH_2CH_2C_6H_5 \quad (13)$$

$$C_6H_5CH{=}CH_2 + C_6H_5CH_2CH_2\cdot \rightarrow C_6H_5\dot{C}HCH_2CH_2CH_2C_6H_5 \quad (14)$$

$$C_6H_5\dot{C}HCH_2CH_2CH_3 + C_6H_5CH{=}CH_2 \rightarrow C_6H_5CH(C_3H_7)CH_2\dot{C}HC_6H_5 \quad (15)$$

A detailed explanation of the primary reactions is presented in the corresponding Technical Progress Report.[2]

The relative yields of the products depend on reaction conditions. At low loading ratios the major reaction products are from the primary reactions. According to the kinetic parameters suggested by Freund and Olmstead,[3] the relative decomposition rates of α, β, γ, and δ-butylbenzene radicals are estimated to be 1:6:7300:13. The decomposition rate of the γ-butylbenzene radical is at least 10^3 times that of the β-butylbenzene radical. Because of their

lower decomposition rates, the α, β, and σ-butylbenzene radicals would have a higher probability of being involved in chain transfer reactions. As a result, the concentrations of the α, β, and δ-butylbenzene radicals participating in the decomposition reactions would decrease, while that of the γ-butylbenzene radical would increase. As pressure increases, this difference in the decomposition steps would be more significant. This is demonstrated by the yield of toluene (from the decomposition of the γ-butylbenzene radical), which increases while those of styrene (from the α-butylbenzene radical) and allylbenzene (from the β-butylbenzene radical) decrease.

At higher pressures the radical addition reactions become significant. As pressure increases, the yields of the secondary products increase as a result of the increased addition rate. The increasing importance of the addition reactions with the increasing pressure also contributes to the decreases in the yields of styrene and allylbenzene.

The radical addition reactions would be favored at lower temperatures because of the low activation energies. Therefore, for the similar conversions, the yields of styrene and allylbenzene would be lower and those of secondary products would be higher at lower temperatures.

The yield of ethylbenzene rapidly increases with the increasing conversion, indicating that ethylbenzene is not only a primary product but also a secondary product. The secondary ethylbenzene could be formed from the decomposition of high-molecular-weight compounds, and/or could be converted from styrene. The formation of ethylbenzene via styrene can be described by the addition of a hydrogen atom to styrene, followed by hydrogen abstraction. This reaction also contributes to the decrease in the yield of styrene.

---

[1] Schobert, H. H. et al. *Advanced Thermally Stable Jet Fuels, Technical Progress Report, August - October 1992.* The Pennsylvania State University. 1993.

[2] Schobert, H. H. et al. *Advanced Thermally Stable Jet Fuels, Technical Progress Report, January - March 1996.* The Pennsylvania State University. 1996.

[3] Freund, H. and W. N. Olmstead. *Int. J. Chem. Kinetics*. 1989. 21. 561-574.

1.31 SUPERCRITICAL PHASE THERMAL DECOMPOSITION OF A MIXTURE OF *N*-DODECANE AND *N*-BUTYLBENZENE

This study is explained in detail in *Advanced Thermally Stable Jet Fuels, Technical Progress Report, January—March 1997*.

Introduction

We previously reported the results from the thermal decomposition of some typical jet fuel model compounds, including C_{10}-C_{14} *n*-alkanes,[1, 2] *n*-butylbenzene,[3] *n*-butylcyclohexane,[4] decalin,[5] and tetralin[6] under near-critical and supercritical conditions. The studies on single model compounds have provided mechanistic information on jet fuel thermal decomposition, but have not addressed the manner in which the hundreds of compounds in jet fuels interact with each other during the thermal reactions.

In this work, the thermal decomposition of a binary mixture of *n*-dodecane (*n*-C_{12}) and *n*-butylbenzene (*n*-BBZ) was studied under supercritical conditions. The mixture consisted of 48.44 wt% of *n*-C_{12}, 51.23 wt% of *n*-BBZ, and small amounts of impurities. The critical properties of the mixture were calculated using the methods recommended in the API Technical Data Book[7] and those of pure compounds. Thermal decomposition experiments were conducted at 425°C in a Pyrex glass tube reactor for 15-60 minutes.

Results and Discussion

1. Reaction Rate. The changes in conversions of individual model compounds with reaction time were obtained from the thermal decomposition of the mixture at 425°C for 15 to 60 minutes with a loading ratio of 0.36. The conversion of each compound was affected by the presence of a second compound. While the conversions from pyrolysis of *n*-C_{12} in the mixture were higher than those for the pyrolysis of *n*-C_{12} alone, the conversions of *n*-BBZ in the mixture were significantly lower than those for the pyrolysis of *n*-BBZ alone. In other words, the presence of *n*-C_{l2} inhibits the decomposition of *n*-BBZ, whereas the presence of *n*-BBZ accelerates the decomposition of *n*-C_{l2}.

2. Product Distributions. The products from the thermal decomposition of the binary mixture included those found in the reaction products of individual compounds and others produced only from the mixture. The GC chromatogram was made of the liquid products from the pyrolysis *n*-C_{l2} and *n*-BBZ mixture at 425°C for 60 minutes with a P_r of 2.04. The products from the decomposition of *n*-C_{12} included series of *n*-alkanes and 1-alkenes lighter than *n*-C_{l2} and some heavier normal and branched alkanes. The products from the decomposition of *n*-BBZ included toluene, styrene, ethylbenzene, benzene, allylbenzene, tetralin, and some secondary products, including *n*-propylbenzene, isopropylbenzene, sec-butylbenzene, isobutylbenzene, *n*-pentylbenzene, 1-propylbutylbenzene, 1,3-diphenylpropane, 1,4-diphenylbutane, and four C_6-diphenyls. Some products unique to the pyrolysis of the mixture were also formed, including six C_{14}-benzenes, a series of high *n*-alkylbenzenes up to *n*-dodecylbenzene, a series of 1-propylalkylbenzenes up to 1-propylundecylbenzene, and some other alkylbenzenes with branched side chains.

Under thermal decomposition at 425°C with a P_r of 2.04, as reaction time increases, the molar yields of *n*-alkanes, toluene, and ethylbenzene increase steadily while the yield of styrene decreases with reaction time. After 15 minutes of reaction, the yields of 1-alkenes and *n*-alkanes are comparable. For 30 minutes of reaction, the yield of *n*-alkanes increases steadily with the increasing reaction time, while the 1-alkenes yields show a slight increase and stay essentially constant up to 60 minutes reaction time. The yields of high-molecular-weight compounds increase with reaction time, but their rates of formation decrease as the reaction time increases.

We examined the product distributions obtained under supercritical and subcritical conditions, with reactions carried out at 425°C for 60 minutes. Two loading ratios were used: 0.36 (supercritical, $P_r = 2.04$) and 0.08 (subcritical, $P_r = 0.77$). The supercritical conditions favor the formation of *n*-alkanes, toluene, and high-molecular-weight compounds, and suppress the formation of 1-alkenes and styrene.

3. Reaction Mechanisms. The observed product distributions can be explained by free radical mechanisms. For the thermal reactions of *n*-C_{12}/*n*-BBZ mixture, initiation reactions could occur by homolytic cleavage of C-C bonds in *n*-C_{12} and C-C bonds in the side chain of *n*-BBZ. A comparison of homolytic bond dissociation energies (BDEs) for different C-C bonds in both compounds reveals that the cleavage of the C_α-C_β bond in the side chain of *n*-BBZ is much easier than the breaking of any other bond in both compounds. This is because the cleavage of this bond produces a resonance-stabilized benzyl radical. Therefore, the major initiation reaction is the breaking of C_α-C_β bond in *n*-BBZ to form a benzyl radical and a 1-propyl radical. Further reactions are described in detail in the corresponding Technical Progress Report.[8]

Styrene seemed to be much more reactive than 1-alkenes in radical addition reactions. The high-molecular-weight compounds formed during pyrolysis of the mixture were not stable, as evidenced by the decreasing production rates for these compounds with the increasing reaction time. Since the hydrogen abstraction and radical addition reactions are favored under high-pressure supercritical conditions, the yields of *n*-alkanes and high-molecular-weight compounds would be expected to be higher and the yields of 1-alkenes and styrene would be lower than those obtained under subcritical conditions. Supercritical conditions produce more toluene than subcritical conditions because of the higher concentrations of high-molecular-weight compounds that undergo further decomposition to form toluene and other compounds.

Conclusions

The pyrolysis of a binary mixture of *n*-C_{12} and *n*-BBZ in Pyrex tubes showed a strong interaction between the components that affects the conversion of individual compounds and those that produced hybrid species which were not found in the products from pyrolysis of pure compounds. In the binary mixture, the conversion of *n*-C_{12} was inhibited, while the conversion of *n*-BBZ was accelerated as compared to those obtained from the pyrolysis of the individual compounds under the same conditions. The composition of the products obtained from the binary mixture under both subcritical and supercritical conditions were likely the result of free radical mechanisms and the relative reactivity of intermediate species produced from the different components of the mixture.

[1] Schobert, H. H. et al. *Advanced Thermally Stable Jet Fuels, Technical Progress Report, January - March 1995*. The Pennsylvania State University. 1995.

[2] Schobert, H. H. et al. *Advanced Thermally Stable Jet Fuels, Technical Progress Report, April - June 1995*, The Pennsylvania State University. 1995

[3] Schobert, H. H. et al. *Advanced Thermally Stable Jet Fuels, Technical Progress Report, January - March 1996.* The Pennsylvania State University. 1996.

[4] Schobert, H. H. et al. *Advanced Thermally Stable Jet Fuels, Technical Progress Report, April - June 1996.* The Pennsylvania State University. 1996.

[5] Schobert, H. H. et al. *Advanced Thermally Stable Jet Fuels, Technical Progress Report, July - September 1996.* The Pennsylvania State University. 1996.

[6] Schobert, H. H. et al. Advanced Thermally Stable Jet Fuels, Technical Progress Report, October - December 1996. The Pennsylvania State University. 1996.

[7] *API Technical Data Book-Petroleum Refining*, 4th ed.; American Petroleum Institute: Washington, DC, 1987.

[8] Schobert, H. H. et al. Advanced Thermally Stable Jet Fuels, Technical Progress Report, January - March 1997. The Pennsylvania State University. 1997.

1.32 SUPERCRITICAL PHASE THERMAL DECOMPOSITION OF A MIXTURE OF *N*-BUTYLBENZENE AND *N*-BUTYLCYCLOHEXANE

This study is explained in detail in *Advanced Thermally Stable Jet Fuels, Technical Progress Report, April—June 1997*.

Introduction

In Section 1.31, we discussed supercritical-phase thermal decomposition of a binary mixture of *n*-dodecane and *n*-butylbenzene. In this work, the mixture thermal decomposition studies were extended to another binary mixture, which consists of 50.49 wt% of *n*-butylbenzene (*n*-BBZ), 49.44 wt % of *n*-butylcyclohexane (*n*-BCH), and small amounts of impurities. The critical properties of the mixture were estimated using the methods recommended in API Technical Data Book,[1] and those of pure compounds. Thermal stressing experiments were carried out in a Pyrex glass tube reactor at 425°C for 15-60 minutes.

Results and Discussion

1. Reaction Rate. We examined the conversions of individual model compounds as a function of reaction time from the thermal decomposition of pure *n*-BBZ, pure *n*-BCH, and an *n*-BBZ/*n*-BCH mixture at 425°C for l5-60 minutes with a loading ratio of 0.36. The conversions for the decomposition of *n*-BCH in the mixture were significantly higher than those for the decomposition of pure *n*-BCH, while the conversions for the decomposition of *n*-BBZ in the mixture were significantly lower than those for the decomposition of pure *n*-BBZ. This means that the presence of *n*-BCH inhibits the decomposition of *n*-BBZ and the presence of *n*-BBZ accelerates the decomposition of *n*-BCH.

Under similarconditions, *n*-C_{l2} and *n*-BCH exhibit a very similar inhibiting effect on the decomposition of *n*-BBZ. This is probably attributable to comparable hydrogen abstraction rates from *n*-C_{l2} and *n*-BCH by free radicals.

2. Product Distributions. The GC chromatogram of the liquid products from the thermal decomposition of the *n*-BBZ/*n*-B CH mixture at 425°C for 60 minutes with a P_r of 1.80 revealed that most of the liquid products produced from the mixture reactions derived from either the decomposition of the *n*-BBZ component or the decomposition of the *n*-BCH component. There were, however, some products that are unique to the reaction of the mixture. Among these are cyclohexylethylbenzene, cyclohexylpropylbenzene, eight cyclohexyl-C_6-benzenes, and several C_7 cyclohexanes.

The yields of most of the light products increased with reaction time. The yield of styrene decreased and the yield of methylenecyclohexane remained unchanged as reaction time increased. The yields of cyclohexylethylbenzene, cyclohexylpropylbenzene, and 1,3-diphenylpropane increased, while the yields of cyclohexyl- C_6-benzenes and C_6-diphenyls first increased, then remained unchanged or decreased with the increasing reaction time.

We compared product distribution between supercritical (i.e., initial supercritical phase) and subcritical (i.e., initial gas phase; temperature is above critical temperature, but pressure is below critical pressure) conditions from the thermal decomposition of *n*-BBZ/*n*-BCH mixture at 425°C for 60 minutes, using two loading ratios: 0.36 for supercritical (P_r = 1.80) and 0.08 for

subcritical ($P_r = 0.77$). Supercritical conditions favor the formation of toluene, C_6-diphenyls, and cyclohexyl-C_6-benzenes, and suppress the formation of styrene, cyclohexylethylbenzene, and other light products. There were no significant differences between supercritical and subcritical conditions in the yields of cyclohexylpropylbenzene and 1,3-diphenylpropane.

3. Reaction Mechanisms. The formation of the products from the thermal decomposition of *n*-BBZ/*n*-BCH mixture can be explained by free radical mechanisms. For the thermal reactions of *n*-BBZ/*n*-BCH mixture, the initiation occurs mainly by homolytic cleavage of C_α-C_β bond in *n*-BBZ because the cleavage of this bond, which produces a resonance-stabilized benzyl radical, occurs much more easily than breaking any other bond in both compounds. The radicals produced by the initiation reactions can abstract hydrogen atoms from *n*-BBZ and *n*-BCH molecules to form various parent radicals, including four phenylbutyl radicals and eight *n*-butylcyclohexane radicals (four cyclohexylbutyl radicals and four butylcyclohexyl radicals). Further reactions are described in detail in the corresponding Technical Progress Report.[2]

Styrene is very reactive while cyclohexene and methylcyclohexenes are not reactive in radical addition reactions. The high-molecular-weight compounds formed in mixture reactions are not stable and their formation rates decrease with reaction time. The cyclohexyl radical seems to be more reactive than the benzyl radical in radical addition reactions with styrene, as evidenced by the fact that the yield of cyclohexylethylbenzene is higher than that of 1,3-diphenylpropane. If both radicals had exhibited comparable reactivity in radical additions, the yield of cyclohexylethylbenzene would have been lower than that of 1,3-diphenylpropane because of the lower concentration of cyclohexyl radical than benzyl radical.

The radical addition reactions between parent radicals (phenylbutyl radicals and 1-butylcyclohexane radicals) and styrene are favored under supercritical conditions because of the higher concentrations of parent radicals, leading to higher yields of C_6-diphenyls and cyclohexyl-C_6-benzenes and low styrene yield. Correspondingly, the formation of decomposition products (light products) is suppressed under supercritical conditions because fewer parent radicals decompose. More toluene is formed under supercritical conditions because more high-molecular weight compounds undergo further decomposition to form toluene and other compounds.

Conclusions

There is some interaction between the individual components during pyrolysis of a binary mixture of *n*-butylbenzene and *n*-butylcyclohexane, as evidenced by the changes in the decomposition rates of these compounds relative to those obtained from the corresponding neat pyrolysis experiments. In addition to observed changes in decomposition rates, the pyrolysis products from the binary mixture were found to contain hybrid compounds, such as cyclohexylethylbenzene, which were produced by cross-reactions between *n*-butylbenzene and *n*-butylcyclohexane species. These results suggest that the solid deposition from the binary mixture can have different characteristics with possible non-additive effects that cannot be predicted from the behavior of the individual compounds.

Substantial differences were observed between the composition of the pyrolysis products obtained from the binary mixtures under a starting supercritical or gas phase. Starting supercritical conditions favor the formation of toluene, C_6-diphenyls, and cyclohexyl-C_6-benzenes, and suppress the formation of styrene, cyclohexylethylbenzene, and other light

products. Depending on the effective solid formation or deposition mechanisms (i.e., catalytic or non-catalytic), these differences in pyrolysis product composition as a function of pressure can also influence the deposit formation.

---

[1] *API Technical Data Book-Petroleum Refining*, 4th ed.; American Petroleum Institute: Washington, DC, 1987.

[2] Schobert, H. H. et al. Advanced Thermally Stable Jet Fuels, Technical Progress Report, April - June 1997. The Pennsylvania State University. 1997.

1.33 DETAILED CHARACTERIZATION OF MINOR LIQUID PRODUCTS FROM THERMAL STRESSING OF AMYLBENZENE AND *N*-HEXYLBENZENE

Introduction

Most liquid products obtained from the thermal stressing were identified and analyzed quantitatively by HP GC and HP GC/MS using the split injection mode. We found that the major products are easily detected and quantified during the analysis. Some minor reaction products, however, were not clearly seen in a single injection because they were present in very limited amounts. Very high selectivities for forming toluene and ethylbenzene were observed for the pyrolysis of alkylbenzenes. Their predominance in a single injection inhibits the identification of other species that are present only in small amounts. These other species although present only in small amounts and, therefore, difficult to identify are nonetheless important. They are likely to be either intermediates in the free radical reactions or high molecular weight products. Their accurate detection and identification can help to further understand the reaction mechanisms and pathways and, more importantly, the pathways of forming high molecular weight products and solid products.

Two major efforts have been made toward these purposes. The first method involved injecting a considerably larger sample into the GC/MS and providing a much longer delay time. The new delay time was just enough to allow the substrate molecule (e.g., amylbenzene or hexylbenzene) to elute from the column. The substrate compounds are usually the most abundant peaks in the resulting product spectrum. The second method was solvent fractionation to obtain and analyze sub-fractions. This work employed both of the aforementioned methods and used GC and GC/MS to perform solvent fractionation on the heavy sub-fractions (fraction 3).

Experimental

The solvent fractionations were conducted using liquid chromatography (LC) columns from Fisher Scientific. Neutral alumina obtained from ICN Biochemical was chosen to be the absorbent. About 130 to 140 g of neutral alumina powder was added to the LC column and about 3.5 g of liquid products from amlybenzene and hexylbenzene was added to the top of the column. **Scheme I** shows the separation process. The three sub-fractions were obtained by the solvent sequence listed in **Table 1.33-1**. Fraction 1 is obtained by difference because it cannot be weighed accurately due to the fact that it contains large amounts of light products such as pentane and hexane. GC and GC/MS were used for the analysis of whole liquids and their fractions.

Results and Discussion

Table 1.33-1 lists the results obtained from LC separation. The majority of products fall into the first fraction (pentane + 5% benzene). Fraction 3 constitutes only a few percent of the whole liquid products, not exceeding 4%. There are small amounts of heavy compounds retained on the LC column.

Figure 1.33-1 compares GC traces obtained three ways. The top trace (a) is the result of direct injection of 0.01 µL neat liquid product from thermal stressing of hexylbenzene at 475¡C for 30 minutes. The middle trace (b) was fraction 2 from the whole liquid. The bottom trace (c)

was also the whole liquid given a much larger amount of injection (1 μL). All of these analyses used the split injection mode. As (a) indicates, almost nothing was detected in the high-retention-time region. The fractionation enables the identification of some of the compounds in this region (b). The proportion of the compounds relative to the parent molecule hexylbenzene changed. Naphthalene was the most abundant species in the high- retention-time region. Large-quantity injection of the whole liquid, while concurrently recording only the high retention time region, (as in the case of HP GC/MS (c)), ensures the accurate detection and identification of the trace compounds in the liquid product.

Figure 1.33-2 shows the results of analyzing the liquid product from the stressing of hexylbenzene at 450 ¡C for 1 hour. From the above discussion, injecting more sample of whole liquid is more accurate than analyzing fraction 2.

Figure 1.33-3 shows the GC/MS TICs of the high retention time regions of liquid products from 450¡C/1hr and 475¡C/30 minutes stressing. We used the same temperature as in the previous analyses and an injection amount of 1 μL. Although both the conversion of substrate and the stressing temperature were different, the types of products formed were identical, indicating that there is not significant change of reaction mechanisms or pathways in this temperature region (450¡C-475¡C). **Figure 1.33-4** shows the corresponding GC/MS TIC traces for hexylbenzene pyrolysis. **Table 1.33-2** lists the major compounds identified from Figure 1.33-3.

Figure 1.33-4 and **Figure 1.33-5** represent the GC/MS traces obtained from fraction 3 of liquid products from amylbenzene and hexylbenzene pyrolysis. Although we doubt that all of the compounds can be detected by the GC/MS, we did detect some 4-ring and 5-ring compounds in fraction 3. The most abundant species were terphenyl, stilbene, phenanthrene and methylphen-anthrenes. **Table 1.33-3** shows the major high molecular weight compounds identified in Figures 1.33-4 and 1.33-5. Most of compounds in fraction 3 were unsubstituted polynuclear compounds or methyl substituted ones. The side chain length on the nuclei did not exceed 2 or 3.

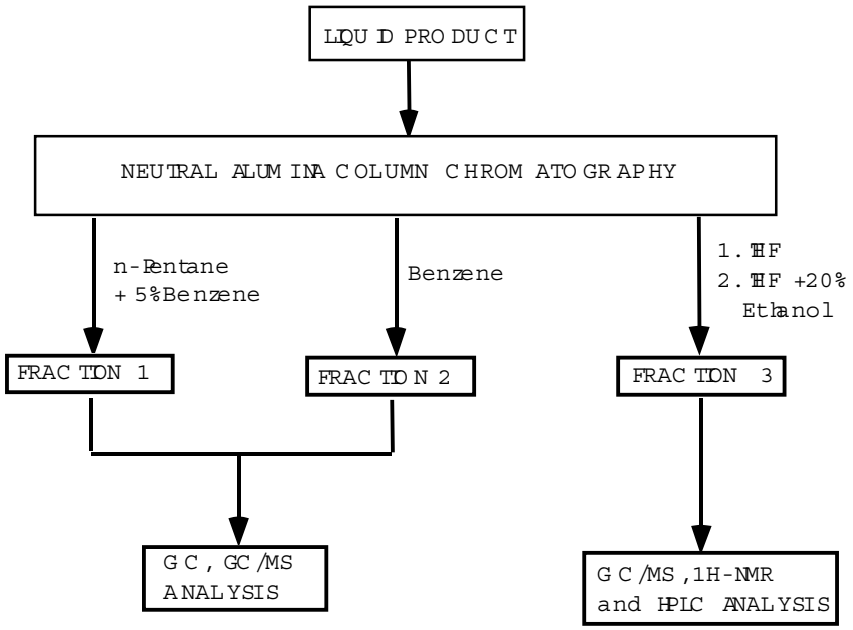

Scheme 1. Fractionation Process of the Liquid Products by Liquid Chromatography

Table 1.33-1. Solvent Fractionation Analysis of Liquid Products from Thermal Stressing of Amylbenzene and Hexylbenzene

Fraction No.	Solvent	Volume of solvent, mL	AB 450¡C —1 hr wt%	HB 450¡C —1 hr wt%	AB 475¡C —30 min wt%	HB 475¡C —30 min wt%
1	Pentane + 5% benzene	200	76.7	79.8	79.5	81.1
2	Benzene	150	20.2	17.4	17.4	16.0
3	THF + THF & 20% Ethanol	300 + 200	3.1	2.8	3.1	2.9

Table 1.33-2. Possible Compounds Identified in the GC/MS High Retention Time Region from Liquid Products of Hexylbenzene Pyrolysis

Peak No.	Mol. Ion	Base Peak	Compound Name
1	176	91	Heptylbenzene
	160	117	Cyclohexylbenzene
2	160	104	Cyclohexylbenzene
	174	104	Dimethylcyclopentylbenzene or Heptenylbenzene
3	160	131	Ethyltetralin
	174	104	Dimethylcyclopentylbenzene or Heptenylbenzene
	144	129	Cyclopentenylbenzene
4	142	142	2-Methylnaphthalene
5	174	104	Dimethylcyclopentylbenzene or Heptenylbenzene
6	142	142	1-Methylnaphthalene
7	190	92	Octylbenzene
	174	104	Dimethylcyclopentylbenzene or Heptenylbenzene
8	156	141	Dimethylnaphthalene
9	154	154	Biphenyl
10	156	141	Dimethylnaphthalene
11	156	141	Dimethylnaphthalene
12	168	168	Dihydrofluorene or Diphenylmethane
	176	105	Phenylhaxanone
	156	141	Dimethylnaphthalene
13	168	168	Methylbiphenyl
14	182	167	1,1'-Diphenylethane
15	168	168	Methylbiphenyl
16	182	91	Bibenzyl
17	196	105	C3-Diphenyl
18	182	167	Dimethylbiphenyl
19	182	167	Dimethylbiphenyl
20	182	182	Methylphenylmethylbenzene
21	166	166	Fluorene
22	180	165	Methylfluorene
23	182	182	Methylphenylmethylbenzene
24	196	92	Diphenylpropane
25	210	105	1-Methyl-1,3-diphenylbenzene
26	180	180	Diphenylethylene
	210	91	Diphenylbutane
27	224	105	C5-Diphenyl
28	224	91	C5-Diphenyl
29	220	91	Alkylbenzene
30	224	91	C5-Diphenyl
31	178	178	Phenanthrene
32	204	203	Phenylnaphthalene
33	266	91	C8-Diphenyl
34	266	91	C8-Diphenyl
35	266	91	C8-Diphenyl
36	204	204	Phenylnaphthalene
37	266	92	C8-Diphenyl
38	266	91	C8-Diphenyl
39	230	230	Terphenyl
40	242	242	Phenylfluorene or Benz(a) anthracene or Triphenylene
41	230	230	Terphenyl
42	244	244	Methylterphenyl

Table 1.33-3. Possible Compounds Identified in the Fraction 3 from Liquid Products of Stressed Amylbenzene and Hexylbenzene

Peak No.	Mol. Ion	Compound Identified	Compound Stucture
1	166	Fluorene	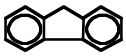
2 3 5 7	180	Fluorene, methyl-	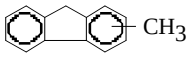
4	180	Benzene, 1,1'-[1,2-ethenediyl]bis-	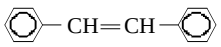
6 10	194	Fluorene, dimethyl-	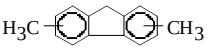
8	178	Phenanthrene	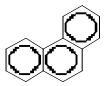
9	178	Anthracene	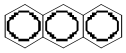
11 12 13 14 15 16	192	1H-Indene,1-phenyl- or Phenanthrene, methyl-or Anthracene, methyl-	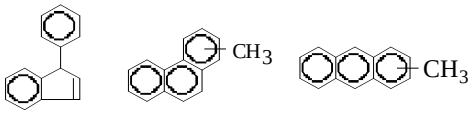
17	206	Anthracene, dimethyl- or Phenanthrene, dimethyl-	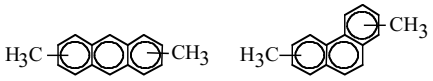
18	204	Naphthalene, phenyl-	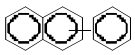
19 21	218	Naphthalene, phenylmethyl-	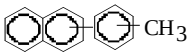
20	202	Fluoranthene	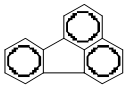
22 26	230	Pyrene, ethyl-	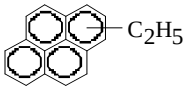
23 33 36 37	242	9H-Fluorene, 9-phenyl- or benz[a]anthracene, methyl- or Triphenylene, methyl-	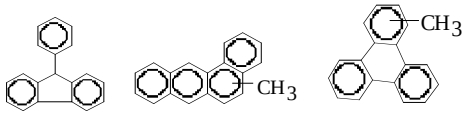
24	202	Pyrene	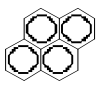

Peak No.	Mol. Ion	Compound Identified	Compound Stucture
25	230	Terphenyl	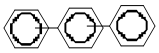
27 28 30 31 32	216	Benzo[b]fluorene or Pyrene, methyl-	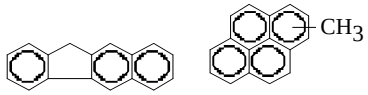
29	230 216	Chrysene, dihydro- and Pyrene, methyl-	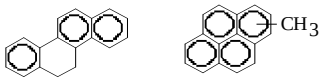
34 35	256	Benz[a]anthracene,-ethyl- or Benzo[c]phenanthrene, dimethyl-	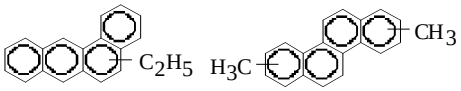
38	228	Benz[a]anthracene or Chrysene	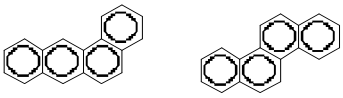
39	256	Benz[a]anthracene, dimethyl- or Benzo[c]phenanthrene, dimethyl-	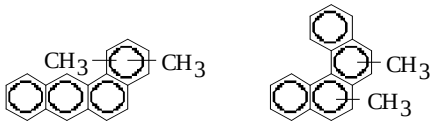
40	228	Triphenylene or Chrysene	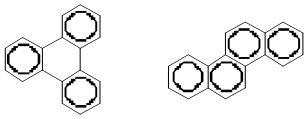
41 42	254	Binaphthalene or Anthracene, phenyl-	
43	268	Clolanthrene, 3-methyl-, or Benzo[j]aceanthrylene	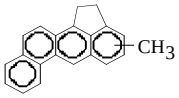
44	252	Benzo[e]pyrene	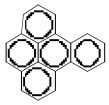
45	280 252	Naphthalene, diphenyl- and Benzo[j]fluoranthene	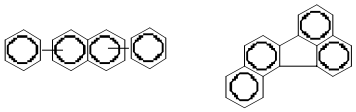
46	278	Benzo[j]triphenylene or Dibenzo[a,h]anthracene	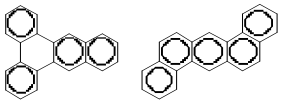

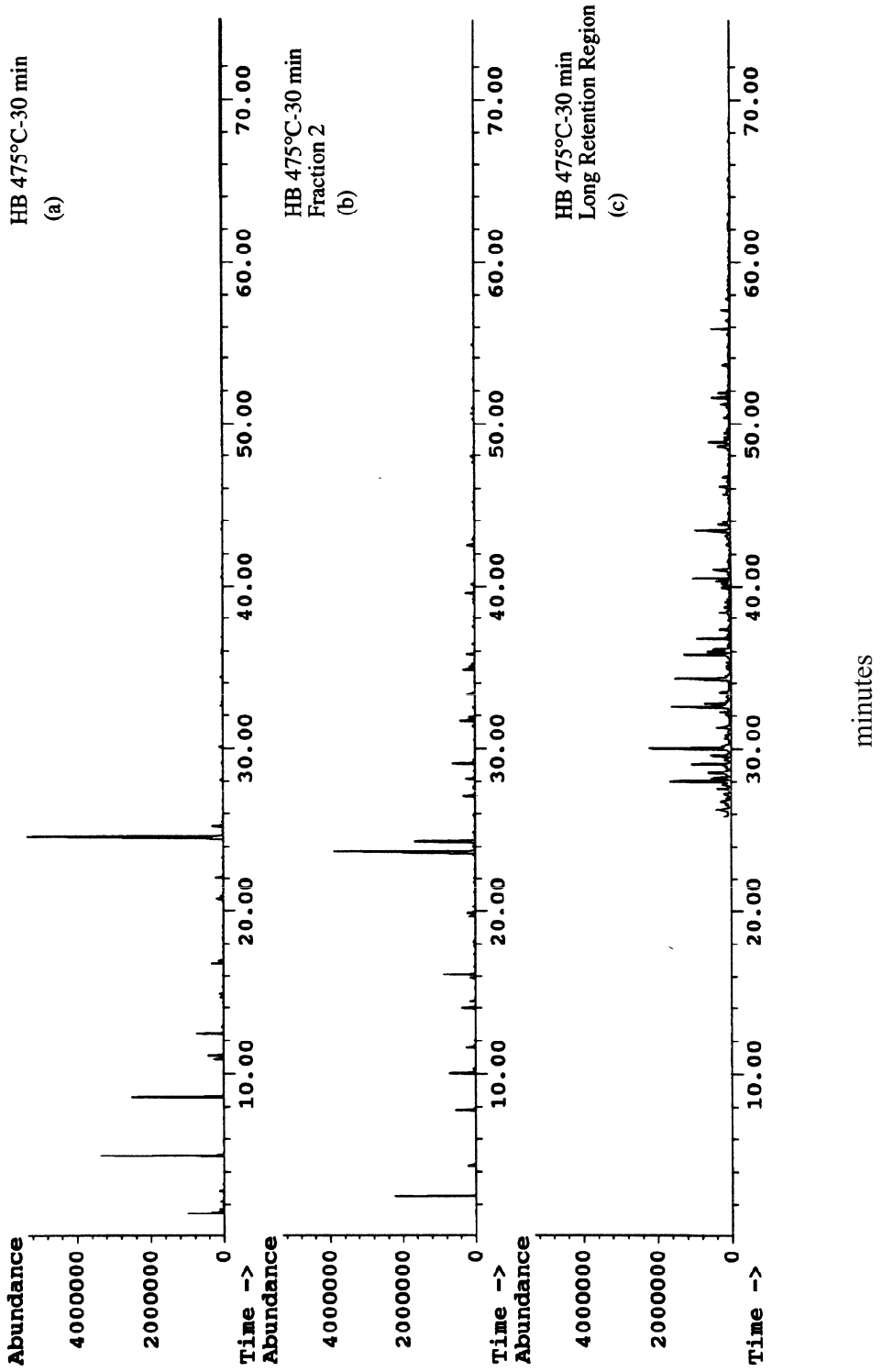

Figure 1.33-1. Hexylbenzene Pyrolysis at 475°C for 30 Minutes

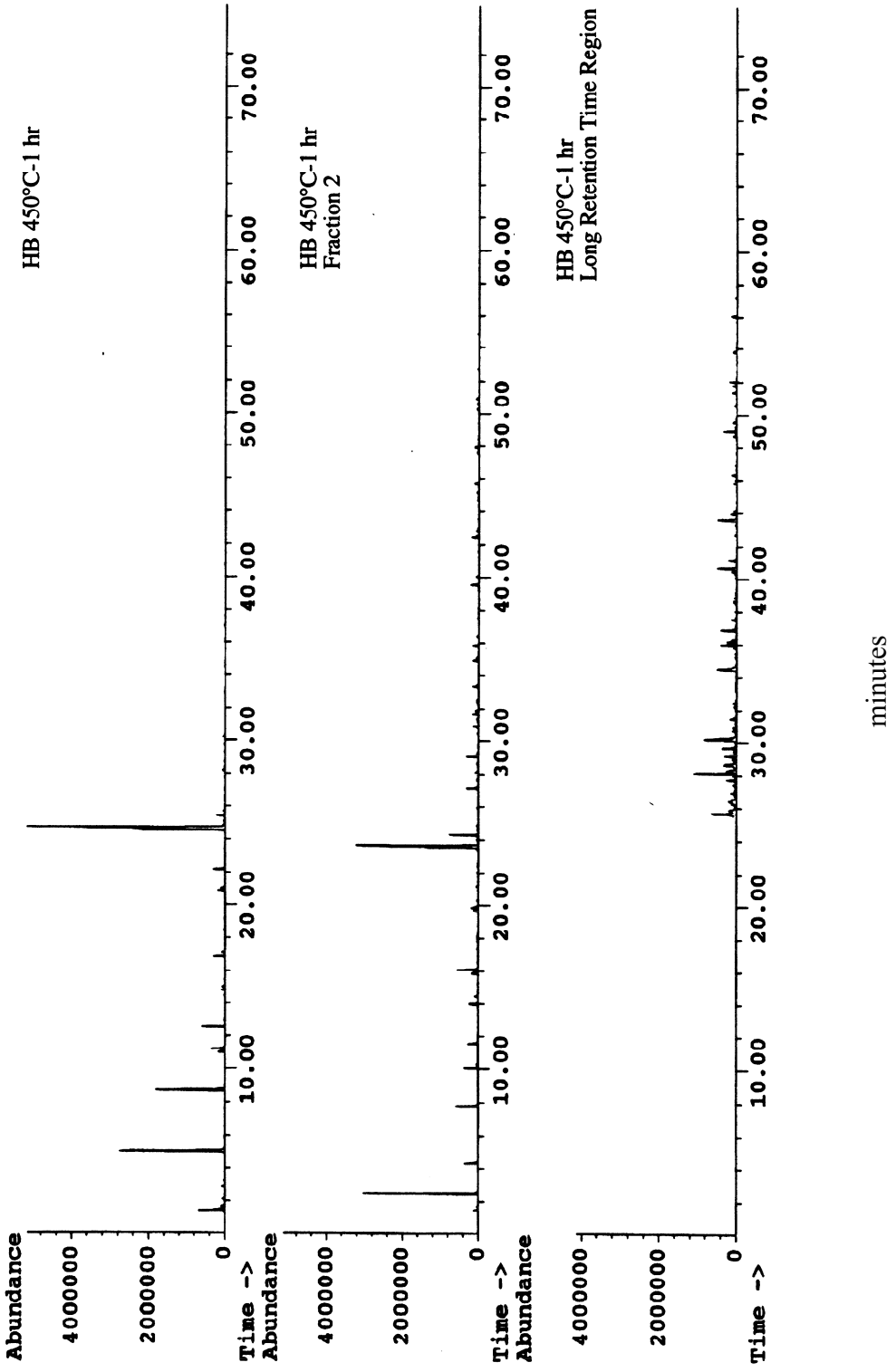

Figure 1.33-2. Hexylbenzene Pyrolysis at 450°C for 1 Hour

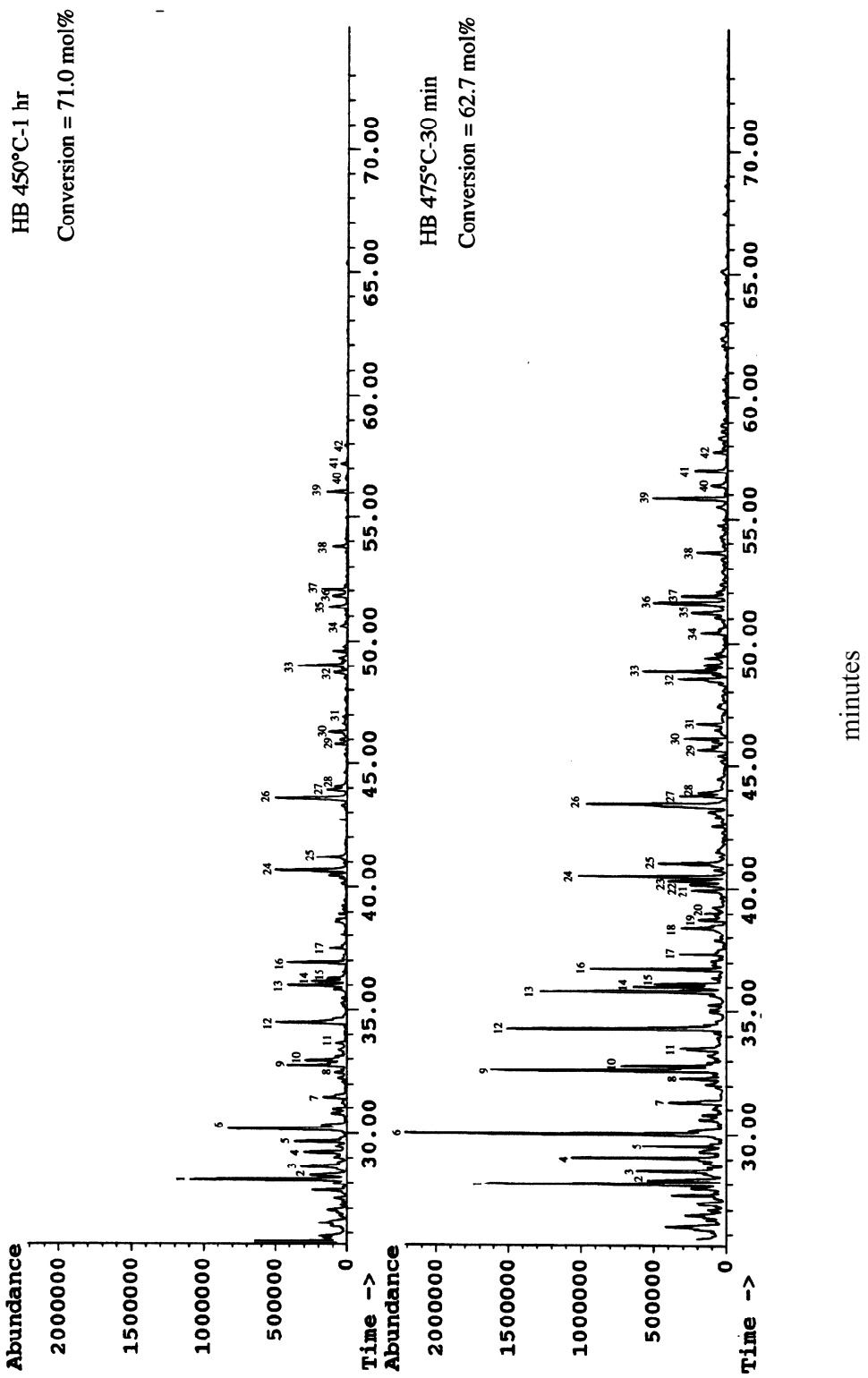

Figure 1.33-3. GC/MS TICs of Liquid Products from the Pyrolysis of Hexylbenzene at High Retention Time Region

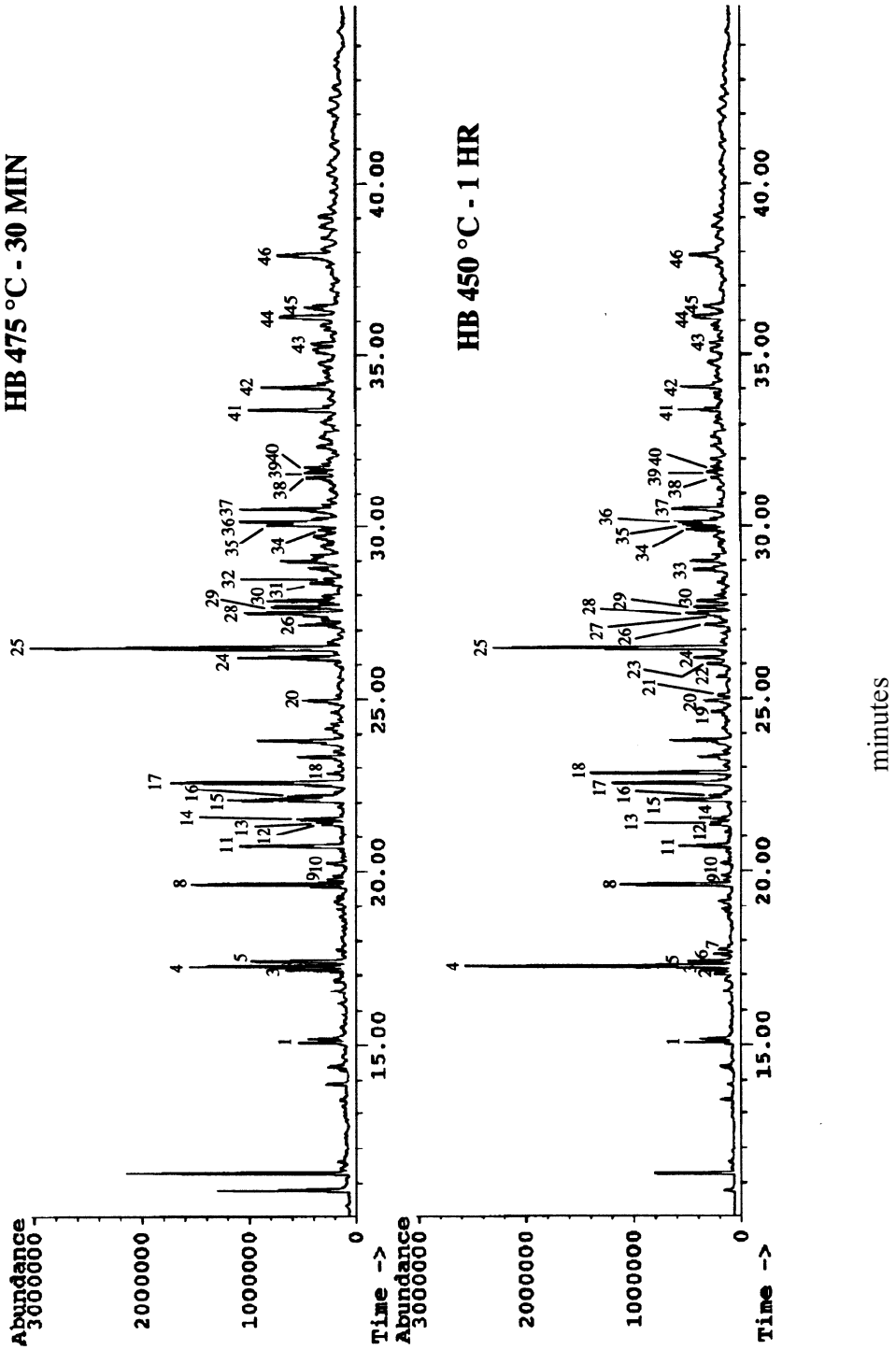

Figure 1.33-4. GC/MS TIC Traces of Fraction 3 of Liquid Products from Hexylbenzene Pyrolysis

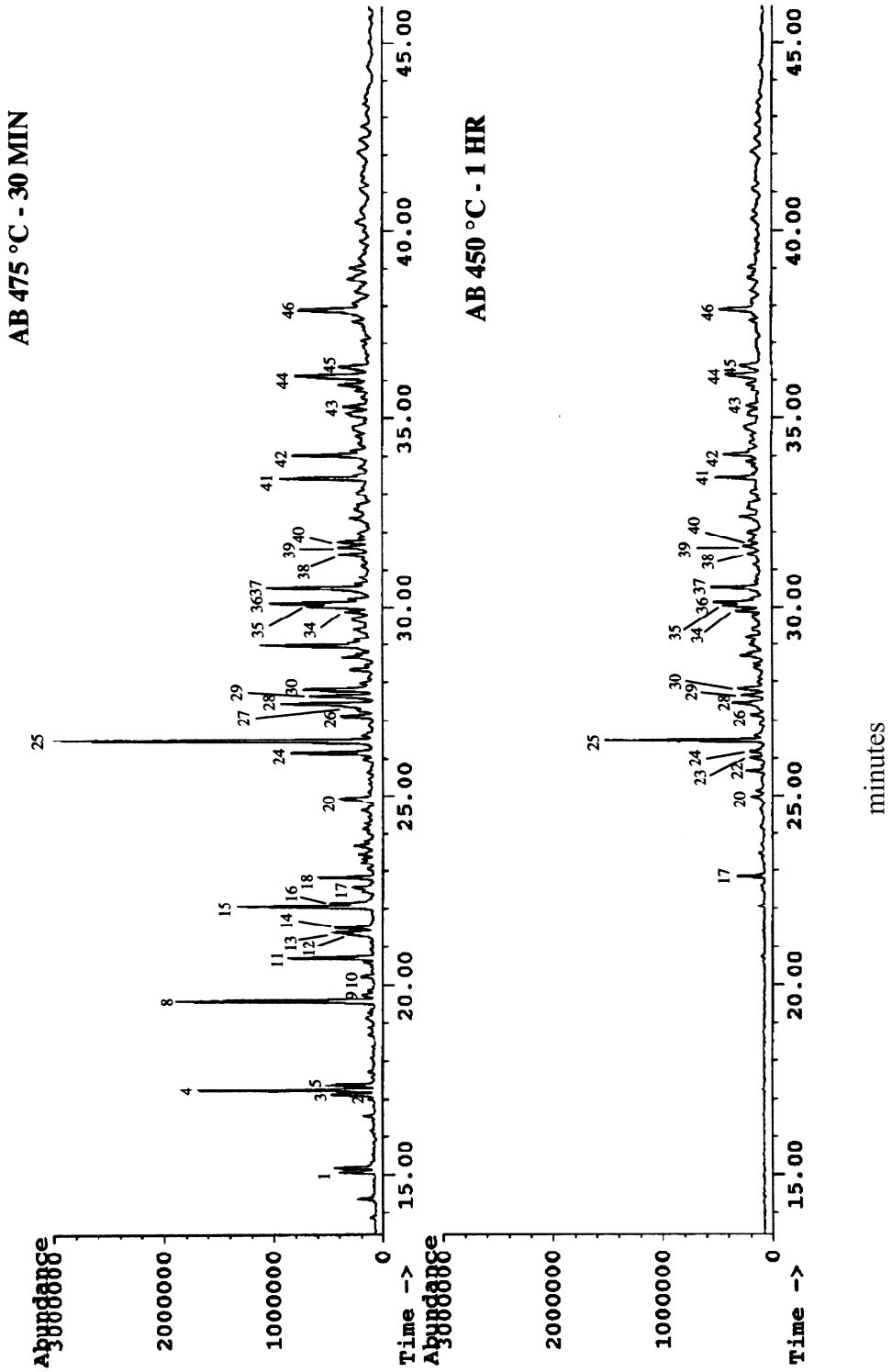

Figure 1.33-5. GC/MS TIC Traces of Fraction 3 of Liquid Products from Amylbenzene Pyrolysis

1.34 USE OF SITE-SPECIFIC ^{13}C-LABELING TO EXAMINE THE THERMAL STRESSING OF 1-PHENYLHEXANE: A CASE STUDY FOR THE DETERMINATION OF REACTION KINETICS IN COMPLEX FUEL MIXTURES VERSUS MODEL COMPOUND STUDIES

This study is explained in detail in *Advanced Thermally Stable Jet Fuels Technical Progress Report, October 1994 — December 1994*

Previous studies involving reaction kinetics and chemical mechanisms for the thermal breakdown of individual hydrocarbons provide an understanding of the chemical reactions of those materials in their most elementary forms and are useful for interpreting general reactions that occur upon thermal alterations.[1 2] While these studies represent an initial first step in comprehending complex radical reactions that occur with the pyrolysis of hydrocarbons, can their results be applied to the same model compounds in complex organic matrices? A 1995 study by Burnham et al[3] showed that the reaction kinetics for the thermal decomposition of hexadecane neat versus crude oil varied by nearly 60 percent.

Improved instrumentation and analytical techniques in recent years have provided a means for tracing the reaction pathways of individual compounds in complex organic matrices using ^{13}C NMR. A major problem with developing methodologies that utilize labeled compound tracer studies is the cost involved with obtaining ^{13}C-labeled compounds at specific sites in the molecules. Many compounds cost as much as $5,000 for only 0.5 g of labeled material, making these methods very costly when applied to fossil fuel systems.

This study had three objectives:

- Develop a synthetic strategy from relatively inexpensive starting materials to incorporate isotopic ^{13}C-labels at specific sites in target molecules
- Demonstrate the applicability of ^{13}C NMR labeling in combination with standard ^{13}C NMR experiments to examine thermally induced changes in jet fuel
- Determine whether reaction kinetics and mechanisms of model compound studies are applicable for the same compounds in complex organic matrices.

Results and Discussion

We obtained a series of ^{13}C NMR spectra for thermally stressed neat 1-phenylhexane, prior to and after 6 hours of thermal stressing at 400°C. The experimental parameters were chosen based on previous model studies with butylbenzene.[4] Prior to stressing, the spectrum showed six sharp signals from 40 ppm to 10 ppm. After six hours of stressing, the spectrum contained a number of additional signals that are characteristic of chemical changes resulting from thermal decomposition. The amount of 1-phenylhexane remaining throughout the thermal stressing is shown in **Table 1.34-1**. After six hours of stressing, only 35% of the 1-phenylhexane remains, thus confirming the presence of thermal decomposition products in the ^{13}C NMR spectra.

The next effort focused on determining whether the decomposition observed for neat 1-phenylhexane was representative of the thermal stressing of this model compound in the presence of a complex reactions matrix, such as that of a jet fuel. Using ^{13}C labeling, we found that when the 1-phenyl-1-^{13}C-hexane was thermally stressed in the presence of JP-8C, the ^{13}C

NMR spectrum obtained after 6 hours of heating is virtually the same as that obtained for the starting material. These results, also shown in Table 1.34-1, clearly demonstrate that only 3.4% of the 1-phenyl-1-^{13}C-hexane underwent any chemical transformation. Comparing the results of thermal stressing experiments with those of the model studies with neat 1-phenylhexane, we found that completely different reaction rates and possibly different reactions occur in the presence of JP-8C.

Conclusions

Site specific isotopic ^{13}C-labeling of organic compounds in complex organic matrices provides an invaluable analytical tool for examining reaction kinetics and mechanisms of those compounds. A complex mixture such as jet fuel constrains the use of conventional analytical methods for examining the thermal degradation of individual hydrocarbons in the mix. We successfully followed the degradation of 1-phenyl-1-^{13}C-hexane mixed with JP-8C at a concentration level of only 1%. Therefore, we were able to examine labeled compounds in the mix at relatively normal concentration levels with respect to other compounds.

The model compound studies at 400°C demonstrated that increased thermal stressing times reduced the amount of 1-phenylhexane by about 65% after 6 hours. In contrast, 1-phenyl-1-^{13}C-hexane remained largely unreacted after the same stressing period. This indicates different reactions kinetics and different mechanisms for thermal degradation for the two systems. In the jet fuel mixture, as radicals were formed in the degradation of 1-phenylhexane, there were quickly quenched by H-donor molecules present in the jet fuel. The neat solution contained no H-donor molecules to retard the thermal breakdown of the 1-phenylhexane.

The thermal degradation data obtained in this study corroborated that of similar studies[5], which also indicate that model compound studies should be used as a first step in understanding reaction kinetics of thermal degradation in complex mixtures. The model compound studies provide preliminary data that can be used to predict which components in the mixture are likely to participate in reactions of interest. The compounds chosen for further study can then be examined using site-specific isotopic labels which allow the reaction products to be analyzed directly, providing an accurate description of the thermal degradation that occurs in the complex fuel mixture.

Table 1.34-1. Thermal Stressing of 1-Phenylhexane at 400°C

Thermal Stressing Time (Min)	% 1-Phenylhexane Neat Thermal Stressing	% 1-Phenylhexane Thermally Stressed in the Presence of JP-8C
0	100	100
60	83.3	99.1
120	66.7	98.4
240	50.6	97.2
360	35.1	96.6

[1] Schobert, H. H. et al. *Advanced Thermally Stable Jet Fuels, Technical Progress Report.* The Pennsylvania State University. July 1994.

[2] Song, S., W. C. Lai, and H. H. Schobert. *Ind. Eng. Chem. Res.* 1994. 33. 534.

[3] Burnham, A. K., H. R. Gregg, and R. L. Braun. *Energy Fuels.* 1994.

[4] Schobert, H. H. et al. *Advanced Thermally Stable Jet Fuels, Technical Progress Report.* The Pennsylvania State University. January 1994.

[5] Burnham, A. K., H. R. Gregg, and R. L. Braun. *Energy Fuels.* 1995.

1.35 PYROLYSIS OF OCTYLBENZENE: EFFECTS OF STRUCTURE OF ALKYL SIDE CHAIN ON THE PYROLYSIS OF ALKYLBENZENES

This study is explained in detail in *Advanced Thermally Stable Jet Fuels Technical Progress Report, November 1992 — January 1993*

We studied the pyrolysis of octylbenzene (OB) at various temperatures 400¡C, 425¡C, and 450¡C. We calculated the reaction kinetics of OB based on this temperature range and analyzed the major chemical processes in its thermal reactions. The experimental apparatus and the analytical procedure employed were identical to those reported in Task 1, Numbers 1-3.

Thermal Stressing of OB at Temperatures 400¡C, 425¡C, and 450¡C.

As expected, temperature plays the most significant role in the degradation process, as shown in **Figure 1.35-1**. The reaction shows only a moderate rate at 400¡C; 8.18 mol% of OB remained after 16 hours of stressing. At 450¡C, however, virtually all OB was consumed after 8 hours of stressing. A rough comparison of the yields (wt%) of gaseous, liquid, and solid products formed (**Figures 1.35-2**, **1.35-3**, and **1.35-4**) shows a uniform increase in product with temperature. For example, a steady increase of the yields (wt%) of gas and solid formation can be observed in Figures 1.35-2 and 1.35-3.

Reaction Kinetics of Octylbenzene

We calculated the global kinetics of the reaction of octylbenzene as follows. The rate of disappearance of octylbenzene in the stressing can generally be expressed by equation (1), where C_A is the concentration of octylbenzene (mol%) at time t (hour), and k is the reaction rate constant, the unit of which depends on the reaction order.

$$-dC_A / dt = kC_A^n \qquad (1)$$

Concentration of OB at time t can also be expressed in terms of its initial concentration, C_{A0} and its conversion X at time t, as shown in equation (2):

$$C_A = C_{A0} (1-X) \qquad (2)$$

Combining equations (1) and (2) results in:

$$dX / dt = kC_{A0}^{n-1}(1-X)^n \qquad (3)$$

By plotting log (dX/dt) against log(1-X), we obtain a straight line with a slope of reaction order n and intercept of kC_{A0}^{n-1}. **Figure 1.35-5** shows the plot in the temperature range of interest.

The previous illustration demonstrates that the reaction order varies from 0.835 at 450¡C to 1.219 at 400¡C. As the temperature of the reaction increases, the reaction order decreases. However, the reaction order can be assumed to be roughly 1. A reaction order of 1 indicates unimolecular decomposition, implying that the major pathway of octylbenzene decomposition is through its thermal breakdown to form benzyl radicals and *n*-heptyl radicals.

The trend of increasing reaction order with decreasing reaction temperature may indicate that bimolecular reactions are gradually enhanced as temperature decreases. A decrease in

temperature lowers the reaction pressure and, therefore, the chance for bimolecular reaction. As such, we can infer that the temperature effect is dominant relative to a pressure effect.

From the intercept of Figure 1.35-5, we can obtain the global reaction rate constants (k« = $kC_{A0}^{n-1)}$. **Figure 1.35-6** shows the Arrhenius plot of the global behavior of octylbenzene based on the first order reaction assumption. An activation energy value (E_a) of 39.56 kcal/mol and pre-exponential factor (A) of $2.664x10^{12}$ hr^{-1} can be achieved. The E_a value obtained is significantly less than the $C\alpha$-$C\beta$ dissociation energy in the side chain of octylbenzene. The participation of secondary reactions, such as H-abstraction, in the consumption of OB may be one of the reasons for the reduction in the global activation energy. Under the reaction conditions used in this work, a high N_2 overpressure greatly facilitated the reactions between OB and other radicals (e.g., H¥, CH3¥). The net effect of these two-body reactions, which have a low E_a, is to greatly decrease the overall E_a value.

Liquid Product Analysis

Table 1.35-1 displays the major products and their amounts in liquid products after 1, 4, and 8 hours of stressing. After 1 hour at 400¡C, the major products are hexane, 1-heptene, toluene, and styrene. As reaction time is prolonged, toluene and hexane increase, whereas their changing patterns with time appear to be similar to the butylbenzenes, except that as the length of the chain increases, greater amounts of smaller products, such as pentane, pentene, and hexane, are formed. They are obviously not observed in the liquid products of the four butylbenzenes.

Table 1.35-1 Yields (mol%) of Major Compounds in Liquid Products for 1, 4, and 8 Hours at 400°C, 425°C and 450°C (continued)

Compound Name	1 hr			4 hr			8 hr		
	400	425	450	400	425	450	400	425	450
Butane + Butene	0.52	4.99	5.67	3.97	8.69	7.45	5.58	7.50	6.73
Pentane + Pentene	0.58	4.00	5.90	3.84	8.85	6.55	5.71	7.19	4.89
2-Methylpentane	0.00	0.00	0.00	0.00	0.16	0.41	0.00	0.54	0.13
Hexane	2.82	14.00	14.90	12.90	20.00	9.57	16.90	15.90	4.80
2 or 3-Hexene	0.00	0.27	0.62	0.24	0.73	0.31	0.51	0.67	0.00
Methylhexane	0.00	0.11	0.46	0.09	0.87	0.80	0.31	0.75	0.90
Heptane	0.06	0.87	1.91	1.15	3.19	1.46	2.96	2.81	0.50
1-Heptene	3.29	6.46	3.13	5.00	1.41	1.13	2.99	1.16	0.79
2-Heptene	0.15	0.85	0.81	1.21	0.40	0.10	1.19	0.33	0.00
3-Heptene	0.10	0.47	0.37	0.57	0.24	0.06	0.53	0.60	0.00
Methylcyclohexane	0.04	0.49	1.04	0.49	1.13	0.88	0.92	1.07	0.51
Ethylcyclopentane	0.00	0.19	0.46	0.21	0.51	0.35	0.46	0.54	0.16
Benzene	0.00	0.33	0.93	0.24	1.12	1.69	0.55	1.66	2.37
Octane	0.03	0.42	0.86	0.42	0.94	0.47	0.90	0.70	0.12
Toluene	5.28	31.90	49.80	31.8	58.20	54.30	51.30	55.4	54.10
Nonane	0.03	0.44	0.66	0.45	0.79	0.21	0.87	0.46	0.04
3-Ethylhexane	0.00	0.00	0.24	0.13	0.28	0.00	0.33	0.16	0.00
Ethylbenzene	0.50	6.10	20.30	6.77	22.30	28.2	15.00	27.5	28.70
Decane	0.00	0.27	0.36	0.30	0.41	0.09	0.51	0.21	0.00
Xylene	0.00	0.00	0.15	0.00	0.16	0.35	0.00	0.28	0.43
Styrene	1.06	1.82	0.84	0.78	0.23	0.17	0.29	0.12	0.13
Isopropylbenzene	0.00	0.54	2.94	0.91	4.10	4.34	2.77	4.97	4.02
n-Propylbenzene	0.21	1.92	4.12	1.81	4.61	4.00	3.67	4.67	2.95
Allybenzene	0.08	0.24	0.36	0.13	0.32	0.00	0.20	0.00	0.00
C3-Benzene	0.00	0.00	0.00	0.00	0.00	0.56	0.00	0.56	0.71
Undecane	0.00	0.00	0.14	0.14	0.18	0.03	0.23	0.08	0.00
Isobutylbenzene	0.00	0.12	0.31	0.11	0.38	0.40	0.28	0.43	0.33
s-Butylbenzene	0.00	0.12	0.49	0.17	0.71	0.44	0.59	0.78	0.20
Methylstyrene	0.13	0.63	0.35	0.31	0.12	0.10	0.12	0.00	0.09
Methylstyrene	0.00	0.13	0.18	0.08	0.07	0.09	0.06	0.21	0.11
C4-Benzene	0.00	0.00	0.00	0.07	0.00	0.00	0.04	0.00	0.00
C4-Benzene	0.00	0.01	0.05	0.01	0.06	0.07	0.00	0.09	0.06
C4-Benzene	0.00	0.00	0.03	0.00	0.04	0.03	0.00	0.05	0.03
n-Butylbenzene	0.40	2.83	3.69	2.51	2.97	0.93	3.46	1.79	0.35
C4-Benzene	0.06	0.14	0.09	0.08	0.06	0.07	0.05	0.08	0.09
Indan	0.00	0.00	0.16	0.05	0.17	0.20	0.11	0.21	0.22
C5-Benzene	0.00	0.00	0.29	0.00	0.30	0.10	0.00	0.19	0.03
C5-Benzene	0.00	0.00	0.00	0.19	0.00	0.00	0.39	0.14	0.00

Table 1.35-1 (cont d) Yields (mol%) of Major Compounds in Liquid Products for 1, 4, and 8 Hours at 400°C, 425°C and 450°C

Dimethylstyrene	0.00	0.00	0.10	0.00	0.00	0.21	0.07	0.25	0.21
5-Methyldodecane	0.02	0.00	0.00	0.18	0.00	0.00	0.20	0.00	0.00
n-Pentylbenzene	0.29	1.91	2.20	1.87	1.95	0.41	2.56	1.03	0.10
2,6,6-Trimethyldodecane	0.02	0.14	0.09	0.17	0.09	0.05	0.17	0.03	0.04
1,3-Dimethylbutylbenzene	0.00	0.15	0.21	0.22	0.21	0.06	0.30	0.13	0.06
1-Pentenylbenzene	0.06	0.19	0.14	0.13	0.06	0.00	0.09	0.02	0.00
nC6-Benzene	0.15	0.64	0.70	0.64	0.61	0.10	0.84	0.28	0.03
Naphthalene	0.00	0.54	1.84	0.49	1.67	2.38	1.00	2.32	2.74
1-Propylpentylbenzene	0.31	0.69	0.36	0.93	0.32	0.00	0.78	0.11	0.00
1-Ethylhexylbenzene	0.03	0.11	0.07	0.17	0.10	0.00	0.19	0.04	0.00
n-Heptylbenzene	0.10	0.42	0.41	0.51	0.30	0.00	0.56	0.11	0.00
3-Methyl-4-pentylbenzene	0.00	0.17	0.26	0.13	0.21	0.00	0.18	0.13	0.00
1-Methylheptylbenzene	0.50	1.20	0.60	1.59	0.49	0.04	1.35	0.14	0.00
2-Methylnaphthalene	0.00	0.00	0.25	0.00	0.25	0.43	0.00	0.47	0.61
C8-Benzene	0.06	0.36	0.19	0.24	0.10	0.00	0.17	0.04	0.00
1-Methylnaphthalene	0.00	0.18	0.70	0.24	0.70	0.89	0.51	1.19	1.02
n-Octylbenzene	88.20	37.30	13.70	44.00	6.13	0.60	19.50	1.12	0.01
Higher Alkylbenzene	0.00	0.15	0.00	0.23	0.09	0.00	0.26	0.00	0.00
Methylnaphthalene	0.00	0.02	0.07	0.00	0.05	0.11	0.00	0.15	0.17
Biphenyl	0.00	0.11	0.40	0.00	0.35	0.61	0.20	0.44	0.89
Methylbiphenyl	0.00	0.10	0.21	0.00	0.17	0.07	0.25	0.12	0.04
Methylnaphthalene	0.00	0.00	0.10	0.00	0.00	0.12	0.07	0.11	0.14
Methylnaphthalene	0.00	0.00	0.10	0.00	0.00	0.10	0.00	0.11	0.15
Methylnaphthalene	0.00	0.05	0.00	0.00	0.10	0.00	0.00	0.17	0.00
1-Octenylbenzene	0.16	0.35	0.25	0.49	0.16	0.00	0.45	0.00	0.00
C9-Alkylbenzenes	0.00	0.00	0.00	0.00	0.00	0.00	0.00	0.00	0.00
Methylbiphenyl	0.00	0.00	0.11	0.00	0.13	0.15	0.09	0.13	0.24
Methylbiphenyl	0.00	0.00	0.26	0.00	0.27	0.36	0.17	0.32	0.56
Methylbiphenyl	0.00	0.00	0.13	0.00	0.12	0.15	0.12	0.13	0.23
Dimethylbiphenyl	0.00	0.00	0.09	0.00	0.09	0.08	0.09	0.09	0.13
Bibenzyl	0.00	0.11	0.18	0.10	0.16	0.04	0.18	0.09	0.06
C9-Benzene	0.05	0.11	0.00	0.11	0.00	0.00	0.08	0.00	0.00
Dimethylbiphenyl	0.00	0.00	0.00	0.00	0.12	0.10	0.00	0.12	0.17
Fluorene	0.00	0.00	0.00	0.00	0.03	0.10	0.00	0.07	0.21
Methylfluorene	0.00	0.00	0.00	0.00	0.04	0.06	0.00	0.08	0.09
Dimethylbiphenyl	0.00	0.00	0.00	0.00	0.08	0.07	0.00	0.08	0.10
Higher Alkylbenzene	0.15	0.38	0.14	0.32	0.04	0.00	0.10	0.02	0.00
Higher Alkylbenzene	0.02	0.16	0.11	0.11	0.05	0.00	0.09	0.00	0.00
Higher Alkylbenzene	0.09	0.14	0.00	0.24	0.00	0.00	0.08	0.00	0.00
Phenylnaphthalene	0.00	0.00	0.00	0.00	0.000	0.04	0.00	0.04	0.07
Phenylnaphthalene	0.00	0.00	0.02	0.02	0.04	0.07	0.03	0.05	0.12
Pyrene	0.00	0.03	0.04	0.03	0.03	0.04	0.03	0.04	0.07
Phenanthrene	0.00	0.00	0.04	0.00	0.03	0.07	0.00	0.06	0.18
Anthracene	0.00	0.00	0.03	0.00	0.03	0.03	0.00	0.04	0.05

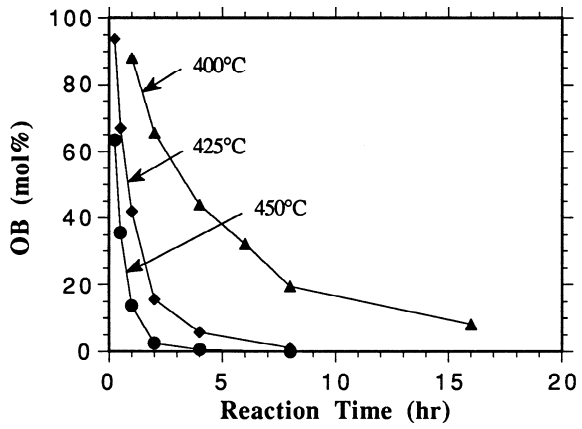

Figure 1.35-1. The Disappearance of Octylbenzene (mol%) at 400°, 425°, and 450°C

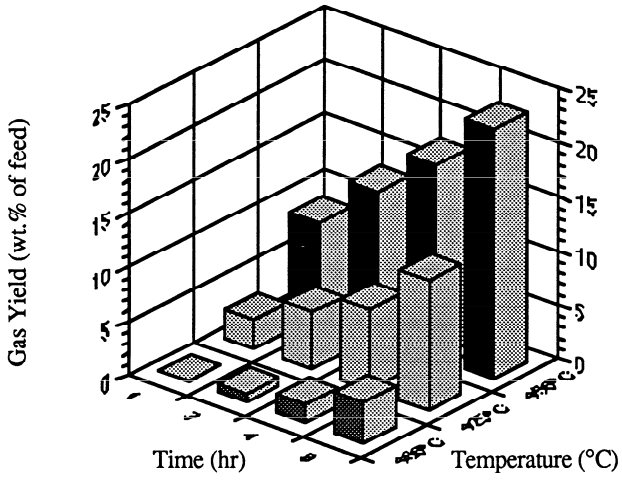

Figure 1.35-2. Relationship of Gas Yield to Reaction Time and Temperature

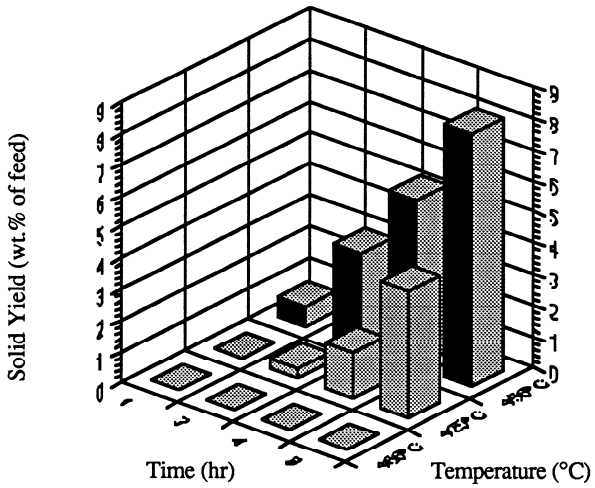

Figure 1.35-3. Relationship of Solid Yield to Reaction Time and Temperature

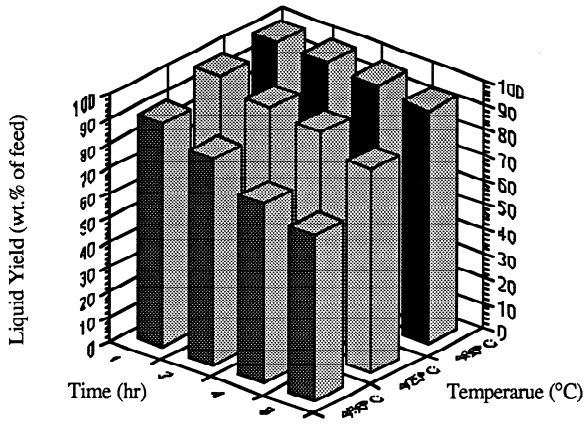

Figure 1.35-4. Relationship of Liquid Yield to Reaction Time and Temperature

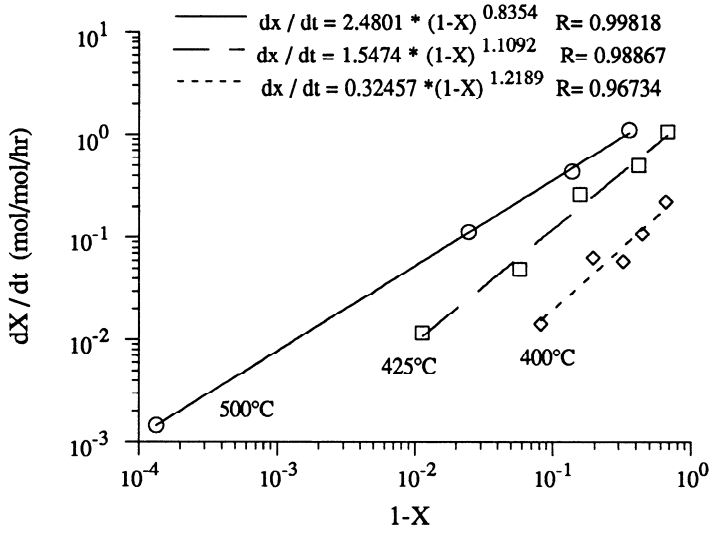

Figure 1.35-5. Reaction Kinetics of Octylbenzene between 400° and 450°C

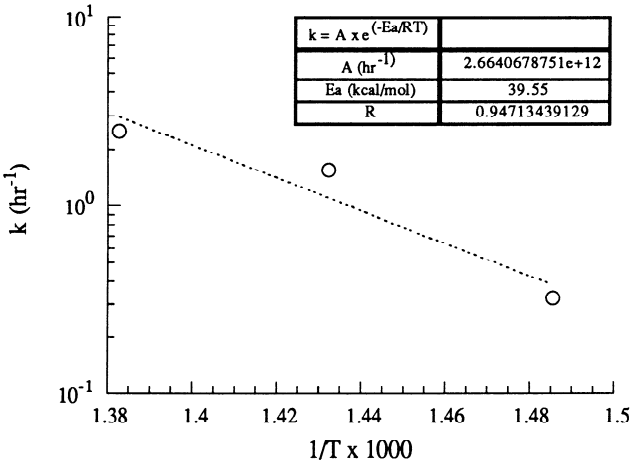

Figure 1.35-6. The Arrhenius Plot for the Pyrolysis of Octylbenzene

1.36 PYROLYSIS OF N-ALKYLBENZENES

This study is explained in detail in *Advanced Thermally Stable Jet Fuels Technical Progress Report, July–September 1994.*

Introduction

This work addressed the effect of the length of the side chain of an alkylbenzene on pathways and kinetics of pyrolysis reactions. Five *n*-alkylbenzenes, typically present in the aromatic fraction of jet fuels, including ethylbenzene, *n*-butylbenzene, *n*-amylbenzene, *n*-hexylbenzene and *n*-octylbenzene, were thermally stressed under a temperature range of 400° to 475°C and batch holding time from 5 minutes to 16 hours. We studied three alkylbenzenes—*n*-amylbenzene, *n*-hexyl, and *n*-octyl-benezene—extensively, using prior results pertaining to *n*-butylbenzene at 450°C for comparison. Reactions were typically monitored by measuring yields of gaseous, liquid, and solid products, and by analyzing the product composition. Thermal stabilities were compared in terms of rate of disappearance of starting materials, global reaction kinetics, and major reaction pathways.

Pyrolysis of *n*-Alkylbenzenes: General Features

1. Ethylbenzene: Toluene is the simplest compound in the *n*-alkylbenzenes family; however, because its high stability at 400°-500°C is widely known, we did not select it as a major candidate model compound. Ethylbenzene was the first compound we examined. It was extremely resistant to reaction compared to other members of the *n*-alkylbenzenes family. Almost no conversion was achieved after 4 hours of reaction at 450°C. Hardly any gases were produced and analysis of the gas products revealed a small amount of methane and C_2 species (ethane and ethylene). More than 99 percent of the condensed liquid after reaction was still constituted of ethylbenzene.

These results contradicted published literature, which indicated that ethylbenzene decomposes at a rate somewhat slower than *n*-propylbenzene. Because of their structural similarities—both contain aliphatic C-C bonds in the side chain that break at similar activation energies—the reaction rates should be comparable. However, the pyrolysis of ethylbenzene proceeded much slower than expected at 450°C, leading us to deduce that the breaking of the aliphatic C-C bonds, as an initiation reaction and rate-controlling step, may not be the only step that causes the tremendous reactivity difference. Some type of radical transfer reactions might exist as a very slow step.

The first step of ethylbenzene decomposition is the homolytic breakdown of the C_α-C_β bonds on the side chain. This is probably followed by a series of hydrogen abstraction and β-scission reactions. By analyzing the likely reactions, shown in reactions (1) through (3) below, we determined that the stability difference of ethylbenzene compared to other *n*-alkylbenzenes might result from the following facts:

a) Reaction (1) has a slightly higher activation energy (E_a) than, for example, the initiation reaction of *n*-propylbenzene, as a result of the stabilizing effect of the extra methylene group in the *n*-propylbenzene molecule. The pre-exponential factors for the two reactions likely are the same. This alone could not account for the

significantly lower reactivity of ethylbenzene. Rates for the initiation reactions are almost equally slow for the two initiation reactions at 450°C in ethyl- and *n*-propylbenzene pyrolysis. Initiation of *n*-propylbenzene proceeded nearly 6 times faster at 800°C, indicating that a more important and unique property of ethylbenzene must exist.

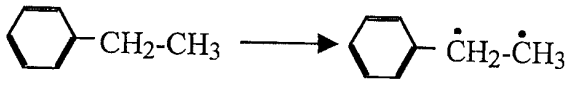

(1)

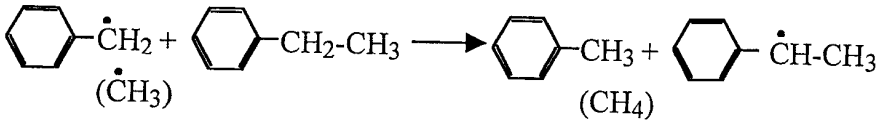

(2)

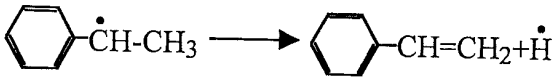

(3)

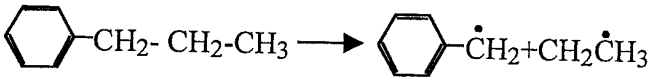

(4)

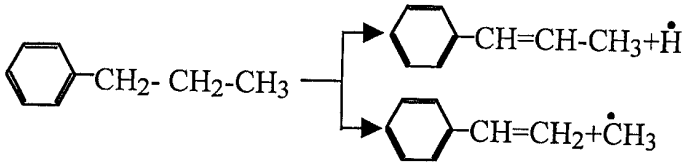

(5)

(6)

b) Reaction (3) is a β-scission reaction that produces a styrene and hydrogen atom by breaking β C-H bonds. Compared with reaction (3), the pyrolysis of other compounds in the series of *n*-alkylbenzene involves a β-scission of both C-H and C-C bonds, as shown in reactions (5) and (6). At a temperature of 450°C, only reaction (6) proceeds at a measurable rate. The rate of β-scission through ejecting hydrogen atoms (reactions (3) and (5)) is very slow. As a result, ethylbenzene barely decomposes at 450°C. At a higher temperature, however, the rate difference between reaction (3) and (6) is much less. Therefore, the βC-C bond cleavage (reaction (6)) is a much easier reaction at 450°C than βC-H cleavage. This probably constitutes the major reactivity difference in ethyl- and *n*-propyl-benzene pyrolysis.

c) Styrene is one of the major condensed reaction products from the pyrolysis of ethylbenzene. Styrene can be rapidly consumed to form ethylbenzene (reaction (7)), explaining the rapid disappearance of styrene as a primary product in the neat batch pyrolysis on *n*-alkylbenzenes and the concurrent steady increase of ethylbenzene as a secondary reaction product. As a result, even though some styrene could be generated from reaction (3), the styrene reacts "back" to form ethylbenzene.

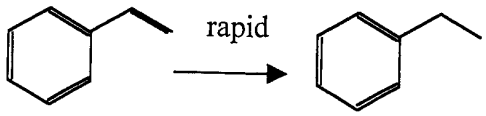

(7)

2. Other *n*-Alkylbenzenes. Other *n*-alkylbenzenes showed a considerably higher degree of reaction in the 400-475°C range, with the extent of the reaction dependent on the actual temperature and the duration of the reactions. The yields of gaseous and solid products increased with reaction time and temperature. In general, findings indicated that the complex interaction between radical fragments thermally produced from various types of compounds in jet fuels determines the solid-forming tendency. Intermediate radicals formed from *n*-alkylbenzene pyrolysis can facilitate the process, either by actively attacking the other radicals in the system of jet fuel pyrolysis or by inactively being attacked by other, more reactive radicals to produce solid products.

Distribution of Major Products

A complete listing of the yields of major products for the pyrolysis of *n*-amylbenzene is presented in **Tables 1.36-1**, **1.36-2**, and **1.36-3**. Butane and 1-butene were frequently detected in high amounts in liquids. The longer the side chain of the *n*-alkylbenzenes, the greater the amounts of these compounds. Major condensed products observed at 425°C for *n*-amylbenzene pyrolysis were toluene and ethylbenzene. Other compounds were found only in significantly smaller yields. Gaseous products resulting from pyrolysis at 425°C for 2 hours included propane, ethane, methane, *n*-butane, 1-butene, propylene, hydrogen, ethylene, and isobutane. Saturated gaseous and liquid products were predominant over unsaturated products at all reaction conditions.

This work examined the temporal variations of the yields of major products for *n*-amylbenzene pyrolysis. The two most abundant products, toluene and ethylbenzene, increased almost linearly. Most oleofinic compounds exhibited a maximum concentration with increasing reaction time. The concentrations of methylethylbenzene and *n*-propylbenzene increased steadily with reaction time. Compounds such as indan and *n*-butylbenzene were formed at short reaction times and disappeared rapidly at high treatment severity. Naphthalene, the only multi-ring compound that could be detected frequently by gas chromotography, consistently increased. Other PAHs were difficult to detect and quantify by GC, either because they were present in limited amounts or had relatively high molecular weights.

The overwhelming predominance of saturated compounds over unsaturated ones is distinctly different from pyrolysis reactions undertaken at low pressures and high temperatures. In high-temperature and low-pressure pyrolysis, the Rice Kossiakoff mechanism (Rice, 1934; Rice, 1935; Kossiakoff, 1943) dominates in the free-radical reactions. β-bond scission is the major mode of the chain propagation reaction; as a result, olefinic products naturally become dominant compounds in the product mixture. In this case, however, the pyrolysis of neat compounds was conducted under 0.69 MPa of UHP N_2 in a closed vessel. The high pressure and comparatively low temperature used could have facilitated the hydrogen-transfer reactions with low activation energies. The net outcome of the pressure increase was the formation of saturated compounds as a direct result of the hydrogen abstraction reactions of various primary and secondary radicals. This process follows the Fabuss-Smith-Satterfield mechanism (Fabuss, 1964).

Based on our findings, we developed a general pyrolysis network for *n*-amylbenzene, which is shown in **Figure 1.36-1**. **Table 1.36-4** lists estimated kinetic parameters and rate constants for some typical hydrogen abstraction reactions in *n*-amylbenzene pyrolysis (Froment,

1991). Benzyl and methyl radicals are probably the most abundant and most active radical chain carriers, with methyl being the more reactive of the two. Based on consistencies with previously published research, we deduced that the formation of a phenyl radical by β-scission of a β-alkylbenzene radical is difficult and may account for the low yield of benzene. Table 1.36-4 lists the relevant kinetic data for β-scission reactions.

Based on the data in Table 1.36-4, the rate of hydrogen abstraction at 450°C at the α-position is about two orders of magnitude higher than at other positions. The rates of hydrogen abstraction at positions other than α were roughly identical (Froment, 1991). Rates of β-scission of the secondary alkylbenzene radicals were different. β-scission of the γ-alkylbenzene radical was significantly faster than other, secondary alkylbenzene radicals. As a result, γ-hydrogen abstraction at 450°C can seemingly be facilitated by the subsequent fast β-scission step. This exemplifies the principle that the operation of the hydrogen abstraction and β-scission determines product distribution. Therefore, hydrogen abstractions at α- and γ- positions, probably by benzyl radicals, at the relatively low conversion of pyrolysis, are two major ways in which the parent *n*-amylbenzene molecules are consumed, as illustrated in Figure 1.36-1. The products formed by the major two steps—styrene, propane, toluene, and 1-butene—dominate the product mixture. Hydrogen abstraction at other places (β, δ, and ε) happens at a lower rate and results in less abundant products.

Possible Major Pathways of Pyrolysis of *n*-Alkylbenzenes

The general features of the pyrolyses for *n*-hexylbenzene and *n*-octylbenzene remain the same as that of *n*-amylbenzene. The thermal reactions of *n*-hexylbenzene and *n*-octylbenzene form toluene and ethylbenzene as major reaction products. The most abundant gaseous products are *n*-butane and *n*-hexane, respectively, at low reaction temperature for the two compounds. The type and amounts of gases formed for *n*-octylbenzene are increased for the longer chain compounds. With one hour reaction at 450°C, for example, methane formation increased from 6 mol% for *n*-amylbenzene to 11 mol% for *n*-hexylbenzene to 14 mol% for *n*-octylbenzene. 1-Pentene is also present in the gaseous product mixture for *n*-hexylbenzene pyrolysis, as is 1-heptene for *n*-octylbenzene. C_1 to C_3 gas formation for the *n*-hexyl- and *n*-octylbenzenes are quite extensive. Their yields increase rapidly with reaction time and temperature. These gases are produced as a result of complex secondary decomposition reactions. The pathways for their formation are very difficult to deduce.

The formation of the major reaction products from *n*-hexyl- and *n*-octylbenzenes can be explained using the steps described for *n*-amylbenzene. The general possible major pathways for the pyrolysis of *n*-alkylbenzenes are shown in **Figure 1.36-2**. This figure demonstrates that the major characteristics of *n*-alkylbenzenes pyrolysis are the same. They have similar initiation reactions and propagation modes. For an *n*-alkylbenzene, α-hydrogen abstraction produces styrene (ethylbenzene) and *n*-2 alkane, and γ-hydrogen abstraction produces toluene and *n*-1 1-alkene. The reactions at the other sites on the side chain produce only minor reaction products. Probably only minor differences exist that cause the difference in the reactivities of the *n*-alkylbenzenes (e.g., the difference in quantity of each major product and number of abstractable hydrogens other than α and γ positions in the side chain). Yet the general mechanism shown in Figure 1.36-2 well explains the major behavior of their pyrolysis characteristics.

Global Reaction Kinetics

Kinetic regression was performed for *n*-amylbenzene, *n*-hexylbenzene , and *n*-octylbenzene based on conversion data obtained from batch thermal treatments. As expected, conversion increases with reaction time and temperature. In comparing the conversion of four *n*-alkylbenzenes at 450°C, *n*-octylbenzene had the highest conversion and *n*-butylbenzene had the lowest. Assuming first-order kinetics, equation (7) is the first-order reaction rate expression in terms of concentration, where C is the reactant concentration (mol/L), *t* is the reaction time (s), and *k* is the first-order rate constant (s^{-1}):

$$-\frac{dC}{dt} = kC \qquad (7)$$

Equation (7) can be transformed into equation (8) by integration, where x is conversion of the reactant:

$$\ln(1-x) = -kt \qquad (8)$$

Plotting ln (1-x) against reaction time, t, our results fit the experimental data to the first-order kinetics well, suggesting that the reactions were, indeed, proceeding according to the first order. The rate constants increased smoothly as reaction temperature increased. As the side chain lengths increased from five to eight, the first-order rate constants increased. The rate constants were correlated with reaction temperature by the Arrhenius equation:

$$K = A_{exp}(-E_a/RT) \qquad (9)$$

where A is the pre-exponential factor (s^{-1}), E_a is the apparent activation energy (kJ/mol), and R is the universal gas constant (J $mol^{-1}k^{-1}$).

The values obtained for E_a and A are listed in **Table 1.36-5**. The E_a values revealed that the activation energies agreed well with those of Banerjee (Banerjee, 1982) for the pyrolysis of *n*-butylbenzene in a flow reactor with a molar ratio of *n*-butylbenzene and diluent inert gas N_2 1:1. The rate constants obtained at 425°C agreed well with other published findings (Savage, 1987), whereas rates at 450°C and 475°C were much lower than the published values. This could account for the low Arrhenius parameters obtained by this study. The apparent disagreement could also be related to the fact that the current work was carried out in a distinctly different reaction condition—a relatively high inert gas pressure—than the studies detailed in the literature. The effect of inert gas pressure on the kinetics of pyrolysis of hydrocarbons is rarely reported; as a result, a comparison of kinetic results obtained from the different procedures may not be useful.

Comparison of Relative Importance of α- and γ-H Abstraction Reactions

The characteristic products ethylbenzene+styrene was employed as an indication of α-hydrogen abstraction. Similarly, toluene was considered as an indication of γ-hydrogen abstraction. The molar ratio of ethylbenzene+styrene over toluene was used as an index to compare the relative importance of hydrogen abstraction reactions at α- and y- positions. The higher the ratio, the more important α-hydrogen abstraction is, and otherwise, the more

important γ-hydrogen abstraction is. **Figure 1.36-3** shows the molar ratio of ethylbenzene+styrene over toluene for three of the *n*-alkylbenzenes from 425°C to 475°C.

Several trends became apparent. For all three compounds, the ratio increased as temperature increased, from 0.39 at 425°C. Likewise, the ratio decreased from 0.77 at 475°C to 0.39 at 425°C at 40% of conversion of *n*-amylbenzene. The ratio changes from 0.6 to 0.36 for *n*-hexylbenzene in the same temperature range. The ratio for *n*-octylbenzene decreases from 0.41 to 0.2, as temperature decreases from 450° to 400°C. This probably indicates that α-hydrogen abstraction is preferred by increasing temperature (i.e., α-hydrogen abstraction has a higher activation energy than γ-hydrogen abstraction). This is explained as follows:

> The α-hydrogen abstraction products, ethylbenzene and styrene, were formed by α-hydrogen abstraction and the subsequent β-scission. The activation energies for them were 63.56 and 157 kJ/mol, respectively. Similarly, γ-hydrogen abstraction product, toluene, was formed by the combination of hydrogen abstraction and β-scission. The activation energies for this process were 90.70 and 117 kJ/mol. The highest activation channel was the β-scission to form styrene; it should also be the most temperature-sensitive reaction. Therefore, when temperature increases, the formation of styrene and ethylbenzene should increase as well.

Another trend observed at similar temperature and conversion was the tendency for the ratio to decrease as the length of the chain increased. This indicates that γ-hydrogen abstraction is relatively easier for a longer chain alkylbenzene. As conversion increases (≤50 percent), the ratio also decreases, indicating the increasing of γ-hydrogen abstraction. The complex reaction processes and the many factors affecting them prevented us from accurately formulating reasons from the mechanistic and kinetic aspects.

Table 1.36-1. Molar Yields (mol%) of Major Products Formed for *n*-Amylbenzene Pyrolysis at 425°C

Compound Name	Reaction Time (hr)				
	0.25	0.50	1.00	2.00	4.00
Methane	0.18	0.41	1.3	3.27	7.31
Ethane	0.51	0.95	2.18	5.20	9.75
Ethylene	0.14	0.22	0.28	0.42	0.41
Propane	2.53	4.12	5.82	17.66	24.12
Propylene	0.37	0.59	0.73	1.97	1.72
i-Butane	0.55	0.49	0.01	0.05	0.17
n-Butane	1.36	2.26	1.56	1.98	3.14
1-Butene	0.29	0.50	5.37	5.56	4.04
Hydrogen	0.21	0.53	1.03	1.24	1.34
Benzene	0.13	0.20	0.58	0.65	1.07
Toluene	0.01	5.66	19.89	26.67	41.33
Ethylbenzene	0.59	1.35	5.85	13.34	30.37
Styrene	2.35	2.67	1.89	0.83	0.00
Methylethylbenzene	0.00	0.07	0.87	2.08	5.62
n-propylbenzene	0.10	0.23	0.94	2.04	4.65
1-ethenyl-2-methylbenzene	0.23	0.20	0.33	0.21	0.00
1-methylethenylbenzene	0.22	0.38	0.61	0.30	0.16
Propenylbenzene	0.04	0.04	0.11	0.13	0.04
n-butylbenzene	0.50	0.67	1.15	1.65	1.79
Indan	0.20	0.23	0.59	0.55	0.33
Naphthalene	0.01	0.04	0.17	0.69	0.00
2-methylnaphthalene	0.00	0.00	0.12	0.13	0.00
1-methylnaphthalene	0.00	0.00	0.00	0.99	0.00

Table 1.36-2. Molar Yields (mol%) of Major Products Formed for *n*-Amylbenzene Pyrolysis at 450°C (continued)

Compound Name	Reaction Time (hr)				
	0.08	0.13	0.25	0.50	1.00
Methane	0.28	0.27	0.75	2.65	5.65
Ethane	0.67	1.04	1.22	3.44	6.78
Ethylene	0.28	0.20	0.34	0.73	0.47
Propane	2.46	2.32	5.91	8.90	17.95
Propylene	0.36	0.39	0.96	1.43	1.68
i-Butane	0.00	0.02	0.00	0.01	0.09
n-Butane	0.54	0.33	0.83	0.76	1.65
1-Butene	0.63	0.81	2.79	2.50	2.48
Hydrogen	0.34	0.39	0.60	1.25	1.10
Benzene	0.03	0.06	0.27	0.42	0.66
Toluene	0.73	1.23	7.61	16.15	21.26
Ethylbenzene	0.23	0.37	2.33	6.73	16.63
Styrene	1.22	1.69	4.14	3.81	1.00
Methylethylbenzene	0.01	0.04	0.13	0.57	2.32
n-propylbenzene	0.00	0.00	0.38	1.13	2.50
1-ethenyl-2-methylbenzene	0.05	0.13	0.23	0.35	0.25
1-methylethenylbenzene	0.05	0.12	0.54	0.00	0.39

Compound Name	Reaction Time (hr)				
	0.08	0.13	0.25	0.50	1.00
Propenylbenzene	0.00	0.00	0.06	0.12	0.12
n-butylbenzene	0.00	0.00	0.81	1.23	1.59
Indan	0.03	0.12	0.34	0.45	0.69
Naphthalene	0.00	0.00	0.07	0.25	1.27
2-methylnaphthalene	0.00	0.00	0.03	0.00	0.20
1-methylnaphthalene	0.00	0.00	0.00	0.00	1.23

Table 1.36-3. Molar Yields (mol%) of Major Products Formed for *n*-Amylbenzene Pyrolysis at 475°C

Compound Name	Reaction Time (hr)				
	0.08	0.17	0.25	0.33	0.50
Methane	0.04	1.07	3.35	2.44	8.42
Ethane	0.11	1.27	3.63	2.47	8.39
Ethylene	0.04	0.47	0.84	0.43	0.79
Propane	1.17	6.35	10.09	9.10	20.36
Propylene	0.15	1.20	1.64	1.44	2.45
i-Butane	0.00	0.00	0.04	0.03	0.13
n-Butane	0.40	0.86	1.29	1.25	1.95
1-Butene	0.51	2.73	2.22	2.69	2.59
Hydrogen	0.04	0.48	1.05	0.49	1.25
Benzene	0.06	0.25	0.34	0.51	0.75
Toluene	0.92	7.80	11.52	14.97	20.55
Ethylbenzene	0.29	3.14	6.18	10.45	17.26
Styrene	1.61	4.09	3.18	2.46	1.56
Methylethylbenzene	0.00	0.39	0.78	1.34	2.09
n-propylbenzene	0.04	0.59	1.10	1.56	2.32
1-ethenyl-2-methylbenzene	0.08	0.50	0.40	0.43	0.32
1-methylethenylbenzene	0.00	0.68	0.70	0.57	0.42
Propenylbenzene	0.00	0.13	0.13	0.24	0.15
n-butylbenzene	0.00	0.93	1.17	1.15	1.07
Indan	0.05	0.58	0.81	0.90	0.66
Naphthalene	0.00	0.32	0.51	0.94	1.56
2-methylnaphthalene	0.00	0.08	028	0.06	0.18
1-methylnaphthalene	0.00	0.00	0.00	0.55	0.92

Table 1.36-4. Some Kinetic Data of Hydrogen Abstraction and β-scission Reactions in *n*-Amylbenzene Pyrolysis

Reaction	E_a (kJ/mol)	log A $m^3/s \cdot kmol$	k (450°C) $m^3/s \cdot kmolor\ s^{-1}$
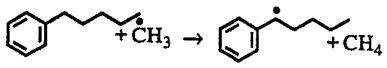	44.25	8.24	1.10×10^5
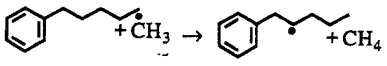	67.77	8.44	3.50×10^3
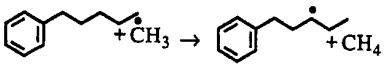	72.53	9.03	6.16×10^3
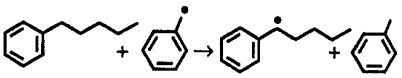	63.56	8.67	1.20×10^4
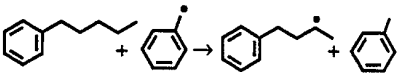	90.70	8.96	2.55×10^2
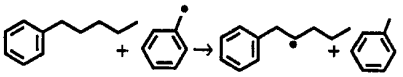	97.27	9.89	7.28×10^2
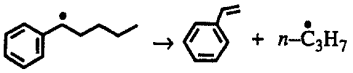	157	14.7	2.27×10^3
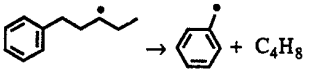	117	15	3.5×10^6
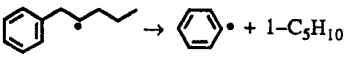	168	14.63	3.10×10^2

Table 1.36-5. Comparison of Kinetic Parameters for n-Alkylbenzene Pyrolysis

Compound	Rate Constants x 10^4, s^{-1}				E_a	A x 10^6
Name	400°C	425°C	450°C	475°C	kJ/mol	s^{-1}
n–amylbenzene		1.25	3.64	7.90	160.09	130
n–hexylbenzene		2.57	5.68	12.99	140.32	8.2
n–octylbenzene	0.84	3.59	7.89		131.98	2.8

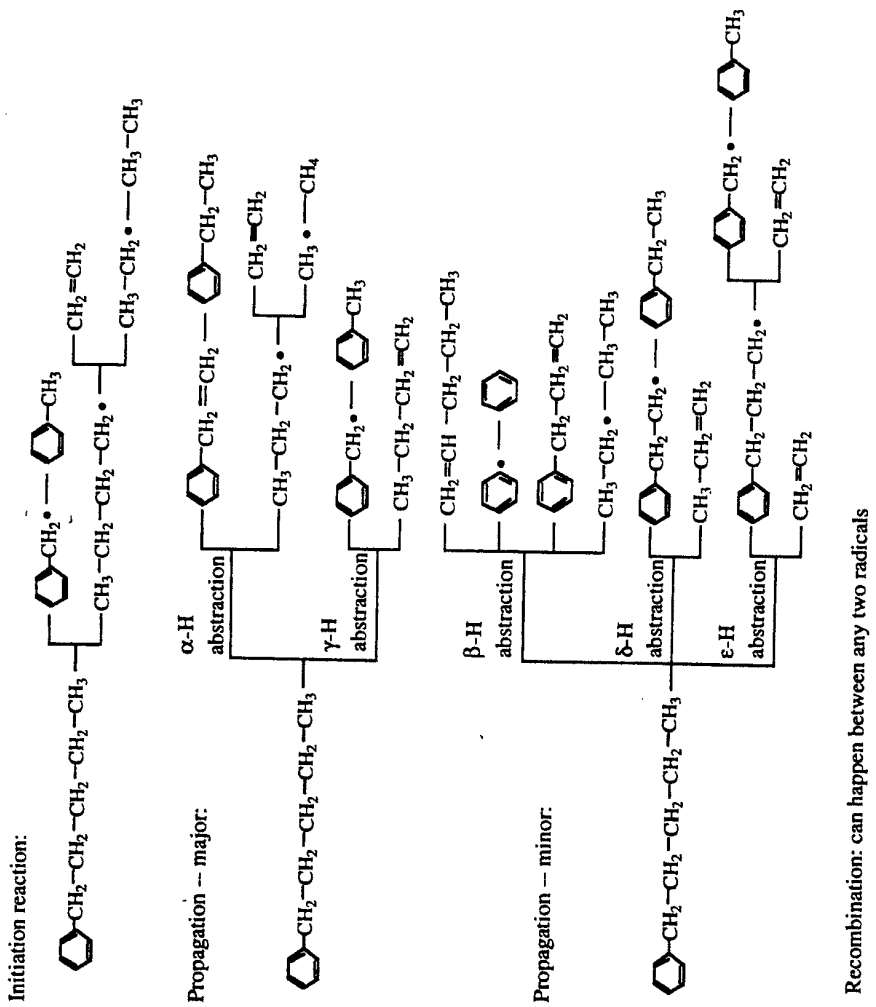

Figure 1.36-1. Possible Pathways to the Formation of Major Products from n-Amylbenzene Pyrolysis

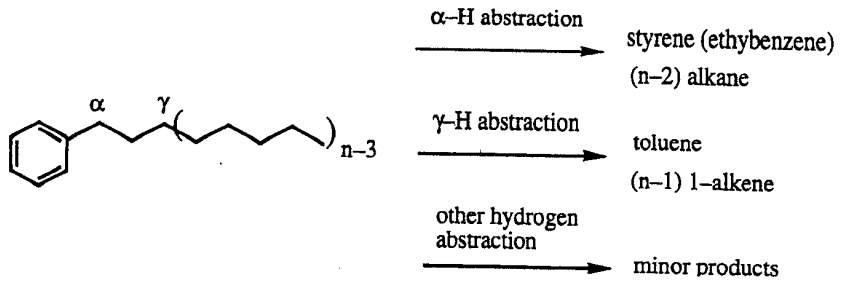

Figure 1.36-2. Possible Major Pathways of Pyrolysis of n-Alkylbenzenes

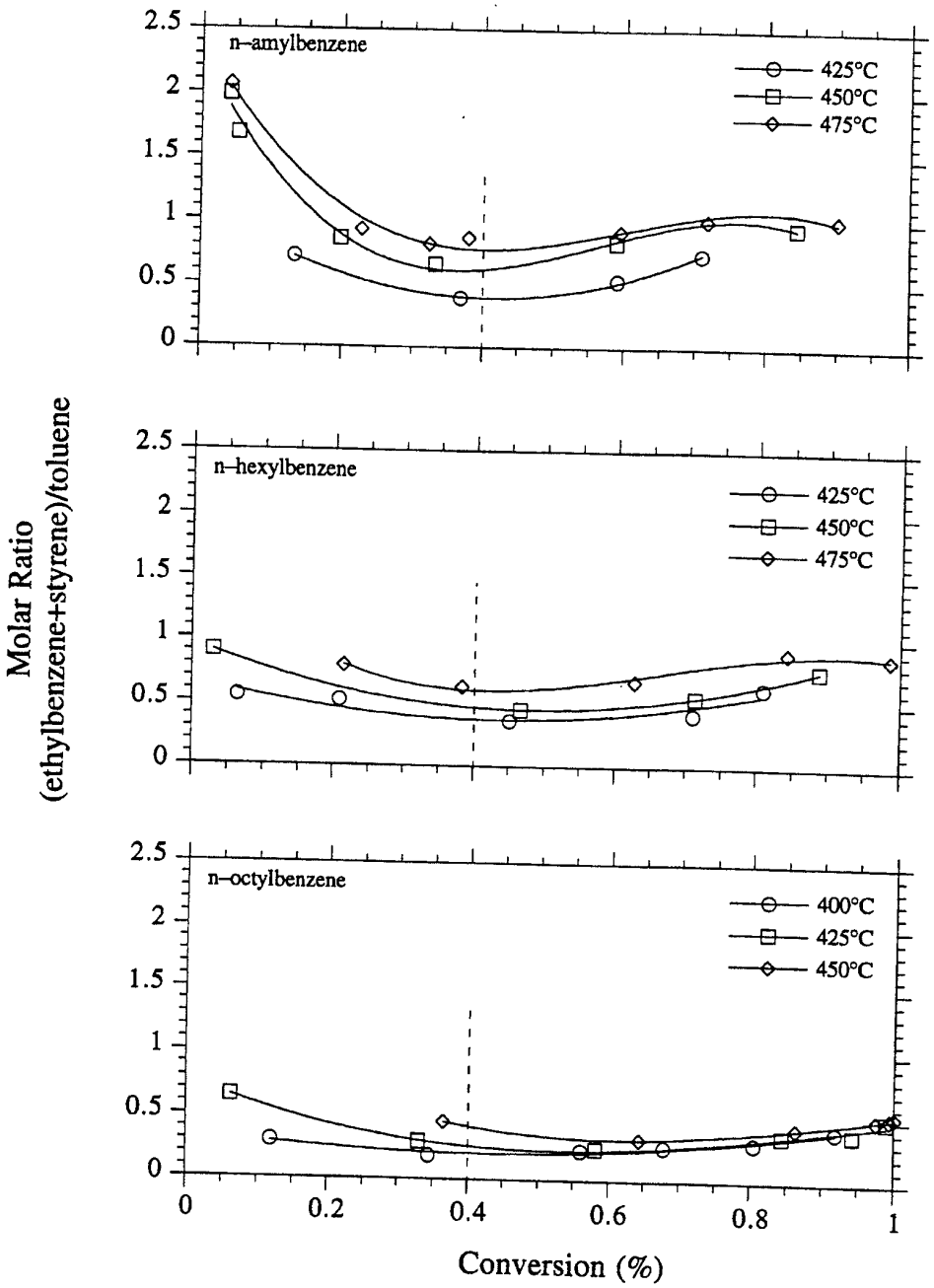

Figure 1.36-3. Comparison of Relative Importance of α- and γ-Hydrogen Abstraction

1.37 Thermal Stability Testing of Napthenic Liquids

This study is explained in detail in *Advanced Thermally Stable Jet Fuels, Technical Progress Report, January – March 1998.*

Introduction

This task included the construction of a flow reactor for studies of jet fuel thermal stability under flowing conditions; use of the flow reactor to examine the thermal stability of various fuel stocks provided by BP Oil Co. and Wright Laboratory individually and in mixtures; and implementation of numerical modeling to interpret the results from the flow reactor studies.

Following construction of the flow reactor and baseline testing, we implemented a numerical model to describe the heat and mass transfer interactions within the flow reactor. We wrote a PC-based boundary layer model in MATLAB and used it to consider the residence time distribution within the reactor tube and variation of exposure to elevated temperature within the flow. Because there were velocity and temperature gradients within the flowing fuel stream, only a fraction of the fuel would be exposed to the most extreme temperature elevations. The model was designed to calculate this fraction and the percent of fuel mass that would likely exceed the stability criteria developed for fuel mixtures and additives under batch reaction conditions. We expected that the analysis would assist us in transitioning from batch reactor studies to flow reactor studies, and in making use of the extensive experience that we have gained thus far in batch systems.

The ultimate goal of the ongoing jet fuel project is to establish a commercial solution to the JP-900 requirement. Our previous research determined that a solution could be found in cyclo-alkane rich fuels, and British Petroleum (BP) was contracted to produce such a fuel from an aromatic petroleum fraction. The approach taken was hydrogenation and dearomatization of a light cycle oil (LCO), as reported in an earlier Technical Progress Report by R. Gregory of BP.[1]

Experimental

The three samples analyzed by GC-MS for characterization were: a light cycle oil; severe hydrotreatment of the LCO at 350°C; and dearomatising (335°C) and further hydrotreatment (320°C) of the HT fraction completed in two successive steps. Approximately 80-90% of the area was investigated, accounting for around 2-300 peaks in each case.

Results and Discussion

The main functional groups present in the samples, which were found from assessing the peaks in the GC-MS traces, primarily correspond with the findings from BP. The LCO was ≈90 mol% aromatic, compared to 80 vol% from the BP data (FIA method). The distribution of mono, di and tri+ aromatics (i.e., benzenes, naphthalenes, and anthracenes or higher, respectively) were in good agreement between the two laboratories. We made a further distinction of bi-phenyls, including indoles, bi-phenyls and fluorenes, which accounted for 13 mol%. The alkanes (saturates) were close—we detected 8 mol% versus BP's 9 vol%, but a large discrepancy was found in the alkanes (olefines) where the findings presented here were only 2 mol%, considerably lower than the 11 vol% published by BP.

The HT fraction displayed around 66 mol% mono aromatics and small amounts of the other aromatic groups, which correspond with BP's findings, although some of our values were higher. The highest discrepancy was observed in the alkane fraction, where BP reported 25 vol%, while we observed only 13 mol%.

For the DA-HT sample, the goal of a highly cycloalkane product with a low aromatic content was obtained, as we found that it contained 61 mol% cycloalkanes compared to 83 vol% at BP. Our observations for both aromatics (all mono) and alkanes (saturates) were in good agreement with those of BP. However, we observed a significant amount of alkenes (olefins) of 17 mol%, compared with 0.3 wt% at BP. This discrepancy can partly be explained by the fact that roughly one-third of the olefins we observed were cyclic. Further, the amount of linear alkanes were more dominant in our studies and about equal in amount with branched alkanes. For the cyclo-alkanes, we differentiated between cyclo-pentanes, cyclo-hexanes and other cyclo-alkanes. The last group included: cyclo-propanes, cyclo-pentanes, cyclo-octanes, spiro-anes, octahydro-indenes and dicyclo-alkyl alkanes. These compounds account for about 16%. Some of these compounds may have been included in the di-cycloparaffins (defined as decalins) in the BP figures, explaining the difference between the amount of decalins we observed (17 mol%) and the di-cycloparaffines at BP (47 wt%). Also the decahydro-anthracenes and larger cyclo-alkane systems concentration was lower in our studies.

In summary, the fuel produced is highly rich in cyclo-alkanes (70-80%) and noncyclo-alkanes (20-30%), indicating that this mixture should have an excellent degree of thermal stability.

---

[1] Schobert, H.H. et al. Advanced Thermally Stable Jet Fuels, Technical Progress Report, January - March 1997. The Pennsylvania State University. U.S DoE, Contract No. DE-FG22-92PC92104. 1997. 49-66.

1.38 Determination of Critical Properties of Jet Fuels

This study is explained in detail in *Advanced Thermally Stable Jet Fuels Technical Progress Report, July–September 1993.*

Introduction

This work was a continuation of our studies related to the exposure of jet fuels to temperatures above the critical temperature with regard to future applications with increased thermal management requirements.[1] At higher temperatures, the fuel decomposes to form detrimental solid deposits. Previous studies have shown that the deposit formation from jet fuels exposed to high-temperature stress has a complex dependence on temperature.[2] In general the deposit formation rate rises with temperature, drops abruptly in a transition region (*e.g.*, 350-425°C), and then increases again with temperature. The sharp drop in deposit formation rates appears to reflect an effect of the transition from the liquid phase to the supercritical phase. Fluids near the critical point exhibit unusual physicochemical properties, such as large partial molar volume, local anisotropy, and high compressibility,[3] which are expected to have a significant influence on the deposit formation in the transition region. The mechanisms of deposit formation from jet fuels under supercritical conditions are not known. In view of the fact that the future jet fuels will encounter supercritical conditions, there is a need to study specifically the effects of supercritical conditions on deposit formation from jet fuels. The critical properties of the jet fuels must be determined to define sub- and supercritical regions before further studies are undertaken.

The are two ways to determine critical properties of substances: experimental measurement and estimation. Suitable experimental methods can produce reliable data, but are rather laborious. Various experimental methods have been developed to determine critical properties of substances ranging from pure compounds to complex mixtures, such as petroleum fractions.[4, 5, 6] In the late 1980s, two novel methods were developed for determining the critical properties of thermally unstable fluids—a rapidly heating sealed tube method and a low residence time flow method.[7] The first measures critical temperature and density; the second determines the critical temperature and pressure. These two methods produce the critical data with high precision for thermally unstable fluids by requiring only a low residence time of the sample in the apparatus before the critical point is reached. For critical temperature measurement of thermally unstable fluids, the results from the flow method seem to be more accurate because the fluids are maintained at their critical temperatures for a short period (e.g., 10-50 seconds), which minimizes thermal decomposition.[8]

Compared to experimental methods, determining the critical properties of fluids using suitable prediction or correlation equations is quite convenient. For complex multicomponent mixtures such as jet fuels, there are no suitable predication equations. Instead, a variety of correlation methods have been developed for estimating critical properties of petroleum fractions. In this work, the critical temperatures of nine jet fuels were measured using a sealed tube method[9, 10] and the critical temperatures and pressures of the fuels were estimated using the methods recommended by the American Petroleum Institute.[11] The measured and estimated critical temperatures were compared to determine the suitability of the estimation method.

Results and Discussion

The apparatus used in this work was constructed by Lyons[12] as an adaptation of the Mogollon apparatus.[13] The apparatus was tested by measuring the critical temperatures of tetralin, *n*-decane, *n*-dodecane, and *n*-tetradecane in comparison to existing, reliable critical data.[14 15] The purities of the samples exceeded 99%.

Some temperature variations occurred along the axial direction of the furnace. In these cases, the thermocouple probe was positioned approximately 3.5 cm away from vapor-liquid meniscus observed just before the critical point was reached. This resulted in a 5°F temperature difference between the two positions, with higher temperature occurring at the position of thermocouple probe. **Table 1.38-1** shows temperature distributions along the axial direction of the furnace. Three tests gave a similar temperature distribution tendency, although different temperature ranges were used. Consequently the observed critical temperature was corrected by subtracting 5°F from the thermometer readout. **Table 1.38-2** shows the comparison between observed critical temperatures and literature values for the four compounds.

The observed critical temperatures of tetralin and *n*-decane did not change with time over 15 minutes and were taken as the true critical temperatures. For *n*-dodecane and *n*-tetradecane, the observed critical temperatures did change with time and the true critical temperatures were determined using the method suggested by Anselme and Teja,[16] except that the critical temperature vs. time curves were extrapolated to zero time for simplicity. **Figure 1.38-1** shows the observed critical temperature vs. time curve for *n*-tetradecane. The results shown in Table 1.38-2 demonstrate that the largest deviation of the measured values from the reported data is 0.32%. This indicated that the apparatus and the extrapolation method were suitable for the purpose of this work.

Table 1.38-3 shows measured and estimated critical temperatures of nine jet fuels. The reproducibility of measurement was satisfactory. The selected value from two runs for each fuel is based on relative reliability, judging from the vapor-liquid meniscus position. Usually sample loading did not deviate from critical loading to a significant degree. The disappearance or reappearance of a meniscus at the critical point occurred near the midpoint of the tube. For two samples of the same fuel, if the meniscus position of one sample was closer to the midpoint of the tube when the critical temperature was measured, then this value was selected as the true critical temperature.

Table 1.38-3 demonstrates that the deviations of the calculated critical temperatures from the measured values were within 10°F for petroleum-derived jet fuels, with the exception of JP-8P, which showed a deviation of 18°F. This agreement between the measured and estimated values is quite satisfactory for complex mixtures such as jet fuels. For three coal-derived jet fuels, however, the calculated critical temperatures were 20-30°F lower than the measured values; this can likely be attributed to the composition of coal-derived jet fuels. The Roess equation was set up on the basis of the measured critical temperatures of many petroleum fractions that are composed primarily of paraffinic compounds. For coal-derived jet fuels, the main components are monocyclic and bicyclic alkanes and some hydroaromatic compounds; in these cases the Roess equation may give larger deviations.

Table 1.38-1. Temperature Distributions along Axial Direction of the Furnace

Distance from Thermocouple Probe (cm)	Temperature (°F)		
	Test 1	Test 2	Test 3
0	776	753	725
1	775	752	724
2	773	750	722
3	771	748	721
4	770	747	720

Table 1.38-2. Critical-Temperature Comparison of Four Compounds

Compound	Measured Tc/Fb		Literature Value Tc/F
	Sample 1	Sample 2	
Tetralin	837	837	836.6[17]
n-Decane	654	654	652.2[15]
n-Dodecane	726	726	725.5[15]
n-Tetradecane	784	784	786.5[15]

Table 1.38-3. Measured and Estimated Critical Temperatures of Jet Fuels

Fuel	Measured Tc/F			Estimated Tc/F
	Sample 1	Sample 2	Selected	
JP-8P	741	740	740	722
JP-8P2	757	757	757	750
Jet A	752	751	752	749
Jet A-1	732	732	732	731
JP-7	761	761	761	751
JPTS	719	719	719	710
JP-8C	762	761	761	738
JP-8CA	754	753	753	725
JP-8CB	773	774	773	752

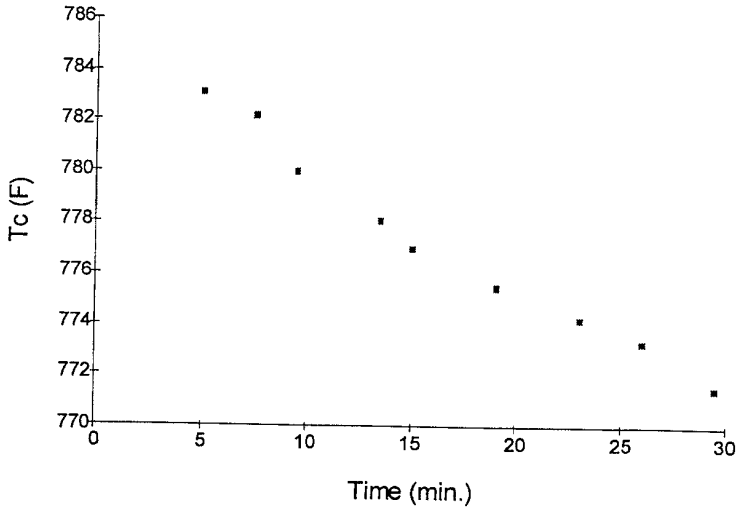

Figure 1.38-1. Change of Observed Critical Temperature with Time for *n*-Tetradecane

---

[1] "Advanced Fuel Composition and Use." *FY 93 New Initiative, Joint AFOSR and WPAFB Announcement, Summer 1991.* 1991.

[2] Taylor, W. F. *Ind. Eng. Chem. Prod. Res. Develop.* 1974. 13, 133.

[3] Brennecke, J. F. *Supercritical Fluid Engineering Science: Fundamentals and Applications.* ACS Symposium Series 514. ACS: Washington, DC. 1993. 201.

[4] Roess, E. E. *J. Inst. Petro. Tech.* 1936. 22, 665.

[5] Kobe, K. A. and R. E. Lynn. *Chem. Rev.* 1953. 52, 117.

[6] Hicks, C. P. and C. L. Young. *Chem. Rev.* 1975. 75, 119.

[7] Teja, A. S., M. Gude, and D. J. Rosenthal. *Fluid Phase Equil.* 1989. 52, 193.

[8] Rosenthal, D. J. and A. S. Teja. *AIChE J.* 1989. 35. 1829.

[9] Hicks, C. P. and C. L. Young. *Chem. Rev.* 1975. 75, 119.

[10] Mogollon, E., W. B. Kay, and A. S. Teja. *Ind. Eng. Chem. Fundam.* 1982. 21, 173.

[11] *Technical Data Book-Petroleum Refining.* 4th Edition. American Petroleum Institute, Division of Refining: Washington, DC. 1987.

[12] Lyons, R. L. *M.S. Thesis.* The Pennsylvania State University: University Park, PA. 1985.

[13] Mogollon, E. *M.S. Thesis.* The Ohio State University: Columbus, Ohio. 1969.

[14] Daubert, T. E. and R. P. Danner. *Physical and Thermodynamic Properties of Pure Chemicals.* AIChE. Design Institute for Physical Property Data. 1992.

[15] Teja, A. S. et al. *Fluid Phase Equil.* 1990. 56, 153.

[16] Anselme, M. and A. S. Teja. Fluid Phase Equil. 1988. 40, 127.

[17] Daubert, T. E. and R. P. Danner. *Physical and Thermodynamic Properties of Pure Chemicals.* AIChE. Design Institute for Physical Property Data. 1992.

1.39 Detection of Polycyclic Aromatic Hydrocarbons Present in Highly Stressed Jet Fuel by High Performance Liquid Chromatography (HPLC) Using Normal-Phase Separation with Diode Array Detection

This study is explained in detail in Advanced Thermally Stable Jet Fuels Technical Progress Report, April–June 1994.

Introduction

The future high-Mach aircraft will require advanced jet fuel with high stability in rigorous thermal environments. To test a fuel's thermal stability, jet fuels are typically stressed at severe temperatures in closed reactor systems or flow reactors, and their subsequent complex liquids are analyzed using either gas chromatography (GC), gas chromatography/mass spectrometry (GC/MS), or 1H and ^{13}C liquid NMR to reveal structural changes in the fuel.[1,2] These analytical techniques can provide valuable information on the relative stability of a given fuel and chemical transformations that occur within that fuel. However, the build-up of large polycyclic aromatic hydrocarbons (PAHs) in thermally stressed jet fuel leads to problems pertaining to GC and GC/MS analysis. As a result, a percentage of highly stressed jet fuel, in the form of large PAHs, can go undetected using GC analysis—a percentage that could trigger the onset of solid deposit formations that are detrimental to the fuel's overall performance.

Since its introduction as an analytical method in the late 1960s and early 1970, high performance liquid chromatography (HPLC) has been widely used in environmental studies, particularly for analyzing PAHs.[3,4] Reverse-phase HPLC on chemically bonded C18 has become the method of choice for the separation of PAHs. However, HPLC has limitations. Analysis is complicated by the fact that elaborate sample preparations of complex fuel-related materials are not usually miscible in acetonitrile, the solvent of choice for reverse-phase HPLC separations of PAHs. And normal-phase and reverse-phase HPLC have depended on either fluorescence detection or monochromatic UV absorbance detection—methods which are too selective and overlook many compounds as a result of the varying optimal wavelengths for the different compounds.

More recent developments—including a full spectrum UV absorbance detector (i.e., a diode array detector or DAD)—have enabled full spectrum detection of HPLC eluates. This technique, which provides UV spectra of separated fractions as a function of time, can identify by spectral comparisons, the molecular components of the eluates, including the isomers of PAHs. When used with reverse-phase HPLC, DAD was able to distinguish between phenanthrene and anthracene, pyrene and fluoranthene, and their substituted homologues.[5] Reverse-phase HPLC, however, is not applicable to more complex fuel mixtures such as highly stressed jet fuels, because these are only slightly soluble in polar solvents required for reverse-phase HPLC. The development of "charge-transfer" stationary phases for separation of π-electron rich PAHs allows for separation of PAHs and their isomers in the normal-phase using solvents that are generally miscible with complex fossil fuel systems.[6]

The objective with this study was to demonstrate a more sensitive method for detectiing the build-up of large ring PAHs that can lead to the onset of solid deposit formations inherent to severe stressing of jet fuel. We used normal-phase separation of PAHs and their alkylated derivatives, present in highly stressed jet fuel, using a tetrachlorophthalimidopropyl (TCCP)-

modified silica column (PAH-2).[7] The column, combined with a UV-diode array detector allowed for more sensitive detection of large PAHs (compared to normal GC and GC/MS detectors) and efficient separation of multi-ring PAHs and their isomers without elaborate sample preparations or on-line coupling of a reverse-phase HPLC system.

Results and Discussion

The resulting chromatogram at maximum UV absorbance for a standard mix of PAHs is shown in **Figure 1.39-1**. Co-elution of several PAHs is obvious, but the chromatogram also demonstrates the use of the TCPP-modified silica phase in separating PAHs. The use of a maximum absorbance plot (maxiplot) is ideal for ensuring that the peak intensities in the 1-D plot are at maximum UV absorbance and, therefore, at maximum intensity.

Knowing that highly stressed jet fuel contains numerous amounts of polynuclear aromatic hydrocarbons and that the PAH-2 column successfully separated PAHs in a known standard, we were optimistic that it could be used for stressed jet fuel samples. **Figure 1.39-2** shows a maxplot of the three samples analyzed by 2D HPLC (0 hrs, 6 hrs, and 12 hrs). These chromatograms show that as the stressing time at 450°C increased, the fuel was being degraded and an increase of PAHs was observed. **Figure 1.39-3**, cut across the UV absorbance region, identifies the number of fused aromatic rings present in Jet A stressed at 450°C for 12 hours, and a general map of where these ring numbers would fall in the chromatogram.

Using the UV-diode array detector, contour plots and 3-D plots can be obtained for each sample, significantly enhancing the ability of the user to detect and identify components that may not be well separated at one specific wavelength. This provides additional perspective and aids in identifying compounds that might not be detected otherwise. For example, **Figures 1.39-4** and **1.39-5** show two different wavelength cuts across the UV absorbance range which tend to highlight specific regions of the chromatogram. The 335 nm cut (Figure 1.39-4) highlights pyrene derivatives and their alkylated isomers and minimizes any interferences from other compounds. After 6 hours, a significant amount of pyrene and alkylated pyrenes is present and their relative concentrations change very little between 6 and 12 hours. The 375 nm cut (Figure 1.39-5) highlights the increase in the concentration of PAHs greater than six rings; PAH build-ups that would not have been detected by normal GC analyses. There was an overall increase in the relative concentrations of large fused ring PAHs from time 0, where there were no large PAH systems, to 12 hours, where there was a complex "hump" of unresolved material representing large PAH systems.

Conclusion

In general, as the time of stressing grew, so did the complexity of the chromatograms. This indicated that a build-up of large PAHs was occurring, as expected, and solid deposit formation was likely increasing. These results could have been determined by GC and GC/MS analyses or by physical observation. However, GC analyses would not have detected the ≥6-ring systems, which were identified by the 2-D HPLC method. Although the concentrations of these larger ring systems is low in comparison to the 1- to 3-ring PAHs (Figure 1.39-3), their significance to the formation of solid deposits during the stressing reactions may be crucial in the determination of a fuel's ability to remain stable at high temperatures.

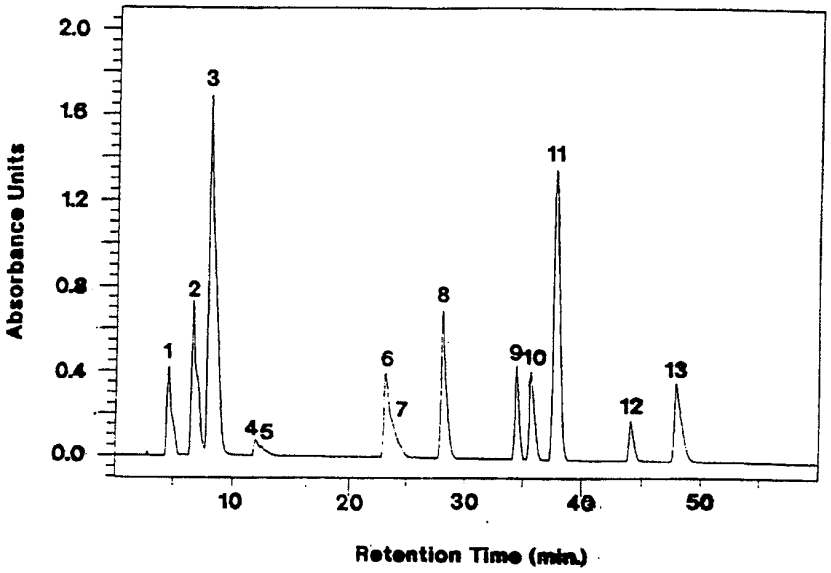

1. Naphthalene
2. Acenaphthalene and Fluorene
3. Acenaphthylene
4. Anthracene
5. Phenanthrene
6. Fluoranthene
7. Pyrene
8. Chrysene and Benzo [a] anthracene
9. Benzo [b] fluoranthene
10. Benzo [k] fluoranthene
11. Dibenzo [a, h] anthracene and Benzo [a] pyrene
12. Indeno [1, 2, 3-cd] pyrene
13. Benzo [g, h, i] perylene

Figure 1.39-1. Chromatogram at Maximum UV Absorbance for a Standard Mixture of PAHs

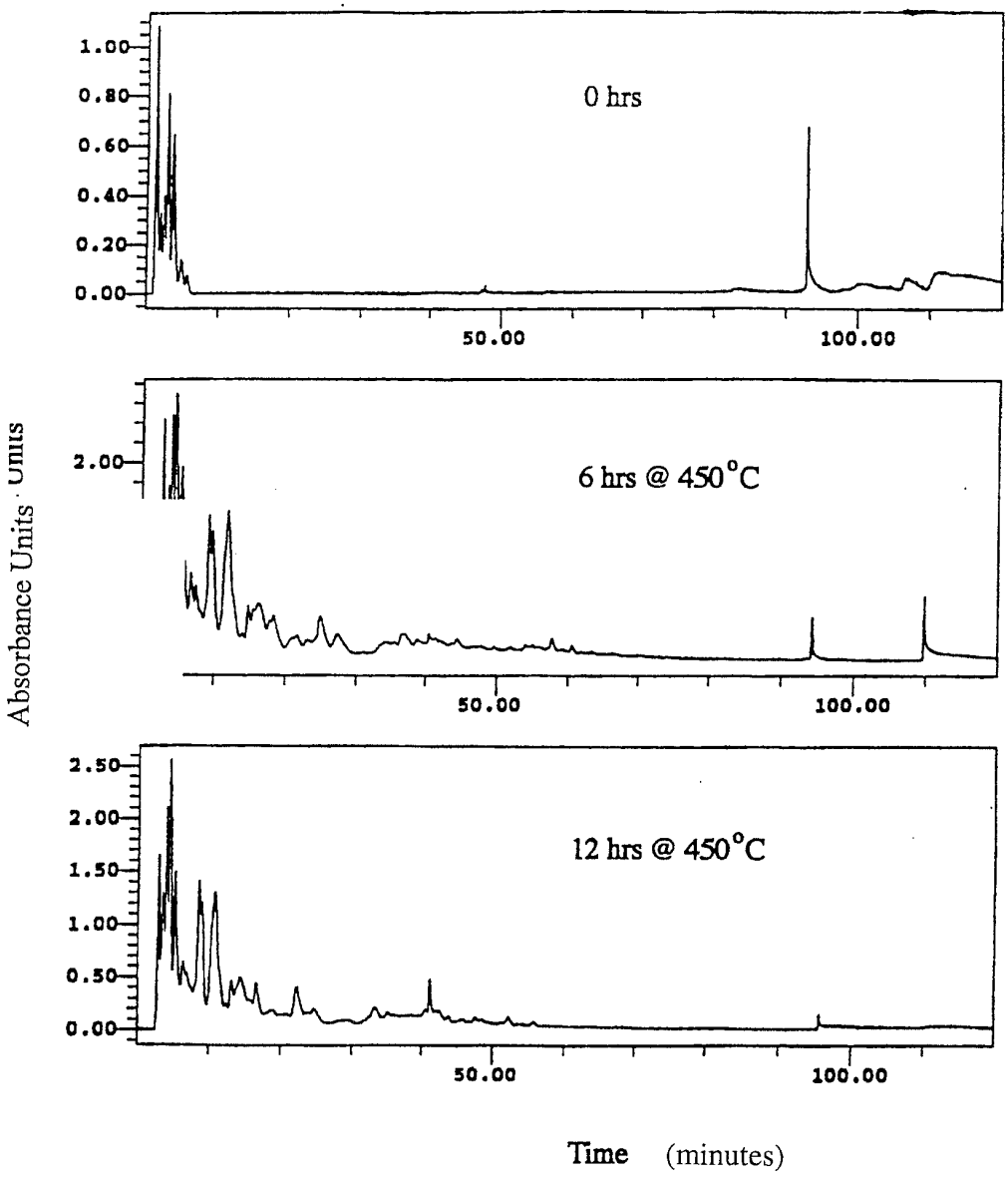

Figure 1.39-2. Max-plots from 2-D HPLC on Jet A Stressed at 450°C for Alotted Times

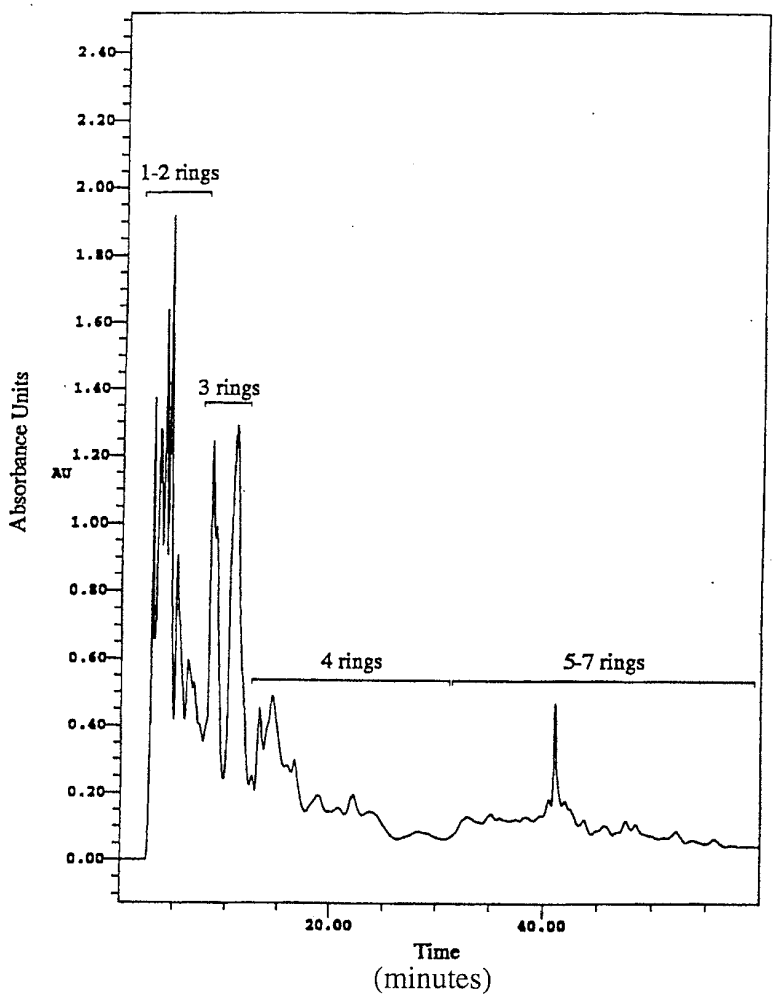

Figure 1.39-3. 254 nm Cut from 2-D HPLC on Jet A Stressed at 450°C for 12 Hours.
(Labels show the number of fused rings.)

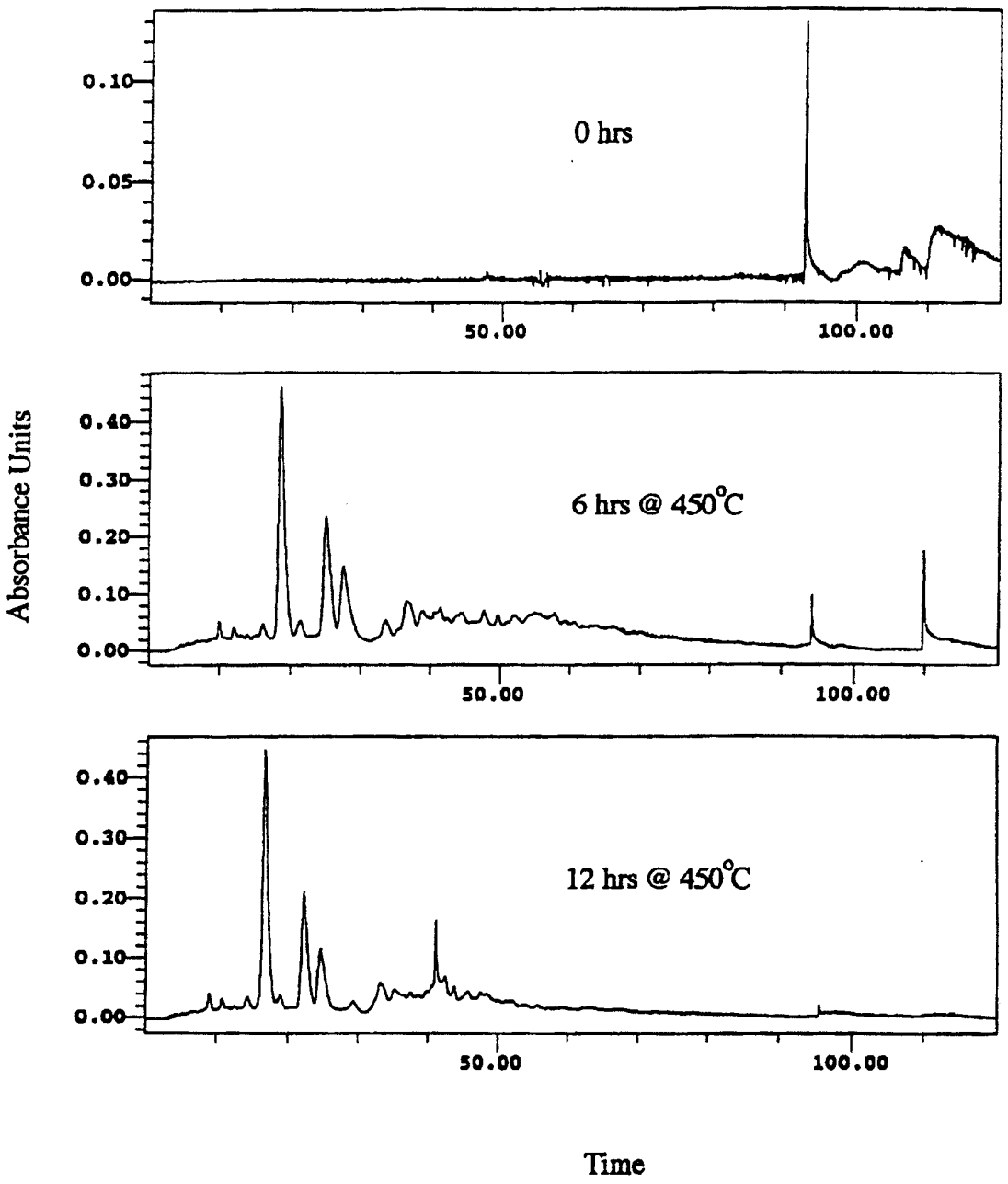

Figure 1.39-4. 335 nm Cut from 2-D HPLC on Jet A Stressed at 450°C

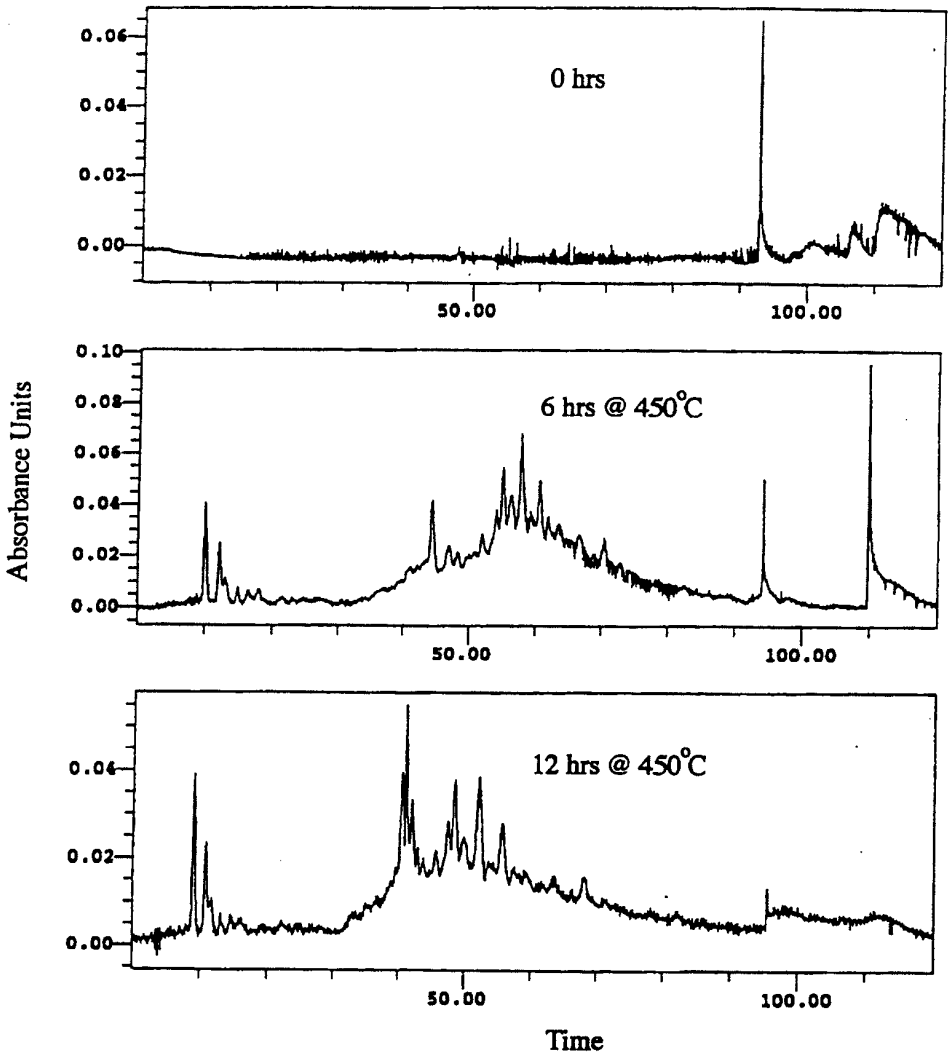

Figure 1.39-5. 375 nm Cut from 2-D HPLC on Jet A Stressed at 450°C

[1] Song, C. et al. *Energy & Fuels.* 1993. 7. 234-243.

[2] McKinney, D. E., J. M. Bortiatynski, and P. G. Hatcher. Energy & Fuels. 1993. 7. 578-581.

[3] Wise, S. A., L. C. Sander, and W. E. May. *J. Chromatogr.* 1993. 642. 329.

[4] Fetzer, J. C. *Chemical Analysis of Polycyclic Aromatic Compounds.* New York: Wiley. 1989. 59.

[5] Liu, Y., S. Eser, and P. G. Hatcher. *Prepr. Pap. – Am. Chem. Soc. Div. Fuel Chem.* 1992. 37(3). 1227.

[6] Holstein, W. *Chromatographia.* 1981. 14. 468-477.
Grizzle, P. L. and J. S. Thomson. *Anal. Letters.* 1987. 20 (8). 1171-1192.

[7] Holstein, W. *Chromatographia.* 1981. 14. 468-477.

1.40 Temperature-Programmed Retention Indices for GC and GC-MS Analysis of Coal- and Petroleum-Derived Jet Fuels

This study is explained in detail in *Advanced Thermally Stable Jet Fuels Technical Progress Report, April-June 1994.*

Introduction

Retention indices are very useful in identifying components in jet fuels by gas chromatography (GC), even when GC is coupled with mass spectrometry (GC-MS). In this work, temperature-programmed retention indices of more than 150 compounds were determined on an intermediately polar capillary column coated with 50% phenyl-50% methyl polysiloxane and a slightly polar column coated with 5% phenyl-95% methyl polysiloxane at three heating rates (2°, 4°, and 6°C/min, from 40° to 310°C).

Results and Discussion

Table 1.40-1 presents the retention indices determined using two columns at three heating rates (2°, 4°, and 6°/min) for 154 compounds generally found in coal- and petroleum-derived jet fuels.

1. Temperature Dependence. Several characteristics are revealed by Table 1.40-1:

a) The small temperature dependence of compounds that are analogous to the reference standards, such as branched alkanes and 1-alkenes, reflects one of the excellent characteristics of the retention index system. **Table 1.40-2** provides the experimental results of retention indices and final elution temperatures for 1-alkenes (ranging from 1-hexene to 1-octadecene) at the three heating rates on the Rtx-50 column. The difference in index values at different elution temperatures is less than ±1 index unit, which is within the experimental error. These data demonstrate the temperature-independent nature of the indices for these compounds, even for a 30°C range.

b) In addition, the other compounds show measurable linear temperature dependence, as shown by **Figure 1.40-1**, which presents the retention index of several representative compounds as a function of elution temperature. The numerical results of the linear temperature dependence for cycloalkanes and benzenes are presented in **Table 1.40-3** for both Rtx-50 and DB-5 columns. In the same manner, **Table 1.40-4** presents the numerical results of the linear temperature dependence for aromatics and NSO compounds (those compounds containing N, S, and O). Examining the data on Rtx-50 reveals that, in general, alkylated cyclohexanes and benzenes displayed a ΔR.I./ΔT of approximately 0.33±0.05 index units/°C, while benzenes with multi-substitution (such as tetramethyl-) and long side-chained (decyl- and dodecyl-) exhibit slightly higher values. Compared with alkylated cyclohexanes and benzenes, the indices for compounds with a two-ring structure exhibit a higher temperature dependence. Multi-ring aromatics exhibit the largest temperature dependence of the retention index among the studied compounds. Four-ring aromatics all display significant temperature dependence judging from the large values of ΔR.I./ΔT (>2.0). Chrysene shows a value as large as 2.88.

c) An important consequence of the observed difference in temperature dependence among the compounds is that compounds that co-eluted at one temperature may be separated at some other temperature. This indicates that co-elution problems that occur at a given heating rate could be eliminated by using another heating rate.

Although the retention indices in Table 1.40-1 were measured under linear temperature programming without an initial isothermal holding period, the results may also be applied to GC analysis with a short initial holding time. **Table 1.40-5** presents the retention times and retention indices measured with 5 minutes of initial isothermal holding time at 40°C, as well as those without initial holding time for 60 representative compounds. We found that adding a 5-minute holding time at low temperature (40°C) has only a small effect on retention indices, although the retention times may differ by as much as 5 minutes. Table 1.40-5 shows that adding an initial holding time only serves to delay the elution of heavier compounds which have retention indices greater than 1400 by as much time as was added (e.g., 5 minutes in this study). For the 154 compounds studied, the retention index was lowered, on average, by about 1 index unit when 5 minutes of holding time was added at the beginning temperature; the retention index decrement for heavier compounds is, in general, negligible. Therefore, the temperature programmed retention indices in Table 1.40-1 may also be applied, with minor adjustment, to the analysis that incorporates a short initial holding time.

2. Column Polarity Dependence. Retention indices exhibit significant dependence on column polarity, as shown in Table 1.40-1. This polarity is characterized by the following:

a) The retention indices of all of the compounds studied decreased as the column polarity decreased (from Rtx-50 to DB-5). Similar to the temperature dependence, the decrement of the retention indices depended on the structure of the compounds. Compared to other compounds, 1-alkenes, which are analogous to the reference standard (*n*-alkanes, in this work), display the smallest polarity dependence. Alkylcyclohexanes (from methylcyclohexane to *n*-decylcyclohexane) also show a small polarity dependence. On the other hand, the retention indices of alkylbenzenes, aromatics, and *N*-, S-, and O-containing compounds are highly dependent on the column polarity. Multi-ring aromatics exhibit the largest polarity dependence of the retention index among the studied compounds. Overall, the behavior of the polarity dependence of retention index can be summarized by the fact that the retention of polar compounds decreases, but that of non-polar compounds (such as *n*-alkanes) increases, when the polarity of stationary phase decreases.

b) The change or shift of compound elution order on different columns can be observed because different compounds display different degrees of retention index changes with column polarity. Based on the knowledge of the shift of compound elution order, compound identification can be improved using columns of different polarity. Another application of the knowledge on the retention indices is that they can facilitate the choice of column phase to reduce or even eliminate co-elution within complex samples.

c) For the two capillary columns studied, in general, the values of ΔR.I./ΔT are larger for Rtx-50 than for DB-5 (i.e., almost all of the compounds studied display higher

temperature sensitivity on the more polar column (Rtx-50) than on the less polar column (DB-5), as can be seen from Tables 1.40-3 and 1.40-4.

3. Characterization of JP-8 Jet Fuels. Retention indices generated in this work can be used to identify compounds in complex mixtures such as jet fuels. In many cases, the unknown compounds may be identified by calculating their retention indices and comparing them with the standards shown in Table 1.40-1. Indices that are within ±2 index units for a given heating rate are considered acceptable matches.

The GC-MS analysis of the whole jet fuel also reveals that many compounds are present in trace amounts or co-eluted with other compounds, making them difficult to identify when analyzing whole fuels. Another approach used in this work is to separate the jet fuels into chemically similar compound classes by liquid column chromatographic separation, which also serves to concentrate the compounds present in whole fuels in very low concentrations and to eliminate or reduce the co-elution of different compounds from the capillary GC column, followed by the GC-MS analysis of the chromatographic fractions. The fuels were separated into several fractions using a neutral alumina gel column and a series of elution solvents.

The results indicate that the coal-derived JP-8C fuel is significantly different from petroleum-based JP-8P in composition. The major compounds in JP-8P saturates are straight-chain and branched alkanes ranging from C_7 to C_{17}. However, the JP-8C saturates consist mainly of monocyclic, bicyclic, and tricyclic alkanes, together with some long-chain alkanes. The aromatics in JP-8P are dominated by alkylbenzenes and alkylnaphthalenes, whereas the JP-8C aromatics are rich in hydroaromatic compounds such as tetralin, alkyltetralins, indans, cyclohexylbenzene, and some partiallly hydrogenated three-ring compounds, together with some alkylbenzenes and alkylnaphthalenes. These results show that jet fuels derived from different sources may have distinctly different molecular composition.

Table 1.40-6 displays the quantitative compositions of the JP-8P and JP-8C fuels based on the major hydrocarbon types found in fuels (e.g., alkanes, cyclohexanes, benzenes, decalinis, tetralins, and indans) and others (e.g., alkylnaphthalenes). The compounds were quantified using the area percent of GC integration results coupled with the comounds' response factors determined from known amounts of standard chemicals. In summary, JP-8P is a paraffinic fuel derived from petroleum with long-chain alkanes as the dominant constituents (61%) and small amounts of cyclohexanes (14%), benzenes (15%), and hydroaromatic compounds. Conversely, the coal-derived JP-8C is composed mainly of monocyclic and bicyclic cyclohexanes (~40%), decalin (15%), tetralin (8%), indans (6%) and alkylbenzenes (~11%). The alkanes only account for about 10% of JP-8C. The qualitative and quantitative information is useful in evaluating and explaining the thermal stability of fuels, which is significantly affected by their chemical composition.[1, 2]

Conclusion

The retention indices of aliphatic compounds are nearly constant at different heating rates, while the retention indices of polycyclic aromatic compounds exhibit relatively strong temperature dependence. The use of a short isothermal holding (5 min) prior to the programmed heat-up does not cause a significant difference in the retention indices. Column polarity can affect retention behavior significantly, depending on the compound type. A relation also exists

between the temperature dependence (or column polarity dependence) of retention indices and the compound type. Almost all of the compounds studied displayed higher temperature sensitivity on the more polar column (Rtx-50) than on the less polar column (DB-5) (i.e., the values of ΔR.I./ΔT are larger for Rtx-50 than for DB-5). Retention indices and their sensitivity to temperature decrease with decreasing column polarity.

Table 1.40-1. Retention Indices of Hydrocarbons Determined for Intermediately Polar (Rtx-50) and Slightly Polar (DB-5) Columns at Three Heating Rates (continued)

Compounds	Molecular Ion	Base Peak	R.I. on Rtx-50			R.I. on DB-5		
			2°C/min	4°C/min	6°C/min	2°C/min	4°C/min	6°C/min
n-Pentane	72	43	500	500	500	500	500	500
n-Hexane	86	43	600	600	600	600	600	600
1-Hexene	84	56	606.4	607.0	607.7	588.2	587.9	587.9
n-Heptane	100	43	700	700	700	700	700	700
Cyclohexane	84	56	705.6	706.3	706.0	655.4	656.2	657.6
1-Heptene	98	56	708.3	708.4	709.5	688.0	689.0	689.4
Cyclohexene	82	67	736.1	740.0	739.3	677.1	676.7	678.8
Methylcyclohexane	98	83	748.1	749.5	752.4	718.3	720.0	720.3
Benzene	78	78	765.7	767.4	769.0	654.2	654.8	656.1
n-Octane	114	43	800	800	800	800	800	800
trans-1,4-Dimethylcyclohexane	112	97	801.8	802.3	803.5	775.6	776.7	777.3
cis-1,3-Dimethylcyclohexane	112	97	801.8	802.3	803.5	772.8	774.7	776.6
1-Octene	112	55	808.2	809.2	809.7	788.3	789.3	789.1
trans-1,2-Dimethylcyclohexane	112	97	820.9	822.4	825.0	796.7	798.0	798.4
1-Methylcyclohexene	96	81	824.1	827.0	829.2	763.9	765.3	766.4
cis-1,4-Dimethylcyclohexane	112	97	828.6	830.5	832.6	804.7	805.3	805.7
trans-1,3-Dimethylcyclohexane	112	97	830.9	832.2	835.4	804.1	805.3	806.2
cis-1,2-Dimethylcyclohexane	112	55	859.1	862.6	866.7	823.1	824.7	827.3
Ethylcyclohexane	112	83	862.3	865.5	867.4	826.9	829.1	830.9
Toluene	92	91	870.5	873.6	875.7	758.9	761.3	761.7
n-Nonane	128	43	900	900	900	900	900	900
Pyridine	79	79	908.9	910.3	913.4	735.6	736.7	739.1
1-Nonene	126	56	909.1	909.5	909.9	888.9	889.5	890.2
n-Propylcyclohexane	126	83	956.9	960.8	963.4	924.2	927.1	929.1
Ethylbenzene	106	91	968.1	971.5	975.2	853.2	856.3	857.2
1,4-Dimethylbenzene (*p*-Xylene)	106	91	972.3	975.7	979.2	861.7	864.4	866.5
1,3-Dimethylbenzene (*m*-Xylene)	106	91	974.2	977.9	981.2	861.7	864.4	866.5
n-Decane	142	43	1000	1000	1000	1000	1000	1000
1,2-Dimethylbenzene (*o*-Xylene)	106	91	1009.2	1012.5	1015.5	888.0	889.9	891.2
1-Decene	140	56	1010.3	1011.0	1011.3	989.2	989.5	990.7
trans-Octahydro-1H-indene	124	67	1011.6	1015.9	1018.8	947.7	952.0	955.3
tert-Butylcyclohexane	140	56	1015.1	1019.3	1022.6	978.1	982.2	985.2
Isopropylbenzene (cumene)	120	105	1028.2	1032.1	1034.7	919.4	922.2	923.6
cis-Octahydro-1H-indene	124	67	1053.0	1059.9	1063.2	981.0	985.8	989.5
n-Propylbenzene	120	91	1058.0	1063.0	1066.1	946.9	950.5	952.3
n-Butylcyclohexane	140	83	1059.5	1064.2	1066.5	1026.6	1030.2	1031.6
1-Ethyl-3-methylbenzene	120	105	1068.7	1073.1	1075.7	955.0	958.5	960.8
1-Ethyl-4-methylbenzene	120	105	1069.8	1074.0	1076.6	956.3	960.0	962.4
1,3,5-Trimethylbenzene (Mesitylene)	120	105	1074.4	1079.2	1081.6	961.5	964.9	967.1
tert-Butylbenzene	134	119	1097.6	1102.3	1104.5	987.1	990.5	992.0
4,5,6,7-Tetrahydroindan	122	79	1097.8	1103.7	1106.9	1008.6	1011.4	1014.8
1-Ethyl-2-methylbenzene	120	105	1098.2	1103.1	1105.3	973.3	977.2	979.7
n-Undecane	156	57	1100	1100	1100	1100	1100	1100
1,2,4-Trimethylbenzene	120	105	1106.8	1111.9	1114.6	987.5	991.1	992.8
1-Undecene	154	41	1110.6	1111.0	1111.0	1090.9	1091.4	1091.4
sec-Butylbenzene	134	105	1112.9	1117.6	1120.3	1006.4	1008.9	1011.7
trans-Decalin	138	138	1114.7	1122.4	1127.2	1045.7	1051.8	1055.9
1,1'-Bicyclopentyl	138	68	1138.6	1145.9	1151.2	1071.8	1077.6	1080.9
1,2,3-Trimethylbenzene	120	105	1147.6	1155.0	1158.9	1016.0	1019.9	1022.7
Phenylethylether	122	94	1150.0	1154.1	1156.9	988.8	991.1	992.4
n-Butylbenzene	134	91	1163.2	1168.6	1171.1	1050.1	1053.7	1055.9
n-Pentylcyclohexane	154	83	1163.7	1169.4	1172.0	1130.2	1134.7	1136.0
cis-Decalin	138	67	1174.6	1184.4	1190.2	1089.5	1096.1	1100.4
Indan	118	117	1180.4	1188.7	1193.5	1027.4	1032.4	1035.5
n-Dodecane	170	57	1200	1200	1200	1200	1200	1200
1-Dodecene	168	55	1211.6	1212.4	1211.9	1191.3	1191.3	1191.3
2-Methylindan	132	117	1212.8	1220.8	1225.8	1074.3	1079.5	1082.0
1-Methylindan	132	117	1222.7	1231.2	1236.5	1079.3	1084.8	1087.1
1,2,4,5-Tetramethylbenzene	134	119	1235.1	1242.4	1247.5	1109.7	1114.1	1115.8
n-Hexylcyclohexane	168	83	1269.0	1274.4	1276.6	1233.9	1237.7	1239.5
1,4-Diisopropylbenzene	162	147	1279.9	1285.1	1288.1	1170.1	1173.4	1174.7
5-Methylindan	132	117	1282.5	1292.7	1298.4	1131.1	1137.1	1139.9
1,2,3,4-Tetramethylbenzene	134	119	1286.4	1296.3	1302.6	1144.2	1149.9	1153.8
2,6-Dimethylphenol	122	107	1297.6	1305.3	1310.7	1102.3	1104.6	1105.5
n-Tridecane	184	57	1300	1300	1300	1300	1300	1300
4-Methylindan	132	117	1301.2	1312.0	1318.8	1141.6	1147.7	1151.4
1-Tridecene	182	55	1311.8	1312.0	1312.4	1291.5	1291.3	1292.2
Tetralin	132	104	1324.1	1336.0	1343.6	1151.7	1158.5	1162.5
1,3,5-Triethylbenzene	162	147	1338.5	1343.6	1346.2	1219.6	1222.3	1224.3
1,2-Dihydronaphthalene	130	130	1345.7	1358.8	1366.2			
n-Hexylbenzene	162	91	1370.1	1376.3	1379.9	1254.6	1258.4	1260.9
Bicyclohexyl	166	82	1377.5	1390.4	1397.4	1293.1	1301.5	1307.8
Naphthalene	128	128	1386.8	1401.2	1410.9	1171.5	1179.7	1183.4
2,4,6-Trimethylphenol	136	121	1397.4	1406.7	1412.2	1199.1	1202.5	1204.1
n-Tetradecane	198	57	1400	1400	1400	1400	1400	1400
1-Tetradecene	196	55	1412.5	1412.8	1412.7	1391.7	1391.4	1392.2
Benzothiophene	134	134	1415.7	1432.0	1442.5	1180.5	1188.3	1192.9
2,3-Dihydroindole	119	118	1455.5	1469.2	1479.2	1195.8	1202.2	1206.6
Cyclohexylbenzene	160	104	1475.5	1489.0	1497.7	1308.9	1317.7	1322.9

Table 1.40-1. (cont'd) Retention Indices of Hydrocarbons Determined for Intermediately Polar (Rtx-50) and Slightly Polar (DB-5) Columns at Three Heating Rates

Compounds	Molecular Ion	Base Peak	R.I. on Rtx-50			R.I. on DB-5		
			2°C/min	4°C/min	6°C/min	2°C/min	4°C/min	6°C/min
1-Indanol	134	133	1476.6	1489.0	1496.8	1224.7	1229.9	1232.9
n-Octylcyclohexane	196	83	1480.1	1485.7	1489.6	1442.4	1447.5	1449.1
Quinoline	129	129	1493.6	1510.6	1521.6	1224.7	1233.0	1237.4
n-Pentadecane	212	57	1500	1500	1500	1500	1500	1500
2-Methylnaphthalene	142	142	1501.0	1517.3	1528.6	1281.5	1290.5	1296.3
1-Pentadecene	210	55	1512.7	1513.1	1513.1	1492.4	1492.5	1492.3
1-Methylnaphthalene	142	142	1530.2	1548.7	1559.6	1297.1	1306.8	1313.4
Dodecahydrofluorene	178	97	1556.9	1576.9	1588.7			
8-Methylquinoline	143	143	1562.7	1580.1	1591.1	1304.5	1313.9	1319.5
1,2-Dicyclohexylethane	194	83	1568.2	1582.1	1589.2	1486.9	1496.3	1501.0
5,6,7,8-Tetrahydro-3-methylquinoline	147	146	1571.5	1586.5	1595.8	1330.2	1338.6	1343.7
n-Octylbenzene	190	92	1580.2	1587.2	1590.6	1461.6	1466.5	1468.2
n-Hexadecane	226	57	1600	1600	1600	1600	1600	1600
1,2,3,4-Tetrahydroquinoline	133	132	1600.0	1617.6	1627.8	1318.5	1326.8	1332.5
2,6-Di-tert-butylphenol	206	191	1603.1	1613.2	1619.7	1433.6	1440.1	1443.2
2-Ethylnaphthalene	156	141	1604.3	1621.6	1632.3	1380.6	1390.6	1396.1
1-Hexadecene	224	55	1613.1	1613.2	1613.1	1591.7	1591.6	1592.7
2,7-Dimethylnaphthalene	156	156	1613.3	1631.8	1641.9	1392.1	1402.2	1409.5
2,6-Dimethylnaphthalene	156	156	1615.5	1633.1	1643.9	1390.6	1400.9	1407.3
1,1'-Biphenyl (Diphenyl)	154	154	1615.7	1631.8	1641.9	1368.5	1377.3	1381.8
2-Methylbiphenyl	168	168	1620.2	1634.5	1644.4	1390.0	1397.6	1402.3
1-Ethylnaphthalene	156	141	1621.0	1639.2	1650.0	1383.6	1393.8	1400.0
1,3-Dimethylnaphthalene	156	156	1642.2	1661.8	1673.2	1405.3	1416.5	1422.3
1,6-Dimethylnaphthalene	156	156	1643.3	1662.5	1675.3	1408.4	1419.6	1427.3
2-Isopropylnaphthalene	170	155	1660.5	1677.4	1687.9	1443.9	1454.0	1459.1
1,4-Dimethylnaphthalene	156	156	1672.6	1692.9	1707.4	1424.2	1436.3	1443.2
1,5-Dimethylnaphthalene	156	156	1678.1	1699.0	1714.2	1428.3	1439.8	1446.4
1-Isopropylnaphthalene	170	155	1684.5	1701.8	1713.7	1451.1	1460.9	1465.9
n-Decylcyclohexane	224	83	1692.2	1698.0	1702.1	1650.7	1656.2	1658.4
1,2-Dimethylnaphthalene	156	156	1692.4	1713.6	1728.6	1439.6	1452.2	1459.1
n-Heptadecane	240	57	1700	1700	1700	1700	1700	1700
5,6,7,8-Tetrahydro-1-naphthol	148	120	1725.3	1743.8	1756.3	1440.8	1447.2	1450.9
3-Methylbiphenyl	168	168	1725.5	1742.3	1753.7	1474.5	1483.5	1487.7
1,8-Dimethylnaphthalene	156	156	1730.1	1752.7	1765.3	1459.7	1472.7	1480.0
4-Methylbiphenyl	168	168	1735.7	1753.4	1766.3	1482.8	1492.2	1497.3
Acenaphthene	154	154	1752.8	1777.6	1794.2	1468.0	1481.4	1488.6
1,2-Diphenylethane (Bibenzyl)	182	91	1758.7	1776.5	1787.9	1508.8	1519.2	1524.3
Dibenzofuran	168	168	1783.4	1808.2	1825.4	1499.4	1513.0	1520.9
n-Decylbenzene	218	92	1791.1	1799.6	1805.5	1669.5	1674.8	1677.7
n-Octadecane	254	57	1800	1800	1800	1800	1800	1800
1-Octadecene	252	55	1814.4	1814.5	1814.9	1792.6	1792.1	1793.5
3,3'-Dimethylbiphenyl	182	182	1837.3	1853.9	1865.7	1580.2	1589.0	1594.2
2-Naphthol	144	144	1849.4	1871.7	1885.6	1514.5	1520.5	1523.8
4,4'-Dimethylbiphenyl	182	182	1856.6	1875.1	1887.8	1596.8	1607.6	1614.2
Fluorene	166	166	1869.3	1895.2	1913.9	1565.2	1579.5	1587.9
n-Nonadecane	268	57	1900	1900	1900	1900	1900	1900
2,6-Diisopropylnaphthalene	212	197	1925.5	1943.7	1956.1	1716.8	1728.0	1735.5
Dibenzylether	198	92	1943.4	1961.4	1974.0	1641.4	1650.3	1656.9
9,10-Dihydroanthracene	180	179	1983.3	2011.1	2028.7	1662.1	1676.6	1685.3
n-Eicosane	282	57	2000	2000	2000	2000	2000	2000
n-Dodecylbenzene	246	92	2005.0	2014.4	2019.5			
9,10-Dihydrophenanthrene	180	180	2010.2	2040.3	2059.1	1673.5	1689.8	1699.5
1,2,3,4,5,6,7,8-Octahydroanthracene	186	186				1680.2	1694.1	1703.2
1,2,3,4,5,6,7,8-Octahydrophenanthrene	186	186				1705.5	1721.1	1730.6
1,2,3,4,5,6,7,8-Octahydroacridine	187	186	2037.8	2067.9	2086.0	1712.2	1726.5	1736.6
1,2,3,4-Tetrahydroanthracene	182	182				1731.3	1748.7	1760.2
1,2,3,4-Tetrahydrophenanthrene	182	182				1737.6	1755.2	1767.7
n-Henicosane	296	57	2100	2100	2100	2100	2100	2100
Phenanthrene	178	178	2136.9	2174.0	2196.8	1756.9	1776.3	1789.2
Anthracene	178	178	2146.5	2183.0	2207.3	1767.0	1786.4	1800.0
1,2,3,4-Tetrahydrocarbazole	171	143	2190.6	2229.6	2250.0	1786.6	1800.4	1811.8
n-Docosane	310	57	2200	2200	2200	2200	2200	2200
1-Phenylnaphthalene	204	204	2224.1	2256.1	2276.0	1841.7	1858.2	1868.0
n-Tricosane	324	57	2300	2300	2300	2300	2300	2300
1-Methylanthracene	192	192				1934.8	1959.3	1976.3
n-Tetracosane	338	57	2400	2400	2400	2400	2400	2400
Fluoranthene	202	202	2494.8	2544.9	2578.2	2032.6	2060.1	2076.5
n-Pentacosane	352	57	2500	2500	2500	2500	2500	2500
Pyrene	202	202	2580.4	2636.3	2673.1	2082.6	2113.4	2132.5
9,10-Dimethylanthracene	206	206	2582.5	2632.1	2664.6	2107.6	2135.5	2152.6
n-Hexacosane	366	57	2600	2600	2600	2600	2600	2600
p-Terphenyl	230	230	2627.1	2665.3	2690.0	2171.1	2190.9	2204.0
n-Triacontane	422	57	3000	3000	3000	3000	3000	3000
Chrysene	228	228	3036.9	3107.4	3153.2	2434.2	2472.3	2494.9
n-Hentriacontane	436	57	3100	3100	3100	3100	3100	3100

Table 1.40-2. Final Elution Temperature and Retention Indices of 1-Alkenes on Rtx-50 Column at Three Heating Rates

	Heating rates					
	2°C/min		4°C/min		6°C/min	
Compounds	T (°C)	R.I.	T (°C)	R.I.	T (°C)	R.I.
1-Hexene	43.7	606.4	47.4	607.0	51.1	607.7
1-Heptene	44.8	708.3	49.3	708.4	53.7	709.5
1-Octene	47.1	808.2	53.4	809.2	59.1	809.7
1-Nonene	51.8	909.1	60.8	909.5	68.1	909.9
1-Decene	59.9	1010.3	71.7	1011.0	80.7	1011.3
1-Undecene	71.0	1110.6	84.9	1111.0	95.0	1111.0
1-Dodecene	83.9	1211.6	99.2	1212.4	109.9	1211.9
1-Tridecene	97.3	1311.8	113.4	1312.0	124.5	1312.4
1-Tetradecene	110.5	1412.5	127.1	1412.8	138.5	1412.7
1-Pentadecene	123.2	1512.7	140.2	1513.1	151.8	1513.1
1-Hexadecene	135.3	1613.1	152.6	1613.2	164.4	1613.1
1-Octadecene	157.9	1814.4	175.6	1814.5	187.8	1814.9

Table 1.40-3. Temperature Dependence of Retention Indices for Cycloalkanes and Benzenes

Compounds	Rtx-50			DB-5		
	Temp. Range (°C)	R.I. Range	ΔR.I./ΔT	Temp. Range (°C)	R.I. Range	ΔR.I./ΔT
Cyclohexane	44.7-53.6	705.6-706.0	0.04	44.6-53.1	655.4-657.6	0.25
Cyclohexene	45.4-55.2	736.1-739.3	0.32	44.9-53.9	677.1-678.8	0.19
Methylcyclohexane	45.6-55.9	748.1-752.4	0.41	46.0-56.3	718.3-720.3	0.19
Benzene	46.0-56.7	765.7-769.0	0.31	44.5-53.0	654.2-656.1	0.22
trans-1,4-Dimethylcyclohexane	46.8-58.6	801.8-803.5	0.14	48.0-60.7	775.6-777.3	0.14
cis-1,3-Dimethylcyclohexane	46.8-58.6	801.8-803.5	0.14	47.9-60.6	772.8-776.6	0.30
trans-1,2-Dimethylcyclohexane	47.7-60.5	820.9-825.0	0.32	48.8-62.3	796.7-798.4	0.13
1-Methylcyclohexene,	47.8-60.8	824.1-829.2	0.39	47.6-59.9	763.9-766.4	0.20
cis-1,4-Dimethylcyclohexane	48.0-61.1	828.6-832.6	0.31	49.2-63.1	804.7-805.7	0.07
trans-1,3-Dimethylcyclohexane	48.1-61.4	830.9-835.4	0.34	49.2-63.2	804.1-806.2	0.15
cis-1,2-Dimethylcyclohexane	49.3-64.1	859.1-866.7	0.51	50.5-65.6	823.1-827.3	0.28
Ethylcyclohexane	49.5-64.1	862.3-867.4	0.35	50.7-66.0	826.9-830.9	0.26
Toluene	49.8-64.8	870.5-875.7	0.35	47.4-59.5	758.9-761.7	0.23
n-Propylcyclohexane	55.5-74.6	956.9-963.4	0.34	58.3-78.2	924.2-929.1	0.24
Ethylbenzene	56.4-76.1	968.1-975.2	0.36	52.5-69.1	853.2-857.2	0.24
1,4-Dimethylbenzene	56.7-76.5	972.3-979.2	0.35	53.1-70.2	861.7-866.5	0.28
1,3-Dimethylbenzene	56.8-76.8	974.2-981.2	0.35	53.1-70.2	861.7-866.5	0.28
1,2-Dimethylbenzene	59.8-81.3	1009.2-1015.5	0.29	54.9-73.1	888.0-891.2	0.18
trans-Octahydro-1H-Indene	60.1-81.8	1011.6-1018.8	0.33	60.7-81.9	947.7-955.3	0.36
tert-Butylcyclohexane	60.4-82.3	1015.1-1022.6	0.34	63.9-86.2	978.1-985.2	0.32
Isopropylbenzene	61.9-84.0	1028.2-1034.7	0.30	57.8-77.4	919.4-923.6	0.21
cis-Octahydro-1H-Indene	64.6-88.1	1053.0-1063.2	0.43	64.2-86.8	981.0-989.5	0.38
n-Propylbenzene	65.1-88.5	1058.0-1066.1	0.35	60.6-81.5	946.9-952.3	0.26
n-Butylcyclohexane	65.3-88.6	1059.5-1066.5	0.30	69.5-93.2	1026.6-1031.6	0.21
1-Ethyl-3-methylbenzene	66.2-89.9	1068.7-1075.7	0.29	61.5-82.7	955.0-960.8	0.27
1-Ethyl-4-methylbenzene	66.4-90.0	1069.8-1076.6	0.29	61.6-83.0	956.3-962.4	0.29
1,3,5-Trimethylbenzene	66.9-90.8	1074.4-1081.6	0.30	62.1-83.6	961.5-967.1	0.26
tert-Butylbenzene	69.4-94.1	1097.6-1104.5	0.28	64.8-87.2	987.1-992.0	0.21
4,5,6,7-Tetrahydroindan	69.4-94.4	1097.8-1106.9	0.36	67.2-90.6	1008.6-1014.8	0.27
1-Ethyl-2-methylbenzene	69.5-94.2	1098.2-1105.3	0.29	63.4-85.4	973.3-979.7	0.29
1,2,4-Trimethylbenzene	70.5-95.6	1106.8-1114.6	0.31	64.8-87.3	987.5-992.8	0.24
sec-Butylbenzene	71.3-96.4	1112.9-1120.3	0.29	67.0-90.1	1006.4-1011.7	0.23
trans-Decalin	71.5-97.4	1114.7-1127.2	0.49	72.0-96.9	1045.7-1055.9	0.41
1,1'-Bicyclopentyl	74.6-101.0	1138.6-1151.2	0.48	75.3-100.7	1071.8-1080.9	0.35
1,2,3-Trimethylbenzene	75.7-102.1	1147.6-1158.9	0.43	68.2-91.8	1016.0-1022.7	0.28
Phenylethylether	76.0-101.8	1150.0-1156.9	0.27	65.0-87.2	988.8-992.4	0.16
n-Butylbenzene	77.7-103.9	1163.2-1171.1	0.30	72.5-96.9	1050.1-1055.9	0.24
n-Pentylcyclohexane	77.7-104.0	1163.7-1172.0	0.31	83.1-109.1	1130.2-1136.0	0.22
cis-Decalin	79.1-106.7	1174.6-1190.2	0.57	77.6-103.7	1089.5-1100.4	0.42
Indan	79.9-107.2	1180.4-1193.5	0.48	69.6-93.8	1027.4-1035.5	0.34
2-Methylindan	84.1-111.9	1212.8-1225.8	0.47	75.6-100.9	1074.3-1082.0	0.30
1-Methylindan	85.4-113.5	1222.7-1236.5	0.49	76.3-101.7	1079.3-1087.1	0.31
1,2,4,5-Tetramethylbenzene	87.0-115.1	1235.1-1247.5	0.44	80.3-106.1	1109.7-1115.8	0.24
n-Hexylcyclohexane	91.6-119.4	1269.0-1276.6	0.28	97.3-124.6	1233.9-1239.5	0.21
1,4-Diisopropylbenzene	93.0-121.1	1279.9-1288.1	0.29	88.6-115.0	1170.1-1174.7	0.18
5-Methylindan	93.4-122.6	1282.5-1298.4	0.54	83.2-109.7	1131.1-1139.9	0.33
1,2,3,4-Tetramethylbenzene	93.9-123.2	1286.4-1302.6	0.55	85.0-111.8	1144.2-1153.8	0.36
4-Methylindan	95.9-125.4	1301.2-1318.8	0.60	84.6-111.5	1141.6-1151.4	0.37
1,3,5-Triethylbenzene	100.8-129.3	1338.5-1346.2	0.27	95.4-122.4	1219.6-1224.3	0.17
n-Hexylbenzene	105.0-134.0	1370.1-1379.9	0.34	100.2-127.7	1254.6-1260.9	0.23
Bicyclohexyl	106.0-136.5	1377.5-1397.4	0.65	105.4-134.5	1293.1-1307.8	0.50
n-Octylcyclohexane	119.1-148.7	1480.1-1489.6	0.32	124.9-153.8	1442.4-1449.1	0.23
1,2-Dicyclohexylethane	129.9-161.5	1568.2-1589.2	0.67	130.5-160.6	1486.9-1501.0	0.47
n-Octylbenzene	131.4-161.7	1580.2-1590.6	0.34	127.3-156.3	1461.6-1468.2	0.23
n-Decylcyclohexane	144.5-175.0	1692.2-1702.1	0.32	149.9-179.7	1650.7-1658.4	0.26
n-Decylbenzene	155.4-186.8	1791.1-1805.5	0.46	152.1-182.0	1669.5-1677.7	0.27
n-Dodecylbenzene	177.4-209.3	2005.0-2019.5	0.45			

Table 1.40-4. Temperature Dependence of Retention Indices for Aromatics and N-, S-, and O-Containing Compounds

Compounds	Rtx-50			DB-5		
	Temp. Range (°C)	R.I. Range	ΔR.I./ΔT	Temp. Range (°C)	R.I. Range	ΔR.I./ΔT
Tetralin	98.9-128.9	1324.1-1343.6	0.65	86.0-113.1	1151.7-1162.5	0.40
1,2-Dihydronaphthalene	101.8-132.1	1345.7-1366.2	0.68			
Naphthalene	107.2-138.3	1386.8-1410.9	0.77	88.8-116.3	1171.5-1183.4	0.43
2-Methylnaphthalene	121.8-153.8	1501.0-1528.6	0.87	103.8-132.9	1281.5-1296.3	0.51
1-Methylnaphthalene	125.3-157.7	1530.2-1559.6	0.91	106.0-135.3	1297.1-1313.4	0.56
Dodecahydrofluorene	128.6-161.4	1556.9-1588.7	0.97			
2-Ethylnaphthalene	134.3-166.7	1604.3-1632.3	0.86	117.0-146.7	1380.6-1396.1	0.52
2,7-Dimethylnaphthalene	135.3-167.9	1613.3-1641.9	0.88	118.5-148.5	1392.1-1409.5	0.58
2,6-Dimethylnaphthalene	135.6-168.1	1615.5-1643.9	0.87	118.3-148.2	1390.6-1407.3	0.56
1,1'-Biphenyl	135.6-167.9	1615.7-1641.9	0.81	115.4-144.8	1368.5-1381.8	0.45
2-Methylbiphenyl	136.1-168.2	1620.2-1644.4	0.76	118.3-147.6	1390.0-1402.3	0.42
1-Ethylnaphthalene	136.2-168.8	1621.0-1650.0	0.89	117.4-147.3	1383.6-1400.0	0.55
1,7-Dimethylnaphthalene	138.3-171.2	1638.6-1670.2	0.96			
1,3-Dimethylnaphthalene	138.7-171.6	1642.2-1673.2	0.94	120.2-150.2	1405.3-1422.3	0.57
1,6-Dimethylnaphthalene	138.8-171.8	1643.3-1675.3	0.97	120.6-150.9	1408.4-1427.3	0.62
2-Isopropylnaphthalene	140.8-173.3	1660.5-1687.9	0.84	125.1-155.1	1443.9-1459.1	0.51
2,3-Dimethylnaphthalene	141.4-174.6	1665.9-1698.5	0.98			
1,4-Dimethylnaphthalene	142.2-175.6	1672.6-1707.4	1.04	122.6-153.0	1424.2-1443.2	0.63
1,5-Dimethylnaphthalene	142.9-176.4	1678.1-1714.2	1.08	123.1-153.4	1428.3-1446.4	0.60
1-Isopropylnaphthalene	143.6-176.3	1684.5-1713.7	0.89	126.0-156.0	1451.1-1465.9	0.49
1,2-Dimethylnaphthalene	144.5-178.1	1692.4-1728.6	1.08	124.6-155.1	1439.6-1459.1	0.64
3-Methylbiphenyl	148.2-180.9	1725.5-1753.7	0.86	128.9-158.9	1474.5-1487.7	0.44
1,8-Dimethylnaphthalene	148.7-182.2	1730.1-1765.3	1.05	127.1-157.8	1459.7-1480.0	0.66
4-Methylbiphenyl	149.3-182.3	1735.7-1766.3	0.93	130.0-160.1	1482.8-1497.3	0.48
Acenaphthene	151.2-185.5	1752.8-1794.2	1.21	128.1-159.0	1468.0-1488.6	0.67
1,2-Diphenylethane (Bibenzyl)	151.8-184.8	1758.7-1787.9	0.89	133.2-163.5	1508.8-1524.3	0.51
3,3'-Dimethylbiphenyl	160.3-193.3	1837.3-1865.7	0.86	141.8-172.1	1580.2-1594.2	0.46
4,4'-Dimethylbiphenyl	162.4-195.7	1856.6-1887.8	0.94	143.8-174.5	1596.8-1614.2	0.57
Fluorene	163.7-198.5	1869.3-1913.9	1.28	140.0-171.3	1565.2-1587.9	0.72
2,6-Diisopropylnaphthalene	169.5-202.8	1925.5-1956.1	0.92	157.4-188.6	1716.8-1735.5	0.60
9,10-Dihydroanthracene	175.2-210.2	1983.3-2028.7	1.30	151.2-182.9	1662.1-1685.3	0.73
9,10-Dihydrophenanthrene	177.9-213.2	2010.2-2059.1	1.39	152.5-184.6	1673.5-1699.5	0.81
1,2,3,4,5,6,7,8-Octahydroanthracene				153.3-185.0	1680.2-1703.2	0.73
1,2,3,4,5,6,7,8-Octahydrophenanthrene				156.1-188.1	1705.5-1730.6	0.79
1,2,3,4-Tetrahydroanthracene				158.9-191.4	1731.3-1760.2	0.89
1,2,3,4-Tetrahydrophenanthrene				159.6-192.2	1737.6-1767.7	0.93
Phenanthrene	189.9-226.4	2136.9-2196.8	1.64	161.7-194.6	1756.9-1789.2	0.98
Anthracene	190.8-227.4	2146.5-2207.3	1.66	162.8-195.8	1767.0-1800.0	1.00
1-Phenylnaphthalene	197.8-233.6	2224.1-2276.0	1.45	170.7-203.1	1841.7-1868.0	0.81
1-Methylanthracene				180.2-214.2	1934.8-1976.3	1.22
Fluoranthene	220.6-259.0	2494.8-2578.2	2.17	189.7-224.1	2032.6-2076.5	1.28
Pyrene	227.3-266.4	2580.4-2673.1	2.37	194.4-229.4	2082.6-2132.5	1.43
9,10-Dimethylanthracene	227.5-265.8	2582.5-2664.6	2.14	196.7-231.2	2107.6-2152.6	1.30
p-Terphenyl	230.9-267.8	2627.1-2690.0	1.71	202.4-236.0	2171.1-2204.0	0.98
Chrysene	259.9-300.2	3036.9-3153.2	2.88	224.6-260.9	2434.2-2494.9	1.67
2,6-Dimethylphenol	95.4-124.3	1297.6-1310.7	0.45	79.2-104.5	1102.3-1105.5	0.13
2,4,6-Trimethylphenol	108.6-138.5	1397.4-1412.2	0.50	92.6-119.4	1199.1-1204.1	0.19
Benzothiophene	110.9-142.5	1415.7-1442.5	0.85	90.0-117.8	1180.5-1192.9	0.45
2,3-Dihydroindole	116.0-147.3	1455.5-1479.2	0.76	92.1-119.8	1195.8-1206.6	0.39
1-Indanol	118.7-149.7	1476.6-1496.8	0.65	96.1-123.6	1224.7-1232.9	0.30
Quinoline	120.9-152.9	1493.6-1521.6	0.88	96.1-124.3	1224.7-1237.4	0.45
8-Methylquinoline	129.3-161.7	1562.7-1591.1	0.87	107.0-136.1	1304.5-1319.5	0.51
5,6,7,8-Tetrahydro-3-methylquinoline	130.3-162.3	1571.5-1595.8	0.76	110.4-139.5	1330.2-1343.7	0.47
1,2,3,4-Tetrahydroquinoline	133.8-166.2	1600.0-1627.8	0.86	108.8-137.9	1318.5-1332.5	0.48
2,6-Di-*tert*-butylphenol	134.2-165.2	1603.1-1619.7	0.53	123.8-153.0	1433.6-1443.2	0.33
5,6,7,8-Tetrahydro-1-naphthol	148.2-181.2	1725.3-1756.3	0.94	124.7-154.0	1440.8-1450.9	0.35
Dibenzofuran	154.6-188.9	1783.4-1825.4	1.22	132.1-163.1	1499.4-1520.9	0.69
2-Naphthol	161.6-195.5	1849.4-1885.6	1.07	133.9-163.4	1514.5-1523.8	0.31
Dibenzylether	171.3-204.7	1943.4-1974.0	0.92	148.9-179.6	1641.4-1656.9	0.50
1,2,3,4,5,6,7,8-Octahydroacridine	180.5-215.9	2037.8-2086.0	1.36	156.9-188.7	1712.2-1736.6	0.77
1,2,3,4-Tetrahydrocarbazole	194.8-231.2	2190.6-2250.0	1.63	164.9-197.1	1786.6-1811.8	0.79

Table 1.40-5. Retention Times and Indices on DB-5 Column Measured at the Heating Rate of 4°C/min. with and without Isothermal Initial Holding Period

Compounds	Retention time (min)			Retention index		
	IH[a]=0	IH=5	difference	IH=0	IH=5	difference
Benzene	2.21	2.34	0.13	654.8	653.8	-0.9
Cyclohexane	2.22	2.35	0.13	656.2	654.9	-1.2
1-Octene	3.88	4.82	0.94	789.3	788.4	-0.9
cis-1,2-Dimethylcyclohexane	4.65	6.09	1.44	824.7	824.4	-0.2
Ethylcyclohexane	4.76	6.25	1.49	829.1	828.4	-0.8
Ethylbenzene	5.43	7.36	1.93	856.3	855.5	-0.8
n-Propylcyclohexane	7.39	10.36	2.97	927.1	926.4	-0.7
1-Ethyl-3-methylbenzene	8.41	11.80	3.39	958.5	958.6	0.2
4,5,6,7-Tetrahydroindan	10.17	14.07	3.90	1011.4	1009.9	-1.5
n-Butylcyclohexane	10.85	14.88	4.03	1030.2	1028.9	-1.3
trans-Decalin	11.63	15.77	4.14	1051.8	1049.8	-2.0
n-Butylbenzene	11.70	15.92	4.22	1053.7	1053.3	-0.5
5-Methylindan	14.74	19.30	4.56	1137.1	1135.1	-2.0
1,2,3,4-Tetramethylbenzene	15.21	19.82	4.61	1149.9	1148.2	-1.6
2,3-Dihydroindole	17.14	21.89	4.75	1202.2	1200.5	-1.7
2,4,6-Trimethylphenol	17.15	21.93	4.78	1202.5	1201.6	-0.9
1,3,5-Triethylbenzene	17.86	22.68	4.82	1222.3	1222.0	-0.4
1-Indanol	18.13	22.92	4.79	1229.9	1228.5	-1.4
n-Hexylcyclohexane	18.41	23.24	4.83	1237.7	1237.1	-0.6
1-Tridecene	20.33	25.26	4.93	1291.3	1291.9	0.5
Bicyclohexyl	20.69	25.60	4.91	1301.5	1301.2	-0.3
1-Methylnaphthalene	20.87	25.75	4.88	1306.8	1305.5	-1.3
1,2,3,4-Tetrahydroquinoline	21.55	26.43	4.88	1326.8	1325.1	-1.7
1,1'-Biphenyl	23.26	28.17	4.91	1377.3	1375.4	-1.9
2-Ethylnaphthalene	23.71	28.66	4.95	1390.6	1389.6	-1.0
1-Ethylnaphthalene	23.82	28.78	4.96	1393.8	1393.1	-0.7
2,6-Dimethylnaphthalene	24.06	29.02	4.96	1400.9	1400.0	-0.9
5,6,7,8-Tetrahydronaphthalenol	25.55	30.51	4.96	1447.2	1446.1	-1.1
n-Octylcyclohexane	25.56	30.54	4.98	1447.5	1447.1	-0.5
1,2-Dimethylnaphthalene	25.71	30.67	4.96	1452.2	1451.1	-1.1
2-Isopropylnaphthalene	25.77	30.75	4.98	1454.0	1453.6	-0.5
n-Octylbenzene	26.17	31.16	4.99	1466.5	1466.3	-0.2
1,8-Dimethylnaphthalene	26.37	31.35	4.98	1472.7	1472.1	-0.5
Acenaphthene	26.65	31.62	4.97	1481.4	1480.5	-0.9
4-Methylbiphenyl	27.00	32.00	5.00	1492.2	1492.3	0.0
1,2-Dicyclohexylethane	27.13	32.09	4.96	1496.3	1495.0	-1.2
Dibenzofuran	27.65	32.62	4.97	1513.0	1512.0	-1.0
2-Naphthol	27.88	32.87	4.99	1520.5	1520.1	-0.3
Fluorene	29.70	34.68	4.98	1579.5	1578.9	-0.6
3,3'-Dimethylbiphenyl	29.99	34.98	4.99	1589.0	1588.6	-0.3
1-Hexadecene	30.07	35.08	5.01	1591.6	1591.9	0.3
Dibenzylether	31.79	36.77	4.98	1650.3	1649.7	-0.7
n-Decylcyclohexane	31.96	36.95	4.99	1656.2	1655.9	-0.3
n-Decylbenzene	32.50	37.49	4.99	1674.8	1674.5	-0.3
9,10-Dihydroanthracene	32.55	37.54	4.99	1676.6	1676.2	-0.3
9,10-Dihydrophenanthrene	32.92	37.90	4.98	1689.3	1688.6	-0.7
1,2,3,4,5,6,7,8-Octahydroanthracene	33.06	38.06	5.00	1694.1	1694.1	0.0
1,2,3,4,5,6,7,8-Octahydroacridine	33.97	38.96	4.99	1726.5	1726.2	-0.4
2,6-Diisopropylnaphthalene	34.01	39.01	5.00	1728.0	1728.0	0.0
1,2,3,4-Tetrahydroanthracene	34.59	39.59	5.00	1748.7	1748.7	0.0
Phenanthrene	35.36	40.36	5.00	1776.3	1776.3	0.0
1-Octadecene	35.80	40.80	5.00	1792.1	1792.1	0.0
1,2,3,4-Tetrahydrocarbazole	36.03	41.02	4.99	1800.4	1800.0	-0.4
1-Phenylnaphthalene	37.54	42.54	5.00	1858.2	1858.2	0.0
Fluoranthene	42.59	47.59	5.00	2060.1	2060.1	0.0
Pyrene	43.85	48.85	5.00	2113.4	2113.4	0.0
9,10-Dimethylanthracene	44.36	49.35	4.99	2135.5	2135.1	-0.4
Dibenzylsulfid	44.62	49.60	4.98	2146.8	2145.9	-0.9
p-Terphenyl	45.64	50.64	5.00	2190.9	2190.9	0.0
Chrysene	51.64	56.63	4.99	2472.3	2471.8	-0.5

a) IH=isothermal initial holding period (minutes)

Table 1.40-6. Compositions and LC and Distillate Fractions of JP-8P and JP-8C Jet Fuels

Compositions (wt%)		
Compound Classes	**JP-8P**	**JP-8C**
Paraffins	61	10
Cyclohexanes	14	40
Benzenes	15	11
Decalins	1	15
Tetralins	<1	8
Indans	1	6
Others[a]	7	10

LC Fraction (wt%)[b]			
Fraction No.	**Elution System Solvent**	**JP-8P**	**JP-8C**
1	n-Pentane	85.2	77.9
2	5% Benzene-Pentane	6.9	9.1
3	Benzene	4.9	11.1
4	1%EtOH-Chloroform	0.7	0.5
5	10% EtOH-THF	1.0	1.0

Distillate Fraction (vol%)		
Temperature (C)	**JP-8P**	**JP-8C**
IBP-165°	8.3	27.0
165-185°	22.2	14.9
185-215°	32.8	22.2
215-240°	22.9	17.1
240°+	13.8	18.8

[a] Including polycyclic alkanes, aromatics, and hydroaromatics, as well as polar compounds (e.g., antioxidants) and trace amounts of unidentified compounds

[b] From separation on neutral alumina column

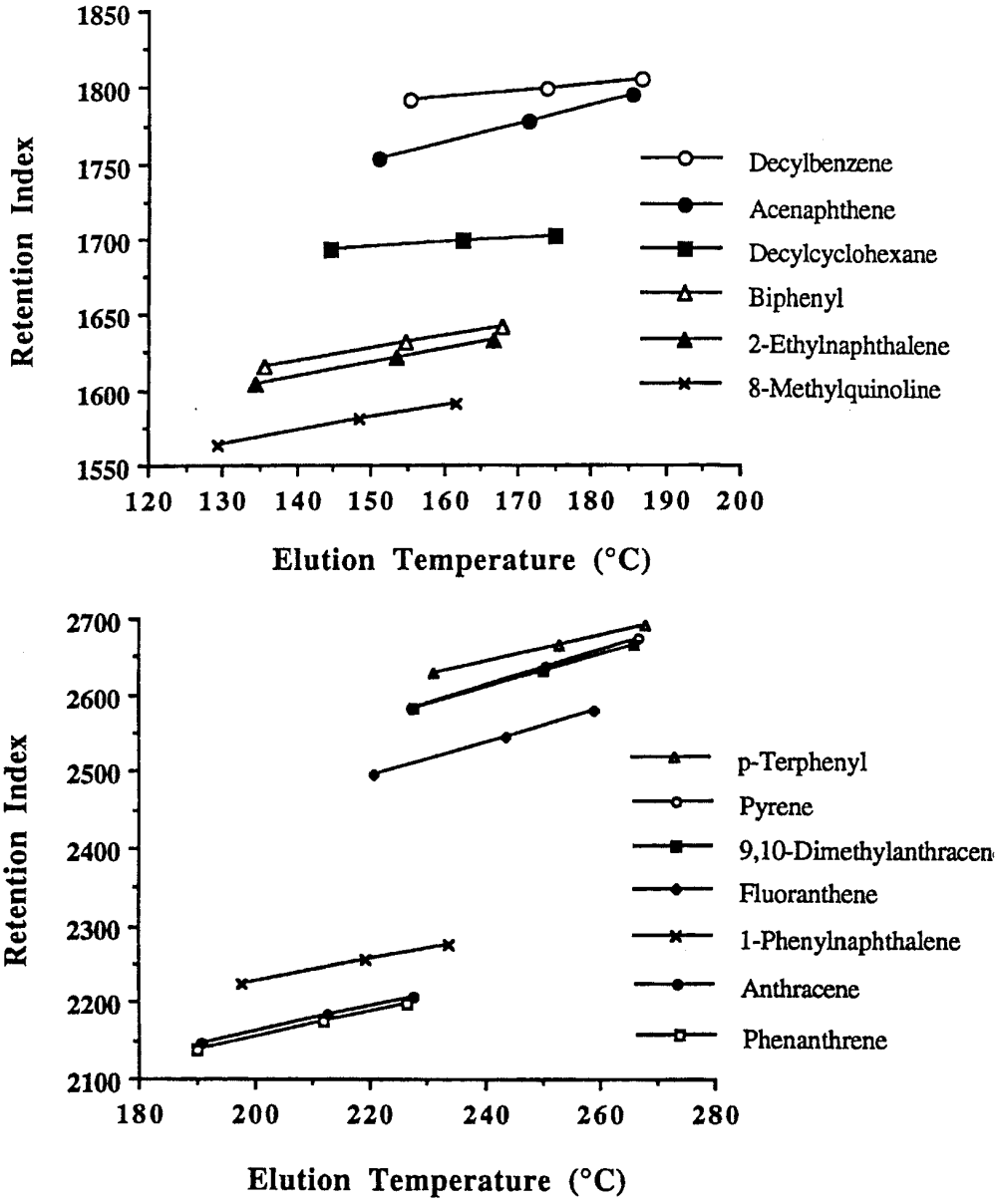

Figure 1.40-1. Retention Index versus Final Elution Temperature (Rtx-50 Column, 40°C to 310°C)

[1] Lai, W. C. et al. *Prepr. Pap. – Am. Chem. Soc. Div Fuel Chem.* 1992. 37(4). 1671-1680.

[2] Song, C. et al. *Energy & Fuels.* 1993. 7. 234-243.

1.41 Literature Review on Thermal Stability of Jet Fuels

This study is explained in detail in *Advanced Thermally Stable Jet Fuels Technical Progress Report, October–December 1994.*

Introduction

The stability of aviation fuel relates to the fuel's tendency to undergo changes in characteristics that affect the efficiency of its performance. These changes can occur during storage or use. The most important changes are those involving formation of insoluble materials that deposit in fuel lines, on heat transfer surfaces, and on injection nozzles.

The various forms of fuel stability are:

- Storage stability – formation of solids during fuel storage
- Thermal stability – instability related to fuel changes at elevated temperatures in aircraft fuel systems (in the absence of either dissolved or input oxygen)
- Thermal oxidative stability – instability when oxygen is present; involved when pyrolysis takes place

The importance of thermal stability will increase in the future, as next-generation high-performance jet engines place more thermal demands on the fuel. Present limits for fuel stability regimes are 436 K for JP-4, JP-5, and JP-8, and 561 K for JP-7.[1] Although the problem has been studied for more than 35 years, more questions than answers remain. There are three primary reasons that no clear physical picture of fouling has evolved:

1. The formation of insoluble material is a complex process that includes several steps. The chemical aspect comprises the decomposition of the components initially present in the bulk fluid and on the hot surfaces of aircraft fuel systems—two very different processes. Jet fuel composition varies from sample to sample and undergoes changes during thermal degradation or oxidative reactions. A detailed kinetic mechanism for a single hydrocarbon could include hundreds of steps; the chemistry of real fuel is much more complicated. The physical aspect of the problem involves transport of precursors of solid deposits to surfaces, either by diffusion or turbulent flows. The formation of solid residue on heated metal surfaces is a highly complicated catalytic process of known initial and unknown intermediate species. The relative importance and interaction of various processes, different by nature, complicate the understanding and prediction of the deposition paths.

2. The empirical data is global in nature. Recent experiments have provided information on thickness of deposits and their thermal resistivity, rates of deposition, dissolved oxygen consumption, and methane production.[2 3 4 5] However, almost no data on chemical composition of the deposits exist. Detailed knowledge of the contents would help to identify the chemical reactions that contribute to the overall deposition rate.

3. The empirical nature of derived correlations involving many adjustable parameters results in very little physical meaning.

Numerical modeling is an alternative method for analyzing the fouling process. A realistic model could help to identify major factors governing the complex process and predict

the system behavior under different conditions. A comprehensive model of real jet fuel decomposition has not been developed because many of the physical and chemical processes involved are not well understood. Therefore, two approaches exist—the accurate description of fluid dynamics with simplified chemistry, and detailed chemical kinetic simulations neglecting flow conditions.

A Computational Fluid Dynamics and Chemistry (CFDC) Model of Thermal Stability

CFDC models have been developed as computational tools for combustor design. They are also used for simulation of carbon deposition processes. These models[6 7] incorporate existing fluid dynamics codes solving the system of conservation equations of mass, momentum, and energy with an averaged Reynolds number and the thermal decomposition model in the simplest form.

The initial one-step CFDC model[6] was produced as a modification of the existing combustion code (block-implicit multigrid method) for two-dimensional, Reynolds averaged Navier-Stokes mass and energy equations in gas flows. The model was modified by supplementing the ideal gas law and gas flow characteristics with fluid properties of viscosity, thermal conductivity, specific heat, and density. These properties are very sensitive to variations in composition.

The CFDC model involves many unknown parameters that can be obtained from experiments with isolated mechanisms, as were performed in the Marteney test program[8] for JP-5 jet fuel. The average rate of carbon deposition in long, thin electrically heated tubes (constant heat flux boundary condition) was found to correlate with the initial wall temperature. The character of dependence reveals behavior typical for two competitive reaction channels with activation energies of 10 kcal/mol for low temperatures (below 533 K) and 40 kcal/mol for higher temperatures. Activation energies of the magnitude 10 kcal/mol are characteristic for heterogeneous processes; this points to the predominance of deposit formation reactions at wall/fluid interface in the low-temperature regime. At higher temperatures, closer to the pyrolysis region, bulk fluid dissociation of products may play an important role.

The CFDC model was calibrated by fixing several model parameters (e.g., deposition coefficient and inlet oxygen) and determining others (e.g., pre-exponential factors and activation energies). When compared with existing experimental data[9], the model qualitatively reproduced the characteristic shape of the experimental curve. The comparison indicates the ability of the model to predict general trends in fuel decomposition rates. However, further refinement of this approach is critical for quantitative analysis. Although the the model seems to closely approximate the real physical processes, it oversimplifies the chemical reactions.

Kinetic Studies of Jet Fuel Stability

Aircraft jet fuels are derived from a relatively high-boiling range distillation of crude oil often referred to as the kerosene fraction. These fuels are composed mostly of hydrocarbons (≤98%), primarily of aliphatic and naphthenic molecules, with aromatic hydrocarbon concentration (20-25%), and olefin (≤5%). The complex mixture likely exhibits a very complicated chemistry.

A simplified description of a thermal cracking mechanism for a model hydrocarbon is constructed according to a free-radical chain mechanism, originally proposed by Rice[10] and later refined by Kossiakoff and Rice.[11] The temperature dependence of rate coefficients, usually described by an Arrhenius relation, varied with the different types of reactions. For monomolecular processes, it was a linear function in low-pressure conditions and a constant under high-pressure conditions.

One approach would involve treating jet fuel as a single compound. Zabarnick[12] modeled the autoxidative processes in jet fuels in the presence (or absence) of an antioxidant, AH, handling the bulk fuel as a single compound, RH, which has chemical properties of a straight-chain alkane. Unfortunately, the time scale in his work was so small that results could not be compared with existing experimental data. In addition, the model describes autoxidation, while the experiments considered air stressed systems. However, the mechanism predicted the general trends in system behavior.

This approach does not give insight into the nature of jet fuel stability because of its oversimplification. More information can be obtained from detailed kinetic modeling of pure hydrocarbons (i.e., paraffin and aromatic compounds).

Rice and Kossiakoff[10, 13] proposed a free-radical mechanism of thermal cracking of paraffins that could possibly be used to predict the product distribution. The theory, in its various extensions, has been developed primarily from studies on paraffins up to C_6. It seems to fit semi-quantitatively for longer paraffins.[14] A better agreement can be obtained when the assumption of isomerization expands the simple chain cracking theory.[15]

The critical issue in constructing a chemical reaction mechanism is knowledge of rate coefficients and thermodynamic data. The major reactions of small hydrocarbon combustion and pyrolysis were extensively studied in recent years, yielding several comprehensive databases. The rate parameters for unknown reactions can also be estimated using modern theoretical methods, such as Benson's rules.[16] Unfortunately, all of these mechanisms hold true only for elementary chemical reactions. For higher hydrocarbons, detailed mechanisms become overly complicated.

The formation of solid deposits suggests that cycloalkanes and aromatics must be included in any attempt at modeling the chemical reactions since the gas-phase formation of carbonaceous materials is presently related to growth of polycyclic aromatic hydrocarbons (PAH).

Three pathways seem to exist—cycloaddition reactions between alkenes and dienes, ion-molecular reactions with very large rate constants, and radical addition to unsaturated hydrocarbons. Based on deficiencies with the first two pathways, attention has focused on the third, radical addition to unsaturated hydrocarbons. The original quarterly report further expounds on this topic and introduces pertinent research efforts.[17]

Non-Traditional Simulation of Chemical Processing

Molecular Level Lumped Modeling. Introduced by Liguras and Allen[18], this approach was designed to combine the advantages of detailed molecular modeling and lumping simulation. It used a 10-class model to describe the heavy hydrocarbon mixture. Rather than use

uniform kinetic parameters for all compounds in a class, Liguras and Allen included the dependence of the rate constants on carbon numbers of reactants and the probability that a reactant will form a product with a definite number of carbon atoms when it undergoes a certain reaction. The model yielded concentration profiles and mean carbon number distribution in compound classes. Although the results of the work were not comparable to current experimental data, the approach seems quite promising.

Structure-Oriented Lumping. Quann and Jaffe[19] developed structure-oriented lumping (SOL), which represents an individual hydrocarbon as a vector function of the structure. The hydrocarbon mixture is represented as a set of such vectors with the appropriate distribution function. This enables construction of reaction networks of the mixtures, using the existing group contribution methods for the estimation of molecular thermodynamic properties, and provides the base for molecular modeling of hydrocarbon mixture reactions. The core of this theory is the description of a complex molecule as a system of structural sybsystems—such as a six-carbon aromatic ring, an alkyl group, different heteroatoms, and many others. SOL is convenient for treating chemical reactions as transformations of the reactant structural increments to the product structural increments. Although the SOL method helps to construct the matrix or rate coefficients in the sense of equal-not equal to zero, it fails to produce values of rate constants. In fact, its purpose is not to resolve the system of rate equations, but to automatically generate a kinetic model.

Kinetic Simulation in Graph Theory Notation. This work by Broadbelt, Stark, and Klein[20] was aimed at developing a computer generator of kinetic mechanisms. This method uses two-dimensional representations for three-dimensional molecular structures, applying the graph theory algorithms to chemical reactions. It uses the bond and electron (BE) matrix to provide descriptions of both the environment of an atom and its formal electronic state.

Statistical Sampling (Monte Carlo) Methods. Monte Carlo methods are a potential alternative to lumping for describing complex reaction systems. There are no documented, direct applications of Monte Carlo methods to the decomposition of jet fuels or pure hydrocarbons; however, a few works focus on complex reaction systems involving heavy oils or polymers.[21 22 23] The first work described asphaltene (heavy hydrocarbon) stock in terms of probability density functions (PDFs). Each asphaltene molecule was characterized by a degree of polymerization, a number of aromatic rings, a number of naphthenic rings, a degree of subsititution, and a chain length for each aliphatic substituent. This information is expressed in PDFs, indicating the probability that the attribute should take on the value of the abscissa or less.

The PDFs were derived experimentally. The Monte Carlo method was used to construct a pool of 10,000 different molecules that represent the generic aphaltene feedstock. After the reactant array was simulated, a structure/reactivity relationship allowed determination of the sequence of rate constants for each reactive site of each component in the stock. The reactions proceeded event-by-event until the final simulation time was reached. Then a new molecule was taken from the stock array and reacted stochastically until all 10,000 molecules had undergone the process. The predicted global coke yield conformed to the laboratory experiments.

Conclusion

The computational fluid dynamics and chemistry model (CFDC) predicts general trends in deposition rates. However, to bring its predictions to the quantitative level and to complete the

picture of the fouling process, a detailed description of chemical reactions in the system is necessary. Detailed kinetic modeling of pure single hydrocarbon systems reasonably agrees with experiments; however, multi-component mixtures reaction mechanisms are highly complicated and involve many uncertain parameters. Structure-oriented lumping and PDF methods allow avoidance of extreme complexity in detailed modeling by using a systematic reactant-reaction description and statistical sampling from a large set of compounds.

---

[1] Roquemore, W. M. et al. "Fouling in Jet Fuels: A New Approach." *Prepr. – Amer. Chem. Soc., Div. Petr. Chem.* 1989. 34. 841.

[2] Chin, J. S., A. H. Lefebvre, and F. T.-Y. Sun. "Temperature Effects on Fuel Thermal Stability." *J. Eng. Gas Tub. Power.* 1992. 114. 353.

[3] Chin, J. S. and A. H. Lefebvre. "Influence of Flow Conditions on Deposits from Heated Hydrocarbon Fuels." *J. Eng. Gas Turb. Power.* 1993. 115. 433.

[4] Heneghan, S. P. et al. "Studies of Jet Fuel Thermal Stability in a Flowing System." *J. Eng. Gas Turb. Power.* 1993. 115. 480.

[5] Klavetter, E. A., S. J. Martin, and Wessendorf. "Monitoring Jet Fuel Thermal Stability Using a Quartz Crystal Microbalance." *Energ. Fuel.* 1993. 7. 582.

[6] Roquemore, W. M. et al. "Fouling in Jet Fuels: A New Approach." *Prepr. – Amer. Chem. Soc., Div. Petr. Chem.* 1989. 34. 841.

[7] Krazinski, J. L. et al. "Computational Fluid Dynamics and Chemistry Model for Jet Fuel Thermal Stability." *J. Eng. Gas Turbines & Power.* 1992. 114. 104.

[8] Marteney, P. J. and L. J. Spadaccini. "Thermal Decomposition of Aircraft Fuel." *J. of Engineering for Gas Turbines and Power.* 1986. 108. 648.

[9] Chin, J. S., A. H. Lefebvre, and F. T.-Y. Sun. "Temperature Effects on Fuel Thermal Stability." *J. Eng. Gas Tub. Power.* 1992. 114. 353.

[10] Rice, F. O. *J. Amer. Chem Soc.* 1933. 55. 3035.

[11] Kossiakoff, A. and F. O. Rice. "Thermal Decomposition of Hydrocarbons, Resonance Stabilization and Isomerization of Free Radicals." *J. Amer. Chem. Soc.* 1943. 65. 590.

[12] Zabarnick, S. "Chemical Kinetic Modeling of Jet Fuel Autooxidation and Antioxidant Chemistry." *Ind. Eng. Chem. Res.* 1993. 32. 1012.

[13] Kossiakoff, A. and F. O. Rice. "Thermal Decomposition of Hydrocarbons, Resonance Stabilization and Isomerization of Free Radicals." *J. Amer. Chem. Soc.* 1943. 65. 590.

[14] Voge, H. H. and G. M. Good. "Thermal Cracking of Higher Paraffins." *J. Amer. Chem. Soc.* 1949. 71. 593.

[15] Doue, F. and G. Guiochon. *"The Mechanism of Pyrolysis of Some Normal and Branched C6 and C9 Alkanes. Composition of Their Pyrolysis Products." J. Phys. Chem.* 1969. 73. 804.

[16] Benson, S. W. *Thermochemical Kinetics.* New York: John Wiley & Sons, 1976.

[17] Schobert, H. H. et al. *Advanced Thermally Stable Jet Fuels, Technical Progress Report, October 1994 – December 1994.* The Pennsylvania State University. 1995.

[18] Liguras, D. K. and D. T. Allen. "Comparisons of Lumped and Molecular Modeling of Hydropyrolysis." *Ind. Eng. Chem. Res.* 1992. 31. 45.

[19] Quann, R. J. and S. B. Jaffe. "Structure-Oriented Lumping Describing the Chemistry of Complex Hydrocarbon Mixtures." *Ind. Eng. Chem. Res.* 1992. 31. 2483.

[20] Broadbelt, L. J., S. M. Stark, and M. T. Klein. "Computer Generated Pyrolysis Modeling: On-the-Fly Generation of Species, Reactions, and Rates." *Ind. Eng. Chem. Res.* 1994. 33. 790.

[21] Neurock, M. et al. "Monte Carlo Simulation of Complex Reaction Systems: Molecular Structure and Reactivity in Modeling Heavy Oils." Chemical Engineering Science. 1990. 45. 2083.

[22] Libanati, C. et al. "Mechanistic Modeling of Polymer Pyrolysis Using Monte Carlo Methods." *Molec. Simulation.* 1993. 11. 187.

[23] Sapre, A. V. and F. J. Krambeck. *Chemical Reactions in Complex Mixtures: The Mobil Workshop.* New York: Van Nostrand Reinhold, 1991.

1.42 Estimation of Critical Temperatures of Jet Fuels

This study is explained in detail in *Advanced Thermally Stable Jet Fuels Technical Progress Report, October–December 1994.*

Introduction

Previous work measured the critical temperatures of nine jet fuels—six petroleum-derived and three coal-derived fuels—using a sealed tube method[1, 2] and the critical temperatures and pressures of fuels were estimated using the methods recommended in API Technical Data Book.[3] The measured results were satisfactory and reproducible; the data book, however, provides satisfactory predictions for petroleum-derived jet fuels but not coal-derived fuels.

This study uses and evaluates five other methods for estimating critical temperatures of jet fuels. The API method is also presented for comparison. In view of the shortcomings of these methods in estimating critical temperatures of coal-derived fuels, we developed a new correlation in the form of a Roess equation[3] using the properties of compounds found in the coal-derived jet fuels.

Critical Temperature Calculations

The five new methods and the API method were used to determine critical temperatures (T_c); all require only specific gravity and boiling point data as input.

API Method:[3]

$$T_c = 186.16 + 1.6667\Delta - 0.7127 \times 10^{-3}\Delta^2 \quad (1)$$

$$\Delta = SG\,(VABP + 100.0) \quad (2)$$

where: T_c is critical temperature (°F)
SG is specific gravity (60°F/60°F)
VABP is volumetric average boiling point (°F) (the average of the ASTM D86 distillation temperatures at 10, 30, 50, 70, and 90 vol% distilled points)

Cavett Correlation:[4]

$$T_c = 768.07121 + 1.7133693T_b - 0.10834003 \times 10^{-2}T_b^2 - 0.89212579 \times 10^{-2}API \times T_b + 0.38890584 \times 10^{-6}T_b^3 + 0.53094920 \times 10^{-5}API \times T_b^2 + 0.32711600 \times 10^{-7}API^2 \times T_b^2 \quad (3)$$

where T_c is in °R, T_b is the boiling point (°F), and API = 141.5 / SG-131.5

Kesler and Lee Correlation:[5]

$$T_c = 341.7 + 811SG + (0.4244+0.1174SG)T_b + (0.4669-3.2623SG) \times 10^5 / T_b \quad (4)$$

where T_c and T_b are in °R.

Riazi and Daubert Correlation:[6]

$$T_c = 24.2787\ T_b^{0.58848} SG^{0.3596} \quad (5)$$

where T_c and T_b are in °R.

Brule Correlation:[7]

$$T_c = 429.138 + 0.886861 T_b - 4.596433 \times 10^{-4} T_b^2 - 2.410089 \times 10^{-3} API \times T_b + 1.630489 \times 10^{-7} T_b^3 - 9.323778 \times 10^{-7} API \times T_b^2 - 1.430628 \times 10^{-8} API^2 \times T_b^2 \quad (6)$$

where T_c is in K and T_b is in °F.

Twu Correlation:[8]

$$T_c = T_c^\circ [(1+2f_T) / (1-2f_T)]^2 \quad (7)$$

$$f_T = \Delta SG_T [-0.362456 / T_b^{1/2} + (0.0398285 - 0.948125 / T_b^{1/2}) \Delta SG_T] \quad (8)$$

$$\Delta SG_T = \exp[5(SG^\circ - SG)] - 1 \quad (9)$$

$$SG^\circ = 0.843593 - 0.128621\alpha - 3.36159\alpha^3 - 13749.5\alpha^{12} \quad (10)$$

$$\alpha = 1 - T_b / T_c^\circ \quad (11)$$

$$T_c^\circ = T_b / (0.533272 + 0.191017 \times 10^{-3} T_b + 0.779681 \times 10^{-7} T_b^2 - 0.284376 \times 10^{-10} T_b^3 + 0.959468 \times 10^{28} / T_b^{13}) \quad (12)$$

where T_c and T_b are in °R.

Results and Discussion

The Roess, Brule and Twu correlations gave satisfactory T_c predictions for the petroleum-derived jet fuels. The Riazi and Daubert correlation and the Cavett correlation predicted T_c moderately well and the Kesler and Lee correlation gave a less satisfactory T_c prediction for petroleum-derived fuels. All of the methods failed to predict T_c satisfactorily for coal-derived jet fuels. The methods were developed either for petroleum fractions—which are composed mainly of paraffinic compounds—or for coal fluids—which consist mainly of aromatic compounds. Because coal-derived jet fuels are dominated by cycloalkanes,[9] the methods presented above may not be applicable to these fuels. While all of the methods predict T_c quite well for the paraffins and aromatics, they all fail to predict T_c satisfactorily for the cycloalkanes. Clearly a new correlation is needed.

The new correlation must be developed based on the properties of coal-derived jet fuel compounds—namely monocyclic and bicyclic alkanes and some hydroaromatics. **Table 1.42-1** shows the selected model compounds and related properties (i.e., specific gravity, boiling point, and critical temperature) which were used to develop the correlation for coal-derived fuels. All data were obtained from the API Technical Data Book[3] and the functional form of the Roess equation[3] was used to regress the T_c data in Table 1.42-1. Using the method of least squares, we obtained the following correlation with a coefficient of 0.99695:

$$T_c = 138.98 + 2.1132\Delta - 1.4085 \times 10\text{-}3\Delta 2 \quad (13)$$

The definition of Δ is given in equation (2). For all 25 compounds in Table 1.42-1, this correlation resulted in an average absolute deviation of 0.86% and a maximum deviation of 2.75%, indicating a good fit of the data and an acceptable prediction of critical temperatures for coal-derived fuel samples.

Table 1.42-1. Model Compounds and Related Properties for Correlation Development for Coal-Derived Jet Fuels.

Compound Name	SG, 60/60 °F[a]	Normal T_b, °F[a]	T_c, °F[a]
cyclohexane	0.7835	177.33	536.70
methylcyclohexane	0.7748	213.68	570.27
ethylcyclohexane	0.7921	269.21	636.80
cis-1,2-dimethylcyclohexane	0.8006	265.51	631.40
trans-1,2-dimethylcyclohexane	0.7803	256.01	613.40
cis-1,3-dimethylcyclohexane	0.7704	248.16	604.40
trans-1,3-dimethylcyclohexane	0.7892	256.01	617.00
cis-1,4-dimethylcyclohexane	0.7873	255.78	617.00
trans-1,4-dimethylcyclohexane	0.7670	246.83	602.60
n-propylcyclohexane	0.7981	314.10	690.80
isopropylcyclohexane	0.8064	310.57	684.90
n-butylcyclohexane	0.8034	357.70	740.93
isobutylcyclohexane	0.8161	340.32	729.05
sec-butylcyclohexane	0.8172	354.70	710.17
tert-butylcyclohexane	0.8168	340.83	702.39
bicyclohexyl	0.8900	462.27	848.93
cis-decalin	0.9018	384.47	804.38
trans-decalin	0.8755	369.16	777.02
1-methyl-cis-decalin	1.0146	469.40	899.53
9-ethyl-cis-decalin	0.8900	451.00	837.77
9-ethyl-trans-decalin	0.8648	437.00	817.27
tetralin	0.9748	405.77	836.60
1-methyl-tetralin	0.9623	429.06	835.25
1-ethyl-tetralin	0.9569	463.23	860.00
1-n-propyl-tetralin	0.9480	493.52	880.36

[a] All data are from API Technical Data Book (1987).

[1] Hicks, C. P. and C. L. Young. "The Gas-Liquid Critical Properties of Binary Mixtures." *Chem. Rev.* 1975. 75. 119.

[2] Mogollon, E., W. B. Kay, and A. S. Teja. "Modified Sealed-Tube Method for the Determination of Critical Temperature." Ind. Eng. Chem. Fundam. 1982. 21. 173.

[3] *API Technical Data Book—Petroleum Refining.* 4th Ed. Washington, DC: American Petroleum Institute. 1987.

[4] Cavett, R. H. "Physical Data for Distillation Calculations: Vapor-Liquid Equilibria." Paper presented to 27th Mid-Year Meeting of the API Div. Ref. 1962. 42(III). 351.

[5] Kesler, M. G. and B. I. Lee. "Improved Prediction of Enthalpy of Fractions." *Hydrocarbon Process.* 1976. 3. 153.

[6] Riazi, M. R. and T. E. Daubert. "Simplify Property Predictions." *Hydrocarbon Process.* 1980. 59. 115.

[7] Brule, M. R. et al. "Multiparameter Corresponding-States Correlations of Coal-Fluid Thermodynamic Properties." AIChE J. 1982. 28. 616.

[8] Twu, C. H. "An Internally Consistent Correlation for Predicting the Critical Properties and Molecular Weights of Petroleum and Coal-Tar Liquids." *Fluid Phase Equil.* 1984. 16. 137.

[9] Lai, W.-C.et al. "Pyrolytic Degradation of Coal- and Petroleum-Derived Jet Fuels and Middle Distillates." *Prepr. – Am. Chem. Soc., Div. Fuel Chem.* 1992. 37. 1671.

1.43 Surface Effects on Deposit Formation in a Flow Reactor System

This study is explained in detail in *Advanced Thermally Stable Jet Fuels Technical Progress Report, October – December 1994.*

Introduction

Flow reactor systems are equally or more valuable than static reactor systems for performing mechanistic studies of jet fuel thermal stability. There are two types of flow reactors—(1) constant-heat-flux, resistant-heated long tube flow reactors[1] and (2) constant-surface-temperature, jacket-heated short tube flow reactors.[2] The constant-surface-temperature type flow reactor generally has better temperature control over the reactor and the fuel. For this study involving metal surface effects on deposit formation from thermal stressing of jet fuel (JP-8P), we used our renovated reactor, which is, in essence, a constant-surface-temperature type reactor.

Results and Discussion

Gas Phase Analysis. A set of JP-8P thermal reactions was run at temperatures from 450°-625°C under varying conditions—first without metal coupons (baseline), then with nickel coupons, copper, and stainless steel coupons inserted in the reactor.

Neither the reaction products nor their distributions changed with the addition of the nickel coupons or changes in reaction time. Using copper and stainless steel surfaces and raising the temperature to 625°C, resulted in greater increases in the conversion of higher end hydrocarbons to smaller compounds compared to earlier nickel tests. However, the cracking products and their distributions did not change with reaction time.

The conversion of large molecules and products distribution with or without metal coupons involved is shown in **Figures 1.43-1** and **1.43-2**. More larger molecules were converted to small compounds (e.g., pentane or hexane) as temperature increased from 600°C with nickel surface to 625°C with copper and stainless steel surfaces. The conversion is lower without any metal coupons than with (1) copper or stainless steel at the same temperature and (2) nickel coupons at a lower temperature. This is not conclusively proven, however, because the mean residence time in the neat jet fuel runs was shorter. Figure 1.43-2 shows that, while the conversion increases with the presence of metal coupons, the distribution of the products does not seem to change. This indicates that the current metal coupon surface does not significantly alter the bulk cracking chemistry; this can likely be attributed to the small area of metal exposed to the reactants. (The metal coupons were 1, 3, 5, 7, and 9 cm long and 0.5 cm wide.)

Deposit Morphology. Less than 1μg of deposit formed on any of the nickel coupons after 5-10 hours of thermal reaction, despite the fact that the coupons were discolored. Using an SEM we observed a few deposit particles scattered on the coupon surface. The particles did not have a preference to the surface sites. After another 10-hour test, aggregates of deposit are visible on the nickel surface. In two cases, the aggregates, which most likely result from gas-phase, chain-like carbon black, grew to cover some extended areas, forming a thick deposit layer taking the shape of a substrate surface. Our findings suggest that the nickel surface has little effect on the incipient deposition on the surface under the conditions we studied.

With the copper coupons, heavy deposition was observed after a 5-hour test at 625°C. For example, 37μg of deposit formed on a 5 x 90mm copper coupon. The coupons became brittle after the reaction and colonies of deposit aggregates were observed on their surfaces. The aggregates were formed of entangled whisk carbon. The copper surface was first covered by a thin layer of arrow-head carbon deposit, similar to those reported by Albright.[3] The copper surface was considerably more active than the nickel surface at a lower temperature.

More deposit was formed with the stainless steel coupons; in fact, the reactor became clogged after 3 hours of reaction. The deposit was spherical and was aggregated in chains to form particulate mound. The deposit most likely formed in the gas stage.

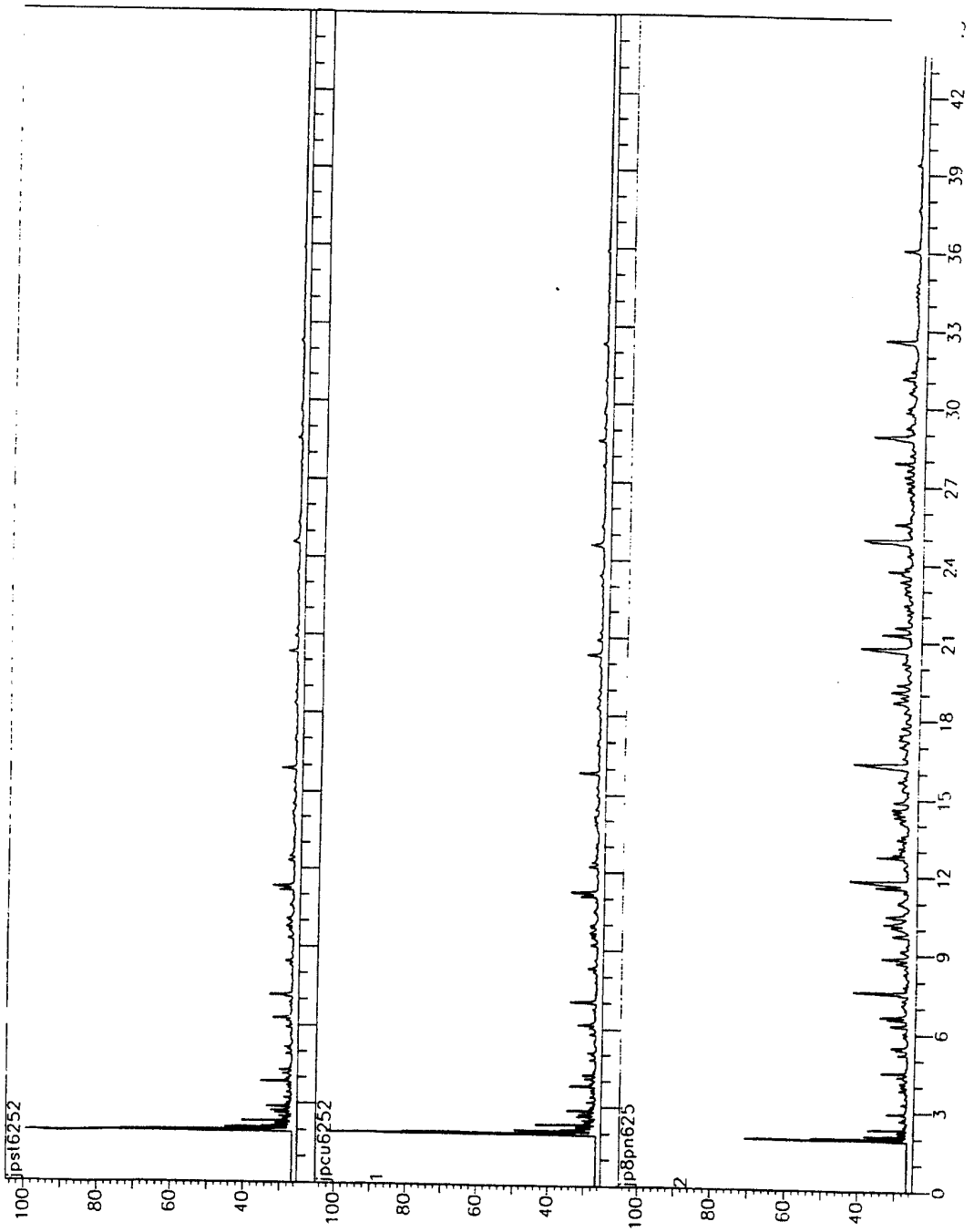

Figure 1.43-1. Comparison of Conversion and Products Distribution of JP-8P after Thermal Reaction without Metal Coupons and with Nickel, Copper, and Stainless Steel in the Flow Reactor

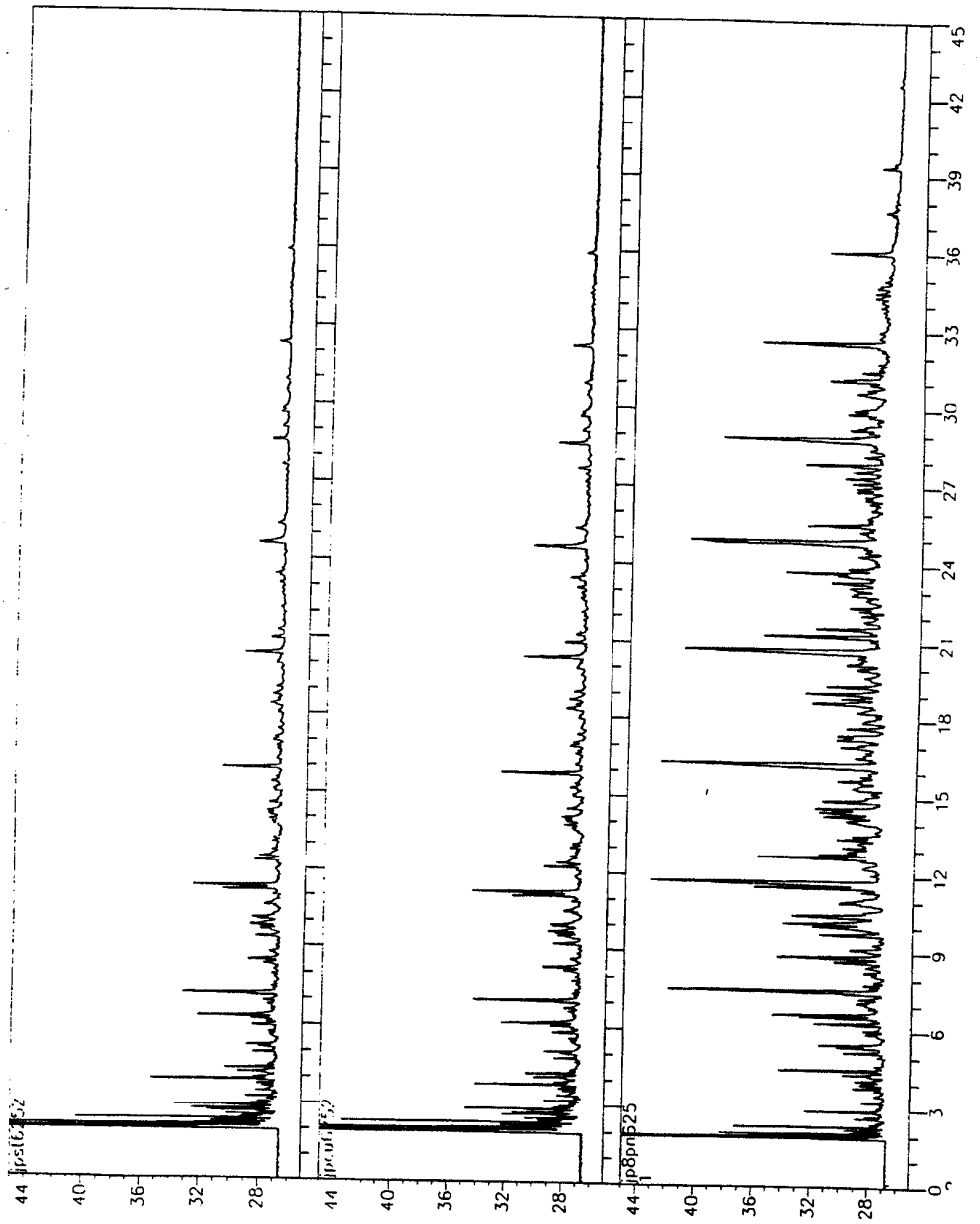

Figure 1.43-2. Zoom In of Figure 1.43-1

[1] Marteney, P. J. and L. J. Spadaccini. J. Eng. Gas Turbines & Power. 1986. 108. 648-653.

[2] Chin, J. S., A. H. Lefebvre, and F. T. Y. Sun. J. Eng. Gas Turvines & Power. 1992. 114. 353-358.

[3] Albright, L. F. and T. C. Tsai. *Pyrolysis: Theory and Industrial Practice.* New York: Academic Press. 1983. 233-254.

1.44 The Study of Quantitative Structure-Thermal Stability Relationships in the Pyrolysis of Hydrocarbons

This study is explained in detail in *Advanced Thermally Stable Jet Fuels Technical Progress Report, January – March 1995.*

Introduction

In this exercise we attempted to apply the Quantitative Structure-Property Relationships (QSPR) method to the study of thermal stability of jet fuels, particularly pure hydrocarbons. The general QSPR method, with a set of united quantum, experimental, and topological descriptors, is the most promising means for developing predictive structure-thermal stability quantitative correlation. The simplest method of chemical structure description in terms of Benson groups was performed in searching for structure-property relationships for a small set of hydrocarbon compounds that we studied previously. Molecular connectivity as a structure-based approach to chemical QSPR analysis was tested and demonstrated the need for further development of both experimental database and computational methods.[1], [2]

Method of Quantitative Structure-Activity or Structure-Prroperty Relationships (OSAR/OSPR)

Molecular mechanisms involved in chemical reactions of complex organic compounds are generally too complex or not sufficiently understood to allow development of a detailed model to predict chemical properties of an untested molecule. Nevertheless, by using a statistical model derived from a large set of molecules (for which the property of interest is known), structure-property relationships can be established. In other words, the molecular structures are characterized by various descriptors used for developing multiple regression model equations to relate the descriptor to the property. The overall approach is shown in **Figure 1.44-1**.[3]

The main steps involved in computer-assisted SPR study are:

1. Input and storage of molecular structures with known property of interest in topological notation
2. Calculation of molecular structure descriptors for each molecule in the data set, testing the descriptors for their significance and considering only those that are not highly correlated with each other
3. Using multivariate regression analysis (both linear and nonlinear) to obtain quantitative structure-property correlations and applying the pattern recognition methods to search for the best set of descriptors
4. Testing the predictive ability of the obtained SP correlation.

Experimental

Our research included the design, testing and application of computer software for the purpose of deriving QSPR and, ultimately, developing the capability to predict thermal stability for unknown compounds. Our approach involved the graphical entry and storage of structures, molecular connectivity descriptor calculation, and multiple linear regression analysis of available experimental data sets.

Conclusions

We attempted to use the method of QSPR; however, the number of available experimental data points would not allow us to generate an equation with good predictive ability. While the structure-property approach revealed a strong potential as a tool for chemical property prediction, it could not be used for eclectic data sets, as was the case in these studies. The absence of reliable experimental data within the range of jet fuel performance conditions precludes using the method effectively.

Given these results, we concluded that a standard procedure of thermal stability should be developed. In particular, we should use the rate of solid deposit formation under standard conditions as the measure of thermal staiblity.

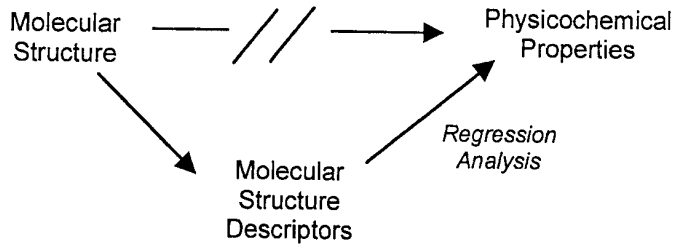

Example Properties: Retention indices, Boiling points, Octane numbers

Example Descriptors: Molecular weight, Surface area, Molecular connectivity indices

Figure 1.44-1. Schematic Diagram of Structure-Property Relationship Study

[1] Kier, L. B. and L. H. Hall. *Molecular Connectivity in Chemistry and Drug Research.* New York: Academic Press. 1976.

[2] Kier, L. B. and L. H. Hall. *Molecular Connectivity in Structure-Activity Analysis.* Letchworth: Research Studies Press Ltd. 1986.

[3] Jurs, P. C., P. J. Hasan, and R. H. Rohrbaugh. *Prediction of Physicochemical Properties of Organic Compounds from Molecular Structure.* Berlin, Schloss Korb, Italy: Springer-Verlag. 1988.

1.45 THE STUDY OF HYDROCARBON DEGRADATION USING THE QUANTITATIVE STRUCTURE-PROPERTY RELATIONSHIP METHOD

This study is explained in detail in *Advanced Thermally Stable Jet Fuels Technical Progress Report, July—September 1995.*

Introduction

This section of the report describes the continuing study of hydrocarbon degradation with the Quantitative Structure-Property Relationship (QSPR) method. As shown previously,[1] this method has a strong potential as a tool for prediction of chemical properties. In this work, the general QSPR analysis was performed using a set of united constitutional, topological, geometrical, electrostatic, and quantum-chemical descriptors. The same experimental data as in the previous study[1] were considered.

Preliminary Results

The first data set represents the experimental conversion results for 13 compounds after 4-hour high-pressure pyrolysis at 450°C.[2] This set was considered for linear regression analysis using comprehensive descriptors. The correlation obtained, based on three descriptors, is given by

$$C = (-134.85 \pm 34.069) + (134.92 \pm 18.437)\alpha_1 - (1237.2 \pm 383.08)\alpha_2 - (5.706 \pm 2.57)\alpha_3 \qquad (1)$$

where α_1 is internal entropy of the molecule at 300 K divided by the number of atoms in the molecule, α_2 is relative positive charge, and α_3 is Kier shape index (order 3). The values of multiple correlation coefficient, R^2, and standard deviation, S^2, are 0.9023 and 174.75, respectively. It is worthwhile to point out that S^2 is an absolute (not relative) standard deviation. **Figure 1.45-1** shows the comparison of the performance of the previously obtained equation,[1] based on topological descriptors only, and equation (1).

The correlation one-descriptor correlation

$$C = (-37.873 \pm 14.819) + (85.957 \pm 12.816)\beta_1 \qquad (2)$$

also shows reasonable agreement in terms of R^2 and S^2 (0.8035, 287.55). The parameter β_1 in equation (2) is the vibrational entropy of the molecule at 300 K divided by the number of atoms in the molecule. **Figure 1.45-2** presents the comparison of predictions of equation (2) and the correlation based on topological descriptors only.[1]

The second experimental data set used for the QSPR search contains the results of the Monsanto group[3] in the form of kinetic parameters and rate constants obtained in static tests (high pressure, 700 K). The linear equations for $\ln(k_0)$ have been generated in the form of

$$\ln(k_0) = 24227. - 6092.9\gamma_1 - 153.17\gamma_2 - 109.78\gamma_3 \qquad (3)$$

where γ_1 is average valency of a C atom, γ_2 is maximum total bond order of a C atom, and γ_3 is average atomic nucleophilic reaction index for a C atom. The multiple correlation coefficient

is 0.9925 and standard deviation is 0.0329. **Figure 1.45-3** shows the performances of the topology-reduced (with 5 descriptors used)[1] and the comprehensive (with 3 descriptors used) QSPR applications.

The similar equation for the average rate constant for decomposition of saturated cyclic hydrocarbons is given by

$$k_{av} = 0.0486 + 0.00835\lambda_1 - 0.0546\lambda_2 - 0.0414\lambda_3 \quad (4)$$

where λ_1 is weighted positive surface area, λ_2 is Kier & Hall index (order 2), and λ_3 is number of rings. The values of R^2 and S^2 are 0.93 and 0.0016, respectively. **Figure 1.45-4** presents the comparison of performance of the topology-based equation[1] and equation (4).

All calculations were carried out with the CODESSA package developed by the group of Prof. A. R. Katritzky at Florida Sate University.[4] The input files for all compounds studied were generated using the MOPAC 5 code.[5]

Conclusion

The QSPR method based on comprehensive descriptors applied to the processes of hydrocarbon thermal degradation demonstrated better performance as compared to the approach based on topological descriptors only. The correlations based on comprehensive descriptors require a smaller number of parameters to obtain the same quality of predictions.

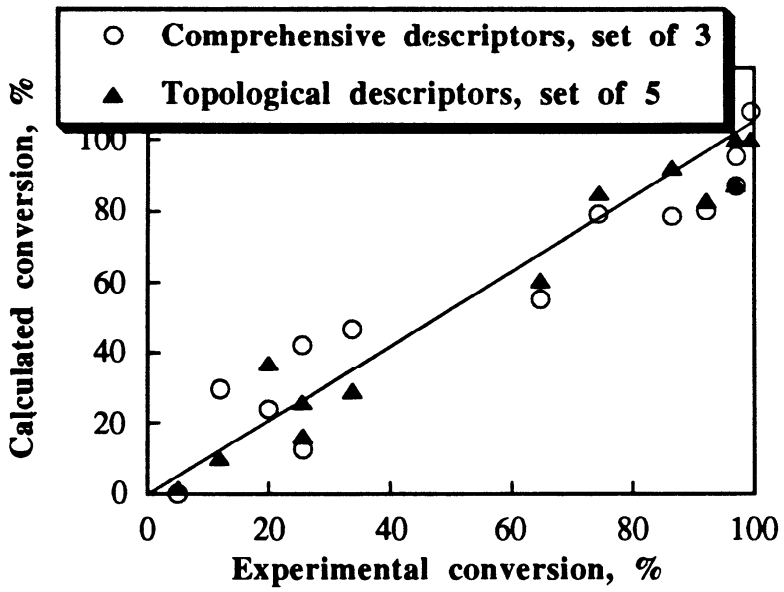

Figure 1.45-1. Comparison of the Calculated and Experimental Conversion after 4-Hour High-Pressure Pyrolysis at 450°C. Correlations with 5 Topological Descriptor Set, 3 Comprehensive Descriptor Set, and In-house Experimental Data.

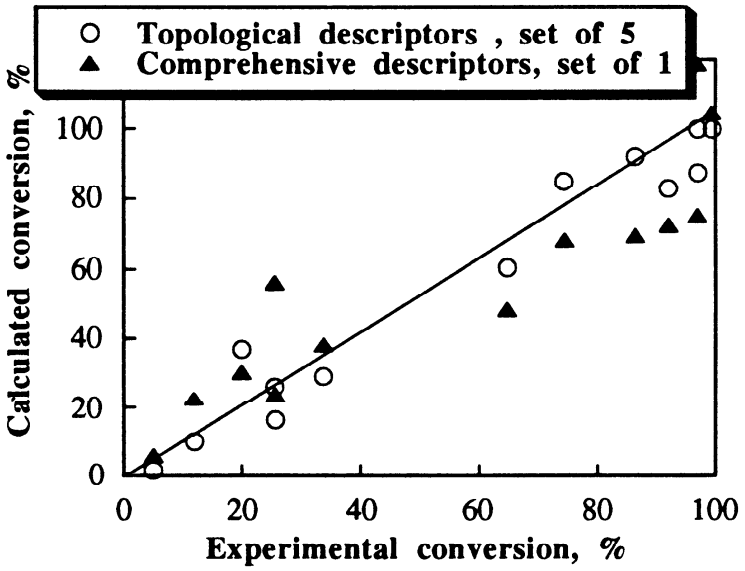

Figure 1.45-2. Comparison of the Calculated and Experimental Conversions. Correlations with 5 Topological Descriptor Set, 1 Comprehensive Descriptor Set, and In-House Experimental.

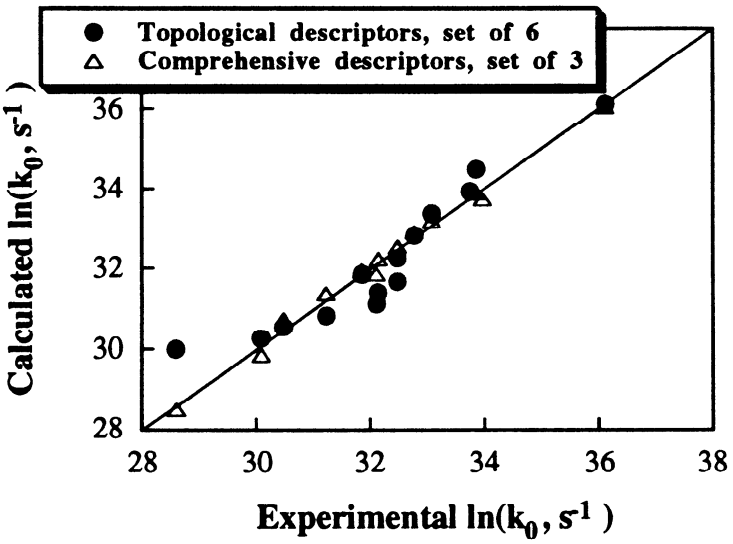

Figure 1.45-3. Comparison of the Calculated and Experimental ln(k_0). Correlations with 5 Topological Descriptor Set, 3 Comprehensive Descriptor Set, and Literature Survey.

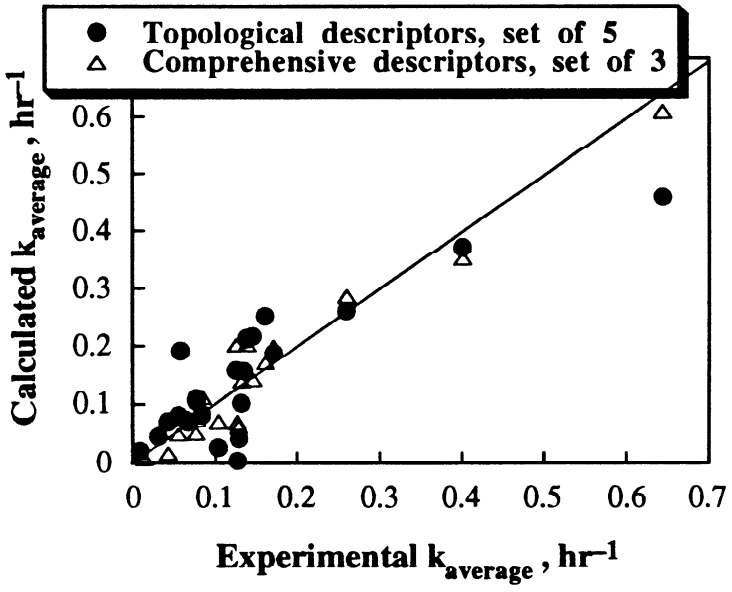

Figure 1.45-4. Comparison of the Calculated and Experimental Average Rate of Decomposition of Saturated Cyclic Hydrocarbons. Correlations with 5 Topological Descriptor Set, 3 Comprehensive Descriptor Set, and Literature Survey.

---

[1] Kazakova, E. *The Study of Quantitative Structure Stability Relationships in the Pyrolysis of Hydrocarbons.* Department of Material Science & Engineering, The Pennsylvania State University. 1995.

[2] Schobert, H. H. et al. *Advanced Thermally Stable Jet Fuels, Technical Progress Report, July — September 1995.* The Pennsylvania State University. #92PC92104-TPR-13. 1995.

[3] Fabuss, B.N., J.O. Smith, and C.N. Satterfield. *Advances in Petroleum Chemistry and Refining.* Eds. Kobe, K.A. & McKetta, J.J. Interscience Publishers: New York. 1964.

[4] Katritzky, A., V. Lobanov, and M. Karelson. *CODESSA*: *Comprehensive Descriptors for Structural and Statistical Analysis*. University of Florida, Gainesville. 1995.

[5] Stewart, J. J. P. Quantum Chemistry Exchange Program. Indiana University, Bloomington, Indiana. 1983. (455).

1.46 CHARACTERIZATION AND DEGRADATION STUDIES OF COAL- AND PETROLEUM-DERIVED AVIATION JET FUELS AND MIDDLE DISTILLATES

This study is explained in detail in *Advanced Thermally Stable Jet Fuels Technical Progress Report, April — June 1995*

Introduction

The thermal stability of jet fuels plays an important role in the design and development of future high Mach aircraft. The fuel in future hypersonic aircraft may experience temperatures in the range of 400-500°C considerably higher than the current maximum operating temperature (< 300°C) for the conventional aviation jet fuels. When fuels are exposed to such high temperatures, serious pyrolytic degradation of the fuels occurs and will result in the formation of solid deposits on critical aircraft systems such as fuel pipelines, filters, and engine parts. As a result, advanced jet fuels will be required for hypersonic aircraft. The development of such fuels warrants detailed study of pyrolytic degradation of hydrocarbon fuels. Future fuels could derive from petroleum or hydrocarbon resources such as coal, tar sands, and oil shale.

This exercise focused on the characterization and degradation of ten fuels four coal-derived fuels and six petroleum-derived military and commercial jet fuels. One objective of this work was to enhance the intrinsic stability of jet fuels by optimizing fuel composition. Many of the physical and chemical properties of fuels (e.g., volatility and critical properties) are determined by distillation curve. Thus, we allowed the distillation curves to serve as guidelines in the formulation of future candidate surrogate distillate fuels, which offer the advantage of exploring the effects of fuel chemical composition on stability at a manageable level because they are composed of relatively fewer hydrocarbons.[1]

Distillation curves generally were obtained from simulated distillation data by GC; however, the results were susceptible to several error sources. In this work, the simulated distillation curves were determined by thermogravimetric analysis (TGA), a reliable and rapid tool for this purpose.

In short, we ranked the stability of current fuels, identified thermally stable compounds in fuels, and elucidated the relative stabilities of the fuels by their chemical composition. The thermal stability study was carried out in tubing bomb reactors at 450°C under N_2. The thermo-oxidation stability of fuels was examined by high-pressure differential scanning calorimetry (DSC). In other words, the onset temperature for the oxidation exotherm of the fuels was used as the oxidation stability criterion and was measured by DSC under dynamic mode (temperature linearly increasing).

Experimental.

Samples. The four coal-derived fuels included JP-8C from hydrotreating of liquids produced from the Great Plains Gasification plant[2] and middle distillates derived either from direct coal liquefaction or indirect coal liquefaction. The six petroleum-derived military and commercial jet fuels included JPTS (thermally stable jet fuel), JP-7, JP-8P, JP-8P2, Jet A, and Jet A-1. The fuel densities ranged from 0.76 g/cm^3 (FI-MD) to 0.96 g/cm^3 (WI-MD), with most

falling in a smaller range of 0.79 to 0.81 g/cm^3 (JPTS, JP-7, JP8P, Jet A, Jet A-1, and JP-8P2). The densities of JP-8C and HRI-MD were 0.84 and 0.92 g/cm^3, respectively.

Thermal analysis. The simulated distillation experiments were carried out with samples of about 7 mg and a purge gas (N_2) flow of 200 cm^3/min. The temperature was programmed from 25° to 425°C at a heating rate of 10°C/min.

Product chemical analysis. The chemical composition of the fuels were characterized using gas chromatography (GC) and gas chromatography - mass spectrometry (GCMS) with the help of temperature-programmed retention indices.[3]

Further details on experimental and analytical procedures are presented in the corresponding Technical Progress Report.[4]

Conclusions

We concluded that the oxidative and thermal stability of the fuels is significantly affected by their chemical composition. The oxidative and thermal stability of ten fuels were studied in a DSC and a tubing bomb reactor, respectively. The compositions of the stressed and neat fuels were all qualitatively and quantitatively characterized by GC-MS and GC and the simulated distillation curves were determined by TGA. All the information is useful in explaining and evaluating the thermal stability of fuels.

The order of oxidative stability is Jet A > JP-8P > Jet A-1 > JP-7 ≈ JPTS > FT-MD > JP-8C. There seems to be an inverse relationship between oxidative stability (in terms of oxidation onset temperature) and thermal stability (in terms of less solid deposit formation). We identified the relative thermal stabilities of the whole fuels and of the hydrocarbons in the fuels. The fuels containing the most 1-3 ring cycloparaffins and/or hydroaromatics were more stable (in terms of less gas formation) than those fuels containing more long-chain paraffins. The former includes JP-8C, HRI-MD and WI-MD, and the latter covers the remaining seven fuels. Among the paraffinic fuels, we observed higher stability (in terms of less gas formation) for those fuels having narrower distribution of paraffins with relatively shorter chains (e.g., Jet A-1). The fuels with lower aromatics content and higher hydrogen-donor compounds exhibited less solid formation . Overall, coal-derived JP-8C and HRI-MD had the best thermal stability among the ten fuels studied, both in terms of less gas and less solid formation.

---

[1] Wood, C. P. et al. *J. Propulsion.* 1989. 5 (4). 399-405.

[2] Song, C. et al. *Energy & Fuels.* 1993. 7. 234-243.

[3] Lai, W.-C. and C. Song. *Fuel.* 1995.

[4] Schobert, H. H. et al. *Advanced Thermally Stable Jet Fuels, Technical Progress Report, April — June 1995.* The Pennsylvania State University. #92PC92104-TPR-12. 1995.

1.47 THE USE OF SITE-SPECIFIC ^{13}C LABELING TO EXAMINE THE THERMAL DEGRADATION OF JET FUEL COMPONENTS

This study is explained in detail in *Advanced Thermally Stable Jet Fuels Technical Progress Report, April—June 1995*.

Introduction

Earlier we made a strong argument in favor of using site-specific ^{13}C labeling to examine the reactions of target components in complex mixtures such as jet fuel (Section 1.23). The ^{13}C label serves as a flag for tracing chemical transformations that occur in complex organic matrices. Two analytical approaches have been used to examine the ^{13}C isotope flags and determine the structural changes that occur during thermal stressing. The method developed by Burnham et al utilizes doubly-^{13}C-labeled substrates and gas chromatography-mass spectrometry to examine thermal stressing reaction kinetics.[1] The second method utilized by McKinney et al employs ^{13}C-labeling in combination with ^{13}C NMR to examine the reaction pathways and kinetics of the thermal stressing of 1-phenyl-1- ^{13}C-hexane in a JP-8C jet fuel.[2] The primary drawback of such studies is the cost of obtaining site specific ^{13}C-labeled substrates to carry out the reactions. This study provided an update of our efforts to obtain additional ^{13}C-labeled jet fuel components for future thermal stressing experiments.

Experimental

General Reaction Scheme. Reagent grade chemicals were purchased from Aldrich Chemicals and each reaction was carried out, first without any ^{13}C-labeled precursor to optimize the reaction conditions for each of the steps shown in Scheme 1.[3] The K^{13}CN was purchased from Isotech, Inc. and will be employed using the optimized reaction conditions.

Detailed descriptions of the optimized reaction conditions for synthesis of 6-^{13}C-dodecane and 1-cyclohexyl-^{13}C-hexane appear in a subsequent report.

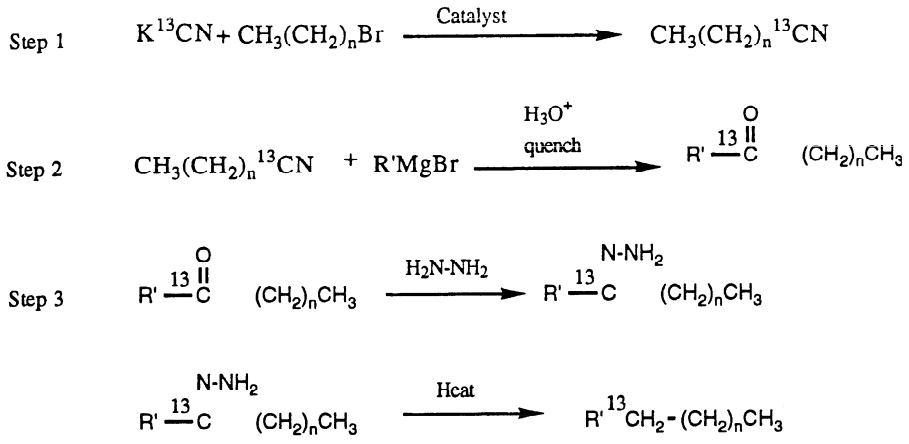

Scheme I

Thermal Stressing 1-Phenyl-1-^{13}C-Hexane for Isotope Ratio Monitoring Mass Spectrometry. Pyrolysis experiments for 1-phenyl-1-^{13}C-hexane were carried out in a 15 mL tubing bomb reactor at 400°C for heating periods of 1, 2, 4, and 6 hours under an initial inert pressure of 6.9 MPa UHP-N_2 (cold). The 15 mL stainless steel reactor was loaded with 5 mL of JP-8C and 0.05 mL of 1-phenyl-1-^{13}C-hexane and purged repetitively with 6.9 MPa UHP-N_2 (3 times) to remove oxygen/air in the reactor or dissolved sample. Following reaction, the reactor was removed from the fluidized sand bath and quenched in a cool water bath. Only the liquid product was collected from the reaction and each bomb was examined by gas chromatography.

Instrumentation. Quantitative gas chromatography (GC) was carried out on each sample using a Hewlett-Packard 5890 II gas chromatograph with flame ionization detection (FID) equipped with a J&W DB-5 fused silica column (30 m, 0.25i.d., 0.25um film thickness).

Results and Discussion

The results of synthesis of 6-^{13}C-dodecane is reported in detail later in this document. Each step was optimized with unlabeled materials to ensure that the maximum amount of ^{13}C-labeled product was produced. Following the synthesis of 6-^{13}C-dodecane, a set of thermal stressing experiments were carried out in JP-8C in an identical manner to those performed on 1-phenyl-1-^{13}C-hexane.[3] The products and kinetics of the pyrolysis reactions were determined by gas chromatography and ^{13}C NMR and are also reported later.

The determination of the optimal synthetic protocol for 1-cyclohexyl-1-^{13}C-hexane was carried out concurrently with the thermal stressing experiments discussed above. Once synthesized, thermal stressing experiments and product analysis were carried out on the 1-cyclohexyl-1-^{13}C-hexane using the conditions established for the ^{13}C-labeling experiments.[3]

In an effort to obtain additional information concerning the thermal stressing of jet fuel components, a second set of pyrolysis experiments was carried out on 1-phenyl-1-^{13}C-hexane. Isotope ratio monitoring experiments was used to examine all of the products that carried the ^{13}C label. This method of analysis is extremely sensitive and enables researchers to identify products that would be difficult to identify using ^{13}C NMR methods, because they are present in such low concentrations. Once identified, a more complete picture of the reaction pathways of the ^{13}C-labeled components can be established.

---

[1] Burnham, A.K., H. R. Gregg, and R. L. Braun. *Energy Fuels.* 1995. 9. 190.

[2] McKinney, D.E., J. M. Bortiatynski, P. G. Hatcher. *Energy Fuels.* 1993. 7. 578

[3] Schobert, H.H. et al. *Advanced Thermally Stable Jet Fuels, Technical Progress Report*. The Pennsylvania State University. #92PC92104-TPR-6. 1994.

1.48 EFFECT OF CARBON SURFACES ON THERMAL DECOMPOSITION OF HYDROCARBONS

This study is explained in detail in *Advanced Thermally Stable Jet Fuels, Technical Progress Report, October—December 1996.*

Introduction

In our previous studies we showed that the presence of high surface area activated carbon PX-21 and other activated carbons prevented solid deposition on reactor walls and reduced the extent of decomposition of *n*-dodecane.[1] We have suggested that the active sites of PX-21 carbon act to stabilize the pyrolysis products and enhance the H-transfer reactions.

Active surface area is one of the important characteristics of solid carbons. Crystallite sizes and structural order of graphitic planes are two major factors that determine the active surface area. The active surface area can be measured by surface cleaning and oxidation followed by a temperature programmed desorption (TPD) experiment. The active sites that contribute to the active surface area are the most probable location for chemisorption on the carbon surface. When high surface activated carbons are exposed to air, all available active sites chemisorb oxygen. These active sites are the same positions that interact with reactive species during thermal decomposition of hydrocarbons.

In this study we investigated the influence of oxygen complexes present on the carbon surface on thermal decomposition of *n*-dodecane and solid deposition during thermal stressing. We also investigated the effects of some other solid carbons (carbon fibers and a carbo*n*-coated monolith) on thermal decomposition of *n*-dodecane.

Experimental

A full explanation of the thermal stressing and analysis appears in the corresponding Technical Progress Report.[2]

Results and Discussion

1. Effects of Carbon Fiber Addition on Thermal Decomposition and Solid Deposition. Assessing the results obtained with the Amoco Thornel Carbon Fibre, the BET surface area measurement showed that all of the fibers had surface areas smaller than 10 m^2/g after activation, indicating that the activation of these fibers was not successful under the conditions used. The GC data of the liquid products from thermal decomposition of dodecane with these fibers also showed that the fiber addition was not effective in inhibiting the conversion of *n*-dodecane, even when approximately 1 gram of fiber was used in the experiments. Deposition of carbon on the reactor was inhibited to some extent because of the amount of carbon fiber placed in the reactor.

Of the other commercially produced carbon fibers that were tested, even those with a higher surface area produced comparable results to those obtained with the activated Amoco Thornel Fiber. The carbonaceous deposit formation on the reactor walls was also inhibited to some extent with these activated carbon fibers, presumably because of the displacement of deposition from metal to the added carbon surface.

Dow Corning s Honeycomb (DCH) monolithic structure was tested with *n*-dodecane. The specific surface area of the monolith was considerably less than those of the other solid

carbons tested. The analysis of the liquid product obtained with the honeycomb structure showed, however, that its performance was comparable to that of PX-21. Since a larger quantity of DCH was used, the total carbon surface area added in the experiments with DCH (620 m^2) was greater than that added by PX-21 (260 M^2). The DCH showed a larger weight gain (300 mg) compared to that by PX-21 (100 mg) in a comparable experiment. The solid deposition on the reactor wall was also much less with DCH than with PX-21. More experiments with DCH are needed to understand the activity of DCH during thermal decomposition of *n*-dodecane before conducting tests with jet fuel samples.

2. Analysis of Hexane Extract of Stressed PX-21 and Characterization of PX-21 before and after Thermal Stressing Using XRD. The stressed PX-21 was extracted with hexane, then the extracted solvent was analyzed by GC/MS. Major components of the extract were naphthalene, long straight chain alkanes up to C_{29}, and some alkylbenzenes. The presence of long straight chain alkanes up to C_{29} is noteworthy. High molecular weight *n*-alkanes and naphthalene tend to concentrate on the PX-21 surface. The longest chain *n*-alkane detected in the liquid products from the experiments with PX-21 was C_{20}. These findings suggest that the recombination of radicals to form longer straight chain alkanes takes place on the carbon surface. The recombination reactions and the adsorption of the resulting long chain alkanes would, in turn, reduce the number of radicals in the reaction system and, thereby, lower the overall rate of thermal decomposition. This result could be taken as another evidence for the stabilizing effect of the added carbon surface on thermal decomposition of hydrocarbons. It should be noted, however, that all of the analyses are carried out on the products which are cooled to room temperature. Some of the products we observed could have formed during quenching of the reactors.

The analysis of PX-21 before and after thermal stressing by XRD demonstrated that approximately the same amount of deposit was collected on the PX-21 surface (100 mg) as that of the initially added PX-21. There were slight, but consistent changes in the crystallite parameters upon stressing PX-21 with *n*-dodecane under different conditions. With the increasing extent of stressing, the stressed PX-21 showed a decreasing crystallite diameter (smaller L_a), but increasing crystallite height (L_c), and interlayer spacing (d). The N_2-BET surface area of PX-21 decreases drastically from 2600 m^2/g to 2 m^2/g in the course of thermal stressing. We concluded that the carbonaceous deposit is a less ordered material than the original PX-21 (smaller L_a and greater d). The progressively increasing crystallite heights of the stressed PX-21 suggest a more or less parallel stacking of the deposited material (consisting presumably of large aromatic ring systems) on PX-21. Unlike other activated carbons, PX-21 has a fairly well ordered structure, because it was derived from an anisotropic petroleum coke.

3. Analysis of Gas Products of Thermal Decomposition of *n*-Dodecane with/without PX-21. The gas products from thermal stressing were analyzed by GC/TCD. The concentration of CO_2 in the gas products obtained from the thermal decomposition of *n*-dodecane with PX-21 results from the desorption of oxygen surface groups, which takes place at high temperatures. Our experiments showed that approximately 1 mmol of CO_2 evolves from the carbon surface when one gram of PX-21 is heated at 450°C for 3 hours in a closed tubing bomb reactor. No CO evolved under these conditions, because the temperature is too low for decomposition of surface groups which produces CO. The desorption of CO_2 creates active sites on the carbon surface

which can readily interact with the reactive species or free radicals generated by pyrolysis of hydrocarbons.

For short reaction times (i.e., 1 and 2 hours), we made two observations regarding the gas product of *n*-dodecane pyrolysis in the presence of PX-21: it contains more H_2, suggesting that the carbon surface is active in hydrogen shuttling/transfer reactions, and methane concentrations are lower. We also observed that the presence of PX-21 produces higher concentrations of ethane, but lower concentrations of ethylene. Higher ethane and lower ethylene concentrations with PX-21 can be attributed to the stabilization of ethyl radicals (formed by β-scission reactions) on the carbon surface.

Conclusions

This study provided additional evidence of the activity of carbon surfaces in stabilizing free radicals during thermal stressing of *n*-dodecane, using different solid carbons, including a Dow Corning carbon-coated ceramic monolith. It appears that the activity of a carbon surface can be closely related to the concentration and nature of surface oxygen groups. Our data suggest that these surface groups decompose at stressing temperatures to create active sites which readily interact with hydrocarbon free radicals.

---

[1] Gergova, K., et al. Preprints, ACS Div. Pet. Chem., New Orleans, LA. 1996. 41(2). 513.

[2] Schobert, H. H. et al. *Advanced Thermally Stable Jet Fuels, Technical Progress Report, October - December 1996.* The Pennsylvania State University. 1996.

1.49 THE STUDY OF QUANTITATIVE STRUCTURE-THERMAL STABILITY RELATIONSHIPS IN THE PYROLYSIS OF HYDROCARBONS

This study is explained in detail in *Advanced Thermally Stable Jet Fuels, Technical Progress Report, July—September 1997*

Introduction

The present limits for fuel stability regimes are 436 K for JP-4, JP-5, JP-8, and 561 K for JP-7.[1] The overall objective of this study is to develop a tool to accurately predict the bulk thermal stability of a complex mixture of hydrocarbons and, thereby, aid in the design of aircraft fuels.

The objective of Step I of the study was to be able to predict thermal stability of pure organic compounds based solely on the knowledge of their molecular structures. This involves the use of all available experimental data and any tests that may be needed to supplement the data. The objective of Step II is to thoroughly test the predictive technique developed in the first part of the study and develop a method for calculating thermal stability of mixtures from the properties of their components. The step included testing of the developed technique.

Background

1. Overall Approach. We chose to use a statistical treatment of a large set of molecules (for which the property of interest is known) to establish structure-property relationships of complex organic compounds. This enabled us to characterize the molecular structures by various descriptors that are used for developing multiple regression model equations to relate the descriptor to the property.

2. Method of Computer-Assisted SPR Study. The main steps involved in the computer-assisted SPR study are:

- Input and storage of molecular structures with known property of interest in topological notation
- Calculation of molecular structure descriptors for each molecule in the data set, testing the descriptors for their significance and considering only those that are not highly correlated with each other
- Utilization of the multivariative regression analysis (both linear and nonlinear models) to obtain quantitative structure-property correlations, application of the pattern recognition methods to search for the best sets of descriptors
- Testing the predictive ability of the obtained SP correlation.

The research included the design, testing and application of computer software for the purpose of deriving QSPR and, thus, developing the capability to predict thermal stability for unknown compounds. The approach involved the graphical entry and storage of structures, the molecular connectivity descriptor calculation, and a multiple linear regression analysis of available experimental data sets.

There are two general aspects that can be identified in a molecule molecular topology and molecular topography. Generally, molecular structure descriptor modules are developed according to the complete information provided by both aspects. Descriptor sets fall into five classes: constitutional, topological, geometrical, electronical, and physicochemical. However, the molecular connectivity method considers dimensional aspects of a structure to be directly dependent on the molecular topology. Therefore, a descriptor module can be reduced to only one class topological descriptor. Although this approach does not work well with heterogeneous data sets, it performs well for properties that have a fundamental additive nature and it is considerably less complex than other approaches in terms of descriptor set. Therefore, we chose to test its performance in searching for the structure-thermal stability correlations and compare the results with those obtained using full descriptor modules.

3. QSPR Terminology. A complete definition of QSPR terms is provided in the corresponding Technical Progress Report.[2]

QSPR Calculations

1. Methodology. We used codes that were developed in-house to carry out the topology index calculation and linear regression analysis in the frame of these indices.[3] The CODESSA software[4] was used to develop the QSPRs within the comprehensive descriptor sets.

We first entered and stored the molecular structures and the dependent variables, using the in-house program GRAPH to store data files in the form of connection tables combined with property columns.

We next performed a descriptor calculation. The search of topology-only based SP correlation was conducted within the frame of Kier and Hall molecular connectivity indices up to the order of 6,[5] as they appear appreciably better than other topological indices in terms of correlation coefficients and standard error. At the same time the comprehensive QSPR study provides the calculation of all types of descriptors. These descriptors are described in detail in the corresponding Technical Progress Report.[2]

Following the descriptor calculation, we used objective feature selection to reduce the multitude of descriptors to a manageable number. The descriptors with a large number of identical values or missing for some compounds in the data set were eliminated from the descriptor module. Various heuristic techniques were used to find the multicollinearities and exclude the related descriptors.[4]

From the remaining descriptors, models were generated using multiple linear regression analysis. The output of the regression analysis included the regression coefficients with their mean square errors and t-values, the standard deviation of the regression S^2, the square of the regression correlation coefficient R^2, and the F-value of the regression. Finally, the derived models had to be validated; we chose to use internal validation procedures.

2. Results. The data for this study were obtained from four different sources:

- Results of experiments on conversion of 13 cyclic hydrocarbons
- Kinetic parameters (14 compound set) and rate constant for 23 saturated cyclic hydrocarbons

- Decomposition reaction rate for 38 saturated hydrocarbons
- Decomposition temperature of 85 hydrocarbons of various nature.

A complete explanation of our attempts to find the QSPR correlation between structure and thermal stability and the resulting models that we developed were presented in the corresponding Technical Progress Report.[2] The same data sources were considered in testing the general QSPR analysis performance.

The first three experimental data sources were used only for the purpose of testing the proposed QSPR method as the possible tool for thermal stability prediction. The limited number of available experimental values within each set did not allow us to statistically validate the obtained correlations.

The last data set was a various hydrocarbon abstraction presented by Fabuss.[6] The property that had been correlated with structure descriptors was the decomposition temperature. Decomposition temperature was determined in a high pressure isoteniscope for 80 naphthenic and 9 paraffinic hydrocarbons, although only 85 experimental points were used in the study described here. When we compared the calculated versus observed values of decomposition temperature, the correlation was poor. Several reasons could account for this: (1)the experimental error (±6 F°), as noted in the Fabuss paper,[6] (2) the isoteniscope decomposition temperature is not the best property to use to measure thermal stability, and (3) the clustering of DT values in the area of 680-750 F° with not enough data outside the pointed range. Based on these reasons, we omitted statistical approval of the model.

3. Conclusions. This study demonstrated the application of QSPR techniques to the problem of thermal stability prediction for groups of hydrocarbons. Multiple linear regression analysis was used to build various mathematical models that describe thermal stability as a linear function of parameters derived from the structure of compounds. The QSPR method, based on comprehensive descriptors applied to hydrocarbon thermal degradation, performed better than the approach based on topological descriptors only. The correlations based on comprehensive descriptors required a smaller number of parameters for the same quality of predictions. The structure-property approach has strong potential as a tool for development of reliable structure-thermal stability correlation.

---

[1] Roquemore, W.M. et al. *Prepr. - Amer. Chem. Soc., Div. Petr. Chem.* 1989. 34. 841.

[2] Schobert, H. H. et al. *Advanced Thermally Stable Jet Fuels, Technical Progress Report, July - September 1997.* The Pennsylvania State University. 1997.

[3] Kazakova, E. Department of Material Science & Engineering, Pennsylvania State University, 1995.

[4] Katritzky, A., V. Lobanov, and M. Karelson. University of Florida, Gainesville. 1995.

[5] Kier, L.B., and L. H. Hall. Molecular Connectivity in Chemistry and Drug Research. Academic Press, New York. 1976.

[6] Fabuss, M.A. et al. *Journal of Chemical and Engineering Data.* 1963. 8. 64.

1.50 CLARIFICATION OF KEY INTERACTIONS AMONG FUEL COMPONENTS

This study is explained in detail in *Advanced Thermally Stable Jet Fuels, Technical Progress Report, January-March 1998*.

Introduction

We previously reported on the importance of cycloalkanes in fuel thermal stability.[1, 2] Decalin was chosen as a representative cycloalkane deriving from hydrogenation of liquids from coal and n-tetradecane from the petroleum stock. In this study, we demonstrate how, at different temperatures, the concentration of cycloalkanes in a mixture plays an important role.

Experimental

Two mixtures containing 5 and 30 mol% of decalin (*cis*-/*tran*-decahydronaphthalene or DHN) added to *n*-tetradecane (TD) to make up a total volume of 5 ml were charged into a 25 mL microautoclaves.[2] To remove entrapped air, the system was degassed 6 times with 1000 psi of ultra high purity N_2. Under a final pressure of 100 psi N_2, the mixtures were stressed for 2 hours with a continuos vertical movement of 40 evolutions per minute in a fluidized sandbath at 400, 450 and 500¡C. After reaction the microautoclaves were rinsed of sand and purged into water for 3-5 seconds. When cooled to ambient temperature, the gas phase and liquid fraction were removed for analysis using GC and GC-MS. The tube and the stem of the microautoclave were washed in pentane until clear color and dried; the amount of solid deposition was determined from the weight gain.

Results and Discussion

At 400¡C, only 1% gas had developed (a broad distribution from methane to butane) for both the 5 and 30 mol % mixtures. Increasing the stressing temperatures to 450¡C resulted in a dramatic rise in the amount of gas produced, where the 5 mol% system contained 27% gas compared to only 17% for the 30 mol%. The former mixture also developed 1% solids at this temperature. The solid deposition becomes important at 500¡C, where the 5 mol% mixture has 12% deposition compared with 10% for the one containing 30% DHN. The latter also produces less gas at this temperature, where the distribution has been shifted to the lighter gases.

The quantitative GC traces show that little degradation had taken place at 400¡C. At 400¡C only alkanes were detected (11-12 wt %) which increased sharply for the 5 mol% mixture to nearly 40% at 450¡C, while the 30% mixture was just around 25%. At this temperature, the aromatic compounds began to gain importance (10-14%), while at 500¡C there were practically no aromatic compounds left. From a stability point of view, the more cycloalkanated mixture retained more liquid yield at different temperatures and more of the original material than the 5 mol% DHN system.

---

[1] Lai, W.C. and C. Song. *Fuel Proc. Tech.* 1996. 48. 1-27.

[2] Song, C. et al. *Energy & Fuels*. 1993. 7. 234-243.

1.51 PHASE EFFECTS ON FUEL DEGRADATION AND SOLID DEPOSITION

This study is explained in detail in *Advanced Thermally Stable Jet Fuels, Technical Progress Report, January—March 1998*.

Fuel thermal degradation under supercritical conditions involves a variety of simultaneous reactions of hundreds of compounds, including long-chain alkanes, alkylbenzenes, alkylcyclohexanes, decalins and tetralins. In order to understand fuel degradation chemistry, we must examine not only the reactions of single model compounds typical of jet fuels, but also those of the mixtures of model compounds. The studies on pure model compounds can provide mechanistic information, while the studies on mixtures can address the question of how individual compounds interact with each other during the thermal reactions of jet fuels.

We previously presented the results from the thermal decomposition of some typical jet fuel model compounds, including C_{10}—C_{14} *n*-alkanes, *n*-butylbenzene (BBZ), *n*-butylcyclohexane (BCH), decalin, and tetralin, under sub-critical and supercritical conditions. In this work, the thermal decomposition of some binary mixtures of jet fuel model compounds was studied under subcritical and supercritical conditions. Five binary mixtures were used in this study, including *n*-C_{12}/*n*-C_{10}, *n*-C_{12}/*n*-C_{14}, *n*-C_{12}/BBZ, *n*-C_{12}/BCH, and BBZ/BCH. Every mixture consisted roughly of 50 wt% of each component. Thermal stressing experiments were carried out in a Pyrex glass tube reactor and reaction products were analyzed by GC and GC/MS.

Reaction Rates. The changes in conversions of individual model compounds with reaction time were obtained from the thermal decomposition of the mixture at 425¡C for 15 to 60 minutes. We found that the conversion of one compound was affected by the presence of the second compound. While the conversions for the decomposition of *n*-C_{12} in the *n*-C_{12}/*n*-C_{14} mixture were higher than those for the decomposition of pure *n*-C_{12}, the conversions of *n*-C_{12} in *n*-C_{12}/*n*-C_{10} mixture were slightly lower than those for the decomposition of pure *n*-C_{12}. This suggested that the lighter alkane inhibited the decomposition of the heavier one while the heavier alkane accelerated the decomposition of the lighter one.

For the thermal reactions of the *n*-C_{12}/BBZ mixture and the *n*-C_{12}/BCH mixture, we found that the presence of BBZ accelerated the decomposition of *n*-C_{12} and the presence of BCH inhibited the decomposition of *n*-C_{12}. The increased decomposition rate of *n*-C_{12} in the presence of BBZ can be explained by the increased radical concentration for the decomposition of *n*-C_{12}, resulting from the much faster initiation reaction of BBZ. The increase in radical concentration leads to an increase in the rates of hydrogen abstraction from *n*-C_{12} and, thus, an increase in *n*-C_{12} decomposition rates. On the other hand, the addition of BCH to *n*-C_{12} reduces the radical concentration for the decomposition of *n*-$C_{12,}$ because some of the radicals produced from *n*-C_{12} decomposition abstract hydrogen atoms from BCH instead of *n*-C_{12}.

For the thermal decomposition of BBZ in the presence of *n*-C_{12} or BCH, we found that *n*-C_{12} and BCH exhibited very similar inhibiting effects on the decomposition of BBZ. This is probably caused by very comparable hydrogen abstraction rates from C_{12} and BCH by free radicals. The decomposition of BBZ is inhibited by the addition of *n*-C_{12} or BCH because some of the radicals, which would abstract hydrogen atoms from BBZ in the absence of *n*-C_{12} or BCH, instead abstract hydrogen atoms from *n*-C_{12} or BCH. The rates of hydrogen abstraction from *n*-

C_{12} and BCH are comparable; therefore, both compounds exhibit similar inhibiting effect on the decomposition of BBZ.

Product Distributions. We identified the major reaction products from sub-critical and supercritical phase thermal decomposition of binary mixtures. For *n*-alkane mixtures, the reaction products were similar to those resulting from thermal reactions of pure compounds. In the case of *n*-C_{12}/BBZ, *n*-C_{12}/BCH, and BBZ/BCH mixtures, the reaction products included both those found in the decomposition of the pure compounds and those found only in the mixture reactions. The product distributions were affected by reaction conditions; supercritical conditions favored the formation of saturated compounds and high-molecular-weight compounds, and sub-critical conditions facilitated the formation of alkenes.

Our thermal decomposition studies on binary mixtures were extended to include the mixtures of *n*-C_{12}/decalin and *n*-C_{12}/tetralin. The *n*-C_{12}/decalin mixture consisted of approximately 50% wt of *n*-C_{12} and 50%wt of decalin (26%wt of *trans*-decalin and 24 %wt of *cis*-decalin), and small amounts of impurities. The *n*-C_{12}/tetralin mixture consisted of approximately 49.2%wt of *n*-C_{12}, 50% wt of tetralin, and small amounts of impurities. Thermal stressing experiments were carried out in glass tube reactors and reaction products were analyzed by GC and GC/MS.

We found that the addition of decalin or tetralin suppressed the decomposition of *n*-$C_{12,}$ although both compounds exhibited different inhibiting effects. While the addition of decalin led to a small reduction in *n*-C_{12} conversion, the addition of tetralin significantly reduced the decomposition of *n*-C_{12}. For example, for the thermal decomposition of pure *n*-C_{12}, the *n*-C_{12}/decalin mixture, and the *n*-C_{12}/tetralin mixture with a loading ratio of 0.36, the conversions of *n*-C_{12} at 425¡C for 60 minutes were 20.9, 17.9, and 4.1, respectively.

The reaction products from thermal decomposition of two mixtures were affected significantly by the reaction conditions. Under low-pressure conditions, the reaction products were mainly those found from the thermal stressing of the pure compounds. Under high-pressure supercritical conditions, however, the reaction products included both those found in the pure compound experiments and those compounds unique to the mixture reactions. For the *n*-C_{12}/decalin mixture, the unique products were a series of alkyldecalins whose detailed molecular structures remain to be determined. In the case of *n*-C_{12}/tetralin mixture, the unique products were two series of alkyltetralins with alkyl chains containing 2—11 carbon atoms. One was 1-alkyltetralin and the other was 2-alkyltetralin. The yields of 1-alkyltetralins were significantly higher than those of 2-alkyltetralins.

TASK 2. INVESTIGATION OF INCIPIENT DEPOSITION

2.1 Growth and Deposition of Particles During Heating of Coal-Derived Aviation Gas Turbine Fuels

This study is explained in detail in *Advanced Thermally Stable Jet Fuels Technical Progress Report, August 1992 – October 1992.*

Introduction

The ultimate objective of this work is to describe particle and deposit growth in sufficient detail and with sufficient accuracy to simulate the fuel composition, pressure, temperature, heating rate, oxygen, impurity and time dependencies of suspended particle concentration. The deposit formation exhibits an induction period, during which deposit formation is slow, followed by a period of rapid growth, then a decline in deposition rate as deposit-forming species are depleted. The ability to simulate this behavior is considered a critical test of any model. The accuracy of a model depends on the uncertainties associated with the measurement of relevant variables, such as weight change, species concentration, particle size, temperature, pressure, and the overall reproducibility of the tubing bomb. Reported uncertainties in experimental measurements demonstrate whether the observed scatter in measured quantities is related to the physical or chemical phenomena occurring in the system or to flaws in the measurement system or experimental protocol.

Deposit formation occurs by addition of reactive species at the wall of the reactor, as well as by gravitational settling of particles formed in bulk phase. Stabilization of reactive species by hydrogen donors present in the fuel occurs simultaneously. Solid formation is determined by the competition among addition of active species to already-formed particles, direct addition to the wall, and stabilization by hydrogen donors.

The following section summarizes a series of studies designed to further define the growth and deposition of particles under conditions comparable to those expected to occur in next generation, high-performance aircraft.

a. Initial Examination of Deposits

This study is explained in detail in *Advanced Thermally Stable Jet Fuels Technical Progress Report, August 1992 – October 1992.*

Purpose: To begin investigating formation and growth of deposits from jet fuels under high temperature conditions

Conditions: 6 hours of heating at 450°C under nitrogen in a tubing bomb reactor

Findings:

- Solid carbonaceous deposits formed on all of the inside surfaces of the reactor
- Deposits on vertical walls were pyrolytic; deposits on the bottom surface contained both pyrolytic carbon and mesophase, suggesting that gravitational settling may be the primary route for deposition of suspended particles on the bottom surface.
- An examination of deposition rate per unit of reactor volume indicated that only a small fraction of suspended particles were in the size range that settles at a significant rate, and

that the primary mechanism of deposit formation was diffusive transport of reactive species or small particles through the fluid to the wall.

b. Quantitative Comparison of Settling and Deposition Rates

This study is explained in detail in *Advanced Thermally Stable Jet Fuels Technical Progress Report, November 1992 – December 1992.*

Purpose: To make a quantitative comparison of settling and deposition rates

Conditions: Mixtures of JP-8C and tetradecane covering the entire range of compositions were stressed for 6 hours at 450°C under nitrogen. The following components were individually collected and weighed:

- Deposit on reactor bottom
- Deposit on side walls of reactor
- Deposit on reactor top
- Suspended particles separated from the liquid by filtration

Findings:

- The product of particle concentration and settling velocity was equated to the average rate of deposit growth per unit area on the bottom of the reactor. Particle sizes were determined to have reached a steady state in 6 hours and varied from 1.7 to 2.1 μm—near the 3 μm peak observed in the size distributions from part (a) of this study.
- The size of the settling particles was insensitive to the particle formation and deposition rates. Settling, therefore, is a plausible mechanism for the growth of deposits on the bottom of the reactor.
- Future analyses should attempt to account for the presence of larger particles (10 μm) in the samples, and a measurement of the density of the particles will be needed to better estimate their settling velocity.

c. Effect of Formation and Deposition Reactions of a Particular Class of Reactive Species on Rate of Deposit Growth and Formation of Suspended Particles

This study is explained in detail in *Advanced Thermally Stable Jet Fuels Technical Progress Report, January 1993 – March 1993.*

The diameter of particles present in suspension at steady state is a function of the concentration of the intermediaries, their diffusion coefficients, the densities of particles and fluid, and the fluid viscosity.

Objective: Determine if the formation and deposition reactions of a particular class of reactive species could explain the observed rate of deposit growth on the walls of the reactor and/or the rate of formation of suspended particles.

Conditions: Mixtures of tetradecane and coal-derived jet fuel containing 18.45 wt% tetradecane were stressed at 450°C under an initial nitrogen pressure of 0.69 MPa. Reactors were purged with nitrogen 8 times to remove residual oxygen. Stress times varied from 2 to 24 hours.

Findings:

- The deposit formation had an induction period of ≈4 hours, followed by a steady rise in solid formation up to 22 hours, after which little additional deposit was formed.
- Particle concentration was measured as a function of time to examine whether the concentration would become steady at long times. The steady value was determined by the competition between particle formation and deposition on the reactor bottom.
- A time dependence of the particle concentration could not be established.
- Additional measurements at short, intermediate, and long times are needed.

d. Further Testing of Gravitational Settling Theory

This study is explained in detail in *Advanced Thermally Stable Jet Fuels Technical Progress Report, April 1993 – June 1993.*

Objective: To further test premise that the growth of deposit on the bottom of a tubing bomb reactor could be explained by gravitational settling of particles formed in suspension, refining both the initial measurements and calculations.

Conditions: Mixtures containing 81.5 wt% of JP-8C and 18.5 wt% of tetradecane were used. The sizes of suspended particles and the masses of deposits on the side walls and bottom of the rector were measured as a function of time, from 2 to 18 hours at 450°C under nitrogen.

Measurements: Measurements consisted of:

- Deposit on reactor bottom
- Deposit on side walls of reactor
- Size distribution of suspended particles
- Concentration of suspended particles at longer times

A particle-sizing instrument was obtained and used to determine the size of suspended particles within an hour of the end of the stressing period. This equipment was not available on-site for previous studies, for which measurements could only be made several days after the stressing period. The benefits of this instrument became apparent when deposit growth was graphed. The graph had a differently shaped curve and indicated that the instantaneous deposition rate at 6 hours was twice the average rate of the period from 0 to 6 hours.

To discriminate settling from direct addition, we subtracted the observed deposit mass per unit area on the vertical wall from the observed deposit mass per unit are on the bottom, to correct for the contribution of direct deposition at the bottom. These data were differentiated by dividing mass/area increments by time increments to determine the time dependence of the deposition rate. This indicated a period of formation of reactive species from precursors in the initial mixture, followed by a period of rapid deposit growth, and, finally, a period of declining deposition rate as the precursors were depleted.

Particle size distribution changed little during the first 8 hours. A period of rapid growth followed, with size increasing 1 to 4 μm from 8 to 12 hours. Little increase occurred from 12 to 16 hours.

Calculations: Settling velocities were calculated as the difference between gravitational and buoyant forces per Stokes' law for viscous drag, assuming fuel vapor completely and uniformly filled the enclosure. Specific-surface-area-weighted-mean particle sizes were used for the calculations.

The average rate of deposit growth per unit area on the bottom, assuming the particle concentration and mean size are uniform throughout the reactor, was calculated as the product of particle concentration and settling velocity.

Findings: The calculated settling rates agreed with the measurements at 8 hours. At the longest times, however, they exceeded the measured rates by a factor of 100. This could be attributed to the fact that many of the large (4 μm) particles that were suspended in the liquid product had actually settled to the bottom of the reactor during stressing, but were not strongly attached to the deposit. Resuspension of these particles on opening and emptying the tubing bomb would cause an overestimation of both the size of suspended particles and the suspended particle concentration, leading to a high value for the calculated deposition rate.

Future studies should focus on shorter times, during which particles are still growing and the mechanism and rate of attachment of particles to a deposit.

e. Further Examination of Initial Stages of Decomposition and the Onset of Deposition

This study is explained in detail in *Advanced Thermally Stable Jet Fuels Technical Progress Report, July 1993 – September 1993.*

Objective: To further refine the measurements of deposit growth, with emphasis on the initial stages of decomposition of the fuel and the onset of deposition.

Conditions: Mixtures containing 81.5 wt% of JP-8C and 18.5 wt% of tetradecane were used.

Measurements: Sizes and concentrations of suspended particles were measured after stressing the mixture for 2, 4, 6, 9, and 24 hours at 450°C under nitrogen. The top of the reactor was simplified by filling in the end cap cavity to create a perfectly flat top surface with only a 4 mm hole to which a pressure gauge is attached. This new design provided more uniform depositions, simplifying sample collection. Assuming that particle size and concentration are quasi-steady, with particle formation from relative species just balanced by loss due to settling, deposition rates per area were calculated as the product of settling velocity and particle concentration.

Findings:

- Deposition on the bottom rose more rapidly in the new design, but the qualitative features of the time dependence were similar in both reactors out to 24 hours.
- Between 4 and 8 hours, the calculated and observed rates closely agreed. Under 4 hours the calculated growth of deposits was underestimated; over 8 hours it was greatly overestimated.
- Two concerns arose with our findings: (1) more measurements were needed during the period when the particles were growing to sizes that settle at significant rates and (2) the sizes of particles separated from the liquid products increased markedly after 12 hours, causing an even more dramatic increase in the calculated settling. (This could be caused by particles that settled to the bottom at long times but were not strongly attached to the

deposit and were, therefore, included in the measurements of suspended material.) Future studies should focus on the formation at times shorter than 8 hours, where the settling model seems to provide a satisfactory estimate of deposition rates.

- Earlier studies showed that the yield of insoluble material was approximately proportional to the initial tetradecane concentration. GC-MS analysis of the liquid remaining after stressing indicated that the early stages of the decomposition were approximately pseudo-first-order, with a characteristic time of 4 hours. Comparison with the deposit growth measurements performed in this study indicate that the time constant for growth is similar, suggesting a relatively simple model consisting of a first-order decomposition step leading to reactive intermediates, followed by reaction of the intermediates to form particles, and settling of the particles.

f. Further Examination of the Onset and Initial Stages of Decomposition

This study is explained in detail in *Advanced Thermally Stable Jet Fuels Technical Progress Report, October 1993 – December 1993.*

Previous studies, which compared the formation rate of the particle surface area with the deposition rate per unit of the wall area, showed that the rates were approximately the same, suggesting that similar species and reactions could be involved in both processes. If so, the wall and suspended particles would compete for the same pool of reactive species.

Objective: To begin development of a global kinetic scheme for quantitatively describing the factors controlling solid formation.

Conditions: Mixtures containing 81.5 wt% of JP-8C and 18.5 wt% of tetradecane treated in a 20 mL batch reactor at 450°C under nitrogen (initially at 100 psi).

Calculations: Precursors in the fuel are assumed to form reactive intermediates that deposit on the surfaces of the reactor and on the surfaces of suspended particles. The reactive intermediates also react with hydrogen donors to form stable products. Ignoring the particles (because the total amount of material forming particles and settling to the bottom is small), the following reactions were calculated:

- Formation of reactive species
- Hydrogenation of reactive species
- Addition of reactive species to surface

Findings:

- Results of the equation are shown in **Figure 2.1-1**. Although the profile exhibits an induction period, during which the pool of intermediates is building up to a steady value, it is much less pronounced than the observed induction period.
- In the simple mechanism, each molecule of tetradecane that disappears produces a reactive intermediate. Because the steady concentration of intermediates is small and the rate of decomposition of tetradecane relatively fast, the calculated concentration of intermediates reaches the steady value very quickly. This indicates that a more detailed mechanics is needed to describe the behavior of the system at short times.

g. Development of a Global Kinetic Scheme for Solid Formation

This study is explained in detail in *Advanced Thermally Stable Jet Fuels Technical Progress Report, January 1994 – March 1994.*

Objective: To refine a global kinetic scheme for quantitatively describing the factors controlling solid formation.

Conditions: Mixtures containing 81.5 wt% of JP-8C and 18.5 wt% of tetradecane heated at 450°C for 6 hours, in a 20 mL batch reactor initially charged with 10 mL of liquid and 100 psi nitrogen.

Figure 2.1-2 shows the measurements of the tetradecane dependence of the total mass of particles and deposits formed under the time and temperature conditions described above. The total mass of solids is approximately linear over the range from the concentration of tetradecane occurring naturally in the jet fuel up to 100% tetradecane. These data suggest that a global model for the system could be useful; however, based on the nonlinear behavior when small amounts of tetradecane were added, a more detailed treatment of the system is likely needed.

Figure 2.1-3 shows the dependence of deposit mass/area on stressing time at a fixed initial concentration of tetradecane in JP-8C (18.5 wt% added, 25.8 wt% total). We were concerned with the wall deposit, choosing to exclude the contribution from settling of particles on the bottom of the reactor. The deposit exhibits and induction period, during which deposit formation is slow, followed by a period of rapid growth, then a decline in deposition rate as deposit-forming species are depleted. Our goal was to develop a model that simulated these results.

The concentration of tetradecane remaining unreacted was determined by gas chromatography/mass spectrometric analysis. The decay was approximately exponential for times up to 6 hours , consistent with a pseudo-first-order reaction. Destruction of a tetradecane molecule, F, is assumed to be directly associated with production of ν_{RF} molecules of reactive intermediates, R, according to the reaction:

$$F \xrightarrow{k_F} \nu_{RF}R$$ Decomposition of fuel precursor and formation of reactive species

The first order rate expression for tetradecane decomposition, with boundary condition $F = F_o$ at $t = 0$, gives $F = F_o \exp(-k_F t)$. The initial concentration of tetradecane, F_o, was 0.43 kmol/m^3. A value, $k_F = 1.1 \times 10^{-4}$ s^{-1}, was estimated for the rate coefficient from a semi-logarithmic plot of the measurements.

The reactive intermediates formed by decomposition of tetradecane may follow three paths:

$\nu_{RH,i}R + H_i \xrightarrow{k_{H,i}}$ stable products	Stabilization of reactive species by hydrogen donor
$R + D \xrightarrow{k_D} D$	Addition of reactive species to deposit on wall
$R + P \xrightarrow{k_P} P$	Particle growth

where H = hydrogen donor
D = deposit
P = particles
F is measured in kmol/m^3
D is measured in kg/m^2
P is measured in kg/m^3

The rate expressions for the formation or disappearance of the four types of species are:

$$\frac{dR}{dt} = \nu_{RF} k_F F - R \Sigma \nu_{RH,i} k_{H,i} H_i - k_D R A_W - k_P R P S_P \quad (1)$$

$$\frac{dH_i}{dt} = - R \Sigma k_{H,i} H_i \quad (2)$$

$$\frac{dD}{dt} = k_D R W_R \quad (3)$$

$$\frac{dP}{dt} = k_P R W_R P S_P \quad (4)$$

The boundary conditions are R = 0, Hi = $H_{i,o}$, D = 0, and P = P_o at t = 0. The stoichiometric coefficient, ν_{RF}, the number of reactive intermediates formed from each tetradecane molecule, was set equal to 2, and the average molecular weight of reactive intermediates, W_R, was assigned the value 99 kg/kmol (one-half of tetradecane). A_W is the area of wall per unit of reactor volume, 240 m^{-1}. S_P is the specific surface area of the particles, $6/(\rho_P d_P)$, where ρ_P is particle density (1300 kg/m^3) and d_P is the specific-surface-area-weighted mean particle size. The time-dependent mean particle size is found by rearranging equation 4, dividing by the number concentration (number of particles per m^3) to obtain the rate of increase in mass of a single particle having the specific-surface-area-weighted mean size:

$$\frac{dm_P}{dt} = k_P R W_R \pi d_P^2 \quad (5)$$

$$\frac{dd_P}{dt} = \frac{2 k_P R W_R}{\rho_P} \quad (6)$$

with boundary condition $d_P = d_{P,o}$ at t = 0. The initial "particles" are species having molecular dimensions (e.g., polycyclic aromatic hydrocarbons present in the fuel), which serve as the nuclei for particle formation through addition of reactive intermediates. The initial size, $d_{P,o}$, was assigned the value 1 nm.

The results were not sensitive to the choice of initial size because the initial volume of a particle soon becomes a negligible part of its total volume. The results, however, were sensitive to the value chosen for the initial particle nucleus concentration, P_o, which determines the number concentration of particles over the entire evolution of the contents of the reactor, in the present model.

Hydrogen donors were divided into two broad groups—tetralin plus substituted tetralins and decalin plus substituted decalins. Their initial concentrations were 0.18 and 0.36 kmol/m^3 (24 and 50 kg/m^3), respectively. The stoichiometric coefficients, $\nu_{RH,1}$ and $\nu_{RH,2}$, the numbers of reactive intermediates stabilized by a single hydrogen donor, were both set equal to 1. There is no allowance in the present mechanism for the formation of tetralins and decalins from other classes of compounds, or the formation of tetralins from decalins.

Integration of equations (1), (2), (3) and (6) gives the evolution of the concentrations of tetralins and decalins, mean particle size, and deposit mass/area. The model was fit to the measurements by adjusting the rate coefficients $k_{H,1}$ and $k_{H,2}$, for reaction of tetralins and decalins with reactive intermediates, the rate coefficients k_D and k_P, for addition of reactive intermediates to deposit and particles, respectively, and the initial concentration of particle nuclei. The values for the rate coefficients were:

$k_{H,1} = 2.5 \times 10^{-4}$ m^3/(kmol s) (tetralins + reactive intermediates)

$k_{H,2} = 1.5 \times 10^{-4}$ m^3/(kmol s) (decalins + reactive intermediates)

$k_D = 3.5 \times 10^{-8}$ m/s (reactive intermediates + deposit)

$k_P = 2 \times 10^{-9}$ m/s (reactive intermediates + particles)

These values are completely dependent on the mechanism and assumptions outlined above, and the values chosen for other adjustable parameters such as the stoichiometric coefficients. Calculations of deposit mass/area, particle size, and concentrations of tetralins and decalins are shown in **Figures 2.1-3, 2.1-4, 2.1-5**. Qualitative features of the formation of the deposit, disappearance of hydrogen donors, and growth of particles were successfully reproduced by the simple mechanism.

Particle growth accounts for destruction of only a small fraction of the reactive intermediates formed from tetradecane at short times. Therefore, the introduction of particles into the mechanism did not significantly influence the rate of deposit growth at short times, and the model does not exhibit the pronounced induction period observed in the measurements of deposit mass/area. A feature of the model associated with this problem is the simple treatment of formation of the reactive intermediates responsible for deposit growth, which were presumed to appear instantaneously on destruction of tetradecane. The induction period can likely be accounted for by introducing two types of intermediates—one intermediate formed directly on decomposition of tetradecane, but slow in reacting with deposits, and another intermediate produced from the first by further reactions, which are the reactive species directly responsible for deposit growth. Another feature that the mechanism lacks is a route for production of particle nuclei (e.g., small polycyclic aromatic hydrocarbons) from other species, in addition to the present assumption that nascent particles are present in the coal-derived fuel.

h. Further Examination of the Onset and Initial Stages of Decomposition

This information was compiled from three quarterly reports:

- *Advanced Thermally Stable Jet Fuels Technical Progress Report, July – September 1994*
- *Advanced Thermally Stable Jet Fuels Technical Progress Report, October – December 1994*
- *Advanced Thermally Stable Jet Fuels Technical Progress Report, January – March 1995*

Basic Mathematics of Error Analysis

We used Moffat's method[1,2] of evaluating uncertainties in experimental results. Suppose X_i is a variable with known uncertainty, δX_i, then X_i and its uncertainty is represented by:

$$X_i = X_i \text{ (measured)} \pm \delta X_i \qquad \text{(20:1 odds)} \qquad (1)$$

This equation asserts:

- The best estimate of X_i is X_i (measured)
- There is an uncertainty in X_i that may be as large as $\pm\delta X_i$
- The odds are 20 to 1 against the possibility of Xi being outside of the range X_i (measured) $\pm$ δX_i.

A full mathematical description of equation (1) has been provided by Schobert et al.[3]

Single Sample and Multiple Sample Analysis

Most exploratory research experiments are single-sample experiments. In this study, single sample analysis was applied to the measurement of species concentrations, weight change of the reactor, and particle size. Multiple sample analysis was applied to the measurement of voltage levels associated with temperature and heater power outputs for the sand bath. Both the thermocouple and heater power outputs of the sand bath are quite steady.

In single sample uncertainty analysis, each measurement is assigned three uncertainty values:

- Zeroth Order Uncertainty – associated with errors introduced by the measurement system (e.g., minimum read-out range on a digital voltmeter, minimum read-out on the weight balance, or minimum demarcation on the particle size analyzer reading). Typically this uncertainty value is well below the overall uncertainty of the measurement and represents a lower limit on the uncertainty obtainable with a given measurement system.
- First Order Uncertainty – associated with the scatter in repeated trial using the same measurement system and experimental procedures, while the experiment is running and held in a stationary state. This uncertainty includes the effects of process unsteadiness and system noise.
- Nth Order Uncertainty – characterizes the overall uncertainty in the result, acknowledging all identified sources of error in the measurement system and including variable errors that arise when the process is running. For reduced quantities—such as the reaction rate—the Nth order uncertainty is the root-sum-square of the Nth order uncertainties of each measured quantity that is used to calculate the reduced quantity.

The multiple and single sample uncertainty analyses developed by Moffat were originally developed for a dynamic system to study fluid mechanics and heat transfer in a flowing system, such as a gas turbine. They cannot be applied to our batch system directly, but the basic principles are applicable.

Refractive Index

We found that particle size measured by the analyzer was extremely sensitive to the refractive index of the black carbonaceous suspended particles. Even the opaque materials, such as metals or black particles, have a certain refractive index.[4] Researchers have made extensive refractive index measurements of soot particles.[5] We used the refractive index of polystyrene polymer in the calculation of size distributions of particles formed during pyrolysis. When a particle absorbs light, its refractive index has a "real" part as well as an "imaginary" part. When a sample consists of particles in the size range of 1 micron to more than 5 microns, a small change in the real or imaginary part of the refractive index can change the size distribution significantly.

Figure 2.1-6 shows particle size distributions calculated for carbon black particles at four different refractive indices—1.18, 1.23-4.13i, 1.12, and 1.3. As the figure clearly illustrates, size distribution is very sensitive to refractive index. Our current database does not have sufficient values of refractive indices to determine the sensitivity coefficient of particle size with respect to refractive index. This database will be updated and uncertainty (with respect to refractive index) will be reported in future studies.

Weight Change Measurement

Another potential problem involves authenticity of the weight change measurement of the reactor after fuel stressing. We have observed weight changes ranging from 15 mg to 500 mg. The weight of the reactor is approximately 170 grams. Therefore, determining deposit formation by recording the weight change can be a problem. Accuracy of the balance was found to be ±0.3 mg and it remains the same regardless of how much weight we measure. During the early stages of deposit growth, deposited material may weigh as little as 15 mg or less. Compared to the uncertainty interval of ±0.3 mg, a deposit weight of 15 mg is substantial with a relative uncertainty of just 2%.

Effects of Thread Lubricant

The effect of anti-seize thread-protecting lubricant on weight change must also be considered, particularly when the weight change is very small. Often the reactor is very difficult to open (particularly after long reaction times) and requires the application of force or a tapping motion. This can alter the weight of the reactor significantly. To address this problem, several dummy tubing bomb reactions were carried out with lubricant on the thread and no sample in the reactor. Standard deviation (2σ) of the weight change process was determined to be ±3.5 mg, which represents a 95% confidence interval for the weight change measurements. An error of ±3.5 mg for weight change of 100 mg is only ±3.5%. Error bars for the deposit measurement on the vertical wall of the tubing bomb are shown in **Figure 2.1-7**. Relatively high error was found for the 16-hour reaction, which can be attributed to the difficulty in opening the reactor without losing some of the deposited material.

Size Measurement and Concentration of Particles

In addition to being sensitive to refractive index, the measurement of particle size is also sensitive to the concentration of particles. The sensitivity of particle size to particle concentration depends on particle size. Larger particles (>20 μm) appeared smaller in size as the percentage of

laser light passing through the solution of suspended particles drops to 70%. When the solution is further concentrated, so that only 35% of the laser light passes through it, the measured median particle size of a 20 μm particle drops to 8 μm. Because the particle size we encountered fell in the range of 0.8 μm to 5 μm, measured particle size will not be sensitive to concentration.

Figures 2.1-8 and **2.1-9** show measured particle size for 100 nm and 900 nm particles at various concentrations. In the case of 900 nm particles, the size drops from 880 nm to 850 nm when the percentage of laser light passing through the solution decreases from 94% to 36%. In the case of 100 nm particles, the size measured changed from 103 nm to 84 nm when the light transmitted is reduced from 98% to 50%. Therefore, provided our studies are in the concentration range that allows greater than 60% laser light to pass, the sample data should be fairly accurate.

The diluent chosen for experimentation can have an effect on the concentration. For example, hexane precipitates significant amounts of soluble gums during the measurement process. In addition, the elapsed time between opening the reactor and making the measurement can affect the measured particle size.

Reactor Immersion

The reactor used to study degradation behavior was considered an ideal batch reactor with no mass transfer effects. However, about 20% of the total volume of the reactor was not immersed in the sand bath; consequently, this portion of the reactor remained cold compared to the portion that was immersed. This can cause thermal and concentration gradients within the reactor. Uncertainty associated with this effect must also be addressed. Once all of the associated uncertainties have been identified and quantified, we can determine the overall uncertainty in data and it effect on our kinetic model using Moffat's method.

Suspended Matter

The amount of suspended matter in the stressed fuel was measured by a solubility method. Stressed fuel was first mixed with 10 parts toluene, allowed to stand in the dark for 10 to 12 hours, and then filtered through 0.1μ filter paper. The amount of toluene insoluble (T.I.) deposit that remained on the filter was obtained by drying the filter paper in a vacuum for 6 to 8 hours and then re-weighing the filter paper and measuring the weight change of filter paper after drying. Toluene was then separated from the filtrate (i.e., mixture of toluene and stressed fuel) by roto-evaporator. The filtrate after toluene removal was mixed with 100 parts pentane and was allowed to stand in the dark for 8 to 10 hours. Pentane was used in large amount to ensure that sufficient pentane was always present in the sample despite evaporation. Pentane-insoluble (P.I.) and toluene-soluble (T.S.) solids precipitate and settle at the bottom of the container.

The T.I. part of suspended matter was found to be negligible. However, the T.S. and P.I. fraction of suspended matter was found to be small but measurable. The P.I.-T.S. soluble portion is small compared to the total solid formed on the wall. The plot shows that under an ultra high purity N_2 environment, deposit formation in the bulk is negligible. As soon as a reactive precursor forms, it goes to the wall and reacts immediately with the deposit layer there. Because the mass of P.I.-T.S. is very small and the rate of formation and disappearance of P.I.-T.S. is equal, the pseudo steady state approximation (PSSA) can be applied.[6] And, because deposit

formation in the bulk is negligible, the particle size distribution measurement will not be significant in this case.

Conclusion

The improved measurement and analysis procedures can be applied to neat jet fuels and mixtures of model compounds within jet fuels, both in pyrolizing and oxidizing environments. Enhanced laboratory analysis will provide the basis for a more sophisticated model for measuring stressed fuel composition using an "internal standard" to quantify species concentration. Statistical analyses can be applied to the chromatographic results to correlate species concentration with deposit formation and growth in the tubing bomb reactor. Compounds will be grouped in terms of their degree of correlation with deposit formation, allowing us to simplify the description of complex fuel chemistry to yield a tractable kinetic model that describes the essential features of the deposition process. These features are the induction period where no deposit forms, followed by a steady increase in the rate of deposition for several hours. A problem with grouping the species is that the model parameters will become very sensitive to the type of reactor and the type of fuel. A more general, kinetic model should include reaction pathways—in terms of several species which can represent the behavior of the fuel—rather than lumping the fuel into several groups. The effects of increasing or decreasing the number of species on the accuracy of the kinetic model warrants further investigation.

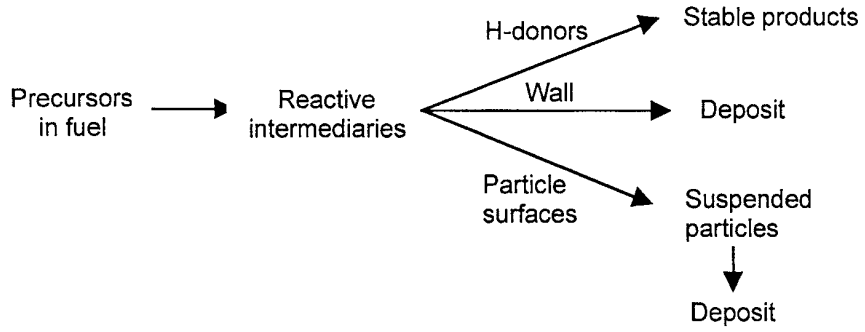

Figure 2.1-1. Simple Mechanism for Simultaneous Formation of Suspended Particles, Deposition of Particles, and Formation of Deposits by Direct Addition of Reactive Species

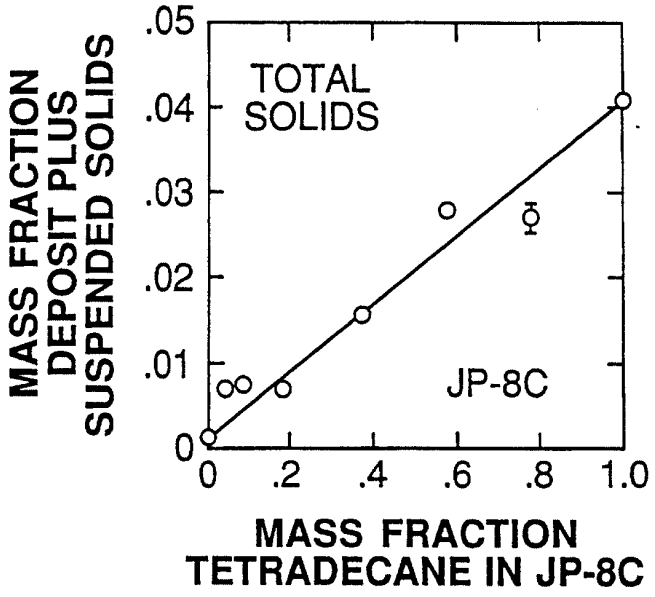

Figure 2.1-2. Mass fraction of the initial charge to a 20 ml batch reactor appearing as insoluble particles and deposits, after thermal treatment for 6 hours at 450°C under nitrogen, vs. the mass fraction of tetradecane added to JP-8C coal-derived fuel. The neat fuel contains 7.3 wt% tetradecane.

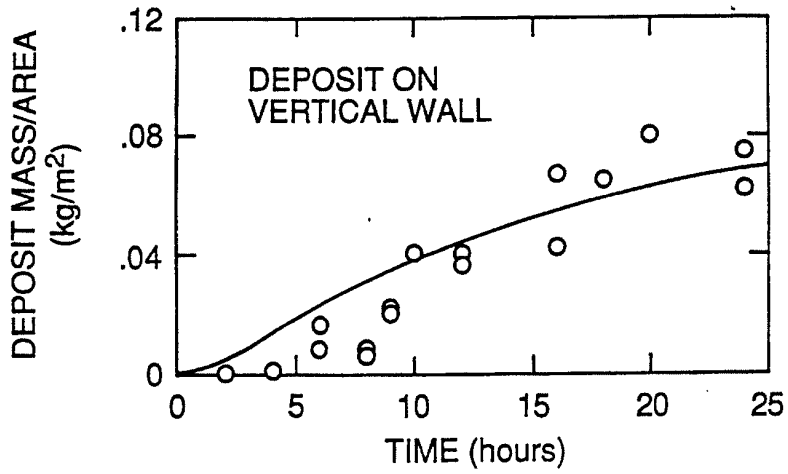

Figure 2.1-3. Measured mass/area of deposits formed on the vertical wall of the 20 ml batch reactor during thermal treatment of mixtures of 81.5 wt% JP-8C and 18.5 wt% tetradecane at 450°C under nitrogen, and comparison with the calculated growth of deposits by addition of reactive species.

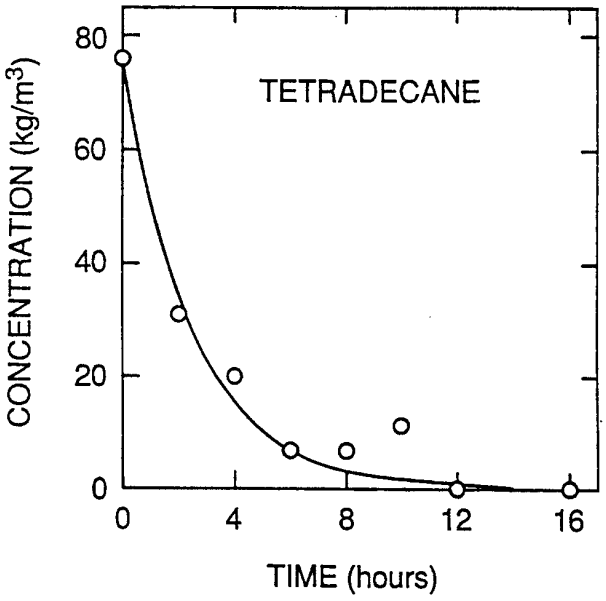

Figure 2.1-4. Disappearance of Tetradecane during Thermal Treatment of Mixtures of 81.5 wt% JP-8C and 28.5 wt% Tetradecane at 450°C. The curve is the fit of a pseudo-first-order decay to the data, with rate coefficient equal to 1.1×10^{-4} s^{-1}.

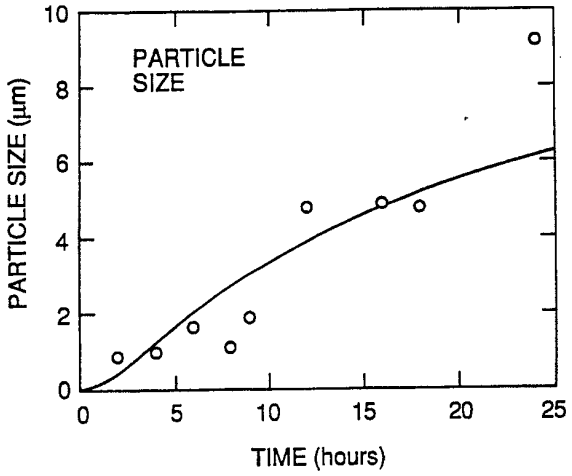

Figure 2.1-5. Measurements of the Mean Size of Particles Suspended in Mixtures of 81.5 wt% JP-8C and 18.5 wt% Tetradecane after Thermal Treatment at 450°C. The sizes were determined by light scattering using a Horiba Model LA-900 Particle Size Analyzer, after diluting the suspended particles and liquid products with *n*-hexane. The curve is the calculated particle growth, assuming an initial size of 1 nm species present in the fuel at a concentration of 0.1 wt ppb.

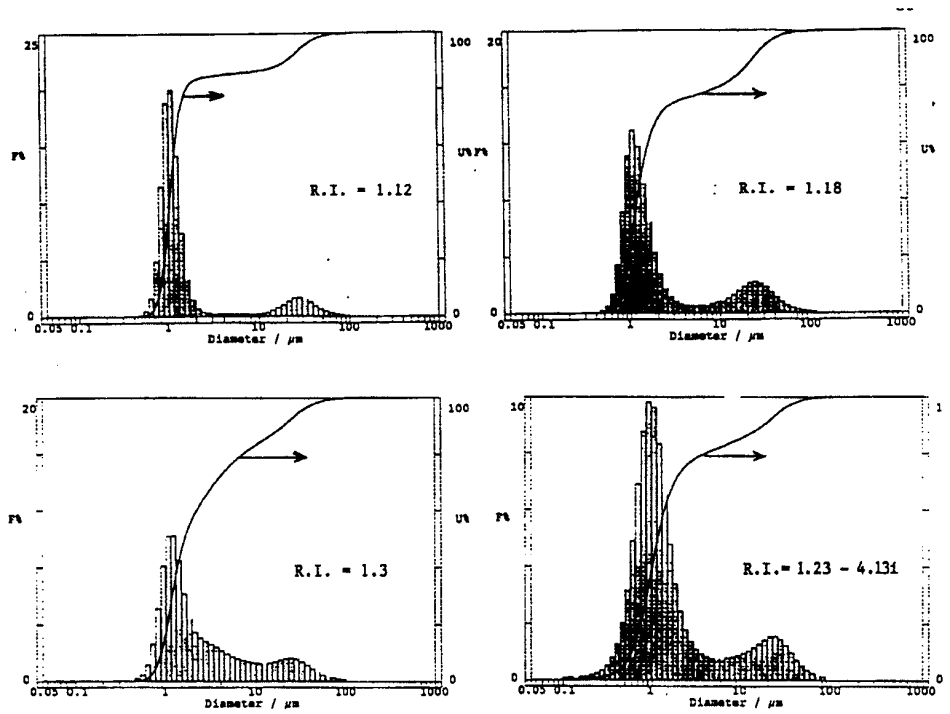

Figure 2.1-6. Size Distributions of Carbon Black Particles for Refractive Index (RI) Values of 1.18, 1.23-4.13i, 1.12, and 1.3. The left vertical axis indicates total particle volume in each size bin (F%) and the right vertical axis is cumulative size distribution (U%).

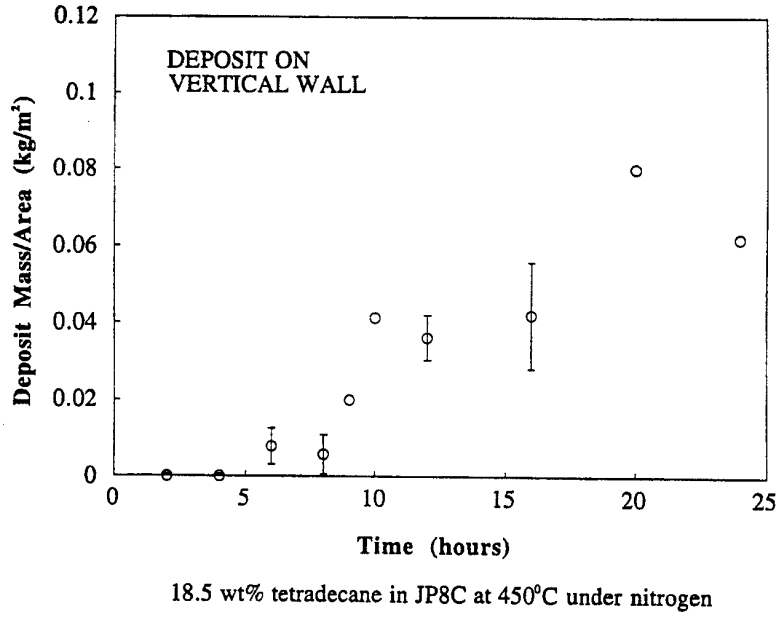

Figure 2.1-7. Errors Involved in Calculating Deposit Formation on the Wall at 6, 8, 12, and 16 Hours

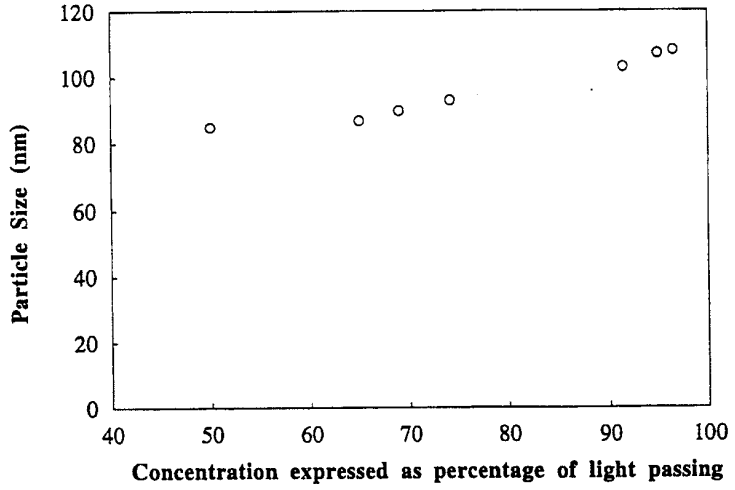

Figure 2.1-8. Variation in Particle Size with Concentration for 100 nm Standard

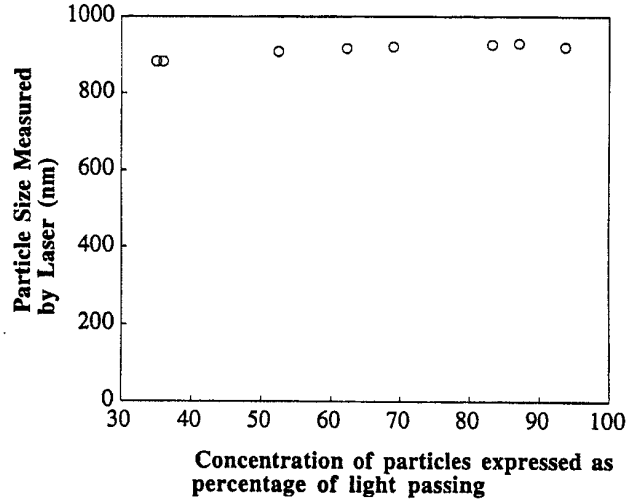

Figure 2.1-9. Variation in Particle Size with Concentration for 900nm Standard

---

[1] Moffat, R. J. *Experimental Thermal and Fluid Science.* 1988. 1 3-17.

[2] Moffat, R. J. *Trans. ASME, J. Fluid Eng.* 1982. 104. 250-260.

[3] Schobert, H. H. et al. *Advanced Thermally Stable Jet Fuels, Technical Progress Report, July 1994-September 1994.* The Pennsylvania State University. 1994

[4] Bohren, C. F. and D. R. Huffman. *Absorption and Scattering of Light by Small Particles.* New York: Wiley. 1983.

[5] Stagg, B. J. and T. T. Charalampopoulos. Combustion and Flame. 1993. 94. 381-396.

[6] Eser, S. *Private Communication.* 1995.

2.2 Deposit Growth During Heating of Coal-Derived Aviation Gas Turbine Fuels

Introduction

Currently jet fuel is used as the primary coolant to cool aircraft components during flight. In high-speed aircraft, cooling requirements have increased significantly and the fuel provides the only practical means of cooling. In future aircraft, the fuel may reach temperatures as high as 700°C for a fraction of a second before its combustion.[1] A portion of the fuel will also experience a moderate heat flux for a long residence time.[2] Under such conditions, the fuel forms carbonaceous coke deposits that foul heat exchangers and reduce the flow through fuel injection nozzles. Coke particles also form in the bulk and can be carried to the turbine combustor, creating performance problems. Because of the increasing thermal management needs in aircraft, there is an increasing need for development of a fundamental model for the prediction of the extent of coke formation in fuel lines.

The ultimate objective of this work is to describe the kinetics of deposit formation in sufficient detail and with sufficient accuracy from a complex mixture such as jet fuel. Development of a satisfactory kinetic model is essential for numerical simulation of complex reactive flows in aircraft fuel systems.

a. Use of Results from Model Compound Studies to Develop Rate Expressions for Deposits Formation from Jet Fuel

This study is explained in detail in *Advanced Thermally Stable Jet Fuels Technical Progress Report, April – June 1995.*

In a previous report, we compared deposit growth on surfaces and in the bulk during pyrolysis of mixtures of tetradecane and coal derived jet fuel (JP8C). Following those studies, we continued to develop an improved analysis technique that could quantify the species concentration.

Previously we were able to correlate decomposition of tetradecane with formation of solids on the wall, indicating that tetradecane is the only contributor to solid formation.[3] This simple model could not simulate the induction period for the onset of significant deposition. The actual fuel contains hundreds of components and any one of these compounds could contribute to solid formation by undergoing decomposition and forming an active radical.

Purpose: To study the effects of deposit growth during heating of coal-derived jet fuels, we examined the results of pyrolytic studies of pure compounds at 450°C in a nitrogen environment.[4] The compounds studied were *n*-decane, *n*-butylbenzene, *n*-butylcyclohexane, decalin, tetralin, naphthalene, t-butylbenzene, ethylcyclohexane and tetradecane.

Findings: The formation of solids from decane depended strongly on temperature. Treatment of decane at 400°C for 72 hours produced only 45mg of solids, whereas heating at 450°C produced 460 mg solids in 10 hours. Fuel degradation reaction occurs through free radical reaction; at 400°C the rate of initiation of free radical reaction is negligible, therefore no deposit forms at that temperature. Heating of butylbenzene at 450°C produced a significant amount of solid. Liquid products from *n*-butylbenzene obtained at 450°C for 4 hours included compounds such as

alkylbenzenes, naphthalene and alkylnaphthalenes, biphenyl and alkyl biphenyls, bibenzyl, phenanthrene and terphenyl.

We found that *n*-butylcyclohexane was fairly stable and produced very little solids. Ethyl cyclohexane was more stable than *n*-butylcyclohexane and produced no apparent solids. Because pyrolysis of alkylated benzenes produced significant quantities of naphthalene and alkylated naphthalenes, we must be familiar with the behavior of naphthalene. Treatment of naphthalene at 425° and 450°C for 48 hours did not produce solids. Similarly, decalin, which is one of the major components of coal-derived jet fuel, did not produce solids for 24 hours at 450°C. Tetralin produced no solids for 48 hours at 450°C. t-Butylbenzene had an induction period of 5 hours when stressed alone.

Knowing the results of individual compound pyrolysis can help understand the behavior of actual fuel. However, when the compound is in a complex mixture it does not necessarily behave in the same manner as it behaves during individual pyrolysis. Perhaps the reason that we could correlate tetradecane decomposition with deposit growth was because tetradecane produced the most solids of any compound in the individual compound studies.

We have mentioned in a previous report the idea of grouping the species in terms of their tendency to form solids, based on a statistical analysis of compound variations during stressing. Because there are so many compounds and many of them coelute in the GC column and ionize to different extents, calculating the ratio of ion abundance and combining it with GCFID results does not always work. As a result, we need to inject the known mixture in several different relative concentrations. This technique will further our efforts to develop a kinetic model for incipient deposition and results of fuel pyrolysis.

b. Calculating Concentrations of Species and Developing Correlations

This study is explained in detail in *Advanced Thermally Stable Jet Fuels Technical Progress Report, July – September 1995.*

Purpose: This study continued our work on development of a kinetic model for deposit formation from coal-derived jet fuel. With the refined analytical method that was based on an internal standard proposed in a previous report, concentrations of species were calculated and correlations were developed in stressed fuel samples.

We studied the kinetics of coke formation from coal-derived jet fuel using statistical methods. We examined the degree of correlation between deposit growth and species concentration and performed detailed composition analysis of neat fuel and tetradecane mixture and pyrolyzed samples using GC and GC/MS.

Findings: Formation of deposits from the mixtures of jet fuel and tetradecane were approximately proportional to the initial concentration of tetradecane present in the mixture of tetradecane and fuel. We found that the decomposition of tetradecane present in the fuel-tetradecane mixture was first order with correlation coefficient of 0.98. Examining tetradecane decomposition at 450°C showed that the change in concentrations of compounds such as cycloalkanes, alkylated C_1, C_2, C_3 benzenes, and alkylated naphathalenes present in the jet fuel mixture at different time intervals were minimal. This led us to conclude that these compounds do not contribute to the solid formation during the pyrolysis of jet fuel. Because tetradecane was found to produce maximum solids in the individual model compound studies and to disappear

more quickly than other compounds during pyrolysis, we concluded that tetradecane is the sole contributor to solids formation. The correlation coefficient between tetradecane concentration and deposit mass was found to be 0.901; therefore, linear correlation between tetradecane and deposit mass is poor.

We also noted that more than 50% of the tetradecane underwent decomposition before an observable mass of deposit formed. This can be attributed to the presence of an induction period prior to significant deposition. Most of the deposit (≈95%) forms by addition of reactive species on already growing films of deposit, rather than via a homogeneous process that occurs to a significant extent during the autoxidation regime.

Summary: The kinetics of coke formation from coal-derived jet fuel were studied using statistical methods. We examined the degree of correlation between deposit (coke) growth and species concentration. Formation of deposits from the mixtures of jet fuel and tetradecane was proportional to the initial concentration of tetradecane present in the fuel. Decomposition of tetradecane was found to be first order with correlation coefficient of 0.98. Other normal alkane species, such as dodecane, tridecane, and pentadecane, which are present in very small amounts also contributed significantly to deposit growth. Cycloalkanes, alkylated C_1, C_2, C_3 benzenes, and alkylated naphathalenes present in coal derived jet fuel were very stable compared to tetradecane. The statistical approach helps in identifying or arranging species in terms of their contribution to deposit formation. Grouping species on the basis of their correlation with deposit formation clarifies the required structure for a general kinetic model of the jet fuel degradation process.

c. Using Statistical Methods and Quantitative Chemical Analysis to Correlate Deposition Kinetics

This study is explained in detail in *Advanced Thermally Stable Jet Fuels Technical Progress Report, October – December 1995.*

Coke formation occurs by secondary reactions. In the case of coal-derived jet fuel, 150 compounds have been identified. Simulating pyrolytic reactions and predicting the elementary reaction steps of individual compounds in coke formation would require us to consider hundreds of reaction steps. The complexity of the network of reactions precludes development of a mechanistic modeling study on fuel pyrolysis and the development of rate equations for the elementary steps. Although some efforts have been made to model deposition in the autoxidation regime[5, 6] the high-temperature pyrolytic domain of fuel decomposition has not been considered.

Purpose: This study used statistical methods and quantitative chemical analysis to correlate deposition kinetics. Deposit formation correlations were developed in terms of the concentrations of the reactive species.

Experimental: The base fuel in these experiments was JP-8C, to which a small amount of tetradecane was added as a reactive species. Experiments were conducted at 450°C (723 K) for periods of 2 to 12 hours in a tubing bomb reactor. Pressures reached values in excess of 1400 psi after two hours and the reaction occurred in the supercritical phase.

This study used a coal-derived jet fuel mixture consisting of 1.5g of tetradecane in 6.68g of neat JP-8C fuel. The reactors were pressurized and purged with nitrogen to remove nearly all

oxygen from the reactor. The tubing bombs were then pressurized to 0.69 MPa with N, before pyrolysis. After the desired reaction time, the reactors were quenched in water at room temperature. The reactors were opened and products were collected separately and analyzed.

In another set of experiments, tetradecane was mixed with JP-8C in different proportions from 0 to 100% tetradecane. These mixtures were also pyrolyzed under similar conditions for 6 hours.

About 3% *n*-decylcyclohexane was added to the pyrolyzed products as an internal standard for quantification. Compounds in the liquid products were identified by capillary gas chromatography-mass spectrometry (GC-MS). Quantification of liquid products was accomplished by using a Perkin Elmer 8500 capillary GC equipped with an FID and a DB- 17 column. Those compounds that coelute in the GC were quantified using single ion monitoring in the mass spectrometer. Gaseous products were analyzed by a gas chromatograph equipped with FID and TCD detectors.

The growth of coke in the bulk fuel was measured by first mixing the stressed fuel with 8 parts toluene and allowing it to stand in the dark for 10-12 hours at room temperature. This mixture was then filtered and the filter paper was dried in vacuum. The amount of toluene insoluble (T.I.) deposit that remained on the filter was determined by weighing the filter after drying. Toluene was removed from the filtrate by a rotary evaporator. The filtrate was then mixed with 100 parts *n*-pentane and was allowed to stand in the dark for 10 hours. This solution of pentane and filtrate was then filtered through 0. 1 g filter paper. The mass of pentane insoluble deposit that remained on the filter paper was reported as toluene soluble and pentane insolubles (T.S.-P.I).

Findings: Deposit formation occurs by the addition of reactive species to the initial deposit layer formed on the reactor wall. Homogeneous processes occurring in the bulk form reactive species, but nucleation of coke particles does not occur at 723K under supercritical conditions. Compounds such as cycloalkanes, xylenes, toluene, and benzene are stable compounds and do not contribute to the formation of solid deposits. Compounds such as indan and C_1- and C_2-indans are very stable and do not trigger formation of radicals that can add to the already growing layer of deposits. However, radicals formed from tetradecane and other comparable alkanes can abstract hydrogen from these stable compounds, thereby forming reactive radicals. However, radicals generated from indans and cycloarmes may not be capable of adding to deposits on reactor walls, as a result of steric factors or some other reason.

From the quantitative analyses of jet fuel pyrolysis performed in this study, we can develop a statistical correlation between conversion of alkanes to cycloalkanes and solid deposits. During this conversion process, compounds such as dodecane and tetradecane form reactive radicals whose natures must be determined. Though deposit formation is proportional to the initial concentration of tetradecane, the direct correlation between deposit mass and tetradecane conversion is very poor. However, using an appropriate functional form that incorporates the induction period for deposition may lead to an improved correlation between these observations. With an appropriate description of the induction process and further statistical analysis, we could likely develop a rate expression for deposit formation in terms of the concentration of reactive compounds such as tetradecane, dodecane, tridecane, undecane, butyl benzenes, and substituted higher benzenes.

d. Refining the Kinetic Model of Deposit Formation

This study is explained in detail in *Advanced Thermally Stable Jet Fuels Technical Progress Report, January – March 1996.*

The ultimate objective of this work is to describe the kinetics of deposit formation in sufficient detail and with sufficient accuracy for a complex mixture such as jet fuel. Development of a satisfactory kinetic model is essential for numerical simulation of complex reactive flows in aircraft fuel systems.

The global model proposed in a previous report[7] for deposit formation was:

$$\phi(\theta) = \sum_{i=1}^{n} \omega_i [C_i^{obs} - C(\theta)]^2 \qquad (3)$$

The values of the best fit parameters obtained were $k_F = 1.1 \times 10^{-4} s^{-1}$, $k_{H,1} = 2.5 \times 10^{-4} m^3/(kmol\ s)$, $k_{H,2} = 1.5 \times 10^{-4} m^3/(kmols)$, and $k_D = 3.5 \times 10^{-8}$ m/s. Based on this information, tetradecane undergoes decomposition and forms radicals that are either stabilized by tetralins or decalins or react to form deposits.

With very low values of k_F, experimental simulation of the induction period would produce such a low radical concentration that too few radicals would remain to form any solids at longer periods of stressing. Therefore, we cannot simulate the observed increase in the deposition rate at longer times. Instead, we can only incorporate enough information about the mechanisms of solid formation to enhance the quality of the model's predictions. This may require postulation of certain radical species that allow the induction period and the increase in deposition at longer times to be described mathematically. Unfortunately, our measurements of stressed fuel compositions do not yield information on radical concentrations. These must be inferred from assumed kinetic pathways.

As a result of these problems, we examined the deposit formation reaction from a statistical viewpoint.[8] Solids formation proceeds mainly through formation of alkylbenzenes as the important intermediate,[9] but during the pyrolysis of mixtures of coal-derived jet fuel and tetradecane, alkyl benzene concentration remained. Therefore, from a statistical viewpoint, we concluded that alkylbenzenes do not play significant role under such circumstances. In previous work on tetradecane pyrolysis, deposit growth did not occur until a significant amount of alkylbenzenes appeared; therefore, we concluded that alkylbenzenes are precursors of deposit formation.[9] Alkylbenzenes also produce significant amounts of solids when they were pyrolyzed individually.[10] However, there have been numerous studies showing that compounds behave differently in mixtures than during neat pyrolysis. Butadiene is an important precursor during coke formation reaction.[11] No butadiene was detected in our stressed fuel samples obtained at various reaction times. This does not necessarily indicate that butadiene was not involved in solid formation process; the butadiene could be so reactive that it does not remain in the sample after the reaction.

Alkenes are a precursor for solid formation. Lower molecular weight alkenes, such as butenes and pentenes, coelute with *n*-alkanes and cycloalkanes. Because of this, we were unable

to quantify alkenes with high confidence. We are working on the use of a different column to separate lower molecular weight alkanes, alkenes and cycloalkanes with good resolution.

The role of lower alkenes and butadiene is still under investigation. In the previous model,[7] cycloalkanes such as C_1- and C_2-cyclohexanes were also included to explore their potential as hydrogen donors. This introduced additional parameters and required the development of a code that can couple ordinary differential equations (ODEs) with an optimization routine. This work is ongoing. When this optimization scheme for kinetic parameters is complete, we will be able to examine the efficacy of various kinetic models. We will also use this code to combine our predictions of deposit formation with statistical analyses of decomposition products to develop a procedure for accurate prediction of jet fuel decomposition.

e. Constructing the Differential Equation Model

This study is explained in detail in *Advanced Thermally Stable Jet Fuels Technical Progress Report, April – June 1996.*

Purpose: This work was a continuation of the development of a kinetic model for deposit formation from complex hydrocarbon mixtures such as jet fuel. Development of a kinetic model requires rate parameter estimation from multi-response data. Parameter estimation from multi-response data has been reported previously.[12, 13]

Parameter estimation from experimental data is considered as the inverse problem of a dynamic model. This can be described as a system of ordinary differential equations (ODE):

$$dC/dt = f(t, C, \theta) \qquad (1)$$

where C is a vector of concentration variables, t is the reaction time, θ is the vector of parameters (e.g., rate coefficients), and f is the functions representing species mass balance. Given the initial conditions of $C = C_0$, we can find the parameter values, θ, such that solution of Eq. 1

$$C = g(\theta, t, C_0) \qquad (2)$$

matches the experimental data, $C = C^{obs}$. Mathematically this is stated as a minimization of an objective function ϕ with respect to the parameters θ, where ϕ is expressed as:

$$\phi(\theta) = \sum_{i=1}^{n} \omega_i [C_i^{obs} - C(\theta)]^2 \qquad (3)$$

where n is the number of experimental observations and ω_i is the weighting factor of the *ith* observation. (3) can be optimized using a search algorithm in a multidimensional space, θ, with a call to a differential equation solver each time new values of parameters θ are evaluated. When the number of parameters to be estimated is small, this method works well. However, when the number of parameters to be estimated increases (>12), this method fails because extremely large numbers of function evaluations are required, which places a large demand on computation time.[14]

To overcome this difficulty a method of solution mapping was proposed.[14] In this work, the method of solution mapping is used for kinetic parameter estimation. C in equation (2) is approximated by simple algebraic expressions:

$$g(\theta, C_0) = \Psi(\theta) \qquad (4)$$

in the subspace, Ω, of parameter space, θ. The approximating functions, $\Psi(\theta)$, are obtained by means of computer experiments known as factorial design.[15] The computer experiments are performed using the complete kinetic model.

On substituting Eq. (4) into Eq. (3), we obtain

$$\phi(\theta) = \sum_{i=1}^{n} \omega_i [C_i^{obs} - \Psi_i(\theta)]^2. \qquad (5)$$

This means optimization of the objective function no longer requires time-consuming numerical integration of differential equations, just straightforward evaluations of $\Psi(\theta)$. In other words, this method decouples the ODE solver from the optimization search.

To illustrate, consider the following problem of parameter estimation from chemical kinetics where k1, k2, k3, and kd need to be determined from experimental values of F, H1, H2, and D:

dF/dt = k1 * (F)

dR/dt = k1 * (F) - k2 * (H1) * (R) - k3 * (H2) * (R) - kd * (R)

dH1/dt = -k2 * (H1) * (R)

dH2/dt = -k3 * (H2) * (R)

dD/dt = kd * R

where F, H1, H2, D represent different species taking part in the reactions. Also values of F, H1, H2, D at time t, where t = t1, t2, t3 ...., are known.

1. Specify the ranges of rate parameters k(1), k(2), k(3) and k(d) as

ln[k1] = ln[k(1,0)] +/- ln[delta(1)]

ln[k2] = ln[k(2,0)] +/- ln[delta(2)]

ln[k3] = ln[k(3,0)] +/- ln[delta(3)]

ln[kd] = ln[k(d,0)] +/- ln[delta(d)]

where k(i,0) is the initial guess of the *ith* rate parameter, and delta(i) is a positive value and is the (arbitrarily) assigned range of rate parameter k(i). Let:

X(i) = ln[k(i)/k(i,0)] / ln [delta(i)]

where X(i) is a factorial variable, such that

X(i) = 1 for k(i) = k(i,0) * delta(i)

X(i) = 0 for k(i) = k(i,0)

X(i) = -1 for k(i) = k(i,0) / delta(i)

2. Make a 2^2 factorial design of X(i).

J	X(1)	X(2)	X(3)	X(d)
1	+1	+1	+1	+1
2	+1	+1	+1	-1
3	+1	+1	-1	+1
4	+1	+1	-1	-1
5	+1	-1	+1	+1
6	+1	-1	+1	-1
7	+1	-1	-1	+1
8	+1	-1	-1	-1
9	-1	+1	+1	+1
10	-1	+1	+1	-1
11	-1	+1	-1	+1
12	-1	+1	-1	-1
13	-1	-1	+1	+1
14	-1	-1	+1	-1
15	-1	-1	-1	+1
16	-1	-1	-1	-1
17	0	0	0	0

Compute the responses (i.e., F(t), H1(t), H2(t) and D(t)) at each design point j (j=1,J) for every time (t1, t2, t3, ...) at which experimental values of F, H1, H2, and D are available. After calculating values for the responses, one will have a table which looks like

J	X(1)	X(2)	X(3)	X(d)	F(t1)	F(t2) ..	H1(t1)	H1(t2) ..	H2(t1)	etc.
1	+1	+1	+1	+1	F11	F12 ..	H111	H112 ..	H211	etc.
2	+1	+1	+1	-1	F21	F22 ..	H121	H122 ..	H212	etc.
3	+1	+1	-1	+1						
4	+1	+1	-1	-1	.....					
5	+1	-1	+1	+1	.....					
6	+1	-1	+1	-1						
7	+1	-1	-1	+1						
8	+1	-1	-1	-1						
9	-1	+1	+1	+1						
10	-1	+1	+1	-1						
11	-1	+1	-1	+1						
12	-1	+1	-1	-1						
13	-1	-1	+1	+1						
14	-1	-1	+1	-1						
15	-1	-1	-1	+1						
16	-1	-1	-1	-1						
17	0	0	0	0						

Using linear regression, one can then obtain a second-order polynomial for each of the responses:

ln[F(t1, polynomial)] = aF0 + aF1 X(1) + aF2 X(2) + aF3 X(3)

+ aF4 X(4) + aF11 X(1)^2 + aF12 X(1)*X(2)

+ .....

where the aFs are polynomial parameters. In essence, this gives the numerical dependence of F, H1, H2 and D on k(i). Because F, H1, H2 and D depend only on k(i) and not on t, costly integration of the ODE system for each optimization search is not required.

3. Optimization: Minimize

L^2 = sum_j [F(tj,polynomial) - F(tj,expt)]^2

+ sum_j [H1(tj,polynomial) - H1(tj,expt)]^2 + sum_j [H2(tj,polynomial) - H2(tj,expt)]^2 + sum_j [D(tj,polynomial) - D(tj,expt)]^2

with respect to k(1), k(2), k(3) and k(d), where F (tj,polynomial) is the developed polynomial and F(tj,expt) is the experimental value at time tj.

We adopted this new method in our problem of kinetic model development.

---

[1] Edwards, T. Personal communication, U.S. Air Force Wright Laboratory, WPAFB. October 1995.

[2] Roquemore, W. M. et al. *Prepr.-Am. Chem. Soc., Div. Pet. Chem.* 1989. 34(4). 841-849.

[3] Schobert, H. H. et al. *Advanced Thermally Stable Jet Fuels, Technical Progress Report, January - March 1994.* The Pennsylvania State University. #92PC92104-TPR-12. 1995.

[4] Eser, S. et al. *Annual Progress Report.* July 1989- June 1990.

[5] Krazinski, J. L. and S.P. Vanka. *Final Report.* WRDC-TR-89-2139. December 1989.

[6] Zabamick, S. Ind. Eng. Chem. Res. 1993. 32. 1012-1017.

[7] Schobert, H. H. et al. *Advanced Thermally Stable Jet Fuels, Technical Progress Report, January - March 1994.* The Pennsylvania State University. #92PC92104-TPR-7. 1994.

[8] Sanghani, P. C. and A. L. Boehman. *Prepr. - Am. Chem. Soc., Div. Pet. Chem.* 1996. 41 (2). 529-533.

[9] Song C., W. C. Lai, and H. H. Schobert. *Ind. Eng. Chem. Res.* 1994. 33. 534-547

[10] Peng, Y. *Ph.D. Dissertation.* Dept. of Materials Science & Engineering, The Pennsylvania State University. 1995.

[11] Froment, G. F. *Reviews in Chemical Engineering.* 1990. 6(4) 293-328.

[12] Ziegel, E. R. and J. W. Gorman. *Technometrics.* 1980. 22(2). 139-151.

[13] Stewart,W. E., M. Caracotsios, and J. P. Sorensen. *AIChe Journal.* 1992. 38(5).

[14] Frenklach M., H. Wang and M. J. Rabinowitz. *Prog. Energy Combust. Sci.* 1992. 18. 47-73.

[15] Box, G. E. P., W. G. Hunter, and J. S. Hunter. *Statistics for Experimenters, An Introduction to Design, Data Analysis, and Model Building.* New York: Wiley. 1978.

2.3 Modeling Heat Transfer to Flowing Jet Fuels

This study is explained in detail in *Advanced Thermally Stable Jet Fuels Technical Progress Report, April–June 1996.*

Introduction

Jet fuel flowing through fuel handling lines in aircraft is exposed to elevated wall temperatures and is heated. This process of heat exchange is controlled by molecular transport, convective transport, and fuel properties. The result can be a substantial change in fuel composition as a result of thermal degradation, but the primary cause of these changes in fuel composition is heat transfer.[1]

As part of our ongoing studies of advanced thermally stable fuels, we began numerical and experimental studies of fuel decomposition in flowing systems. Here we report preliminary results from calculations of heat transfer to a flowing fuel from heated stainless steel tubing. We compare our results to those of experiments performed at Wright Laboratory, WPAFB.[2]

The basis for our calculations was the entry length heat and mass transfer model for flow in tubes, STANTUBE, developed by Kays and Crawford.[3] STANTUBE is a cylindrical coordinates version of the STAN5 boundary layer heat and mass transfer code. STANTUBE solves the governing equations for internal flows in cylindrical, axisymmetric tubes using finite differencing. It can consider developed, developing, laminar and turbulent flows. Turbulence is modeled by one of three means: (1) Prandtl mixing-length approximation, (2) a turbulent kinetic energy (TKE) scheme, or (3) an eddy diffusivity function. In the latter two models, the mixing-length approximation is used in the laminar sublayer region.

STANTUBE is an interactive program that produces a complex summary output file. A second interactive program, TUBETRAN, and subsequently, TUBETRA2, have been developed to read and manipulate the output from STANTUBE so that particularly useful details can be extracted from the output file. These important features of the modeling calculations include: residence time distributions; mass distributions of times spent at particular temperatures; and depths of thermal penetration into fluid where temperatures that exceed those where decomposition reactions become greatly accelerated.

Experimental

Measured tube wall temperature data serve as the wall temperature boundary condition for the STANTUBE solution. The experiments were performed on Norpar-13 flowing at 12 mL/min and 700 psig through 1/4" stainless steel tubing. The Wright Laboratory calculations used variable fuel property data for *n*-dodecane from a NIST hydrocarbon property database. The STANTUBE calculation used fixed property databased on the mean fluid temperature reached halfway through the heated tube. The STANTUBE prediction of T_{mean} compared well with the Wright Laboratory prediction, taking into account the difference in the handling of thermal properties. Near the entrance to the heated tube, the temperature-dependent properties yielded a Prandtl number of 8.9, although we assumed 4.99 throughout the solution. Near the exit of the tube, temperature-dependent properties give a value of 2.8 for Prandtl number. Correspondingly, STANTUBE predicted a lower mean fuel temperature near the inlet and a higher mean fuel temperature near the exit.

This comparison demonstrated our capability to calculate thermal transport to jet fuel in flowing systems. From these initial calculations, we began building a flow reactor model for comparison to our flow reactor experiments and for formulation of kinetic models that describe pyrolytic jet fuel degradation in flowing systems.

---

[1] Hazlett, R. N. *Thermal Oxidation Stability of Aviation Turbine Fuels.* Philadelphia: ASTM Publications. 1991. 1-21.

[2] Atria, J. V. and T. Edwards. "High Temperature Cracking and Deposition Behavior of an *n*-Alkane Mixture." *Prepr. - Am. Chem. Soc., Div. Pet. Chem.* 1996. 41(2). 498-501.

[3] Crawford, M.E. and W.M. Kays. *STAN5 - a Program for Numerical Computation of Two-Dimensional Intemal/Extemal Boundary Layer Flows.* Thermosciences Division, Department of Mechanical Engineering, Stanford University, Stanford, California. Report No. HMT-23. 1975.

2.4 INVESTIGATION OF INCIPIENT DEPOSITION

a. Studying Incipient Deposition using Model Compounds

This study is explained in detail in *Advanced Thermally Stable Jet Fuels Technical Progress Report, July – September 1996.*

In our previous work, we proposed a global kinetic scheme to describe the kinetics of solid formation from coal-derived jet fuel (JP8C). From a practical standpoint, future jet fuels likely will be made by blending various hydrocarbon streams in petroleum refineries. These blends probably will contain components that serve as hydrogen donors within mixtures of various long chain alkanes. In addition, these mixtures may also contain several hydrogen donor additives, such as tetrahydroquinoline (THQ), tetralin, decalin, benzenedimethanol (BDM), and dihydrophenanthrene (DHP), all of which may serve as thermal stabilizers. The effectiveness of additives decreases with increases in temperature. The amount of additives will depend on cost and also on their interactions with other additives and components of the jet fuel. Temperatures in the fuel handling system aboard future aircraft will also be an important factor in deciding additive proportions.

At 450°C, coal-derived jet fuel has been found to be more thermally stable than petroleum-derived jet fuel. This is attributable, at least in part, to the presence of hydrogen donor compounds in the coal-derived jet fuel. To anticipate how petroleum derived feedstocks would be blended, and the amounts and types of additives these fuel blends will require to achieve the desired degree of thermal stability, we must understand the pyrolytic decomposition process. To this end, development of superior hydrogen donor mixtures to minimize deposit formation will depend on understanding the fundamentals of incipient deposition. The complexity of jet fuel makes it difficult to fundamentally investigate incipient deposition. Because of this, we will use model compounds, rather than complex fuel mixtures, to study incipient deposition. Our results will help us to understand the thermal stability behavior of jet fuels and how to effectively produce fuel blends that achieve the desired degree of thermal stability.

Purpose: Use model compounds to study incipient deposition and better understand the thermal stability behavior of complex jet fuels.

Experimental: Tetradecane, tetralin, decalin, and tetrahydroquinoline (THQ) were stressed at 450°C under a nitrogen environment. First, about 5.46 gram of tetradecane was pyrolyzed neat, then mixtures of tetradecane + tetralin and tetradecane + THQ were pyrolyzed for two hours. About 1 gram of -16μm 316 stainless steel (SS316) powder was charged into a tubing bomb reactor for each test. The reactor was shaken at 60 strokes per minute.

Deposits formed preferentially on the steel powder because of its high surface area. Because decalin is an inferior hydrogen donor compared with tetralin, mixtures of decalin and tetradecane were not pyrolyzed.

In another set of experiments, mixtures using, tetradecane, tetralin, decalin, and THQ were pyrolyzed. In these tests, the amount of tetradecane charged remained constant 5.46 grams). Two levels of additive concentrations were used—4 mole% and 10 mole%.

Incipient deposition was examined by measuring the amount of deposit formed on the SS316 powder. About 30mg of powder was scraped from the wall of tubing bomb and loaded on an alumina crucible for TGA analysis. The sample was heated under air from 25°C to 800°C at the rate of 10°C per minute with an air flow rate of 100ml/min. The mass of deposit was measured by observing the weight loss from 350°C onwards. By assuming uniform deposition, the total amount of solid formed on 1 gram of the SS316 powder could then be determined.

Findings: Results of the preliminary tests are shown in **Table 2.4-1**. In 2 hours, neat tetradecane forms 12.24 mg of deposit. Addition of 4 mol% tetralin to tetradecane did not reduce the deposit formation in 2 hours. These results seem to contradict those reported earlier about the role of tetralin in suppressing deposit formation. Further investigation is needed, although a potential explanation for this discrepancy is that the amount of deposit reported here is very small, about 12 mb, and the small amount of deposit may lead to a substantial relative uncertainty. Earlier work reported deposit amounts of about 50 mg.

In this work, 4 mole% THQ retarded deposit formation significantly during the stressing of tetradecane at 450°C and no deposit was observed in the TGA. Addition of three hydrogen donor additives to tetradecane was also quite effective in eliminating deposit formation. These results also indicate that tests on higher levels (10 mol%) of additives will not be necessary at 450°C and higher temperatures.

The deposits that are mentioned here refer to the amount collected on the SS316 powder, as evidenced by the weight change of the powder during heating in air. Small amounts of deposit also formed on the walls of tubing bomb, but these deposits were not reported here. Tests with 500 and 700 mg powder charged in the reactor should give some idea of how much deposition is occurring on the wall, although the likely amounts would be difficult to directly measure due to low mass.

b. Blending THQ and Other Additives to Achieve Cost Effective Thermal Stability

This study is explained in detail in *Advanced Thermally Stable Jet Fuels Technical Progress Report, January – March 1997.*

Based on our experimentation, we have found tetrahydroquinoline (THQ) to be a superior high temperature jet fuel thermal stabilizer in terms of its ability to prevent carbon (deposit) formation. However, based on the cost of THQ, the expense of use 10-20 weight % THQ as an additive in jet fuels would be prohibitive.

Purpose: Determine whether blending THQ with other practical thermal stabilizers (additives) could achieve the same thermal stability as that achieved using only THQ.

Because future jet fuels likely will be made by blending various hydrocarbon streams in petroleum refineries, these hydrocarbon streams will have a wide range of stability. It is necessary to know the quantity of stable mixture that should be added to unstable mixtures to prevent incipient carbon deposition. Understanding the kinetics of these processes is a prerequisite for predicting the fuel behavior. Kinetic study is a next step for this work.

Experimental: Various mixtures of tetradecane, tetralin, decalin, and tetrahydroquinoline (THQ) were stressed at 450° and 478°C under a nitrogen environment. All mixtures were fixed at 5.46

g of $C_{14}H_{30}$. Additives were used at 4, 10 and 20 mol% concentrations. About 600-700 milligrams of -16μm stainless steel (SS316) powder was charged into a microautoclave reactor for each test. Deposits formed preferentially on the steel powder because of its high surface area. Incipient carbon deposition was examined by measuring the amount of deposit formed on the SS316 powder using TGA.

Findings: THQ and mixtures of three additives at 4 mol% worked well in preventing incipient deposition at 450°C. Although tetralin is a well-known hydrogen donor, 4 mol% tetralin did not prevent deposits—perhaps because hydrogen donation from tetralin is slower than the degradation of tetradecane. Also, the amount of carbon reported here is fairly low, merely 10 mg.

At 478°C the additives did not work as well. Carbon formation from neat $C_{14}H_{30}$ was not measured at 478°C because neat $C_{14}H_{30}$ produces significant deposits (>300mg) and no longer represents incipient deposition. Mixtures with 10 mol% additive did not show improvement in preventing incipient deposition from $C_{14}H_{30}$ over the 4mol% case—an indication of a decrease in effectiveness of the additives with an increase in temperature. The 20 mol% THQ and tetralin reduced carbon deposition from $C_{14}H_{30}$ by a factor of 2. The 10 mol% THQ and tetralin were better than three additives at 10 mol%, which is also an indication of the poorer stabilizing capacity of decalin.

Mixtures of tetradecane and 3 additives at the 10 mol% level were pyrolyzed for time periods of 12 to 90 minutes. Very little carbon appeared before 50 minutes. After 60 minutes, carbon deposition increased rapidly. Therefore as soon as the system starts building carbon, it is very difficult to control the process further.

GC and GC/MS were performed on liquid products obtained after pyrolysis. The concentration of tetradecane dropped to a very low level in 50 minutes. Concentrations of tetralin, *trans*-decalin, and THQ were present. THQ disappeared faster than tetralin and *trans*-decalin. In about 60 minutes, both THQ and tetralin concentrations had decreased significantly. After 60 minutes, very little THQ or tetralin remained available. During the same period, we observed the rapid rise in deposit mass.

In summary, the ability of additives to stabilize fuel is a strong function of temperature. Additives that work at 450°C may not work at all at 500°C. Sufficient amounts of additive must be present at all times to stop carbon deposition. By blending tetralin and decalin with THQ, stabilization can be achieved at 450°C.

Table 2.4-1. Preliminary Results from Incipient Deposition Studies

Mixture	Amount of Deposit (mg)
Neat tetradecane ($C_{14}H_{30}$)	12.24
$C_{14}H_{30}$ + tetralin (4 mol%)	12.41
$C_{14}H_{30}$ + THQ (4 mol%)	0.00
$C_{14}H_{30}$ + tetralin (4 mol%) + decalin (4 mol%) + THQ (4 mol%)	0.00

2.5 Study of Hydrocarbon Fuel Degradation in the Presence of Hydrogen Donors as Stabilizers

This study is explained in detail in *Advanced Thermally Stable Jet Fuels Technical Progress Report, July – September 1997.*

Introduction

The primary objective of this work was to study fuel decomposition in the presence of various fuel stabilizers and determine the amount of fuel stabilizers needed to prevent incipient carbon formation from jet fuel.

This work is part of an ongoing project on the development of advanced thermally stable jet fuels for future high-speed aircraft. To date, we have learned that at 450°C addition of 50 vol% of tetralin or decalin prevents or minimizes carbon deposits for up to 4 hours. The addition of 50 vol% of tetralin or decalins amounts to about 47 wt% of these additives—a significant amount of hydrogen donor compound, which, based on cost and availability, may not be feasible. Coleman and coworkers developed thermal stabilizers for jet fuels above 400°C.[1] They tested a number of additives and established that the addition of benzyl alcohol, benzenedimethanol and the classic hydrogen donors—tetrahydroquinoline (THQ) and tetralin—significantly retards carbonaceous solid formation from jet fuels. Using deuterated compound studies they showed that benzyl alcohol retards dodecane degradation by hydrogen transfer from benzyl carbon, thereby converting to benzaldehyde. In their study, additives were evaluated by measuring the amount of unreacted fuel (dodecane) remaining after a specific reaction time.

Although we have found THQ to be the best fuel stabilizer, we also know that adding significant amounts of THQ to jet fuel is prohibitive in terms of cost and availability. Furthermore, additive effectiveness decreases with temperature. That means additives that work at 400-450°C could perform very poorly at 475°C. For example, at 450°C the amounts of decalin and tetralin needed to stop carbon formation will be much higher than the amount needed at 425°C. The goal of this experiment was to quantify the effectiveness of additives with increasing temperature.

Experimental

The mixtures of hydrocarbons (tetradecane plus three additives at various concentration levels) were charged into microautoclave reactors and immersed into a fluidized sand bath set at the desired heat treatment temperature. The three additives used for study are tetrahydroquinoline (THQ), tetralin, and decalin. All mixtures were fixed at 5.46 g of $C_{14}H_{30}$. Additives were used at 4, 10 and 20 mol% concentrations. Tests were conducted at 450°C and 477°C. Tetradecane was used instead of jet fuel for the study because jet fuel contains more than 100 identifiable compounds. This multitude of different components makes a fundamental study of incipient deposition very difficult.

About 650-750 milligrams of -16μm stainless steel (SS316) powder were charged into a microautoclave reactor for each test. The reactor was shaken vigorously during pyrolysis tests to ensure that the steel powder was always suspended in the reactor and the entire surface of the powder was available to capture carbon deposits. After the specific reaction time intervals,

liquid and gaseous products were collected separately. The steel powder was also collected and washed with pentane. Incipient carbon deposition was examined by measuring the amount of deposit formed on the SS316 powder using TGA. About 25 mg powder was used for each TGA run and the mass of carbon deposited was measured by observing the weight loss from 300 to 600°C.

n-Decylcyclohexane was added to liquid products for analysis as an internal standard. Compounds in the liquid products were identified by GC-MS. Mass spectrometric identification was confirmed by injecting 60 different compounds and comparing their spectra and retention times with the unknown compounds of liquid products of the pyrolyzed fuel. Compounds such as substituted decalins, tetralins, indans, and cycloalkanes, for which standards are not available were identified using knowledge of their fragmentation patterns. Quantification of liquid products was accomplished using a capillary GC equipped with an FID and a DB-17 column. Those compounds that coelute in the GC were quantified using single ion monitoring in the mass spectrometer.

The absolute amount of product compound present in the liquid products was determined by:

$$Wt_{un} = \frac{Area_{un} * W_{IS}}{A_{IS} * RF} \qquad (1)$$

where $Area_{un}$, A_{IS}, W_{IS}, RF, and Wt_{un} are the area of the unknown compound peak, area of internal standard peak, weight of internal standard added, response factor of unknown with respect to internal standard, and weight of unknown, respectively.

The molar yield of unknown was determined as:

$$\text{Yield}_{un}(\text{mol}\%) = \frac{Wt_{un}/MW_{un}}{Wt_{re}/MW_{re}} * 100 \qquad (2)$$

where Yield_{un}, Wt_{un}, MW_{un}, Wt_{re}, and MW_{re}, are the molar yield of the unknown, weight of the unknown, molecular weight of the unknown, weight of the reactant, molecular weight of the reactant, respectively. The unknown compound formation occurs from a reactant that depends on the nature of the unknown. The reactant (i.e., Wt_{re} and MW_{re}) used in equation (2) to calculate molar yield of unknown was the same as that compound (i.e., tetradecane, tetralin, decalin, or THQ) from which the unknown forms. For example, in calculating the naphthalene yield, tetralin was used as the reactant, quinoline was calculated based on THQ, substituted decalins were calculated based on decalin and n-alkanes were calculated based on tetradecane as the reactant. The uncertainty in this GC analysis can be as high as 15% of the plotted value.

Gaseous products were analyzed using a gas chromatograph equipped with FID and TCD detectors. The TCD column was used to quantify hydrogen and ethylene.

Results

A mixture of 3 additives at 4 mol% addition was successful in stopping carbon formation at 450°C for two hours. The temperature of the tests was increased to 477°C and carbon deposit was measured at the end of 2 hours of pyrolysis. A mere 25°C rise in temperature led to significant carbon formation. In fact, a 10 mol% mixture of 3 additives produced more carbon deposit (263 mg) than 10 mol% of THQ and tetralin (155 mg) added to tetradecane. Thus, elimination of decalin from the 3 additive mixture actually reduced the total mass of deposits.

Results obtained from these tests motivated us to further examine the pyrolysis chemistry of mixtures of tetradecane and these three additives. To understand fuel degradation in the presence of additives, tests were first conducted on the following hydrocarbon mixtures at 477°C for time periods of 10-60 minutes:

- Neat tetradecane
- Tetradecane and 3 additives (10 mol%)
- Tetradecane and decalin (10 mol%)

We measured the mass of carbon deposits and the species compositions. TGA was run on the liquid products of the pyrolysis reactions to determine any dissolved deposits in the liquid products. To derive a pyrolysis mechanism, mixtures of tetradecane and 10 mol% tetralin were also pyrolyzed for 20 and 40 minutes.

Examining the amount of carbon deposit on the steel powder for hydrocarbon mixtures of tetradecane and 3 additives (at 10 mole% concentration) at 477°C, we realized that carbon formation has an apparent induction period of 50-60 minutes. After 60 minutes of pyrolysis, deposit mass increased more rapidly.

An examination of the molar yield of tetradecane remaining for different hydrocarbon mixtures at 477°C showed that tetradecane yield reduced most slowly for the hydrocarbon mixture that contained three additives. At 20 minutes, the yields of tetradecane for samples containing neat tetradecane, tetradecane + tetralin, tetradecane + decalin were the same. However, from 0 to 20 minutes, tetradecane disappeared faster for neat tetradecane than for the mixture of tetradecane with tetralin or decalin.

The deposits that remained soluble in the liquid products were similar in nature to asphaltene, because they were soluble in aromatic solvents and insoluble in pentane. These soluble deposits appeared in 20 minutes and rose to significant levels in 50 minutes.

We examined the molar yields of THQ, tetralin and decalin for hydrocarbon mixtures containing tetradecane and thee three additives. The yield of THQ decreased most rapidly. More than 90% of THQ was already converted at the end of 40 minutes. The molar yield of tetralin also reduced rapidly, but less rapidly than THQ. Decalin was found to be less reactive than THQ or tetralin. At the end of 40 minutes, a significant amount of decalin was detected in the liquid products.

Examining the deposit mass formed on steel powder and the molar yield of n-alkanes from C2-CI3 measured for 15 minutes of pyrolysis of neat tetradecane, tetradecane and decalin, tetradecane and three additives, we concluded the following:

- These additives work by retarding the decomposition of tetradecane
- Decalin performed the worst among the additives.
- Practically no additive was available at the end of 60 minutes of test.

Also, after 60 minutes, there was a significant rise in deposit mass, which may be attributed to either: (1) The fact that no hydrogen donor was available or (2) The dissolved deposit (i.e. asphaltene) increased to such a level that dissolved mass exceeded the solubility limit and, therefore, precipitated. Therefore, if we want to evaluate additives, we should concentrate studies on the point of pyrolysis at which no additive remains.

In order to understand tetradecane pyrolysis in the presence of the three additives, pyrolysis of neat tetradecane, tetradecane + decalin, and tetradecane + tetralin was used as a baseline. We examined product distributions of Cl-Cl3 normal alkanes from neat tetradecane pyrolysis for 5 and 15 minutes of reaction time at 477°C. At 5 minutes, the yield of C4, C5, and C6 normal alkanes is highest among all the alkanes. After 15 minutes of reaction time, the yield of C2 and C3 n-alkanes increased significantly and equaled C4-C6 n-alkanes. From 5 to 15 minutes of pyrolysis, the yield of all normal alkanes from Cl-C13 increased. The yield of *n*-alkanes from Cl-C13 at the end of 35 minutes was as high as 50%. Tetradecane conversion at 477°C after 35 minutes of pyrolysis was 90%.

Product distributions were determined from mixtures of tetradecane and decalin pyrolyzed for 10 and 15 minutes at 477°C. The amount and distribution pattern of n-alkanes obtained from pyrolysis of the mixture of tetradecane and decalin is very similar to the amount and distribution of n-alkanes obtained from pyrolysis of neat tetradecane after a reaction time of 15 minutes. The molar yield of C2 and C3 alkanes is slightly higher for neat tetradecane than for the tetradecane + decalin sample after 25 minutes of pyrolysis. However, considering the experimental uncertainties involved, the molar yield of C1, C4-C13 *n*-alkanes was the same in both cases. We then examined the distributions of C1-C13 normal alkanes from a mixture of tetradecane and three additives (decalin, tetralin and THQ) for 12, 20, and 30 minutes. For up to 30 minutes of pyrolysis time, the yield of Cl-C13 *n*-alkanes was much smaller than values determined for neat tetradecane and the tetradecane + decalin mixture.

From pyrolysis of mixtures of tetradecane and three additives, at 12 minutes of reaction time, the distribution of C3 to C11 alkanes was equimolar (i.e., the molar yield of C3-C 11 normal alkanes was similar). Values of C2-C6 *n*-alkanes were the same up to 30 minutes. At longer pyrolysis times, the yield of C3 was highest, followed by C2 and C4 *n*-alkanes. Among the ring products, selectivity for naphthalene (molar yield 44%) and quinoline (molar yield 64%) was highest. The yield of single ring aromatics such as benzene, toluene, xylenes, and benzene-C4 was similar in all four cases of pyrolysis (i.e., neat tetradecane, tetradecane + decalin, tetradecane + tetralin, and tetradecane + 3 additives). To understand the formation of ring structures and their possible precursors, information available in the literature was combined with results obtained from our study on neat tetradecane, tetradecane + decalin, and tetradecane + tetralin.

During neat tetradecane pyrolysis insignificant amounts of naphthalene, indan, methyl naphthalene, dimethylnaphthalene (molar yield < 0.2%) formed. Significant amounts of naphthalene were detected as products from pyrolysis of mixtures of tetradecane + tetralin and tetradecane + three additives. Hillebrand conducted pyrolysis of neat tetralin and neat

transdecalin at temperature range of 700-850°C.[2] They found naphthalene as a major significant product (molar yield 42%) during pyrolysis of tetralin. During *trans*-decalin pyrolysis, they found significant amounts of mono-ring aromatics (molar yield 30%).

Reaction Mechanism. Based on the observed product distributions, we proposed a reaction mechanism for pyrolysis of mixtures of tetradecane in the presence of three additives. Results obtained by Yoon et al[3] and Yu and Eser[4] were used as starting point for the construction of mechanism. Our goal was not to predict product distributions from tetradecane decomposition, but to account for the disappearance of the three additives in the presence of tetradecane and the disappearance of tetradecane. The mechanism proposed in Scheme 1 was written with this goal in mind. The pertinent Technical Progress Report explains the mechanism step-by-step.[5]

Conclusion

Additives work by retarding the initial decomposition of tetradecane. After additives are consumed, carbon formation is difficult to retard without further addition of hydrogen donors. For the pyrolysis of mixtures of tetradecane and 10 mol% of three additives at 477°C, the total sum of mass of quinoline, substituted quinolines, dihydronaphthalene, methylindan, *cis*-decalin, naphthalene, substituted naphthalenes, methylperhydroindan, substituted decalins, unreacted tetralin, unreacted THQ, and unreacted *trans*-decalin accounted for 92% of the initial mass of the three additives added to tetradecane for time periods of 10 to 50 minutes. Total mass accounts for 82% of the initial mass of three additives charged to the reactor after 60 minutes of pyrolysis. This implies that up to 50 minutes, the reaction pathways we developed for these additives during pyrolytic reaction are reasonably accurate.

All of the reactions mentioned in the mechanism are elementary reactions. Values of kinetic parameters for elementary reactions can be determined from the literature. Some parameter values may not be available or may not be reliable. These values become adjustable parameters. When the reaction pathway consists of elementary reactions, our model becomes more generalized and will have fewer adjustable parameters.[6]

---

[1] Coleman, M. M. et al. *Energy & Fuels.* 1996. 10.

[2] Hillebrand, W., W. Hodek, and G. Kolling. *Fuel.* 1984. 63. 756.

[3] Yoon, E. et al. *Energy & Fuels.* 1996. 10. 806-811.

[4] Yu, J. and S. Eser. *Ind. Eng. Chem Res.* 1997. 36. 574-591.

[5] Schobert, H. H. et al. *Advanced Thermally Stable Jet Fuels, Technical Progress Report, July – September 1997.* The Pennsylvania State University. 92PC92104-TPR-21. 1997.

[6] Froment, G. F. *Chemical Reactions in Complex Mixtures.* New York: Van Nostrand Reinhold. Chapter 5. Editors: A. V. Sapre and F. J. Krambeck. 1991.

2.6 KINETICS OF DEPOSIT FORMATION FROM JET FUEL

This study is explained in detail in *Advanced Thermally Stable Jet Fuels Technical Progress Report, October – December 1997.*

Introduction

In future aircraft the fuel will reach temperatures as high as 700°C for a fraction of a second before combustion. A portion of the fuel will also experience a moderate heat flux for a long residence time. Under such conditions, fuel undergoes pyrolytic reactions that lead to the formation of carbonaceous coke-like solids, known as deposit, which foul heat exchangers and reduce the flow through fuel injection nozzles. Coke particles also form in the bulk and can be carried to the turbine combustor, creating performance problems. Because of the increasing thermal management needs in aircraft, there is an increasing need for development of a fundamental model to predict the extent of coke formation in fuel lines. Development of an accurate kinetic model for deposit formation also could help to reduce costly engine tests to determine the rate of deposit formation. In this study, the words "deposit," "coke" or "solids" all refer to a layer of carbon formed on metal surfaces by fuel decomposition.

Although deposit formation from jet fuel has been studied for more than five decades, the kinetics of solid formation are not well understood. Mechanisms of solid formation from jet fuel depend on temperature, pressure, oxygen, nature of the fuel, and additive presence. Deposit formation from coal derived jet fuel is studied under an inert environment of nitrogen in the vicinity of 450°C (723°K) and autogenous pressure of 2000 psi. Thermal stressing (pyrolysis) of the fuel is carried out in tubing bomb reactors. About 10 ml of fuel sample is heated in a nitogen environment for a time period varying from 2 to 12 hours. Reaction products are analyzed using GC and GC/MS for identification and quantification. Coke formed on the reactor wall is determined by measuring the weight change of the reactor before and after the reactions. The amount of deposit that formed but remained within the bulk was determined by solvent extraction.

Approaches to the Problem

A commonly accepted explanation is that coke formation during hydrocarbon pyrolysis occurs by free radical reactions. Development of a kinetic model for deposit formation during hydrocarbon pyrolysis requires consideration of several reaction steps. A number of people have studied the kinetics of hydrocarbon pyrolysis in terms of elementary reactions. Savage[1] considered 170 elementary reactions to predict product distributions from joint pyrolysis of tridecyl cyclohexane and pentadecyl benzene. All of the reactions considered were primary reactions whose rate constants can be determined from the literature. Coke forms by secondary reactions of hydrocarbon pyrolysis. Coal-derived jet fuel (JP-8C) contains approximately 150 identifiable compounds. To simulate pyrolytic reactions and predict coke formation in terms of elementary reaction steps of individual compounds would require consideration of hundreds of reaction steps. Because of the complexity of the network of reactions and the absence of widely accepted chemistry, a mechanistic modeling study on fuel pyrolysis to develop rate equations in terms of elementary steps is not possible. Although some efforts have been made to model deposition in the autoxidation regime, the high temperature pyrolytic domain of fuel decomposition has not been considered.[2, 3]

In this study, 10 ml of fuel and mixtures of fuel and reactive compounds were stressed in tubing bomb reactors at 450°C and an initial nitrogen pressure of 100 psi. Gaseous and liquid products formed during thermal decomposition were collected separately and analyzed by GC-MS. Because insignificant amounts of solids remain in the bulk after pyrolysis, solvent extraction was not employed to characterize the solids further.

From measurements of the concentration history and the knowledge of mechanisms of deposit formation, a kinetic model for solid formation will be constructed from a reaction engineering viewpoint. In the kinetic model, species will be categorized by their tendency towards deposit formation.

Hirt and Palmer[4] found direct correlation between homogeneous decomposition of methane and coke formation, and derived an activation energy of 103 kcal/mole for coke formation between 890° and1100°C. Froment and coworkers developed an overall rate equation for coke formation from ethane and propane in terms of propylene concentration over a temperature range of 750° to 850°C.[5, 6] However, the decomposition of hydrocarbon alone or evolution of olefins alone is unable to explain the induction period. This study is aimed at simulating both the induction period as well as, the rise in deposit mass at longer times and extrapolating the proposed rate equation to other fuel mixtures and different temperatures.

The study was carried out in two parts. The first part involved development of proper experimental methods and data analysis using GC and GC/MS. Under the assumption that pyrolysis chemistry is going to be complex, the second part was devoted to the development of a suitable computational method to describe the kinetics with sufficient accuracy.

Part 1: Development of Proper Experimental Methods and Data Analysis

Deposits can form by surface reactions on the reactor walls as well as by homogeneous reactions occurring in the bulk. Because two kinds of reactions occur during coke formation, it was necessary to determine the amount of solid formed on the wall and the amount that remained suspended in the particulate form in the pyrolyzed fuel (i.e., solid remaining in the bulk).

Deposits formed on the reactor walls were found to be insoluble in solvents like toluene and THF. No toluene insolubles were found in the stressed fuel. However, small but measurable amounts of pentane-insoluble and toluene-soluble compounds were found in the stressed liquid product, but not on the wall. Solid growth occurred directly on the wall rather than through a homogeneous nucleation, such as occurs during soot formation. Thus, as soon as the reactive species form they go to the wall and react with the deposit mass present there. This does not mean than deposit formation is a heterogeneous process. Stainless steel surfaces (SS 316) remain inert during pyrolysis.[7] However when Ni and Cu are present, these surfaces do catalyze deposit formation.[8] The initial layer of deposit on the wall acts as a sink for reactive species.

We next had to identify the reactive species or the compounds that could furnish such reactive species during pyrolysis. Coal-derived fuel contains at least 150 identifiable compounds which we suspect can each contribute to deposit formation. Also, the knowledge of the degree to which a particular family of hydrocarbon contributes to solid formation helps in determining the groupings of hydrocarbons for the kinetic analysis.

To resolve which species are involved we used a number of model compound studies to elucidate the degree to which many of these compounds contribute to deposit formation. During these model compound studies, tetradecane, dodecane, and *n*-butylbenzene were found to produce the maximum amount of solids during pyrolysis at 450°C for 4 hours. JP-8C was predominantly a mixture of cycloalkanes, decalins, and tetralins, with small amounts of normal alkanes and alkylated aromatics. JP-8C's abundance of hydrogenated ring compounds and lack of appreciable *n*-alkanes and alkyl aromatics make it a very stable fuel under pyrolytic conditions. Neat coal-derived jet fuel was found to produce deposits only after 8 hours of stressing. Because tetradecane was found to produce more solids, we concluded that tetradecane would act as a reactive species during coke formation in a complex mixture such as jet fuel. Results of deposit formation for an initial concentration of tetradecane added to the neat jet fuel showed that deposit formation was directly proportional to the concentration of tetradecane present in the fuel. Mixtures of 18% tetradecane in neat JP-8C were pyrolyzed at 450°C for different time periods. The natural logarithm of concentration of the tetradecane remaining in the mixture at a specific time was plotted and the correlation coefficient for tetradecane decomposition versus time was found to be 0.98. Therefore, tetradecane decomposition is first order under these conditions.

The highly correlated relationship between initial tetradecane concentration and deposition of solids led us to examine other compounds in the fuel and stressed fuel products from a statistical viewpoint. The concentration of compounds such as hexane, heptane, octane, nonane, decane, undecane, dodecane, tridecane, cyclohexane, methyl cyclohexane, ethylcyclohexane, propylcyclohexane, benzene, toluene, xylenes, ethylbenzene, ethylmethyl cyclohexanes, dimethylcyclohexanes, tetralin, decalin, tetralins c1, tetralins c2, decalins c1, decalins c2, naphthalene, naphthalenes c1, and naphthalenes c2, were measured at various time intervals and plotted. We then set out to determine what role these compounds play in the stressed fuel during pyrolysis, based on observations of the time history of their concentration. We looked for the degree to which concentration correlated with deposit mass over time.

When drawing a conclusion about coking tendency of a compound under pyrolytic conditions, we assumed that when the concentration of a particular species continuously increases or decreases very slowly, that species will likely be stable during pyrolysis (i.e., it will not undergo rapid thermal decomposition). When a compound is stable, it cannot contribute to coke formation. When the concentration of a compound decreases relatively quickly, it likely will be an unstable compound and, therefore, will contribute to deposit formation.

The reason for determining the degree or contribution that particular species makes toward deposit formation is that this will allow us to selectively eliminate large numbers of species from our kinetic model. Obviously it is unrealistic to follow pathways for each species. The kinetics of solid formation can be described in terms of the pathways of a few species. Their degree of contribution is not measured quantitatively. The qualitative estimate of this degree is made from the concentration history, coupled with the knowledge of the model compound studies and bond dissociation energy, and the number of possible ways the organic compound decomposes. All of the discussion that follows refers to 450°C (723°K).

The concentration of methylcyclopentane steadily increased with time. Methylcyclopentane forms from cyclization reaction of radicals formed from tetradecane, tridecane and dodecane.[9] Cyclohexane and methyl cyclohexane concentrations remained

constant for 6 to 9 hours and then decreased slightly. The concentrations of compounds such as ethylcyclohexane, propylcyclohexane, and methylethyl cyclohexane decrease slowly but steadily with time. Ethyl, propyl, and ethylmethyl cyclohexane concentrations either decreased very slowly or increased continuously. There was no direct correlation between the initial concentration of cycloalkanes and the deposit formed. Therefore, these cycloalkanes will not contribute to deposit formation.

The concentration of toluene, xylenes, ethylbenzene, naphthalenes and substituted naphthalenes increased with reaction time. Naphthalene, naphthalene c1, naphthalene c2, and indan c1 are primary products of the fuel decomposition reactions. Naphthalene and substituted naphthalenes were found to be very stable in individual model compound studies and, because their concentration increases with time, these compounds will not contribute to deposit formation. Concentrations of toluene, xylenes, and ethylbenzene increased with time, and we concluded that they do not contribute to deposit formation. However, this hypothesis was not correct, as reported by Coleman and coworkers[10] during their study on dodecane pyrolysis that deposit formation begins with the evolution of aromatics. Can their results be extrapolated for different mixtures? This issue requires further consideration before any conclusion can be drawn. We grouped xylenes and ethylbenzene together as one compound because of difficulty in quantifying them separately due to their similar mass spectra.

The concentrations of tetralin, decalin, decalins cl, decalins c2, tetralins cl, and tetralins c2 decreased steadily with time. It has already been shown by Song et al. that compounds such as tetralin and decalin function as hydrogen donors and that they inhibit deposit formation.[9] These two compounds are converted to naphthalene, which is thermally stable. Substituted tetralins and decalins will be converted to substituted naphthalenes and are, therefore, less likely to form reactive species. The concentrations of indan, indans cl, indans c2 decrease slightly. These compounds might be converted to naphthalene and naphthalenes c1, which should preclude them from forming deposits.

The concentrations of dodecane, tridecane, and undecane decreased very quickly compared to cycloalkanes. We have shown that the amount of solid formation is directly proportional to the initial concentration of tetradecane in JP-8C; it was also proportional to dodecane and tridecane concentration.

Solids formation proceeds mainly through formation of alkylbenzenes as the important intermediate. But during the pyrolysis of mixtures of coal-derived jet fuel and tetradecane, we found that alkylbenzene concentration remained constant and was fairly small. Therefore, we concluded that alkyl-benzenes do not play a significant role under these specific circumstances. In the previous work on tetradecane pyrolysis, deposit growth did not occur until a significant amount of alkyl benzenes appeared; in that case we concluded that alkyl benzenes were precursors of deposit formation. Alkyl benzenes also produced significant amounts of solids when they were pyrolyzed individually.[11]

The concentrations of normal hexane, heptane, octane, nonane, decane, and undecane increased from 0 to 4 hours and then began to decrease. In the individual model compound studies, coking tendency was found to decrease with a decrease in carbon number. Therefore hexane, heptane, and octane might not contribute to solid formation. Only nonane, decane, and

undecane could contribute to solid formation among the normal alkanes from hexane to undecane.

Because the initial concentration of tetradecane was fairly high (60 kg/m^3) and concentrations of other well-known deposit-forming precursors (such as alkylaromatics, nC10, and higher alkanes) were very low (< 12 kg/m^3), the preliminary reaction model shown in Scheme 1 was proposed for deposit growth.

$$F \xrightarrow{k_F} R \qquad \text{F = Tetradecane, R = Radical}$$

$$R + H_i \xrightarrow{k_{H_i}} \text{Stable Products} \qquad H_i = \text{Tetralins and Decalins}$$

$$R + D \xrightarrow{k_D} D \qquad \text{D = solids}$$

$$\frac{dR}{dt} = k_F F - R\Sigma k_{Hi} H_i - k_D R$$

$$\frac{dH_i}{dt} = -R\Sigma k_{Hi} H_i$$

$$\frac{dD}{dt} = k_D R$$

Scheme I. Preliminary Kinetic Model for Deposit Formation from Tetradecane in a Fuel Mixture

The values of the best fit parameters obtained were $k_F = 1.1 \times 10^{-4} s^{-1}$, $k_{H,1} = 2.5 \times 10^{-4} m^3/(kmol\ s)$, $k_{H,2} = 1.5 \times 10^{-4} m^3/(kmols)$, and $k_D = 3.5 \times 10^{-8}$ m/s. We were able to qualitatively describe the disappearance of tetradecane and hydrogen donors such as tetralins, decalins, and the growth of deposits. Here we assumed that tetradecane undergoes decomposition and forms a radical that is either stabilized by tetralins or decalins or reacts and forms deposits. However, an attempt to model deposit growth based solely on tetradecane concentration failed to reproduce the observed induction period shown. During the induction period, tetradecane decomposed prior to significant deposit formation. Deposit selectivity, calculated as the mass of coke produced divided by the initial mass of tetradecane present, was plotted against the conversion of tetradecane. From that curve we deduced that a measurable amount (> 4 mg) of deposit appears only after 63% conversion of tetradecane. This means that the reactive species formed from tetradecane will form more reactive radicals. Because of the complexity of the JP8C-$C_{14}H_{30}$ mixture and lack of a proper experimental probe, we could not speculate on the nature of radicals formed based on the very first radicals formed by decomposition.

Although we could reasonably assume that tetradecane is the sole contributor to deposit formation from mixtures of JP-8C and tetradecane, we could not quantitatively describe deposit formation based on this assumption. We can accurately model the induction period using the evolution of toluene and xylenes, because these compounds increased in concentration after 3

hours of pyrolysis. This type of molecular reaction model is more effective than the model shown in Scheme 1. However, can the kinetic parameters obtained from this information be extrapolated to other mixtures or temperatures? Furthermore, are the values of the kinetic parameters independent of concentration? To answer such questions, we need a more detailed description of fuel decomposition chemistry. Because the chemistry is expected to be complex and several groupings of species will be necessary to describe the kinetics, the second part of the study was devoted to the development of a suitable computational method.

Part 2: Development of a Suitable Computational Method for Decomposition Chemistry

Development of a kinetic model requires rate parameter estimation from multiresponse data. Parameter estimation from multiresponse data has been studied previously.[12, 13] Parameter estimation from experimental data is considered to be the inverse problem of a dynamic model. It can be described as a system of ordinary differential equations (ODE):

$$dC/dt = f(t, C, \theta) \qquad (1)$$

where C is a vector of concentration variables, t is reaction time, θ is the vector of parameters (e.g. rate coefficients), and f is the functions representing mass balance of species. Given the initial conditions of $C = C_0$ we can find the values of parameter θ such that solution of equation (1)

$$C = g(\theta, t, C_0) \qquad (2)$$

matches the experimental data, $C = C^{obs}$. Mathematically this is stated as the minimization of an objective function ϕ with respect to the parameters θ. ϕ is expressed as:

$$\phi(\theta) = \sum_{i=1}^{n} \omega_i [C_i^{obs} - C(\theta)]^2 \qquad (3)$$

where n is the number of experimental observations and ω_i is the weighting factor of the *ith* observation.

Optimization of (3) can be performed via a search algorithm in a multidimensional space, θ, with a call to a differential equation solver each time new values of parameters are evaluated. When the number of parameters to be estimated is small, this method works well. However, when the number of parameters to be estimated increases (>12), this method fails because the extremely large number of function evaluations required places a large demand on computation time.[14]

To overcome this difficulty, a method of solution mapping was proposed.[14] In this work, the solution mapping method will be used for kinetic parameter estimation. In this technique, C in equation (2) is approximated by simple algebraic expressions:

$$g(\theta, C_0) = \psi(\theta) \qquad (4)$$

in the subspace Ω of parameter space θ. The approximating functions $\psi(\theta)$ are obtained by means of computer experiments known as factorial design performed using a complete kinetic model.[15]

By substituting equation (4) into equation (3), we obtained:

$$\phi(\theta) = \sum_{i=1}^{n} \omega_i [C_i^{obs} - \Psi_i(\theta)]^2. \qquad (5)$$

which means that optimization of the objective function no longer requires time consuming numerical integration of differential equations, but rather straightforward evaluations of $\psi(\theta)$. That is, this method decouples the ODE solver from the optimization search.

As an illustration, consider the following problem of parameter estimation from chemical kinetics where k1, k2, k3 and kd need to be determined from experimental values of F, H1, H2, and D:

dF/dt = k1 * (F)

dR/dt = kl * (F) - k2 * (HI) * (R) - k3 * (H2) * (R) - kd * (R)

dHl/dt = -k2 * (H1) * (R)

dH2/dt = -k3 * (H2) * (R)

dD/dt = kd * R

where F, H1, H2, and D represent different species taking part in reactions. Also values of F, H1, H2, and D at time, t, where t = tl, t2, t3 ...., are known.

1. Specify the ranges of rate parameters k(l), k(2), k(3) and k(d)

ln[kl] = ln[k(1,0)] +/- ln[delta(l)]
ln[k2] = ln[k(2,0)] +/- ln[delta(2)]
ln[k3] = ln[k(3,0)] +/- ln[delta(3)]
ln[kd] = ln[k(d,0)] +/- ln[delta(d)]

where k(i,0) is the initial guess of the i*th* rate parameter, and delta(i) is a positive value and is the (arbitrarily) assigned range of rate parameter k(i).

Let X(i) = ln[k(i)/k(i,0)] / ln [delta(i)]

where X(i) is a factorial variable, such that

X(i) = 1 for k(i) = k(i,0) * delta(i)

X(i) = 0 for k(i) = k(i,0)

X(i) = -1 for k(i) = k(i,0) / delta(i)

2. Make a 2^2 factorial design of X(i)

J	X(t)	X(2)	X(3)	X(d)
1	+1	+1	+1	+1
2	+1	+1	+1	-1
3	+1	+1	-1	+1
4	+1	+1	-1	-1
5	+1	-1	+1	+1
6	+1	-1	+1	-1
7	+1	-1	-1	+1
8	+1	-1	-1	-1
9	-1	+1	+1	+1
10	-1	+1	+1	-1
11	-1	+1	-1	+1
12	-1	+1	-1	-1
13	-1	-1	+1	+1
14	-1	-1	+1	-1
15	-1	-1	-1	+1
16	-1	-1	-1	-1
17	0	0	0	0

Compute the responses [i.e., F(t), HI(t), H2(t) and D(t)] at each design point, j (j=1,J) for every time tl, t2, t3 .... at which experimental values of F, H1, H2, and D are available. After calculating values of responses, you will have a table that looks like this:

J	X(l)	X(2)	X(3)	X(d)	F(t1)	F(t2)	..	H1(t1)	H1(t2)	..	H2(t1)	etc.
1	+1	+1	+1	+1	Fll	F12	..	Hlll	H112	..	H211	etc
2	+1	+1	+1	-1	F21	F22	..	H121	H122	..	H212	etc
3	+1	+1	-1	+1								
4	+1	+1	-1	-1								
5	+1	-1	+1	+1								
6	+1	-1	+1	-1								
7	+1	-1	-1	+1								
8	+1	-1	-1	-1								
9	-1	+1	+1	+1								
10	-1	+1	+1	-1								
11	-1	+1	-1	+1								
12	-1	+1	-t	-1								
13	-1	-1	+1	+1								
14	-1	-1	+1	-1								
15	-1	-1	-1	+1								
16	-1	-1	-1	-1								
17	0	0	0	0								

Using the linear regression technique, you can then obtain a second-order polynomial for each of the responses, for example:

ln[F(tl, polynomial)] = aF0 + aFl X(l) + aF2 X(2) + aF3 X(3) + aF4 X(4) + aF11 X(1)^2 + aF12 X(1) *X(2) + ...

where aF represents polynomial parameters. In essence, the above exercise gives the numerical dependence of F, H1, H_2, and D on k(i). Because F, HI, H2 and D depend only on k(i), and not on t, costly integration of ODE for each optimization search is not required.

3. Optimization: Minimize

L^2 = sum_j [F(tj,polynomial) - F(tj,expt)]^2 + sum_j [Hl(tj,polynomial) - Hl(tj,expt)]^2 + sum_j [H2(tj,polynomial) - H2(tj,expt)]^2 + sum_j [D(tj,polynomial) - D(tj,expt)]^ 2

with respect to k(l), k(2), k(3) and k(d), where F(tj,polynomial) etc. is the developed polynomial and F(tj,expt) is the experimental value at time tj.

This new method will be used in our problem of kinetic model development.

Summary and Conclusion:

Kinetics of deposit formation can be described qualitatively in terms of the thermal decomposition of unstable compounds. In the study discussed here, tetradecane was an unstable compound that was also present in large amount (18% by weight). Despite its abundance in the mixture, the decomposition of tetradecane could only provide a qualitative description of deposit formation. Alkanes having greater than nine carbons and substituted alkyl benzenes produce significant amounts of coke. Thus, when the mixture has a high concentration of these compounds, the initial decomposition alone is a poor approximation for kinetics.

For mixtures of tetradecane and JP-8C, further development of the kinetic model will focus on the formation of toluene and xylenes from tetradecane, and subsequent formation of deposit from these compounds. Formation of alkanes lighter than n-hexane will also be included in the model. We may also have to include the formation of other compounds from xylenes and toluene to apply the results to other mixtures. The difficulty involved in speculating the formation of secondary radicals from the primary radical, the reaction model described in Scheme 1 will not be easy to implement.

---

[1] Edwards, T., Personal communication, U.S. Air Force Wright Laboratory, WPAFB, October 1995.

[2] Krazinski, J. L., and S. P. Vanka. *Final Report.* WRDC-TR-89-2139. December 1989.

[3] Zabamick, S. *Ind. Eng. Chem. Res.* 1993. 32. 1012-1017.

[4] Hirt, T. J. and H. B. Palmer. *Carbon.* 1963. 1. 65.

[5] Froment, G. F., K. M. Sundaram, and P. S. Van Damme. *AIChe Journal.* 1981. 27. 94, 951.

[6] Froment, G. F., and K. M. Sundaram. *Chemical Engineering Science.* 1979. 34. 635-644.

[7] Eser, S. Personal communication. Pennsylvania State University, Fuel Science Program. 1995.

[8] Li, J. and S. Eser. *Extended Abstracts: 21st Biennial Conference on Carbon.* American Carbon Society. 1993. 527.

[9] Song, C., W. Lai, and H. H. Schobert. *I & EC Research.* 1994. 33. 534-547.

[10] Coleman M. M. et al. *Energy and Fuels.* 1992. 6. 535-539.

[11] Peng, Y. *Ph.D. Dissertation.* Dept. of Materials Science & Engineering, The Pennsylvania State University. 1995

[12] Ziegel, E. R. and J. W. Gonnan. Technometrics. 1980. 22(2). 139-151.

[13] Stewart, W. E., M. Caracotsios and J. P. Sorensen. *AlChe Journal.* 1992. 38(5).

[14] Frenklach, M., H. Wang, and M. J. Rabinowitz. *Prog. Energy Combust. Sci.* 1992. 18. 47-73.

[15] Box, G. E. P., W. G. Hunter and J. S. Hunter. *Statistics for Experimenters, An Introduction to Design, Data Analysis, and Model Building.* New York: Wiley. 1978.

TASK 3. CHARACTERIZATION OF SOLID GUMS, SEDIMENTS, AND CARBONACEOUS DEPOSITS

3.1 SEM Study of the Deposits on Stainless Steel Flow Reactor Tube Surface

This study is explained in detail in *Advanced Thermally Stable Jet Fuels Technical Progress Report, August 1992 – October 1992.*

Introduction

This study involved the analysis of carbon deposits, morphologies on metal grids, and flow reactor deposits with regard to the flow reactor tube used throughout our research. Our analysis was conducted on one half of a stainless steel reaction tube deposited with carbon from thermal stressing of a jet fuel, which we obtained from Sandia National Laboratories. The tube was cut into segments and examined by SEM to obtain a morphology profile of the deposits along the tube.

Results and Discussion

The inner surface of the reactor tube appeared rough with protrusions like extended hills and various sized "buttons" (grains), which were scattered on and between the hills. Black spots also appeared on the surface. The deposits were primarily of three types:

- Mobile Carbon Island
- Carbon Mound
- Particulate Carbon – which can be divided into coalesced particulate clusters, continuous grown particulate carbon layer, and finely dispersed particulate carbon

The mobile carbon islands were observed at both ends of the reactor tube. They deposited around the edges of the buttons (metal grain boundaries) and coalesce and move, trying to form an extended network. The growth of this type of deposit is the initial and final stage of the deposition process. Thus, it is incomplete and is soon replaced by the dominant growth pattern—particulate growth. Mobile carbon island likely did not grow on the buttons because the edges, which are grain boundaries, are more favorable sites for deposit growth.

Carbon mound was observed at the boundaries of the deposition and was visible to the naked eye. This type of deposit was not observed at the exit end of the tube.

Particulate carbon's distinct feature is its layered deposit structure. Typically, coalesced particulate clusters are covered by a continually grown particulate carbon layer. In this case, however, the holes of the top layer did not necessarily correspond to the buttons. Lahaye and Prado[1] suggested that this could be caused by the competition between the formation of surface pyrolytic carbon and the gas-borne carbon. Deposition of pyrolytic carbon on the substrate results in a decrease of surface area, thereby inhibiting further adsorbtion and growth of the surface carbon. Meanwhile, gradually more finely dispersed carbon forms in the gas phase. A portion of the carbon becomes absorbed on the formerly deposited carbon. Consequently, the surface area temporarily increases, and conditions for the formation of a new layer of surface carbon are resumed. In addition, gas-borne carbons likely adhere to the surface protrusions (the buttons).[2] This indicates that the particulate around the button edges must not be formed in the gas phase. Rather they are probably the surface pyrolytic carbon. As fuel flows deeply into the tube (i.e., the latter half of the reactor tube), more finely dispersed carbon is formed. This type

of carbon is easy to deposit on the imperfect carbon substrate, thereby filling the holes of the layers to form a continuous growing carbon layer.

---

[1] Lahaye, J. and G. Prado. "Mechanism of Carbon Black Formation." *Chemistry and Physics of Carbon.* P. L. Walker, Jr., ed. 1978. 14. 167.

[2] Bokros, J. C. *Chemistry and Physics of Carbon.* P. L. Walker, Jr., ed. 1969. 5. 1.

3.2 Surface Effects on the Formation of Carbon Deposits—A Literature Review

This study is explained in detail in *Advanced Thermally Stable Jet Fuels Technical Progress Report, February–March 1993.*

Introduction

Jet fuels are mixtures of hundreds of hydrocarbons, including paraffins and aromatics. Under severe thermal stressing—as anticipated in future high-performance aircraft—these hydrocarbon species could undergo a hydrogen redistribution process, resulting in a hydrogen-rich gas/liquid phase and a hydrogen-poor carbonaceous solid.[1 2 3] Carbonaceous deposit formation is a minor reaction relative to the main fuel degradation, but its ability to lead to system malfunctions makes it an important reaction.[4] The rate of formation, however depends on the fuel and the environment the fuel serves. Inhibiting deposit formation can only be achieved by gaining a full understanding of the mechanisms of catalytic and non-catalytic deposit formation.

Carbon deposits can form via two opposite routes—decomposition of the hydrocarbons to elemental carbon and hydrogen, or polymerization to large planar polycyclic aromatic hydrocarbons (PAHs), which then nucleate and grow to carbonaceous deposits. A critical factor determining the formation of catalytic or non-catalytic carbon deposits is the characteristic of the substrate surface. A non-catalytic surface may affect the heat or mass transfer in the system and serve to collect the carbon deposit formed in the bulk phase. In contrast, a catalytic surface could also interact with the bulk phase, promote the deposit formation, and, finally, be deactivated to a non-catalytic surface as a result of the encapsulation of carbon deposits.

We reviewed existing literature on the mechanisms of carbonaceous deposit formation in the jet fuel range, catalytic and non-catalytic deposit formation from related light or heavy hydrocarbons, and comparisons of catalytic and non-catalytic deposit formation. Our findings are detailed in *Advanced Thermally Stable Jet Fuels Technical Progress Report, February – March 1993*; space constraints require us to summarize our findings for the purpose of this report.[5]

Conclusions

Figure 3.2-1 provides a schematic overview of catalytic and non-catalytic carbonaceous deposit formation from thermal stressing of hydrocarbons. Autooxidation and pyrolysis of jet fuels under thermal stressing can lead to the formation of carbonaceous deposits. The mechanisms of deposit formation were relatively well documented as they pertain to autoxidation of jet fuels, but are not fully understood from a pyrolysis standpoint. In general, free radical decomposition, polymerization, and condensation reactions produce PAHs, which nucleate and grow to form a carbonaceous deposit under pyrolysis conditions.

Catalytic carbon deposits from pyrolysis of light hydrocarbons include filamentous, laminar graphitic, and amorphous carbons. Filamentous carbon forms via the bulk diffusion of elemental carbon atoms through the metal particles. The driving force behind this diffusion process continues to be debated. A metastable metal carbide likely helps to establish the concentration gradient from the leading to the trailing face of the metal particle. For the

formation of laminar graphitic deposit, both dissolution-precipitation and surface diffusion are likely part of the mechanisms. Finally, amorphous carbon may form through the polymerization of small hydrocarbon species.

Non-catalytic pyrolytic carbons come from two sources: gas-born carbon and surface carbon. These two distinct forms of carbon may have different precursors, nucleation of the precursors, and the growth patterns. For gas-born carbon, the precursors are probably PAHs, and homogenous nucleation and agglomeration have been suggested as its nucleation and growth mechanisms. For surface carbon, the precursors are probably more diverse, and nucleation and growth processes can better be described as chemical in nature. During the carbonization of heavy hydrocarbons, liquid phase mesophase carbon and precipitated tars are found to be the predominant carbon deposits.

Studies of the deposit formation from jet fuel pyrolysis have explored a new field in the spectrum of carbon formation from hydrocarbon pyrolysis. These studies are important for their practical applications, as well as their potential to provide new insights into various carbon formation processes.

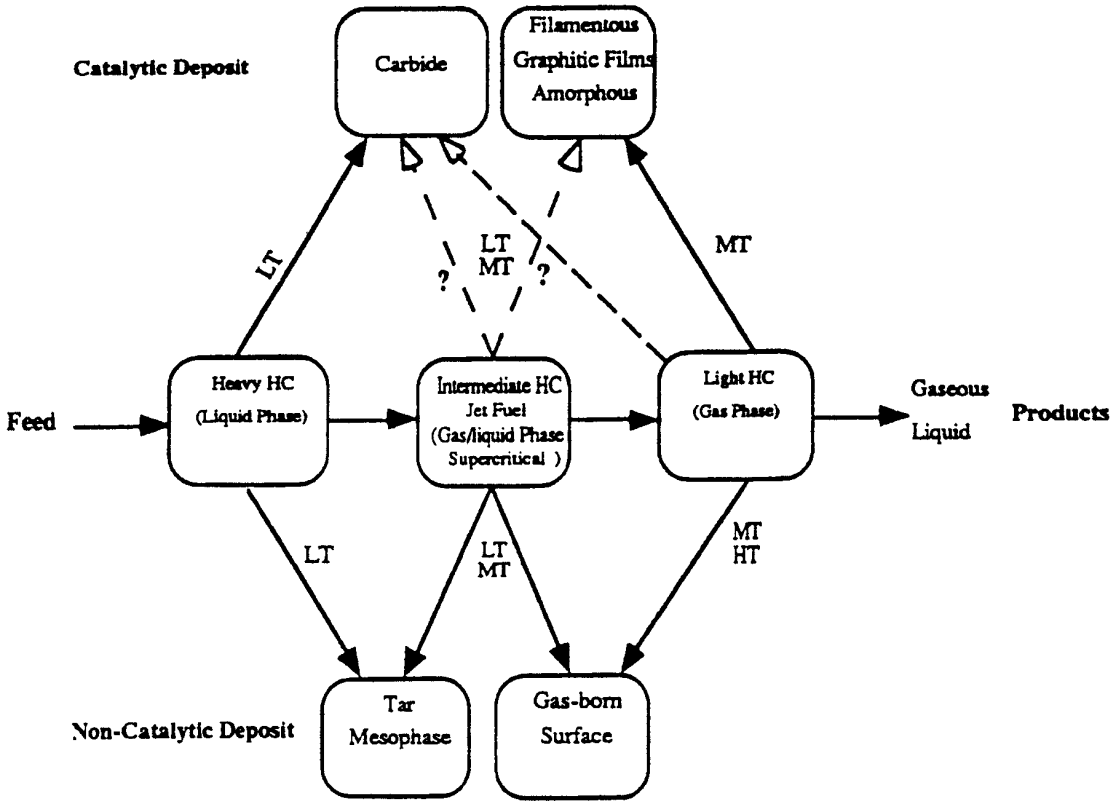

Figure 3.2-1. Schematic Diagram of the Mechanisms of Catalytic and Non-Catalytic Carbon Deposit Formation in Pyrolysis of Hydrocarbons, LT, Low Temperature: <400°C; MT, Intermediate Temperature: 400-800°C; HT, High Temperature: >800°C.

[1] Fitzer, E., K. Mueller, and W. Schaffer. *The Chemistry and Physics of Carbon.* New York: Dekker. 1971. 237-383.

[2] Faith, L. E. et al. *Hydrocarbon Fuels for Advanced Systems.* Aero Propulsion Laboratory. AFAPL-TR-70-71, Part III. 1972.

[3] Taylor, P. H. and W. A. Rubey. *Energy & Fuels.* 1988. 2(6). 723-728.

[4] *CRC Literature Survey on the Thermal Oxidation Stability of Jet Fuel.* Atlanta: Coordinating Research Council, Inc. CRC Report No. 509. 1979.

[5] Schobert, H. H. et al. *Advanced Thermally Stable Jet Fuels Technical Progress Report, February 1993 – March 1993.* The Pennsylvania State University. 1993. 15-35.

3.3 Carbonaceous Deposit Formation on Metal Foils from Thermal Stressing of Coal-Derived Jet Fuels (JP-8C)

Our previous work indicated that the chemical composition of a metal surface and the types of reactants had a significant effect on carbon deposit formation during thermal stressing of Jet A and *n*-dodecane.[1] In addition, we found that the deposit formation from dodecane thermal stressing on a metal surface could be a two step process—an initial catalytic deposition step on some clean metal surfaces and a subsequent deposition step on the previously formed deposit surface.[2] Filamentous carbon and fibrous carbon were detected on nickel and copper surfaces respectively, which may be as a result of the catalytic effects of these two metal surfaces in the system. Meanwhile, a common feature of carbon deposit on all of the metal surfaces studied was found to be the circular or oval ring structure, which is probably related to the further growth of deposit on previously formed carbon deposit surface.

a. Deposits on Pure Metal and Stainless Steel Foils

This study appears in Appendix IV of *Advanced Thermally Stable Jet Fuels Technical Progress Report, October– December 1993.*

Purpose: Continue study of surface effects of deposit formation, using pure metal and stainless steel foils, rather than grids and wires, as substrates.

Experimental: *N*-dodecane was thermally stressed in 20 mL stainless steel tubing bomb reactors using 5 mL deoxygenated samples and 100 psi UHP N_2 as the initial pressure. Nickel (NI), copper (Cu), aluminum (Al), titanium (Ti), and stainless steels 304 (Fe/Cr18/Ni10), 316 (Fe/Cr 18/Ni 8/Mo 3), and 321 (Fe/Cr 18/Ni 8/Ti) foils were used. Two foil coupons were suspended at both the top and bottom of the reactor for each run.

Results: We identified clear indications of both initial and subsequent deposit formation on different metal surface from dodecane thermal stressing. Initially, nickel surface can catalyze the deposition by forming fibrous carbon; copper surface can likely catalyze the deposition by forming fibrous carbon. Stainless steel, on the other hand, has no catalytic effects on the deposit formation process. A feature common to all of the metal surfaces was the formation of rings on the deposit layer. The ring formation process is probably related to the steady-state growth of deposit on all metal surfaces. The mechanism of ring formation is not yet understood.

b. Two-Step Deposition Process

This study appears in Appendix IV of *Advanced Thermally Stable Jet Fuels Technical Progress Report, January – March 1994.*

Purpose: In this work, a coal-derived jet fuel, JP-8C, was studied to test the proposition of a two-step deposition process on metal surfaces.

Experimental: Thermal stressing of JP-8C was conducted isothermally in 20 mL stainless steel tubing bomb reactors heated in a fluidized sand bath. A 5 mL sample was used for all of the tests. The sample was deoxygenated by repetitive pressurization and purging with ultra-high purity (UHP) nitrogen, and left with 0.69 MPa (100 psi) UHP N_2 as the initial pressure. At the end of the reaction, the reactor was quenched in cold water. Nickel, copper, aluminum, titanium,

and stainless steel foils were used as the substrate surface. For each run, two coupons were hung at the top of the reactor, just below the reducer and two were placed in the bottom of the reactor.

Results:

Carbon deposition on nickel surface. After 3 hours' reaction, nickel surfaces both on top and at the bottom of the reactor are covered by deposit with a honey comb shape. The deposit seemed to have a glassy layer. Deposits grew significantly by 5 hours. The nickel surface at the top of the reactor ("top surface") had numerous sticky deposit particles scattered on the glassy layer; no such deposit was seen on the nickel surfaces at the bottom of the reactor ("bottom surfaces"). No glassy layer develops on surfaces of other metals, indicating that a nickel surface cannot only affect the deposition process itself, but also alter the chemistry that leads to the deposition formation.

Carbon deposition on titanium, aluminum, and copper surfaces. After 3 hours, no carbon deposit was apparent on any of the three surfaces. After 5 hours, thick deposit layers had formed on both the top and bottom metal surfaces. The carbon deposit on titanium and copper was bulky with random cracks. The deposit on the aluminum surface was also bulky, but contained regular straight strips. On all surfaces, an extra layer of loosely coalesced or aggregated particulate carbon (about 1 μ in diameter) was scattered on the bulky layer of the top surfaces, but not on the bottom surfaces.

Carbon Deposition on Stainless Steel Surfaces. Three different stainless steel foils were used; none showed any deposits after 3 hours of reaction. After 5 hours, deposits were similar to those found on titanium, aluminum, and copper. The bottom surfaces had a smooth, bulky deposit with random cracks. Top surfaces had an extra layer of porous particulate partilcate carbon on the smooth, bulky carbon layer. Unlike the bottom surface, the top surface's bulky layer was not flat. Its particulate carbon was much larger than that seen on the other top surfaces and seemed to have grown from the bulky deposit layer.

Conclusion: The results obtained in these experiments on JP-8C differed from our experiments on dodecane. JP-8C is generally more stable than dodecane. Deposition occurs only after three hours of thermal stressing for JP-8C. Nickel surfaces were the only surfaces tested that amassed a glassy layer of material over their deposit, suggesting that nickel is involved in the thermal degradation chemistry. In general, the other metal surfaces all had a smooth, bulky layer of deposit on both the top and bottom surfaces; the top surfaces, however, also had a loose particulate carbon layer. This difference can probably be attributed to a phase separation that existed between the top and bottom of the reactor.

---

[1] Schobert, H. H. et al. *Advanced Thermally Stable Jet Fuels, Technical Progress Report, August 1992 – October 1992*. The Pennsylvania State University, 1992.

[2] Schobert, H. H. et al. *Advanced Thermally Stable Jet Fuels, Technical Progress Report, July 1993 – September 1993*. The Pennsylvania State University, 1993.

3.4 Surface Effects on Deposit Formation in a Flow Reactor System

This study is explained in detail in *Advanced Thermally Stable Jet Fuels Technical Progress Report, October – December 1995.*

Introduction

This study extends our experimentation regarding metal surface effects on deposit formation from thermal stressing of jet fuel. This work involved thermal stressing in a flow reactor using Norpar 13 (a mixture of C_{12}-C_{15} *n*-alkanes) to study the metal surface effects on deposit formation.

Experimental

The reactant used in the experiments was Norpar 13, a mixture of C_{11}-C_{15} *n*-alkanes (0.32 %wt *n*-C_{11}, 11.3 %wt *n*-C_{12}, 49.51 %wt *n*-C_{13}, 38.47 %wt *n*-C_{14}, and 0.39 %wt *n*-C_{15}). Liquid reactants were pumped into the reactor system at a flow rate of 2 mL/min. UHP N_2 was also fed to the reactor with Norpar 13 during the reaction (N_2 was used before the reaction to purge and stabilize the reactor system). The effects of temperature, pressure, and the metal surface on the pyrolysis of Norpar 13 and on deposit formation were studied. The parameters we studied included temperatures from 500 to 600 °C, pressures from 0 to 1000 psig, and with/without the insertion of nickel coupons. Space time was approximately 25 seconds when studying the effects of temperature, and 5–50 seconds when studying the effects of pressure.

Using an on-line GC capillary column with a FID and a packed column with a TCD enabled us to fully determine the distribution of reaction products. The liquid products collected from the gas/liquid separator of the reactor system were analyzed with a UV-VIS spectrophotometer. Deposits collected from the reactor (walls) and foils were analyzed by polarized-light microscopy (PLM), SEM, and TEM. Results and Discussion

Results

Response Factors. The response factors for different compounds eluting from a capillary column with FID depended on the column used and the operation conditions. We used a standard mixture containing C_6–C_{16} normal alkanes to determine the response factor for each alkane. The differences between the response factors for different alkanes under the typical GC conditions used (GC temperature program, carrier gas pressure, FID cell temperature, Air/H_2 ratio) were significant. In addition, as a result of the vaporization of the light alkanes (C_6 and C_7), the response factors for hexane and heptane could be determined more accurately by extrapolation than those obtained by direct measurement. Therefore, the response factors for pentane, hexane, and heptane were calculated from the extrapolated data. The response factors for 1-alkenes were assumed to be the same as those of *n*-alkanes with the same carbon number. These response factors are listed in **Table 3.4-1**.

For the packed column with a TCD, the relative response factor (determined using benzene as an internal standard and helium as a carrier) appeared to be independent of the experimental parameters.[1] Relative response factors that were used in this analysis also appear in Table 3.15-1.

Because the reaction products were mostly kept in vapor state during the reaction (before being sent to the GC columns), TCD and FID actually analyzed the same compositions of reaction products. The TCD and FID data were correlated using pentene as a reference component and then normalized. We later confirmed that the errors of the quantitative analyses were within 10%.

Gas Phase Analysis. Four sets of experiments were conducted:

1. Temperature effects (500, 525, 550, 575, 600°C) without the presence of nickel coupons
2. Pressure effects (0, 250, 500, 750, 1000 psig.) without the presence of nickel coupons
3. Temperature effects (500, 525, 550, 575 °C) with the presence of nickel coupons
4. Pressure effects (0, 500, 1000 psig.) with the presence of nickel coupons.

A typical GC chromatogram (Norpar 13, 550°C, 500 psig., no metal coupons, 25 second space time, 1 hour run) of the reaction products showed that the packed column with TCD can separate C_1–C_6 *n*-alkanes and 1-alkenes well. Reaction products included C_1–C_{15} *n*-alkanes and C_2–C_{11} 1-alkenes. Very small amounts of heavier components (>C_{15}) were detected. The amounts of aromatic products were too small to be detected by the online GC.

The product distribution was consistent with those expected from well-known radical reaction mechanisms and the effects of temperature and pressure. High temperature favored β-scission reactions, leading to higher 1-alkenes and ethylene and lower *n*-alkane yields. For example, at 600° and 500 psig., the ethylene yield was as high as 3.99% (wt). The butene yield under the same conditions was 5.29%, although butane is only 2.99%. High pressures favored bimolecular hydrogen abstraction reactions and radical addition reactions, leading to a higher *n*-alkane yield and lower 1-alkene yield. For example the ethylene yield was only 0.74% (wt) at 550 °C and 1000 psig, while the ethane yield was 2.53% (wt).

Liquid Phase Analysis. The liquid products collected from the gas /liquid separator were analyzed using GC and GC/MS to identify the aromatic products. No aromatic peaks were detected, perhaps as a result of the very low concentration of these products. Since UV absorption is very sensitive to the aromatic compounds, we used a UV spectrophotometer to analyze the liquid products. We found that aromatics were present in the liquid products. The concentration was in the order of ppm (based on the comparison with a naphthalene standard). With or without the presence of nickel coupons, the concentration of the aromatic compounds appeared to increase exponentially with the reaction temperature, but linearly with the reaction pressure. A preliminary HPLC analysis of the liquid products suggested that one-ring aromatics (benzene and alkylbenzenes) were the most abundant aromatic compounds.

Deposit Characterization. Consistently large amounts of carbon deposit (around 900 mg) were formed at 550 °C, under 500 psig for 5 hours. The morphology of the deposit formed under these conditions was typical; the deposit took predominately two forms: filamentous carbon and segregated platelets. The mechanism of filamentous carbon formation is well known, but we were surprised that filaments were formed under the experimental conditions used in the flow reactor.

Similarly, the formation of a large amount of platelet carbon is not normally expected under the conditions we used. These platelets were quite different from those reported in the literature. They are much thicker than those formed on catalytic nickel surfaces.[2, 3, 4, 5] Therefore, the proposed dissolution-precipitation model[4] or surface diffusion model[6] likely cannot fully explain platelet formation in this case. TEM micrographs show that these platelets are not attached to any metal particles. The cracks at one side of the platelets appear to have been caused by growth cones of pyrolytic carbon. Polarized-light optical microscopy reveals that these platelets are highly anisotropic; the entire block of the platelets is in either yellow or blue color. This indicates that the platelets are highly ordered, perhaps in graphitic structure and/or in the form of pyrolytic carbon. The existence of aromatics in the reaction products indicates that the formation of carbon by aromatization and polymerization is also a possible route. It is, therefore, plausible that the formation of these thick platelets takes place through a combination of catalytic initiation and pyrolytic growth processes.

Experiments also show that there is a narrow temperature window for the formation of large amounts of filamentous carbon and especially thick carbon platelets. At 525 °C and 575°C, no collectable amount of carbon deposits were formed in the reactor tube. Morphologies of deposits on nickel coupons were mostly filamentous.

Table 3.4-1. The Response Factors of the FIC and TCD

Compound	RRF9 for FID*	RWR for TCD**
CH4		2.25
C2H4		1.71
C2H6		1.70
C3H6		1.53
C3H8		1.48
C4H8	1.21	1.44
C4H10	1.21	1.47
C5H10	1.17	1.41
C5H12	1.17	1.46
C6H12	1.12	1.39
C6H14	1.12	1.43
C7H14	1.07	
C7H16	1.07	
C8H16	1.03	
C8H18	1.03	
C9H18	1.00	
C9H20	1.00	
C10H20	0.94	
C10H22	0.94	
C11H22	0.88	
C11H24	0.88	
C12H24	0.83	
C12H26	0.83	
C13H28	0.78	
C14H30	0.74	
C15H32	0.70	

* C4-C7 response factors are extrapolated data
** From ref. 2 with He as a carrier gas

[1] Rosie, D. M. and E. F. Barry. *J. Chromatographic Sci.* 1973. 11. 237-250.

[2] Robertson, S. D. *Carbon.* 1970. 8. 365-374.

[3] Baird, T. *Fuel.* 1984. 63. 1081-1099.

[4] Derbyshire, F. J., A. E. B. Presland, and D. L. Trimm. *Carbon.* 1975. 13. 111-113.

[5] A. E. B. Presland and P. L. Walker Jr. *Carbon.* 1969. 7. 1-8.

3.5 Surface Effects on the Formation of Carbonaceous Solid from Thermally Stressed Jet Fuels and Model Compounds

This study is explained in detail in *Advanced Thermally Stable Jet Fuels Technical Progress Report, July–September 1997.*

Introduction

The formation of carbonaceous deposits on metallic surfaces resulting from thermal degradation/pyrolysis of jet fuels is a major concern in the development of advanced high-mach jet aircraft, in which the fuel will be used as a heat sink. Understanding the effects of metal surfaces on deposit formation, especially at high temperatures (> 400°C), is necessary to determine the possible catalytic aspects of the deposit formation mechanisms. The principal objective of this work was to examine the metal surface effects on deposit formation from thermally stressed jet fuels and model compounds.

The carbonaceous deposit on a metal surface conceals considerable information linked to formation or deposition mechanisms. Some important characteristics include: hydrogen content and hydrogen distribution, short range coordination of carbon-carbon atoms, medium range orientation of carbon atoms (clusters), and interfacial bonding between the deposit and the substrate surface. Many of these characteristics are reflected by the microstructure of the deposit. The reaction system for carbon deposition is crucial in collecting and interpreting the experimental data.

Experimental

This two-phase study involved:

1. An exploratory study to determine what effects different metallic surfaces have on the formation of carbon deposit from jet fuels and model compounds
2. Investigations probing why and how a metallic surface affects carbon deposition.

In Phase 1, solid carbons from thermal stressing of a model compound *n*-dodecane and commercial jet fuel Jet A were deposited onto different metal surfaces—nickel (Ni), titanium (Ti), copper (Cu), aluminum (Al), gold (Au), and stainless steel—in a tubing bomb reactor at elevated temperatures and autogenerous pressures. We used TEM grids as metal substrates to accommodate three dimensional deposit growth. We studied morphologies of the carbon deposit on the metal grids and the reactor walls.

In Phase 2, carbon solids from dodecane and jet fuel JP-8P were deposited on selected metal surfaces in the form of foils, wires, powders, and tubes, based on the results from the Phase I study. Most experiments were conducted in the tubing bomb reactors.

In addition to performing batch reactor experiments, we used a constant-surface-temperature type flow reactor system to carry out reactions in the 5 ml "isothermal" section of a reactor tube at high temperatures (up to 700°C) and high pressures (up to 1500 psi) with online gas chromatography.

We used elemental analysis, FTIR, ^{13}C NMR, micro-Raman, Polarized-Light Optical Microscopy (PLM), Scanning Electron Microprobe, SEM, and TEM in deposit characterization. With these techniques, we obtained the compositional and structural data, which are linked to surface effects on carbon deposition. Carbon deposits from an engine fuel line, nozzle, and afterburner were also analyzed.

Conclusions

The deposits consisted primarily of aromatic structures with a significant amount of hydrogen present in substituent $-CH_3$ groups. As deposition proceeded, the deposits became less ordered, but more aromatic. The final deposit reached a H/C ratio of about 0.55.

The nickel surface had strong catalytic activity in the formation of carbonaceous deposits from *n*-dodecane. Deposits formed on the surface consisted of two different layers: an initial dense and well-oriented anisotropic layer and a subsequent porous isotropic layer. The initial layer resulted from the catalytic activity of nickel. This layer also contained filamentous carbon, which appeared to have a strong adhesion to the metal surface.

The copper surface showed some catalytic activity in deposit formation. The initial deposit contained small whiskers with anisotropic structures. No particular catalytic activity was observed on a stainless steel surface under the stressing conditions used.

Both batch and flow reactors exhibited similar results: nickel and copper surfaces were the most active in deposit formation, while stainless steel surfaces did not show any particular activity in solid deposition. However, higher stressing temperatures, used in more recent experiments, showed a strong catalytic activity of stainless steel surfaces in flow reactors, leading to the formation of filamentous carbon, from stressing of *n*-paraffins. The most severe deposition in an actual engine fuel line appeared to be associated with catalytic activity of the metal surface.

3.6 Surface Effects on Fuel Decomposition

This study is explained in detail in *Advanced Thermally Stable Jet Fuels Technical Progress Report, July–September 1997.*

Introduction

The purpose of this work was to conduct thermal stressing of a commercial JP-8 fuel in the presence of the coupons of selected high temperature alloys and metal tubes to determine surface effects on fuel decomposition.

Experimental

Thermal stressing of a commercial JP-8 fuel sample was carried out in a flow reactor in the presence of both 1/4" (OD) tubes and coupons of selected high temperature superalloys. The tubes were SS 304, SS 316, nickel, copper, glass-lined SS and Silcosteel. Thermal stressing experiments were conducted at 500°C and 500 psig for 5 hours at a liquid flow rate of 1 cc/min. The 2.5 cm sections of stressed tubes were analyzed by LECO-Multiphase Carbon analyzer to determine the amount of carbon deposit collected along the total length of the tubes.

Foils of the following high-temperature alloys were used for JP-8 thermal stressing experiments in a flow reactor to obtain data that could be compared with that of the 316 stainless steel and nickel foils:

MoRe: Mo 52.5 / Re 47.5
Waspalloy: Ni 58 / Cr 19 / Co 14 / Mo / Ti / Al / Fe
Hastelloy C: Ni 57 / Mo 17 / Cr 16 / Fe / W / Mn
Inconel 600: Ni 72 / Cr 16 / Fe 8
Inconel 718: Ni 53 / Fe 19 / Cr 19 / Nb / Mo / Ti
Havar: Co 42.5 / Cr 20 / Ni 13 / Fe / W / Mo / Mn
Fecralloy: Fe 72.6 / Cr 22 / Al 4.8 / Si 0.3 / Y 0.3

The superalloy foils were cut into 3 mm x 15 cm coupons and placed in glass lined stainless steel tubes (OD=1/4") in a flow reactor with the JP-8 sample for thermal stressing at 500°C and 500 psig for 5 hours at a liquid flow rate of 4 cc/min.

For batch reactor experiments, the foils of Hastelloy C, Inconel 600, Inconel 718, and FeCr alloy were cut into in 1 cm x 5 cm coupons and placed in the batch reactor for thermal stressing experiments at 480°C for residence times from 30 to 90 minutes.

Results and Discussion

Metal Tubes. In the thermal stressing experiments involving the metal tubes, we observed the most deposition on the nickel surface, followed by SS 316 and SS 304. Silcosteel and copper gave substantially lower levels of deposition compared to those of nickel and the two stainless steel tubes. There was very little deposition on the glass-lined stainless steel tube.

The LECO-multiphase carbon analysis of the stressed tubes showed that the nature of the deposits also changed depending on the type of the surface exposed and the position of the deposit along the length of the tubes. For example, nickel, SS 316, and SS 304 showed three

different kinds of deposits, the relative proportions of which changed as a function of position along the tubes. In contrast, copper, Silcosteel, and glass-lined stainless steel tubes appeared to contain only one kind of deposit.

The same stressing experiments were repeated to examine the tubes by SEM. The tubes were cut longitudinally to observe the inner surface under the microscope. The SEM images showed different deposit morphologies on different tubing materials. The nickel surface was covered with both filamentous and plate-like deposits, indicating catalytic deposition. Both SS 316 and 304 showed globular and plate-like deposits, while the copper surface showed only plate-like deposits. In contrast with metal or alloy surfaces, the Silcosteel surface showed only spherical particles, likely indicating non-catalytic deposition.

Foil – Flow Reactor. Among the foils, Inconel 718 gave the least amount of carbon deposition, whereas Inconel 600 gave the largest amount. There were also differences in the types of deposits collected on different surfaces, as shown by the LECO-multiphase carbon analysis results and SEM examination of the stressed foils. This large spread in deposition among different alloys could have resulted from differences in the composition of the alloys and/or from differences in surface roughness or other physical properties of the foils. We are planning experiments to decouple the effects of surface roughness and surface composition on carbon deposition.

Foil – Batch Reactor. The FeCr alloy generated considerably more deposit than the other alloys and the Inconel 718 alloy produced the least amount of deposit. The Hastelloy C gave lower amounts of deposit than the Inconel 600 alloy. There appears to be some similarities in deposition trends on these alloys between flow and batch reactor experiments. Before we can draw conclusions about the role of a particular alloy component, we need to understand the role that surface roughness (and possibly other physical properties) plays in deposition, before concentrating on the role of alloy composition.

3.7 Effects of Pretreatment with High Surface Area Activated Carbon PX-21 on Thermal Stressing of JPTS Jet Fuel

This study is explained in detail in *Advanced Thermally Stable Jet Fuels Technical Progress Report, July–September 1993.*

Introduction

In previous studies we have shown that the addition of high-surface-area activated carbon PX-21 to jet fuel stops the formation of carbonaceous solids on the reactor walls resulting from thermal stressing. The addition of PX-21 also inhibits thermal degradation of JPTS jet fuel, even under severe conditions (>400°C). The performance of an additive depends on a number of factors, including type of fuel, fuel composition, additive concentration, and temperature of stressing. Fuels that have the highest degree of instability have the highest free radical concentration.[1] We assume that the presence of an activated carbon during thermal stressing terminates the free radical chain reactions by stabilizing the reactive species on active carbon surfaces.[2] The behavior of several carbons added to jet fuel during thermal stressing has shown that the surface area of an added carbon is an important parameter in determining the carbon's effectiveness.[3] Spiro reported that the surface area of carbons plays an important role in carbon catalytic activity.[4]

The amount of activated carbon PX-21 which must be added to JPTS jet fuel depends on the temperature of thermal stressing. We studied two relatively high temperatures and long stressing times (425°C and 450°C for 5 hours). There was no visible change in the color of the initial jet fuel mixed with 50 mg PX-21 after thermal stressing at 425°C for 5 hours. At 450°C for 5 hours, 100 mg PX-21 was sufficient to prevent carbon deposition on the reactor walls and enhance the thermal stability of jet fuel.[5] Thermal degradation of jet fuels is typically more severe or occurs at a much lower temperature if the fuel is saturated with air.[6] The addition of PX-21 delayed the degradation of JPTS more effectively in nitrogen than in air. However, even at 450°C in air, no carbonaceous deposit was observed on the reactor walls after stressing JPTS with PX-21.

Considering that high surface area activated carbons adsorb significant quantities of fuel and, depending on the surface properties of the carbon, selective adsorption of a certain species in a given fuel may strongly affect its thermal stability. If reactive compounds (e.g., heteroatom species) can be removed by adsorption on a surface, the stability of fuels at high temperatures can be increased substantially.

This work involved contacting jet fuel with PX-21 in a batch system over a prolonged time period to determine the effect on the fuel's thermal stability during subsequent thermal stressing of the filtered fuel. Two simultaneous sets of experiments were carried out on JPTS at 425°C for 5 hours in nitrogen atmosphere. One set of experiments involved stressing a mixture of 10 mL JPTS mixed with 50 mg PX-21.

In the other set, 15 mL samples of JPTS were mixed separately with 50, 100, and 200 mg PX-21. The mixtures were stored in a nitrogen atmosphere for three days. The jet fuel samples were then filtered to remove the activated carbon, and 10 mL samples of filtered JPTS was stressed alone at 425°C for 5 hours in a nitrogen atmosphere. For this series of experiments, the

JPTS jet fuel was pretreated with 50 mg PX-21. Additionally, JPTS was treated for 3 days with 100, 150, 200, 300, and 500 mg PX-21 and stressed at 450°C for 5 hours in a nitrogen atmosphere.

Conclusions

The results of stressing experiments of JPTS jet fuel pretreated with PX-21 showed that pretreatment of 15 mL JPTS with 50 mg PX-21 activated carbon delayed the degradation processes and prevented carbon deposition during thermal stressing at 425°C for 5 hours in nitrogen and air atmospheres. Apparently the 15 mL JPTS had to be pretreated with 300 mg of PX-21 activated carbon in order to delay degradation processes at 450°C. After pretreatment, no carbonaceous deposit was observed on the reactor walls when the fuel is stressed at 450°C for 5 hours. GC and GC/MS analysis of liquid products after stressing at 450°C were not conducted; however, the color of the liquids obtained was darker than the liquids obtained after stressing of pretreated JPTS at 425°C.

The examination of the surface of PX-21 before and after stressing with JPTS showed that it was covered with a thin layer of carbonaceous deposit and small discrete particles when activated carbon is stressed with jet fuel. This suggests that the carbonaceous solid formed during thermal stressing is deposited on the activated carbon surface. The activated carbon treated with JPTS showed the same microstructure as the original activated carbon. Although we could not observe the micropores with SEM, we deduced that small concentrations of jet fuel compounds were likely adsorbed on the microporous structure of activated carbon, decreasing the carbon surface area.

---

[1] Batts, B. D. and A. Fathoni Zuhdan. *Energy and Fuels.* 1991. 5. 2.

[2] Schobert, H. H. et al. *Advanced Thermally Stable Jet Fuels, Technical Progress Report, Novermber 1992 – January 1993.* The Pennsylvania State University. 1993.

[3] Schobert, H. H. et al. *Advanced Thermally Stable Jet Fuels, Technical Progress Report, February 1993 – March 1993.* The Pennsylvania State University. 1993.

[4] Spiro, M. *Catalysts Today.* 1990. 7. 167.

[5] Schobert, H. H. et al. *Advanced Thermally Stable Jet Fuels, Technical Progress Report, April 1993 – June 1993.* The Pennsylvania State University. 1993.

[6] Mayo, F. R. *Free Radical Autoxidation of Hydrocarbons, Accounts of Research.* 1968. 7. 193.

3.8 Effects of High Surface Area Activated Carbon as a Catalyst during Thermal Stressing of *n*-Octane and *n*-Dodecane

This study is explained in detail in *Advanced Thermally Stable Jet Fuels Technical Progress Report, April–June 1994.*

Introduction

Our previous studies showed that addition of high surface area activated carbon PX-21 is effective in slowing thermal degradation reactions of jet fuel heated to a high temperature (450°C) even for periods of time (≈5 hours).[1,2] The primary use of activated carbons is as adsorbents, but they can also promote a variety of surface reactions. Their role as catalyst is different in different reactions. The catalytic reactions have been classified as: oxidation reactions, combination reactions, decomposition reactions, and elimination reactions.

The performance of an activated carbon as catalyst depends on a number of factors, such as the nature of the carbon surface, the presence of carbon-oxygen surface structures, the availability of the active sites, and the surface area. To better understand the role of activated carbon as catalyst during thermal stressing of jet fuel, we used model compounds *n*-dodecane and *n*-octane. Using model compounds instead of jet fuel simplifies the study of the details of activated carbons' catalytic reactions and their mechanisms. We added 5% decalin to the model compounds in order to test the ability of activated carbon PX-21 to catalyze the transformation of decalin to naphthalene. Samples of jet fuel and dodecane were stressed for only 1 hour at 450°C, because the complicated mixture of compounds obtained after 5 hours did not allow insight into catalytic reactions of activated carbon.

Results

1. *n*-Octane Mixed with 5% Decalin. Adding PX-21 considerably reduced the pressure increase during stressing of *n*-octane and, as shown by **Table 3.8-1**, the formation of lighter compounds, such as C4, C5 alkanes was also reduced. The difference in the weight percent of decomposed *n*-octane stressed with and without carbon is 2.5-4.5% in the sample stressed with activated carbon. The final product of H transfer reaction of the polycyclic hydrocarbon decalin, which acts as hydrogen donor, is naphthalene. The higher amount of naphthalene and the lower percent decalin indicates that PX-21 catalyzes the H transfer reactions. However, when the activated carbon is present, the effect of decreasing hydrocarbon degradation considerably increases, as indicated by the much lighter color of the liquid obtained from stressing *n*-octane with PX-21.

Figure 3.8-1 shows the increase of naphthalene and tetralin in the stressed liquids when different amounts of activated carbon are added to constant amounts of the same compounds in the liquid obtained after stressing of *n*-octane and decalin alone. The amount of carbon added does not seem to have a significant effect on the catalytic reactions, although the catalytic ability increases as the amount of carbon is increased up to 150 mg. The increase, however, is not large enough to justify the necessity of adding more than 50 mg of activated carbon.

The liquids from the repeated experiments of *n*-octane+decalin and *n*-octane+decalin+PX-21 were separated and we obtained two fractions. In the hexane fraction we detected the same compounds with no significant difference in their concentration (although

quantitative analysis was not performed based on the high risk of error). The toluene+THF fraction showed more interesting results. There was a huge difference in the concentrations of naphthalene between the two samples. The sample stressed with PX-21 was considerably higher in naphthalene than the sample stressed without. This confirms that the activated carbon added during thermal stressing of *n*-octane+decalin contributes to the H transfer and conversion of decalin to naphthalene. In addition, further increases of PX-21 were not found to produce higher naphthalene concentration.

The structure of activated carbons can explain their role as hydrogen carrier. Activated carbons have a structure consisting of sheets of aromatic condensed ring systems stacked in nonpolar layers. These sheets have edges and defects, dislocations and discontinuities—characterized by unpaired electrons and residual valencies—and are richer in potential energy. The carbon atoms are highly reactive and constitute active sites/centers.

2. Cis/Trans Dodecan Mixed with 200 µL Decalin d_{18}. The 9.8 ml dodecane mixed with 200 µL decalin d_{18} was stressed for 450°C for 1 hour alone and with 250 mg PX-21. The percent of short alkanes+alkenes (C_3-C_5) was higher for the sample stressed without carbon; the concentration of long-chain alkanes, starting from C6, was higher in the liquid stressed with PX-21.

After adding the PX-21 and stressing for 1 hour, there were noticeable differences from the results achieved by stressing the dodecane+decalin alone. Following stressing with the addition of PX-21, we observed that no dodecane and coeluted n-alkanes were present and the formation of hexane, octane, nonane, decane, and undecane was significantly suppressed. This variation of product distribution can likely be attributed to the distinction between different radicals. The primary radicals were more stable than the secondary. This also explains the lower concentration of light compounds (C_3-C_5) in the liquid obtained from stressing of dodecane+decalin+PX-21. The concentration of C_6-C_{10} alkenes was higher in the liquid stressed without carbon. This suggests that the active sites of PX-21 initialize the cracking process, since the concentration of dodecane in the liquid obtained after stressing of *n*-dodecane+decalin d_{18} is nearly 3% higher than the concentration of dodecane in the liquid stressed with PX-21. However, after initializing the cracking process, PX-21 stabilizes the primary pyrolysis products.

In examining the percent area of naphthalene and *cis*-and *trans*-decalins for the liquids obtained from stressing dodecane with and without PX-21, we deduced that activated carbon enhanced the H-transfer. There was a lower concentration of *cis*-and *trans*-decalins and a higher concentration of naphthalene for the sample stressed with carbon. The naphthalene was d_{18} naphthalene.

When both liquids were separated, we found a higher concentration of alkanes in the hexane fraction of the liquid product obtained from stressing of *n*-octane, but the same compounds were identified in both liquids. In the toluene+THF fraction, no phenanthrene, pyrene, or other heavy compounds were detected, with the exception of naphthalene. This is probably attributable to the addition of decalin, which is an H-donor and helps to slow the dodecane degradation. In fact, no carbonacous deposit was found after the stressing of dodecane with PX-21 in the presence of decalin; only a negligible amount was detected after stressing dodecane without PX-21 in the presence of decalin. The concentration of naphthalene in the

toluene+THF fraction of the liquid obtained from stressing of dodecane+PX-21 was very high, while the concentration of naphthalene in the liquid product from stressing dodecane without activated carbon was almost undetectable.

Table 3.8-1. Percent Weight of the Compounds Identified in the Liquids after Thermal Stressing of n-Octane+Decalin Alone and with 50, 150, and 250 mg PX-21 (continued)

Compounds identified	n octane+ decalin	n octane+ decalin+ 50 mg PX21	n octane+ decalin+ 150 mg PX-21	n octane+ decalin+ 250 mg PX-21
n propane+propene	0.70	0.03	0.46	0.63
n butane+butene	3.18	1.15	2.51	2.76
2 methyl butene	0.24	0.12	0.19	0.13
n pentane+pentene	5.92	5.44	4.74	4.86
pentene	0.46	0.06	0.19	0.06
2 methyl pentane	0.15	0.09	0.09	0.10
3.methyl pentane	0.17	0.06	0.07	0.10
n hexane	1.98	2.29	2.64	2.29
hexene	1.00	0.58	0.42	0.69
hexene	0.59	0.34	0.27	0.27
hexene	0.22	0.11	0.08	0.09
methyl cyclopentane	0.44	0.33	0.24	0.18
3 methyl hexane	0.44	0.26	0.18	0.21
n heptane	1.28	1.19	1.06	0.97
dimethyl cyclopentane	0.60	0.47	0.34	0.30
heptane	0.10	0.06	0.04	0.04
heptene	0.25	0.16	0.10	0.10
dimethyl cyclopentene	0.15	0.10	0.05	0.03
methyl cyclohexane+methyl cyclohexene	0.04	0.02	0.01	0.01
4 methyl heptane	0.40	0.29	0.25	0.19
3 methyl heptane	1.28	1.28	1.21	1.17
n octane	65.55	71.03	73.01	73.28
octene	0.24	0.10	0.09	0.05
octene	0.21	0.19	0.22	0.24
octene+dimethyl cyclohexane	0.28	0.37	0.40	0.41
octene	0.23	0.22	0.24	0.26
octene	0.11	0.10	0.11	0.13
4 methyl octane	0.42	0.35	0.30	0.26
ethyl cyclohexane+br. alkane	0.31	0.28	0.23	0.20
toluene	0.18	0.20	0.13	0.09
n nonane	0.75	0.60	0.41	0.37
nonene	0.14	0.13	0.07	0.07
c3 cyclohexane+nonene	0.10	0.08	0.08	0.04
nonene	0.02	0.06	0.01	0.01
5 methyl nonane	0.13	0.11	0.07	0.07
4 methyl nonane	0.19	0.16	0.11	0.10
3 methyl nonane+ethyl benzene	0.38	0.31	0.23	0.21
xylenes	0.14	0.20	0.15	0.09
n decane	0.52	0.43	0.29	0.29
decene	0.13	0.09	0.05	0.03
o xylene	0.06	0.13	0.11	0.08

Table 3.8-1. (con't) Percent Weight of the Compounds Identified in the Liquids after Thermal Stressing of n-Octane+Decalin Alone and with 50, 150, and 250 mg PX-21

Compounds identified	n octane+ decalin	n octane+ decalin+ 50 mg PX21	n octane+ decalin+ 150 mg PX-21	n octane+ decalin+ 250 mg PX-21
decene	0.08	0.04	0.02	0.02
c3 cyclohexane	0.03	0.05	0.03	0.01
br. alkane	0.18	0.14	0.11	0.08
dimethyl nonane	0.29	0.20	0.11	0.12
5 methyl decane	0.13	0.10	0.06	0.06
4 methyl decane	0.66	0.41	0.27	0.29
br alkane	0.07	0.10	0.05	0.06
c3 benzene	0.05	0.08	0.05	0.03
n butyl cyclohexene	0.02	0.03	0.01	0.01
c3 benzene	0.07	0.02	0.03	0.03
n undecane	0.56	0.42	0.30	0.27
trans decalin	3.35	3.41	2.82	2.93
br alkane	0.22	0.15	0.08	0.12
br alkane	0.14	0.09	0.06	0.07
dimethyl decane	0.35	0.22	0.16	0.16
n butyl benzene	0.10	0.11	0.07	0.07
cis decalin	1.76	1.94	1.62	1.44
n dodecane	0.31	0.25	0.16	0.16
br alkane	0.09	0.06	0.04	0.04
br alkane	0.18	0.11	0.06	0.08
6 methyl dodecane	0.24	0.16	0.09	0.14
n tridecane	0.17	0.13	0.08	0.07
br alkane	0.10	0.06	0.05	0.05
6 methyl tridecane	0.12	0.08	0.03	0.05
tetralin	0.10	0.18	0.12	0.15
dimethyl dodecane	0.27	0.17	0.09	0.11
c3 decalin	0.10	0.07	0.03	0.03
c3 decalin	0.04	0.04	0.02	0.02
naphthalene	0.17	1.23	1.71	1.66
n tetradecane	0.04	0.04	0.01	0.01
br alkane	0.03	0.03	0.02	0.01
c3 decalin	0.04	0.03	0.01	0.01
br alkane	0.10	0.08	0.04	0.04
c3 decalin	0.02	0.04	0.01	0.02
n pentadecane	0.05	0.03	0.02	0.02
2 methyl naphthalene	0.01	0.06	0.06	0.03
1 methyl naphthalene	0.02	0.07	0.06	0.04
br alkane	0.03	0.03	0.01	0.01
	100.00	100.00	100.00	100.00

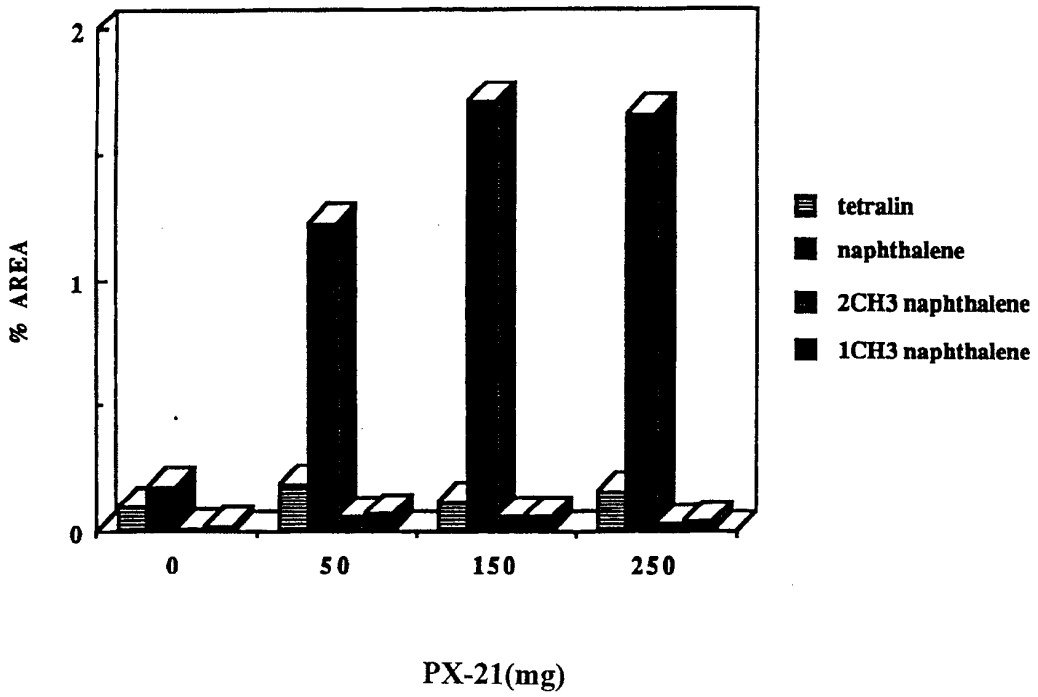

Figure 3.8-1. Effect of PX-21 on the Naphthalene and Tetralin Concentration in the Liquids Obtained from Thermal Stressing of n-Octane with Decalin

---

[1] Schobert, H. H. et al. *Advanced Thermally Stable Jet Fuels, Technical Progress Report, November 1992 – January 1993.* The Pennsylvania State University. 1993.

[2] Schobert, H. H. et al. *Advanced Thermally Stable Jet Fuels, Technical Progress Report, February 1993 – March 1993.* The Pennsylvania State University. 1993.

3.9 Effects of High Surface Area Activated Carbon and Decalin on Thermal Degradation of Jet A-1 Fuel and *n*-Dodecane

This study is explained in detail in *Advanced Thermally Stable Jet Fuels Technical Progress Report, July–September 1994.*

Introduction

Jet fuel degradation occurs under long-term, low-temperature (oxidative) storage conditions and short-term, high-temperature (pyrolytic) stress. During both storage and exposure to high temperatures, jet fuel decomposes, forming insoluble material that could deposit in fuel lines or on other surfaces. The higher temperatures required by high-performance aircraft in the future could further complicate the problem. Many chemicals have been used as additives, antioxidants, metal deactivators, dispersants, and passivators for fuel applications in the oxidative regime. They must be used cautiously, particularly for fuels that will enter the pyrolytic region, where the oxygen plays a complex role and participates in many side reactions.[1] The performance of an additive depends on various factors, such as type of fuel, fuel composition, additive concentration, and temperature of stressing.

The objective of this work is to study the thermal degradation of commercial petroleum-derived Jet A-1 jet fuel and model compounds *n*-dodecane in the presence of decalin and high-surface-area activated carbon PX-21. Thermal stressing was carried out on 10 mL samples of a commercial petroleum-derived Jet A-1 fuel and dodecane at 450°C for 1 hour.

Conclusions

In studying the presence of the hydrogen donor, decalin, with PX-21 activated carbon during thermal stressing of Jet A-1 fuel and *n*-dodecane, the following was noted:

The color of the liquids obtained after stressing Jet A-1 + 5% decalin with different amounts of PX-21 activated carbon is clearly different and becomes lighter with increasing amounts of carbon added. Adding decalin, an H-donor, further reduced the extent of the decomposition of *n*-dodecane and jet fuel. The activated carbon addition appears to promote H-transfer reactions during the thermal treatment. Our data also suggested that during thermal degradation of Jet A-1 and *n*-dodecane, the primary radicals are stabilized on carbon surfaces. The active sites of PX-21 carbon likely promote the H-transfer reactions and some cracking reactions, in addition to stabilizing some free radicals. The degree of thermal degradation of Jet A-1 and n-dodecane depends on both the amount of activated carbon and the amount of decalin added.

Thermogravimetric analysis of stressed PX-21 carbon showed that:

- The heating rate 10°C/min leads to the highest weight loss compared to the heating rate 20° and 30°C/min (i.e., to most complete desorbtion of the adsorbed species)
- The samples stressed with 50% decalin adsorbed higher amounts of liquid than the carbon stressed with 5% decalin.
- The stressed samples lose weight during heating in N_2 in 2-3 steps, while the unstressed carbon loses weight continuously up to 1000°C.

These data led us to conclude that the adsorbed compounds are most likely inside of the pore structure of PX-21 carbon and the longer time is needed for their desorption. There seems to be a synergistic effect between activated carbon and decalin addition in suppressing the thermal degradation reactions. The stressed samples lose weight in 2-3 steps, most probably due to the presence of different types of active sites on the activated carbon surface.

---

[1] Hazlett, R. N. *Thermal Oxidation Stability of Aviation Turbine Fuels.* Ann Arbor, MI: ASTM Publications. 1991.

3.10 Studies of Surface Chemistry of PX-21 Activated Carbon during Thermal Degradation of Jet A-1 Fuel and *n*-Dodecane

This study is explained in detail in *Advanced Thermally Stable Jet Fuels Technical Progress Report, October 1994 – December 1994.*

Introduction

Our previous studies demonstrated that the presence of high surface area activated carbon PX-21, combined with the hydrogen donor decalin, prevented solid deposition on reactor walls and reduced the extent of decomposition of *n*-dodecane and jet fuel even after 5 hours at 450°C.[1] Adding decalin as H donor also reduced the extent of decomposition of jet fuel and *n*-dodecane in the presence of the carbon only. The activated carbon appears to promote H transfer reactions during thermal treatment.[2] We suggested that the active sites of PX-21 carbon act to stabilize the pyrolysis products, enhance the H-transfer reactions, and promote some cracking reactions.

The thermogravimetric studies of PX-21 from stressed *n*-dodecane or Jet A-1 fuel mixed with decalin showed that some compounds are adsorbed into the pore structure of the carbon. The desorption of these compounds during heating in N_2 up to 1000°C took place in two or three steps, most likely resulting from the presence of different types of active sites or porosity.

Chemisorption of oxygen on carbon surfaces and the manufacturing process lead to generation of oxygen surface groups.[3,4]

A distinct catalytic effect of activated carbon was observed in different reactions.[5,6] Although the nature of the carbon surface and the presence of carbon-oxygen surface structures play dominant roles in some reactions, the surface area and accessibility of the active sites are important factors in other reactions. Goughlin suggested that the catalytic carbon properties could also be related to the electronic structure of the materials.[7]

However, many solid carbon properties, including their catalytic activities, are related to the presence of surface complexes. Perhaps the most important surface property of carbons as related to the surface complexes is their acid/base character. The changes on carbon surfaces occur over a range of temperature with the exact properties depending on the carbon and the pretreatment conditions.

In this study, we investigated the influence of outgassing PX-21 activated carbon at 900°C for 2 hours in N_2 on the degradation chemistry of jet fuel and model compound *n*-dodecane at 425°C as compared to the activity of untreated PX-21. Thermal stressing experiments were carried out on 10 mL dodecane and petroleum derived Jet A-1 fuel mixed with 5% decalin and 50 mg PX-21. In some experiments, PX-21 was added after outgassing at 900°C for 2 hours in N_2 in a stainless steel vertical reactor place in a tube furnace. The experiments used microautoclave reactors pressurized with N_2 to 100 psi.

Conclusion

The nature and activity of the activated carbon surface is one of the most important parameters under thermal stressing conditions. We found that surface oxygen concentration can be reduced by outgassing PX-21 at a high temperature (900°C) in N_2. The activity of PX-21

carbon in preventing carbon deposition increases considerably with such pretreatment. The outgassed carbon showed lower catalytic activity in promoting H transfer reactions and converting decalin into naphthalene. Apparently, surface complexes on the carbon surface act as active sites for H transfer reactions.

The original PX-21 carbon contained appreciable amounts of chemisorbed oxygen, which was removed during outgassing, rendering the active sites available for the free radicals. Faster termination of free radical chains likely reduced the degradation of model compounds and jet fuel stressed with 5% decalin.

The optical and scanning electron microscopy of stressed carbons showed that outgassed PX-21 not only suppressed the carbon deposition on the reactor walls, it also significantly reduced the formation of carbonaceous solids. The carbonaceous solid, in the form of discrete particles, deposited on the surface of original PX-21. The increase of solid weight of original PX-21 after stressing with dodecane or jet fuel and decalin can be attributed to solid deposition, while the increase of solid weight of outgassed PX-21 is caused primarily by adsorption of selective compounds during thermal stressing. The thermogravimetric analysis and the surface area measurements of original and outgassed PX-21 before and after thermal stressing with dodecane+decalin strongly agree with the results obtained from optical and scanning electron microscopy.

---

[1] Schobert, H. H. et al. *Advanced Thermally Stable Jet Fuels, Technical Progress Report, July 1994 – September 1994.* The Pennsylvania State University. 1994.

[2] Gergova, K. et al. *Effect of High Surface Area Activated Carbon on the Thermal Stability of Jet Fuel*, 5th National Conference on Stability and Handling of Liquid Fuels, Rotterdam, The Netherlands, 1994.

[3] Puri, B. R. *Chemistry and Physics of Carbon.* New York: Marcel Dekker. 1970. 6. 191.

[4] Kinoshita, K. *Carbon, Electrochemical and Physicochemical Properties.* New York: John Wiley and Sons. 1988. 86.

[5] Szymanski, G. and G. Rychlicki. *Carbon.* 1991. 29. 489.

[6] Guerrero-Ruiz, A. and J. Rodriguez-Ramos. *Carbon.* 1994. 32. 23.

[7] Goughlin, R. W. Proc. *4th International Conference on Catalysts.* Moscow. 1968.

3.11 Effects of Surface Changes and Toluene Extraction of PX-21 Carbon on Thermal Stressing of Model Compounds

This study is explained in detail in *Advanced Thermally Stable Jet Fuels Technical Progress Report, January–March 1995.*

Introduction

Our previous studies on the effects of surface chemistry of PX-21 activated carbon focused on the role that the surface complexes play during thermal degradation of jet fuel and model compounds. We concluded that the activity of a carbon surface is dependent on its surface area and the nature of the surface.[1] The outgassing of carbon at high temperatures leads to the removal of chemisorbed oxygen and creates active sites for free radical reactions.

We anticipated that the carbonaceous solid deposited on the surface of activated carbon during thermal stressing would also affect the degradation reactions. Carbonaceous overlayers had always been associated with catalytic poisoning; however, in some cases, they have catalytic activity.[2]

Small amounts of aromatic and/or PAH contaminates can be released from the activated carbon structure into the jet fuel mixture during thermal stressing. When we extracted activated carbons with benzene and separated the PAH via chromatographic methods, we confirmed that fluoranthene and benzoflouranthene were present in small quantities.[3]

This study investigated the effect of the carbonaceous deposit overlayer on PX-21 surfaces and the removal of aromatic and PAH contaminants from PX-21 carbon in the thermal degradation of model compounds dodecane and decalin.

Experimental

We performed thermal stressing experiments on 10 mL of dodecane mixed with 5% decalin and 100 mg PX-21 at 425°C. The outgassed and original PX-21 carbon was used and, as a preliminary step, was stressed with dodecane + 5% decalin at 450°C. The second set of experiments was carried out on 10 mL of dodecane + 5% decalin and 100 mg PX-21 extracted with toluene for 24 hours. In all experiments, the 10 mL + 5% decalin alone were stressed for comparison.

Gas chromatography (GC) and a mass detector were used to analyze the liquid products. Thermogravimetric (TGA) analysis was performed, increasing the temperature of the TGA experiments from 30° to 1000°C at 10°C/minute. The microstructure of the PX-21 carbon after stressing was analyzed using a polarized-light microscope and a scanning electron microscope (SEM).

Conclusions

Considerably higher amounts of carbonaceous solid were associated with the original PX-21 than with the outgassed PX-21 after thermal stressing. We found evidence that the carbonaceous overlayer formed on the PX-21 surface after thermal stressing of model compounds + decalin can inhibit further deposition more effectively than the original PX-21. Surface oxygen complexes, formed on the carbonaceous overlayer, appeared to be the active

species during thermal stressing. Unlike the case of oxygen functional groups on the surface of original activated carbon, the deposit overlayer renewed the activity of the carbon. The TGA experiments indicated that the used activated carbon appears to adsorb less liquid during thermal stressing than the original PX-21. This carbon feature could prove extremely valuable in preventing solid deposition and stabilizing jet fuel during thermal stressing.

SEM micrographs of the activated carbon stressed subsequently with dodecane and decalin mixtures showed unusual carbon filaments (or fibers), which seem to originate from a carbonaceous overlayer formed during the first stressing. The formation of carbon filaments on activated carbon surfaces at the relatively low temperatures used in this study (≈425°C) had not previously been reported.

The PX-21 carbon contained nickel (Ni) and vanadium (V) as trace metals (0.02% and 0.01%, respectively), which are not expected to exhibit strong catalytic effects during thermal stressing. However, the extraction of PX-21 with toluene proved the presence of some aromatic hydrocarbons possibly diminishes the activity of PX-21 during thermal stressing. The comparison of the alkane concentration in the liquids obtained from thermal stressing of dodecane + decalin in the presence of extracted and original PX-21 showed that the dodecane concentration of the liquid produced by thermal stressing at 450°C for 0.5 and 1 hour was considerably higher in the presence of extracted PC-21. The concentration of short-chain alkanes was also lower in the liquid obtained after thermal stressing in the presence of the extracted carbon. This difference diminished when longer stressing times were applied. Optical microscopy showed more carbon deposition in the presence of the original PX-21 compared to that of extracted PX-21.

---

[1] Schobert, H. H. et al. *Advanced Thermally Stable Jet Fuels, Technical Progress Report, October – December 1994.* The Pennsylvania State University. #92PC92104-TPR-10. 1995.

[2] Trimm, D. L. *Catal. Rev. Sci. Eng.* 1977. 16. 155.

[3] Borneff, J. *Activated Carbon Adsorption of Organics from the Aqueous Phase.* Ann Arbor: Ann Arbor Science Publishers, Inc. J. H. Suffet and M. J. McGuire, Eds. 1980. Vol I.

3.12 Catalytic Effects of Carbon Surfaces in Organic Reactions—A Literature Review

This study is explained in detail in *Advanced Thermally Stable Jet Fuels Technical Progress Report, January – March 1995.*

Introduction

In addition to being known as adsorbents and catalyst supports, solid carbons have served as catalysts for many reactions (e.g., decomposition of hydrogen peroxide and oxidation of oxalic acid) for some time.[1, 2] However, less known are the catalytic effects in some organic reactions, such as substitution and isomerization.

This study summarized the literature on known organic reactions that are catalyzed by various carbons and compared the catalytic activities of carbons with those of other catalysts. For the purposes of this study, we did not examine literature pertaining to inorganic reactions catalyzed by solid carbons.

The original Technical Progress Report[3] contained a full discussion pertaining to types and classification of catalysts. It also expounded on the organic reactions catalyzed by carbons, including:

- Redox Reactions – hydrogenation-dehydrogenation, oxydative hehydrogenation, hydrodehydroxylation and hydrodehalogenation, and oxidation
- Substitution Reactions – halogenation, hydrolysis, and solvolysis
- Addition-Elimination Reactions – dehydration, polymerization, and hydrogen halide elimination
- Molecular Rearrangement – recemization and isomerization
- Other Reactions

We then examined how the various catalytic activities result from the physical and chemical properties of carbon, including its surface chemistry, electronic properties, pore structure, and crystal structure.

Conclusion

Carbon possesses the properties to catalyze many organic reactions, from dehydration to polymerization. Surprisingly, carbon exhibits varieties of catalytic activities, as shown in **Table 3.12-1**. Solid carbons catalyze reactions mainly catalyzed by metal to acid catalysts. The responsible sites and mechanisms for the reactions vary from one reaction to another. In the case of one reaction (e.g., oxidation and dehydrogenation), use of different reactants will change the active site of catalysis. The selectivity, as well as catalytic activity, is influenced by the chemical and physical properties of the carbon. Pore size and distribution in solid carbon affects the shape selectivity of the catalytic reaction. Surface functional groups and impurities incorporated directly influence the catalytic activity.

Based on the information we gathered from the 46 sources cited in the original Technical Progress Report,[3] we can predict other reactions in which ordinary catalysts can be replaced by

carbon. Because solid carbons possess properties of metals, metal oxides, and acidic catalysts, all of the heterogeneous catalytic reactions shown in Table 3.11-1 could be catalyzed by carbon. However, the feasibility of carbon acting as a catalyst for a certain reaction is heavily dependent on the reactions involved.

Electronic properties are not the only factors used to determine the catalytic activity of carbon; however, they do provide some interesting considerations. Solid carbons may possess electronic properties ranging from conductor to insulator, depending on the method of preparation and treatment. Different electronic properties may exist in a single microcrystalline carbon sample. Hence, proper treatment of carbon catalysts alters their electronic properties; further, it alters their catalytic activity and selectivity for a particular reaction. For example, heat treatment and graphitization of carbon leads to a metallic property, and oxidation and the formation of oxide would lead to more semiconductivity. Manufacturing highly disordered carbon could result in an insulator type of carbon.

Because solid carbons have high adsorption capability, considerable amounts of products and/or reactants are adsorbed during the reactions, often leading to false kinetic conclusions, particularly for reactions in solution. As a result, kinetic studies of catalytic reactions with carbon should be carefully studied to avoid false kinetic conclusions.

There are two primary disadvantages to using solid carbons as catalysts. First, although solid carbons are inert materials for a wide range of temperatures, they are easily oxidized to form unwanted surface functional groups, creating problems like difficulty in tailoring of surface groups. Second, if solid carbons are used for certain reactions in the industry, regeneration of carbon catalysts could become a problem, because metal ions during reaction often become incorporated within the carbon structure during the regeneration process; consequently, the regenerated carbons can differ from the original carbon catalyst.

Table 3.12-1. A Classification of Heterogeneous Catalysts

Class	Conductivity	Functions	Examples
Metals	Conductors	Hydrogenation Dehydrogenation Hydrogenolysis (Oxidation)	Fe, Ni, Pt, Pd, Cu, Ag
Metal oxides & sulfides	Semiconductors	Oxidation Reduction Dehydrogenation Cyclization Desulphurization (Hydrogenation)	NiO, ZnO, CuO, Cr_2O_3, WS_2
Metal oxides	Insulators	Dehydration	Al_2O_3, SiO_2, MgO
Acids		Polymerization Isomerization Cracking Alkylation Halogenation Hydrogen transfer	SiO_2-Al_2O_3, zeolites

[1] Larson, E. C. and J. H. Walton. *J. Phys. Chem.* 1940. 44. 70-85.

[2] Rideal, E. K. and W. M. Wright. *J. Chem. Soc.* 1926. 128. 1813-1821.

[3] Schobert, H. H. et al. *Advanced Thermally Stable Jet Fuels, Technical Progress Report, January – March 1995.* The Pennsylvania State University. #92PC92104-TPR-11. 1995.

3.13 Effects of High Surface Area Activated Carbons on Thermal Stressing of Model Compounds

This study is explained in detail in *Advanced Thermally Stable Jet Fuels Technical Progress Report, April – June 1995.*

Introduction

In our previous work, we studied the effect of high surface area activated carbon PX-21 (BET surface area 2090 m^2/g) addition on thermal decomposition reactions. We established that activated carbon addition promoted a variety of reactions during thermal treatment of jet fuels and model compounds. The reactivity of an activated carbon depends on the nature of the carbon surface, presence of carbon-oxygen surface groups, availability of the active sites, and surface areas. Activated carbon surface area is an important parameter that determines, to a large extent, the effectiveness of added carbon in suppressing solid deposition during thermal stressing at high temperatures.[1]

In this study, we used three new high surface area activated carbons—two granulated carbons, Maxsorb 94-06 and Maxsorb 94-20, and one powdered carbon, Maxsorb 92-11A. These activated carbons had the following BET surface area:

Maxsorb 94-20	2080 m^2/g
Maxsorb 94-06	2320 m^2/g
Maxsorb 92-11A	3190 m^2/g

We also studied the effect of the hydrogen donor, decalin, in addition to high-surface-area activated carbon, PX-21, during thermal stressing. The activated carbon addition appears to promote H-transfer reactions during thermal stressing.[2] There seems to be a synergistic effect between activated carbon and decalin addition in suppressing the thermal degradation reactions.

Experimental

We added 5% decalin to dodecane and stressed the mixture with 100 mg of each Maxsorb carbon at 450°C for 1 hour. Initially colorless, all dodecane samples turned yellow after thermal stressing. The darkest was the liquid stressed with Maxsorb 92-11A, followed by Maxsorb 94-20, and Maxsorb 94-06.

All liquids stressed with activated carbons were lighter in color than the liquids stressed without carbons, which appeared brown in color. There was no deposit formation on the reactor walls after thermal stressing of dodecane + 5% decalin in contrast to 20 mg of deposit on the reactor walls after thermal stressing without carbon.

Gas chromatography(GC) was used to identify compounds in the liquid samples. Mass spectrometry (GC-MS) was carried out using a Hewlett-Packard 5090 11 GC coupled with HP 5971 A mass selective detector.

Conclusions

The high-surface-area activated carbons Maxsorb 94-20, 94-06, and 92-11A were stressed with the model compounds dodecane and 5% decalin at 450°C for 1 hour and 425°C for

5 hours. The activated carbons suppressed carbon deposition and helped retard the degradation of dodecane. These carbons showed the same effect as the PX-21 carbon used in our previous work. The considerable difference in the surface area of Maxsorb carbons (1000 m^2/g) did not affect the performance of activated carbons during thermal stressing. This indicates that surface area higher than 2000 m^2/g does not increase the catalytic effect and the ability of carbon to suppress carbon deposition during thermal stressing.

The concentration of naphthalene in the stressed liquids depends on both the H-transfer reactions and degradation processes that took place during thermal stressing. The toluene extraction of activated carbons before thermal stressing resulted in an increase in the effectiveness of activated carbon added before thermal stressing. Unusual tubular deposits were formed on the carbonaccous overlayer of Maxsorb carbons, as well as PX-21 carbon, after they were stressed subsequently with dodecane and decalin at 425°C.

---

[1] Schobert, H. H. et al. Advanced Thermally Stable Jet Fuels, Technical Progress Report, November 1992 – January 1993. The Pennsylvania State University. #P2PC92104-TPR-2. 1993.

[2] Schobert, H. H. et al. Advanced Thermally Stable Jet Fuels, Technical Progress Report, July – September 1994. The Pennsylvania State University. #P2PC92104-TPR-9. 1994.

3.14 Effects of Solid Carbon Surfaces on Thermal Decomposition of *n*-Dodecane

This study is explained in detail in *Advanced Thermally Stable Jet Fuels Technical Progress Report, July–September 1995.*

Introduction

The presence of different solid carbons added to *n*-alkanes during thermal stressing at temperatures higher than 400°C causes substantial changes in decomposition reactions. The high surface area activated carbons (2000-3000 m^2/g) were found to be very effective in suppressing thermal degradation of *n*-alkanes and preventing carbonaceous solid formation on metal surfaces. In addition, the hydrogen transferring pyrolysis of *n*-alkanes in the presence of decalin and high surface area carbons showed that the active carbon surfaces catalyze hydrogen transfer. Although the surface area and accessibility of the active sites are important factors in some reactions, the nature of the carbon surfaces and the presence of surface oxygen groups play a dominant role in other reactions. The carbonaceous solid deposited on the surface of activated carbons during thermal stressing also affects the degradation reactions. The carbonaceous overlayer has always been associated with catalytic poisoning, but in some cases, the overlayer seems to have catalytic activity. There is evidence that carbon deposited on a catalyst surface is also catalytically active. Some hydrogenation reactions were catalyzed by carbon overlayers. The most obvious catalytic role of carbon is in promoting the deposition of solid carbons. In other cases, the surface complexes may be the active catalysts. Cariaso and Walker found that impurities in the carbon could also have a strong influence on the catalytic reactions. (Note: The sources of the information presented in this paragraph can be found in the original Technical Progress Report.[1])

The ability of carbon surfaces to promote a variety of surface reactions has been studied over many years and many catalytic reactions of carbon have been reported. We have located no studies reported in the literature on the effect of carbon surfaces on pyrolysis of jet fuel range hydrocarbons.

The focus of this work is to study the effects of active carbon surfaces during thermal decomposition of *n*-dodecane. First, we examined the results of thermal stressing of *n*-dodecane in the presence of high-surface-area activated carbons that were subjected to various treatments. Second, we evaluated the effects of previously deposited carbonaceous solids on further solid deposition from *n*-dodecane. The experimental methodology and detailed findings of our discussions are presented in the pertinent Technical Progress Report.[1]

Conclusions

High surface-area-activated carbons PX-21 and Maxsorb 92-11A, 94-06, and 94-20 strongly affected decomposition reactions during thermal stressing of *n*-alkanes at high temperatures (425°C and 450°C). The surface area and surface functionalities are the two most important parameters that influence the carbon activity. The higher the surface area of activated carbon, the more prominent the effect of activated carbon used. However, activated carbons with very high surface area (> 2000 m^2/g) do not differ in their performance during thermal stressing.

The addition of the hydrogen donor decalin showed that the active carbon surfaces catalyze hydrogen-transfer reactions. The treatment of activated carbon at high temperatures in a N_2 atmosphere led to the removal of oxygen complexes on the carbon surfaces. Compared to original carbons, outgassed carbons showed higher activity during thermal stressing of *n*-dodecane at 450°C for 1 hour, but lower activity at 450°C for 4-hour stressing. Oxidation of PX-21 decreased its effectiveness in stabilizing *n*-dodecane.

The carbonaceous solid deposited on the carbon surfaces during thermal stressing also played a catalytic role, which can be attributed to specific oxygen functionality on the carbon overlayer as well as adsorbed species. The surface area and porosity of activated carbon measured before and after thermal stressing with *n*-alkanes showed that carbonaceous solid deposited on the carbon surfaces and extraction of original carbon in toluene leads to a sharp decrease of N_2 BET surface area. Although the meso- and/or macroporosity of activated carbons covered with carbonaceous solid is blocked selectively during thermal stressing, extraction decreases the porosity of the carbon uniformly as a result of adsorption of small amounts of toluene. The N_2 adsorption isotherms are type I, which is characteristic of microporous solids, and they do not exhibit hysteresis, indicating absence of considerable mesoporosity.

The 316 stainless surface of the reactors coated with carbonaceous deposits appeared to attract more deposition, especially in the bottom plug, than a clean metal surface. Presumably, condensed-phase pyrolysis reactions were responsible for the observed increase in the amount of carbonaceous deposits collected on a carbon coated metal surface.

---

[1] Schobert, H. H. et al. Advanced Thermally Stable Jet Fuels, Technical Progress Report, July – September 1995.. The Pennsylvania State University. #P2PC92104-TPR-13. 1995.

3.15 Effect of Carbon Surfaces on Thermal Decomposition of Hydrocarbons

This study is explained in detail in *Advanced Thermally Stable Jet Fuels Technical Progress Report, January–March 1997.*

Introduction

We previously showed that the presence of high surface area activated carbon (PX-21 and other activated carbons) prevented solid deposition on reactor walls and reduced the extent of decomposition of *n*-alkanes.[1] We have suggested that the active sites of PX-21 carbon act to stabilize the pyrolysis products and enhance the H-transfer reactions. In this study, we compared the effects of activated carbon addition on thermal decomposition of cyclohexane and ethylbenzene, as models of other types of hydrocarbons present in jet fuels.

Experimental

Thermal stressing tests were performed on 10 mL cyclohexane and ethylbenzene at 450°C for 2 to 23 hours. The experiments were carried out in microautoclave reactors purged five times with ultra-high purity grade nitrogen to 1000 psi. We conducted gas chromatography (GC) of liquid samples, GCTCD analysis of gas samples, and capillary gas chromatography/ mass spectrometry (GC/MS) of compounds in the liquid products.

Results and Discussion

Effects of PX-21 Addition on Thermal Decomposition of Cyclohexane. Thermal stressing of cyclohexane with/without PX-21 gave similar results to those obtained from stressing *n*-dodecane. The addition of PX-21 inhibited the thermal cracking of cyclohexane and gave much higher concentrations of benzene in the liquid products. The dehydrogenation activity of PX-21 produced, in long duration experiments, almost 30 times higher benzene concentrations compared to that obtained without PX-21. Strong isomerization activity was observed with/without PX-21 (e.g., cyclohexane to methylcyclopentane). The isomerization activity was reduced when PX-21 was present in the pyrolysis of cyclohexane.

The mechanism for methylcyclopentane production from cyclohexane can be explained by ring opening of cyclohexane followed by ring closing back to C5 ring with a methyl group substituent. A proposed pathway for the isomerization reaction, shown in **Figure 3.15-1**, is initiated by hydrogen abstraction from cyclohexane by a free radical followed by ring opening and closing to form methylcyclopentane as the final product. We can infer from the proposed pathway that lower free radical concentration in the pyrolysis system results in lower extents of isomerization and, thus, lower concentration of methylcyclopentane in the final liquid product. Addition of PX-21 reduces the concentration of methylcyclopentane in the product, presumably by reducing the free radical concentration in the reactor.

The gaseous products obtained by adding PX-21 contained higher hydrogen and ethane concentrations and lower ethylene concentration than those obtained without PX-21. The higher ethane and lower ethylene concentrations can be attributed to the stabilization of ethyl radicals (formed by β-scission reactions) on the carbon surface. Combined with the data on the concentrations of cycloalkanes and aromatics in the liquid products, the gas analysis suggests that the carbon surface is active in both dehydrogenation (e.g., of cycloalkanes) and

hydrogenation (e.g., of ethyl radicals) reactions. One possible mechanism for the proposed hydrogen shuttling activity is the sequential hydrogenation and dehydrogenation of aromatic ring systems on the carbon surface. The stabilization of free radicals on a carbon surface can explain why thermal decomposition of hydrocarbons is suppressed with inhibition of solid deposition on metal surfaces.

2. Effects of PX-21 Addition on Thermal Decomposition of Ethylbenzene. In contrast to the results obtained from stressing *n*-dodecane and cyclohexane, the addition of PX-21 promoted cracking reactions of ethlybenzene and increased the amount of carbonaceous deposit on the reactor wall. The liquid products obtained with PX-21 were much darker. Much higher concentrations of benzene, methylbenzene, dimethylbenzene, styrene, and methylethylbenzene were obtained when PX21 was added to ethylbenzene. The major product was dimethylbenzene.

The gas analyses showed the same trends as those observed with *n*-dodecane and cyclohexane—when PX-21 was present, we obtained higher concentrations of hydrogen and ethane (and methane), and lower concentrations of ethylene. Almost no ethylene was present in the gases obtained with PX-21. The carbon surface seems to continue to act as a hydrogen shuttler to methyl and ethyl radicals, but compared to *n*-dodecane and cyclohexane reactions, there was much less hydrogen to shuttle. We surmised that the major reactions were: demethylation of the ethyl group (producing a resonance-stabilized benzyl radical) and methylation, which subsequently formed methylbenzene (to produce dimethylbenzene). The higher extents of cracking observed with PX-21 can be attributed to the abstraction of hydrogen by the carbon surface which, in this case, appears to destabilize the pyrolysis system. Alternatively, the alkyl group on the benzene ring might become more vulnerable to cracking when ethylbenzene is adsorbed on the carbon surface.

Conclusions

Thermal decomposition behavior of hydrocarbons is strongly influenced by the presence of an activated carbon, PX-21. The addition of PX-21 inhibits thermal decomposition of cyclohexane and solid formation on reactor walls, but promotes the decomposition of, and solid formation from, ethylbenzene. The increased stability of cyclohexane systems is explained by effective hydrogen shuttling on the carbon surface. Increased extents of cracking and solid formation from ethylbenzene can be attributed to the relative hydrogen deficiency of this aromatic compound compared to the two alkanes. The adsorption of ethylbenzene on the carbon surface also could have enhanced the cracking of the alkyl group on ethylbenzene.

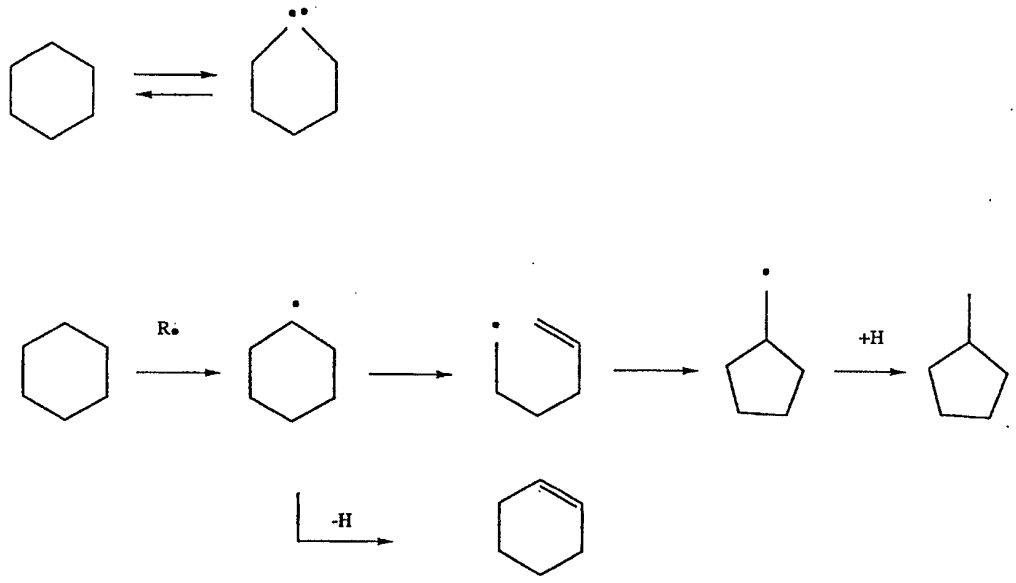

Figure 3.15-1. Proposed Pathways for Cyclohexane at 450°C

[1] Gergova, K. et al. *Preprints.* New Orleans: ACS Div. of Pet. Chem. 1996. 41(2). 513.

3.16 Effects of Adding Solid Carbons on Thermal Degradation of Jet Fuel

Introduction

Earlier studies involving thermal stressing of JP-8 jet fuel with model compound *n*-dodecane in the presence of two different activated carbons—carbon black and graphite spectroscopic powder, SP-1—demonstrated that the presence of solid carbons, particularly activated carbons, causes substantial changes in the degradation reactions. Adding carbon prevented solid deposition on the metallic reactor surfaces, even after rather severe thermal stressing of JP-8 jet fuel at 450°C for 5 hours. The different microstructures of the deposits observed on the added solid carbons indicated that the deposition mechanisms were also affected by the presence of the carbons during thermal stressing.

a. Thermal Stressing in the Presence of Alumina and Carbonaceous Deposits

This study is explained in detail in *Advanced Thermally Stable Jet Fuels Technical Progress Report, August 1992 – October 1992.*

Purpose: We performed additional thermal stressing experiments on JP-8 jet fuel in the presence of alumina and carbonaceous deposits produced previously from thermal stressing of JP-8 jet fuel alone to provide further insight into the role of initial carbonaceous deposits on further formation and deposition of solids during thermal stressing.

Conditions: Thermal stressing of 10 ml of JP-8 jet fuel mixed with 1 g alumina and, in another trial, 200 mg carbonaceous deposit, both carried out at 450°C for 5 hours. Carbonaceous solids were examined by optical microscopy.

Findings: In general, the addition of alumina and carbonaceous deposit obtained from stressing of jet fuel provided more attractive areas for carbon deposition than stainless steel reactor surfaces. As a result, a considerable increase in the amount of carbonaceous solid was seen in these two situations. Of the two additions, the deposit addition produced more solids than the alumina did.

In comparing the deposits obtained from the two trials with the deposits obtained from thermal stressing of JP-8 alone, we found that all three deposits had anisotropic microstructures. However, the carbonaceous solids formed on the metallic surface had finer grained structures than the solids formed during stressing with alumna and carbonaceous deposits. This would indicate different deposit mechanisms.

JP-8 alone. The deposits showed signs of gas phase nucleation in the form of liquid droplets that collect on metal surfaces and continue carbonization on the surface to form continuous band of solids.

With alumina. Solids were either long, thin particles with fine texture deposited from the gas phase, or larger, isometric particles consisting of large-grain anisotropy formed primarily by liquid phase carbonization on alumina particles. Alumina particles contain acidic sites that are active in catalyzing cracking reactions.

With carbonaceous deposits. The new deposits were formed by a gas phase deposition processes on the added solids.

The solid resulting from stressing JP-8 alone measured 84 mg; the solids resulting from the addition of alumina and carbonaceous deposits were 150 and 218 mg, respectively. Despite alumina's tendency to catalyze cracking reactions, more solids were formed with the addition of the carbonaceous deposits.

Yield and Composition of Liquid Products. The yield of liquids obtained after stressing of JP-8 with the activated carbon at 450°C for 1 hour is 16% lower than the yield of liquid obtained after stressing of JP-8 alone. This difference remained virtually unchanged after 5 hours of stressing. The lower liquid yield obtained with added activated carbon could be attributed to the adsorbtion of stressed products on active surfaces and the catalysis of recombination reactions on carbon surfaces to produce more gases. Generally, the addition of solid carbons leads to the production of less C_1 and C_2 and more C_3, C_4, and C_5. The concentration of long-chain paraffins was higher when JP-8 was mixed with activated carbon. The addition of carbon had little effect on the concentration of alkylbenzenes.

Short chain-alkanes, not present in the original JP-8 (neat), are produced by cracking reactions during thermal stressing. The concentration of short-chain alkanes is higher in the samples obtained from thermal stressing of JP-8 alone. Higher concentrations of long-chain alkanes occurred in the liquids produced in the presence of activated carbon. However, the concentration of the alkanes with fewer than seven carbon atoms was higher for the jet fuel stressed alone than with activated carbon. This is an indication that the addition of activated carbon leads to preservation of the compounds present in the initial fuel sample. In general, all alkanes showed higher product yields for the liquid obtained after stressing of JP-8 without carbon.

The concentration of alkenes and cycloalkanes in the liquid obtained after stressing of JP-8 with activated carbon was equal to or higher than that in the liquids obtained from thermal stressing of JP-8 alone.

b. The Effect of Carbon Surface on Deposition Mechanism

This study is explained in detail in *Advanced Thermally Stable Jet Fuels Technical Progress Report, November 1992 – January 1993.*

Purpose: Previous studies have shown that solid carbons with the most disordered structure and highest surface reactivity (i.e., activated carbons) produced the most significant effect on thermal degradation. The activated carbon surfaces appear to be effective in stabilizing the free radicals or catalyzing the recombination reactions to form more gases and to preserve constituent paraffins in the fuel at 450°C. We undertook this study to:

- Investigate the effects of the surface area and pore distribution of activated carbons on solid deposition
- Gain more insight into the thermal behavior of commercial jet fuels A-1 and JPTS in the presence of different solid carbons
- Substantially decrease the amount of activated carbon added to jet fuels before thermal stressing at 450°C

Conditions: Thermal stressing at 450°C for 5 hours of:

- 10 mL samples of JP-8 jet fuel mixed with 1 g samples of activated carbons from cherry stones, grape seeds, almond shells, and anthracite
- 10 mL JPTS jet fuels samples mixed with 1 g and 200 mg of activated carbon from apricot stones with particle size 1-3 mm, powdered activated carbon, and a commercially activated carbon sample (Calgon)
- 10 mL JPTS and A-1 jet fuel stressed with 100 and 200 mg of high surface area activated carbon, PX-21 (produced by Amoco Oil Company; has a BET N_2 surface area of 3000 m^2/g)

Findings: The specific surface areas of activated carbons used as additives is the most important determinant of the carbons' ability to suppress solid deposition. Activated carbons with high specific surface areas and microporous structures appear to be the most effective carbon additives for inhibiting solid formation. The differences in liquid product composition when solid carbons are added indicate a catalytic effect of the carbon surfaces during thermal degradation of jet fuels. Higher concentrations of paraffins and lower concentrations of alkylated aromatics are associated with the liquid products obtained in the presence of activated carbons.

1. Thermal Stressing of JP-8 Mixed with Different Activated Carbons. The activated carbons provided a wide variation of BET N_2 surface areas and pore size distributions. Thermal stressing of JP-8 jet fuel with 1 g of activated carbon from apricot stones and the commercial activated carbon resulted in prevention of solid deposition and preservation of the compounds present in the initial fuel sample. The stabilizing effect could not be fully attributed to either the activated carbon's stabilization of free radicals or its specific pore size distribution.

All of the solid carbons gained weight during thermal stressing. Part of the weight gained by the activated carbons could be attributed to solid carbon deposit on the carbon surfaces. This was particularly apparent on the surface of activated carbons from grape seeds and cherry stones—which have predominantly macro-and mesoporous structures—and almond shells—which contain primarily meso- and microporous structures. Activated anthracite gained considerably less weight than the other activated carbons. Because anthracite has a higher BET N_2 surface area than the other activated carbons, we concluded that it adsorbs more liquid during thermal stressing. The activated carbons with lower BET surface and predominantly meso- and macroporous structures created higher gas pressures in the reactors; therefore, these carbons are most likely to promote the cracking processes and increase the possibility of solid deposition on reactor walls.

The deposits from the cherry stone and almond shell carbons had more closed structures with irregularly distributed pores than the grape seed carbons, but showed similar deposition of carbonaceous solids on their outer surfaces. All three provided more attractive surfaces for carbon deposition than stainless steel reactor surfaces. The deposit structures suggest liquid-phase carbonization reactions on the surface of the activated carbons of the deposit precursors, which are mostly initiated in a vapor phase. Microporous carbons (apricot stone and commercial activated carbon) did not show any significant solid deposition on their surfaces.

The carbonaceous deposits recovered with activated anthracite particles have different microstructures from those seen with the other activated carbons. These deposits have thin flaky solids mixed with activated anthracites, which are smaller and more loosely attached to the reactor walls than the deposits resulting from the other activated carbons. However, similar to the behavior of other microporous carbons, anthracite suppressed the formation of carbonaceous deposits without any apparent deposition on the added carbon surfaces.

2. Thermal Stressing of JPTS Jet Fuel with Activated Carbons. The activity of carbons in suppressing deposit formation depends on surface area. Activated carbon from apricot stones (1-3 mm in size) inhibited solid deposition and slowed the degradation of jet fuel, while activated carbon from powdered apricot stones did not. The former had isotropic structures and no carbonaceous solid deposited on its surfaces; the latter had large quantities of carbonaceous solid deposited on the activated carbon surfaces.

3. Thermal Stressing of Jet Fuel Samples with 100 and 200 mg of High Surface Area Activated Carbons. In general, the polyaromatics—particularly the alkylated polyaromatics (which were probably more complex in structure than those identified in the liquid product obtained after thermal stressing) were most likely the precursors to solid deposits. The concentration of short-chain alkanes was higher in the sample obtained from thermal stressing of A-1 alone. Comparing the stressing of A-1 alone with activated carbon PX-21, we found similar results as with the stressing of JP-8 both with and without activated carbon; however, the amount of activated carbon added to A-1 jet fuel was just 20% of the amount added to JP-8 jet fuel.

The concentration of long-chain paraffins was higher in the liquid obtained from stressing of A-1 with activated carbon. The same was true for alkenes. While the nonene and decene were predominantly in higher concentration in the liquid obtained from A-1 stressed with activated carbon, pentane and hexane are in higher concentration in the liquid obtained from A-1 stressed alone. There was no clear predominance of cycloalkanes in either of the samples. However, the liquid obtained from stressing of neat A-1 consists of higher concentrations of alkyl benzenes and naphthalenes.

c. The Effectiveness of Adding Activated Carbons in the Presence of Oxygen

This study is explained in detail in *Advanced Thermally Stable Jet Fuels Technical Progress Report, February 1993 – March 1993.*

Purpose: Determine the effectiveness of adding an activated carbon in the presence of oxygen, by stressing JPTS jet fuel with PX-21 in an air atmosphere at two different temperatures.

Conditions: 10 mL samples of JPTS mixed with 100 mg of activated carbon PX-21 at 450°C for 5 hours in an air atmosphere and 10 mL samples of JPTS mixed with 50 mg of activated carbon PX-21 at 425°C for 5 hours in air and nitrogen atmosphere

Findings:

The addition of a high-surface-area activated carbon, PX-21, is highly effective in enhancing the thermal stability of JPTS at high temperatures in both nitrogen and air atmospheres. A concentration of 50 mg per 10 mL of fuel is sufficient for almost complete suppression of thermal decomposition after stressing for five hours at 425°C in nitrogen and for preventing solid deposition on the reactor walls after stressing in air at 425°C for 5 hours. A 100 mg/10 mL

addition appears to be necessary to prevent solid deposition in air at 450°C for 5 hours. The increased stability by activated carbon addition can be explained by the termination of free radical chain reactions on active carbon surfaces.

d. Products Obtained from Thermal Stressing of JPTS Jet Fuel

This study is explained in detail in *Advanced Thermally Stable Jet Fuels Technical Progress Report, April–June 1993.*

Purpose: Determine the liquid, gaseous, and solid products obtained after thermal stressing of JPTS jet fuel at 450°C and 425°C for 5 hours.

Conditions: 10 mL JPTS alone and mixed with 50 mg high surface area activated carbon PX-21 in stainless steel microautoclaves under 100 psi of nitrogen and air at 425°C for 5 hours and 450°C for 5 hours.

Findings: The PX-21 addition effectively stops the formation of carbonaceous solids on the reactor walls. It also increases stability and suppresses the thermal degradation of jet fuel after stressing at 425°C and 450°C for 5 hours. The 50 mg of PX-21 was sufficient to prevent carbon deposition and stabilize JPTS jet fuel during thermal stressing at 425°C.

The experimental data suggest that at least 100 mg PX-21 is necessary for preventing solid deposition at 450°C. The processes of thermal degradation of JPTS were delayed more in the nitrogen atmosphere than in the air atmosphere. However, the results obtained for JPTS stressed in air, even at 450°C, showed that no carbonaceous solid was observed on the reactor walls.

The data for the gaseous products obtained after thermal stressing of JPTS with and without PX-21 at 425°C for 5 hours show that the reactions during thermal stressing of JPTS with high surface area activated carbon are quite different from those occurring in the absence of added carbon.

3.17 CARBONACEOUS DEPOSIT CHARACTERIZATION

This study is explained in detail in *Advanced Thermally Stable Jet Fuels Technical Progress Report, January–March 1994.*

Introduction

Previous studies concluded that deposit formation from dodecane thermal stressing on metal surfaces could be a two step process involving an initial catalytic deposition step on some clean metal surfaces and a subsequent deposition step on previously formed deposit surface.[1] This did not hold true for thermal stressing of JP-8C, a coal-derived jet fuel. Filamentous carbon and fibrous carbon were detected on nickel and copper surfaces, respectively, indicating catalytic effects of the two metal surfaces on initial deposition.[2] A common feature of the carbonaceous deposits found on all metal surfaces studied was the presence of circular or oval ring structures, as part of the solid growth on previously formed carbonaceous deposits.

This work focuses on characterizing carbonaceous deposits formed on different metal surfaces from thermal stressing of dodecane and JP-8C. We chose to use micro-Raman spectroscopy and static secondary ion mass spectroscopy (SIMS) in our investigation, because both techniques are surface-sensitive and location-specific. These attributes were important in revealing the chemical characteristics of specific features, such as the "ring" structures on the deposit surfaces. We also studied deposition from tetradecane and butylbenzene on a hot nickel surface and gasification of the deposit formed on a metal surface using a hot-stage environmental scanning electron microscope (ESEM)—a useful tools for monitoring deposition dynamics, including initial deposit formation.

Micro-Raman Spectroscopy

Raman spectra were measured on an Instruments SA Raman or U-1000 spectrometer; excitation was by means of the 514.5 nm line of an argon ion laser with an output power range of 100-500 mW. The instrument's microscope had a focal spot size of a few micrometers; initial laser power was adjusted to 10 mW. Multiple scans were collected and co-added between 1000 and 1700 cm^{-1}.

Figure 3.17-1 shows the Raman spectra of the deposit on nickel (Ni) foil at the top (T) of the tubing bomb reactor from thermal stressing of dodecane (D) and JP-8C (C) for 3 and 5 hours. Two broad bands can be seen—one in the 1600 cm^{-1} region reflects the stretching mode of the individaul sheets of graphitic crystallite; the other indicates the breakdown of the $k = 0$ selection rule for Raman scattering, as a result of the turbostratic nature of the deposit. There was no difference in the wave numbers of the G band and only a small downshift in the D-band as thermal stressing time increased for both dodecane and JP-8C. A shoulder peak around 1240 cm^{-1} appears after three hours reaction for both dodecane and JP-8C and disappears after 5 hours of reaction. A similar shoulder peak was reported by Dischler et al[3] on hydrogenated amorphous carbon films prepared by plasma deposition and assigned as sp^4 amorphous carbon (hydrogenated amorphous carbon films have been confirmed to consist of a mixture of tetranedral and trigonal bonding structures).[4]

We calculated the integrated intensities by digitizing the spectra with Un-Plot-It and using a combination of Gaussian and Lorentzian fit. The ratio of intensities $R = A_{1360}/A_{1580}$,

plotted in **Figure 3.17-2**, increases with reaction time, indicating an increase in structural disorder both for dodecane and JP-8C as the deposition continues (i.e., the top layers of the deposit after 5 hours are more disordered than those at 3 hours). This could be caused by a decrease in the rate of continuing carbonation of deposit or an increase in the rate of deposition of smaller, more disorganized crystallines.

In studying the ring structures at the 3-hour stressing time, we found that there was no significant difference in the shape and location of the D and G bands. The G bands were located at roughly 1600 cm^{-1}, which was higher than the G bands from the deposit on nickel surface. The D bands were around 1370 cm^{-1}. Based on the ratio intensities, structural disorder increases from carbon mound to carbon ring to bulky carbon substrate, with disk carbon substrate—which defined the perimeter of the ring—being the most ordered deposit. Differences in the order of molecular structures on different positions in the deposit suggest different precursors/mechanisms of solid deposition, depending on the location on the substrate, as well as the time of deposition. The variations observed in molecular order may be associated with different chemical constitution of the deposit, particularly its hydrogen content.

Static Secondary Ion Mass Spectroscopy (SIMS)

SIMS uses a beam of energetic ions to bombard a material's surface and perform mass analysis of the sputtered ions and neutral atoms and molecules. For static SIMS, incident ion flux is kept below 1% of the number of molecules needed to create one layer, ensuring that the amount of material removed during analysis is sub-monolayer.[5]

Using static SIMS, we found that at 5 hours stressing time, the desorbed ions consist of groups of saturate and unsaturated hydrocarbons ranging from C1 to C9, the C2 group being most abundant. No polyaromatic ions were detected. At 3 hours stressing time, the groups of hydrocarbon ions were very similar. The spectra indicated that the fragmentation of the deposit on the layer surface is easy. No PAHs can remain intact under the bombardment of Ga+ ions. Lower Ga+ ions will be used in future experimentation to investigate the possibility of removing larger molecular species from the deposit surface.

We investigated possible chemical differences in the deposits both on and off the ring structure, examining deposit from thermal stressing of dodecane on 321 stainless steel at 450°C for 5 hours. The general characteristics of the ion peaks were similar; however, the intensities of the peaks were different. Ions from off of the ring count more than twice those from on the ring, agreeing with the conclusion that carbon substrate is more disordered than the carbon ring.

Hot-Stage Environmental Scanning Electron Microscopy (SEM)

Cooling a specimen after thermal reaction may influence the observed morphologies and lead to erroneous conclusions on deposition mechanisms; therefore, observing solid deposit in-situ using a hot-stage SEM is useful for monitoring the fluid/surface interaction. These experiments take place under reduced pressure in the microscope (1-5 torrs) and observations may not apply at higher pressures.

In this case, a nickel coupon was placed in a crucible attached to a platinum heating wire. The temperature of the crucible can reach 1200°C. Liquid reactants (tetradecane or butylbenzene) were injected onto the nickel surface inside the vacuum camber by a Fullam

microinjector. Reaction products on the surface could be imaged continuously and videotaped at pressures near 3 Torr. Relatively high temperatures (600°-700°C) were employed to observe deposition within a reasonable time period.

The deposit formation from *n*-butylbenzene on nickel had the following characteristics:

- A rough surface
- Umbrella shaped grains were visible before deposition
- Deposition first observed approximately 30 minutes after the heater reached 650°C
- Initial deposit particles grew to form ridges on the grain surface and covered the grain surface in two hours
- No preferential deposition on the grain boundaries was observed, although these regions are known for their higher reactivities.

Two experimental difficulties hampered the in-situ experiments—the low retention time of the reactant gases on metal surface and the lack of control of the flow of liquid that is constantly sucked into the chamber by the vacuum.

In microautoclave experiments, the deposition of the carbonaceous solids takes place over a relatively long time period (1-5 hours), while the accumulation occurs layer by layer. Therefore, studying the gasification of microautoclave deposits by in-situ SEM can provide very useful information on the structure of the deposits. The carbonaceous deposit formed on nickel surface after 3 hours thermal stressing of dodecane at 450°C was heated in the microscope stage to 900°C in a water vapor atmosphere. The observed gasification mode of the deposit can be characterized as "edge recession"—a mechanism observed for highly ordered solid carbons, such as graphites. Preferential gasification of the edges of the cracks found in the deposits led to widening of these cracks to reveal, eventually, the nickel surface on which the deposition had started.

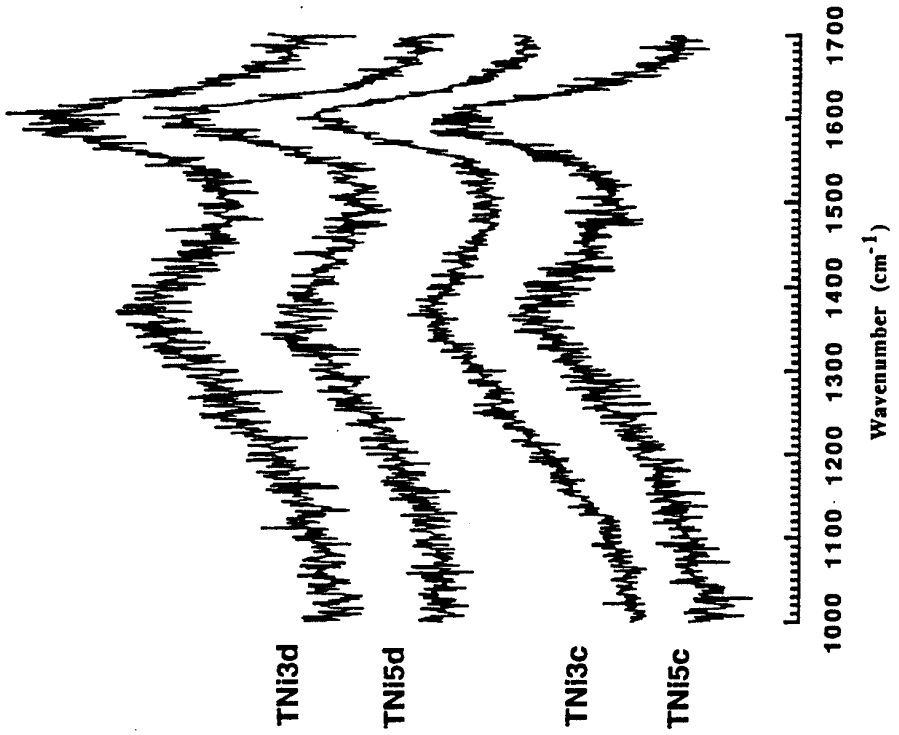

Figure 3.17-1. Raman Spectra of Deposit on Nickel Foil
(T: top, d: dodecane, c: JP-8C, 3: 3 hours, 5: 5 hours)

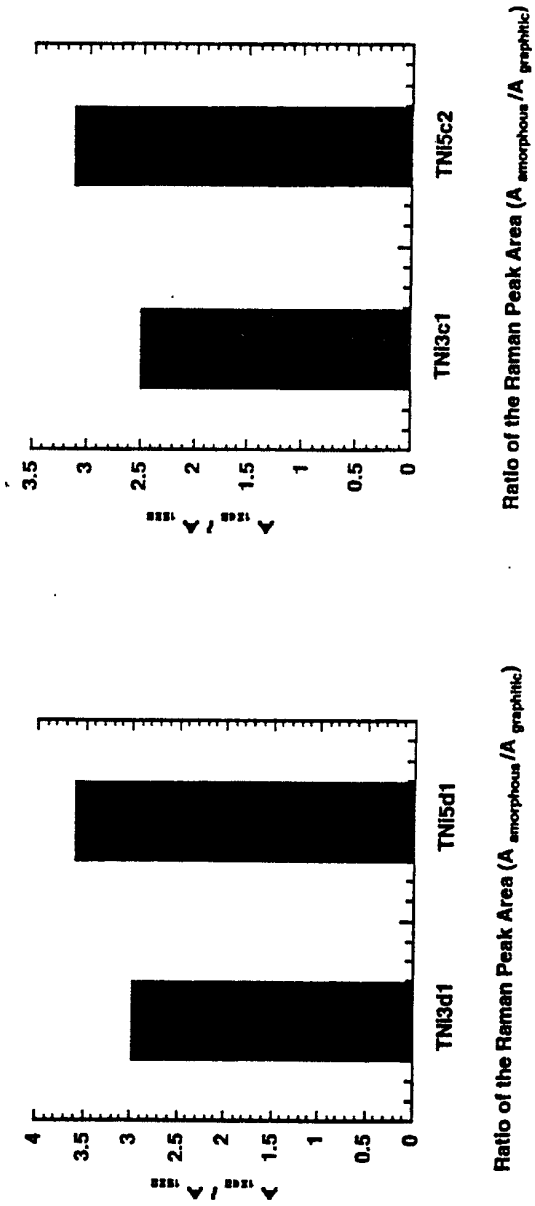

Figure 3.17-2. Ratio of Integrated Intensities of D Band to G Band

---

[1] Schobert, H. H. et al. *Advanced Thermally Stable Jet Fuels, Technical Progress Report, July 1993 – September 1993.* The Pennsylvania State University. 1993.

[2] Schobert, H. H. et al. *Advanced Thermally Stable Jet Fuels, Technical Progress Report, October 1993 – December 1993.* The Pennsylvania State University. 1993.

[3] Dischler, B. et al. *Inter. Sym. Plasma Chem.* ISPC-7 Eindhoven. Paper # A-1-4. 1985.

[4] Yoshikawa, M. et al. *Phy. Rev. B.* 1992. 46(11). 7169-7174.

[5] Winograd, N. Analy. Chem. 1993. 65. 622A-629A.

3.18 Characterization of Actual Engine Deposits

This study is explained in detail in *Advanced Thermally Stable Jet Fuels Technical Progress Report, July–September 1995.*

Introduction

Earlier we presented the results of characterization of deposits produced in a tubing bomb reactor[1] and in a flow reactor.[2] This study focuses on data from characterization of actual engine deposits. Characterization of actual engine deposits can serve two general purposes. It can help to identify the main cause of deposition in the engine systems as a means of developing measures to prevent deposit formation. It also serves as a check to ensure the relevancy of our studies to the solid deposition observed in actual engine fuel systems. We previously established that different solid formation and deposition mechanisms can be responsible for deposition accumulation on different parts or components of the fuel system in an aircraft.

Experimental

Two types of actual engine deposits were examined: deposits from a fuel line and deposits from a fuel nozzle. The nozzle deposits are further classified into two categories—main tip deposits and metering set deposits. Part of the carbonaceous deposits on these engine parts were scraped off, mixed with KBr to make a 1% deposit pellet, and examined using Fourier transform infrared spectroscopy (FTIR). The deposits from the engine parts were also made into an epoxy pellet for examination by polarized-light microscopy. The morphology of the deposits was examined using scanning electron microscopy (SEM) coupled, in some cases, with an energy-dispersive x-ray (EDX) detector for element mapping.

Conclusion

Characterization of deposits from actual engine parts show that different reaction and deposition mechanisms prevail in different sections of the fuel system. Metal surface seems to be an important factor for the formation of deposits inside the main tip. Temperature and oxygen concentrations are the other important factors that govern deposition on different parts of an engine fuel system. Results from the deposits obtained with model compounds heated in the presence of metal foils bear resemblance to those from actual engine deposits in that a two-layer deposit structure is observed on an active metal substrate, such as nickel.

---

[1] Schobert, H. H. et al. Advanced Thermally Stable Jet Fuels, Technical Progress Report. The Pennsylvania State University. #P2PC92104-TPR-5 and P2PC92104-TPR-7. 1993.

[2] Schobert, H. H. et al. Advanced Thermally Stable Jet Fuels, Technical Progress Report. The Pennsylvania State University. #P2PC92104-TPR-5 and P2PC92104-TPR-10. 1995.

3.19 Nature of High Temperature Deposits from *n*-Alkanes in a Flow Reactor

This study is explained in detail in *Advanced Thermally Stable Jet Fuels Technical Progress Report, October – December 1995.*

Introduction

Higher temperatures in jet engines increase concerns about system fouling due to carbon deposits in heat exchangers, nozzles, and fuel lines. Current aircraft can heat the fuel to temperatures around 150°C, but future designs may cause the fuel to heat up to temperatures approaching 540°C prior to combustion.[1] At 150°C, carbon deposits form from autoxidative reactions. At 540°C. the fuel begins to thermally break down under pyrolysis and form gas, which leads to gas-phase or pyrolitic carbon deposits.

An Exxon solvent, Norpar-13, which consists of C_{12}-C_{15} normal alkanes, was used to help model the pyrolitic deposition of jet fuel in a single-tube flow reactor. Norpar-13 forms large amounts of pyrolytic deposits, but remains stable in the autoxidation regime. This stability qualifies it as a good model mixture to observe the chemistry and deposit formation of jet fuels under pyrolytic conditions.

Thermal stability of a fuel, as measured by deposit formation, can be increased different ways. Higher thermally stable components can be engineered into the jet fuel, additives can be added to the fuel to stabilize radicals formed by thermal stressing, or surface effects from the metal walls—which can cause catalytic decomposition of the fuel at high temperatures—can be mitigated. This work investigated the surface catalytic effects of stainless steel on the deposition behavior and deposit morphology of Norpar-13. The behavior of an inert fused silica coating called Silcosteel, from the Restek Corporation, was also investigated. Experimentation with Silcosteel in the oxidative regime on thermally stressed jet fuels has been conducted.[2] In addition, the morphology of the pyrolytic deposits were compared with oxidative deposits formed from a Jet A fuel.

Experimental

The flow reactor apparatus consisted mainly of a fuel tank and a single tube running through a Lindberg laboratory furnace with a 91.5 cm actively heated zone. The fuel was pumped through the system with a SSI high-pressure liquid chromatography pump, and the system pressure was regulated by a back pressure valve. Liquid and gas products were sampled through a three-way valve downstream of the back pressure valve. Tube wall temperatures were determined by type K thermocouples spot welded to the outside of the tube, and a thermocouple was inserted at the end tube section to measure the final fuel temperature. The fuel in the tank could be sparged with either air or nitrogen (70 ppm O_2 (w/w) in air-saturated fuel (0.0018 molar) and the system was sparged with nitrogen prior to each test.

The Norpar-13 was made up of 0.2 wt% undecane, 14.4% dodecane, 52.9% tridecane, 32.0% tetradecane, and 0.5% pentadecane. Each test was run for 5 hours at a final fuel temperature of 550°C, which corresponded to a maximum wall temperature from 600°C to 620°C. These conditions created linear flow through the tube, with the Norpar-13 reaching supercritical conditions in the pyrolytic regime at temperatures greater than 400°C. The gas

formation (cracking) of Norpar-13 was calculated as the volume percent of the liquid that was converted to gas (C_1-C_6) and was determined by measuring the fuel flow before and after reaction through the tube.

Further procedural and analytic detail can be obtained from the corresponding Technical Progress Report.[3]

Conclusions

Norpar-13 stressed above 450°C in stainless steel flow reactor tubes created a large amount of catalytic filament deposits. The addition of a sufficiently thick fused silica coating in the Silcosteel reactor tubes created a barrier from the catalytic stainless steel surface, eliminating filament formation and greatly reducing the amount of pyrolytic deposits formed. Oxidative deposits from a Jet A fuel were very different in morphology than the pyrolytic deposits from Norpar-13. The oxidative deposits were made up of submicron carbon bundles that seemed to condense together.

---

[1] Edwards, T. and Atria, J. V. *Preprints.* Div. of Petrol. Chem., ACS. 1995. 40(4). 649.

[2] Jones, G. E., W. J. Balster, and W. A. Rubey. *Preprints.* Div. of Petrol. Chem., ACS. 1995. 40(4). 655.

[3] Schobert, H. H. et al. *Advanced Thermally Stable Jet Fuels, Technical Progress Report, October – December 1995.* The Pennsylvania State University. #92PC92104-TPR-14. 1996.

3.20 Thermal Decomposition of Tetralin in Near-Critical and Supercritical Regions: Product Distributions and Reaction Mechanisms

This study is explained in detail in *Advanced Thermally Stable Jet Fuels Technical Progress Report, October–December 1996.*

Introduction

Earlier we presented the results from the thermal decomposition of some typical jet fuel model compounds, including C_{10}-C_{14} *n*-alkanes, *n*-butylbenzene, *n*-butylcyclohexane, and decalin under near-critical and supercritical conditions. In this study, thermal decomposition experiments were performed on another model compound, tetralin.

Previous Work. Tetralin is the simplest model for hydroaromatic structures in coal and has also been used widely as a hydrogen donor solvent in coal liquefaction experiments. Most previous thermal decomposition experiments of tetralin were carried out under low temperature, high-pressure conditions relevant to coal processing. The major products from the pyrolysis of tetralin at low temperatures and high pressures are 1-methylindan and naphthalene.[1, 2, 3, 4] Other products, including *n*-butylbenzene, ethylbenzene, indan, toluene, and small amounts of gases, were also observed.[1, 3] On the other hand, when tetralin was pyrolyzed under high-temperature, low-pressure conditions—which are of interest for industrial thermal cracking—the major products were naphthalene and 1,2-dihydronaphthalene, followed by indene, styrene, and some monoaromatics.[5, 6] Gaseous products were also formed, including hydrogen, methane, ethane, and ethylene.

The product distributions from tetralin pyrolysis have been explained by a free radical mechanism that involves three main pathways: dehydrogenation to naphthalene and 1,2-dihydronaphthalene, isomerization to 1-methylindan, and naphthenic-ring opening to *n*-butylbenzene and other cracking products.[1, 6] The relative importance of these three pathways depends on reaction conditions. Low-temperature, high-pressure conditions favor the isomerization, while high-temperature, low-pressure conditions facilitate dehydrogenation. The cracking pathway is always less important at temperatures below 850°C. The cracking reactions are accelerated substantially in the presence of hydrogen.[2, 7]

Experimental

The experiments were carried out at 425-474°C in a Pyrex glass tube reactor for different times. We studied the effects of pressure at 450°C for 30 minutes.

Results and Discussion

1. Product Distributions

Analysis of the original tetralin sample showed that it contained approximately 1.1 wt% impurities, including naphthalene, 1,2-dihydronaphthalene, 1-methylindan, *cis*- and *trans*-decalin, ethylbenzene, toluene, benzene, and an unidentified compound that eluted between *cis*-decalin and 1-methylindan from the GC column. As the reactions proceeded, *cis*-decalin was isomerized to *trans*-decalin, and 1,2-dihydronaphthalene, benzene, and the unidentified

compound remained unchanged, while the yields of all other aforementioned compounds increased.

The most abundant product from thermal decomposition of tetralin under the conditions employed was 1-methylindan, followed by naphthalene, n-butylbenzene, and 2-methylindan. Also appearing, but in lower yields, were *n*-propylbenzene, ethylbenzene, and toluene. The yields of the reaction products changed with pressure, temperature, and residence time.

Product Distributions as a Function of Pressure. The product distributions as a function of pressure from the thermal decomposition of tetralin at 450°C for 30 minutes showed that as pressure increased, the yield of 1-methylindan increased while those of naphthalene, n-butylbenzene, and 2-methylindan decreased. (Note that the yields of 1-methylindan and naphthalene were adjusted to account for the feed impurities.) In the pressure range examined, the major products were 1-methylindan and naphthalene, and the yield of 1-methylindan was always higher than that of naphthalene. This indicated that, under the conditions used, the major reactions were ring isomerization and dehydrogenation.

Product Distributions as a Function of Temperature. The yield of 1-methylindan decreased while that of 2-methylindan increased with an increase in temperature. The yields of naphthalene and *n*-butylbenzene did not change significantly with temperature.

Product Distributions as a Function of Conversion. We plotted the product distributions as a function of conversion from the thermal decomposition of tetralin at 450°C with a loading ratio of 0.36 (P_r=1.16). The yield of 1-methylindan increased slightly and that of naphthalene decreased with the increasing conversion. The yields of *n*-butylbenzene and 2-methylindan did not change significantly with the conversion.

2. Reaction Mechanisms

In considering the potential reaction mechanisms involved in thermal decomposition of tetralin (see **Figure 3.20-1**), we determined that initiation occurs by homolytic cleavage of the α carbon-hydrogen bond to form a 1-tetralyl radical and a hydrogen atom. These radicals then abstract hydrogen atoms from tetralin to form 1-tetralyl and 2-tetralyl radicals. The 2-tetralyl radical could be converted to 1-methylindan by a neophilic rearrangement,[8] followed by hydrogen abstraction. The 1-tetralyl radical could undergo dehydrogenation reactions to form naphthalene. The formation of *n*-butylbenzene can be explained by hydrogen atom addition to tetralin, followed by decomposition and subsequent hydrogen abstraction. The 2-methylindan could be formed by P-scission of the 2-tetralyl radical, followed by ring closure and subsequent hydrogen abstraction.

Effect of Pressure. The product distributions were affected by pressure. Increasing pressure increased the yield of 1-methylindan, because the formation of the cyclohexadienyl intermediate from the 2-tetralyl radical is favored at high pressures. The yields of naphthalene and 2-methylindan decreased with the increasing pressure, because dehydrogenation and P-scission reactions are suppressed at high pressures. The yield of *n*-butylbenzene decreased as pressure increases, because of the decreased concentration of hydrogen atoms with the increasing pressure (resulting from the depressed dehydrogenation reaction at high pressures).

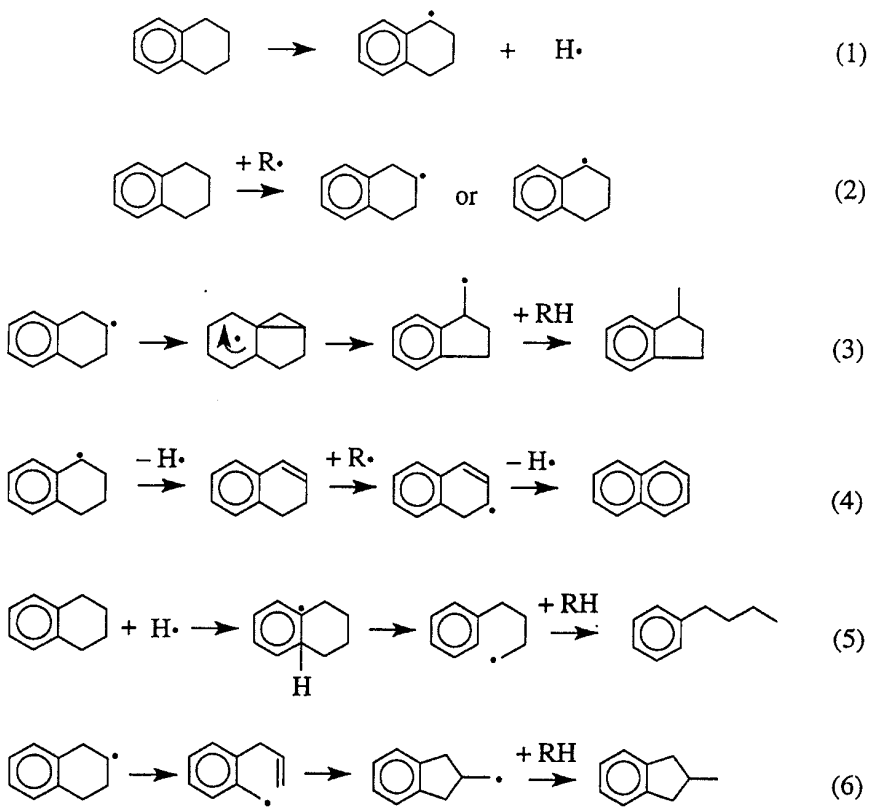

Figure 3.20-1. Reaction Mechanisms for Tetralin Thermal Decomposition

[1] Hooper, R. J.; H. A. J. Battaerd, and D. G. Evans. *Fuel.* 1979. 58. 132.

[2] Penninger, J. M. L. *Int. J. Chem. Kinetics.* 1982. 14. 761.

[3] de Vlieger, J. J., A. P. G. Kieboom, and H. van Bekkum. *Fuel.* 1984. 63. 334.

[4] Brodzki, D. et al. *Fuel.* 1994. 73. 789.

[5] Bredael, P. and T. H. Vinh. *Fuel.* 1979. 58. 211.

[6] Hillebrand, W., W. Hodek, and G. Kolling. *Fuel.* 1984. *63.* 756.

[7] Grigorieva, E. N. et al. *Fuel Processing Technology.* 1994. *38.* 85.

[8] Franz, J. A. and D. M. Camaioni. *Fuel.* 1980. 59. 803.

TASK 4. COAL-BASED FUEL STABILIZATION STUDIES

4.1 USE OF ^{13}C LABELS TO TRACE REACTIONS OF POTENTIAL ANTIOXIDANTS FOR JET FUELS

This study is explained in detail in *Advanced Thermally Stable Jet Fuels Technical Progress Report, August 1992 – October 1992.*

Introduction

Addition of antioxidants to retard cracking of the complex assemblage of hydrocarbons comprising jet fuels is a strategy being examined to prevent or delay the formation of solid deposits. Coleman et al demonstrated that benzyl alcohol and 1,4-benzenedimethanol are effective additives for the retardation of solid-deposit formation in jet fuel subjected to a temperature of 425°C.[1, 2] Their use of infrared spectroscopy, H NMR, and gas chromatography/mass spectrometry, prevented them from fully identifying reaction mechanisms, due to the fact that the complexity of jet fuel components obscures the various reaction intermediates. This inability to quantitatively differentiate all of the reaction intermediates from compounds present in the jet fuels prior to thermal stressing limited the researchers' ability to assess reaction mechanisms.

In this study, we chose instead to apply ^{13}C-labeled compounds to examine the reactivity of specific compounds in complex mixtures, based on our previous experience.[3] Reactions involving the ^{13}C-labeled carbon lead to significant changes in the chemical shift of this carbon in ^{13}C NMR spectra. By enriching the reactive compound with 100% ^{13}C at the one reactive site, an enhancement in the ^{13}C NMR sensitivity is realized for the labeled carbon. Unlabeled carbons are reduced to near-background level in the spectra, allowing reactions at the labeled site to be clearly discerned.

We examined the thermal reactivity of the benzyl alcohol additive with thermally stressed jet fuel in experiments identical to those described by Coleman et al.[1, 4] We used benzyl alcohol labeled with 100% ^{13}C at the (α) benzylic carbon.

Results

The fuel in our experiment behaved as described by Coleman from the previous study[1]—addition of 5% benzyl alcohol delayed formation of carbonaceous residues for up to 6 hours. Coleman's research indicated that a delay of carbonization reactions is linked to the thermal degradation of benzyl alcohol.

Addition of α-labeled benzyl alcohol to Jet A-1 fuel provided a ^{13}C NMR spectrum (**Figure 4.1-1**) dominated by the peak of the labeled α carbon at 65.3 ppm. Other peaks were those natural abundance carbons in the jet fuel as a result of hydrocarbons and the unlabeled carbons of the benzyl alcohol. The relative intensity of the labeled α carbon was 71.4% of the total intensity of all peaks.

As the jet fuel/benzyl alcohol mixture was thermally stressed at 425°C for varying times, the ^{13}C NMR spectra changed dramatically, as shown in Figure 4.1-1. The peak for the labeled α carbon gradually diminished over a period of 6 hours and eventually disappeared after 12 hours. During this period, other peaks emerged.

Previous studies showed that thermal stressing of jet fuel for the time periods used in our study led to significant alteration of the fuel-derived hydrocarbons. However, we did not observe a significant change in the relative distribution of the unlabeled peaks assigned to jet fuel hydrocarbons over the course of 12 hours. We also did not observe the evolution of olefins that would give peaks in the range of 90-140 ppm, in contrast to the observations made by Coleman.[1]

While both our study and previous studies determined that benzyl alcohol is thermally degraded to benzaldehyde and subsequently oxidized to benzoic acid, only our study observed toluene and benzene—other research methods were unable to distinguish benzyl-alcohol-derived toluene and benzene from the toluene and benzene naturally present in jet fuel.

Perhaps the most significant advantage ^{13}C NMR and use of labels have over other techniques is the ability to quantify the reaction products to trace reaction mechanisms. Furthermore, the tracking of the label can be made quantitatively in the presence of complex mixtures of materials containing natural abundance carbons. **Table 4.1-1** shows the yield of peaks assigned to specific carbons of individual compounds normalized to the total intensity of peaks in the NMR spectra for each aliquot taken over the course of time during the reaction. This table demonstrates the growth and loss of both labeled and unlabeled carbons. The steady loss of benzyl alcohol was accompanied by a rise in toluene as the next most abundant product. Benzaldehyde increased during thermal stressing, but the amount of benzaldehyde was not as significant as the amount of toluene. After 6 hours of heating, the benzaldehyde concentration decreased while the concentration of both benzene and benzoic acid increased slightly.

Conclusions

Using ^{13}C labeling, we can quantify products formed as a result of thermal alteration of benzyl alcohol, following the α-^{13}C-labeled carbon over the given time intervals for thermal stressing. The distribution of all of the identified labeled and unlabeled reaction products indicates that thermal stressing of benzyl alcohol in the presence of jet fuel leads to the production of toluene and benzene as the major species—two products which had gone undetected using other forms of analysis. Benzaldehyde and benzoic acid were determined to be intermediates.

The detailed mechanism responsible for producing these compounds and the reason for retardation of solid deposit formations were not determined in this work. However, we did demonstrate the value of using labeled substrates in complex systems (e.g., jet fuels) to trace products formed, without interference from other unlabeled portions of the fuel . This is a major first step in determining the influence of a reacting species such as benzyl alcohol and the mechanism by which retardation of thermal degradation occurs.

Table 4.1-1. Intensity of ^{13}C NMR Data of Specific Carbons Normalized to the Total Peak Intensity of the Spectrum

Time (min)	α-Carbon of Benzyl Alcohol (65.3 ppm)	α-Carbon of Benzyl-dehyde (192 ppm)	α-Carbon of Toluene (21.4 ppm)	α-Carbon of Benzoic Acid (170 ppm)	Benzene (128.35 ppm)	Σ Label
0	71.4	0.0	0.0	0.0	0.0	71.4
10	62.0	1.3	4.2	0.0	0.2	67.5
60	44.5	4.0	8.8	0.0	0.4	57.3
180	26.1	6.8	17.3	0.6	1.9	50.8
360	6.1	4.4	31.7	1.3	5.4	43.5
720	0.0	0.0	38.5	1.0	6.6	39.5

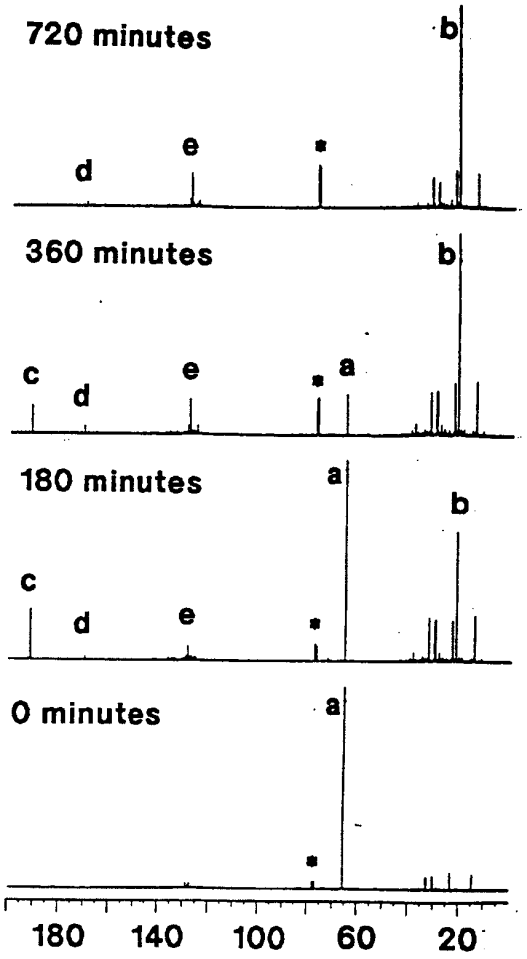

Figure 4.1-1. ^{13}C NMR Spectra of Thermally Stressed Jet A-1 with 0.25 mL of 100% Labeled α-^{13}C-Benzyl Alcohol

(a = benzyl alcohol, b=toluene, c=benzaldehyde, d=benzoic acid, *=chloroform)

[1] Coleman, M. M. et al. *Energy and Fuels.* 1992. 6. 535-539.

[2] Coleman, M. M. et al. *Prepr. Paper – Am. Chem. Soc., Div. Fuel Chem.* 1992. 37(4). 1664-1670.

[3] Bortiatynski, J. M. et al. *6th International Meeting of the International Humic Substances Society Abstracts.* 1992. 293.

[4] Coleman, M. M. et al. *Prepr. Paper – Am. Chem. Soc., Div. Fuel Chem.* 1992. 37(4). 1664-1670.

4.2 The Mechanism of Hydrogen Transfer from Hydroaromatic Compounds—A Literature Review

This study is explained in detail in *Advanced Thermally Stable Jet Fuels Technical Progress Report, August 1992 – October 1992.*

Introduction

Our interest in the mechanism of hydrogen transfer from hydroaromatic compounds derives from the potential to use hydrogen transfer to stabilize jet fuels during thermal stressing. Much of the recent literature on hydrogen transfer from hydroaromatics derives from coal liquefaction studies.

Coal liquefaction depends on a supply of hydrogen atoms proportionate with the rate of free-radical formation, which is a function of coal structure and reaction temperature. The bridges linking the cyclical units of coals are ruptured when heated to 400-450°C. Bond rupture forms free radicals, which can be stabilized by the addition of a hydrogen atom. If hydrogen capture does not occur, the radicals combine to form stable, high molecular mass products. One hydrogen source is the liquefaction solvent. The liquefaction solvent not only provides a transport medium for the coal and facilitates heat transfer, it also serves as an important source of transferable hydrogen and it disperses the liquefaction products.[1] This hydrogen-donor solvent serves as a hydrogen source and transfer agent for the degrading coal and it inhibits the retrograde reactions that lead to solid, unreactive carbonaceous residue.

Hydrogen-donor solvents are known to donate hydrogen to the coal liquefaction system without having to add external hydrogen gas to the system.[2] The value of hydrogen-donor solvents has long been recognized, and their activity is related to the degree of saturation and to the number of condensed rings.[3, 4] The degree of saturation is related to the degree of hydrogenation on multiaromatic ring systems. The most effective hydrogen-donor compounds are those with a partially hydrogenated aromatic structure—such as tetrahydronaphthalene (tetralin), dihydropyrene, and 9,10-dihydrophenanthrene.[2, 5, 6, 7] The hydroaromatic hydrogens are easily abstracted, leading to stable aromatic compounds and stabilizing the coal free radicals.[8] Neither the parent aromatic compound nor the fully hydrogenated derivative is a good hydrogen donor.[9]

There are other applications of hydroaromatics in coal liquefaction. Hydroaromatics such as tetralin and octahydrophenanthrene play the role of inhibitor in the autoxidation of hydrocarbons and effectively suppress the formation of colored and high molecular weight products.[10] The inhibiting abilities of heavy hydroaromatics from petroleum have been applied to rubbers and plastics.[11] Research continues on the application of hydroaromatics to improve the thermal stability of aviation jet fuels.[12]

Conclusion

The mechanisms of hydrogen transfer from donor solvents to various coal structures remain largely unspecified, although many researchers have investigated this subject. Much discussion of donor solvent coal liquefaction has focused on thermal scission of covalent bonds, followed by capping the free radicals by hydrogen atom abstraction from the donor solvent. This line of reasoning continues, although a number of researchers have pointed out alternative

possibilities, such as radical chain processes (usually involving a β-scission of the chain carriers), hydrogen atom and radical addition-elimination processes, hydride transfer, and concerted H_2-transfer processes. Recent work has focused on direct transfer of hydrogen atoms from solvent-derived radicals to substituted positions in aromatic rings as preliminary steps in depolymerizing coal structures. Based on recent and ongoing research, none of these mechanisms can be singled out and considered exclusively; all remain plausible.

---

[1] Whitehurst, D. D., T. O. Mitchell, and M. Farcasiu. *Coal Liquefaction.* New York: Academic Press. 1980.

[2] Bockrath, B. C. *Coal Science.* 1982. 2. 65-124.

[3] Curran, G. P. , R. T. Struck, and E. Gorin. *Ind. Eng. Chem. Process Dev. Div.* 1967. 6. 166.

[4] Obara, T., T. Yokono, and Y. Sanada. *Fuel.* 1983. 62. 813.

[5] Curran, G. P. , R. T. Struck, and E. Gorin. *Ind. Eng. Chem. Process Dev. Div.* 1967. 6. 166.

[6] Gorin, E. *Chemistry of Coal Utilization.* New York: J. Wiley and Sons. 1981. 2nd suppl vol. 1845-1918.

[7] Neavel, R. C. *Fuel.* 1976. 55. 237.

[8] Neavel, R. C. *Philos. Trans. R. Soc. London, Ser. A.* 1981. 300. 141.

[9] Burgess, C. E. M. S. Thesis, The Pennsylvania State University. 1991.

[10] Kubo, J. *Fuel Proc. Tech.* 1991. 27. 263.

[11] Kubo, J. *Fuel Proc. Tech.* 1991. 28. 19.

[12] Song, C., W.-C. Lai, and H. H. Schobert. Paper submitted at 204th ACS National Meeting, Washington, DC, August 1992.

4.3 Thermal Stability Studies Using the Model Compound Dodecane

Introduction

The typical jet fuel is a highly complex mixture, which makes the analysis of the products of thermal degradation in the presence of additives very complicated. Having successfully performed scouting studies to find additives that retard the thermal degradation of the jet fuel at 425°C, we decided to simplify the experimental methodology in our attempt to elucidate the underlying mechanisms involved. Understanding how benzyl alcohol and similar molecules retard the formation of carbonaceous solids in hydrocarbon mixtures at high temperatures is important and should point the way to the design of superior additives in the future. Dodecane was chosen as the model compound, as it is the most abundant hydrocarbon in jet fuels and there have been numerous studies performed on dodecane as a model.

Summary

FTIR studies indicated that during the thermal degradation of dodecane, alkenes form, followed by subsequent cyclization, aromatization, and condensation. In the case of the dodecane experiments, aromatic species were directly derived from the parent hydrocarbon upon thermal stressing (in contrast, analogous studies on pure jet A-1 fuel are complicated by the aromatic species present in the jet fuel). Parallel ^{1}H NMR studies were performed to assist in the interpretation of the changes observed in the infrared spectra as a function of thermal stressing. GC-MS studies were performed on the liquid samples to gain insight on the components of the liquid sample. Finally, the ^{1}H NMR and the GC-MS data are discussed and the mechanistic ramifications of our results are considered.

a. Analysis Involving Infrared, 1H NMR,, and Gas Chromatographic Studies

This study is explained in detail in *Advanced Thermally Stable Jet Fuels Technical Progress Report, November 1992 – January 1993.*

Experimental: Two sets of experiments were performed: the first on pure dodecane and the second on dodecane with 5% benzyl alcohol by volume, each stressed as a function of time. Thermal stressing was performed on 10 mL samples at 425°C in 15 mL type 316 stainless steel microreactors under 100 psi of air or nitrogen. The microreactor containing the sample was purged with UHP-grade N_2 five times at 1000 psi to minimize the presence of dissolved oxygen, then pressurized with 100 psi of air. It was placed in a preheated sand bath at 425°C for the specified reaction time and then quenched in cold water and depressurized to remove head-space gases.

Results: The following results have supported further experiments with deuterated dodecane. Preliminary results are very encouraging and appear to offer several mechanistic insights.

Infrared Studies. The room temperature infrared spectra of samples thermally stressed under air after 0, 1, 3, 6, 12, and 18 hours at 425°C is shown in **Figure 4.3-1**. The growing band at approximately 1642 cm^{-1} recorded between 1 and 6 hours represents a C=C stretching vibration resulting from the formation of alkenes during thermal stressing. The band increases from 6 to 18 hours, then diminishes after 18 hours. At about 6 hours, other bands appear at approximately 1600 cm^{-1} which grown in intensity from 6 to 18 hours of stressing time. These

bands were assigned to the ring stretching vibrations of aromatic compounds. They indicate that during the thermal degradation of dodecane, olefins form, followed by subsequent cyclization and aromatization. In the dodecane experiments, aromatic species are directly derived from the parent hydrocarbons, whereas the "pure" jet fuel already contains aromatic species, which complicates interpretation.

Figure 4.3-2 shows the infrared spectra of dodecane stressed with 5% benzyl alcohol. The band at 1710 cm^{-1} represents the carbonyl stretching vibration of benzaldehyde. The intensity of this band increases to a maximum after approximately 3 hours of stressing at 425°C, decreases at 6 hours, and is only a minor component by 12 hours. Concurrently, the band assigned to the C=C stretching vibration (1642 cm^{-1}) is detected at 1 hour, rises to a maximum at about 6 hours and is only a minor component by 18 hours of thermal stressing. Comparing Figures 4.3-1 and 4.3-2 shows that the rise and fall in intensity of the band at 1642 cm^{-1} is retarded with dodecane in the presence of 5% benxyl alcohol. After about 6 hours, a band is detected at approximately 1695 cm^{-1} that is likely associated with benzoic acid—the product of the oxidation of benzaldehyde.

Figure 4.3-3 shows the results of a quantitative analysis using the infrared band at 1642 cm^{-1} for dodedane neat (top) and dodecane with 5% benzyl alcohol (bottom). In the absence of the additive, the intensity of the olefinic band maximizes at 3 hours of thermal stressing, whereas in the presence of the additive this band reaches a maximum after approximately 6 hours of stressing—a retardation of about 3 hours.

^{1}H NMR Studies. These studies indicated that the formation of alkenes maximized between 3 and 6 hours. In the presence of benzyl alcohol, a maximum concentration occurred at 6 hours, which is consistent with infrared results.

Gas Chromatographic Studies. These studies showed that the addition of 5% benzyl alcohol retards the degradation of dodecane and, unsurprisingly, the effect is more pronounced under a nitrogen atmosphere. The products of benzyl alcohol degradation were clearly identified for dodecane with 5% benzyl alcohol stressed for 3 hours under 100 psi air; they were ≈3 min benzene, ≈6 min toluene, ≈18 min benzaldehyde, ≈20 min dodecane, ≈21 min benzyl alcohol, and ≈44 min dibenzyl ether. These compounds were confirmed using mass spectroscopy.

b. Pyrolysis with Deuterated Dodecane

This study is explained in detail in *Advanced Thermally Stable Jet Fuels Technical Progress Report, February 1993 – March 1993.*

Purpose: Dodecane has been used as a model compound to investigate the effect of the additive, benzyl alcohol, during pyrolysis under an atmosphere of air. The changes observed in the yields of the major products obtained upon stressing dodecane at elevated temperatures with and without benzyl alcohol were investigated as a function of time. The pyrolysis products of benzyl alcohol in the reaction medium were also studied. The results obtained are useful in elucidating the underlying reaction mechanisms. In this study, deuterated dodecane was used to probe the hydrogen-donating character of benzyl alcohol.

Experimental: Conditions were identical to 4.3a, above.

Results:

Pyrolysis of Dodecane with and without Benzyl Alcohol. Gas chromatographic analyses of neat dodecane and dodecane with 5 vol% benzyl alcohol indicated that the major pyrolysis products are *n*-alkanes and 1-alkenes ($<C_{12}$) for short periods of time (<6 hours) of thermal stressing. Longer periods of stressing favored higher yields of *n*-alkanes and over 12 hours, 1-alkenes were barely detectable. In the presence of benzyl alcohol, the degradation of dodecane to *n*-alkanes is retarded for about 6 hours of stressing. The longer the thermal stressing, the greater the cracking of dodecane into low molecular weight alkanes. The abundance of paraffins increases in a linear fashion with stressing time after an short initial induction period without benzyl alcohol. With benzyl alcohol, the induction period is expanded to approximately 6 hours.

Benzyl alcohol retards the formation of 1-alkenes. In contract to alkanes, the concentration of 1-alkenes maximizes between 1 to 3 hours of stressing without benzyl alcohol, between 3 to 6 hours with benzyl alcohol. This is consistent with the data previously obtained via Fourier transform infrared (FTIR) spectroscopy. The disappearance of alkenes after longer stressing periods can be attributed to their conversions into other products by condensation, cyclization, and aromatization reactions. Gas chromatography also indicated that benzyl alcohol retards the formation of gaseous hydrocarbons for about 6 hours of stressing.

Benzyl Alcohol Degradation in the Reaction Mixture. The benzyl alcohol is nearly completely consumed after 6 hours of reaction. It has a dramatic effect on the degradation of dodecane and, although a significant concentration of benzyl alcohol exists in the mixture, it acts as a "sacrificial lamb" to retard the degradation of dodecane. In the time interval that benzyl alcohol functions as an effective additive in retarding the degradation of dodecane, the major reaction product is benzaldehyde. As a result, we inferred that benzyl alcohol donates hydrogen to molecular species containing free radicals that are formed in the reaction medium prior to being oxidized to benzaldehyde. After a longer stressing time, benzene and toluene were the only products observed by gas chromatographic analysis; FTIR indicated that some benzoic acid is also formed. Benzene and toluene are obtained via the pyrolysis of benzaldehyde and dibenzylether; benzoic acid results from the simple oxidation of benzaldehyde.

Mechanistic Studies Using Deuterated Dodecane. **Figure 4.3-4** summarizes the proposed primary reaction scheme for thermal degradation of deuterated dodecane in the presence of benzyl alcohol. Under these conditions, pyrolysis of dodecane proceeds via free radical mechanisms. The first step is initiation resulting in the formation of free radical (R•). This radical abstracts a deuterium from the deuterated dodecane molecule. At this stage, the free radical either abstracts the benzylic hydrogen from benzyl alcohol and forms an alkane (m-1) or it undergoes β-scission, forming a completely deuterated alkene and a free radical, which, in turn, can abstract hydrogen from benzyl alcohol, resulting in the formation of an alkane (m-1). Deuterium can also be abstracted from the alkene, resulting in a radical that can abstract hydrogen from benzyl alcohol, resulting in an alkene (m-1). These (m-1) species can further undergo the same cycle, producing (m-2) and other species. Evidence that benzyl alcohol donates hydrogen to the reaction system in the manner depicted in Figure 4.3-4 was obtained from a related study, which provides strong proof that benzyl alcohol donates hydrogen and acts as a free radical scavenger.[1]

c. Thermal Stability of Second Generation Fuel Additives

This study is explained in detail in *Advanced Thermally Stable Jet Fuels Technical Progress Report, April 1993 – June 1993.*

Purpose: Summarize research pertaining to the development of a second generation of antioxidants.

In an effort to further probe and improve upon the nature of benzyl alcohol stabilization of jet fuel, a second generation of antioxidants has been identified and is being investigated. Early findings are presented here; thermal stressing of these additives was not yet conducted. Several examples of the new stabilizers are shown in Scheme III, **Figure 4.3-5**, each of which could have several additional benefits beyond those offered by benzyl alcohol.

As with benzyl alcohol, Compound 1—1,2,3,4-tetrahydro-1-napthol—has the benzylic proton we believe is responsible for antioxidant properties. Moreover, it possesses two tetralynic protons that may further enhance its ability to scavenge radicals, thereby increasing its antioxidant potential.

Compound 2—9,10-phenanthrenediol—also contains two benzylic protons, but after the initial radical abstraction, the newly formed benzylic radical should have an attenuated stability as a result of resonance throughout the phenanthrene ring system. This added stability should thermodynamically permit a more facile regeneration of the in tact hydrocarbon jet fuel.

Compound 3—phthalan—contains four benzylic protons, rather than the two present in benzyl alcohol. This could permit one molecule of phthalan to prevent the decomposition of twice the amount of jet fuel that is possible with benzyl alcohol. Additionally, the polar hydroxyl substituent of benzyl alcohol has now been replaced with a relatively nonpolar furan ring, providing increased solubility in the rather nonpolar jet fuel. Compound 3 is commercially available.

Compound 4—1,2-benzenedimethanol—also has four benzylic protons. Moreover, after an initial oxidation of one of the benzene methanol substituents of Compound 4 to an aldehyde (the transformation demonstrated to occur for benzyl alcohol), the remaining benzyl alcohol-like protons induce an intramolecular self-reduction to provide the starting benzenedimethanol. Compound 4 is commercially available.

d. Final Analysis of Findings and Mechanistic Ramifications

This study is explained in detail in *Advanced Thermally Stable Jet Fuels Technical Progress Report, October 1993 – December 1993.*

Purpose: Present the ^{1}H NMR and the GC-MS data, summarize our conclusions, and consider the mechanistic ramifications of our results.

Experimental: Thermal stressing conditions were identical to those described in 4.3a, above. A Hewlett Packard GC with mass selective detector was used for the GC-MS analysis. The initial temperature was 40°C, initial isothermal holding time was 5 minutes, heating rate was 4°C/min to 280°C, and the final isothermal holding time was 10 minutes. The split mode of injection was used.

Thermal Stressing of Neat Dodecane and Dodecane / Benzyl Alcohol Mixtures at 425°C.

^{1}H NMR Studies. Using the liquid sample, we found that olefinic protons resonate between 6 and 4.5 ppm, a region which can be very useful to monitor the formation and elimination of olefinic bonds. **Figure 4.3-6** shows ^{1}H NMR spectra of dodecane thermally stressed under air for periods of 0 and 20 minutes, and 1, 3, 6, 12, and 18 hours at 425° C. NMR resonances that can be attributed to internal and external alkenes are obvious and, in common with the infrared results, the concentration of alkenes appears to maximized at approximately 6 hours.

Figure 4.3-7 shows ^{1}H NMR spectra of dodecane-benzyl alcohol mixtures thermally stressed under air after period of 0, 1, 3, 6, 12, and 18 hours. The trends observed for the olefinic resonances are consistent with those seen in the infrared results. More interesting, however, is the fact that benzyl alcohol has a convenient characteristic resonance at 4.74 ppm attributable to benzylic protons. The intensity of this line at 4.74 ppm decreases as a function of thermal stressing, which verifies that benzyl alcohol is being consumed, but is still detectable after 6 hours at 425 °C. This implies that the benzyl alcohol is remarkably stable in the mixture and gradually transforms to benzylaldehyde (and other products) over a period greater than 6 hours. Furthermore, the amount of benzyl alcohol present after 12 hours of thermal stressing is insignificant. This suggests that as long as benzyl alcohol is present, the onset of the formation of carbonaceous solids is suppressed. These data strongly support the results obtained from simple quantitative GC analyses of thermally stressed samples of dodecane and mixtures with benzyl alcohol.

GC-MS studies. All liquid samples were qualitatively examined by GC-MS. The results obtained on stressing pure dodecane for 1, 3, 6, and 12 hours at 425°C indicate that in the first hour of stressing some cracking of dodecane to smaller alkanes and alkenes takes place. After 3 hours, alkylcycloalkanes were detected (predominantly alkylcyclohexanes and some alkylcyclopentanes). After 6 hours, C_2 to C_4 alkylbenzenes and some indane begin to appear, in addition to alkylcyloalkanes and alkylcyclopentanes. After stressing for 12 hours we also observed the presence of alkylnaphthalenes.

These results provide strong evidence that degradation of dodecane at 425°C proceeds as follows: initial cracking into lower alkanes and alkenes; cyclization reactions to form alkylcycloalkanes (and alkylcycloalkenes); dehydrogenation to form alkylbenzenes; and, finally, condensation to form the polyaromatics that presumably result in the formation of carbonaceous solids. This result is consistent with the reaction pathways proposed in a recent study of solid formation from paraffinic jet fuels.[2] The analogous GC-MS results for the dodecane-benzyl alcohol (5% v/v) mixture that was stressed for 6 hours clearly showed that in the presence of benzyl alcohol, no significant amount of alkylcyclohexanes, alkyl cyclopentanes or alkylbenzenes were detected.

Mechanistic Implications. The mechanism that could explain the stabilization of dodecane by benzyl alcohol at temperatures above 400 °C is depicted in **Figure 4.3-8**, Scheme I. Thermolysis of dodecane initially leads to the generation of a secondary radical. In the presence of benzyl alcohol, further reactions can follow either pathway A or B.

If pathway A is followed, the secondary radical could proceed, through a thermodynamically favored process, to abstract a benzylic proton from benzyl alcohol, thus regenerating the dodecane and producing a resonance stabilized benzylic radical. The O-H

proton of the benzylic radical is then abstracted, probably via a second dodecane radical, to produce benzaldehyde.

However, if pathway B is followed, the initially generated secondary radical could undergo a β-scission to provide a terminal alkene and a primary radical. The primary radical would then abstract a benzylic proton from benzyl alcohol, thereby regenerating a saturated hydrocarbon and the benzylic radical as discussed previously. Abstraction of an allylic proton from the terminal alkene produced from the ß-scission of dodecane would give an allylic radical, which could either react with benzyl alcohol as before, or undergo further dissociative reactions.

Consequently, we propose that benzyl alcohol has acted as a suicide-free radical scavenger via proton donation during the thermal stressing of dodecane at 425 °C. Supporting evidence that benzyl alcohol donates hydrogen to the reaction system in the manner depicted above was obtained from earlier studies using labeled dodecane.[1]

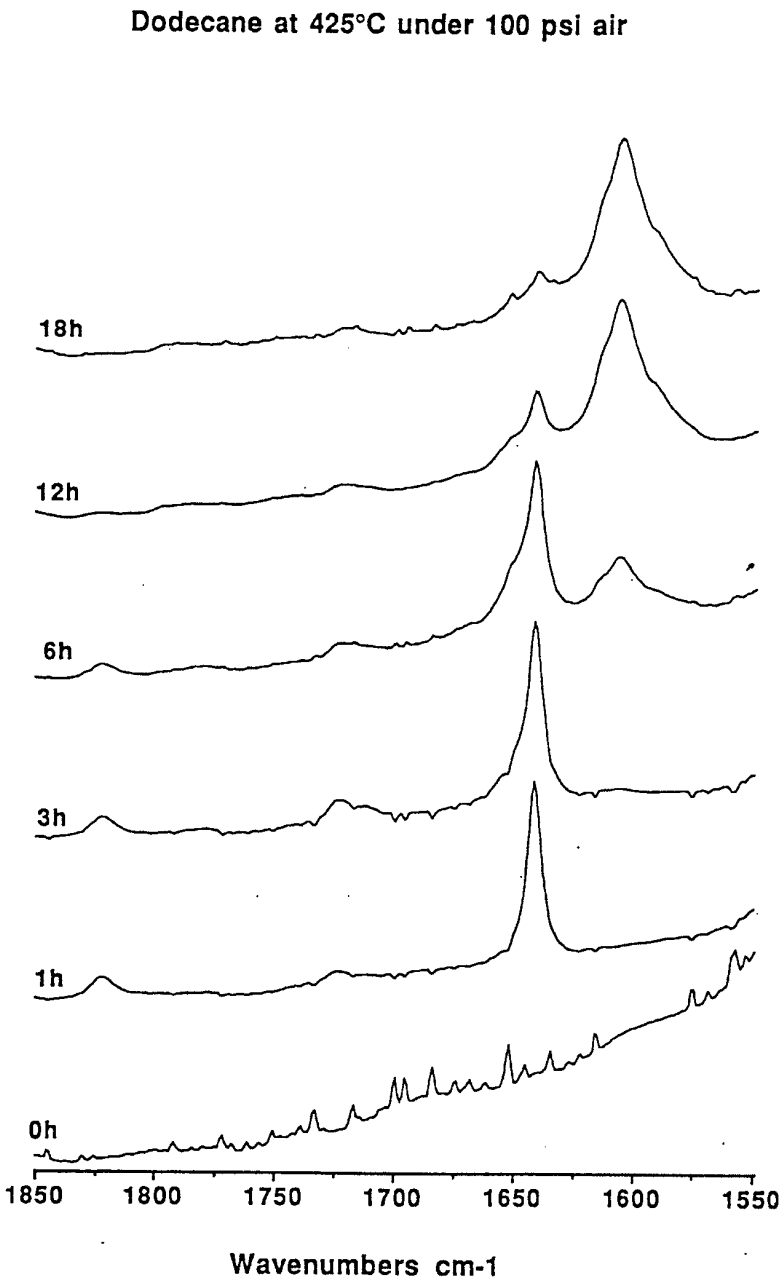

Figure 4.3-1. Infrared Spectra of Dodecane Samples Stressed under 100 psi Air at 425°C for 0, 1, 3, 6, 12, and 18 Hours

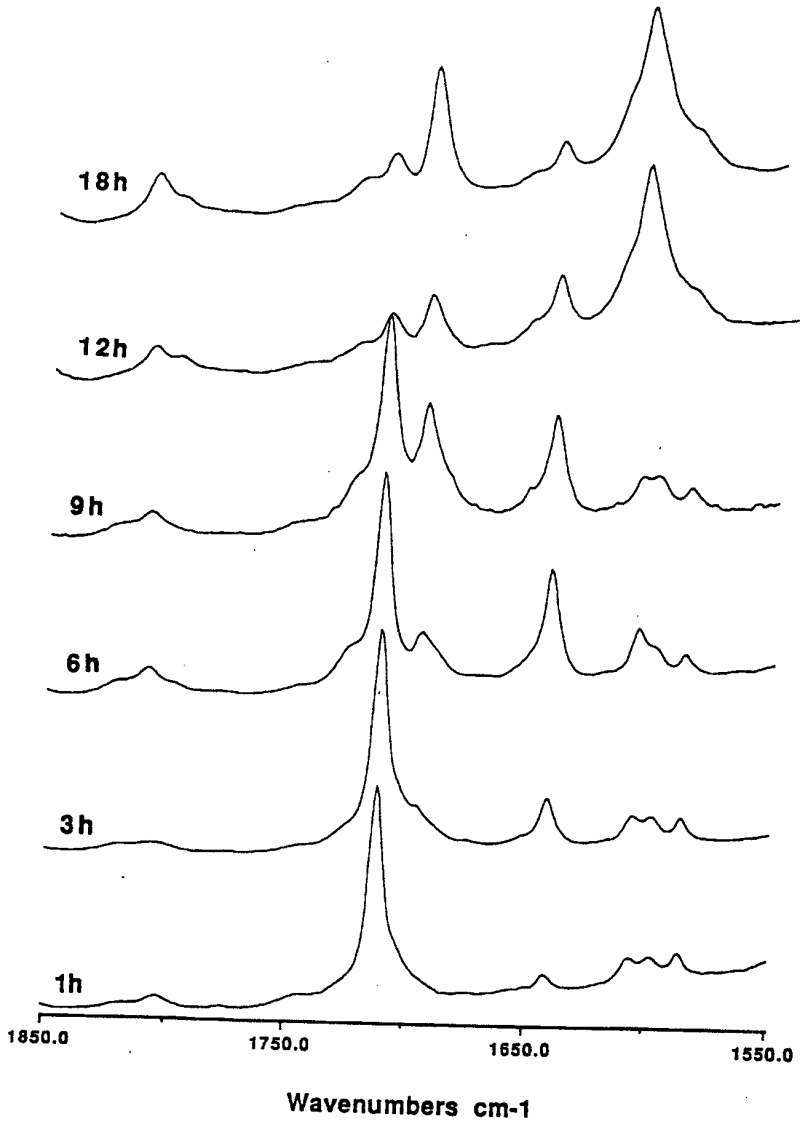

Figure 4.3-2. Infrared Spectra of Dodecane + 5% Benzyl Alcohol Samples Stressed Under 100 psi Air at 425°C for 1, 3, 6, 9, 12, and 18 Hours

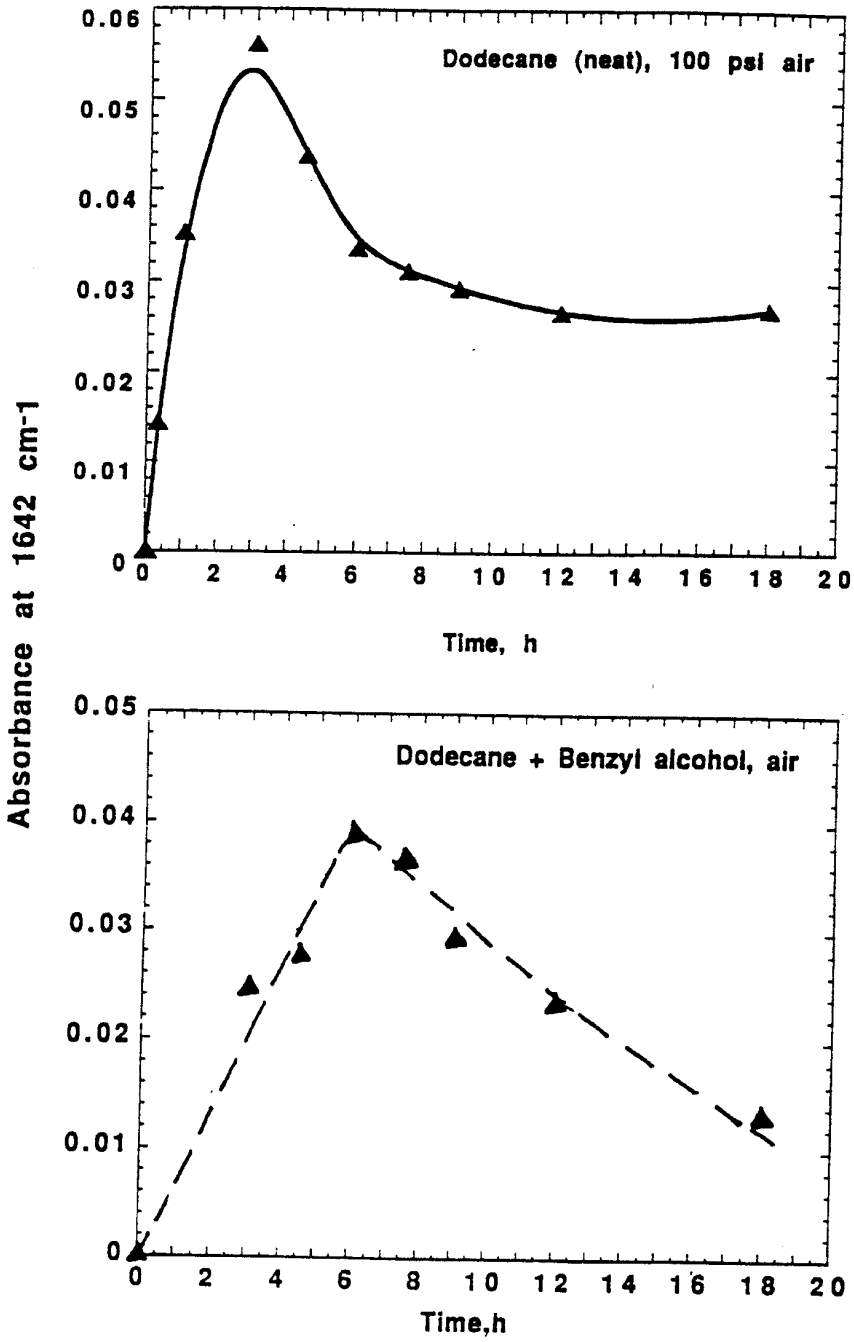

Figure 4.3-3. A Plot of Absorbance of Infrared Band at 1642 cm^{-1} vs. Time of Stressing for (top) Dodecane Samples Stressed Under 100 psi Air at 425°C and (bottom) for Samples of Dodecane + 5% Benzyl Alcohol Stressed Under 100 psi Air

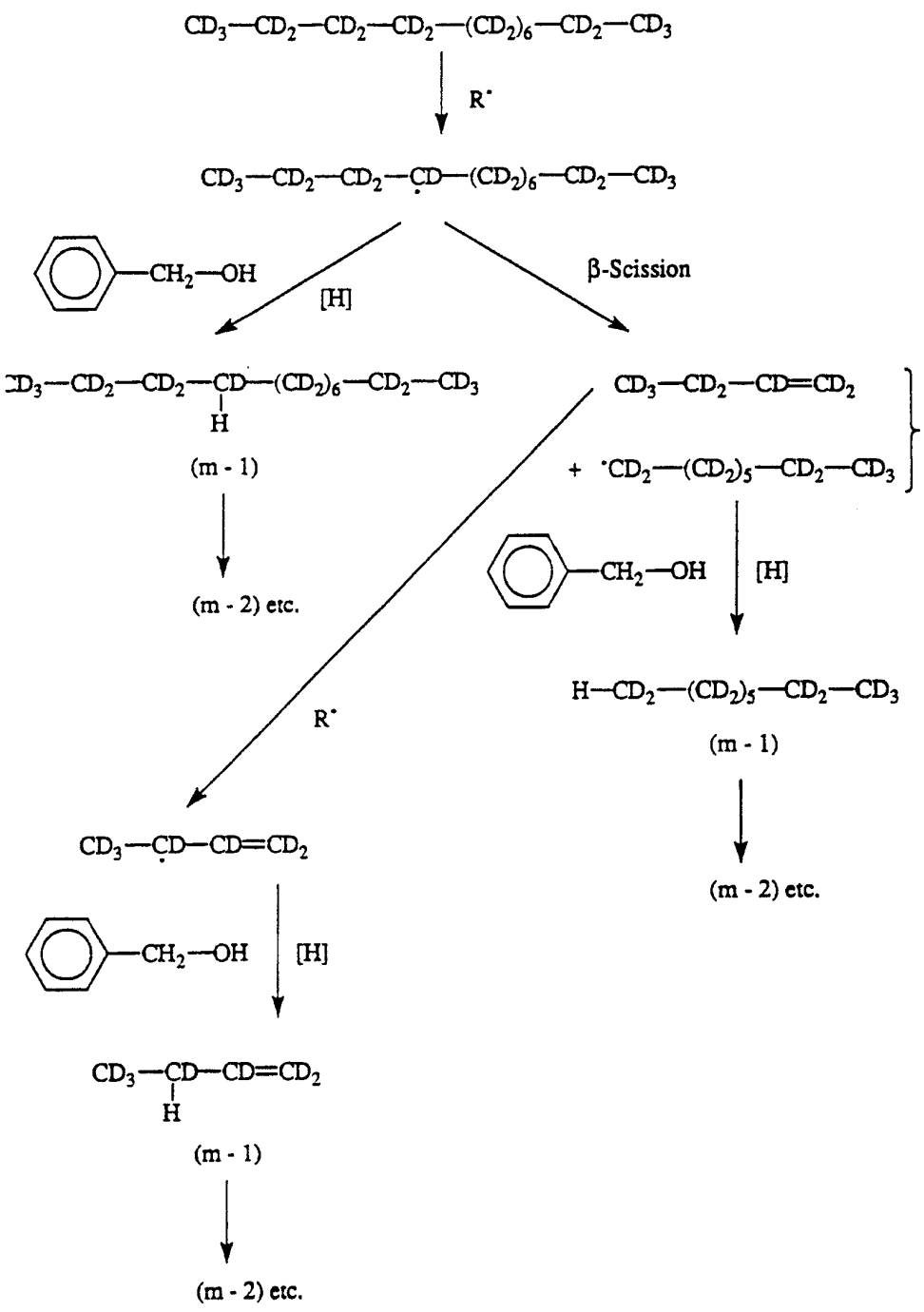

Figure 4.3-4. Primary Reaction Scheme for the Degradation of Dodecane in the Presence of Benzyl Alcohol

Scheme III

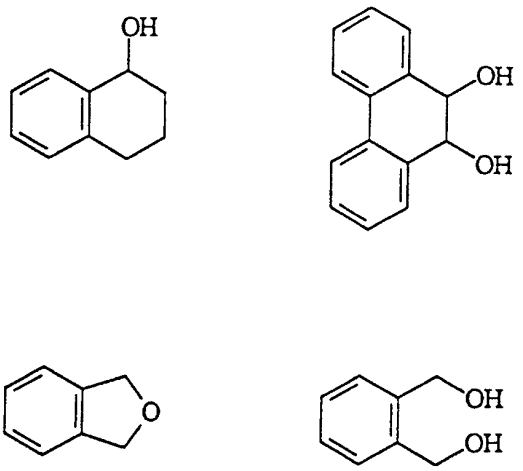

Scheme IV

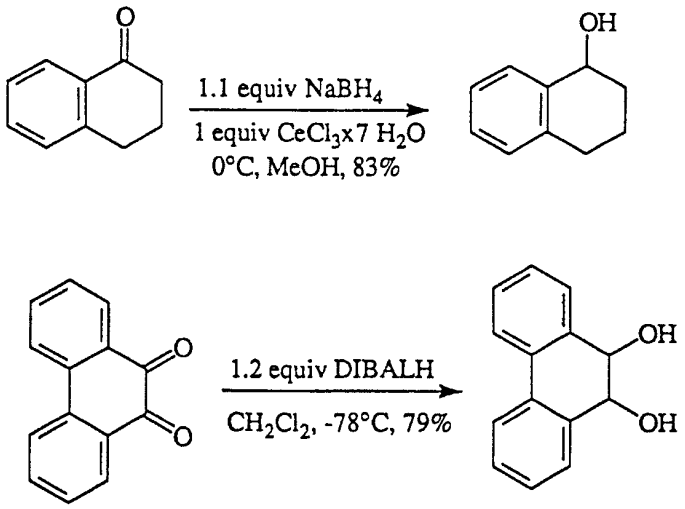

Figure 4.3-5. The Chemical Structure of the Proposed Stabilizers and the Method of Synthesis of 1,2,3,4-Tetrahydro-1-napthol and Phenanthrenediol

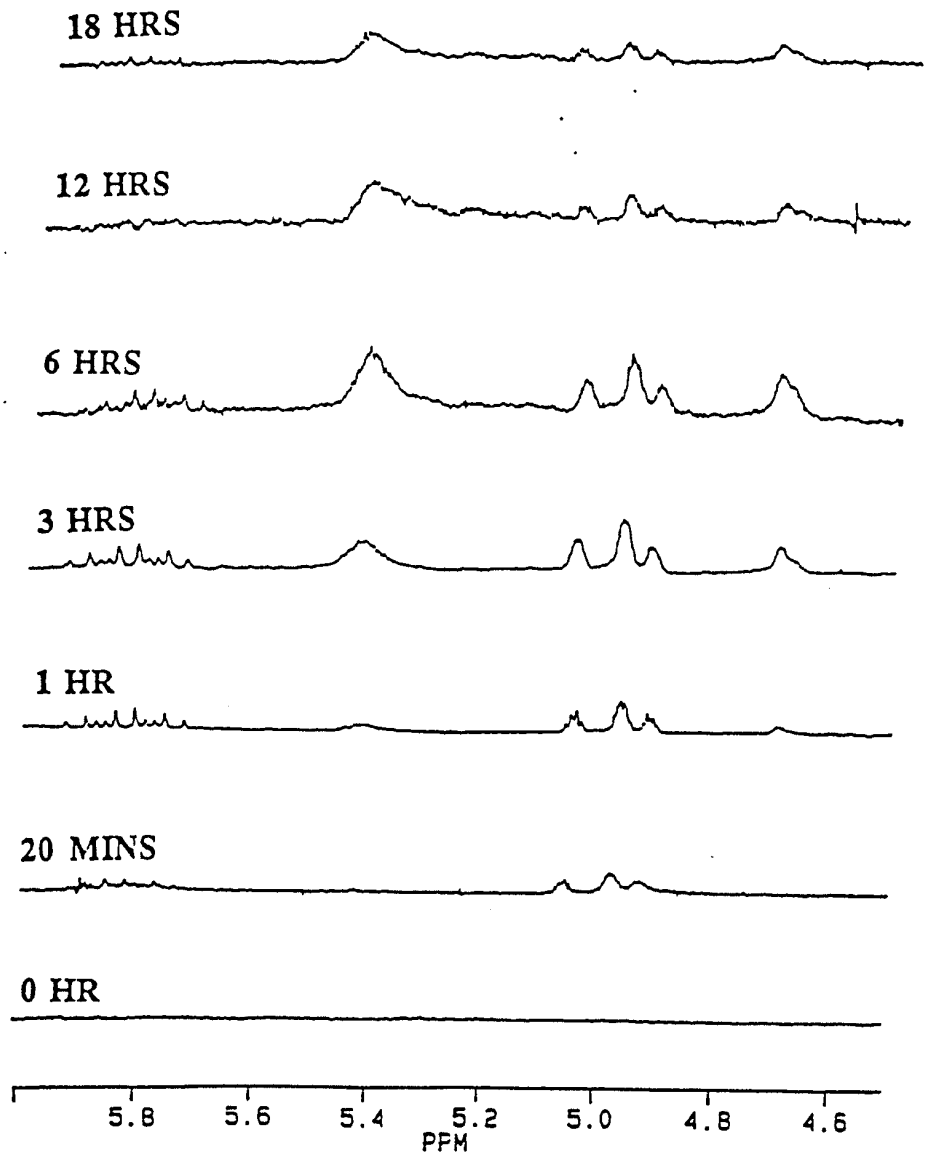

Figure 4.3-6. Scale Expanded ^{1}H NMR Spectra in the Olefinic Region of Neat Dodecane Thermally Stressed for the Times Indicated under Air at 425°C

Figure 4.3-7. Scale Expanded ^{1}H NMR Spectra in the Olefinic Region of Dodecane Containing 5% Benzyl Alcohol Thermally Stressed for Times Indicated over Air at 425°C.

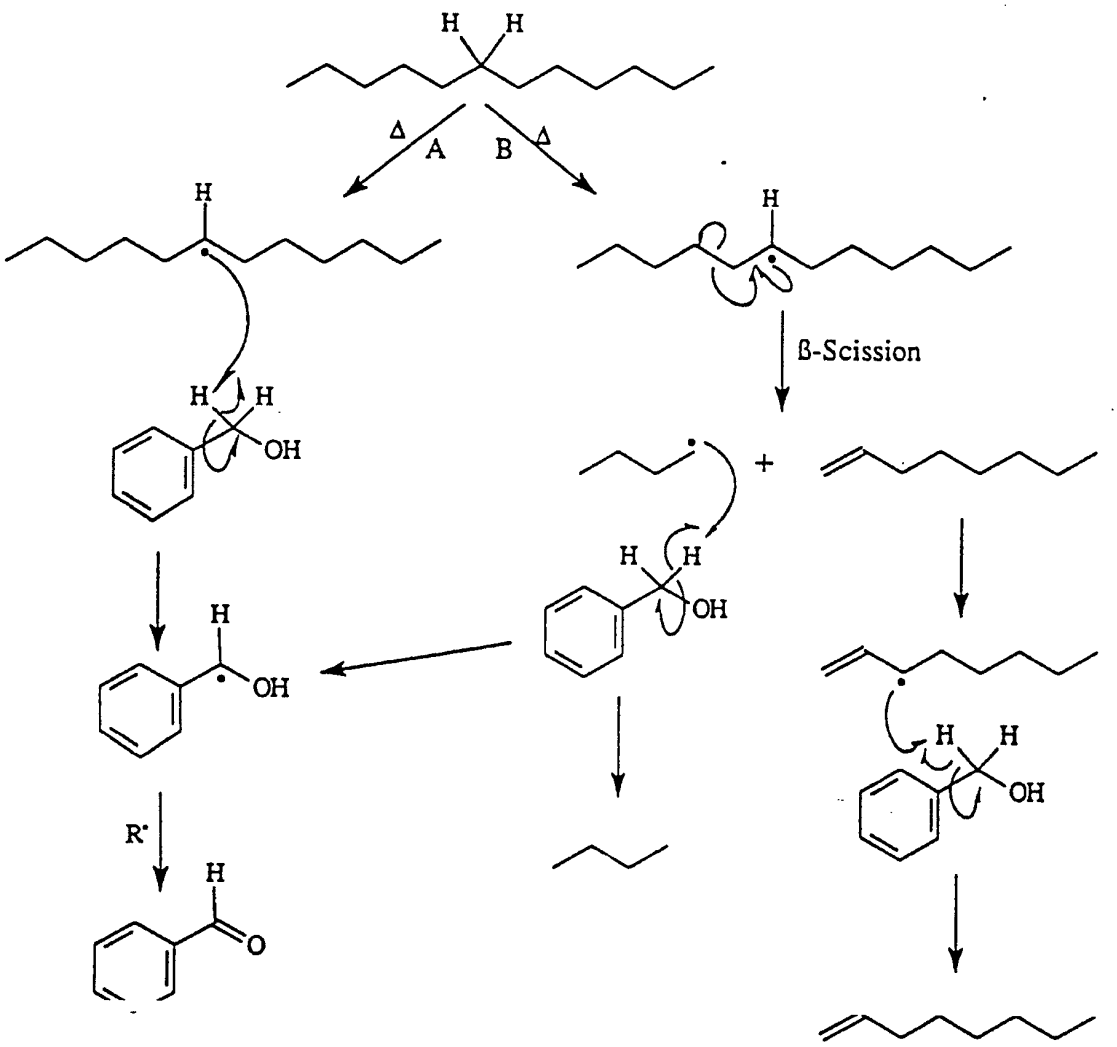

Figure 4.3-8. Scheme I

[1] Schobert, H. H. et al. *Advanced Thermally Stable Jet Fuels Technical Progress Report, February 1993 – March 1993.* The Pennsylvania State University. 1993. 43.

[2] Song, C. et al. *Energy & Fuels.* 1993. 7(2). 234.

4.4 Hydrogen-Transferring Pyrolysis of Tetradecane—Enhancing High-Temperature Stability of Jet Fuels by H-Donors

This study is explained in detail in *Advanced Thermally Stable Jet Fuels Technical Progress Report, November 1992 – January 1993.*

Introduction

In studying the pyrolytic degradation of coal- and petroleum-derived jet fuels, we suspected that hydrogen transfer from H-donors, such as those present in coal-derived JP-8C jet fuel, could play an important role in suppressing thermal decomposition of hydrocarbon components and in inhibiting solid formation.[1, 2] Until recently, the major concerns of jet fuel stability involved only thermal oxidation stability and storage stability, because the operating temperature of commercial and military jet fuels was under 300°C, where fuel degradation is controlled by autoxidation reactions. Recent interest in developing high-Mach aircraft has made thermal stability more crucial.

This study examined the following:

- The products from pyrolytic degradation of tetradecane
- The effects of H-donors on the decomposition of n-tetradecane (n-C_{14})
- The inhibiting effects of H-donors on the solid deposition from n-C_{14}
- The mechanisms of the H-transferring pyrolysis of n-C_{14} and the effects of reactive compounds on the thermal reactions of H-donors

The experimental conditions used in this work were characterized by condensed or supercritical phases, relatively high pressure, a static reactor, and long residence times. Such conditions are distinctly different from those used in most previous alkane pyrolysis work.

Experimental

Thermal stressing was conducted on 5 mL of n-tetradecane. For hydrogen-transferring pyrolysis, a 5 mL mixture of a compound or JP-8P jet fuel and a H-donor agent (usually 10% by volume) were used. Pyrolysis was conducted at 450°C for 6 to 240 minutes under 0.69 MPa UHP-N_2 (cold) in 25 mL tubing bombs. Additional detail is provided in the original report.[3]

Results

This study revealed two significant features of the hydrogen-transferring pyrolysis related to the pyrolysis of pure paraffinic jet fuel components: the much lower rate of decomposition of the starting materials, and the substantially reduced amounts of solid deposit. When stressed alone, hydrogen donors—such as tetralin—were quite stable and acted as radical scavengers by donating hydrogen to the radicals from reactive compounds. Therefore, the radicals from reactive compounds, via H-abstraction, enhanced the dehydrogenation reaction of tetralin or decalin.

The results of H-transferring pyrolysis of reactive compounds in the presence of H-donors provided some very important information. Adding H-donors—such as tetralin or

decalin—to conventional jet fuel significantly reduced or even eliminated the formation of carbonaceous deposits at 450°C and decreased the extent of fuel decomposition and gas formation, which lead to substantial increase in fuel stability. For runs at 450°C for 4 hours, adding 10 vol% tetralin to JP-8, *n*-C_{14}, and *n*-BB reduced the formation of deposits by 94% (from 3.1 to 0.2 wt%), 77% (from 3.0 to 0.7 wt%), and 54% (from 5.6 to 2.6 wt%), respectively. The enhanced stability can be attributed to the stabilization of the reactive radicals via H-abstraction from tetralin- or decalin-type compounds, which contributes mainly to inhibiting the radical decomposition, cyclization, aromatization, and condensation reactions. These results clearly demonstrate that via hydrogen-transferring pyrolysis, hydrocarbon jet fuels can be used at high operating temperatures with little or no solid deposition.

---

[1] Song, C. et al. "Thermal Stability of Petroleum- and Coal-Derived Jet Fuels at High Temperatures." *Am. Chem. Soc. Div. Petrol. Chem. Prepr.* 1992. 37(2) 540-547.

[2] Song, et al. "Pyrolytic Degradation Studies of a Coal- and a Petroleum-Derived Aviation Jet Fuel." *Energy and Fuels.* 1993.

[3] Schobert, H. H. et al. *Advanced Thermally Stable Jet Fuels Technical Progress Report, November 1992 – January 1993.* The Pennsylvania State University. 1993.

4.5 Screening Potential Jet Fuel Stabilizers Using the Model Compound Dodecane

Introduction

Following several qualitative studies that considered classic antioxidants, coal liquefaction reagents, and some alcohols as potential thermal stabilizers for jet fuels,[1] we performed quantitative studies on each of the potential stabilizers. In each of the three studies described, we used dodecane as a model compound, based on the fact that it is the most abundant hydrocarbon in jet fuels.

a. Volume-based Study on Quantitative Effects of Potential Jet Fuel Additives

This study is explained in detail in *Advanced Thermally Stable Jet Fuels Technical Progress Report, February 1993 – March 1993.*

Purpose: Determine the quantitative effects of six additives, using dodecane as the model compound. The additives were tetralin, benzyl alcohol, 9,10-dihydrophenanthrene, and tetrahydroquinoline, and Mark 1901 (alkyltin mercaptide).

Experimental: Thermal stressing was performed at 450°C in 25 mL type 316 stainless steel microreactors under 1.0 MPa of UHP-grade N_2. Based on the volume of dodecane, 5 vol% of each additive was used. The microreactor containing the sample was purged five times with UHP-grade N_2 at 7.0 MPa to minimize the presence of dissolved oxygen and then pressurized with 1.0 MPa of N_2. It was placed in a preheated sand bath at 450°C for 10 to 40 minutes and quenched in cold water.

Quantification of the liquid products was performed using a Hewlett Packard GC with a FID detector; an RTS-50 column was used. The column temperature was programmed from 40° to 280°C at a heating rate of 4°C/min. Split mode of injection was used to inject approximately 0.1µl into the column. The molar yields of the dodecane were calculated as follows:

$$\text{Molar yield (\%)} = [(A\%_{dd} * W_{liquid})/MW_{dd}]\, N_{dd}$$

where $_{dd}$ indicates the dodecane, $A\%_{dd}$ is th integrated area % of dodecane, W_{liquid} is the total weight of the liquid product, and N_{dd} is the number of moles of reactant dodecane. Dodecane conversion was calculated as:

$$\text{Dodecane conversion (mol\%)} = 100\% - \text{molar yield (\%)}$$

Results:

Dodecane Conversion. Without additives, the conversion of dodecane ranged from 4 to 44% between 10 and 40 minutes, respectively. The conversion decreased with each of the additives, except the classical antioxidant Mark 1901, which was the only additive that caused black carbonaceous deposits to form. The other samples produced only gas and liquid products. Based on the 5 vol% additives used, tetrahydroquinoline inhibited the dodecane decomposition the most. Our findings are summarized in **Figure 4.5-1**.

Reaction Kinetics. The assumption of first-order kinetics was made for the reaction at 450°C from 10 to 40 minutes. Using the first-order rate expression:

$$dx/dt = k(1-x) \quad (1)$$

where x is the dodecane conversion, t is time (seconds), and k is the first order rate constant sec^{-1}, we obtained the following equation for isothermal reactions:

$$\ln[1/(10-x)] = kt + c \quad (2)$$

The rate of dodecane disappearance decreases in the order of"

Dodecane neat > dodecane + tetralin>dodecane + benyzl alcohol>dodecane + 9,10-dihydrophenanthrene > dodecane tetrahydroquinoline.

b. Molar Equivalent Studies of Jet Fuel Additives

This study is explained in detail in *Advanced Thermally Stable Jet Fuels Technical Progress Report, July 1993 – September 1993.*

Purpose: To further evaluate potential jet fuel additives via studies based on molar equivalents.

Experimental: The reactants used were:

Dodecane
1,2,3,4-tetrahydronaphthalene (I)
9,10-dihydrophenanthrene (II)
1,2,3,4-tetrahydroquinoline (III)
Benzyl alcohol (IV)
Benzaldehyde dimethyl acetal (V)
Phthalan (VI)
1,2,3,4-tetrahydro-1-naphthol (VII)

Stressing conditions and the method of calculating dodecane conversion were the same as those employed in (a).

Results: Compared to stressing dodecane alone, with the exception of Compound V (benzaldehyde dimethyl acetal), each of the additives significantly increased the amount of dodecane remaining after stressing. Additive V was completely ineffective as a radical scavenger, probably as a result of the cleavage of the side group at 450°C. Compounds II and III were superior to the other additives, as indicated by the results below. Compounds I, IV, and VI performed in the middle range, and Compound VI, although reasonably effective at inhibiting dodecane decomposition, proved to be a poor radical scavenger. Both Compounds VII and VI decomposed too quickly to qualify as viable fuel additives.

The superior performance of Compound II (9,10-dihydrophenanthrene) can likely be attributed to its excellent thermal stability at 450°C, combined with the increase in resonance stabilization of the radical scavenger relative to benzyl alcohol. The cause of Compound III's effectiveness, however, remains unknown. It is thermally stable at 450°C and quinoline is a reaction product.

	Additive Compounds	Original Dodecane Remaining after 45 Min. of Stressing
II.	9,10-dihydrophenanthrene	92 mol%
III.	1,2,3,4-tetrahydroquinoline	(superior)
I.	1,2,3,4-tetrahydronaphthalene	70 mol%
IV.	Benzyl alcohol	(moderate)
VII.	1,2,3,4-tetrahydro-1-naphthol	
VI.	Phthalan	65 mol% (poor radical scavenger)

c. Examining the Effects of 13 New Hydrogen Donor Additives

This study is explained in detail in *Advanced Thermally Stable Jet Fuels Technical Progress Report, July 1994 - September 1994.*

Purpose: Evaluate the effects of 13 new hydrogen donor additives:

1. 3-pyridylcarbinol
2. 4-pyridylcarbinol
3. 2-hydroxybenzyl alcohol
4. 1,2,3,4-tetrahydroquinoline
5. 2-chlorobenzyl alcohol
6. 4-chlorobenzyl alcohol
7. anthrone
8. 1-naphthalenemethanol
9. 9-anthracenemethanol
10. 9-hydroxyfluorene
11. indene
12. 9,10-dihydrophenanthrene
13. benzyl alcohol

We placed both electron donating (#1-4) and electron withdrawing substitutents on or in the aromatic ring, as well as additional aromatic rings in succession (#7-12). In doing so, we hoped to gain more insight into the properties necessary for an efficient additive.

Experimental: Ten mol% of each additive was used. Thermal stressing was performed at 425°C in 25 mL type 316 stainless steel reactors under 0.69 MPa of UHP-grade N_2. Purging and pressurization were performed as in (a), above.

Results: **Figure 4.5-2** shows the results of 6 hours of thermal stressing of dodecane in the presence of additives 1-6, 8, and 10-13. Compounds 7 and 9 were insoluble in dodecane, even after stressing at 425°C for 6 hours, and resulted in the formation of various solids. The results for the remaining 11 additives are presented in the table that follows.

From these results, we drew the following conclusions:

- Based on the inability of Compounds 5 and 6 to act as efficient radical scavengers, we concluded that the presence of electron-withdrawing substituents on the aromatic ring facilitates and accelerates side group cleavage.
- Compound 3 reinforces our earlier finding that any side groups on additives will undergo thermal cleavage at 425°C, resulting in degradation of the additive and, thus, decreased stabilization of dodecane.

Compound #	Molar Yield of Dodecane	Byproducts / Benefits & Drawbacks
1, 2	Relative increase	Pyridine, methylpyridine, and pyridinecarboxaldehyde (suggesting an acceleration in side group cleavage compared to benzyl alcohol)
3	35%	Benzyl alcohol, benzene, and toluene
4	93%	Quinoline / Far better molar yield than benzyl alcohol (93% vs. 48%) and 78% of additive remained after 6 hours of stressing
5, 6	30%, 20%	Benzene, toluene, chlorobenzene, and chloromethylbenzene, products of additive degradation and proof of these compounds' inability to act as efficient radical scavengers.
8	Relative increase	Naphthalene and methyl naphthalene
10	No significant increase	Flourene (from loss of OH) and fluorenone (product of oxidation)
11	Relative increase	Unidentified (resulting from additive decomposition)
12	Similar to benzyl alcohol	Phenanthrene / Only 20% of the additive remained after 6 hours stressing of compared to 48% of benzyl alcohol
13 (benzyl alcohol)	48%	

- Based on Compound 12, we concluded that a correlation exists between additive efficiency and the overall thermal stability of the additive. Compound 4 supports this theory.
- Compound 4 performed significantly better than benzyl alcohol, both in terms of its molar yield of dodecane and the amount of the additive remaining after 6 hours of stressing. There are two plausible explanations for this: (1) Compound 4 exhibits super thermal stability at 425°C, which increases the lifetime of the additive. (2) Compound 4 has four hydrogen atoms available for abstraction, instead of the two offered by benzyl alcohol.

To summarize, the following set of parameters seem to predict the effectiveness of organic additives that can be used to thermally stabilize hydrocarbon fuels and prevent the formation of carbonaceous solids:

1. Additives must be thermally sable at temperatures above 400°C (i.e., they must not possess any side groups that could undergo cleavage and promote degradation).
2. Additives must have hydrogen atoms that can be transferred or abstracted by hydrocarbon radicals. The greater the number of hydrogen atoms available, the better.
3. The radicals generated from hydrogen atom abstraction should be stabilized by resonance.

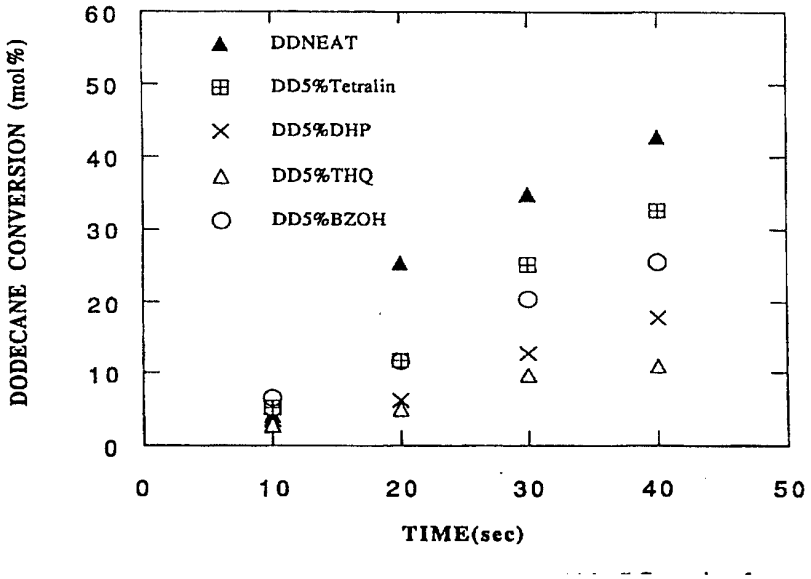

Figure 4.5-1. Effects of Hydrogen Donor Additives on the Molar % Conversion of Dodecane at 450°C Under Initial N_2 Pressure of 1.0 MPa (145 psi)

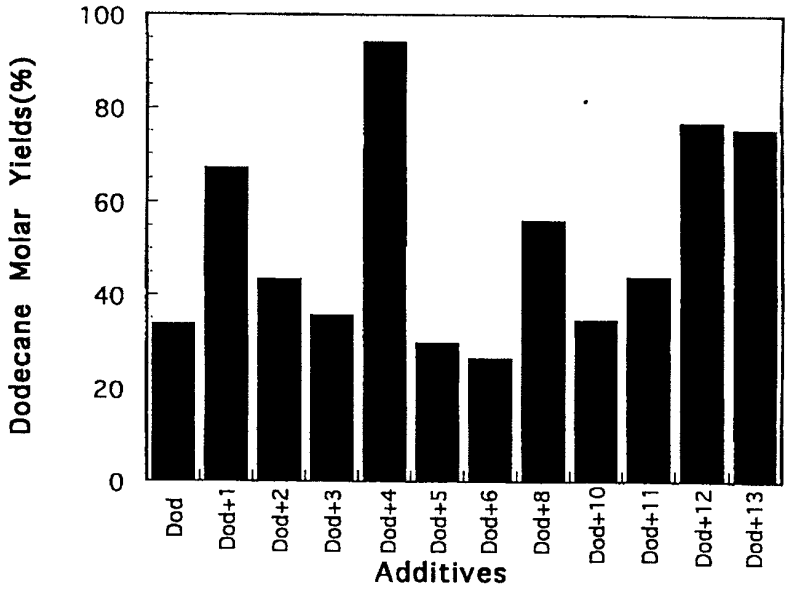

Figure 4.5-2. Effects of Hydrogen Donor Additives 1 Through 13 on the Molar Yields of Dodecane at 425°C for 6 Hours under Initial N_2 Pressure of 0.69 MPa

[1] Coleman, M. M. et al. Energy and Fuels. 1992. 6. 535-539.

4.6 THEORETICAL MODELS TO STUDY THE PHASE BEHAVIOR OF JET FUEL

This study is explained in detail in Advanced Thermally Stable Jet Fuels Technical Progress Report, April 1993 – June 1993.

Introduction

From our fuel stabilization studies, we know that benzyl alcohol can retard the degradation of jet fuel for at least 6 hours at elevated temperature.[1] The phase behavior of jet fuel is a matter of considerable practical importance. Critical issues involving next generation jet fuels pertain to the phase behavior of mixtures of benzyl alcohol and dodecane. Ultimately, we need to determine whether these mixtures exhibit one- or two-phase behavior under conditions involving high pressure, high temperature, and lengthy stressing times.

The purpose of this work was to predict the phase behavior of benzyl alcohol and dodecane in the first step of pyrolysis. Among the various theories of solutions, two most widely used ones are Flory's and Sanchez and Lacombe's Lattice Fluid models.[2, 3, 4, 5] We performed an exhaustive comparison of the models, which are presented in full in our original report.[6] Our conclusions are summarized below.

Conclusion

Both the Flory and Sanchez and Lacombe Lattice Fluid (LF) theories use a van der Waals type of potential energy for the fluid mixture, but differ in their representation of the volume-dependent part of the entropy of the mixture. The Flory treatment essentially assumes that the system's free volume is distributed among each of the system's lattice sites or cells, as shown in **Figure 4.6-1**, whereas the LF model allows for empty lattice sites or holes, as in **Figure 4.6-2**. Both theories require three equation-of-state parameters for each pure component. Therefore, it is very important that these parameters for a given system be evaluated from experimental values of ρ, α, and β (or γ) determined at the same temperature and pressure.

Both the LF theory and the Flory theory can qualitatively explain the feature of the upper and lower critical phase phenomena in nonpolar systems. However, the LF model has an initial advantage over the Flory model because it converges to the ideal gas law at low densities. The Flory model assumes a certain amount of order to exist and is, therefore, limited to densities found in the solid state and in liquids far below their critical temperatures. The LF model also has advantages over the Flory model in that it does not introduce the reduced degrees of freedom parameter, c, and the molecular surface contact parameter, s, which are both difficult to measure and estimate.

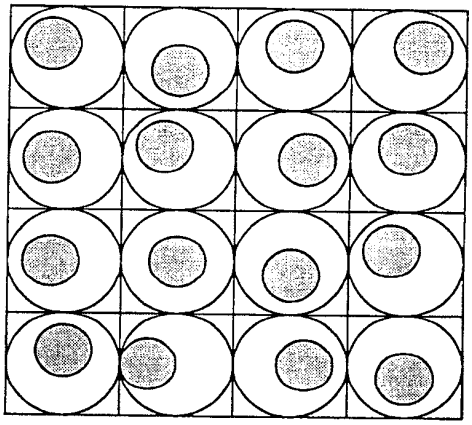

Figure 4.6-1. The Flory Model. Each Lattice Site Holds a Cell that Contains the Free Volume for the Site's Particle.

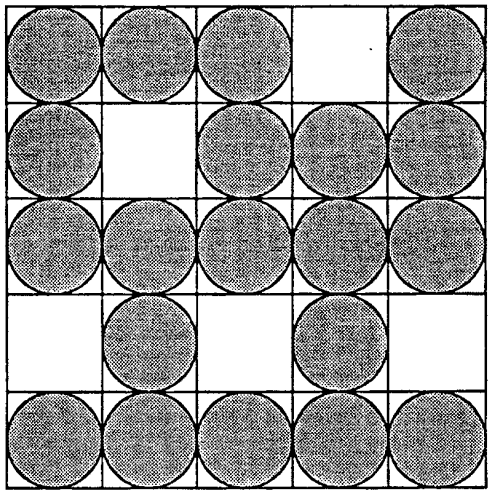

Figure 4.6-2. The Sanchez-Lacombe Model. The Vacant Lattice Sites, or Holes, Represent the Free Volume of the System.

[1] Coleman, M. M. et al. *Energy & Fuels.* 1992. 6535-6539.

[2] Flory, P., J., R. A. Orwoll, and A. J. Vrij. *Amer. Chem. Soc.* 1964. 86. 3515.

[3] Flory, P. J. *Amer, J., Chem. Soc.* 1965. 87. 1833.

[4] Eichinger, B. E. and P. J. Flory. *Trans. Faraday Soc.* 1968. 64. 2035.

[5] Lacombe, R. H. and I. C. Sanchez. *J. Phys. Chem.* 1976. 80. 2568.

[6] Schobert, H. H. et al. Advanced Thermally Stable Jet Fuels, Technical Progress Report, April– June 1993. Pennsylvania State University. 1993. 23-34.

4.7 Study of the Phase Behavior of Jet Fuels Using the Lattice Fluid Method

This study is explained in detail in *Advanced Thermally Stable Jet Fuels Technical Progress Report, January 1994 – March 1994.*

Introduction

Section 4.6 outlined and compared two theories concerning the phase behaviors of liquid mixtures—the Lattice Fluid (LF) theory and the Flory theory. The Flory theory, which assumes a certain degree of real-space order in the liquid, does not take into account the free volume effect and only applies to the densities found in solids and liquids. The LF theory converges to the ideal gas law as the density of the fluid approaches zero. Our first approach was to understand the phase behavior of jet fuel, and then consider the mixture of jet fuel and additives.

Phase behavior is usually represented by a phase diagram, which is a plot of thermodynamic quantities. In the case of two-dimensional plots, a phase diagram is a graph of one state variable (e.g., temperature) versus another (e.g., composition) while the other remaining variables are kept constant (e.g., pressure).

There are many ways to choose the combination of thermodynamic state variables to plot two-dimensional phase diagrams, such as temperature vs. composition or pressure vs. volume at constant temperature. In keeping with our experimental jet fuel stability studies conducted at 425°C, we chose pressure and density to represent the phase diagram at 425°C. Our detailed calculations were presented in the initial report on this study[1]; our results are summarized below.

Results

The characteristics for the four mixtures, calculated by combination rules, are shown in **Table 4.7-1**. The phase diagrams of the four mixtures (dodecane/benzene, dodecane/toluene, dodecane/ethylbenzene, and dodecane/phenol), the spinodal line of pressure versus density at 425°C, are shown in **Figures 4.7-1**, **4.7-2**, **4.7-3**, **4.7-4**, and **4.7-5**.

The characteristic parameters of three of the four mixtures are very close to one another, dodecane/phenol being the exception. This can be attributed to the small amount (5%) of additives in the dodecane, which enables dodecane to determine the major physical characteristics. This, in turn, indicates that the spinodal lines of the hydrocarbon mixtures are also very close. The dodecane/phenol mixture was significantly different from the analogous hydrocarbon mixtures.

Table 4.7-1. Calculated Characteristic Parameters of the Mixtures and Spinodal Density

	T* (K)	P* (MPa)	ρ* (kg/m3)	r	Spinodal Density (kg/m3) at 100 MPA, 425°C
Dodecane (95%)/benzene (5%)	525.0	291.5	857.2	12.66	342.94
Dodecane (95%)/toluene (5%)	525.0	290.0	856.6	12.71	321.39
Dodecane (95%)/ethylbenzene (5%)	525.4	290.5	856.5	12.85	334.11
Dodecane (95%)/phenol(5%)	525.2	295.8	860.4	13.11	435.64

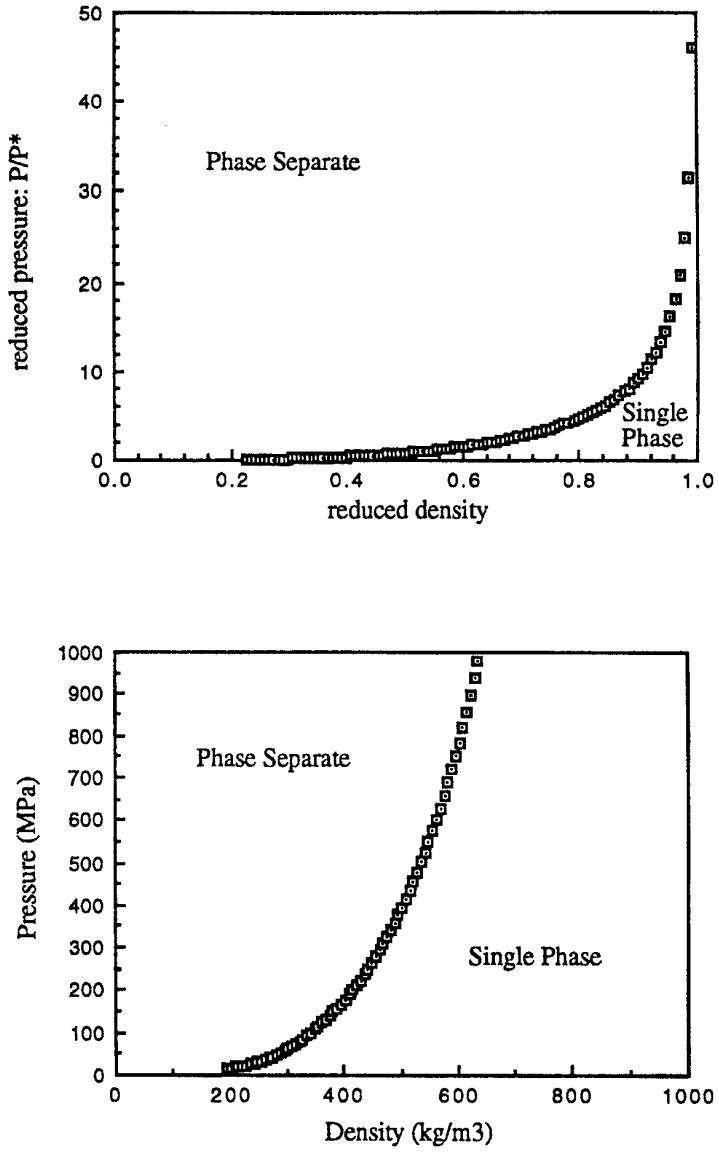

Figure 4.7-1. The Spinodal Line Calculated at 425°C of Pressure vs. Density for the Mixture of Dodecane (95%) / Benzene (5%)

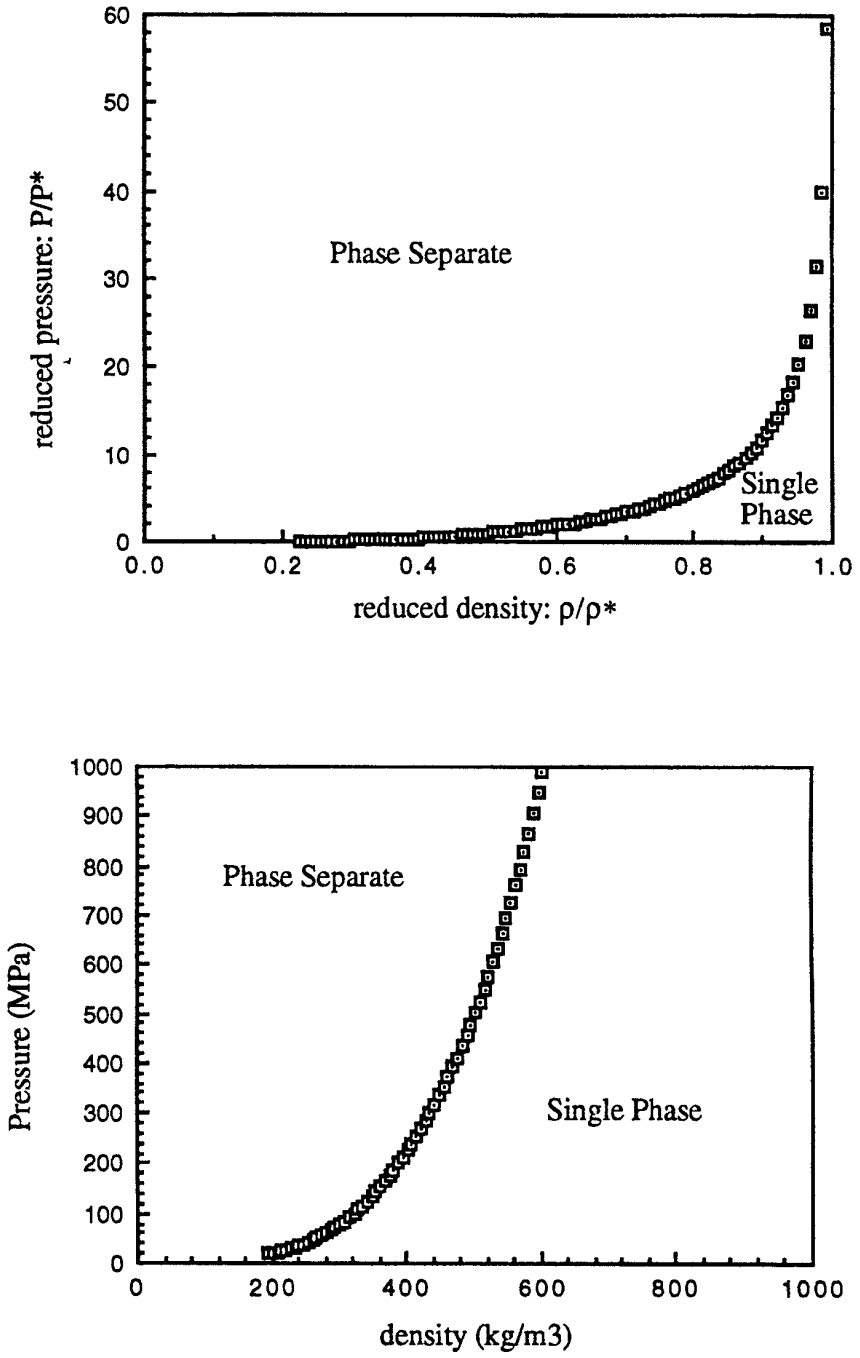

Figure 4.7-2. The Spinodal Line Calculated at 425°C of Pressure vs. Density for the Mixture of Dodecane (95%) / Toluene (5%)

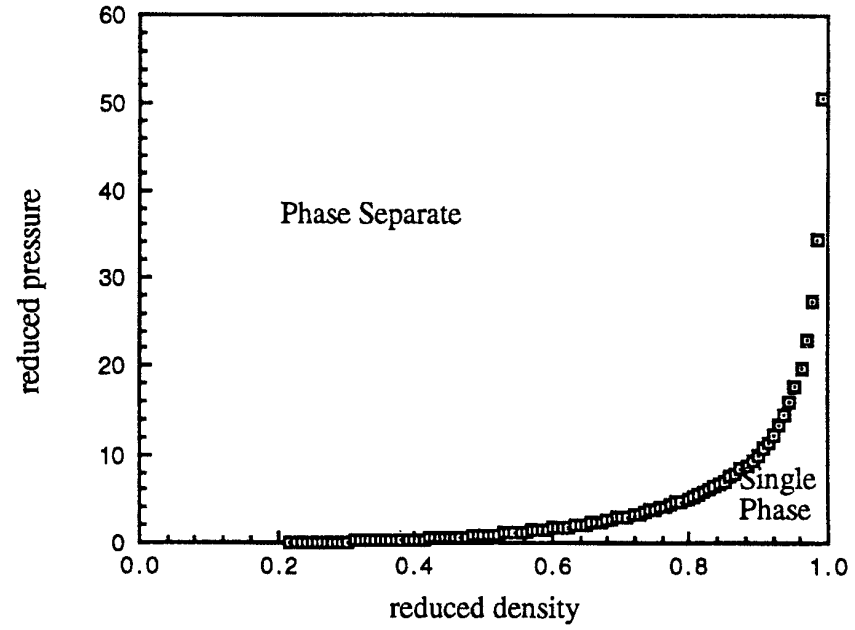

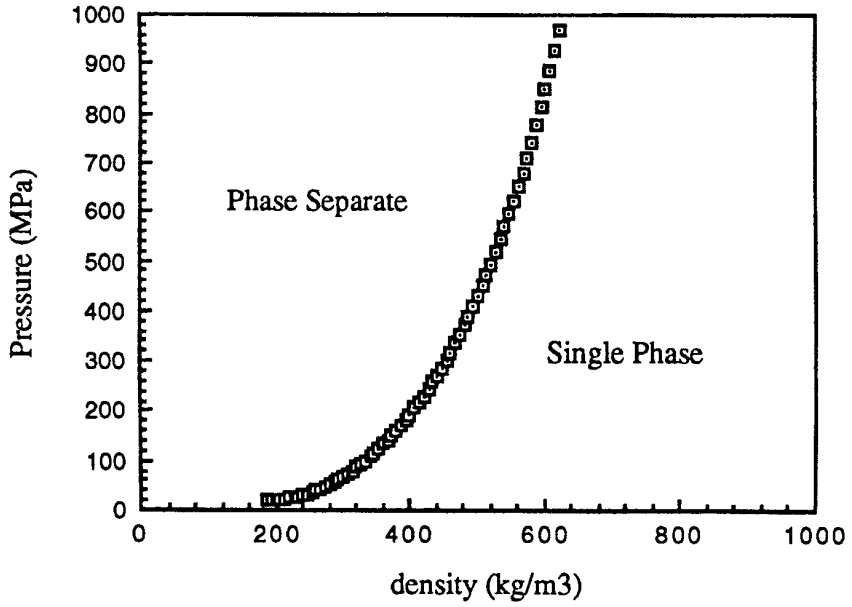

Figure 4.7-3. The Spinodal Line Calculated at 425°C of Pressure vs. Density for the Mixture of Dodecane (95%) / Ethylbenzene (5%)

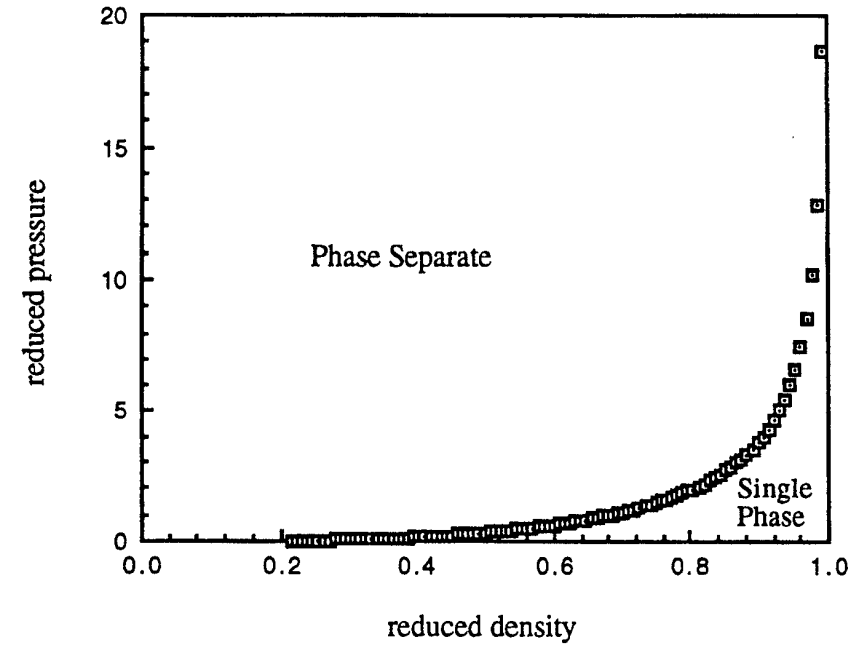

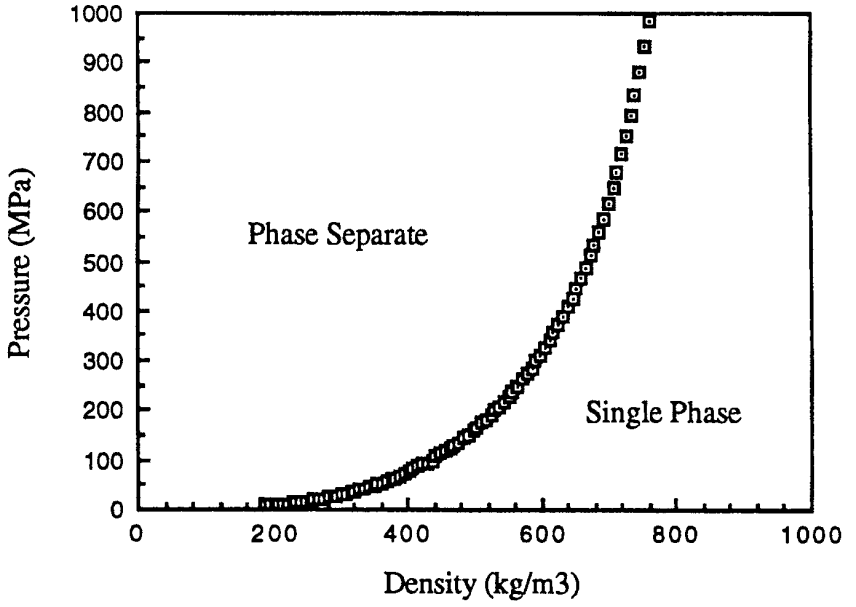

Figure 4.7-4. The Spinodal Line Calculated at 425°C of Pressure vs. Density for the Mixture of Dodecane (95%) / Phenol (5%)

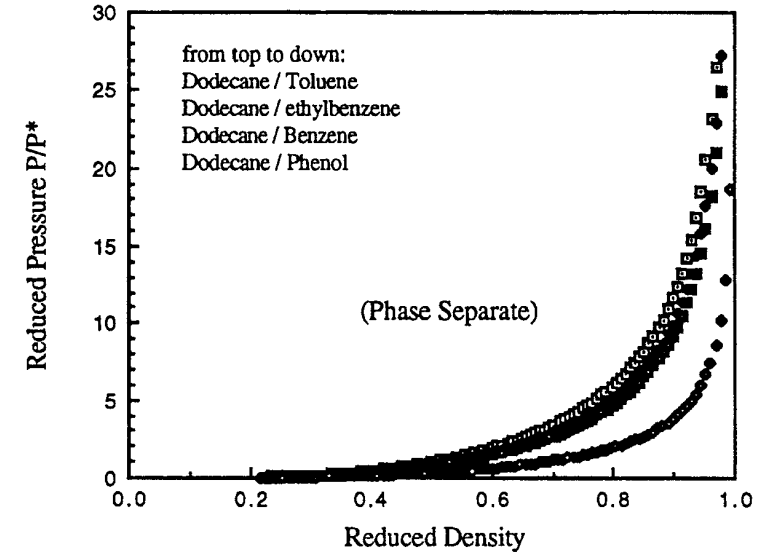

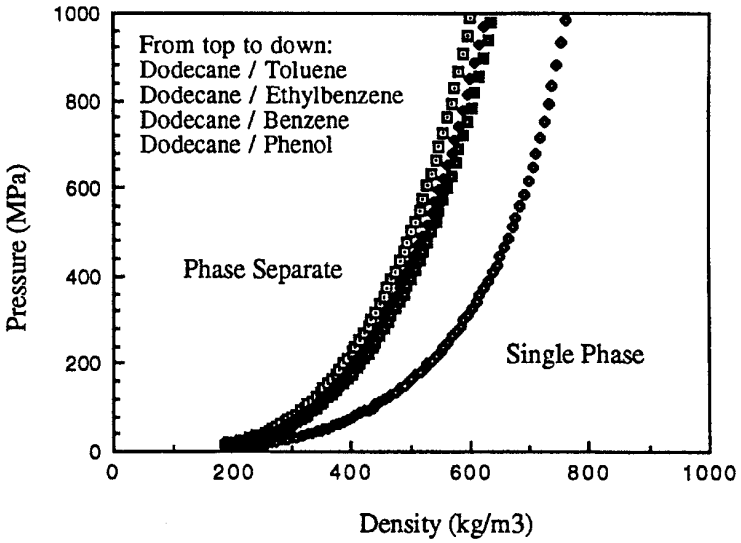

Figure 4.7-5. The Spinodal Line Calculated at 425°C of Pressure vs. Density for the Mixtures of Dodecane (95%) with Benzene (5%), Toluene (5%), Ethylbenzene (5%), and Phenol (5%) Respectively

[1] Schobert, H. H. et al. Advanced Thermally Stable Jet Fuels, Technical Progress Report, January 1994 –March 1994. The Pennsylvania State University. 1994. 28-31.

4.8 In Situ Regeneration of the Thermal Stabilizer Benzyl Alcohol

This study is explained in detail in *Advanced Thermally Stable Jet Fuels Technical Progress Report, April–June 1994.*

Introduction

Earlier research indicated that benzyl alcohol and 1,4-benzenedimethanol function as efficient stabilizers at temperatures above 400°C and enhance the thermal stability of jet fuels and the model compound, dodecane.[1, 2] In contrast, other alcohols have been found to be poor stabilizers.[3] However, the addition of ethanol to hydrocarbon/benzyl alcohol mixtures has a significant effect on the thermal stabilization of jet fuels and related materials at temperatures above 400°C. Ethanol appears to function in a redox fashion by reducing the benzaldehyde formed during the degradation of the benzyl alcohol/hydrocarbon mixtures. This regenerates benzyl alcohol. In other words, in the presence of ethanol, less benzyl alcohol is required for thermal stabilization of the fuel.

In this study, we performed thermal stressing on dodecane with benzyl alcohol, ethanol, and mixtures of benzyl alcohol and ethanol as stabilizers.

Experimental

The molar concentration of the stabilizers was kept constant at 0.0072 M, and only their molar ratio (benzyl alcohol:ethanol) was varied. The stressing experiments were performed for 6 hours on 10 mL dodecane samples containing known amounts of stabilizers at 425°C using 15 mL type 316 stainless steel microreactors under 100 psi of air. The temperature program used was: initial temperature, 40°C; initial isotime, 5 minutes; heating rate, 4°C/min to 280°C; and the final isotime, 10 minutes.

Results

Thermal Stressing of Dodecane with Benzyl Alcohol – Ethanol Mixtures. The molar ratios of benzyl alcohol:ethanol for the samples were:

Sample	Molar Ratio
1	3 : 0
2	2.5 : 0.5
3	1 : 2
4	0.5 : 2.5
5	0 : 3

The liquid products obtained after thermal stressing were quantitatively analyzed using GC. **Figure 4.8-1** shows a histogram depicting the mol% of uncracked dodecane after thermal stressing. In the first three samples, only about 10 mol% of the dedcane had degraded. In samples 4 and 5, 44 mol% and 56 mol% of the original dodecane had cracked, respectively. **Figure 4.8-2** shows the corresponding mol% of heptane, octane, nonane, decane, and undecane formed from samples 1 through 5.

Earlier studies demonstrated that degradation reactions are retarded as long as an appreciable concentration of benzyl alcohol is present in the reaction mixture.[4] The thermal

stability observed in Sample 1 can be attributed to the high initial concentration of benzyl alcohol. At the other extreme, the relatively poor thermal stability of Sample 5 results from the fact that ethanol is an inefficient stabilizer. In Samples 2 and 3, which contain mixtures of benzyl alcohol and ethanol, ethanol appears to act in a synergistic fashion.

When 10 mL of dodecane was stressed under the same conditions with benzyl alcohol alone (Sample 6), key results compared to Sample 3 characteristics as follows:

	Sample 6	Sample 3
uncracked dodecane	69 mol%	88 mol%
unreacted benzyl alcohol	14 mol%	43 mol%

There was a 19 mol% increase in the concentration of uncracked dodecane and a 29 mol% increase in the concentration of unreacted benzyl alcohol for Sample 3, compared to Sample 6.

Proposed Reaction Mechanism for the In Situ Regeneration of Benzyl Alcohol. Malwitz and Metzger reported that carbonyl compounds can be reduced by alcohols via a thermally initiated free radical reaction.[5] They investigated the thermal reduction of benzaldehyde in the presence of 2-propanol to provide benzyl alcohol and acetone as the only two products.

In our reaction system, we expect ethanol to react in a similar fashion with benzaldehyde, thus regenerating benzyl alcohol in the system. The proposed mechanism is shown in **Scheme II**. After hydrogen atom abstraction of benzyl alcohol by the hydrocarbon free radicals, benzaldehyde is initially formed. In the presence of ethanol, a reduction of the benzaldehyde occurs with ethanol donating two protons to regenerate several molecules of benzyl alcohol and further yielding acetaldehyde. By this route, ethanol can regenerate bnezyl alcohol by an in situ reduction.

Thermal Stressing of Ethanol-Benzaldehyde Mixture at 425°C. When the liquid samples were analyzed, we found that in addition to ethanol and benzaldehyde, benzyl alcohol is the major reaction product, while benzene and toluene are the minor products. This indicates that ethanol can generate a significant amount of benzyl alcohol in the presence of benzaldehyde.

Thermal Stressing of Dodecane with Benzyl Alcohol and Labeled Ethanol (CH_3CD_2OH). From the results of this stressing, we concluded that ethanol donates two hydrogens to benzaldehyde and, thus, regenerates benzyl alcohol in the system per Scheme II. As a result, ethanol is oxidized to acetaldehyde and its degradation products. In the presence of ethanol, therefore, less benzyl alcohol is required for thermal stabilization of fuel.

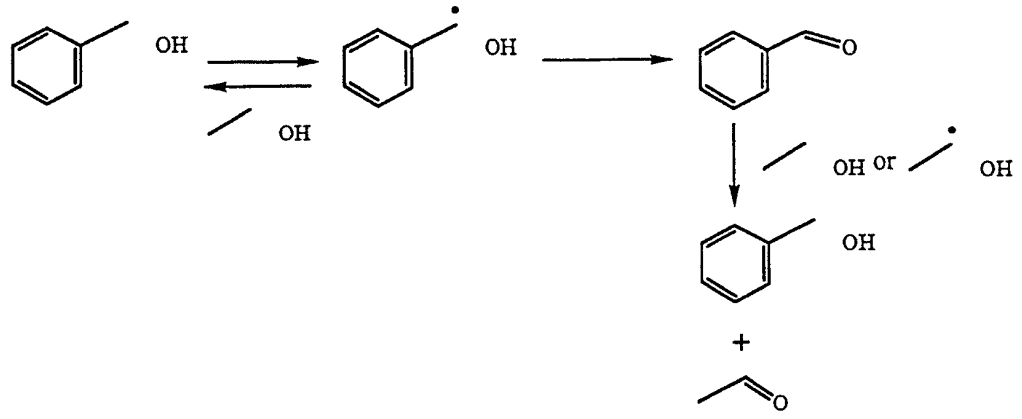

Scheme II

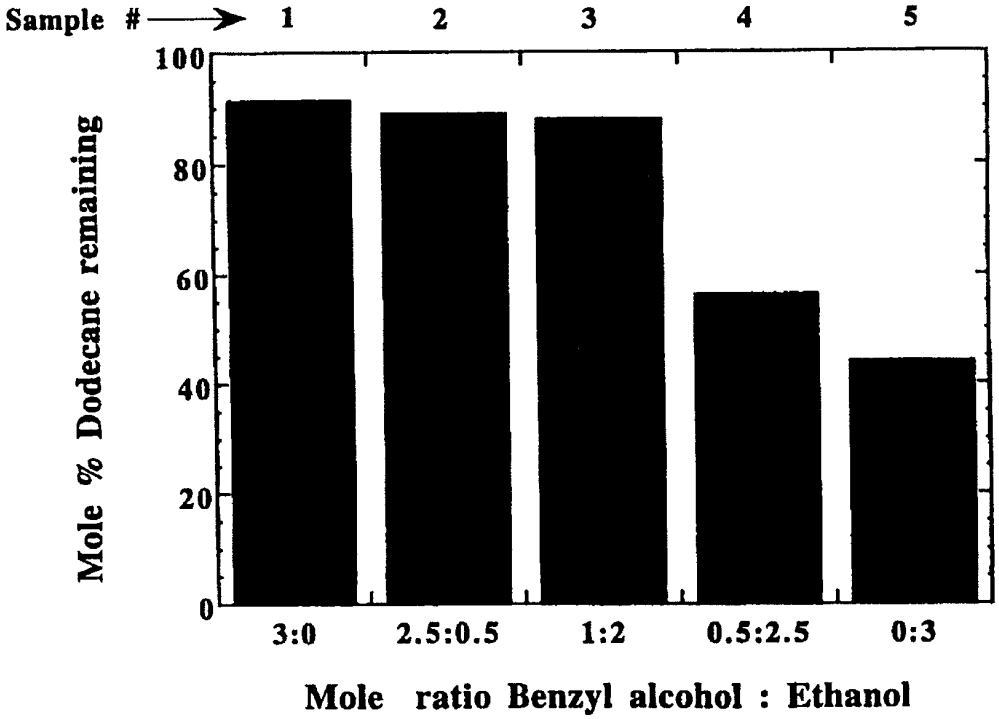

Figure 4.8-1. The Amount of Dodecane Remaining as Determined by GC Analyses. Samples of Dodecane Stressed with Stabilizer Mixtures after Thermal Stressing at 425°C under 100 psi Air for 6 Hours.

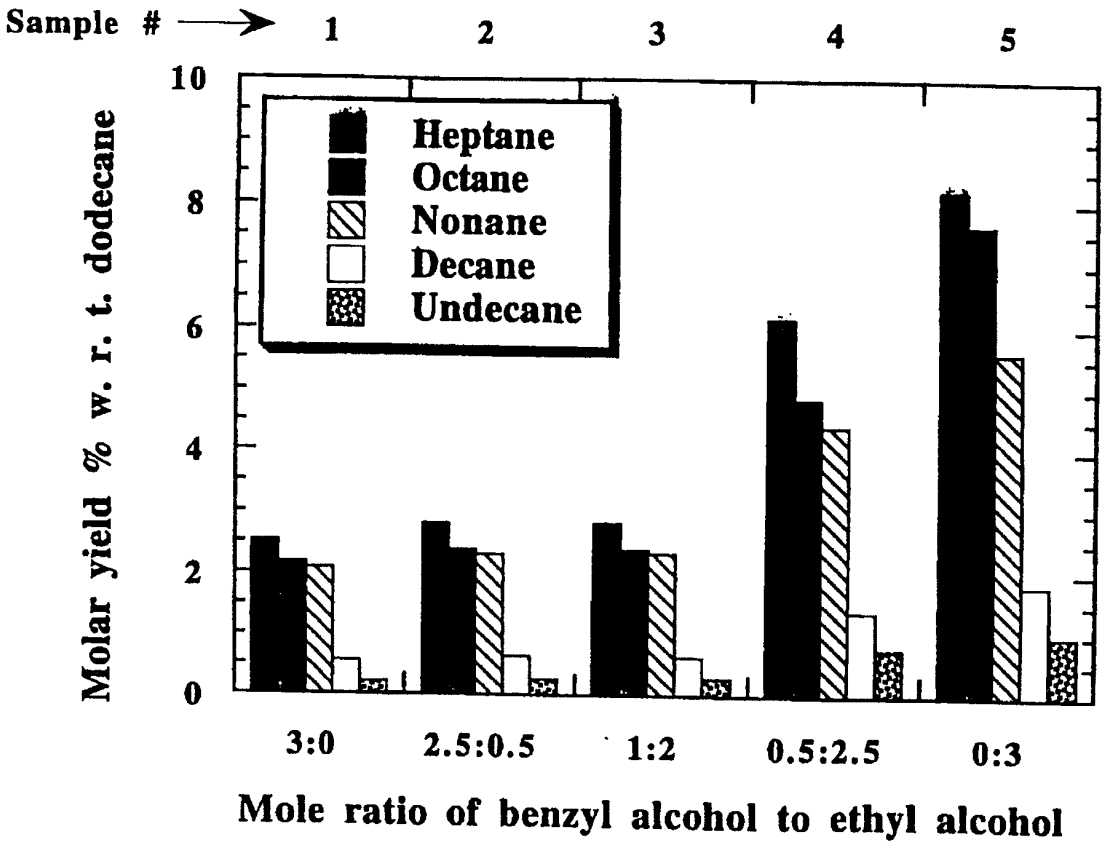

Figure 4.8-2. The Amount of C7 to C11 Alkanes Remaining as Determined by GC Analyses. Samples of Dodecane Stressed with Stabilizer Mixtures after Thermal Stressing at 425°C under 100 psi Air for 6 Hours.

---

[1] Coleman, M. M. et al. *Energy & Fuels.* 1992. 6(5). 535.

[2] Selvaraj, L. et al. *Energy & Fuels.* 1994.

[3] Coleman, M. M. et al. *Energy & Fuels.* 1992. 6(5). 535.

[4] Selvaraj, L. et al. *Energy & Fuels.* 1994.

[5] Malwitx, D. and J. O. Metzger. *Chem. Ber.* 1986. 119. 3558.

4.9 Exploratory Screening and Development of Potential Jet Fuel Thermal Stabilizers Over 400°C

This study is explained in detail in *Advanced Thermally Stable Jet Fuels Technical Progress Report, October 1994 – December 1994.*

Introduction

The techniques or processes for attaining suitable thermal stability in jet fuels will be chosen based on such factors as economy, logistics, and safety. Hydrogenation and additive treatments are potential techniques, because they could be performed at a refinery. However, hydrogenation is costly and hydrogen may be in short supply in the future, as the refining industry reduces reforming for gasoline production, in response to environmental concerns.[1] Additive treatments can be inexpensive, but a more thorough understanding of additive functions at high temperatures is required before additive treatments become a viable option. The objective of this study is to screen and develop a superior potential jet fuel stabilizer.

Summary of Research Performed to Date.

1. Exploratory Screening of Potential Jet Fuel Stabilizers. We initially screened thermal stabilizers and well-established antioxidants used to protect polymers and rubbers against degradation. After thermal stressing, we determined that none of the compounds tested had any significant advantageous effect on the rate of degradation of Jet A-1 fuel, and some antioxidants even promoted the rate of degradation. This could be attributed to the fact that most of these antioxidants were designed to function at much lower temperatures.

We next chose to test the classic hydrogenation agents employed in coal liquefaction and oil products. Tetralin and 1,2,3,4-tetrahydroquinoline, both classic liquefaction reagents, inhibited the degradation of Jet A-1 and showed similar effects as benzyl alcohol, another potential thermal stabilizer.

2. Preliminary Studies of Potential Jet Fuel Stabilizers using Dodecane as a Model Compound. Based on jet fuel's intricate chemical mixtures of hydrocarbons, which become more complex following thermal stressing at high temperatures, we chose dodecane, a major component of Jet A-1 fuel, as a model compound to quantitatively evaluate different potential thermal stabilizers. Of the potential stabilizers, 1,2,3,4- tetrahydroquinoline inhibited dodecane decomposition the most.

3. Quantitative Studies of Potential Jet Fuel Stabilizers Based on Molar Equivalents and Using Dodecane as a Model Compound. Of the addititives considered (tetralin, 9,10-dihydro-phenanthrene, 1,2,3,4-tetrahydroquinoline, benzyl alcohol, benzaldehyde dimethyl acetal, phthalan, and 1,2,3,4-tetrahydro-1-naphthol), with the exception of benzaldehyde dimethyl acetal, all of the additives significantly reduced the amount of dodecane conversion. Benzaldehyde dimethyl acetal was likely ineffective as a result of the cleavage of the side group at 450°C. The two most effective additives were 9,10-dihydro-phenanthrene and 1,2,3,4-tetrahydroquinoline. The other three additives merely retard degradation and are less effective as thermal stabilizers. The 9,10-dihydro-phenanthrene and 1,2,3,4-tetrahydroquinoline additives' superior performance could be attributed to their excellent thermal stability at 450°C, in

conjunction with an increase in resonance stabilization of the radical scavenger relative to benzyl alcohol.

4. Additional Studies of Potential Jet Fuel Stabilizers. We tested 13 additives, studying both electron-donating (1,2,3,4) and electron-withdrawing (5,6) substituents on or in the aromatic ring, as well as additional aromatic rings in succession (7,8,9,10,11,12) to probe their effects on radical stability. **Figure 4.9-1** shows the results from 6 hours of thermal stressing of dodecane at 425°C in the presence of 11 of the additives. The other two compounds—anthrone and anthracene methanol—were insoluble in dodecane even after stressing at 425°C for 6 hours, and resulted in the formation of various solids.

1,2,3,4-tetrahydroquinoline (Dod+4) was the most effective (93% molar yield), showing a dramatic improvement over benzyl alcohol (75%). And 78% of the tetrahydroquinoline remained after 8 hours stressing vs. 48% of benzyl alcohol. The major byproduct from stressing tetrahydroquinoline was quinoline. There are two reasons for tetrahydroquinoline's effectiveness—it exhibits superior thermal stability at 425°C, which implies an increased lifetime of the additive, and it has four hydrogen atoms available for abstraction vs. the two hydrogen atoms that benzyl alcohol has.

We developed this set of parameters to predict the effectiveness of organic additives that can be used to thermally stabilize hydrocarbon fuels and prevent formation of carbonaceous solids. A good additive should:

- Be thermally stable at temperatures above 400°C
- Have hydrogen atoms that can be transferred or abstracted by hydrocarbon radicals (the more the better)
- Enable the radicals generated from hydrogen atom abstraction to be stabilized by resonance

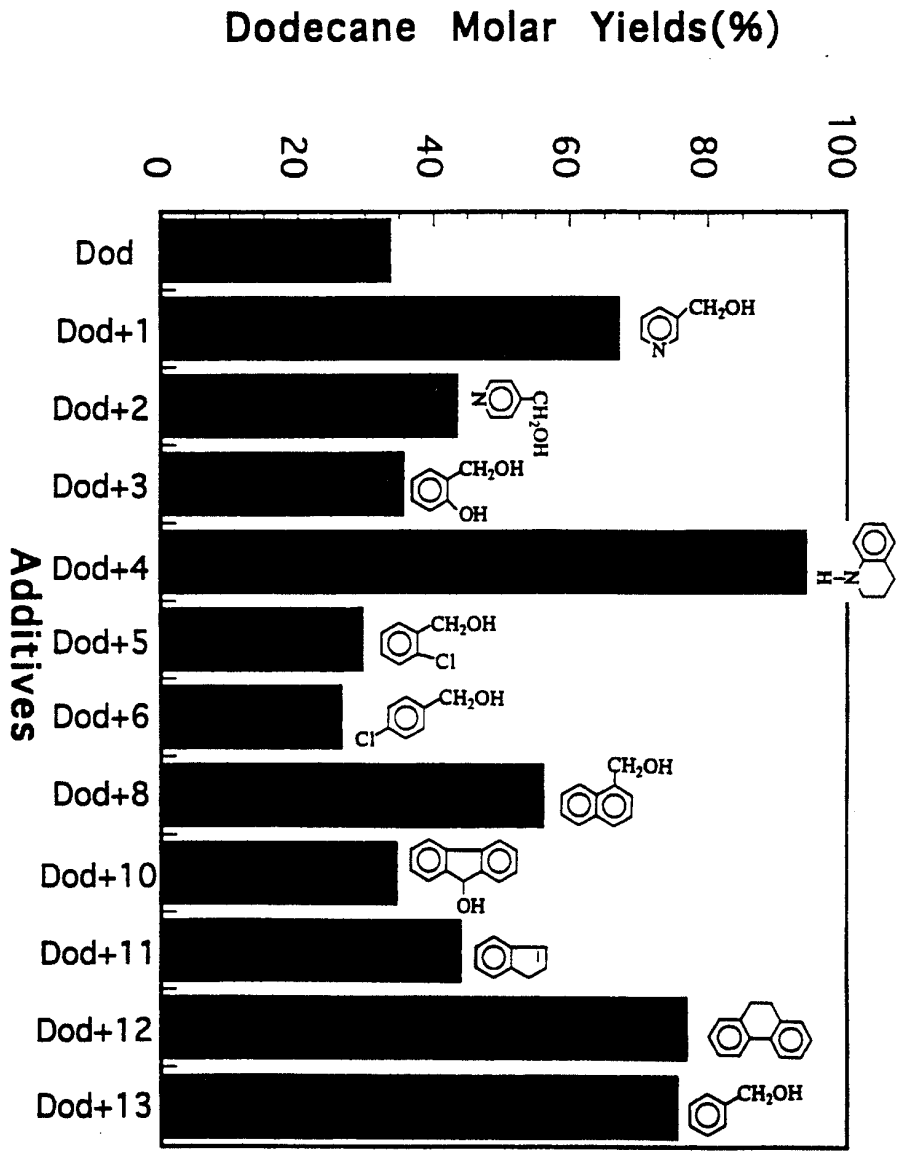

Figure 4.9-1. Effects of Hydrogen Donor Additives 1 through 13 on the Molar Yields of Dodecane at 425°C for 6 Hours under Initial N_2 Pressure of 0.69 MPa

[1] Hazlett, R. N. Thermal Oxidation Stability of Aviation Turbine Fuels. ASTM Mongraph 1. Philadelphia: ASTM. 1991.

4.10 KINETIC STUDIES ON POTENTIAL JET FUEL STABILIZERS

a. Comparing the Thermal Stability of THQ and Dodecane

This study appeared in *Advanced Thermally Stable Jet Fuels Technical Progress Report, January – March 1995.*

Introduction

In previous studies, we demonstrated that 1,2,3,4-tetrahydroquinoline (THQ) is a more efficient thermal stabilizer than benzyl alcohol at 425°C when employed in comparable concentrations in dodecane.[1] In this exercise, we performed preliminary optimization and kinetics studies.

Results

1. Optimization Studies of THQ in Dodecane. Thermal stressing experiments were performed on dodecane samples containing various amounts of THQ at 425°C for 6 hours. The concentration of THQ was varied from 1 to 10 mol%. The liquid products were quantitatively analyzed using GC.

Above about 2 mol% THQ, the amount of dodecane remaining after 6 hours at 425°C was between 75 and 85 mol% with only a slight dependence on the concentration of THQ. Below 2 mol%, however, a large increase in the degradation of dodecane occurred—a phenomenon that supports the hypothesis that we were below the critical concentration required to prevent significant cracking of dodecane.

Observing the mol% of THQ remaining in the dodecane/THQ mixtures after 6 hours at 425°C demonstrates that, as in the benzyl alcohol studies performed earlier, while a significant amount of the additive (THQ or benzyl alcohol) remains, degradation of dodecane is suppressed.

2. Kinetic Studies of Model Compound Dodecane in the Presence of THQ. The thermal stability of THQ, abenzyl alcohol and similar compounds at temperatures above 400°C is one of the most important factors in designing effective thermal stabilizers. Accordingly, we performed kinetic studies of dodecane/THQ mixtures at different temperatures in the range of 400-500°C. Mixtures containing 10 mol% THQ were stressed at temperatures of 400°, 425°, and 450°C for the required reaction time. The concentration of dodecane (C_A) after specific degradation periods was calculated using GC data. Assuming the reaction is first-order, we used the following equation to calculate the rate constant, k:

$$C_A = C_{A0}e^{-kt} \quad (1)$$

or

$$\ln(C_A/C_{A0}) = -kt \quad (2)$$

Plots of $\ln C_A$ versus time should be linear with a slope equal to (-k) and an intercept equal to $\ln C_{A0}$.[2] Values of $9.4*10^{-7}$, $7.2*10^{-6}$, and $4.6*10^{-5}$ sec^{-1} were obtained for k at 400°, 425°, and 450°C, respectively. As the temperature increased from 400° to 450°C, the rate constant, k, increased significantly. Further experimentation will explore different temperatures and THQ

concentrations and determine activation energies from these data. Similar experiments were planned for benzyl alcohol. Ultimately we hope to determine the relative stability of THQ vis-à-vis benzyl alcohol in hydrocarbons at temperatures of 400°-500°C.

b. Kinetic Studies of Dodecane Neat, Dodecane/THQ Mixtures, and Dodecane/Benzyl Alcohol Mixtures

This study appeared in *Advanced Thermally Stable Jet Fuels Technical Progress Report, July – September 1995.*

Introduction

We reported in (a.), above, that 1,2,3,4-tetrahydroquinoline (THQ) is the superior thermal stabilizer among the hydrogen donor compounds screened for jet fuels at temperatures ranging from 400° to 500°C. We performed kinetic studies on dodecane neat, dodecane/THQ mixtures, and dodecane/benzyl alcohol mixtures and calculated the rate constants and Arrhenius parameters.

Results

Thermal stressing was performed on 10 mL dodecane samples with and without additives at different temperatures in the 400°-500°C range for the required reaction time. The liquid products were analyzed using a GC with a FID detector.

In observing the mole percent of dodecane remaining after thermal stressing at different temperatures, we noticed that the degradation of dodecane, with or without additives, increases with time and temperature. The rate of dodecane degradation is retarded in the presence of benzyl alcohol and THQ. There is a strong temperature dependence in dodecane degradation, even in the presence of THQ or BzOH.

Assuming the reaction is first-order, equations (1) and (2) can be used to calculate the rate constant, k. The concentration of dodecane (C_A) after specific degradation periods was calculated using GC data. First-order reaction plots of $\ln(C_A/C_{A0})$ versus time were linear with a slope equal to (-k). With the increase in temperature, the rate constant, k, increases significantly. From these data, we calculated apparent activation energies for each reaction. The rate constant, k, was expressed in the Arrhenius form:

$$k = Ae^{-Ea/RT}; \qquad (3)$$

where E_a is the activation energy, A is the pre-exponential factor for the reaction, R is the gas constant, and T is the absolute temperature. The variation of k with temperature can be determined by differentiating the logarithmic form of equation (3).

$$\frac{d\ \ln k}{d\left(\frac{1}{T}\right)} = -\frac{E_a}{R} \qquad (4)$$

Plots of (ln k) versus 1/T give a slope of $(-E_a/R)$. Accordingly, activation energies, E_a, can be calculated. The activation energies increased in the order of $E_{a'Dod} < E_{a'Dod+BzOH} < E_{a'Dod+THQ}$. The rate constants decreased in the order of $k_{Dod} > k_{Dod+BzOH} > k_{Dod+THQ}$. The

pre-exponential factor increased in the same order as activation energy. These kinetic results demonstrated that dodecane degradation is retarded in the presence of BzOH, and to an even greater degree in the presence of THQ.

The rate constants and Arrhenius parameters we calculated for THQ degradation in dodecane showed that THQ degradation increases with time and temperature. This information serves as the basis for additional research and analysis.

---

[1] Yoon, E. M. and M. M. Coleman. Advanced Thermally Stable Jet Fuels, Technical Progress Report, October – December 1994. The Pennsylvania State University. 92PC92104-TPR-10. 1995.

[2] Hill, Jr., C. G. An Introduction of Chemical Engineering Kinetics and Reactor Design. New York: John Wiley & Sons. 1977.

4.11 FURTHER STUDIES ON POTENTIAL JET FUEL STABILIZERS

This study appeared in *Advanced Thermally Stable Jet Fuels, Technical Progress Report, April – June 1995.*

Introduction

We previously demonstrated that 1,2,3,4-tetrahydroquinoline (THQ) is an effective thermal stabilizer for jet fuels between 400° and 500°C.[1] Understanding why THQ is an outstanding thermal stabilizer at high temperatures is important; therefore, we evaluated number of compounds as potential additives in the model compound dodecane. This study was intended to enhance our understanding of the underlying mechanisms involved in the thermal stability of jet fuels.

Results and Discussions

The compounds evaluated were 5,6,7,8-tetrahydroquinoline **(2),** 1,2,3,4-tetrahydroisoquinoline **(3),** 5,6,7,8-tetrahydroisoquinoline **(4),** 1,2,3,4-tetrahydronaphthalene **(5),** 1,2,3,4,5,6,7,8-octahydrophenanthrene **(6),** 9,10-dihydrophenanthrene **(7),** along with 1,2,3,4-tetrahydroquinoline **(1),** benzyl alcohol **(8),** and 1,4-benzenedimethanol **(9).**

Thermal stressing was performed on 10 mL dodecane samples containing the additive (10 mol% with respect to dodecane) at 425°C for various periods of time (3 to 9 hours). The total weight of gases formed upon thermal stressing was obtained by measuring the weight difference of the reactor before and after venting the gases upon thermal stressing. The liquid products were analyzed using a Perkin-Elmer GC with a FID detector. The reaction products were analyzed using GC/MS.

Isomers of THQ **(2, 3, 4)** were evaluated to study the effect of N atom position in the ring. Tetralin **(5),** which has a structure similar to THQ but without the N atom in the ring, was studied in order to probe the effect of N atom position on hydrogen transfer. Similarly, the importance of the number of transferable hydrogens and the type of ring system present was probed using the compounds **6-9.** Based on the amount of gases formed after 3 hours at 425°C, THQ **(1)** proved to be the most effective thermal stabilizer. Additives **5, 6, 7,** and **9** appeared reasonable, while additives **2, 3, 4,** and **8** were poor. After 6 hours at 425°C, only THQ **(1)** and possibly compound **7** were superior thermal stabilizers at a concentration of 10 mol%.

We examined the amount (mol%) of dodecane remaining in the recovered liquid after 3 hours and 6 hours of thermal stressing at 425°C, respectively. Approximately 96 mol% of dodecane remained in the presence of THQ after 3 hours at 425°C. In contrast, the dodecane mixtures containing additives **2, 3, 4, 5, 6,** and **8** have only about 65-85 mol% dodecane remaining. This effect is more dramatic after 6 hours at 425°C. At that point, approximately 90 mol% of dodecane remained in the presence of THQ, while only 35-55 mol% of dodecane remained in the presence of the other additives. Compounds **7** (9,10-dihydrophenanthrene) and **9** (1,4-benzenedimethanol) were not soluble in dodecane even after thermal stressing; therefore, liquid analysis data could not be collected for these compounds.

The relative thermal stabilities of the additives and the reaction products formed during thermal stressing were determined by GC and GC/MS. By analyzing these products, we were

able to rationalize the superior thermal stability of THQ as an additive over the other compounds. Although compounds **1-4** have the same number of hydrogens available for hydrogen transfer, the results indicated that the position of the N atom in the ring system is important.

Compound **3** (1,2,3,4-tetrahydroisoquinoline) is not as stable as compound **1** (THQ), because the ring opens to form 1,2-dimethylbenzene, 1-ethyl-2-methyl-benzene, 1-ethenyl-2-methylbenzene, *o*-ethylbenzonitrile, and isoquinoline. When compound **3** loses the H-atom from the N-H bond, the resultant radical is not resonance stabilized whereas the radical from compound 1 (THQ) is resonance stabilized by delocalization through the aromatic ring.

Compounds **2** and **4** are not stable at 425°C as they convert quickly to quinoline and isoquinoline, respectively. In compounds **2** and **4,** the hydrogen transfer occurs from the C-H bond, where the bond dissociation energy of C-H is 96-99 kcal/mol while compound 1 (THQ) loses a H-atom from the N-H bond which has the bond dissociation energy of 84 kcal/mol [2]. Consequently, it is more difficult to abstract H-atoms from compounds **2** and **4** compared to compound 1 (THQ).

Compound **5** (tetralin) also is not stable at 425°C, because it forms methyl indene, methyl naphthalene and naphthalene. Since compound **5** (tetralin) does not have a N-atom in the ring, the hydrogen transfer again occurs from C-H bond. Therefore, tetralin is not as effective as a thermal stabilizer as THQ.

Although compound **6** (OHP) has eight hydrogens available for hydrogen transfer, it is not stable at 425°C. In addition to its dehydrogenation products like 1,2,3,4-tetrahydro-phenanthrene and phenanthrene, it degrades to form products like alkyl naphthalenes and alkyl benzenes.

Compounds **8** and **9** are effective stabilizers, but when they are compared to compound 1 (THQ), they are not as stable as THQ at high temperatures. Compound **8** (benzyl alcohol) produced benzene, methylbenzene, ethylbenzene and benzaldehyde. Compound **9** (1,4-benzenedimethanol) is a more effective stabilizer than compound **8** (benzyl alcohol), primarily because of the doubling of the transferable hydrogens.

We conclude, therefore, that compound 1 (THQ) is a superior additive in inhibiting the thermal degradation of dodecane because: (a) it has four transferable hydrogens, (b) it is relatively stable at 425°C, (c) the N-H bond is weaker than the C-H bond, and (d) the radicals formed are stabilized by delocalization through the aromatic ring.

---

[1] Yoon, E. M. and M. M. Coleman. Advanced Thermally Stable Jet Fuels, Technical Progress Report, October – December 1994. The Pennsylvania State University. 92PC92104-TPR-10. 1995.

4.12 Toward the Design of Thermally Stable Jet Fuels at Both Moderate (<250°C) and High (>400°C) Temperatures

a. Developing a Simple Screening Test

This study appeared in *Advanced Thermally Stable Jet Fuels, Technical Progress Report, October–December 1995.*

We previously demonstrated that if certain hydrogen donors—the most effective being 1,2,3,4-tetrahydroquinoline (THQ)—are blended into jet fuels (or similar hydrocarbon mixtures) they enhance thermal stability and retard the formation of carbonaceous solids at temperatures of 400–500°C. The superior performance of THQ in the pyrolysis regime was predicated on a number of factors. First, THQ and its dominant reaction product, quinoline, are highly stable at 400–450°C and there are no substituents on the aromatic or aliphatic rings that can be cleaved at these temperatures to produce radicals and promote degradation. Second, THQ is an efficient radical scavenger at these temperatures. Initial hydrogen atom transfer to an aliphatic hydrocarbon radical is facile and the THQ radical formed after initial hydrogen abstraction is well stabilized by resonance through delocalization into the aromatic ring. Finally, the transfer of three more hydrogens to hydrocarbon radicals is also facile, with excellent resonance stabilization at every step towards the formation of quinoline. Details of screening and kinetic studies have been presented previously.[1,2]

Having successfully discovered compounds that act as thermal stabilizers for hydrocarbon mixtures at temperatures in excess of 400°C, we faced a number of questions that have important ramifications in the design, formulation, and development of commercially viable, high temperature stable jet fuels. Such fuels must be stable (both thermally and oxidatively) at storage and moderately elevated temperatures (from ambient to ≈300°C) which is in the autoxidative regime. Will high temperature (> 400°C) thermal stabilizers such as THQ and benzyl alcohol (BzOH) also act as antioxidants at these lower temperatures? If THQ and BzOH are inherently poor antioxidants at the lower temperatures, will the relatively high concentration (≈1–10 mol% compared to <500 ppm for a classic antioxidant) of the hydrogen donor offset this drawback? This represents the next real challenge, because classic antioxidants like the sterically hindered phenolics that operate well in the autoxidation regime actually *promote* free radical reactions in the pyrolysis regime. In other words, the additive introduced to prevent degradation of the fuel in storage and at moderately elevated temperatures can adversely affect the efficacy of the additive put in to retard the formation of carbonaceous solids at high temperatures (>400°C).

We surmised that we could conceivably find solutions to these problems in a related field—vulcanization chemistry. In the vulcanization of diene elastomers, accelerators (e.g., mercaptobenzothiazole and tetramethylthiuram disulfide) are used in conjunction with sulphur and other activators to produce the active crosslinking agent. In mixing the ingredients on a two-roll mill, premature vulcanization, or as it commonly called "scorch," is prevented by adding a "retarder" (often a sulphenamide). The retarder entirely mops up any active crosslinking agent until the retarder is fully consumed, thus delaying the onset of normal vulcanization. This would be similar to a jet fuel formulation that contains a relatively small amount (<500 ppm) of a classic antioxidant (e.g., a sterically hindered phenolic) and a relatively large amount (≈5%) of a high temperature stabilizer (e.g., THQ). The former should work well in the autoxidative regime,

but as the temperature rises and approaches 400°C, cleavage of the antioxidant side groups will occur and the free radicals formed must be capped by hydrogen donation from the high temperature stabilizer. In effect, some of the THQ will be sacrificed to mop up the excess radicals formed by the cracking of the antioxidant at the higher temperatures.

Purpose: Before we could test any of these ideas, we needed to develop a simple screening test, similar to the tubing bomb methodology used in our high-temperature screening of thermal stabilizers at 400–500°C. The test had to be capable of being reproduced in a reasonable time period at temperatures of 200–300°C. The screening methodology employed at 400–500°C would not be applicable at 200–300°C, because of the inordinately long time periods required to produce measurable changes.

Experimental: We adopted the following simple procedure to accelerate the oxidative degradation process. Samples of pure Dod (or Jet A-1 fuel) and mixtures containing 5 vol% of THQ or BzOH based on Dod (or Jet A-1) were prepared. Thermal stressing was performed at 250°C in 25 mL type 316 stainless steel microreactors. The microreactor containing the sample was purged five times with UHP-grade N_2 at 1000 psi to minimize the presence of dissolved oxygen and finally pressurized with air at various specific pressures from 100 to 400 psi. The microreactor was placed in a preheated oil bath at 250°C for 1 hour, then quenched in cold water. The liquid products were examined visually in terms of color and the absence or presence of oils or solids.

Findings: Comparing the preliminary results obtained from neat Dod and the Dod mixtures, we found no evidence that carbonaceous solid formation occurs in the samples of neat Dod thermally stressed at 250°C under air pressures up to 200 psi. There is some discoloration of the liquid at 150 and 200 psi, however. At 250 psi air, a trace of carbonaceous solids was observed and the liquid was yellow. At 300 and 400 psi air, obvious amounts of carbonaceous solids were present and the liquids were highly colored.

In the Dod mixtures with THQ, there were no large amounts of carbonaceous solids formed up to pressures of 400 psi, but the liquids were colored throughout and there was evidence of a small amount of oily material in the samples subjected to the higher air pressures. At that stage, before further analysis of the products, we presumed that THQ was reacting with oxygen and retarding the formation of carbonaceous solids. The Dod/BzOH mixtures were clear and contained no carbonaceous solids at 100 psi air, but at 200 psi and above, both the presence of oil and carbonaceous solids was apparent and the liquid was discolored. This did not represent an improvement over neat Dod.

The analogous results for the neat Jet A-1 and mixtures with THQ and BzOH indicated that, in the case of the neat Jet A-1 fuel, there was no evidence that carbonaceous solid formation occurred in the samples of neat Dod thermally stressed at 250°C under an air pressure of 100 psi. However, there was some discoloration of the liquid. Above 100 psi air, carbonaceous solids were apparent and the liquids were highly colored. The Jet A-1 fuel mixtures with both THQ and BzOH seemed to represent a significant improvement. While the liquids were highly colored, carbonaceous solid formation appeared to be retarded vis-à-vis neat Jet A-1 fuel.

These preliminary results were encouraging and served as the precursor to the systematic experiments of the type described at 250°C under an initial air pressure of 200 psi as a function of time.

b. Further Experimentation to Achieve Thermal Stability in Both the Autoxidative and Pyrolysis Regimes

This study appeared in *Advanced Thermally Stable Jet Fuels, Technical Progress Report, January – March 1996.*

Purpose: Previously, we showed that when mixtures of dodecane (Dod) with THQ and Jet A-1 fuel with both THQ and BzOH are stressed at 250°C under air pressures of 100, 200, 300 and 400 psi for 1 hour, no large amounts of carbonaceous solids formed. These preliminary results were encouraging and we continued to perform systematic experiments of the type described above at 250°C under an initial air pressure of 200 psi as a function of time. The object of these experiments was to formulate a jet fuel that will offer enhanced thermal stability in both the autoxidative and pyrolysis regimes.

Experimental: Samples of pure Dod or Jet A- 1 and mixtures containing 5 vol % of THQ or BzOH based on Dod (or Jet A- 1) were thermally stressed at 250°C under 200 psi air for 1, 2, 3 and 4 hours using the method described in (a).

Findings: In the Dod mixtures with THQ, no large amount of carbonaceous solids formed up to 4 hours; however, the liquids were colored throughout and there was evidence of small amount of oily smear on the reactor walls after 3 hours of stressing. The smear was soluble in acetone. The Dod/ BzOH mixtures stressed under the same conditions showed the presence of oil and carbonaceous solids. BzOH was not miscible with Dod at ambient temperature and there was little to no improvement in stability over neat Dod.

A significant improvement was observed in the Jet A-1 fuel mixtures with both THQ and BzOH. Although the liquid was colored, carbonaceous solid formation appeared to be retarded compared to that of neat Jet A- I fuel.

Classic antioxidants such as the sterically hindered phenolics operate well in the autoxidation regime (<250°C). Will the addition of such antioxidants like 2,6-di-*tert*-butyl-*p*-hydroxytoluene (BHT) to THQ and BzOH further improve their performance at the lower temperature (<300°C)? We conducted a series of experiments where samples of dodecane mixtures containing 5% vol of THQ and BzOH were compared to analogous ternary mixtures containing 200 ppm BHT. These mixtures were stressed at 250°C under air pressure of 100 psi for 1 hour.

The addition of 200 ppm BHT to the mixtures of Dod with THQ produced clear, less colored liquids compared to the binary mixture of Dod with THQ. The mixture of Dod with BzOH produced in a less pronounced difference, probably as a result of the limited solubility of BzOH in Dod at ambient temperatures. The next step in our investigation was to characterize the mixtures based on their major reactions.

c. Determining Benzyl Alcohol's Susceptibility to Oxydation at 250°C in Comparison to THQ and Tetralin

This study appeared in *Advanced Thermally Stable Jet Fuels, Technical Progress Report, July – September 1996.*

We previously concluded that the chemical and structural characteristics that make tetrahydroquinoline (THQ), tetralin, and similar hydrogen donors effective thermal stabilizers in the pyrolysis regime also render them highly susceptible to oxidation in the autoxidation regime. Furthermore, the addition of phenolic antioxidants does not improve matters. Therefore, we deduced that if THQ or tetralin is to be used as a high temperature stabilizer in jet fuels, oxygen would have to be eliminated in the fuel or the hydrogen donor would have to be added in situ just before the fuel experiences high temperatures (>400°C). We also pointed out that benzyl alcohol (BzOH), while not as efficient as THQ as a high temperature stabilizer (>400°C), is not considered a classic hydrogen donor, although it donates hydrogen to the alkyl free radicals formed at high temperatures while being transformed to benzaldehyde.

Purpose: Undertake a series of experiments to address the following questions arising from our studies described in (a) and (b): "Is BzOH less susceptible to oxidation at 250°C than THQ or tetralin?," "If so, what are the mechanistic implications?," and "Can we use this information to design superior simultaneous low and high temperature stabilizers ?"

Experimental: Using the same tubing bomb methodology as in our high-temperature screening of thermal stabilizers at 400–500°C , we thermally stressed neat BzOH at 250°C for 1 hour under initial air pressures of 100, 200, 300, and 400 psi.

Findings: After 1 hour at 250°C, under an initial 100 psi air, BzOH appeared to only be slightly affected. The sample had a very pale yellow appearance and there were no signs of solid, oil, or gel formation. This provides a significant contrast to the analogous experiments for neat THQ, which became a dark black liquid with a measurable amount of suspended black solids, and tetralin, which became a dark brown/black liquid.[3] At higher pressures of air, up to an initial pressure of 400 psi (i.e. higher concentration of oxygen), BzOH did demonstrate significant degradation, eventually transforming into a black liquid that could contain small suspended particles. Nonetheless, BzOH represented an obvious improvement in terms of oxidative stability over THQ and tetralin.

Experimental: We performed a second set of experiments, holding the initial pressure of air constant at 100 psi and varying the stressing time from 1 to 4 hours.

Findings: In contrast to the results observed for neat THQ and tetralin, the BzOH sample increased in color from pale yellow (after l hour) to a reddish brown liquid (after 4 hours), but there was no evidence of any solids. BzOH appeared to be far less susceptible to oxidative degradation than either tetralin or THQ.

Experimental: The role of oxygen was briefly explored by thermally stressing BzOH under different atmospheres. Neat BzOH were stressed at 250°C under an initial pressure of 100 psi of air, nitrogen, and argon for periods of 10, 15, 30 and 60 minutes.

Findings: Under nitrogen, the BzOH sample became slightly colored after 60 minutes, but had no evidence of solid carbonaceous materials. Under argon, no changes were observed visually. Again, BzOH appeared inherently more stable at 250°C than either THQ or tetralin.

Experimental: Finally, classic antioxidants, such as the sterically hindered phenolics, are known to work well in the autoxidation regime (< 250°C). We undertook another series of experiments to determine whether the addition of 200 ppm of such an antioxidant (e.g., 2,6-di-*tert*-butyl-*p*-hydroxytoluene (BHT)) could improve the oxidative stability of BzOH at 250°C. We thermally stressed BzOH in the presence and absence of 200 ppm BHT at 250°C for 1 hour under an initial pressure of 100 psi of air.

Findings: The addition of the antioxidant did not appear to improve the oxidate stability of BzOH. The THQ/BHT mixture was highly colored and appeared visually to be more oxidatively degraded than neat BzOH. Additional characterization will be needed to substantiate this conclusion.

d. Determining the Effect on Thermal Oxidative Stability at 250°C of Adding Ethanol (as Compared to Pure Benzyl Alcohol)

This study appeared in *Advanced Thermally Stable Jet Fuels, Technical Progress Report, October – December 1996.*

Benzyl alcohol (BzOH) appears to be the best candidate for the high temperature stabilization of jet fuels in the pyrolysis regime, because it is less susceptible then either tetrahydroquinoline (THQ) or tetralin to oxidative degradation in the autoxidation regime (150-350°C). Moreover, in our initial scouting studies of potential high temperature stabilizers, we observed that ethanol (EtOH) was a marginal high temperature thermal stabilizer for Jet A-1 fuel at 425°C,[4] but, unfortunately, phase separation of fuel mixtures was evident after thermal stressing and subsequent cooling to room temperature. Selvaraj et al., showed that the problem of phase separation can be solved by using a mixture of ethanol and benzyl alcohol.[5] Furthermore, there was added advantage in that in situ regeneration of benzyl alcohol occurs in ethanol/benzyl alcohol mixtures.

Purpose: Address the question, "Compared to pure BzOH, does the addition of EtOH have any positive or detrimental effect on thermal oxidative stability at 250°C?" To answer this question, we performed a set of thermal stressing experiments using neat ethanol and various ethanol-benzyl alcohol mixtures. Results were also obtained with ethanol-benzyl alcohol mixtures in dodecane and Jet A-1 fuel.

Experimental: Employing the same tubing bomb methodology as described previously, we thermally stressed samples of neat EtOH at 250°C under an initial air pressure of 100 psi for 1, 2, 3, and 4 hours. Analogous experiments were performed on neat BzOH/EtOH mixtures which were thermally stressed under the same conditions for 1 hr. The molar ratio of BzOH:EtOH was varied as 3:0, 2.5:0.5, 2:1, 1: 1, 1:2, 0.5:2.5, and 0:3.

Findings: Pure EtOH appeared to be only slightly affected by the thermal stressing. There was no evidence of the presence of any solids and the liquids remained essentially colorless up to 3 hours. After 4 hours at 250°C the EtOH sample exhibited an increase in color from colorless to pale yellow, but gave no evidence of any solids.

Liquids obtained after thermal stressing of BzOH/EtOH mixtures were generally more colored than those from the neat alcohols. Apparently, there is no advantage to using BzOH/EtOH mixtures in the autoxidation regime.

Experimental: Although our previous results were discouraging, we added BzOH/EtOH mixtures at a concentration of 5 weight % to dodecane and Jet A-1 fuel and thermally stressed them under the same conditions described above.

Findings: In all of the dodecane mixtures, with the exception of the one containing 2:1 BzOH/EtOH, two phase liquids (a major liquid phase with a minor oil phase) were produced. In the case of the Jet A-1 mixtures, there was no observed phase separation up to BzOH:EtOH ratios of 1:1. In the Jet A-1 mixtures containing BzOH:EtOH concentrations of less than 1:1, two phases were observed. These phase behavior differences can likely be attributed to simple solubility considerations.

In summary, ethanol-benzyl alcohol mixtures have no promising advantages as thermal jet fuel stabilizers in the autoxidation regime at 250°C.

e. Further Thermal Stressing Experimentation Using Model Jet Fuel Compound Dodecane

This study appeared in *Advanced Thermally Stable Jet Fuels, Technical Progress Report, January – March 1997.*

In our studies involving thermal stressing of tetrahydroquinoline (THQ), tetralin (TRL) and benzyl alcohol (BzOH), we have found that THQ is the best high temperature jet fuel stabilizer in the pyrolysis regime (> 400°C), yet the most susceptible to oxidative degradation in the autoxidation regime (150-350°C). Pure TRL performed better at 250°C under 100 psi air, but still transformed into a brown/black liquid containing a trace of solids after 1 hour. Finally, BzOH, the least efficient high temperature thermal stabilizer of the three in the pyrolysis regime (but nevertheless still quite effective), was found to be the most stable to oxidative degradation in the autoxidation regime. With these results in mind, we performed a series of simple systematic thermal stressing experiments at 250°C under 100 psi air using the model jet fuel compound dodecane (Dod) and employing the same tubing bomb methodology as described previously.

1. Pure Dod. To establish a "baseline," samples of pure dodecane were thermally stressed at 250°C under an initial air pressure of 100 psi for 1, 2, 3 and 4 hours. After 1 hour, Dod remained a clear liquid with no evidence of oil or solids formation. After 2 hours, the sample was slightly more colored (pale yellow), but offered no evidence of oil or solids formation. After 3 hours, the sample was more highly colored and exhibited an oily phase. Finally, after 4 hours, the sample resembled a poor emulsion—it was cloudy with the obvious presence of an oily phase. In summary, pure Dod (i.e., containing no additives such as an antioxidants or thermal stabilizers), was reasonably stable (i.e., formed no oils, gels or carbonaceous solids) at 250°C under 100 psi air for periods of up to 2 hours.

2. Dod + 200 ppm BHT. Hindered phenols, such as 2,6-di-*tert*-butyl-4-hydroxytoluene (BHT), act as radical scavengers and are commonly employed in the 100-500 ppm range as antioxidants to improve the storage stability of jet fuels.[6] Like the high temperature stabilizers THQ, TRL, and BzOH, BHT and similar hindered phenolics are also hydrogen-donating

molecules, but the temperature range over which they operate efficiently (i.e., donate hydrogen atoms and form stable products that do not initiate further degradation) is very different. BHT and the like operate well in jet fuels (i.e., they significantly retard the onset of gel and carbonaceous solid formation) in the autoxidative range, but actually promote degradation in the pyrolysis range (> 400°C) because radicals are produced from the cleavage of the *tert*-butyl side groups. The mechanism of BHT antioxidation is complex, but the essential features are:

$$ROO\bullet + RH \xrightarrow{k_1} ROOH + R\bullet$$

$$ROO\bullet + AH \xrightarrow{k_2} ROOH + A\bullet$$

AH denotes the phenolic (or secondary amine) antioxidant, and as k_2 is very much larger than k_1, only relatively small concentrations of AH are required in the autoxidative regime to adequately stabilize jet fuels and similar hydrocarbon mixtures. Steric hindrance of the phenolic hydroxyl group with at least one bulky side group in the 2 or 6 position decreases the ability of the phenoxy radical to abstract a hydrogen atom from the hydrocarbon fuel and produce an alkyl radical. This and the excellent resonance stabilization of the phenoxy radical are important factors for good antioxidants.

For baseline purposes, samples of dodecane containing 200 ppm BHT were thermally stressed at 250°C under an initial air pressure 100 psi for 1, 2, 3 and 4 hours. After 1 and 2 hours, the Dod/BHT mixture remained a clear colorless liquid with no evidence of oil or solids formation. Between 2 and 4 hours, the sample had a very pale yellow color, but still exhibited no evidence of oil or solids formation.

In summary, as expected, adding 200 ppm BHT enhances the thermal stabilization of Dod at 250°C and the mixture is reasonably stable under 100 psi air for periods of up to 4 hours. BHT does, however, promote degradation in the pyrolysis regime (> 400°C).

3. Dod + 5 wt % THQ. At temperatures of 400-500°C (i.e., in the pyrolysis regime), in the presence of oxygen, blends of jet fuel containing appreciable quantities of the hydrogen-donating molecule THQ (1-5%) have been found to be the most thermally stable.[7] However, as mentioned above, pure THQ has been shown to be highly susceptible to oxidation in the autoxidative regime. What happens to a mixture of Dod and THQ (5%) when it is thermally stressed at 250°C in the presence of air?

Samples of dodecane containing 5% THQ were thermally stressed at 250°C under an initial air pressure 100 psi for 1, 2, 3 and 4 hours. After 1 hour, the Dod/THQ mixture, an initially clear colorless liquid, transformed into a brown/yellow liquid containing a brown oil. Between 1 and 4 hours, the sample became increasingly colored (yellowish brown) and the oil had a brownish black appearance. The amount of brownish/black oil present appeared to correspond roughly to the amount of THQ originally introduced. Most likely, as indicated above, the THQ has preferentially oxidized to form a polar species that phase separated from the non-polar Dod.

4. Dod + 5 wt % THL. We previously demonstrated that the hydrogen-donating molecule tetralin (THL) was an effective thermal stabilizer for jet fuel in the pyrolysis regime, but that it was not as effective as THQ.[7] Although pure TRL is also susceptible to oxidation in the autoxidative regime at 250°C (pure THL transforms into a brown/black liquid after 1 hour under an initial pressure of 100 psi), it is not as sensitive as THQ.

Does a mixture of Dod and THL (5%) perform better than the analogous Dod/THQ mixture when thermally stressed at 250°C in the presence of air? Indeed it does. Samples of dodecane containing 5% THL were thermally stressed at 250°C under an initial air pressure 100 psi for 1, 2, 3 and 4 hours. The Dod/THL mixture remained a clear, very pale yellow liquid containing no oils or solids for up to 3 hours. Between 3 and 4 hours, the sample became increasingly colored (bright yellow) and exhibited a small amount of solid and/or oil particles. Hydrogen donation appeared less facile in the case of THL compared to THQ, making THL a less efficient high-temperature stabilizer in the pyrolysis regime and less susceptible to oxidation in the autoxidation regime.

5. Dod + 5 wt % BzOH. BzOH, the third candidate for a potential high temperature jet fuel stabilizer, is also a hydrogen-donating molecule.[3] Unlike THQ and THL, however, BzOH is a polar molecule that contains an oxygen atom and is not considered a classic hydrogen-donating molecule (which might be considered for liquefaction processes). Neat BzOH thermally stressed at 250°C under an initial pressure of 100 psi air becomes more colored as a function of time, but we have samples that have been stressed for as much as 12 hours without the presence of obvious solids.

Samples of dodecane containing 5% BzOH were thermally stressed at 250°C under an initial air pressure 100 psi for 1, 2, 3 and 4 hours. Unfortunately, BzOH is not miscible with Dod and forms a two-phase system at room temperature. (It is, however, miscible with jet A- 1 fuel.) Whether or not the mixture is one phase at 250°C under an initial air pressure 100 psi is unknown at this time, but we suspect that it is. Up to a least 4 hours of thermal stressing at 250°C and upon cooling to ambient temperature, the Dod/BzOH mixtures remain clear, colorless liquids with a yellow colored oil. This oil is not the result of major chemical modification (oxidation) of the BzOH, but rather the fact that pure BzOH is not miscible with Dod in the first place.

6. Dod + 200 ppm phenol, 2,6-dimethylphenol and 2,4,6-trimethylphenol. As mentioned in (2), above, BHT is an effective antioxidant for jet fuels in the autoxidation regime, but is ineffective in the pyrolysis regime, because the tert-butyl side groups cleave, produce additional radicals, and accentuate degradation. While sterically hindered phenolic molecules in the 2 and 6 positions have been found to be the most effective antioxidants at relatively low temperatures, other phenolic molecules have shown at least some antioxidative activity. We surmised that phenolic molecules without cleavable side groups might protect, at the additive level ($\approx$ 200 ppm), both the jet fuel and the high temperature stabilizer (THQ, THL, BzOH, etc.) as the fuel temperature passes through the autoxidation regime. Accordingly, initial scouting experiments were performed on Dod mixtures (our model jet fuel) containing 200 ppm of phenol (Ph), 2,6-dimethylphenol (DMPh) and 2,4,6-trimethylphenol (TMPh).

Results of thermally stressing the mixtures at 250°C under an initial air pressure 100 psi for 1, 2, 3 and 4 hours revealed that Dod/Ph mixtures remained clear, slightly colored (very pale

yellow) liquids with no evidence of oil or solid formation for time periods of up to at least 4 hours. This was a distinct improvement on the results for neat Dod and indicates that phenol does offer at least some protection to oxidation at 250°C. Similar results were obtained for the Dod/DMPh mixtures, although the liquids were somewhat more colored (pale yellow). There was no evidence of either oil or solid formation up to 4 hours stressing at 250°C. In contrast, and rather surprisingly, Dod mixtures did not appear as stable. Dod/TMPh mixtures remained clear, colorless liquids with no evidence of oil or solid formation for time periods of up to 2 hours. Between 2 and 4 hours, however, the presence of a phase-separated oil was detected.

The results from the Dod mixtures containing 200 ppm of phenol and 2,6-dimethylphenol show promise. We next chose to investigate ternary mixtures with THQ, TBL, and BzOH in the autoxidative and pyrolysis regimes.

---

[1] Yoon, E. M. et al. "High Temperature Stabilizers for Jet Fuels and Similar Hydrocarbon Mixtures. 1. Comparative Studies of Hydrogen Donors." *Energy & Fuels*. Submitted 1996.

[2] Yoon, E. M. et al. "High Temperature Stabilizers for Jet Fuels and Similar Hydrocarbon Mixtures. 2. Kinetic Studies." *Energy & Fuels*. Submitted 1996.

[3] Sobkowiak, M. and M. M.Coleman. *Advanced Therinally Stable Jet Fuels, Technical Progress Report, October – December 1995*. The Pennsylvania State University. 92PC92104-TPR-14. 1996.

[4] Coleman, M M. et al. "Potential Stabilizers for Jet Fuels Subjected to Thermal Stress Above 400°C." *Energy & Fuels*. 1992. 6 535-539.

[5] Selvaraj, J. B. et al. "In Situ Regeneration of the Thermal Stabilizer Benzyl Alcohol Via Ethanol in Simulated Jet Fuels Above 400°C." Fuel Processing Technology. 1997. 50 153-162.

[6] Nixon, A. C. *Autoxidation and Antioxidants*. New York: Interscience, W. O. Lundenberg, Ed. 11. 1962.

[7] Yoon, E. M. et al. *Energy & Fuels. 1996. 10.* 806, 812.

4.13 Design and Synthesis of second Generation Jet Fuel Stabilizers

This study appeared in *Advanced Thermally Stable Jet Fuels, Technical Progress Report, April – June 1995.*

In recent years we have identified several novel additives as important leads in the development of a practical high-temperature thermal stabilizer for jet fuels.[1] Three in particular have proven effective in model studies at elevated temperature: tetrahydroquinoline (THQ), tetrahydronaphthalene (tetralin), and benzyl alcohol (BzOH). Examining thermolysis products confirmed our belief that all three operate by donation of multiple hydrogen atoms to quench the radical species responsible for fuel degradation.

THQ and tetralin are excellent hydrogen donors in the pyrolysis regime (> 400°C); however, their outstanding reactivity makes them susceptible to autoxidation at lower temperatures (250°C) and, thus, limits their application.[2] BzOH, although not quite as effective under pyrolysis conditions, readily survives passage through the autoxidation regime.[3] This is probably a direct indication of the distinct chemical mechanisms involved in each case. Whereas THQ and tetralin each donate four hydrogens with formation of stable aromatic compounds (quinoline and naphthalene, respectively) as the ultimate driving force, the mechanism of BzOH stabilization is somewhat more obscure, an analogous stepwise loss of two hydrogens resulting in a formal oxidation to benzaldehyde. Further oxidation, disproportionation, combination, and other processes of this intermediate product may all play an important role, which clearly requires further clarification.

This contrasting efficiency over a range of temperatures has led us to consider a number of questions: What if the crucial structural elements necessary for stabilization in both autoxidative and pyrolysis regimes are combined within the same molecule? Will complementary antioxidant abilities allow access to the full range of stabilization? In addition, will synergistic effects then come into play, whereby enhanced capabilities are observed? What are the effects of the substitution pattern? How will all of this differ from direct use of admixtures? Finally, can relative efficiency be predicted with the aid of molecular modeling as opposed to exhaustive exploratory testing?

With these questions in mind, we undertook a series of studies aimed at the development of novel "hybrid" stabilizers based on a combination of two or more of our existing candidate additives. For example, "crossing" BzOH with tetralin led to three new compounds—THN, α-hybrid, and β-hybrid—each containing the necessary features of their "parents" (i.e., a benzylic alcohol moiety and a partially reduced naphthalene). Indeed, some precedent for this approach existed in our previous studies—we demonstrated that 1,2,3,4-tetrahydro-1-naphthol (THN) proves marginally more effective in preventing dodecane degradation at high temperatures (450°C under 1 MPa of N_2).

Although THN is commercially available, provision of the other hybrids in the quantities required for preliminary degradation studies required an expedient synthetic route. Thorough examination of the literature revealed both to be known compounds, although no direct synthesis was available. Reduction of the corresponding carbonyl compounds proved a viable alternative. In the case of the β-hybrid, a modified Friedel-Crafts type formulation of tetralin[4] unexpectedly yielded a mixture of the 2 aldehydes. Sodium borohydride reduction[5] (under slightly acidic

conditions to preclude competing acetal formation) followed by distillation (110°-12°C at 300-400 miliTorr) yielded the require alcohol in 64% overall.

For the α-hybrid, a less direct approach was required, as Friedel-Crafts chemistry was known to sterically favor the β position. However, the corresponding bromide had been reported with remarkable and exclusive regioselectivity.[6] An ensuing carbonylation, either of the Grignard type or palladium mediated, would yield the necessary substrates for reduction. Bromination proceeded and we investigated carbon monoxide insertion to produce the ester. Although an in situ generation technique failed,[7] use of higher pressures[8] revealed some interesting features. In addition to some simple over-reduction to tetralin, a mixture of three carbonylation products was produced: both the α- and β-hybrids, and a symmetrical diester, of unconfirmed regiochemistry. Either the bromination is not as selective as expected, or some unusual mechanism is at work in the palladium-mediated carbonylation.

One solution to the question of regioselectivity involves starting with the commercially available reduced α-naphthol and proceeding via its triflate,[9] similar in reactivity to the corresponding halide. A standard triflation,[10] followed by palladium mediated carbonylation[11] yielded the α-ester in moderate yield. Simple lithium-aluminum hydride reduction afforded the required benzylic alcohol.

With sufficient quantities of the tetralin-BzOH hybrids in hand, we turned our attention to the complementary THQ-BzOH species, of which there were five possibilities, although this chemistry was expected to be more complex as a result of the necessity to use *N*-protecting groups.

---

[1] Coleman, M. M. et al. Energy & Fuels. 1992. 6. 536.

[2] Sobkowiak, M. and M. M. Coleman. *Advanced Thermally Stable Jet Fuels, Technical Progress Report, October – December 1995.* The Pennsylvania State University. 92PC92104-TPR-14. 1996.

[3] Sobkowiak, M. and M. M. Coleman. *Advanced Thermally Stable Jet Fuels, Technical Progress Report, January – March 1996.* The Pennsylvania State University. 92PC92104-TPR-15. 1996.

[4] Monte, A. P. et al. *J. Med. Chem.* 1993. 36. 3700.

[5] Jensen, E. H., P. H. Nielsen, and R. Hohlweg. *Heterocycles.* 1995. 41. 2441.

[6] Ranu, B. C., D. C. Sarkar, and R. Chakraborty. *Synth. Commun.* 1992. 22. 1095.

[7] Carpentier, J.-F. et al. *Tetrahedron Lett.* 1991. 32. 4705.

[8] Schoenberg, A., I. Bartoletti, and R. F. Heck. *J. Org. Chem.* 1974. 39. 3318.

[9] Hanack, M. and R. Rieth. *Chem. Ber.* 1987. 120. 1659.

[10] Hanack, M. *Chem. Ber.* 1984. 117. 3004.

[11] Dolle, R. E., S. J. Schmidt, and L. I. Kruse. *J. Chem. Soc., Chem. Commun.* 1987. 904.

4.14 FUNDAMENTALS OF HIGH-TEMPERATURE STABILITY

This study appeared in *Advanced Thermally Stable Jet Fuels, Technical Progress Report, January – March 1998.*

Introduction

We have studied the stabilization of jet fuels in the pyrolysis regime (> 400°C) through the addition of hydrogen donors such as tetrahydroquinoline (THQ), tetralin (THN), and benzyl alcohol (BzOH). While the results have been promising, kinetic studies have revealed that the rate of hydrocarbon decomposition is a very strong function of temperature in the range from 400 to 500°C.[1] In fact, satisfactory stabilization of jet fuels seemed infeasible using organic hydrogen donors at temperatures exceeding 475-500°C. At relatively low temperatures in the pyrolysis regime (e.g., 400°C), the degradation of jet fuel proceeded through a chain reaction with formation of free radicals. If we can "kill" those free radicals, especially at the point of inception, we can, in principle, inhibit degradation of jet fuels. This, of course, is the function of the hydrogen donor. However, at relatively high temperatures (> 500°C) significant spontaneous breakup of C–H (and C–C) bonds takes place. Both the hydrocarbon and the organic hydrogen donor stabilizer are susceptible to significant bond cleavage. The question addressed here is can we estimate the highest temperature attainable for hydrogen donor stabilized jet fuels? We start these studies by first estimating this temperature using a very simple model with the following assumptions:

1. The stabilizer (hydrogen donor) is 100 % effective—all free radicals formed under pyrolysis are immediately captured and do not participate in further fuel degradation.
2. The only cause of fuel degradation is the thermal breakup of C–H bonds.

We can calculate the characteristic time of the elementary reaction for breaking the bond as:[2]

$$\tau = \tau_0 e^{W/kT} \tag{1}$$

where τ_0 is the period of elementary vibration for the molecule:

$$\tau_0 = 10^{-12} \ldots 10^{-13} \text{ sec} \tag{2}$$

W is the height of the barrier, k is the Boltzmann constant, and T is the temperature. From this formula we have:

$$T = \frac{W}{k} \frac{1}{\ln(\tau / \tau_0)} \tag{3}$$

The strength of the C–H bond, generally speaking, depends on the environment. Nevertheless a good estimation[3] for it is:

$$\frac{W}{k} \sim 40.76 \times 10^3 \text{K} \tag{4}$$

This led to the following temperature values for various values of τ:

τ (sec)	T (°C)
1	1090
60	920
3600	800
36000	730

In this model the amount of unaffected jet fuel exponentially decreases with time. The parameter τ is the time after which only 1/e = 0.37 of the original hydrocarbons remains unaffected. In other words, 63% of the original fuel has degraded. At a temperature of ≈1000°C, two-thirds of the fuel has degraded in the first second. At ≈900 °C it happens in about one minute, at ≈800 °C in the first hour, and at ≈700 °C after more than 10 hours. In subsequent work, we planned to produce degradation vs. time curves at different temperatures, consider more exact estimates for lower temperatures, and introduce less than 100% effective stabilizers in the model.

---

[1] Yoon, E, M. et al. *Energy & Fuels*. 1996. 10. 812.

[2] Clark, I. D. and R. P. Wayne. "The Theory of Elementary Reactions in Solution." *Comprehensive Chemical Kinetics*. Amsterdam, London, New York: Elsevier. C. H. Bamford and C. F. H. Tipper, Eds. 1969.

[3] Zeldovich, Y. B. et al. *The Mathematical Theory of Combustion and Explosions*. Consultants Bureau: New York; London. 1985.

4.15 DESIGN OF SUPERIOR STABILIZERS

This study appeared in *Advanced Thermally Stable Jet Fuels, Technical Progress Report, January – March 1998.*

Introduction

Although tetralin (THN) and benzyl alcohol (BzOH) exhibit contrasting stabilities in the pyrolysis and autoxidation regimes respectively, a simple combination of the pertinent structural features of both molecules, in a series of novel hybrids, may lead to enhanced complementary stabilization across a broader range of temperatures. We previously investigated several speculative synthetic routes to the compounds of interest; in this study we focus on producing practical quantities necessary for a wide range of exploratory testing.

Our initial route to the β-hybrid **1**, Scheme 1, may be more problematic than first expected, as it appears a mixture of both α- and β-isomers are produced, in contrast to the reported literature. We are seeking an improved separation technique, although we still intend to test this initial mixture in its own right.

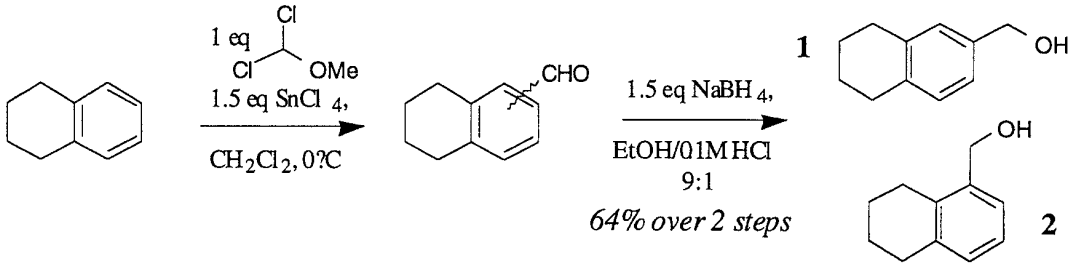

Scheme 1

A solution already presented to the issue of regioselective control is the direct carbonylation of triflate **3**, Scheme 2. After some initial optimization this reaction was found to proceed well on a small scale, under 1 atmosphere of carbon monoxide. However, attempts to increase scale resulted in exclusive reduction to tetralin.

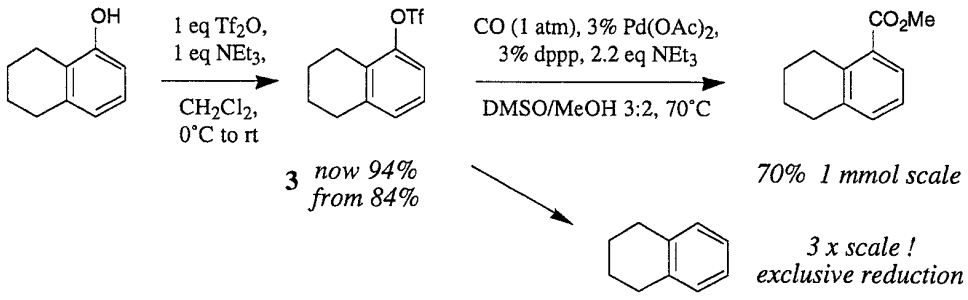

Scheme 2

We surmised that this was simply a problem of CO availability in the reaction vessel. Indeed, we found that use of higher pressures (≈40 psi) in a sealed apparatus (Parr high pressure reactor) under otherwise identical conditions afforded the required ester in near-quantitative yields (10 x scale). A simple reduction furnishes the α-hybrid. An analogous route to the β-hybrid **2** is currently sought, thus avoiding the problems of regioselectivity previously experienced.

Because we previously investigated several speculative synthetic routes to a series of novel hybrid stabilizers with enhanced capabilities across a broader range of temperatures, practical production of quantities necessary for a wide range of exploratory testing now proved paramount. With pure α-hybrid **1** at hand, as well as an expedient mixture of the two isomers, only the β-hybrid **2** remained to be synthesized.

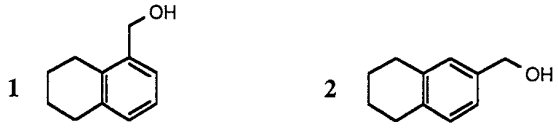

Our initial route to the β-hybrid **2** exhibited poor regioselective control, so we resolved the issue by direct carbonylation of triflate **4**, Scheme 1. An analogous approach to the α-hybrid had proved satisfactory, whereas use of moderate pressures (about 40 psi CO) in a sealed apparatus (Parr high-pressure reactor) afforded the required α-ester in near quantitative yields, application of this methodology in the β-case under otherwise identical conditions gave a significantly lower yield.

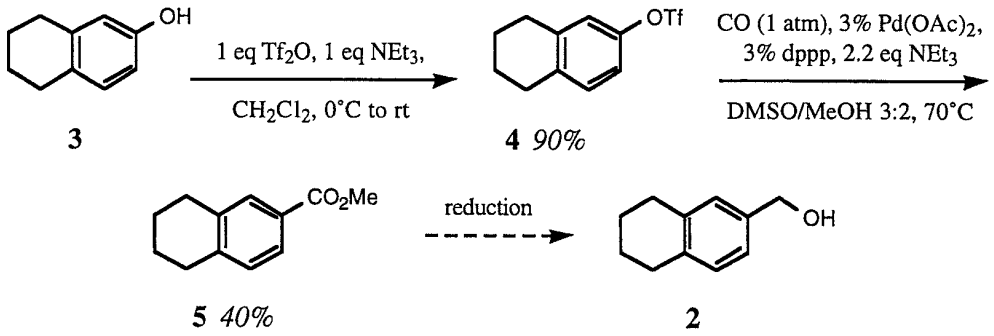

Scheme 1

One possible explanation for this apparent difference in reactivity can be invoked upon consideration of the catalytic pathways involved, Scheme 2. As can be seen in the α-case, equilibration from an initial Pd(II) complex to the acyl palladium species is driven by release of considerable *peri*-type steric strain; in the β-case no such incentive exists, thus leading to the overall slower rate of ester formation.

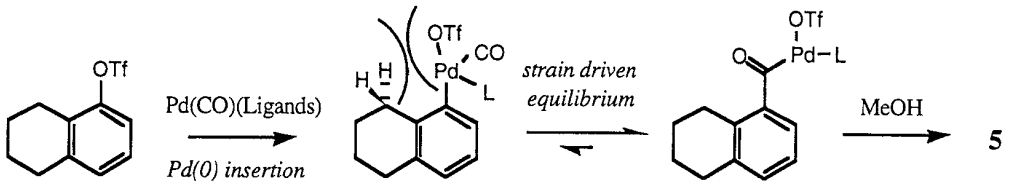

Scheme 2

Of particular concern was a rather disappointing carbonylation in our route to the β-hybrid **2**. Whereas use of moderate pressures (≈40 psi CO) in a sealed apparatus (Parr high pressure reactor) afforded the analogous α-ester **3** in near quantitative yields, application of this methodology in the β-case under otherwise identical conditions proved somewhat less adequate. Fortunately, a simple doubling of the initial catalyst loading (6%) and increased reaction time (3 days) afforded the intermediate ester **4** quantitatively. Ensuing hydride reduction furnished the required alcohol **2** (albeit in somewhat lower isolated yield due to some accidental sample loss.) Routes to both regio-isomers **1** and **2** are shown below, in Scheme 1.

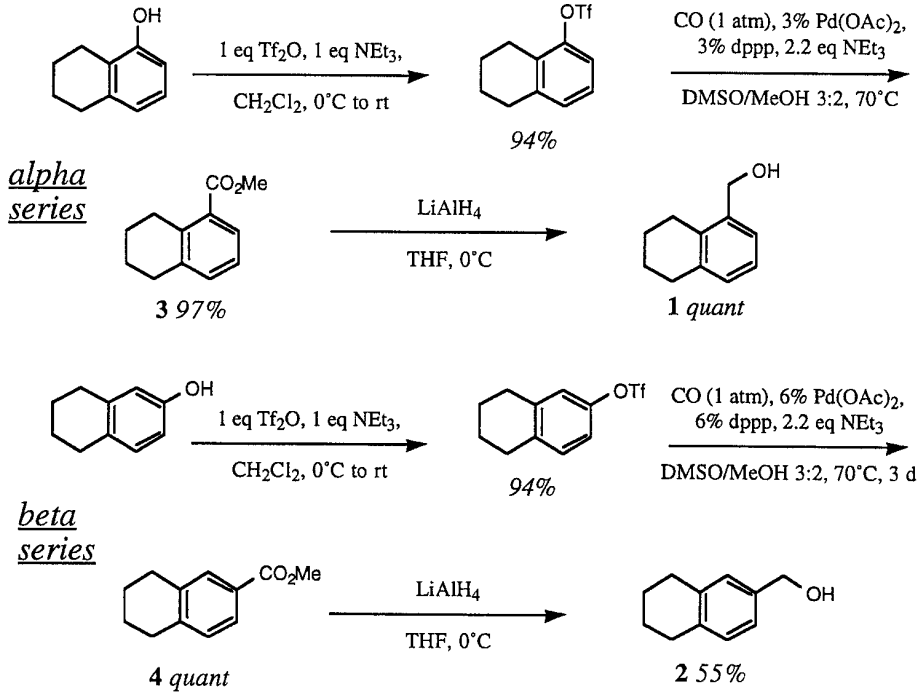

Scheme 1

4.16 Low-Temperature Oxidation Resistance of Thermal Stabilizers

This study appeared in *Advanced Thermally Stable Jet Fuels, Technical Progress Report, January – March 1998.*

Introduction

Hindered phenols such as 2,6-di-*t*-butyl-4-hydroxytoluene (BHT) are effective antioxidants for jet fuels in the autoxidative regime, but unfortunately accentuate degradation in the pyrolysis regime, because the *t*-butyl side groups cleave at high temperatures and are an additional source of free radicals. While we have found sterically hindered phenolic molecules in the 2 and 6 positions to be the most effective antioxidants at relatively low temperatures, other phenolic molecules have shown at least some antioxidative activity. We surmised that phenolic molecules without cleavable side groups might protect both the jet fuel and the high temperature stabilizers—benzyl alcohol (BzOH), tetralin (THN), and tetrahydroquinoline (THQ)—as the fuel passes through the autoxidative temperature regime. Initial results from scouting experiments demonstrated that Dod mixtures containing 200 ppm of phenol (PhOH) or 2,6-dimethylphenol (DMPh) remained clear (albeit slightly colored) liquids with no evidence of phase separation or solid formation for up to 4 hours at 250°C under an initial pressure of 100 psi air. This was an improvement over the results obtained for neat Dod, which showed evidence of phase separation after 3 hours of thermal stressing at 250°C.

The important issue became whether the addition of PhOH to a Dod mixture containing BzOH, THN, or THQ, could protect both the hydrocarbon fuel and the high temperature stabilizer while the mixture passed through the autoxidative regime. To date, our results indicate that this is not possible. In the case of Dod mixtures containing 5% THQ and varying amounts of PhOH ranging from 200 ppm to 1%, the mixtures became highly colored with obvious phase separation after 1 hour at 250°C under 100 psi air. Evidently, as discussed in previous reports, THQ preferentially oxidizes and the PhOH is not an effective antioxidant for THQ. The effect of PhOH in the analogous THN and BzOH mixtures was less obvious, but appears to follow a similar trend.

In recent years we have identified several hydrogen donors that have considerable potential as high temperature thermal stabilizers for jet fuels.[1] Three in particular have proven effective in model studies at temperatures above 400°C: tetrahydroquinoline (THQ), tetralin (THN), and benzyl alcohol (BzOH). Although THQ and tetralin are excellent hydrogen donors in the pyrolysis regime (> 400°C), this outstanding reactivity makes them susceptible to autoxidation at lower temperatures (250°C).[2] Conversely, BzOH, although not quite as effective under pyrolysis conditions, readily survives passage through the autoxidation regime. Hindered phenols such as 2,6-di-tert-butyl-4-hydrotoluene (BHT) are effective antioxidants for jet fuels in the autoxidative regime, but actually accentuate degradation in the pyrolysis regime because the t-butyl side groups cleave and produce additional radicals.[2]

Bearing this in mind, we considered whether it was possible to prevent the degradation of jet fuels over a broad temperature range by using a combination of high and low temperature additives. Our concept involved the possibility that the low temperature additive would protect the fuel in the autoxidative regime and the large excess of high temperature stabilizer would "mop up" any additional free radicals formed in the pyrolysis regime. Accordingly, we initiated

a program to stress jet fuels containing both low and high temperature additives in tubing bombs during a temperature ramp from room temperature to 425 °C over a period of time (initially 1 hour). The experimental methodology has not yet been refined to our satisfaction, but some preliminary experiments have been performed with jet fuel containing BzOH and BHT. Reproducibility is a concern and these experiments will require the design of a more sophisticated piece of equipment than currently exists.

Experimental

The overall concept of the scouting program designed to test jet fuel mixtures containing both low and high temperature stabilizers is straightforward. For these simple scouting studies, we intend to subject tubing bombs containing the fuel mixtures in the presence of air to a temperature ramp over a relatively short period of time (< 15 minutes) from room temperature (or a moderately elevated temperature such as 250°C) to 425°C. This has turned out to be a more formidable task than originally thought, but some progress has been made. Heating of the tubing bombs was accomplished using three 1000-watt heating elements in an air-fluidized sand bath unit fitted with a temperature controller. The existing temperature controller does not permit the setting of a constant rate of heating and the sand bath can only be heated at the variable rate of 3°-8°C per minute. Under these conditions, 2 hours are required to ramp from ambient temperature to 425°C. Making some adjustments, we managed to accentuate the rate of heating from room to 425°C time to approximately one hour, but this is still not satisfactory for our purposes.

Preliminary experiments of jet fuel mixtures containing 200 ppm 2,6-di-tert-butyl-4-hydrotoluene (BHT) with 5% wt of either benzyl alcohol (BzOH), tetraline (THN), or tetrahydroquinoline (THQ) performed under 100 psi of air showed slight improvement, but were not very encouraging. However, any conclusions would be premature prior to improving the heating rate and reproducibility of the current sand bath equipment.

---

[1] Coleman, M. M., L.Selvaraj, and M.Sobkowiak. *Advanced Thermally Stable Jet Fuels, Technical Progress Report, October – December 1995*. 92PC92104-TPR-14. 1996

[2] Nixon, A. C. *Autoxidation and Antioxidants*. New York: Interscience. W.O.Ludenberg, Ed. 1962. II.

TASK 5. EXPLORATORY STUDIES ON THE DIRECT CONVERSION OF COAL TO HIGH QUALITY JET FUELS

5.1 PRODUCTION OF JET FUELS FROM COAL

This study is explained in detail in *Advanced Thermally Stable Jet Fuels Technical Progress Report, August–October 1992.*

Introduction

Cycloalkanes (cyclohexanes and decalins) are jet fuel components that possess high thermal stability. Using coal as the parent material to produce these compounds is desirable, because coals contain aromatic and hydroaromatic molecules that, in principle, could be hydrogenated to cycloalkanes. Coals are diverse in composition, so we must characterize candidate feed stock coals to determine the best candidates for jet fuel production (i.e., those that have high populations of small aromatic units that could be converted to the desired cycloalkanes). This work begins the process of comparing products from liquefaction and determining the optimum reaction conditions and the best catalyst to use for the production of high quantities of thermally stable jet fuel.

Experimental

We analyzed two coals—DECS-6 (Blind Canyon) and DECS-12 (Pittsburgh #8). The coals were reacted at two different reaction conditions for baseline experiments—360°C for 1 hour and 425°C for 1 hour. Specifics of the experimental conditions can be obtained from the original report.[1]

Results

The ^{13}C-NMR indicated that the Pittsburgh #8 (DECS-12) coal was more aromatic than the Blind Canyon (DECS-6). Both contain phenol and ether functional groups, while DECS-6 also contains carbonyl and carboxyl functional groups. The main difference between the two coals, as observed by NMR data, is that DECS-6 is relatively more alkane-like than DECS-12.

There was a marked increase in conversion when stressed at 425°C versus 360°C. This increase is accompanied by a decrease in the yield of THF-soluble DCM insolubles and an increase in the DCM solubles + gas.

In the analysis of the residues, the hexane-soluble fraction and distillate reflected the changes that occur from raw coal to the reaction at 360°C to the reaction at 425°C:

DCS-6. The raw coal had a high percentage of alkanes with some occurrence of phenol, alkyl phenols, alkyl benzenes, and alkyl naphthalenes. In the residue produced at 360°C stressing, the phenols, alkyl naphthalenes, alkyl benzenes and alkanes/alkenes were no longer present when observed in the residue flash pyrolysis and NMR, yet the hexane-soluble fraction showed an increase in some of these same compounds. The residue at 425°C showed even fewer products of pyrolysis (i.e., alkanes/alkenes), while the hexane-soluble fraction had a definite increase in alkanes, alkyl naphthalenes, and prist-1-ene.

DCS-12. The raw coal was characterized by phenols, alkyl naphthalenes, and alkyl benzenes, but no alkanes. However, like DCS-6, the loss of these compounds was obvious in the

flash pyrolysis of the residue at 425°C, and a corresponding increase also occurred in the distillate and hexane-soluble fraction.

Future studies will seek to determine whether the liquefaction products are produced entirely from the "mobile phase" of coal, or whether some of the products result from the cracking of the heavier THF-soluble/DCM-insoluble fraction or from the coal itself.

---

[1] Schobert, H. H. et al. *Advanced Thermally Stable Jet Fuels, Technical Progress Report, August 1992 – October 1992*. 1992. 63.

5.2 Characterization of Isolated Resinite Maceral

This study is explained in detail in *Advanced Thermally Stable Jet Fuels Technical Progress Report, November–January 1993.*

Introduction

The resinite maceral, which composes at least 5% of the Blind Canyon DECS-16 (Utah) coal, has previously been shown by spectroscopic techniques to be sesquiterpenoid in nature. The structure of sesquiterpenoid resinites is comprised of a polycadinene-like polymer, as well as a significant portion of mobile bicyclic alkanes that are representative of the polycadinene backbone.[1] Because of the cycloparaffinic nature of sesquiterpenoid resinites and the thermal stability of these compounds, coals that are rich in resinite are possible precursors in the production of thermally stable jet fuel from coal.

This study attempted to isolate the resinite maceral from the Blind Canyon coal by hand-picking and analyzing the pure product to determine whether or not the resinite is composed primarily of a polycadinene polymer and a bicyclic sesquiterpenoid volatile fraction, other researchers suggest. From this data we hope to obtain a molecular model of the resinite maceral.

Experimental

The resinite maceral was isolated from the coal by hand-picking and purified by extraction with hexane. The hexane-soluble fraction, which contained the pure resinite, was filtered by passing it through a 0.2 μm filter attached to a 10 mL syringe. The hexane was then evaporated from the resinite and the pure sample was dried in a drying oven at 110°C for 10 hours to remove any remaining solvent or moisture. Pyrolysis GC/MS was then carried out on the sample at temperatures of 710°C and 310°C for 10 seconds. The pyrolyzate was separated using a DB-17 capillary column coupled to a mass spectrometer fitted with a Technivent Vector 1 data system for detection and compound identification. Sample masses of 0.414 mg and 0.427 mg were used in the pyrolysis at 710°C and 310°C, respectively.

Solid state ^{13}C NMR experiments employing cross polarization with magic angle spinning (CPMAS) and dipolar dephasing (DDMAS) were performed with the experimental conditions described in the full report on this study.[2] The samples were analyzed using liquid and solid-state nuclear magnetic resonance spectrometry (NMR) and pyrolysis/gas chromatography/mass spectrometry (py-GC/MS)

Conclusions

From the data presented above, we concluded that the DECS-16 resinite does contain a substantial amount of occluded material, which appeared to be cadinene dimers and triterpenoids that are easily removed from the polymer backbone. Pyrolysis at 710°C increased the yield of bicyclic naphthalenes and hydronaphthalenes, suggesting that the polymeric make-up of this particular resinite is loosely based on polycadinene. It appears as if dehydrogenation induced by thermal maturation has occurred to some extent throughout the cadinene polymer. Solid-state NMR showed that approximately three out every 15 carbons were olefinic and less than one of the three olefinic carbons is protonated. This again suggests a deviation from the polycadinene structure. The data obtained from the liquid NMR analyses have aided in the assignment of

carbon functional groups that can be qualitatively related to a cadinene polymer and will be essential to the quantitative studies that follow.

To properly model the Blind Canyon DECS-16 resinite, we must remove the occluded material from the resinite polymer and repeat the experiments described above. The volatile compounds can then be analyzed by GC/MS, which will provide a better understanding of their contribution to the pyrolysis spectra and the solid and liquid-state NMR spectra. With this data, we can then create a computer model of the resinite polymer that is consistent with all of the acquired analytical data and, eventually, establish a computer model of the whole resinite.

---

[1] Anderson, K. B, Re. E. Winans, and R. E. Botto. "The Nature and Fate of Natural Resins in the Geosphere-II. Identification, Classification and Nomenclature of Resinites." *Organic Geochem.* 1992. 18(6). 829-841.

Crelling J. C. et al. "The Chemical Structure and Petrology of Resinite from the Hiawatha 'B' Coal Seam." *Energy & Fuels.* 1991. 5. 688-694.

Meuzelaar H. L. C. et al. "Chemical Composition and Origin of Fossil Resins from Utah Wasatch Plateau Coal." *Fuel Processing Technology.* 1991. 28. 119-134.

[2] Schobert, H. H. et al. Advanced Thermally Stable Jet Fuels, Technical Progress Report, February 1993 – March 1993. 1993. 46-47.

5.3 Statistical Models for Bituminous Coal: A Three-Dimensional Evaluation of Structural and Physical Properties Based on Computer-Generated Structures

This study is explained in detail in *Advanced Thermally Stable Jet Fuels Technical Progress Report, November 1992 – January 1993.*

Introduction

Coal is a highly heterogeneous material. Its structure depends on the diverse composite material entering into its composition (minerals and macerals) and also on its degree of maturation (rank). Even within a single maceral and rank there is a considerable degree of complexity. Nevertheless, many attempts have been made to model coal structure.

Given,[1] Wiser,[2] Solomon,[3] and Shinn[4] specifically attempted to model high-volatile bituminous coal, our subject of interest. Their models were constructed by a trial-and-error technique of manually fitting the analytical data. The amount of data for each model is small compared to the actual complexity of coal, and for all of the models, more than one structure can be built. The process for choosing one structure over another is unclear. All of the authors agree that their structure was just intended to represent an "average" coal model, with "average" defined as the mean value for a certain characteristic. However, because this value cannot be calculated if the size of the total population is not known (as was the case in the four studies), the models are more "arbitrary"than "average."

Computer-aided molecular design (CAMD) has been used to model in three dimensions the previously published coal structures.[1-4] The structures were refined by molecular mechanics and dynamics. Potential energy, true density, and microporosity were evaluated for each model.[5] Prior to using CAMD software, researchers must first determine the connectivity (i.e. the structural formula) of the studied molecule. This information is lacking for coal.

Many computer-aided structure elucidation (CASE) studies have been conducted in the past three decades to resolve, by computer, the general problem of retrieving a structure from analytical data. The technique can construct large molecular models from analytical structural data. In theory, any kind of quantitative and qualitative structural information can be introduced into the computer program. In practice, the computer technique successfully employs physicochemical analyses such as elemental analysis, functional group analysis, ^{1}H and ^{13}C NMR, and flash pyrolysis coupled with gas chromatography and mass spectrometry (flash pyrolysis/gc/ms). Generally, more than one model can be built from a set of analytical data, particularly in the case of macromolecules such as coal. Knowledge of the number of possibilities is crucial for a true elucidation.

The SIGNATURE program was developed to achieve true elucidation. It is based on an isomer generator[6] and can determine the number of possible models that can be built from a set of analytical data. Knowing the number of possibilities, the user can request depiction of one, several, or all of the models.

In a study of vitrinite from HvC bituminous coal, this program was used to generate 3D models for a molecule containing between 140 and 180 carbon atoms.[7] The analytical data used as input to the program were provided by elemental analysis, ^{13}C NMR, and flash

pyrolysis/gc/ms provided from a study by Hatcher et al.[8] Even with this reasonably small number of atoms, the number of possible models was enormous—nearly one million. Clearly, for coal, even for a specific rank and a pure maceral, the number of models is too large to build all of them, and too large to chose one model as representative of all the possibilities. This purpose of this study was to determine how many and which structures must be selected and constructed.

Method

The SIGNATURE program was used to generate models from analytical data, to define a sample design, to compute molecular formulas and molecular weights, and to define energetic and physical characteristics. A full explanation of these activities appears in the original report.[9]

Results

Our intention was to focus exclusively on a sample of models for vitrinite from HvC bituminous coal, rather than attempting to define an "average" coal model. We used a piece of coalified wood, a fossil stem recovered from a lacustrine shale from the Midland Formation (Triassic) near Culpeper, Virginia. In a previous report, we assumed that this sample was representative of vitrinite coalified to a rank of hvC bituminous coal.[10]

The analytical data supplied to the SIGNATURE program are summarized in **Table 5.3-1**. The SIGNATURE program was run and all of the solutions containing 333 carbon atoms were searched. This number of carbons was chosen considering the computational time and the fact that all of the fragments listed in Table 5.3-1 must be present in the models. The best solution of the signature equation, $C_{333}H_{302}O_{16}$, is listed in column 2 of the table. The deviation between model and analytical data is listed in column 3. The SIGNATURE equation can provide a large number of solutions with different deviations between model and data. The program was asked to determine all of the solutions containing 333 carbon atoms and having an average deviation between model and quantitative analytical data of less than one percent. Five solutions were found, as shown in **Table 5.3-2**. The average deviations between models and quantitative analytical data are listed in the last row of the table. Each solution contains the same quantity of each fragment as listed in Table 5.3-1, but different quantities of inter-fragment bonds.

The fragments that form the models are mainly alkylbenzenes and alkylphenols. These types of fragments, when randomly connected, generate a highly cross-linked structure (molecular weight between cross-link less than 150 amu) with a high potential energy (more than 10 kcal/atom-mole). However, a systematic construction of hydroaromatic sub-structures built from the aromatic fragments enables the molecular weight per cross-link to increase an average of 1000 amu and the potential energy to decrease nearly 2 kcal/atom mole.

Considering all of these previous observations, the SIGNATURE program was set up to build models using a two-stage procedure. First, a fragment was randomly chosen and successively connected to other fragments. The program retained only the combinations that formed new five- or six-membered rings. This first stage was repeated for all of the fragments until no more possibilities of forming new ring systems remained. Using this procedure, the program constructed six disconnected hydroaromatic sub-structures using all of the fragments and 81 inter-fragment bonds. At this point only a few inter-fragments bonds remained. These

were used in the second stage to link or cross-link the hydroaromatic sub-structures. An illustrative example of this first stage procedure is diagrammed in **Figure 5.3-1**.

In the second stage, the final models were constructed by connecting and eventually cross-linking the hydroaromatic sub-structures together using the remaining inter-fragment bonds. Depending on the different solutions of the signature equation (Table 5.3-2), the six hydroaromatic sub-structures were connected using five to nine remaining inter-fragment bonds. **Figure 5.3-2** provides an example of this procedure for model $C_{333}H_{302}O_{16}$ in which nine inter-fragment bonds remained after performing the first-stage operation.

Computing the number of possible non-identical models that can be constructed is time consuming; the problem has an exponential algorithmic complexity. Limited by the computational power of our workstation, the number of possible models was evaluated only for the second stage of the construction procedure (after building hydroaromatic sub-structures). The total number of possible models that could be built during the second stage was 319,318.

The population of possible coal models is subdivided into five different C_{333} structures, which represent five different solutions of the signature equation. To build a sample which is a good representation of the entire population, the sample size of each C_{333} structure has to be proportional to the corresponding population of all of its possible isomers. Considering the population size of each C_{333} structure and the computational time required to build the structures and evaluate the different characteristics, we chose to build a sample of n1 = 15 structures comprising the following: 2 structures of $C_{333}H_{302}O_{16}$, 10 structures of $C_{333}H_{304}O_{16}$, 1 structure of $C_{333}H_{306}O_{16}$, 1 structure of $C_{333}H_{308}O_{16}$, and 1 structure of $C_{333}H_{310}O_{16}$. For each of the 15 models, minimum energy conformations were calculated and structural, energetic, and physical characteristics were evaluated, as were their means and variances. In short, with a sample of 15 structures, the mean potential energy of the entire population of models is 2.03 ± 0.03 kcal/atom-mole with a population deviation of 0.12 kcal/atom-mole.

Conclusion

All 15 of the constructed C_{333} models matched well with the quantitative analytical data with an average deviation of less than one percent. The cross-link densities we found were a direct consequence of the analytical data. From a structural point of view, a cross-link is a bond between the hydroaromatic substructures (i.e. an inter-fragment bond). The total number of inter-fragment bonds determined by the signature equation depends on the quantitative analytical data; therefore, greater or lesser amounts of inter-fragment bonds would produce more or less cross-links and larger deviations between models and data. The number of cross-links varies only between 2.5 and 5 for each C_{333} structure, and the molecular weight per cross-link averages 1205 amu with a standard deviation of 254 amu. This value agrees well with swelling experiments for acetylated and pyridine extracted bituminous coal, where the molecular weight per covalent cross-link ranges between 900 and 1500 amu.[11] Furthermore, the average number of aromatic fragments between cross-links (7.9) is in the range of values obtained from swelling experiments (4-8 aromatic fragments between cross-links).[12]

The potential energy increased slightly with the number of cross-links (1.85 kcal/atom for the model having 2.5 cross-links and 2.14–2.16 kcal/atom for the two models having 5 cross-links). The reverse trend was observed for the contribution of the non-bonded energy (49–51% for the models with 2.5 cross-links and 57 % for the two models with 5 cross-links). However,

overall, the energy values were clustered, and as a direct consequence, the variances were small. Another interesting point was observed when the structures were depicted on the computer monitor. Independent of the cross-link density, the global conformations appeared very similar. It was impossible to visually identify the structures containing the lower cross-link density. This suggests that even when the structures are not highly covalently cross-linked, they are held together by van der Waals interactions. A related observation is that no major changes in helium density and porosity were observed for the models containing different cross-link densities.

The computed helium density averaged 1.26 g/cc for all 15 C_{333} structures constructed and the population deviation was less than 2 percent of this value. This closely agreed with experimental results found for vitrinite at a rank of bituminous coal (1.25 - 1.30 g/cc).[13] The closed microporosity was almost nonexistent for most of the 15 models and was lower than 7% of the total micropore volume. The computed micropore volume average was 0.030 cc/g with a population deviation of 13 percent. The micropore volume was slightly lower than experimental values found for HvC bituminous rank (0.039-0.070 cc/g).[14] The low microporosity may have been caused by our model sizes; they were rather small compared to the particle sizes used in porosimetry experiments.

In summary, the physical properties that we calculated agreed well with experimental data. Further, the energetics and physical characteristics found for the different models were relatively close to each other and the variances were small. These observations suggest that each model is a reasonable representation of vitrinite. Perhaps the most important conclusion, however, is that we have successfully developed a technique that uses computing power to create a number of molecular models for coal based on actual quantitative and qualitative experimental data. And we have proven that the models, from a statistical viewpoint, are a good representation of the coal structure. Previous attempts at definitions of coal molecular structure, including previous computer models, necessarily included investigator bias and could not be proven to be representative or average coal structures. We concluded that, for the physical properties investigated, a sample of 15 structures is sufficient to statistically represent the entire population of vitrinite from HvC bituminous.

Table 5. Quantitative and Qualitative Analytical Data for HvC Bituminous Coalified Wood (Midland Stem). [22]

Parameter	Analytical Data	Model ($C_{333}H_{302}O_{16}$)	Deviation Analytical data - Model
	Quantitative data (normalized for 100 carbon atoms)		
C	100.0	100.0	-
H	92.0	91.8	0.2
O	5.0	4.6	0.4
f_a	62.5	63.0	-0.5
f_a^H	28.0	27.6	0.4
f_a^P	7.5	7.5	0.0
f_{al}	37.5	37.4	0.1
f_{al}^H	26.0	26.2	-0.2
f_{al}^*	11.5	11.2	0.3
Average deviation			± 0.26
	Qualitative data (weight % normalized to total aromatic fragments)		
benzene	3.3	2.0 (1)	1.3
totuene	4.8	4.8 (2)	0.0
C-2 benzenes	5.2	8.3 (3)	-3.1
C-3 benzenes	3.9	6.3 (2)	-2.4
phenol	3.6	2.5 (1)	1.1
o -cresol	5.7	2.8 (1)	2.9
m + *p* -cresol	13.0	8.5 (3)	4.5
2,4 dimethylphenol	12.0	9.6 (3)	2.4
other C-2 phenols	10.3	6.4 (2)	3.9
C-3 phenols	10.9	14.2 (4)	-3.3
C-4 phenols	4.8	3.9 (1)	0.9
alkylnaphthalenes	17.0	24.4 (6)	-7.4
alkyldibenzofurans	5.2	6.2 (1)	-1.0
methyl	-	(7)	
ethyl	-	(9)	
propyl	-	(3)	
C4-C22	-	(0)	

f_a = aromatic carbon, f_{al} = aliphatic carbon, f_a^H = protonated aromatic carbon, f_a^P = phenolic or phenolic ether, f_{al}^H = aliphatic carbon in CH or CH_2, and f_{al}^* = aliphatic carbon as methyl. As mentioned in the text, the weight percentages given by pyrolysis results are not an accurate representation of the quantities of fragments present in coal. For this reason, the values listed here are not taken quantitatively, and the SIGNATURE program considers the list of fragments only as qualitative information. Values indicated in parentheses are the quantities of each fragment corresponding to a molecule containing 333 carbon atoms.

Table 5.3-2. Solutions of the Signature Equation

Inter-fragment bonds	$C_{333}H_{302}O_{16}$	$C_{333}H_{304}O_{16}$	$C_{333}H_{306}O_{16}$	$C_{333}H_{308}O_{16}$	$C_{333}H_{310}O_{16}$
phenyl-phenyl	5	5	5	5	5
phenyl-alkyl	29	29	29	29	28
phenyl-oxygen	9	9	9	9	9
alkyl-alkyl	41	40	39	38	38
alkyl-oxygen	6	6	6	6	6
Total	90	89	88	87	86
Average deviation[a]	0.26	0.29	0.39	0.49	0.71

[a] The deviation is the average deviation between model and quantitative analytical data as calculated in Table 1.

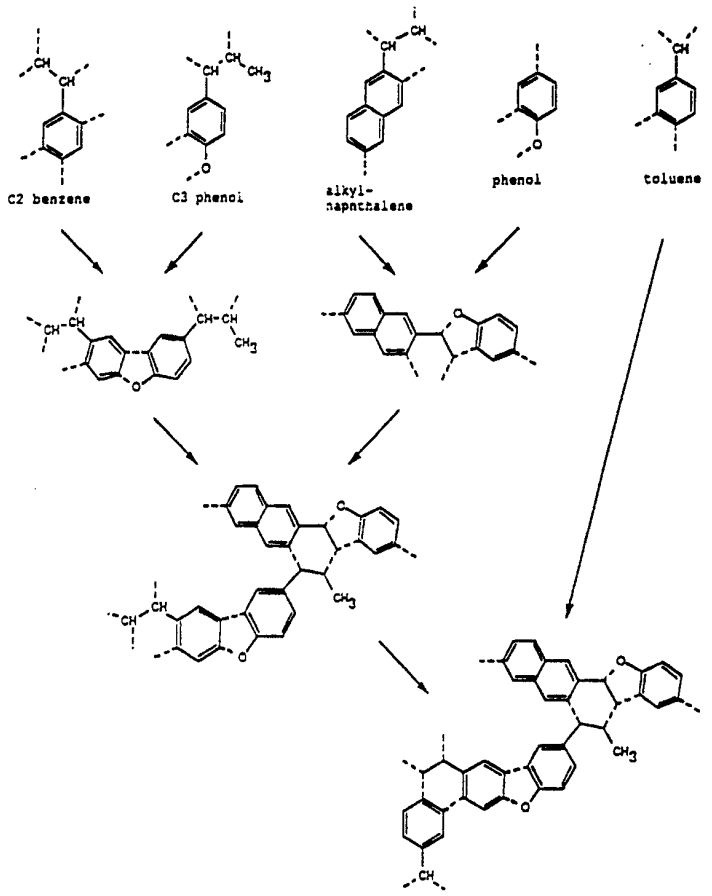

Figure 5.3-1. The Construction of a Hydroaromatic Substructure.

The initial fragments (at top) are identified by pyrolysis/GC/MS analysis. Dashed lines represent bonding sites. Our models were built using 86 to 90 inter-fragment bonds as determined by the signature equation. Each inter-fragment bond requires two binding sites to be created; therefore, the total number of bonding sites is 172 to 180. The bonding sites were chosen arbitrarily. Overall, there are 49 fragments and an average of 3.5 to 3.7 bonding sites per fragment.

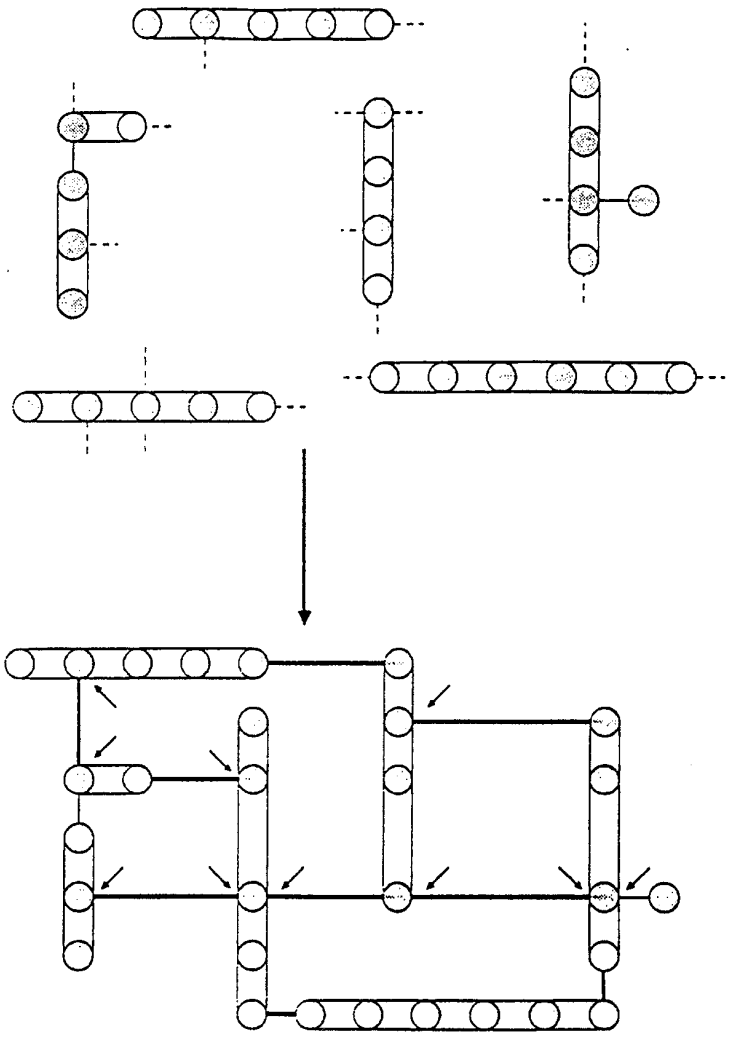

Figure 5.3-2. Example of Connection of Hydroaromatic Substructures. Using the convention of Flory and Rehner, there are five cross-links in this structure. The location of each 1/2 cross-link is noted by an arrow.

---

[1] Given, P. H. *Fuel.* 1960. 39. 147.

[2] Wiser, W. H. *NATO ASI Series C.* 1983. 124. 325.

[3] Solomon, P.R. *New Approaches in Coal Chemistry*, ACS Symposium Series No. 169. Washington, DC: American Chemical Society. 1981. 61.

[4] Shinn, J. H. *Fuel.* 1981. 63. 1187.

[5] Carlson, G. A. *Energy Fuels.* 1992. 6. 771.

[6] Faulon, J. L. *J. Chem. Inf. Comput. Sci.* 1992. 32. 338.

[7] Faulon, J. L. et al. *Fuel Process.Technology.* 1993.

[8] Hatcher, P. G. et al. *Energy Fuels.* 1992. 6. 813.

[9] Schobert, H. H. et al. *Advanced Thermally Stable Jet Fuels, Technical Progress Report, February 1993 – March 1993.* 1993.

[10] Hatcher, P. G. et al. *Energy Fuels.* 1992. 6. 813.

[11] Larsen, J. W., T. K. Green, and J. Kovac. *J. Org. Chem.* 1985. 50. 4729.

[12] Larsen, J. W., T. K. Green, and J. Kovac. *J. Org. Chem.* 1985. 50. 4729.

Green, T. K., J. Kovac, and J. W. Larsen. *Fuel.* 1984. 63. 935.

Brenner, D. *Fuel.* 1985. 64. 167.

Lucht, L. M. and N. A. Peppas. *Fuel.* 1987. 66. 803.

Lucht, L. M., J. M. Larsen, and N. A. Peppas. *Energy & Fuels.* 1987. 1. 56.

Hall, P. J., H. Marsh, and K. M. Thomas, K. M. *Fuel.* 1988. 67. 863.

[13] Crelling, J. C. *Proc 1987 Int. Conf. Coal Sci.* 1987. 119.

[14] Gan, H., S. P. Nandi, and P. L. Walker, Jr. *Fuel.* 1972. 51. 272.

5.4 Direct Coal Liquefaction: A Potential Route to Thermally Stable Jet Fuel

This study is explained in detail in *Advanced Thermally Stable Jet Fuels Technical Progress Report, April 1993 – June 1993.*

Introduction

The principal mechanism of fuel degradation at temperatures above 300°C is pyrolytic decomposition. Cycloalkanes are much more resistant to thermal degradation than are *n*-alkanes or alkylaromatics.[1] Indeed, decalin shows remarkable thermal stability even at 450°. Hydroaromatics, such as tetralin, are also quite stable at these temperatures when reacted neat[1, 2] and can suppress the thermal degradation of other compound classes, such as *n*-alkanes, in hydrogen-transferring pyrolysis.[3] Thus, high concentrations of cycloalkanes and hydroaromatics in a real fuel (which may contain dozens of components) could provide significant thermal stability.

Direct liquefaction of coal could potentially provide a facile route to liquids boiling in the jet range and containing the desired cycloalkanes and hydroaromatics. The key chemical steps in this process would be the liberation of the aromatic units by cleavage of whatever crosslinks or other interactions hold them in the coal structure, and the hydrogenation of the aromatics to cycloalkanes or hydroaromatics. Clearly, coals showing good reactivity during liquefaction are desirable. Selecting coals containing a relatively low population of crosslinks would facilitate liberation of the aromatic ring systems. Using coals in which a preponderance of the aromatic structures are naphthalene derivatives allows direct hydrogenation to decalins and tetralins, minimizing the downstream processing required. Similarly, a low content of heteroatoms minimizes downstream treatment of the liquids. Not all of these features are available in coals of a given rank. High reactivity and small aromatic units are characteristics of coals at the low end of the rank range. Low crosslink density and relatively low heteroatom content are more likely found in the bituminous rank range. Thus the selection of potential feedstocks may involve a compromise to achieve a reasonable balance among these desired characteristics.

We conducted an exploratory study to test the hypothesis that forming high yields of cycloalkanes and hydroaromatics that boil in the jet range is possible by (1) selecting feedstocks that contain a high proportion of small aromatic units and relatively few crosslinks and (2) choosing catalyst and reaction conditions to liberate the desirable structural features of the coal. In this study, we subjected two bituminous coals to temperature-programmed liquefaction and reported the reactions, particularly the effects of coal, solvent, and catalyst on conversion, product slate, and product quality.

Experimental

The coals we studied were DECS-6 (Blind Canyon) and DECS-12 (Pittsburgh #8). Pyrene and 9,10-dihydrophenanthrene (DHP) were used as liquefaction solvents. The reactors were charged with 4 g coal and 4g of the desired solvent. For those reactions in which a catalyst was used, coal was dried and impregnated with ammonium tetrathiomolybdate (ATTM) or $NiCl_2$. The reactors were pressurized to 7 MPa with H_2 at ambient temperature. The reactor is immersed in a sand bath preheated to 200°C and held for 15 minutes. The temperature is then ramped to 425° at 7°/min, and is held at 425° for 30 or 60 minutes. At the end of a reaction, the

reactor is quenched by immersion in cold water. For the sake of brevity, further details of the experiment and analysis can be obtained from the original Technical Progress Report.[4]

Results and Discussion

The principal experimental results are summarized in **Table 5.4-1**. The DCM-solubles include gas yields, and gas yields were ≤5% for all reactions. The principal compound classes identified in the hexane-soluble portions of the DCM-soluble products are summarized in **Table 5.4-2**. For convenience, we refer to three ratios:

1. THF-solubles to the sum of the DCM-solubles expressed as THF/DCM
2. Aromatic compounds of one ring to those with two rings or more (i.e., benzenes + phenols to naphthalenes + phenanthrenes + polynuclear aromatics), expressed as B+P/≥2-ring
3. The total aromatic compounds to alkanes, expressed as ΣAro/ΣAli.

For reactions without a catalyst, conversions to DCM-solubles depend mainly on solvent. For a given solvent, conversions of the two coals are similar. However, DHP is clearly superior to pyrene for increasing conversions. Although pyrene is well known as a hydrogen shuttler, DHP is a potent hydrogen donor. Furthermore, in non-catalytic reactions, most of the hydrogen consumption comes from the solvent rather than gas-phase H_2, so DHP's substantially higher conversions are not surprising.

Although the conversions of the two coals in a given solvent are comparable, and the comparative effects of pyrene versus DHP are comparable, the change in product slates with increased conversion is quite different between the two coals. With DECS-6, the increased conversion effected by DHP comes largely via formation of THF-solubles. In contrast, THF/DCM is essentially unchanged for reactions of DECS-12 in these solvents.

	Solvent	DECS-6	DECS-12
THF/DCM Ratio	Pyrene	0.23	0.37
	DHP	0.64	0.33
B+P/≥2-Ring Ratio	Pyrene	0.98	1.19
	DHP	0.73	0.83
ΣAro/ΣAli Ratio	Pyrene	1.46	1.19
	DHP	1.80	0.83

DHP reduces the proportion of aromatics with ≥2 rings in the DCP-solubles, and increases the proportion of total aromatics to alkanes, relative to the results obtained using pyrene. The effect of solvent on the B+P/≥2-ring ratio for DECS-12 is quite similar.

A remarkable difference is seen in the ΣAro/ΣAli ratio for DECS-12 relative to DECS-6. For both coals, reaction in DHP increases this ratio relative to reaction in pyrene, but the products from reaction of DECS-12 have so few n-alkanes that there is an order-of-magnitude difference in the ΣAro/ΣAli ratios. Characterization of these two coals by flash pyrolysis GC/MS has shown the preponderence of n-alkanes in DECS-6 relative to DECS-12.[5]

For reactions in pyrene, the addition of catalyst enhances conversion of both coals. Using either MoS_2 or $NiCl_2$, the conversion of DECS-6 increases by about 30 percent. Both catalysts increase the conversion in the hydrogen-shuttling solvent pyrene to the same level as obtained by using the strong hydrogen donor solvent DHP without a catalyst. However, the two catalysts have quite different effects on the product slate. $NiCl_2$ appears to increase the depolymerization of DECS-6, but not alter the relative proportion of products; in comparison, MoS2 seems both to increase the depolymerization and shift the product slate toward lighter products.

An important point to remember is the fact that these product classifications are based on solubility behavior, which could possibly mask differences in molecular composition. For $NiCl_2$/pyrene reaction of DECS-6, there is a substantial increase in the amount of naphthalenes in the DCM-solubles relative to the MoS_2-catalyzed reaction, which actually decreases the B+P/≥2-ring ratio. With DECS-12, catalytic reaction in pyrene also increases conversion to about the same value as obtained in non-catalytic reaction in DHP. Use of MoS_2 shifts the product slate to lighter products, as occurred with DECS-6, although the effect is not quite so pronounced for DECS-12. With $NiCl_2$, however, the proportion of preasphaltenes in the product is actually enhanced relative to reaction without catalyst. In this case, the effect of $NiCl_2$ catalysis is quite different for the two coals. However, when product composition is examined, a reduction of the B+P/≥2-ring ratio is observed for $NiCl_2$-catalyzed reaction of DECS-12 in pyrene relative to MoS_2. This can (as in the case of DECS-6) be attributed to a large increase in naphthalenes and a loss of phenols in the DCM-solubles. The reduction of phenols and the concurrent increase in THF/DCM ratio could indicate that retrogressive reactions are promoted by the $NiCl_2$ cracking without the stabilization of hydrogen from an H-donor or hydrogenation catalyst.

The effect of reaction time was evaluated only for DECS-6, by comparing reactions with high-temperature holding times of 30 and 60 minutes for both MoS_2 and $NiCl_2$ in pyrene. Little change was observed in either conversion or product slate. The slight changes in conversion or product slate observed after 60 minutes would not likely compensate for the additional processing costs associated with a doubling of the residence time at 425°.

The combination of the MoS_2 hydrogenation catalyst and DHP donor solvent in reaction of DECS-6 provided the highest conversion observed in the present work, 95%. The product slate was about the same as that obtained for MoS_2 and pyrene, with THF/DCM of 0.06. Liquefaction of DECS-6 in DHP without catalyst actually increased the THF/DCM ratio relative to non-catalytic reaction in pyrene. Consequently, the catalytic effect of the added MoS_2 seems important for shifting the product slate to lighter—on the basis of solubility classifications—products, regardless of whether a hydrogen donor or hydrogen shuttler is used as solvent.

Using DHP with $NiCl_2$ produced no increase in conversion relative to that of $NiCl_2$ and pyrene. There is, however, a shifting of the THF/DCM ratio to 0.15, compared with 0.19 for $NiCl_2$/pyrene, and 0.23 for non-catalytic reaction in pyrene. The combination of catalyst and donor solvent produces the lowest values of the B+P/≥2-ring ratio observed for this coal, 0.46 for MoS_2-catalysis and 0.53 for $NiCl_2$. Thus, 40–43% of the DCM-solubles from DECS-6 for catalytic reaction in DHP are naphthalene derivatives.

For liquefaction of DECS-12 in pyrene, $NiCl_2$ provided higher conversions than MoS_2, 84 and 77%, respectively. The same superiority of $NiCl_2$ is observed when DHP is used as the

solvent, the conversions being 89 and 85%, respectively. For both coals, a change of solvent from pyrene to DHP when MoS_2 is used as the catalyst produces essentially the same effect—an additional 6-8% of conversion, and a reduction of THF/DCM to 0.06. On the other hand, the change of solvent has different effects for the coals when $NiCl_2$ is used as the catalyst. For DECS-12, an increase in conversion and significant shift of THF/DCM is observed when DHP is used instead of pyrene. The combination of a catalyst and donor solvent causes significant reductions in the B+P/≥2-ring ratio, as was seen for DECS-6. Indeed, nearly 50% of the DCM-solubles from MoS_2/DHP reaction of DECS-12 are naphthalene derivatives.

An additional aspect of $NiCl_2$ catalysis is its ability to reduce yields of phenols relative to similar reactions in the presence of MoS_2. For all but one coal/solvent combination, the concentration of phenols in the DCM-solubles is lower for the $NiCl_2$-catalyzed reaction relative to MoS_2, the single exception being DECS-6/DHP. But if there is a reduction in phenols when using $NiCl_2$, and a concurrent increase in THF/DCM, the lost phenols could be participating in retrogressive reactions by crosslinking to THF-solubles. Soloman et al[6] have suggested that functional groups containing oxygen participate in retrogressive reactions. These crosslinking reactions apparently are repressed when a donor solvent or a good hydrogenation catalyst is used.

Conclusions

Attaining the highest conversion with either coal under these reaction conditions clearly requires the presence of the donor solvent in addition to a catalyst. For DECS-6, 95% conversion is achieved for MoS_2/DHP reaction. Any other combination of solvent, catalyst, or both provides conversions in the range 83–89%. For DECS-12, the highest conversion, 89%, was obtained in $NiCl_2$/DHP reaction; the other combinations of solvent and catalyst gave conversions of 77–85%. For either coal and either solvent, the lowest values of THF/DCM are invariably obtained with MoS_2 catalysis. THF/DCM ratios of 0.06 can be achieved for either coal with this catalyst, along with conversions in the 85–95% range. Furthermore, MoS_2/DHP liquefaction produces DCM-solubles that are 40–50% naphthalene derivatives. The subsequent hydrogenation of this product could, in principle, provide a liquid that contains ≈50% of the desirable, high-thermal-stability decalins and tetralins.

With careful selection of the feedstock, we can achieve 85–95% conversions with THF/DCM ratios <0.1 and 40-50% of the DCM-solubles being naphthalenes. We have not yet attempted to improve these results by optimizing reaction conditions. The DCM-solubles are highly aromatic, with ΣAro/ΣAli approaching 30 for some reactions of DECS-12. Both a hydrogenation of the product and a hydrodeoxygenation to remove phenols, neither of which is an insignificant operation, must still be investigated. Nevertheless, if these two further transformations can be effected, either by some alteration of reaction strategy such as "reverse temperature staging"[6] or by separate subsequent reactions, the prospect exists for direct conversion of bituminous coals to high yields of liquids containing high concentrations of desirable decalins and tetralins. Such a product could be the foundation of a jet fuel with excellent high-temperature stability characteristics.

Table 5.4-1. Liquefaction Conversion Data for DECS-6 and DECS-12

Expt #	Temp	Catalyst	Solvent	TC	THF-Sol	DCM-Sol	THF/DCM
tb 6-8	TPL, 425-30	none	pyrene	55.2	10.5	44.7	0.235
tb 6-9	TPL, 425-30	none	DHP	83.0	32.5	50.5	0.644
tb 6-3	TPL, 425-30	MoS_2	pyrene	89.3	5.1	84.2	0.061
tb 6-4a	TPL, 425-30	$NiCl_2$	pyrene	83.0	13.1	69.9	0.187
tb 6-10	TPL, 425-30	MoS_2	DHP	95.0	5.7	89.3	0.064
tb 6-11	TPL, 425-30	$NiCl_2$	DHP	83.2	11.0	72.2	0.152
tb 6-6	TPL, 425-60	MoS_2	pyrene	88.2	3.6	84.6	0.043
tb 6-7	TPL, 425-60	$NiCl_2$	pyrene	87.3	12.7	74.6	0.170
tb 12-5	TPL, 425-30	none	pyrene	51.9	14.0	37.9	0.369
tb 12-6	TPL, 425-30	none	DHP	81.7	20.1	61.6	0.326
tb 12-3	TPL, 425-30	MoS_2	pyrene	76.8	14.5	62.3	0.233
tb 12-4	TPL, 425-30	$NiCl_2$	pyrene	84.2	28.3	55.9	0.506
tb 12-7	TPL, 425-30	MoS_2	DHP	85.4	5.1	80.3	0.064
tb 12-8	TPL, 425-30	$NiCl_2$	DHP	88.7	13.1	75.6	0.173

TC = total conversion

DCM-Sol = DCM-Solubles + Gas Yield

THF/DCM = ratio of THF-Solubles to DCM-Solubles

Table 5.4-2. Percent Area of Major Compounds in GC of Hexane-Solubles

Expts	Benzenes	Phenols	2-Ring	3-Ring	4-Ring +	Alkanes	B+P/2-Ring	ΣAro/ΣAli
tb 6-8	3.7	25.6	27.7	2.3	0.0	40.6	0.98	1.46
tb 6-9	8.9	18.2	35.4	n.d.	1.8	35.8	0.73	1.80
tb 6-3	14.6	30.6	21.0	3.2	0.0	30.5	1.87	2.28
tb 6-4	19.2	25.8	29.4	3.8	0.9	21.0	1.32	3.77
tb 6-10	0.5	19.4	40.5	n.d.	3.1	36.6	0.46	1.73
tb 6-11	2.6	20.5	43.4	n.d.	0.0	33.4	0.53	1.99
tb 6-6	2.7	44.7	22.8	3.9	2.9	23.0	1.60	3.35
tb 6-7	8.6	29.5	34.5	3.9	0.0	23.5	0.99	3.26
tb 12-5	8.3	41.8	20.7	20.8	0.6	7.8	1.19	11.8
tb 12-6	15.4	28.3	46.7	n.d.	6.2	3.3	0.83	29.3
tb 12-3	5.0	46.4	29.2	2.2	4.5	12.8	1.43	6.82
tb 12-4	6.3	32.2	38.6	6.6	4.4	11.9	0.78	7.40
tb 12-7	2.4	30.1	48.1	n.d.	10.4	9.1	0.56	10.0
tb12-8	2.6	23.4	39.5	n.d.	31.1	3.4	0.37	28.4

2-Ring = alkylated aromatics and hydroaromatics composed of two rings

3-Ring = alkylated aromatics and hydroaromatics composed of three rings

4-Ring = alkylated aromatics and hydroaromatics composed of four rings and other polynuclear aron

n.d. = not determined

B+P/≥2-Ring = Benzenes + Phenols/2-Ring + 3-Ring + 4-Ring+

ΣAro/ΣAli = Total Aromatics/ Total Alkanes

[1] Given, P.H. *Fuel.* 1960. 39. 147.

[2] Shinn, J.H. *Fuel.* 1984. 63. 1187.

[3] Solomon, P.R. *New Approaches in Coal Chemistry.* Washington, DC: ACS Symposium Series No. 169. 1981. 61.

van Krevelen, D.W. *Coal: Typology-Chemistry-Physics-Constitution.* The Netherlands: Elsevier Scientific Publishing Co. 1981.

[4] Schobert, H. H. et al. *Advanced Thermally Stable Jet Fuels, Technical Progress Report, April 1993 – June 1993.*

[5] Burgess, C.et al. *Proceedings of the 7th International Conference on Coal Science.* September 1993.

[6] Solomon, P.R. et al. *Coal Science II.* ACS Symposium Series No. 461, American Chemical Society, Washington, D.C. 1991. 193.

5.5 Structural Correlation of Coal Liquefaction Oils with Flash Pyrolysis Products

This study is explained in detail in *Advanced Thermally Stable Jet Fuels Technical Progress Report, April 1993 – June 1993.*

Introduction

Many studies have attempted to elucidate the average structure of different ranks of coal; these models provide general guidelines pertaining to the typical functional groups and the size of the aromatic ring clusters for different ranks of coal. There has also been much work done on analysis of coal liquids, mainly the light oil fractions; however, there is limited data on the comparison of liquefaction products to structural features of different coals. The most well known work to date is by Given and coworkers.[1] Anderson et al.[2] and Calkins et al.[3] used NMR to correlate coal characteristics to coal liquefaction or pyrolysis products. Flash pyrolysis GC/MS has been used as a technique for coal analysis to monitor the transformation of certain maceral groups through coalification.[4]

We surmised that flash pyrolysis GC/MS could provide information related to the lighter liquefaction products. The focus of this work is the comparison of structural features of coals (rank that ranges between subbituminous C to HvA bituminous) to the structural features of the light liquids obtained from coal liquefaction.

Experimental

Five coals were provided by the Penn State Coal Data Bank along with rank and elemental and maceral compositions. These coals and related structural information are listed in **Table 5.5-1**. The coals were then characterized by several methods. ^{13}C-NMR CPMAS parameters were a contact time of 1000 μs, a 90° pulse of 5-7 μs, and a pulse delay of 1 second. For dipolar dephasing, the parameters used were the same, and t was varied from 2.5 μs to 2 ms. We used a DuPont GC/MS with the pyroprobe connected to the injection port of the GC/MS for flash pyrolysis GC/MS. The sample was pyrolyzed for 10 seconds at 610 °C. The conditions of the GC used were a rate of 4 °C/min from 30 to 280°C.

The liquefaction conditions were 425°C for 1 hour in a 75 ml microautoclave, with pyrene as a solvent (10g:10g coal-to-solvent-ratio) and cold H_2 pressure 7MPa. The reactors were heated in a fluidized sandbath, and the time required to heat the reactors to the reaction temperature was about 10 minutes. The reactors were quenched in cold water at the end of reaction. Products were emptied from the tubing bomb into a dry tared thimble using dichloromethane (DCM) and extracted with DCM for about 36-48 hours until the extracted solvent appeared clear. The products were then extracted with tetrahydrofuran (THF) for about 24–36 hour until the extracted solvent appeared clear. The DCM was rotoevaporated from the DCM-solubles, and then the sample was extracted with hexane. The residue was rinsed with acetone and pentane and dried at 100°C for 12 hours. The THF-soluble fractions were dried for 1 hour at 60°C.

The hexane-soluble fractions were analyzed by GC/FID and GC/MS. The conditions of the GC used were a rate of 4 °C/min from 40 to 280 °C. The residues were analyzed by CPMAS ^{13}C-NMR and flash pyrolysis GC/MS under the same conditions as described previously.

Results and Discussion

The discussion will focus on two coals (DECS-6 and -12); the others follow a similar pattern of behavior.

DECS-6. ^{13}C-NMR of DECS-6 could indicate that the aromatic clusters are not highly condensed, or that the functional groups on the aromatic rings contain long chains of aliphatic groups instead of the aliphatics being attached at several spots on the rings. The dominant feature of the flash pyrolysis products is the series of n-alkanes/alkenes and the biomarkers prist-1-ene and cadalene. Phenols make up the bulk of the remaining products. The dominance of the alkanes/alkenes also suggests the aliphatic portion of the coal could be long-chain aliphatics.

DECS-12. ^{13}C-NMR of DECS-12 seems to indicate that the aromatic rings are more condensed, and that most of the attached functional groups will be oxygen or shorter alkyl groups. The dominant features of the pyrolysis products are naphthalenes, benzenes, and phenols. The presence of alkanes/alkenes is less in DECS-12 than in DECS-6.

Conversions. The highest conversions were obtained with DECS-6 and -12 at 425 °C for 1 h with pyrene. For DECS-6, the dominant products in the hexane-soluble fraction were alkanes with some contribution from phenols and naphthalenes. For DECS-12, the dominant products were phenols and naphthalenes. The ^{13}C-NMR of both residues indicate loss of aliphatics and oxygen compounds.

Other coals. Coals DECS-9, PSOC-831, and PSOC-1379, had lower conversion and fewer DCM-solubles than DECS-6 and DECS-12. DECS-9 and PSOC-1379 have a higher oxygen content. At 425°C, the loss of oxygen functional groups (e.g., by thermal cleavage of bonds) creates nascent reactive sites, which, if not capped by H•, can be sites for retrogressive crosslinking reactions. Alkanes and phenols were dominant components for the hexane-solubles from DECS-9. PSOC-1379 behaved in a similar manner to DECS-6. For PSOC-1379, the hexane-solubles contain alkanes, naphthalenes, and phenols. For PSOC-831, alkanes and phenols dominate the hexane-solubles. ^{13}C-NMR of the residues from these reactions indicates the loss during liquefaction of those structures or functional groups that were identified in the unreacted coal by flash pyrolysis GC/MS.

The flash pyrolysis GC/MS pyrograms for each coal showed compositional features very similar to GC/MS chromatagrams of the light fractions, with the exception of PSOC-831. If the pyrograms of unreacted coal indicated an abundance of alkanes/alkenes, the oils produced during liquefaction were found to have abundant alkanes, and the residue had almost no aliphatic carbon. The flash pyrolysis of the raw coal can be a good indicator of the compositional features of the hexane-soluble liquid products from non-catalytic reactions when using liquefaction conditions. The similarity of product compositions for liquefaction at 425°C in hydrogen and flash pyrolysis at 610°C suggests both non-catalytic liquefaction and pyrolysis follow similar decomposition mechanisms. Use of these techniques could possibly provide more specific information regarding the mechanistic pathway of catalytic liquefaction. By altering the temperature regime of the pyrolysis and by using different liquefaction reaction conditions in future studies, we may be able to understand liquefaciton reaction pathways at the molecular level. This information could be used for more rational selection of feedstocks and appropriate reaction conditions for coal liquefaction.

Table 5.5-1. ^{13}C-NMR and H/C Ratio Data for Coals and Liquefaction Residues.

Experiment	Coal	Reaction Cond	f_a	f_{CO}	f_{OH}	f_{ha}	H/C Res
Raw Coal	Pittsburgh #8	None	0.70	0.00	0.03	0.29	0.794
TB12-2		425°C, 1h, pyrene	0.81	0.00	0.11		0.584
Raw Coal	Blind Canyon	None	0.65	0.01	0.05	0.41	0.905
TB6-2		425°C, 1h, pyrene	0.84	0.03	0.02		0.58
Raw Coal	Deitz, Mt	None	0.57	0.08	0.05	0.21	0.803
TB9-2		425°C, 1h, pyrene	0.81	0.07	0.09		0.546
Raw Coal	Colorado F	None	0.67	0.11	0.08	0.16	0.770
TB1379-2		425°C, 1h, pyrene	0.82	0.04	0.11		0.542
Raw Coal	Brazil Block	None	0.72	0.01	0.06	0.22	0.704
TB831-2		425°C, 1h, pyrene	0.86	0.02	0.03		0.526

f_{CO} - fraction carboxyls, f_{OH} - fraction phenols/ethers

[1] Mudamburi, Z. and P. H. Given. *Org. Geochem.* 1985. 8. 221.

Shadle, L. J., P. H. Neill, amd P. H. Given. *Fuel.* 1988. 67. 1465.

Yarzab, R. F.et al. *Fuel.* 1980. 59. 81.

[2] Anderson, L. L. et al. *NewApproaches in Coal Chemistry.* ACS Symposium Series No. 169, American Chemical Society, Washington, D.C. 1981. 223.

[3] Calkins, W. H. *American Chemical Society, Division of Fuel Chemistry, Preprints.* 1983. 28(5). 85.

[4] Hatcher, P. G. and H. E. Lerch, III. *Coal Science II.* ACS Symposium Series No. 461, American Chemical Society, Washington, D.C. 1991. 9.

Hatcher, P. G. et al. *Fuel.* 1988. 67. 1069.

Anderson, K. B., R. E. Winans, and R. E. Botto. *Org. Geochem.* 1992. 18. 829.

van Aarssen, B. K. G., J. W. de Leeuw, and B. Horsfield. *J. Anal. Appl. Pyrol.* 1990. 20. 125.

5.6 A Study of the Molecular Structure of Polycadinene from Dammar Resin: The First Phase of a Comparative Study to Understand the Chemistry and Structure of Resin from Blind Coal Samples

This study is explained in detail in *Advanced Thermally Stable Jet Fuels Technical Progress Report, July 1993 – September 1993.*

Introduction

We chose Blind Canyon coals as a potential liquefaction feedstock for jet fuels because they are rich in resinite. Resins and resinites (fossilized resins) seem to contain readily cleaved cycloparaffinic structures, which are desirable components in jet fuels because of their thermal stability. In this study, we examined the structure of the resinite present in Blind Canyon coal in an effort to understand the chemistry of its conversion during liquefaction.

The general consensus regarding the structure of sesquiterpenoid resinites (i.e., the resinite from DECS-16 coal) is that the maceral exists as two fractions. One fraction consists of a high molecular weight (HMW) polymer, thought to be polycadinene (PC)[1] and the second fraction is composed of low molecular weight compounds shown by gas chromatography/mass spectrometry (GC/MS) to be dimers and trimers of cadinene and functionalized triterpenoids.[2] We previously demonstrated by spectroscopic techniques that the resinite maceral isolated from the Blind Canyon coal is a sesquiterpenoid resinite having a polycadinene-like backbone enveloped by a large proportion of volatile and occluded material.[3] In that study, we did not separate the resinite sample into its respective fractions, because we hoped to gain an overall understanding of the chemical constituents contributing the maceral in bulk. In this work, we did isolate each fraction of the fossilized Blind Canyon resinite and fractions of a recent resin and subjected them to analyses similar to those applied to the intact sample.

This study included a series of experiments designed to characterize a recent (extant), less-mature resin. By examining the structure of polycadinene from a young resin such as Dammar resin, we could compare its structural characteristics with those of the Blind Canyon resin. From this comparison, the chemical changes that accompany the coalification process could be identified, further aiding in the structural identification of the Blind Canyon coal's resinite maceral.

The Dammar resin was chosen due to its availability in a relatively pure form and its high solubility in CDCl3—an important consideration because NMR was chosen as the primary structural tool. NMR is a powerful structural elucidation tool because it is nondestructive and is not restrictive in terms of examining high molecular weight or polar species, problems often incurred with GC/MS analysis of complex materials. NMR techniques, which include one- and two-dimensional NMR spectra, were used in this study to determine the consistency of the structure of the HMW methanol-insoluble fraction of the Dammar resin with that of a pure, theoretical polycadinene polymer and to propose possible chemical alterations induced during coalification.

Experimental

Sample Isolation. Commercially available Dammar resin was dissolved in 50 mL of hexane, to which approximately 5 mL of methanol was added to precipitate the polymer as a

white powder following the procedure described by van Aarrssen et. al.[4] The powder was then separated by centrifugation and washed with methanol. The methanol was evaporated and replaced with approximately 0.6 mL of CDCl3, a solvent suitable for NMR spectroscopy.

Elemental Analysis. Elemental analysis of the polycadinene isolated from Dammar resin was carried out using a Leco Model CHN-600 elemental analyzer.

NMR Analysis. The high-resolution liquid ^{1}H and ^{13}C NMR experiments were performed on a Bruker AMX-360 spectrometer equipped with a 5mm inverse-detected probe. The one-dimensional single pulse ^{1}H and ^{13}C experiments were carried out using a 30°flip angle. The pertinent parameters in the measurement of the ^{1}H NMR spectrum were as follows: a 2.8 μs (30°) pulse width, 2 second pulse delay, 15 ppm sweep width, 32 scans and 32K data points. The pertinent parameters for the ^{13}C spectra were as follows: 2.2 μs (30°) pulse width, 5 second pulse delay, 250 ppm sweep width, 32K FID data points. An inverse-gated decoupling pulse sequence was utilized to obtain quantitative ^{13}C NMR spectra. The ^{13}C distortionless polarization transfer (DEPT) experiments were carried out using 45° (3.3 μs), 90° (6.6 μs), and 135° (16.5 μs) ^{13}C read pulses, respectively. A solid-state ^{13}C CPMAS spectrum was obtained on a Chemagnetics M-100 NMR spectrometer. The pertinent parameters are found elsewhere.[5]

A two-dimensional high resolution liquid experiment COSY (homonuclear correlation) with a 45° read pulse was performed on the polycadinene isolated from the Dammar resin using a standard Bruker experiment. The spectral resolution in the F1 dimension is 8.4 Hz/point while the resolution in the F2 dimension is 2.1 Hz/point. The total experimental time for the COSY45 was 14 hours.

A full explanation of the findings from the analyses is available in the original report.[6]

Conclusions

The NMR data for Dammar PC, a purified sesquiterpenoid polymer thought to be the primary component of fossil resin, indicated that proposed structures[5] were not entirely correct. Quantitative estimation of the number of olefinic carbons indicated that approximately 1.5 olefins were present per C15 substructure. This implied that one out of the C15 sesquiterpenoid units was fully saturated. Also, the presence of 4 olefinic peaks of nearly equal intensity in the ^{13}C NMR spectrum clearly indicated that the internal double bonds were not located at the same positions in the two substructures containing olefinic carbons. The DEPT spectra gave us clues that at least half of the olefins were quaternary. Thus, the information provided from the NMR studies indicates that a new structural composition must be proposed for the polycadinene-like resin polymers from Dammar resin. Considering the fact that the Dammar PC is very similar to resinite from the Blind Canyon coal, we now have a working structural model for this component of a potential coal feedstock for liquefaction to jet fuels.

---

[1] van Aarssen, B.G.K. et al. "A Cadinene Biopolymer of Fossil and Extant Dammar Resins as a Source for Cadinanes and Bicadinanes in Crude Oils from South East Asia." *Geochem. Cosmochim. Acta.* 1991. 54. 3021-3031.

Anderson, K.B., R. E. Winans, and R. E. Botto. "The Nature and Fate of Natural Resins in the Geosphere-II. Identification, Classification and Nomenclature of Resinites." *Org. Geochem.* 1992. 18(6). 829-841.

[2] Crelling, J.C. et al. "The Chemical Structure and Petrology of Resinite from the Hiawatha 'B' Coal Seam." *Energy & Fuels.* 1991. 5. 688-694.

Meuzelaar, H.L.C. et al. "Chemical Composition and Origin of Fossil Resins from Utah Wasatch Plateau Coal." *Fuel Proc. Technol.* 1991. 28. 119-134.

[3] Clifford, D.J.et al. "Characterization of Isolated Resinite Maceral." Advanced Thermally Stable Jet Fuels, Technical Progress Report, February 1993 - March 1993. The Pennsylvania State University. 1993. 46-50.

[4] van Aarssen, B.G.K. et al. "A Cadinene Biopolymer of Fossil and Extant Dammar Resins as a Source for Cadinanes and Bicadinanes in Crude Oils from South East Asia." *Geochem. Cosmochim. Acta.* 1991. 54. 3021-3031.

[5] van Aarssen, B.G.K. et al. "A Cadinene Biopolymer of Fossil and Extant Dammar Resins as a Source for Cadinanes and Bicadinanes in Crude Oils from South East Asia." *Geochem. Cosmochim. Acta.* 1991. 54. 3021-3031.

[6] Schobert, H. H. et al. *Advanced Thermally Stable Jet Fuels, Technical Progress Report, July 1993 – September 1993.*

5.7 Preliminary Investigation into Producing Cycloalkanes from Dammar Resin

This study is explained in detail in *Advanced Thermally Stable Jet Fuels Technical Progress Report, October–December 1993.*

Introduction

The Blind Canyon coal was chosen for liquefaction based primarily on its high concentration of resinite. The resinite in this coal is believed to exist as two fractions—a high molecular weight polymer and low molecular weight compounds. The high molecular weight polymer is thought to be polycadinene.[1,2] This structure is made up of substituted hydronaphthalene monomers that could be liberated upon liquefaction. The second fraction is composed of low molecular weight compounds shown by GC/MS to be dimers and trimers of cadinene and functionalized triterpenoids.[3,4]

To optimize a process for producing cycloalkanes from resinite, we needed to learn more about the reaction chemistry of the process. Because obtaining enough resinite to carry out reactions would be difficult, we selected Dammar resin as a suitable substitute that is commercially available in large quantities. Dammar resin contains a polymer similar to that found in Utah resinite and serves as a good model to study the liquefaction behavior of the resinite. This investigation involved three primary tasks:

1. Preliminary investigation into behavior of Dammar under conditions of liquefaction.
2. More detailed investigation to ascertain the best conditions to produce bicyclic and monocyclic structures.
3. Hydrogenation of products to produce cycloalkanes.

Experimental

Dammar resin was loaded into a 25 mL tubing bomb reactor, which was purged twice with nitrogen and then pressurized to 1000 psi with hydrogen. The reactor was heated in a fluidized sand bath. After reactions at 450°C at various times, the reactor was quenched and the products were extracted into hexane-solubles and -insolubles. The hexane-soluble fraction was analysed by GC/MS. Dammar resin was dissolved in methanol and the insoluble fraction separated by filtration. The soluble fraction was recovered by rotary evaporation. The methanol-insoluble fraction was liquefied for 60 minutes at 450°C.

Results

We examined the total ion chromatograms (TICs) of the hexane solubles from liquefaction of the whole Dammar resin at 450° C for reaction times 10, 20, 40 and 60 minutes. The major peak assignments are shown in **Table 5.7-1**.

The TICs can be broken into four distinct sections:

1. RT 0-20 minutes: C_1–C_4 benzenes
2. RT 20-30 minutes: C_1–C_4 indenes
3. RT 30-45 minutes: C_1–C_5 naphthalenes/tetralins

4. RT 60-80 minutes: Dimers and trimers of cadinene and other high molecular weight compounds

After a reaction time of 10 minutes, peaks were observed in all four sections. As time of reaction increased, the concentration of peaks in Section 4 dropped. After 40 minutes, all GC-amenable products that elute in Section 4 were almost gone. C_1–C_4 benzenes increased in concentration up to 40 minutes, as did naphthalenes and indenes. After 60 minutes of reaction, the product distribution had changed significantly. GC/MS identification of peaks showed that C_2-biphenyl and dimethylanthracene were being formed. This was accompanied by a decrease Section 1 of the TIC. The concentration of toluene and other substituted benzenes has decreased in relation to other products.

A thorough explanation of the investigation is difficult, but several ideas have emerged. The methylbenzenes could have reacted together to produce biphenyls. Dimethylanthracene could have been produced by cracking of the large molecular weight dimers, such as bicadinane. These two reactions would only occur at high temperatures and long reaction times. The recombination reactions are undesirable, but cracking of the high molecular weight fraction of the resin is required if compounds are to be formed that can be upgraded to desirable cycloalkanes boiling in the jet fuel range. **Scheme I** shows a possible reaction mechanism. (Dashed arrows indicate product formation after one hour of reaction.)

The liquefied methanol insoluble fraction was the high molecular weight polymer proposed to be polycadinene. Thermal stress caused the polymer to break down into monomeric, dimeric, trimeric and oligomeric cadinenes. Aromatization of the compounds released by depolymerization led to the formation of cadalene via 1,6-dimethyl, 4-isopropyltetralin. Previous reports indicated that removal of the isopropyl group and hydrogen atoms was possible under these conditions, as demonstrated by the formation of dimethylnaphthalene in high concentration.[5] **Scheme II** shows a possible reaction mechanism of the depolymerization reaction of polycadinene.

The formation of cadinane under these conditions could be explained in two ways. Cadinene released by depolymerisation reactions could hydrogenate to cadinane. Also, a cadinane moiety may exist in the polymeric structure, and upon release by depolymerization, be thermally stable enough to resist dehydrogenation to cadinene and, further, to dimethylnaphthalene. The second explanation is more likely under these conditions, because hydrogenation to any great extent is less favorable than dehydrogenation, which is seen by the formation of dimethylnaphthalene.

Conclusions

Dammar resin consists of two fractions. The products that occurred in the reactions of the whole resin, but not in the reactions of the polymeric component, must have originated in the second fraction (i.e., low molecular weight dimers and trimers of cadinene). The chromatograms showed that as time of reaction increased, the second fraction began to crack from bicadinanes/tricadinanes to naphthalenes and benzenes. At long reaction times, undesirable recombination reactions occurred, but the second fraction has almost totally been converted to compounds that can be upgraded to cycloalkanes. The polymeric fraction is converted to dimethylnaphthalene and cadinane.

These preliminary findings offer guidance on how resinite in coal would behave under liquefaction conditions. The sesquiterpenoid polymer that makes up Utah resinite would break apart to produce cadinene, which dehydrogenates and dealkylates to dimethylnaphthalenes, and to a smaller extent substituted decalins. The extent of the depolymerization reaction was not known at this stage of the investigation. Future investigations would focus on reactions at lower temperatures, catalytic upgrading of products and a more detailed investigation into the depolymerisation of polycadinene.

Table 5.7-1. Major peak assignments of TICs of Dammar resin hydrogenated at 450°C for various times

Peak Number	Retention Time (min.)	Peak Assignment
1	8.3	Benzene
2	14.3	Benzene
3	15.2	Benzene (p-cymene)
4	18.3	Benzene
5	23.6	Indene
6	28.3	Dihydroindene
7	33.6	Naphthalene
8	38.0	Naphthalene
9	40.7	dalene
10	44.2	Biphenyl
11	49.7	Anthracene
—	>60	ıers + trimers (e.g., bicadinanes)

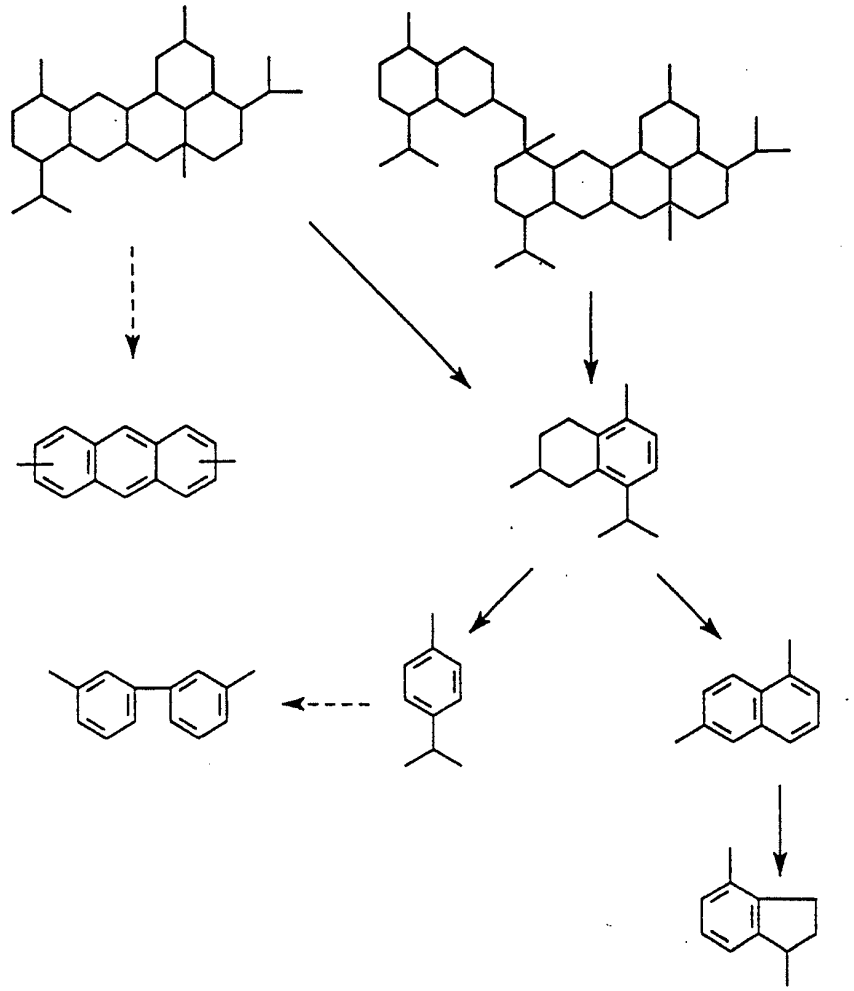

Scheme I. Possible Reaction Pathway of Dimers and Trimers of Cadinene in Dammar

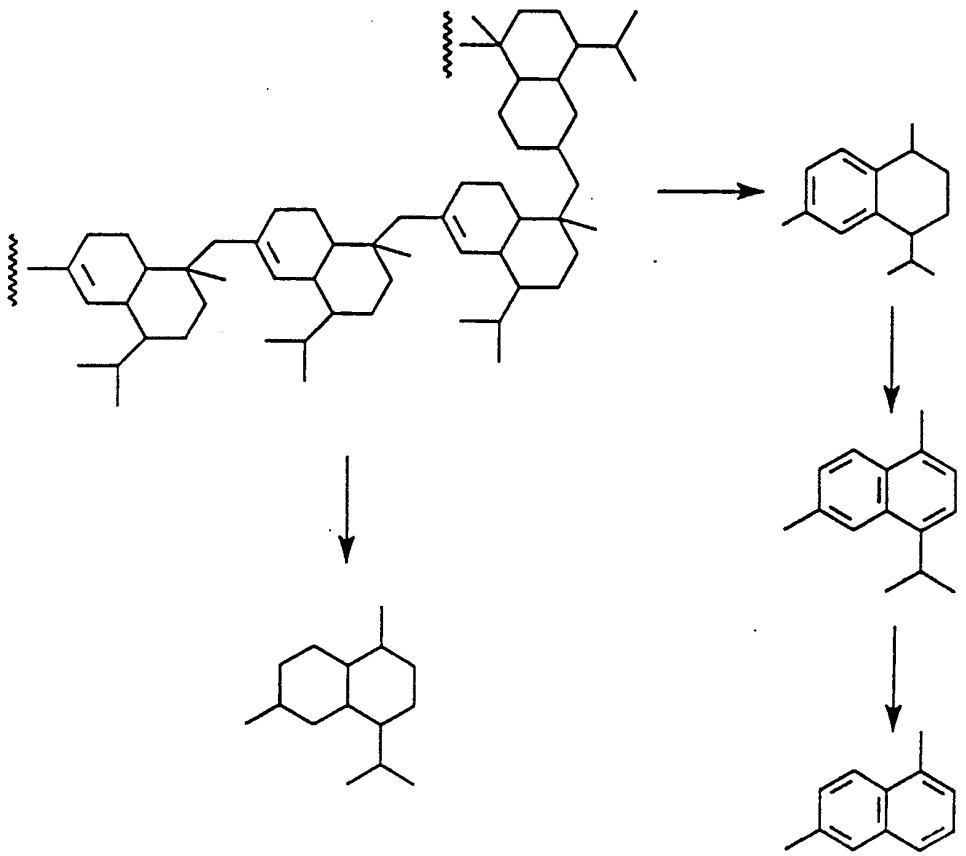

Scheme II. Possible Reaction Pathway of Polymeric Component of Dammar Resin

---

[1] van Aarssen, B.G.K. et al. *Geochem. Cosmochim. Acta.* 1991. 54. 3021. 1991.

[2] Anderson, K.B. Winans, R.E., and Botto, R.E. *Org. Geochem.* 18(6), 829, 1992.

[3] Crelling, J.C., Pugmire, R.J., Meuzelaar, H.L.C., McClennen, W.H., Huai, H. and Daras, J. *Energy Fuels.* 5, 688, 1991.

[4] Meuzelaar, H.L.C., Huai, H., Lo, R., and Dworzanski, J.P. *Fuel. Proc. Technol.* 28, 119, 1991.

[5] Cocker, W., Cross, B.E., and McCormick. J. The elimination of non-angular alkyl groups in aromatisation reaction. Part 1. *J. Chem. Soc.* 72-77, 1952.

5.8 Design of Batch Mode and Continuous Mode Three-Phase Reactor Systems for the Liquefaction of Coal and Upgrading of Coal Liquids

This study is explained in detail in *Advanced Thermally Stable Jet Fuels Technical Progress Report, October 1994 – December 1994.*

Introduction

Extensive research studies on various aspects of the liquefaction of coal in the presence of a solvent and dispersed catalyst have been conducted,[1] including the effect of temperature programmed liquefaction (TPL) of coal.[2] All of these experiments were conducted in a 25 ml tubing bomb microautoclave reactor.

To simulate conditions prevalent in an industrial-type reaction atmosphere, coal liquefaction experiments and the upgrading of coal liquids must be conducted in a continuous reactor system. In a continuous flow reactor system the catalyst moves with the products, rather than staying in the reactor for extended periods, thus prolonging the life of the catalyst and enhancing once-through reactor productivity. The reactor system can be operated continuously (feed in, product out) for a substantially longer time, leading to an increase in product quantities. If the coal liquefaction products remain in the reactor for a prolonged period of time, retrograde reaction occurs that converts desirable small product molecules into less desirable, larger macromolecules, be recombining two small product molecules or adding these product molecules back onto the coal.[3] The coal liquefaction products that are formed are continuously removed from the flow reactor system, alleviating the effect of the retrograde reactions and increasing the yield and quality of coal-derived liquids.

This study includes the early stages of design of two reactor systems for performing studies in the liquefaction of coal process. These systems will enable us to better understand the results obtained from the 25 mL tubing bomb microautoclave reactor and to apply them to a larger scale reactor system. This study describes the design and assembly of a 300 mL batch autoclave reactor system. The original Technical Progress Report[4] provides a description of all major aspects of the reactor system and a description of coal liquefaction and upgrading of coal liquids facilities in Alabama, New Jersey, and Pittsburgh, PA. A conceptual diagram of the reactor system is shown in Figure 5.8-1.

Results

A conceptual process flow diagram (PFD) of a continuous mode reactor scheme for the liquefaction of coal is presented in **Figure 5.8-1**. This PDF is only a preliminary representation; it will likely change, as necessary, to satisfy our requirements.

Brief Description of the Proposed Novel Multistage Continuous Flow Reactor for the Coal Liquefaction Process. A mixture of coal (30 wt%)-catalyst-solvent slurry is prepared and stored in a slurry feed mix tank. The slurry is fed into a preheater by a slurry pump. In addition, a mixture of H_2 and H_2S (for iron catalysts) or plain H_2 (for molybdenum catalysts) is fed into the coal slurry feed line. The mixture of gas and slurry, preheated to 200°C, flows into an intermediate activation reactor and then a coal liquefaction reactor (for iron catalyst), or directly into the coal liquefaction reactor (for molybdenum catalysts).

After a specified residence time, the contents of the reactor exit through an overflow line at the bottom of the reactor and into a high pressure (HP) product recovery vessel (V/L separator), where the gas escapes from the top and flows through a condenser. Prior to entering the condenser, water is added through a high-pressure water pump to condense H_2S and NH_3. The light oils and other condensables are collected in the HP light oil recovery vessel, from which the coal liquid flows into the low-pressure (LP) recovery vessel. The vapors from this vessel flow through a condenser into a flash gas meter and are vented to atmosphere. The vapors exiting the HP light oil recovery vessel flow through a back pressure controller into a tail gas meter and are vented.

The heavy slurry product from the HP product recovery vessel flows into the LP recovery vessel. The vapors from this vessel are connected to the vapors exiting the other LP recovery vessel. The slurry from the LP recovery vessel is filtered to separate the coal liquids from the unconverted coal, the dispersed catalysts, ash, and other insolubles. The coal liquids from both the LP recovery vessels are collected and analyzed.

Mini-Pilot Plant for Coal Liquefaction. Our process couples two technologies in an attempt to develop a more economical coal liquefaction process than currently exists. The two technologies are temperature programmed liquefaction (TPL) of coal and the addition of water to the coal liquefaction process. Microautoclave studies performed prior to, and in support of, the bench scale unit operation will help to provide some basic information in guiding the selection of operating conditions for the continuous unit. The key parameters of the continuous unit that would benefit from the microautoclave runs include: temperature of the 1st and 2nd stage reactors, pressure of the feed gas in the reactor system, quantity of water to be added to the liquefaction runs, size of coal particles, size of catalyst particles, type of solvent, and concentration of coal and catalyst in the solvent.

Conclusion

The significant features of the proposed continuous flow reactor scheme for the coal liquefaction process include:

- Use of dispersed catalysts in the coal-solvent slurry
- Temperature-programmed liquefaction (TPL) of coal in a two-stage reactor scheme
- Ability to add water to coal-catalyst-solvent slurry in the 1st stage reactor
- Incorporation of an interstage separator between the two stages of the reactor to primarily remove water previously fed into the 1st stage reactor
- A feed gas blending (syngas – H_2 + CO) and compression (H_2 or syngas) system to allow syngas or pure H_2 to be fed into the 1st stage reactor at elevated temperatures
- Continuous sampling and GC analysis of gas and liquid from the slurry lines at several vantage points to periodically monitor the progress of the reaction.

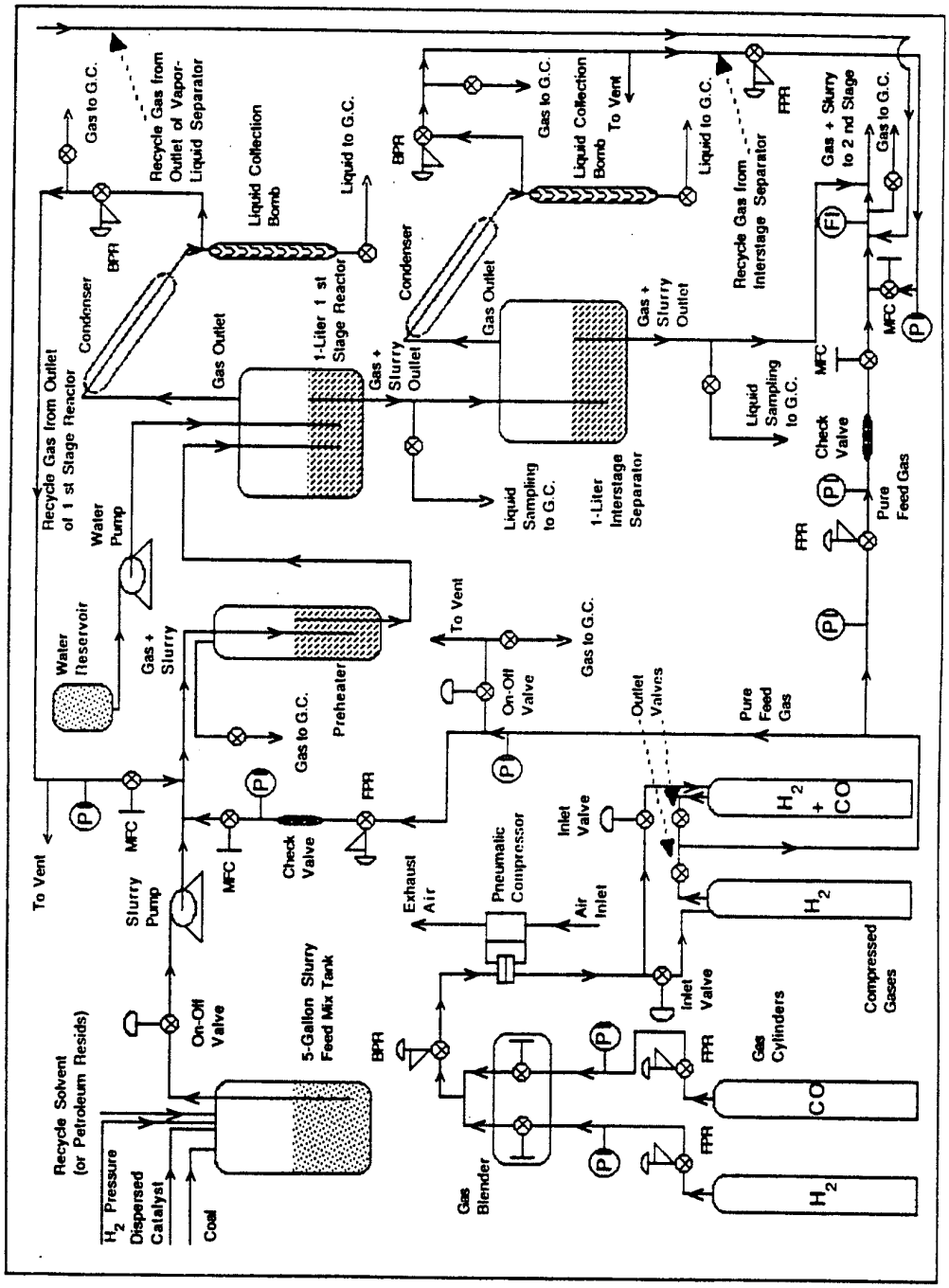

Figure 5.8-1. Conceptual Process Flow Diagram of the Proposed Mini-Pilot Plant for a Coal Liquefaction Process in a Continuous Mode (continued)

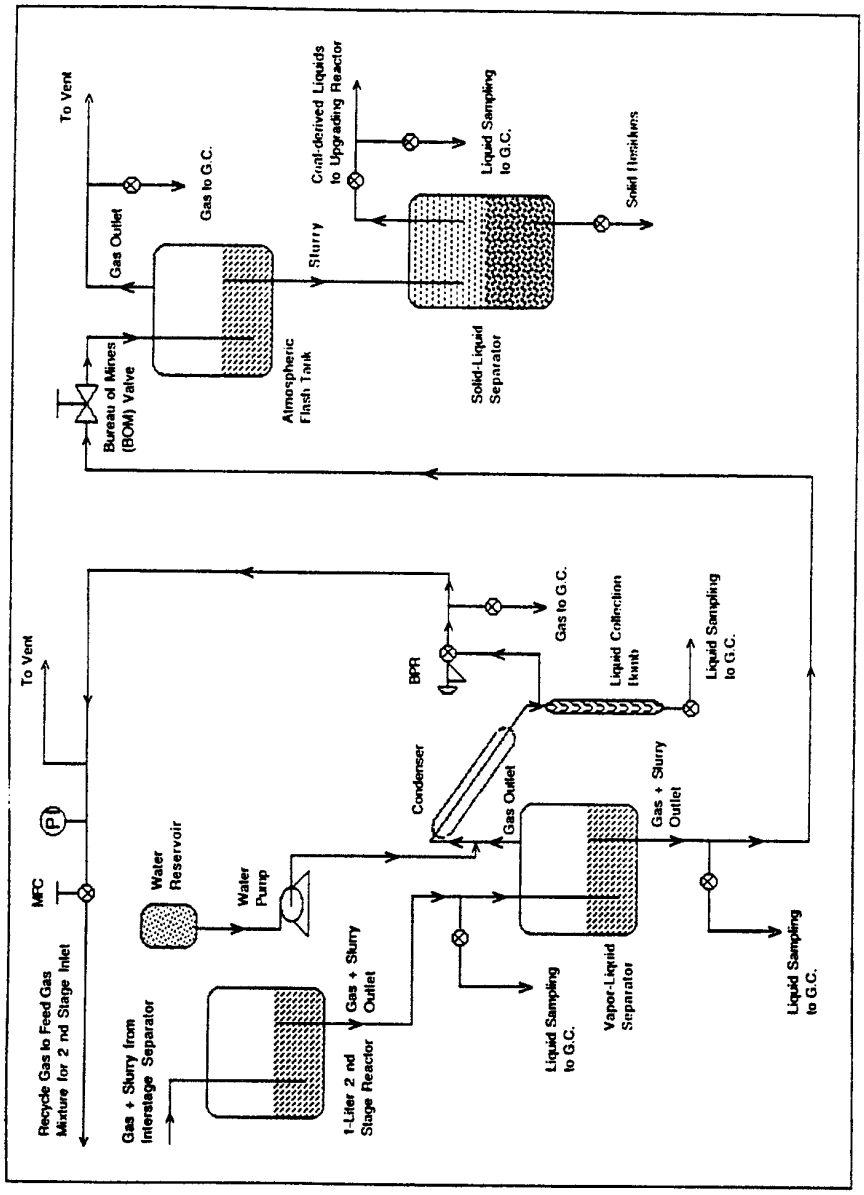

Figure 5.8-1. (cont'd) Conceptual Process Flow Diagram of the Proposed Mini-Pilot Plant for a Coal Liquefaction Process in a Continuous Mode

---

[1] Derbyshire, F. J. "Catalysis in Coal Liquefaction." *IEA Coal Research Pub.* IEACR/08. 1988.

[2] Kresge, C. T. et al. Nature, 1992. 359. 710.

[3] Beck, J. S. et al. J. Am. Chem. Soc. 1992. 114. 10834.

[4] Schobert, H. H. et al. *Advanced Thermally Stable Jet Fuels, Technical Progress Report, October 1994 – December 1994.* The Pennsylvania State University. 1995.

5.9 Design, Assembly, and Operation of a Batch Mode and a Continuous Mode Three-Phase Reactor System for the Liquefaction of Coal and Upgrading of Coal Liquids

This study is explained in detail in *Advanced Thermally Stable Jet Fuels Technical Progress Report, January 1995 – March 1995.*

Introduction

A previous report addressed in detail the design of a batch mode mini-pilot plant scale reactor system for liquefaction of coal and a continuous mode mini pilot plant scale reactor scheme for liquefaction of coal and upgrading of coal liquids.[1] It also described existing coal liquefaction and coal liquids upgrading units in Alabama, New Jersey, and Pennsylvania.

This exercise describes the assembly and operation of the batch-mode mini-pilot plant scale reactor system and provides an overview of the design of experiments and analysis of gases, liquids, and solid products to be performed in the reactor. We modified the continuous flow mini-pilot plant reactor system, which was developed earlier, to meet our requirements. In addition to describing this new design, we provided a cost analysis of related equipment and accessories.

Experimental

Experiment Design. The batch mode mechanically agitated slurry reactor system was assembled as planned.[1] Based on experiments conducted earlier in a 25 mL tubing bomb microautoclave reactor, a series of experiments was designed to address a wide range of variables, including:

- Raw coal or vacuum-dried coal
- Single-stage liquefaction (SSL)
- Temperature-programmed liquefaction (TPL)
- With and without the addition of catalyst (Molyvan L)
- With and without the addition of water
- Using H_2 or syngas (H_2 + CO) in the SSL and in the 1st stage of TPL
- Temperature range: 350°-450°C
- Duration of experimental run: 30-60 minutes

Details of the experimental runs are provided in the relevant Technical Progress Report.[2]

Analysis of Products. When the slurry reactor cools down, some of the gases are collected in a sampling bag and analyzed using both TCD (H_2, CH_4, CO, and CO_2) and FID (C_1-C_4 hydrocarbon gases) detectors. To analyze the liquid and solid products from the slurry reactor, we devised a detailed, multi-step filtration process capable of handling larger quantities of samples than the traditional Soxhlet extraction procedure. Collection and analysis of gas, liquid, and solid products were performed at the conclusion of each experimental run to determine the conversion of H_2, composition of product gases, quantity of oil produced, amount of asphaltene and preasphaltene formed, and the conversion of coal.

Modified Process Design of the Continuous-Mode Reactor Scheme. Based on our previous design scheme[1], we made the following modifications to suit our process/budgetary limitations:

- Eliminated all recycle gas streams and the compressors in those lines based on budgetary and space limitations
- Eliminated the gas outlet/recycle stream and accessories from the 1st stage reactor
- Added a condenser to the process stream exiting the vapor-liquid separator and flowing through the BOM valve in the atmospheric flash tank to help in reducing the temperature and pressure of the stream exiting the V/L separator and assist in the condensation of the desired product vapors.
- Placed a filter bag in the exit of the atmospheric flash tank to aid in the separation of liquids from the solids.

These changes are reflected in the process flow diagram presented in **Figure 5.9-1.**

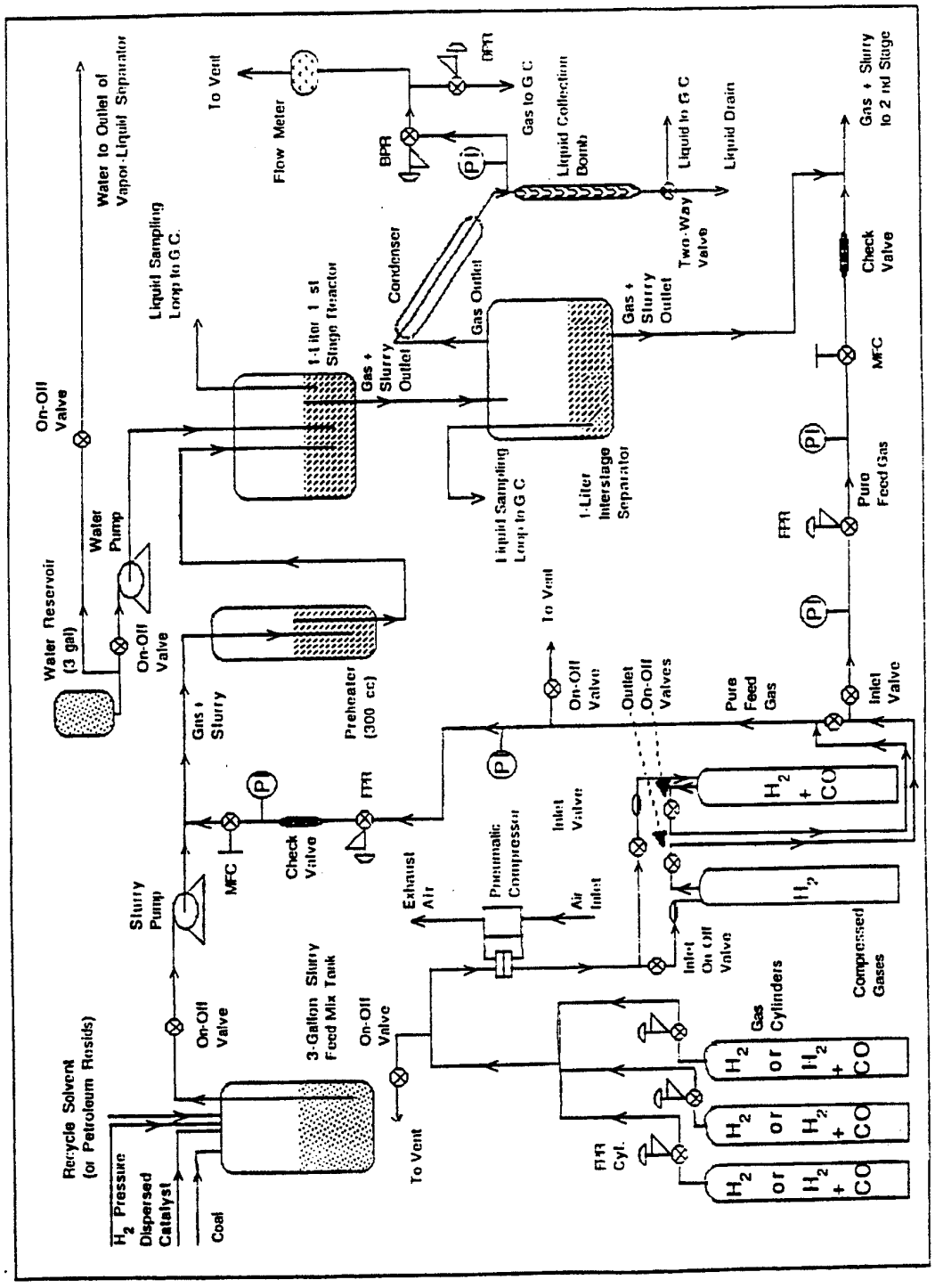

Figure 5.9-1. Process Flow Diagram of the Mini-Pilot Plant for Liquefaction of Coal in a Continuous Mode (continued)

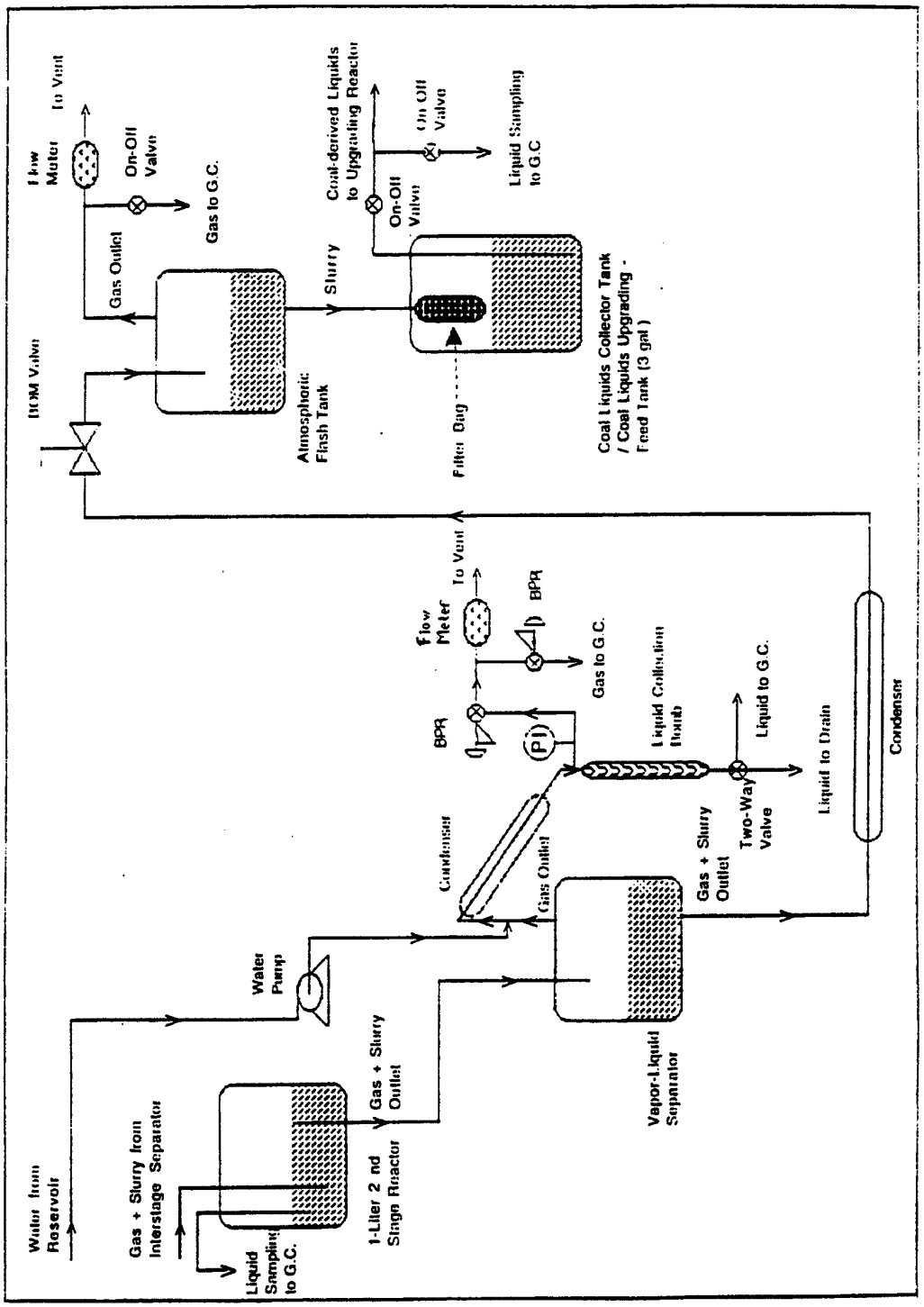

Figure 5.9-1. (cont'd) Process Flow Diagram of the Mini-Pilot Plant for Liquefaction of Coal in a Continuous Mode

[1] Schobert, H. H. et al. *Advanced Thermally Stable Jet Fuels, Technical Progress Report, October 1994 – December 1994.* The Pennsylvania State University. 1994.

[2] Schobert, H. H. et al. *Advanced Thermally Stable Jet Fuels, Technical Progress Report, January 1995 – March 1995.* The Pennsylvania State University. 1995.

5.10 Contribution of Mineral Matter to Low Temperature Liquefaction Mechanisms

This study is explained in detail in *Advanced Thermally Stable Jet Fuels Technical Progress Report, January – March 1996.*

Introduction

During coal conversion, the coal undergoes structural changes through reactions between coal constituents and solvent species or through catalytic reactions accelerated by added catalysts or the inherent mineral components. To date, the exact role of much of the mineral matter in coals remains unclear.[1, 2, 3] Typical interactions of mineral constituents and their behavior at high temperatures is summarized in **Table 5.10-1**.

These mineral and inorganic species can act as catalysts or poisons during liquefaction, depending on reaction conditions. For example, minerals could act physically to block access to pores or reaction sites. Conversely, the chemical roles of inorganics include clays that can act as cracking catalysts and the hydrogenation catalyst, pyrite. Removal of naturally occurring cations such as Na^+, Ca^{2+} and K+ enhances liquefaction conversions[2, 4] and several authors have observed a favorable influence of demineralization on coal depolymerization. Shams et al. reported that the treatment of coals with methanol and HCl removes virtually all of the calcium species, leading to retardation of the retrogressive reactions Ca was proposed to catalyze.[5]

This work evaluated the nature and distribution of coal mineral matter in both untreated and treated (demineralized) samples of Wyodak coal and considered the influence of these compounds by assessing their possible catalytic effect. A previous series of experiments compared the effect of demineralization on coal conversion at low temperatures (300-350°C); preliminary results indicated that conversions were comparable upon pretreatment.

Experimental

Wyodak coal (DECS-8) was obtained and demineralized via successive acid treatments—an HCl wash and an HF wash. Both the untreated and demineralized samples were analyzed by ICPAAS to more clearly identify the mineralogical distribution changes upon acid treatments. Ash samples were obtained using a lithium metaborate fusion technique and analyzed using a inductively coupled plasma spectrophotometer (ICP).

Experimental procedures for liquefaction in tubing bombs were outlined in a corresponding Technical Progress Report.[6] The conversion of coal into soluble products and gases was calculated on the basis of recovered THF-insoluble residue and reported on a dmmf basis. Residues were further analyzed by FTIR and ^{13}C NMR.

Conclusions

As anticipated, relative to runs at 350°C with untreated coal, demineralization afforded higher overall conversions; this trend became more apparent when either an H-donor (tetralin) or non-donor (1-mn) solvent was used. Specifically, there was no evident

mineral matter effect on solvent H donation. Thus, initial results between the two sets of data suggested that the reactions undergone at 350°C are not mineral matter catalyzed. With respect to mineral matter identification, further ICP-AAS studies have been conducted, in association with CC-SEM and XRD determinations, to identify the mineral phases and species contributing to possible low temperature hydrogenation mechanisms.

Table 5.10-1. General Behavior of Minerals at High Temperatures

Inorganic Species	Behavior on Heating
Clays	Loose structural OH groups with rearrangements of strucutre and release of H_2O.
Carbonates	Decompose with loss of CO2; residual oxides fix some organic and pyritic S as sulphate.
Quartz	Possible reaction with iron oxides from pyrite
Pyrite	In air, burns to Fe2O3 and SO2
Metal Oxides	May react with silicates
Metal Carboxylates	Decompose

[1] Maldonado-Hodar, F.J. et al. *Fuel.* 1995. 74(6). 818 (and references therein).

[2] Mochida, I. et al. *Fuel.* 1988. 67. 114.

[3] Serio, M.A. et al. *Am. Chem. Soc., Div. Fuel Chem., Prep.* 1990. 35(l). 61.

[4] Joseph, J. T. and T. R. Forrai. *Fuel.* 1992. 71. 75.

[5] Shams, K., R. L. Miller, and R. M. Baldwin. *Fuel.* 1992. 71. 1015.

[6] Schobert, H. H. et al. *Advanced Thermally Stable Jet Fuels, Technical Progress Report, January – March 1995.* 92PC92104-TPR-11. 74.

5.11 HYDROGENATION/DEHYDROGENATION REACTIONS OF ROSIN

Introduction

Cycloalkanes are desirable components of advanced jet fuels because they offer high thermal stability. If cycloalkanes can be produced in high yield in direct liquefaction, downstream processing of the product would be reduced. Resinite, which has predominantly alphatic and hydroaromatic structures, can be characterized and classified according to its structure and origin. One major class of resinite is diterpenoid in nature. If the behavior of diterpenoids under liquefaction conditions can be determined and understood, a highly efficient liquefaction could be developed. Coals with a high resinite concentration could be liquefied, and the cycloparaffinic products from resinite could be extracted into the oil fraction and into the jet fuel boiling range. The resulting liquid would likely be thermally stable and could be a high quality jet fuel.

In order to gain more insight into resinite, which is a very complex mixture of polymerized diterpenoids, and enable us to analyze products and reaction pathways more easily, we chose to study commercially-available rosin. Rosin contains 90% diterpenoids (isomeric with abietic acid) and is, in a sense, a simplified resin. As a result, its hydrogenation/dehydrogenation behavior should offer valuable insight into resinite liquefaction.

a. Study of the Hydrogenation/Dehydrogenation Behavior of Rosin

This study is explained in detail in *Advanced Thermally Stable Jet Fuels Technical Progress Report, August 1992 – October 1992.*

Purpose: Determine the hydrogenation/dehydrogenation behavior of rosin to gain insight into resinite liquefaction.

Experimental: Rosin gum was used as reactant; all reactions were carried out in standard microautoclave reactors under 1000 psi hydrogen pressure. Reactions were carried out at varying temperatures and reaction times. The products were dissolved in acetone and analyzed by GC/MS.

Findings: To produce compounds that make good jet fuel from diterpenoid structures, we must hydrocrack the 3-ring compounds to naphthalenes and benzenes. Based on the results of this study, we know that cracking requires a high temperature, which concurrently promotes dehydrogenation of cycloparaffinic compounds to unwanted fully aromatic compounds. Therefore, we envisioned a two-stage reaction:

1. A high temperature cracking reaction to yield a "backbone" of naphthalenes and benzenes. This requires a reaction temperature of at least 450°C and a reaction time of at least 45 minutes.

2. A low temperature hydrogenation stage in which naphthalenes and benzenes from stage 1 would be catalytically hydrogenated to cycloalkanes and tetralins. The final products should fall into the jet fuel boiling range, yielding a thermally stable fuel.

From these conclusions, we developed proposed reaction pathways, shown in **Figures 5.11-1** and **5.11-2**. Figure 5.11-1 shows the dehydrogenation pathway of abietic acid. One

aspect of the reaction, the decarboxylation of abietic, is not addressed here, but warrants further investigation. Figure 5.11-2 focuses on the possible route of cracking of the 3-ring compounds.

b. Aromatization/Cracking/Isomerization Reactions of Rosin Compounds

This study is explained in detail in *Advanced Thermally Stable Jet Fuels Technical Progress Report, November 1992 – January 1993.*

Purpose: Examine the aromatization/cracking/isomerization reactions of rosin compounds with various catalysts.

Experimental: Rosin was hydrogenated under different conditions with NiMo/Al2O3, Ni-Y zeolite and ammonium tetrathiomoybdate. All reactions were carried out in standard microautoclave reactors, with a cold hydrogen pressure of 7 MPa. The products were analyzed by CG/MS and quantified using heptadecane as an internal standard.

Findings: Diterpenoid compounds can be successfully hydrogenated and cracked to jet fuel compounds using NiMo and Ni-Y catalysts. With careful tailoring of the process temperature and time of reaction, high quality distillate can be obtained. A temperature-staged reaction with optimum conditions chosen from the plots of product distribution could yield maximum concentration of cycloalkanes and hydronaphthalenes. Fully aromatic compounds could be kept to a minimum.

Diterpenoids are the most common resins in the geosphere. In addition to appearing in some coal resinites, they can be found as ambers or as modern pine resins (i.e., rosin). Their chemical properties can be used in developing high-quality fuels, either by direct hydrocracking or as a blending additive in a coal liquefaction process. Some of the reactions occurring in rosin hydrocracking (e.g., dealkylation/isomerization) could prove to be useful in determining the best way to study liquefaction behavior of sesquiterpenoid resinites, which are found in some Utah coals.

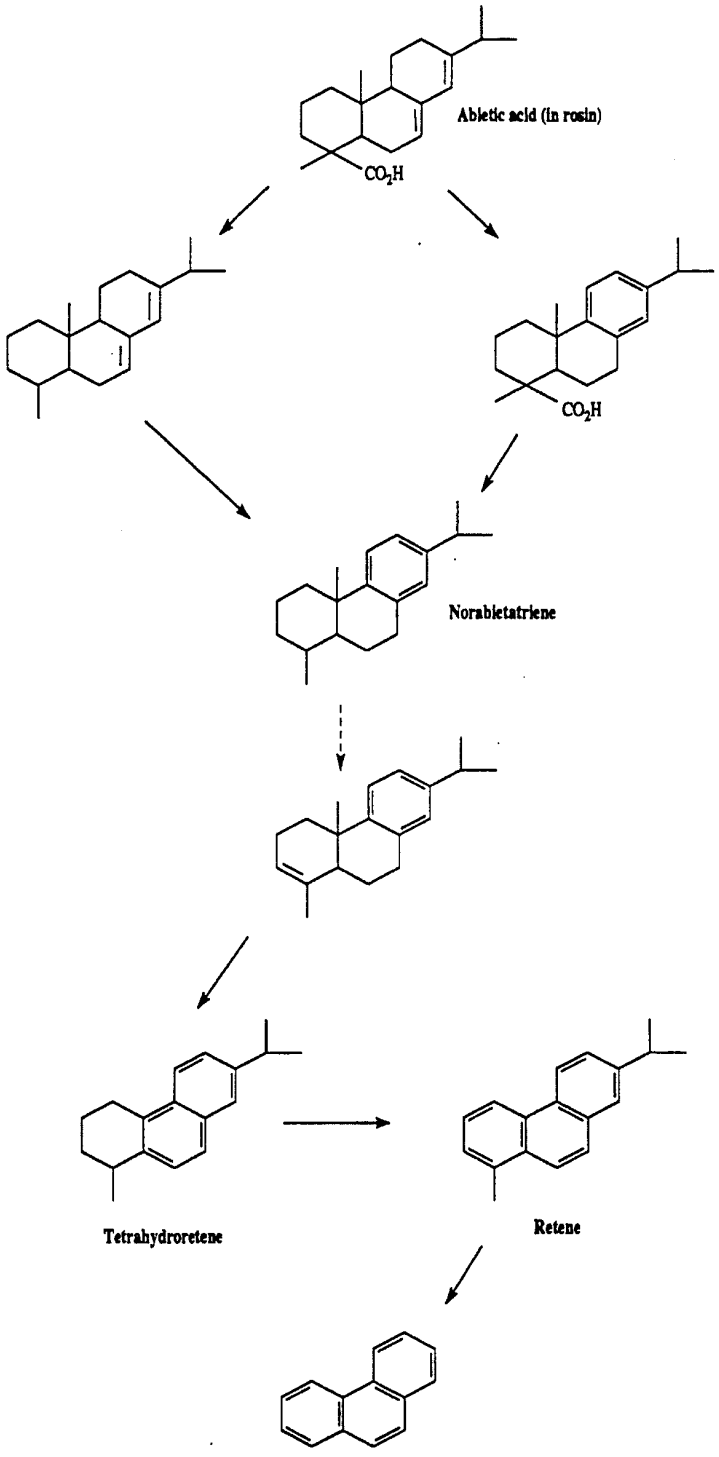

Figure 5.11-1. Hydrogenation Reaction Pathway of Abietic Acid in Rosin

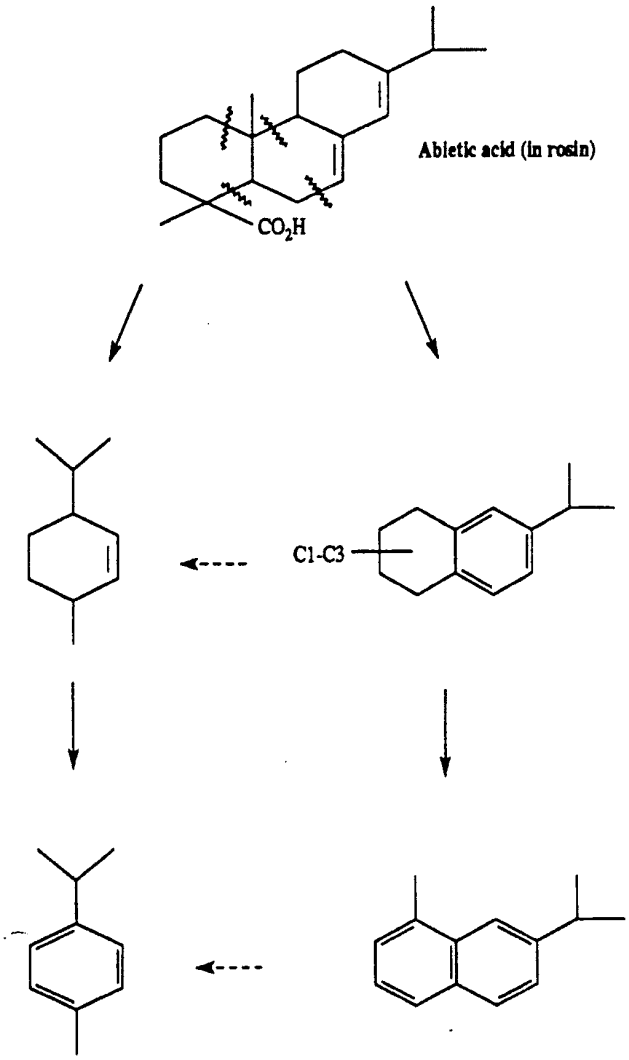

Figure 5.11-2. Cracking Reaction Pathway of Abietic Acid in Rosin

5.12 Hydrotreatment of Multicyclic Compounds to Produce Cycloalkanes

This study is explained in detail in *Advanced Thermally Stable Jet Fuels Technical Progress Report, January–March 1994.*

Introduction

With the increasing need to develop advanced jet fuel comes an increasing need to find new feedstocks that can be converted to thermally stable compounds. Jet fuels are traditionally produced from petroleum and contain a large proportion of alkanes, which are thermally unstable at elevated temperatures.[1] Previous work has shown decalin, tetralin, and cyclohexanes to be stable when stressed at high temperatures.[1] Therefore, selecting a feedstock that can be converted to one of these products quickly and easily would be advantageous. If cycloalkanes are to be produced efficiently, compounds that are predominantly cycloparaffinic would make ideal feedstocks.

As discussed in previous sections of Task 5, the potential feedstocks we have identified include resins, petroleum fractions, and model compounds representing coal/resin liquids. This study was designed to test all three.

Experimental

In this work, resins, petroleum fractions, and model compounds were hydrotreated and underwent time, temperature, and catalyst conditions chosen to provide high yields of desired jet fuel components, or compounds that could be easily converted to cycloparaffins. After initial studies of the chemistry involved in the reactions, we compared the yield and composition of the liquid products for each feedstock at the chosen optimum condition. The final test for each reaction system involved comparing the thermal stability of surrogate liquids blended to have the same composition as the optimum feedstock products.

All reactions were carried out in 25 mL microautoclave reactors under hydrogen pressure of 7 MPa (cold). Various catalysts were used, depending on their effectiveness in each reaction system. Products were separated into liquid and solid fractions. Chemical composition and concentration of liquid products were determined using GC and GC/MS. HPLC was used to determine whether high molecular weight compounds were produced. Liquid NMR was used to determine the aromaticity of liquid products.

Results

1. Hydrogenation, Dehydrogenation, and Cracking of Rosin. Rosin is composed primarily of isomers of abietic acid. We studied the decarboxylation and cracking reactions and the hydrogenation/dehydrogenation behavior of rosin and its products to determine whether mono and bicyclic compounds could be produced from them. Details of the conditions used can be found in the original Technical Progress Report.[2]

In all cases, as temperature and time increased, the concentration of benzenes and naphthalenes in the liquid products increase. Benzenes are produced first in the cracking reaction. **Scheme I** shows the probable route of formation of benzenes.

Naphthalenes are produced later in the reaction for the non-catalytic and NiMo experiments. This can be attributed to the cracking of the terminal ring in norabietatriene and tetrahydroretene to produce substituted naphthalenes (noncatalytic) and tetralins (catalytic). When Ni-Y was used as a catalyst, cracking reactions were predominant in the first 10 minutes. Dehydrogenation and isomerization reactions predominated for the remainder of the reaction time.

Based on these results, we concluded that a catalytic stage is necessary to crack the three-ring structures to desirable benzenes and naphthalenes. This requires a high temperature, which favors dehydrogenation of cycloalkanes to aromatics. Therefore, the reaction must be stopped at an optimum point (predicted from the product distribution graphs), the temperature must be lowered to a point that favors hydrogenation over dehydrogenation, and a suitable catalyst must be added to hydrogenate the products from the first stage to produce cycloalkanes. This process is termed reverse temperature staging.

2. Hydrocracking Reactions of Dammar. Of Dammar's two fractions, the methanol-insoluble fraction is suspected of being a polymer called polycadinene. It is composed of low molecular weight compounds shown by GC/MS to be dimers and trimers of cadinene and functionalized triterpenoids. The polymer constitutes approximately 16% of the whole resin.[3] Research focused on:

1. Hydrocracking of whole Dammar at various temperatures and times
2. Separating Dammar into methanol-soluble fractions, followed by hydrocracking of the two fractions.
3. Analyzing liquids by GC/MS and HPLC. Product distributions were analyzed and reaction pathways were proposed.
4. Using Dammar to predict the behavior of resinite under liquefaction conditions. Results were compared to samples of resinite obtained from coal by solvent extraction.

Conclusion

As temperature increased, the large molecular weight compounds were cracked into benzenes and naphthalenes. The naphthalenes were probably cracked products of polycadinene, although the extent of depolymerization cannot be known until reactions on this individual fraction are undertaken. Napththalenes could also be produced from bicadinanes from this soluble fraction.

Saturated naphthalene compounds are the likely source of benzenes in the cracking products. Most of the high molecular weight compounds are cracked to dimers and trimers after only 10 minures. These dimers and trimers crack to produce naphthalenes, usually within the first 30 miutes of reaction time. Benezenes, which are produced from cracking of tetralins, steadily increase in concentration.

These results clearly indicate that a reverse temperature stage reaction is the best method for producing cycloalkanes, because most of the cracking reactions are complete after 30 minutes. If the reaction were allowed to continue, unnecessary dehydrogenation reactions would

occur, making the upgrading stage more difficult. **Figure 5.12-1** shows chromatograms of the naphthalenes in products before and after an upgrading step with palladium on carbon catalyst (300°C, 3 hours). The C_2 and C_3 naphthalenes have been almost entirely converted to tetralins. The benezene fraction did not hydrogenate under these conditions.

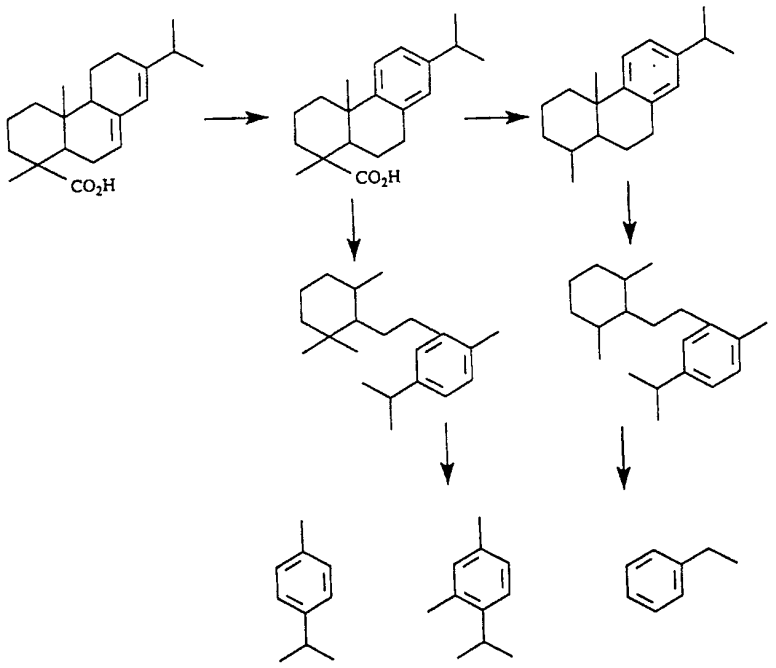

Scheme I. Formation of Benzenes from Rosin

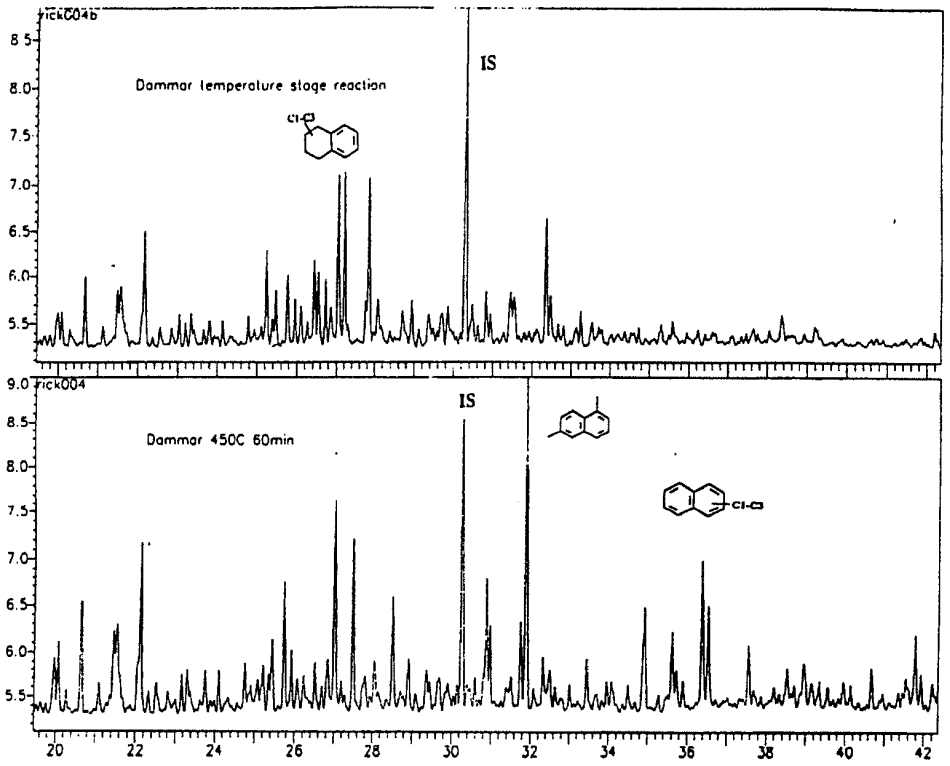

Figure 5.12-1. Bicyclic Products of Reverse Temperature Stage Hydrogenation of Drammar

---

[1] Song, C. et al. *Prepr. Pap. American Chem. Soc., Div. Pet. Chem.* 1992. 37(2). 484.

[2] Schobert, H. H. et al. *Advanced Thermally Stable Jet Fuels, Technical Progress Report, April 1994 – June 1994.* The Pennsylvania State University. 1994.

[3] Van Aarssen, B. G. K. et al. *Geochem. Cosmochim. Acta.* 1991. 54. 3021.

5.13 HYDROGENATION/DEHYDROGENATION OF POLYCYCLIC COMPOUNDS USING MoS_2 AS CATALYST

This study is explained in detail in *Advanced Thermally Stable Jet Fuels Technical Progress Report, January—March 1995.*

Introduction

Coal liquefaction is a viable means of producing advanced fuels only if the coal macromolecule can be broken into low molecular weight fragments and hydrogenated to decrease the concentration of aromatics in the final product. Previous studies have used various catalysts and conditions to aid in the initial breakdown of coal. However, to achieve a very high quality distillate as the final product, the coal liquids need further hydrotreatment.

One way of improving quality involves adding a step in the liquefaction process, employing a very active catalyst to hydrogenate the products from the first liquefaction stage. To minimize operating costs, though, the coal fragments could be hydrogenated as they are being released during the first stage of liquefaction. This would decrease the amount of hydrogen and the related cost required for the second stage. Ammonium tetrathiomolybdate can be used as a catalyst precursor for coal liquefaction to produce a pre-jet fuel. [1] Using this method, we observed coal conversion as high as 95%; however, the products were aromatic and contained some phenols.

Various temperature strategies have been formulated for coal liquefaction, the majority of which concern the depolymerization of coal and the avoidance of retrogressive reactions. The thermodynamic behavior of the released coal fragments is an important aspect of temperature strategies; a trade-off must be made between kinetics and thermodynamics. Fine tuning the reaction conditions could conceivably provide advantageous thermodynamics in the system and reasonably fast kinetics of depolymerization of the coal macromolecule. A study of model compounds could aid in understanding the fundamental behavior of coal fragments during coal liquefaction and coal liquids upgrading.

This study analyzed the hydrogenation/dehydrogenation behavior of 2-, 3-, 4-, and 5-ring compounds. We calculated kinetic and thermodynamic parameters from the product distribution trends, enabling us to outline a possible reaction strategy that allows the compounds to remain in their hydroaromatic states during a coal liquefaction operation. We hoped to determine what conditions would be required (once the hydrogen was in the system) to allow the hydrogen to remain there and what conditions favor rehydrogenation reactions.

Experimental

Reactions were carried out in 25 mL stainlessmicroautoclave reactors using 3±0.01 g naphthalene or pyrene and 0.075±0.005 g ammonium tetrahiomolybdate. The reactor was pressurized with hydrogen to 7 MPa. The reactor was heated in a fluidized sand bath and, after the specified reaction time, cooled in a cold water bath. The products were removed from the reactor using THF. The THF was removed by rotary evaporation and the product weighed. In all cases, the weight of the products equaled the weight of the original pyrene before reaction. The products were dissolved in acetone and GC analyzed. As all of the compounds in the

products were detected, we observed that the responses of the compounds were similar and that their peak areas gave mass fractions directly. This was confirmed by injecting standard mixtures of naphthalene and tetraline.

To determine the dehydrogenation behavior of the hydrogenated pyrenes, the products from pyrene hydrogenated at 350°C for 60 minutes, 400°C for 80 minutes, and 450°C for 40 minutes were catalytically dehydrogenated under N_2 (using the same reactors used in hydrogenation). The products were weighed into the reactor with 1 wt% of ATTM and the reactor was pressurized with 3 MPa N_2 and immersed in a heated sandbath. After the specified time, the reactor was quenched and the products were removed using THF and GC analyzed, as before. The dehydrogenation behavior of tetralin was similarly investigated.

Results

1. Naphthalene

Thermodynamics. At reaction temperatures of 350°, 400°, and 450°C and reaction times up to 3 hours, tetralin was a hydrogenation product of naphthalene. No decalin was observed. Cracking/isomerization products of tetralin were observed at 450°C, but total concentration did not exceed 5 wt%. At 450°C, conversion of naphthalene to tetralin reaches a maximum of 51%. At 400°C, conversion was 62% and at 350°C, it did not reach equilibrium, but was 72% after 3 hours. The resulting Kp values decreased with increasing temperature, reflecting the fact that thermodynamics controls the extent of the reaction as temperature increases.

Kinetics. We proposed a simple pseudo-first-order reaction for the hydrogenation of naphthalene to tetralin:

$$\text{naphthalene} + 2H_2 \rightarrow \text{tetralin}$$

$$d\,[\text{naphthalene}]/dt = -k\,[H_2]\,[\text{naphthalene}] = -k'[\text{naphthalene}]$$

$$-d[\text{naphthalene}]/[\text{naphthalene}] = k'\,dt$$

$$\ln [\text{naphthalene}]_t / [\text{naphthalene}]_0 = -kt$$

When the data for each time were plotted, deviation from the straight line was observed, which could have resulted from heat-up effects, change in overall pressure as hydrogenation proceeds, and thermodynamics pulling the reaction away from first-order behavior. The reaction at 450°C is affected sooner than that at 400°C and the reaction at 400°C is affected earlier than the reaction at 350°C. This suggested that the effect of thermodynamics increases at time and temperature increase. An activation energy of 12.6 kcal/mol was calculated from the slope of the corresponding Arrhenius plot.

Kinetics vs. Thermodynamics. To produce hydroaromatics from aromatics, we must first consider two factors conversion and length of time to reach the desired conversion level. Conversion decreases with increasing temperature, but the kinetics of the reaction are slower at lower temperatures. Based on our data, high temperatures are desirable for the first 40 minutes of reaction, but after 40 minutes, thermodynamics limits the conversion. At that point, the temperature should be dropped below 400°C so naphthalene converson to tetralin can continue

as in the 350°C reaction. To hydrogenate at 350°C would take too long 120 minutes of reaction at 350°C is equal to 60 minutes at 450°C. Therefore, in hydrogenating naphthalene to tetralin, we propose a two-stage reaction:

Stage 1: 400°C, 40 minutes
Stage 2: 350°C, 60 minutes

Dehydrogenation Reactions of Tetralin. As temperature increases, the rate of dehydrogenation increases and the conversion of tetralin to naphthalene increases. At 350° and 400°C, conversion to naphthalene does not exceed 13%, but at 450°C, conversion reaches 42%. This explains the rapid approach to equilibrium seen in the hydrogenating reactions and the relatively low conversions seen at the high temperature (450°).

2. Pyrene

Thermodynamics. The distribution of pyrene, dihydropyrene, tetrahydropyrene, and hexahydropyrene products demonstrated that temperature affects the conversion of pyrene to hydrogenated pyrenes. Similar to naphthalene hydrogenation, as temperature increases, the conversion of pyrene decreases, but the rate of reaction increases.

Kinetics. As temperature increases, the rate constant increases from 0.0088 min^{-1} (350°) to 0.014 min^{-1} (400°C) and 0.019 min^{-1} (450°C). An activation energy of 6.88 kcal/mol was calculated from the slope of the corresponding Arrhenius plot.

Kinetics v. Thermodynamics. Similar to naphthalene, we recommend a reverse temperature stage reaction:

Stage 1: 400°C, 20 minutes
Stage 2: 350°C, reaction time set for desired conversion

Dehydrogenation of Hydropyrenes. Dehydrogenation is rapid and complete at 450°C. At lower temperatures, dehydrogenation is slower and complete dehydrogenation to pyrene was not observed in the 30-minute reaction time. Dehydrogenation constants were similar for dihydropyrene, tetrahydropyrene, and hexahydropyrene.

Comparison of Naphthalene and Pyrene

As ring size increases, enthalpy of reaction decreases and activation energy decreases. Plots of the dehydrogenation rate/hydrogenation rate vs. temperature demonstrate the susceptibility of compounds to dehydrogenation. Pyrene is more readily hydrogenated than naphthalene, and the effect of increasing temperature increases as ring size increases.

[1] Burgess, C. Pennsylvania State University. 1994.

5.14 EXPLORATORY STUDIES ON THE POSSIBILITY OF NON-RADICAL HYDROGEN TRANSFER UNDER LOW TEMPERATURE LIQUEFACTION CONDITIONS

Introduction

Gaseous hydrogen reacts with coals under low temperature conditions in preference to hydrogen from donor solvents such as tetralin. In the presence of a catalyst in a hydrogen atmosphere, transfer of hydrogen can occur via one of two possible scenarios:

- Hydrogen could directly hydrogenate the sample using a catalyst
- An aromatic solvent could hydrogenate into a donor species, then hydrogenate the samples

Neither of these pathways has been proven conclusively, leaving these questions: Which is the main pathway of hydrogen transfer from donor or from gaseous hydrogen? And why does preferential donation from gaseous hydrogen occur in some, but not all, cases?

Previous studies indicate that this phenomenon may rely on the catalyst activity and the type of donor or sample. Hydrogen transfer mechanisms were studied using tritium tracers to determine whether radicals produced in polycondensed aromatic hydrocarbons could behave as catalysts for the dissociation of hydrogen molecules.[1] Hydrogen exchange between gas phase and coal components proceeded before hydrogen migration among the system components, indicating that the hydrogen atoms in large coal molecules (with structures resembling polycondensed aromatics) could be highly exchangeable with gaseous hydrogen, even without a catalyst. However, the complex nature of the coal structure makes the use of model compounds more practical than obtaining a transfer mechanism.

Previous observations have all been based on experiments conducted in the presence of catalysts under the premise that the initial steps for coal hydrogenation have occurred via radical hydrogen transfer. Recently, however, the existence of non-radical pathways for hydrogen incorporation has been proposed. Reactions of coals are not necessarily limited to free radical processes. Generally, radical reactions are dominant at 350°C or higher. If non-radical reaction pathways exist, they could explain a higher gas-phase H_2 consumption observed in comparative non-catalytic runs with raw and dried coals at 350°C.[2] Reactions involving charge separation (i.e., ionic reactions) could play a key role in coal conversion processes, given the polar functionalities in coals. Because many of the oxygen-containing constituents of coal liquids are phenolid, structures that could possibly participate in non-radical pathways include β-naphthols and 1,3- and 1,4-dihydroxy aromatics. These structures could possibly add H_2 through a concerted pathway, forming enols which then convert to ketones.

a. Investigating the Possibility of Non-Radical Hydrogen Transfer in Coal Liquefaction

This study is explained in detail in *Advanced Thermally Stable Jet Fuels Technical Progress Report, January 1995 — March 1995.*

Purpose: Test the hypothesis of non-radical hydrogen transfer in coal liquefaction of DECS-8 Wyodak coal, which is rich in phenolic structures.

Experimental: The DECS-8 was reacted at low temperature (350°C) without the presence of a catalyst to observe an increase in carbonyl content. The FT-IR difference spectrum between the whole product and the vacuum dried, unreacted coal indicated that the reaction involved the loss of hydrozyl groups and the increase of aliphatic C-H groups. No increase in carbonyl groups was observed. A detected formation of CO indicates that this could be attributed, at least in part, to decarbonylation at 350°C.

Further experiments were conducted in a nitrogen atmosphere to determine whether the results with hydrogen could be attributed to hydrogenation or thermal reactions. We found that the gas formation in both runs could be attributed to thermally driven reactions alone. The CO formation in the experiment conducted under H_2 at 350°C apparently did not result from decarbonlyation of newly formed ketones.

Findings: Under the conditions employed, our experiments did not produce significant ketone, which is the product of non-radical incorporation of molecular H_2 into coal.

The next step in this investigation should involve examining the possibility that the reactions of H_2 could be a mineral matter-catalyzed reaction. Tests should be conducted on demineralized coal samples and representative model compounds. The objective of demineralization is to isolate the kerogen by making the miner matter phase soluble, while minimizing modifications in the chemical composition of the organic matter.

b. Initial Determination of Whether Thermal Reactions at 350°C Are Mineral Matter Catalyzed

This study is explained in detail in *Advanced Thermally Stable Jet Fuels Technical Progress Report, April — June 1995.*

Purpose: The pathways by which coal macromolecules can be depolymerized to give lighter products and the precise roles of individual functional groups in the reactions continue to be investigated. Generally, radical reactions for hydrogen incorporation are dominant at temperatures at or above 350°C. Recently, however, the existence of non-radical pathways has been proposed. Phenols may be one such species that participates in concerted reactions, undergoing conversion to ketones via an enol intermediate. This mechanism could be facilitated by molecular hydrogen, thus serving as the basis of a possible non-radical hydrogenation of coal.

Preliminary studies had been conducted on Wyodak coal, known to be rich in phenolic species, to determine whether such mechanisms occur under low temperature liquefaction conditions (350°C, 1000 psi H_2, 30 minutes).[3] However, no definite conclusions were drawn from this work.

The purpose of this study was to examine the possibility that the reaction with H_2 may be a mineral matter catalyzed reaction. Demineralization is based on the premise that the kerogen can be isolated via dissolution of the mineral matter phase, a process commonly facilitated by consumption of carbonates, sulphides, oxides, and hydroxides in HCl, followed by silicates in HF. Demineralization is typically carried out at a temperature sufficient to dissolve the carbonates, but not high enough to oxidize the organic matter (approximately 60°C).

Findings: Initial results indicated a comparative level of conversion between the two sets of data, suggesting that the thermal reactions undergone at 350°C are not mineral matter catalyzed. The seemingly higher conversion reported for the demineralized coal in the absence of solvent compared to the untreated coal may have been caused by water present in the sample due to insufficient drying an area that warrants further investigation.

For the demineralized coal reacted in the presence of the non-hydrogen donor solvent (i.e., 1-methylnaphthalene), C_1-C_4 gas production was greater by an order of magnitude than for the other reactions. However, GC results are not fully reliable for gaseous products, because the reproducibility of the calculated product distribution was inconsistent. Furthermore, the net hydrogen consumption from tetralin was not calculated, which would better illustrate if non-radical pathways effectively participate during hydrogenation.

Drawing any firm conclusions at this early stage in the experiment would have been unwise, because comparative data with untreated coal had not yet been completed for this set of experiments. However, the level of conversion attained with the demineralized coal was comparable to the untreated coal. Further characterization was carried out on the parent demineralized coal and certain products by FRIR and NMR.

The ^{13}C CP-MAS spectrum of the demineralized Wyodak coal displayed many similarities to that of the untreated coal.[2] The first region (0 and 80 ppm) consisted primarily of aliphatic carbons (e.g., methoxy groups). The second region (90 to 170 ppm) resulted from the presence of aromatic carbon. The shoulders present on the side of the aromatic band could be attributed to specific functionalities (e.g., catechol groups at 142 ppm and phenolic groups at 210 ppm). The carboxylic functionality was prominent at 180 ppm and the carbonyl was prominent near 210 ppm. Upon liquefaction under H_2 without solvent, the primary features illustrated by the product were as follows. In the aliphatic band, the symmetry observed for the parent coal was lost, and the appearance of a shoulder at ≈25 ppm was observed. This may be attributed to a number of groups, including CH_3-Ar side chains (20-21 ppm) or CH_3-CO_2-R acetates (20-22 ppm). Furthermore, the distinct shoulders observed in the aromatic region had virtually disappeared, indicating a loss of oxygen functionalities.

Comparative FTIR spectra of the whole demineralized coal indicated the presence of most of the groups of interest in this study, such as:

Hydroxyl groups	3300-3600 cm^{-1}
Aromatics	3030 cm^{-1} and associated bands at 1450-1600 cm^{-1}
Aliphatics	2920, 2850 cm^{-1}
Carboxylic acids	1710-1760 cm^{-1}
Conjugated Ketones	1715 cm^{-1}
Esters, Lactones	1712-1735 cm^{-1}
	(present as a shoulder on the C=O band)

After reaction under H_2 at 350°C, the most notable feature of the whole product spectrum was a decrease in hydroxyl concentration, in part attributed to a loss of H_20. Further examination of the THF-insoluble residue from this experiment confirmed the loss of OH functionality, coupled with the disappearance of the ester shoulder.

The FTIR spectrum of the THF-insoluble residue from the reaction conducted with tetralin displayed somewhat contrasting features. The carboxyl stretching region was much broader; moreover, the ester shoulder was more pronounced and the carbonyl region was much more defined. Generating the difference spectrum between the demineralized coal and the respective products could better illustrate the changes in structure undergone during reaction.

These results to date on the demineralized coal suggest that conversion to products at temperatures such as 350°C are not mineral matter catalyzed. Complete liquefaction tests for the full set of variables (i.e., both treated and untreated coal in the presence and absence of solvent) will provide much more conclusive data to either verify or disprove the possibility of non-radical hydrogenation in coal liquefaction.

c. Further Exploration of Possible Hydrogenation Mechanisms

This study is explained in detail in *Advanced Thermally Stable Jet Fuels Technical Progress Report, October — December 1995.*

In view of the economic constraints placed on current coal processing, attractive options for the future include reducing production temperature and H_2 consumption. To date, the exact role of much of the mineral matter in coals remains unclear. Catalytic activity, mainly attributed to pyrite, has been well-documented.[4, 5] Conversely, removal of naturally occurring cations, such as Na^+, Ca^{2+} and K^+, has been shown to enhance liquefaction conversions.[6] In recent tests, a higher gas-phase H_2 consumption was observed in comparative non-catalytic runs, with raw and dried low rank coals at 350°C. Preliminary studies were subsequently conducted on a demineralized sample to examine the possibility that the reaction with H_2 may be mineral matter catalyzed. We observed that demineralization had no serious detrimental effect on liquefaction under low temperature conditions.[7, 8] In terms of liquid product distribution, tests conducted in the presence of 1-methylnaphthalene yielded the best results. Perhaps elimination of such species allows for better access for gaseous H_2. However, questions regarding possible hydrogenation mechanisms remain.

Purpose: To further explore hydrogenation mechanisms under low temperature liquefaction conditions.

Experimental: During the last reporting period, a series of non-catalytic baseline tests were conducted at 300°C, again with Wyodak (DECS-8) coal. Refer to that study for an explanation of experimental procedures.[3]

Findings: In terms of total conversion (dmmf wt%), the product distribution for the tests (completed at 300° and 350°C, 1000 psi H_2, 30 minutes) complemented those reported previously by Saini et al.[9] However, product distributions, especially in the case where no solvent was present, varied from previous results.

Determination of liquid product distribution shows that the most significant changes occurred in the presence of solvent, both H-donor and non-donor. Oil yield increases the most with the H-donor solvent (≈4 wt%), almost double that observed at 350°C. Non-donor solvent afforded little change (≈1.2 wt%). However, oils yields from both runs (i.e., in the presence of both solvents and under two temperatures) were comparable. Asphaltene concentration increased by approximately 1.5 % in the presence of both tetralin and 1-methylnaphthalene; the

corresponding increases were 5 wt% and 3.2 wt%, respectively, for the runs at 350°C. The yield of pre-asphaltenes (THF-sols) in the presence of both solvent systems decreases approximately 2 wt%. This contrasts with the earlier results, where, at 350°C, the presence of 1-methylnaphthalene was shown to exert a favorable influence on conversion to preasphaltene. Therefore, as anticipated, relative to runs at 300°C, 350°C runs afforded higher overall conversions and better liquid product distribution. This trend was more apparent when either an H-donor (tetralin) or non-donor (1-mn) solvent was used.

The FRIR spectra of the THF-extracted raw coal and the residues from the runs conducted at 350°C revealed that under all conditions (i.e., in both the presence and absence of solvent), no marked changes were evident. The residue from this set of experiments was later analyzed by PY-GCMS to evaluate in more detail the fundamental differences in speciation resulting from non-catalytic treatment under different regimes.

5.15 LOW TEMPERATURE ROUTES TO HYDROGENATION OF PITTSBURGH NO. 8 COAL

This study is explained in detail in *Advanced Thermally Stable Jet Fuels Technical Progress Report, April—June 1995.*

Introduction

Hydrogenation of coal with gaseous hydrogen at high pressure and temperature is a difficult and costly process from a technological point of view. The high pressure, high temperature process of hydrogenation is hazardous and requires the construction of thick-walled reactors. Cost, inconvenience, and potential hazard encouraged us to develop new methods for hydrogenation methods that used lower temperatures and lower pressures. This work explored the feasibility of low-temperature routes to hydrogenation of Pittsburgh #8 coal.

Experimental

Pittsburgh # 8 (DECS-12) coal samples were used. The experiment was carried out at 300°C, with a starting pressure of hydrogen in the batch reactor of 1000 psi. The time of reaction was 30 minutes. No catalyst or solvent was used. Changes of reaction pressure are presented in **Table 5.15-1**. The residue was analyzed by NMR and pyrolysis-GC/MS.

Results and discussion

No significant changes were observed in the hydrocarbon structure of coal at 300°C, indicating that the hydrogenation will not occur at or below 300°C in the absence of a solvent or catalyst two common means of reducing the temperature of hydrogenation. (Later experiments with DECS-12 coal were carried out in presence of hydrogen-donor solvent 9,10dihydrophenanthrene.)

There is another way to decrease temperature of hydrogenation and increase the rate of reaction of hydrogenation. Using microwave energy enables us to increase the rates of some organic reactions several times. Preliminary research using microwave energy found that the oxidation of coal occurs at 150°C, but using microwave energy decreases the temperature of reaction and increases the rate of reaction. Microwave energy should, therefore, be considered a factor in increasing the rate of hydrogenation and decreasing the temperature of reaction to the other factors (catalysts, solvents).

Conclusions

This work demonstrated that hydrogenation does not occur in the absence of catalysts or hydrogen-donor solvents. There are two common ways to decrease temperature of hydrogenation use catalysts or use hydrogen-donor solvents. Based on preliminary reasearch, there may be other ways to achieve the same goal, including the use of microwave energy.

Table 5.15-1. Changes of Reaction Pressure

Time (min)	Pressure (psi)
0	1000
1	1500
2	1510
3	1520
4	1525
5	1526
6	1532
8	1539
10	1540
15	1540
20	1539
25	1540
30	1540
Pressure after reaction	990

[1] Yamamoto, K. et al. *Coal Science Technology.* Proc. 1987 ICCS. 1987. 211.

[2] Song, C., A. K. Saini, and H. H. Schobert. *Energy & Fuels.* 1994. 8. 301.

[3] Martin, S.C., and H.H. Schobert. Advanced Thermally Stable Jet Fuels, Technical Progress Report, January— March 1995. 1995. 74.

[4] Maldonado-Hodar, F.J. et al. *Fuel*. 1995. 74(6). 818.

[5] Garcia, A. B., and H. H. Schobert. *Fuel*. 1989. 68. 1613.

[6] Joseph, J. T. and T. R. Forrai. *Fuel*. 1992. 71. 75.

[7] Martin, S.C., and H.H. Schobert. Advanced Thermally Stable Jet Fuels, Technical Progress Report, April— June 1995. 1995. 35.

[8] Martin, S.C., and H.H. Schobert. Advanced Thermally Stable Jet Fuels, Technical Progress Report, July— September 1995. 1995. 22.

[9] Saini, A. J., C. Song, and H. H. Schobert. *Am. Chem. Soc. Div. Fuel Chem. Prep.* 1992. 37(3). 1235.

5.16 THE STUDY OF COAL USING LOW-TEMPERATURE HYDROGENATION IN THE PRESENCE OF HYDROGEN-DONOR SOLVENTS

This study is explained in detail in *Advanced Thermally Stable Jet Fuels Technical Progress Report, July — September 1995.*

Introduction

Pittsburgh No. 8 coal does not seem to react with molecular hydrogen at temperatures below 300¡C.[1] This confirms that hydrogenation of coal requires the use of atomic hydrogen or protons formed during some reactions.[2] For example, some kinds of organic solvents (e.g., tetrahydro-naphthalene, 9,10-dihydrophenanthrene, and dihydropyrene) might play the role of hydrogen-donors during the hydrogenation process. A possible mechanism of the donation process is:

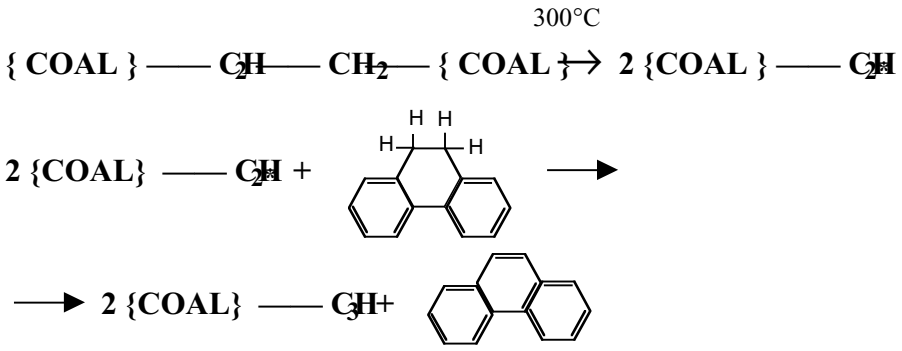

In the presence of gaseous molecular hydrogen the following reaction might occur:

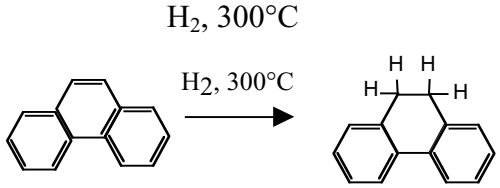

This reaction could not occur, or would occur very slowly, without a catalyst. If the catalyst was not added to the system, perhaps some naturally occurring catalysts contained in coal could speed up the reduction of phenanthrene. One possible catalyst is FeS_2, which is originally present in coal mineral matter. FeS, a compound that could be formed from FeS_2, could act as the catalyst for transforming phenanthrene to 9,10-dihydrophenanthrene.

In the type of process discussed above radicals are formed in coal by breaking C—C bonds by heating. These radicals are stabilized by hydrogen produced from the reaction of dehydrogenation of 9,10-dihydrophenanthrene (hydrogen-donor solvent). Phenanthrene is formed during this reaction; the phenanthrene then is reduced to 9,10-dihydrophenanthrene by molecular hydrogen.

The experiments described here were based on this mechanism of hydrogenation.

Experimental

Two coal samples with different rank were used for the experiments: Pittsburgh # 8 (DECS-12, hvAb rank) and Wyodak (DECS-8, subC rank). The experiments were carried out at 300°C in the batch reactors. The starting pressures in the reactors were:

Reactor # 1 (DECS-12): 1150 psi;
Reactor # 2 (DECS-8): 890 psi

Time of reactions was 30 minutes. 9,10-dihydrophenanthrene was used as a hydrogen-donor solvent. No catalyst was used for the experiment. The residues were investigated by CP/MAS NMR spectroscopy.

Conclusions

9,10-dihydrophenanthrene allows the process of hydrogenation to occur at 300°C without a catalyst. The average percentage of aromatics converted during hydrogenation is 5%. The effectiveness of the hydrogenation process at given conditions seems to increase with decreasing rank of coal (Pittsburgh #8 is high volatile bituminous coal, Wyodak is subbituminous coal): low-rank coal produces a larger amount of low molecular weight aliphatic molecules than high rank coal.

The amount of oxygen-substituted aromatics also changes during low-temperature hydrogenation. This process also depends on coal rank: for Pittsburgh #8 the amount of oxygen-substituted aromatics decreased from 3.6% to 3.4% (0.2%), for Wyodak this value was 7.12% (from 10.3% to 3.18%).

In summary, low-temperature hydrogenation occurs at 300°C in the presence of the hydrogen-donor solvent 9,10-dihydrophenanthrene. This solvent was not effective under present conditions (300°C, without catalyst) a low percentage of aromatics converted to aliphatics. Increasing the effectiveness of the solvent may require a catalyst.

---

[1] Schobert, H. H. et al. *Advanced Thermally Stable Jet Fuels, Technical Progress Report, April — June 1995.* The Pennsylvania State University. 1995.

[2] Aronov, S. G. and L. L. Nesterenko. *Chemistry of Solid Fossil Fuels.* Khar kov: University of Khar kov. 1960.

5.17 HYDROGENATION/DEHYDROGENATION OF POLYCYCLIC AROMATIC HYDROCARBONS USING AMMONIUM TETRATHIOMOLYBDATE AS CATALYST PRECURSOR

This study is explained in detail in *Advanced Thermally Stable Jet Fuels Technical Progress Report, July — September 1995.*

The hydrogenation and dehydrogenation behavior of naphthalene, phenanthrene, and pyrene was investigated via their product distribution and kinetic and thermodynamic parameters. Hydrogenation reactions were carried out in 25 mL microautoclave reactors at 350, 400, and 450°C for various times up to equilibrium conditions. A global kinetic model was used to determine forward and reverse rate constants, which were then used to determine Arrhenius parameters. Enthalpy data were obtained and compared to values calculated in the literature. It was found that the temperature where dehydrogenation became favorable over hydrogenation reactions decreased with increasing ring size. This was also shown by an increasing thermodynamic control over the reactions as ring size increased.

Introduction

Coal liquefaction can be considered a technically viable alternative for the production of liquid transportation fuels if the coal macromolecule can be broken into low molecular weight fragments, and the fragments can then be hydrogenated to decrease the concentration of aromatics and heteroatoms (nitrogen, sulfur, and oxygen) in the final product. The liquefaction process can be facilitated using various sulfided catalysts, which are generally resistant to poisoning by heteroatomic compounds. The exact role of the catalyst is still under question. The catalyst is thought not to participate in bond cleavage directly. The breaking of these bonds in the coal macromolecule is generally considered to be a thermally driven process. However, the use of a catalyst, along with a hydrogen-donor solvent, does improve conversion to liquid products. In fact, if the coal is relatively easy to convert, a catalyst will improve conversion without a good donor solvent present.[1] Therefore, research into catalyst development and the effects of catalysts on coal dissolution and upgrading of primary products is an important component of coal liquefaction development.

Molybdenum has long been a focus of research into catalytic coal liquefaction. Liquefaction improves with an increase in molybdenum concentration, but limits exist beyond which further increases in molybdenum no longer have a significant effect.[2, 3, 4] Because the catalytically active form, MoS_2, is insoluble, a dispersion of molybdenum onto coal particles is often effected using so-called catalyst precursors. The precursors are soluble compounds of molybdenum that may have little or no catalytic activity themselves, but are presumed to convert to a catalytically active form at liquefaction temperatures. Ammonium heptamolybdate (AHM) has been used in liquefaction research. Ammonium tetrathiomolybdate (ATTM), created by sulfiding AHM with H_2S, produces higher conversions than AHM. The mechanism by which ATTM decomposes to its active form is MoS_2.

In our research, through careful coal selection, we achieved coal conversions of up to 95% in catalytic reactions, although the hexane-soluble oils produced in the process still remained aromatic. The aromatics in the coal liquids have to be removed if they are to be used for liquid transportation fuels. Coal may be the preferred feedstock for advanced generation jet fuels that would be able to withstand severe thermal stressing without decomposing to

carbonaceous solids; however, aromatics have been shown to be precursors to solid deposition in fuels at elevated temperatures.[5, 6, 7] Upgrading processes would have to hydrogenate the aromatics produced during liquefaction. This step would involve catalytic hydrotreating of the primary liquid products from coal. However, hydrogenating as many of the coal fragments as possible during the liquefaction step itself would be more economically advantageous; that is, as the coal fragments are released during the depolymerisation of the coal macromolecule.

Various strategies have been formulated for application of temperature during liquefaction. These strategies are concerned with optimizing depolymerization of coal, upgrading primary products, and avoiding retrogressive reactions. The retrogressive reactions represent the recombination of reactive free radicals to form a carbonaceous char that resists further reaction. Such reactions often occur because the rate of hydrogenation cannot catch up to that of free radical formation. In temperature-staged and temperature-programmed liquefaction, a low-temperature pretreatment stage is followed by a high-temperature reaction stage. Conditions during the second stage are responsible for the quality of the coal liquids produced. Careful fine tuning of the reaction conditions could result in advantageous thermodynamics in the system, combined with reasonably fast kinetics of depolymerization of the coal macromolecule. Basically, a trade-off between kinetics and thermodynamics is possible.

Given the complexity of the macromolecular structures of coals, the likely existence of numerous parallel reactions during liquefaction, and the production of dozens of individual compounds in the coal-derived liquids, the use of model compounds facilitates research into the effect of various reaction conditions. Hydrogenation of aromatics has been studied for many years, focusing on kinetic, thermodynamic, and product distribution analysis. Correlations among the reactivities of 2-, 3-, and 4-ring compounds were lacking. In some cases, the research only employed a single temperature. We now know that an investigation of temperature effects is vital to understanding hydrogenation/dehydrogenation reactions.

This work focused on the hydrogenation and dehydrogenation reactions of naphthalene, phenanthrene, and pyrene using ATTM as the catalyst precursor. This choice stemmed from our previous investigation of the behavior of a variety of polycyclic compounds, aimed at investigating some of the fundamental chemical processes involved in various aspects of fuel utilization. These included direct coal liquefaction,[1, 8] stability of aviation fuels[5-7] and carbonization or graphitization reactions leading to carbon materials.[9]

Experimental

All reactions were carried out in 25 mL microautoclave reactors. In all runs, 3–0.01g reactant and 0.075–0.005g ammonium tetrathiomolybdate were weighed into the reactor. The reactor was then purged with hydrogen twice, before the final pressurization with hydrogen to 7MPa. Heating was accomplished by lowering the reactor into a fluidized sand bath preheated to the desired temperature. After a measured reaction time, the reactor was removed from the sandbath and quenched to room temperature by immersing it in a cold water bath. The products from the reaction were removed from the reactor using tetrahydrofuran (THF). The THF was removed by rotary evaporation and the product was weighed. It was found that in all cases the weight of the products equaled the weight of the original compound before reaction. The products were dissolved in acetone and analysed using a Perkin-Elmer 8500 gas chromatograph.

Products were identified using a Hewlett-Packard 5890II gas chromatograph coupled with a HP 5791A mass selective detector.

To determine the dehydrogenation behavior of the hydrogenated pyrenes, the products from pyrene hydrogenated at 350°C and 60 minutes, 400°C and 80 minutes, and 450°C and 40 minutes, were catalytically dehydrogenated under N_2. This was accomplished using the same reactors and heating and cooling processes as in the hydrogenation step. The products from the three hydrogenations listed above were weighed into the reactor with a 1wt% (metal) loading of ATTM. The reactor was pressurized with approximately 3 MPa N_2. After reaction, the products were removed using THF and analysed using GC. The dehydrogenation behavior of tetralin was investigated in a similar way to the hydrogenated pyrenes.

Conclusions

The main objective of this work was to compare 2-, 3-, and 4-ring systems and try to extrapolate our findings to larger ring systems. From a kinetic standpoint, the rate of reaction appears to be the most important factor for bicyclic compounds. As ring size increases, kinetics play a less important role, and thermodynamics becomes the driving force for the outcome of the reaction. In fact, the data for pyrene showed that even at the low temperature of 372°C, dehydrogenation reactions predominate. This implies that if even larger ring systems are hydrogenated, equilibrium considerations will become dominant.

This shift in relative importance of thermodynamic and kinetic considerations can be attributed, in part, to the heats of formation of the various polycyclic compounds and their hydrogenated species. Shaw et al. reported these values, revealing a clear trend of increasing thermodynamic control over hydrogenation reactions with increasing ring size.[10] The enthalpy data from the present work correlates well with Shaw s data. The following thermodynamic trends also were revealed:

- When adding 1 mol H_2, dihydrophenanthrene is more readily formed than dihydropyrene.
- When adding 2 mol H_2, tetrahydronaphthalene is more readily formed than tetrahydrophenanthrene, which is more readily formed than tetrahydropyrene.

In terms of coal liquefaction, temperature effects are very important when hydrogenating 3- and 4-ring systems, whereas the kinetics of hydrogenation of 2-ring systems are very important. Therefore, a tradeoff between kinetics, thermodynamics, and product selectivity is necessary.

In determining a coal liquefaction process, the type of product required is a significant consideration. If coal is to be converted, not simply to a synthetic crude oil, but to some specific product slate, then the coal has to be selected on a basis of its molecular architecture. For example, a product that requires a large concentration of tetralin and decalin, a coal-derived jet fuel for example, requires a feedstock in which bicyclic components dominate in its structure. Conditions for liquefaction can then be determined to match the desired reaction chemistry of the selected feedstock. Data from this work suggest that the important factor is depolymerization kinetics and subsequent hydrogenation kinetics. A product that requires larger ring structures as part of its composition would require a coal that has these large polycyclic moieties as part of its

structure. Our data suggest that for hydrogenation of the fragments to take place, the temperature of the reaction must be precise.

A possible reaction strategy for consideration in the future, particularly for direct production of high yields of hydroaromatic or fully hydrogenated compounds, would be a reverse temperature program that would have a low-temperature final stage to avoid dehydrogenation reactions.

---

[1] Huang, L. PhD Dissertation, The Pennsylvania State University, University Park, PA. 1995.

[2] Derbyshire, F. J. et al. *Applied Catalysis.* 1986. 27. 117.

[3] Abotsi, G. M. K. PhD Dissertation, The Pennsylvania State University, University Park, PA. 1987.

[4] Garcia, A. B. and H. H. Schobert. *Coal Preparation*. 1989. 7. 47.

[5] Song, C. et al. *Prepr. Pap.- Am. Chem. Soc., Div. Pet. Chem*. 1992. 37. 484.

[6] Song, C. and P. G. Hatcher. *Prepr. Pap.- Am. Chem. Soc., Div. Pet. Chem.* 1992. 37. 529.

[7] Song, C. et al. *Energy Fuels.* 1993. 7. 234.

[8] Burgess, C. PhD Dissertation, The Pennsylvania State University, University Park, PA. 1994.

[9] Atria, J. V. M.S. Thesis, The Pennsylvania State University, University Park, PA. 1994.

[10] Shaw, R., D. M. Golden, and S. W. Benson. *J. Phys. Chem.* 1977. 81.

5.18 HYDROGENATION OF COAL AT MILD CONDITIONS

This study is explained in detail in *Advanced Thermally Stable Jet Fuels Technical Progress Report, July — September 1997.*

Introduction

Hydrogenation is important as a source of synthetic liquid fuels. Thus, studies of coal hydrogenation mechanisms are very important from a practical point of view.

The interaction of hydrogen as a reductive agent with coals depends on the reactivity of coal organic matter, conditions of the process, and the form in which hydrogen reacts with coals. Molecular hydrogen does not react with coal at normal conditions and atomic hydrogen is very reactive; therefore, we must create conditions that will support the transformation of molecular hydrogen to the atomic form.

Berthelot (1870) was the first researcher to investigate the treatment of coal by atomic hydrogen.[1] He used hydrogen iodide as a reductive agent. Later Bergius (1913) developed a new approach to liquefaction and hydrogenation of coals based on treatment with molecular hydrogen at 450°-470°C and pressure of 200 atm, and in the presence of catalysts.[2] Historically, Bergius method was the first used for industrial production of liquid oils and synthetic fuels from coal. The majority of methods now used for coal liquefaction and hydrogenation are based on modifications of Bergius approach. A number of methods of catalytic hydrogenation at mild conditions (300°-350°C) were developed and used by researchers over the past 60 years. Hydrogen-donor solvents are also used by many present-day researchers.

Problems persist with coal hydrogenation, especially in hydrogenation at mild conditions. As we research and develop next-generation jet fuels, the search for more effective catalysts and solvents and more effective methods for obtaining structural information require us to concentrate our attention on hydrogenation studies.

Background on Conventional Hydrogenation

A number of factors affect hydrogenation, including such coal characteristics as petrological composition, coal rank, and mineral matter. Some types of coals undergo chemical and physical transformation more readily then others. Coals also have variations in yield and in product properties. The reasons for these phenomena lie in the petrological composition and rank of coals.

Petrological Composition. The organic material of coal is made up of macerals; studies of individual macerals enable us to determine their chemical and physical properties. We can also identify correlations between different forms and structures of macerals and particular fossil plants and vegetable materials. There are three groups of macerals with similar origin or chemical composition: *vitrinite, liptinite, and inertinite.* In a group of macerals with the same rank, where vitrinite contains 84% carbon, hydrogen content will be: 7% liptinite, 5.5% vitrinite, and 3.9% inertinite. Such differences in chemical composition lead to different behavior of macerals during coal hydrogenation.

Liptinite is more reactive in hydrogenation and liquefaction processes, because it is more aliphatic and hydrogen-rich. The reactivity of vitrinite is lower than liptinite, but higher than inertinite, because vitrinite is moderately aromatic, mostly oxygen-rich, and has a moderate hydrogen content. Macerals from the inertinite group are generally inert in the process described. However, some variations exist within the inertinite group, including micrinite and macrinite.

In conclusion, liptinite-rich coal will undergo the hydrogenolysis more readily than inertinite-rich coal. The amount and rank of vitrinite will also influence the rate of process, composition and amount of final products of hydrogenation.

Coal Rank. Rank of coal depends of the age of the coal and conditions of its formation. The most acceptable coal rank classification is ASTM (American Society for Testing and Materials) system. This system, shown in **Table 5.18-1**, classifies coals on the basis of its behavior as a fuel. In general, the lowest hydrogenation yields are obtained from the highest rank coals. Many researchers agree that the optimum conversion is obtained from lignite and high-volatile bituminous coal, because high-rank coal has a highly aromatic structure with large-ring condensation. Low rank coal, in contrast, has a more aliphatic structure, which is very significant in hydrogenation process.

Mineral Matter. Mineral matter includes all inorganic minerals present in coal and inorganic elements that can nevertheless be present in organic compounds (for instance, sulfur or nitrogen). Carbon, hydrogen, and oxygen form organic matter of coal can also be present in mineral matter in form of carbonates, water, oxides, sulfates, and other minerals.[3]

Mineral matter in coal can be divided into three classes of inorganic constituents: bulk inorganic mineral phases, microscopic mineral phases mixed with the organic constituents (macerals) of coal, and inorganic elements bonded to the organic matrix. All inorganic elements present in coal mineral matter can be divided into two groups main elements (> 0.1%) (e.g., carbon, hydrogen, oxygen, nitrogen, sulfur, silicon, aluminum, iron, magnesium, sodium, potassium, titanium, and calcium), and trace elements (> 0.1%), which also can be divided into three subgroups in order of decreasing concentration in coal:

1. Boron, fluorine, phosphorus, chlorine, vanadium, chromium, manganese, nickel, copper, zinc, arsenic, lead, barium, zirconium
2. Lithium, beryllium, scandium, cobalt, gallium, germanium, selenium, strontium, bromine, rubidium, yttrium, niobium, molybdenum, cadmium, tin, antimony, iodine, cesium, lanthanum, tungsten, bismuth, uranium, ytterbium
3. Silver, gold, indium, rhenium, mercury, iridium, platinum

Concentrations of each element and types of compounds formed by these elements depend on physical-chemical and chemical-biological conditions of coal formation. Also, composition and relationship of mineral matter with organic matter are very specific for each coal and depend on a number of factors.

Mineral matter plays a variety of important roles in all coal utilization processes, including the hydrogenation process. Actually, this aspect of mineral matter science is not clear. Some workers reported that demineralization of coal before utilization positively influences coal

depolymerization, and provides good contact between demineralized coal and hydrogen-donor solvent.[4] However, other authors have shown that only minerals containing iron have a catalytic effect on coal hydrogenation. Iron (Fe) is present in mineral matter mainly in form of pyrite and pyrrhotite. Hydrogenation conversion increases with Fe content in mineral matter. Authors assumed that pyrite has a double catalytic role in both homogeneous and heterogeneous catalysis.[5] A number of authors have established the catalytic effect of mineral matter, particularly pyrite, indicating that demineralization of coal before hydrogenation seems is not required and may be undesirable.

Effect of Catalysts

Catalysts that are typically used in organic hydrogenation reactions in organic chemistry, are useless in coal hydrogenation because they are poisoned by sulfur contained in coal. Normally, molybdenum, iron, and tin compounds are used as catalysts for this process. Before the reaction, catalysts are dispersed as a precursors, then the catalyst precursors transform during the hydrogenation process to form the active catalysts. This method of dispersed catalysts is very effective, unfortunately, molybdenum catalysts are expensive. Iron catalysts are much cheaper and are used more often in hydrogenation and liquefaction processes. In the hydrogenation processes, this group of catalysts is thought to make hydrogen radicals from molecular hydrogen, leading to direct reaction between hydrogen radicals and coal free radicals generated by heat. Catalysts also help to break the bonds of the macromolecular structure of coal. The liquefaction experiments by Weller and Pelipetz suggest that molybdenum catalysts take part in depolymerization processes and help to hydrogenate heavier products by forming a lighter oil fraction.[6] All these assumptions have some supporting evidence in the literature, but there is still no clear theory describing the catalytic mechanisms of this type of catalysts.

Another important group of catalysts are acid catalysts. This group includes metal halides ($NiCl_2$, $ZnCl_2$, $SnCl_2$), which are highly active and selective catalysts. The highest activity of such catalysts can be realized at their high concentration, but, unfortunately, a high concentration of catalysts increases the contamination of undesirable chlorides in the liquid fuel. Acid catalysts act by ionic mechanisms. Metal halide reacts with water or with hydrogen halide with the formation of Lewis or Bronsted acids.

An additional type of catalysts is the internal catalyst. Hydrogenation can be catalyzed by mineral components present in coal.

Effect of Solvents

H-donor solvents play an important role in coal hydrogenation, performing three principal functions: providing additional hydrogen atoms, stabilizing reactive molecular fragments formed during coal structure degradation, and dissoluting the resulting fragments in the reaction medium. However, solvents cannot donate hydrogen into the system without adding external hydrogen gas. This external source is needed for reduction of the solvent molecule after the donation of coal molecular fragments.

The best H-donor solvents are partially hydrogenated condensed aromatics, such as tetralin, 9,10-dihydrophenanthrene or tetrahydrofluoranthene. The ring system of solvent also plays an important role in the ability of solvents to donate hydrogen: the bigger ring a system gets, the greater its ability to dissolve coal liquids. Therefore, tetrahydrofluoranthene is a better

H-donor solvent than 9,10-dihydrophenanthrene and tetralin,9,10-dihydrophenanthrene is better than tetralin..

Another group of solvents called hydrogen shuttlers cannot be H-donors but do make some contribution to the process of hydrogenation. During hydrogenation these compounds react with molecular hydrogen from the gas phase and transfer atomic hydrogen to the coal. Moreover, hydrogen shuttlers can react with other organic compounds, which can be dehydrogenated, and also transfer hydrogen from this reaction to coal. Two types of organic compounds can be the hydrogen shuttlers polycyclic aromatics (such as naphthalene and phenanthrene) and low molecular weight compounds like phenols.[7]

Chemical Composition of Hydrogenation Products

The final goal of coal hydrogenation is the conversion of solid coal into liquid product. The coal macromolecular network must be broken into smaller and less aromatic (more aliphatic) fragments. Because of the complex chemical structure of original coal, the products of coal hydrogenation consist of a number of different organic compounds. All are classified on the basis of their solubility in different solvents. The fraction that cannot be soluble in major organic solvents is usually called tar and includes highly aromatic, comparatively high-molecular compounds.

The difference between soluble and insoluble fractions of products may correspond to the difference between the chemical structures of both fractions.[8] The structure of potentially soluble material is more likely branching, in contrast to the structure of the insoluble fraction which tends toward crosslinking.

Historical Approaches to Mild Hydrogenation

One of the main goals of coal hydrogenation is to prevent retrogressive reactions from occurring during the coal heat treatment. Decreasing the temperature of the process and ensuring sufficient hydrogen donation to coal radicals formed during the heating are the keys to obtaining more complete structural information, suppressing retrogressive reactions, and precluding chemical changes during coal hydrogenation.

R*estricted hydrogenolysis* involves using an autoclave with a cold-head receiver, which allows the products of coal hydrogenation to leave the high temperature reaction zone by distillation as soon as the process of hydrogenation has advanced. Further chemical transformation of hydrogenation products is precluded by such a procedure. The temperature range of restricted hydrogenation is 350°-375°C.

Multiple hydrogenolysis involves using the lowest possible temperature during the process and stopping the experiment after a short time. The distinction of this method over others is the series of hydrogenation reactions carried out on residue using a fresh amount of catalyst in every reaction. This allows us to extract most of extractable materials at the mildest conditions (325°C and 400 atm pressure) and separate them into a number of fractions: hexane-soluble, ether-soluble, benzene soluble, etc.

Extractive hydrogenolysis is based on an even lower temperature (300°C) than that of multiple hydrogenolysis. The factors which allow use of such a low temperature are pyridine as

a reaction medium, very long reaction time (15 hours in the experiments of Meys et al.[9]), and very large amount of catalyst.

Hydro-iodolysis is a combination of Berthelot s method of reduction of coal structure with HI and new advances in coal hydrogenation. Geerards, VanKrevelen and Waterman (1958) reported that iodine as a catalyst under hydrogenation conditions (350°C and 200 atm hydrogen pressure) leads to successive yield of liquid products from coal.[10] The mechanism of hydro-iodolysis was studied on model compounds and then applied to coal. The behavior of coal during hydroiodolysis was similar to the behavior of substances like phenanthrene and chrysene and different from that of anthracene and pyrene. On the whole, the model compounds showed a high degree of cyclization, especially for carbohydrates, but also a splitting of some aromatic rings took place in fully aromatic compounds.

New Ideas in Coal Hydrogenation

Computer Simulation of the Molecular Structure. Computer simulation of coal molecular structure can help to predict the behavior of coals during conversion processes. Also molecular models can form the basis for the development of new methods in coal conversion, particularly in liquefaction and hydrogenation processes. For material with unknown structural formulas, such as coal, we must first use molecular simulation to study the three-dimensional organization of these compounds.

Coal is a highly heterogeneous material containing a number of individual macerals. Developing structural models for individual macerals may eliminate some heterogeneity. As a result, vitrinite is commonly chosen for molecular simulation; however, coalified wood serves as a superior substitute for vitrinite, offering more homogeniety than vitrinite. Structural models were developed from a lignin template lignin is a major source of chemical structures in coalified wood.

Construction of a computer model of coal or of an individual maceral requires the list of fragments and interfragment bonds derived from Py/GC/MS results, and data from elemental analysis, solid state NMR techniques, pychometry, mercury intrusion, SAXS (small-angle X-ray scattering), and SANS (small-angle neutron scattering). Computer simulated molecular structures are based on models of the chemical structure of coal developed earlier.

The physical parameters of coal also influence the computer model. Nakamura et al. suggested the physical density of coals as one of the most significant parameters which could be evaluated based on experimentally observed values.[11] Authors reported a number of interesting conclusions based on the density-energy approach to computer-aided molecular design. Coal model molecules were presented as composed of polyaromatic hydrocarbons and polymethylene bridges.

One of the possible directions of computer modeling investigations is the determination of electronic density of coal structures. Knowledge about the distribution of electronic density in the coal structure may help to predict with high probability the products of pyrolysis and the behavior of coal during coal conversion. Also, this method of coal investigation may open new horizons in coal chemistry.

Hydroboration-Protonolysis

Most modern methods of coal hydrogenation are based on the direct donation of molecular hydrogen into the coal structure. The variations of these methods are catalytic hydrogenation where catalysts mostly act as accelerators of the process, and hydrogenation with solvents where solvents are the additional sources of hydrogen atoms. Most investigations in this field have focused on finding the most successful catalyst or the most powerful solvent or the best combination of: temperature, pressure, concentrations of reagents, type and concentration of catalysts, and type and concentration of solvents or solvent mixture.

One recommended alternative to these old coal hydrogenation approaches is the application of hydroboranes as a hydrogen donor. The chemistry of boron hydride allows us to use them in the reductive reactions with reagents that contain double or triple bonds. The simplest hydroborane is BH_3, which exists in the form of diborane. A number of organboranes, such as boranetetrahydrofurane ($H_3B.THF$) or boranedimethylsulfide ($H_3B.Sme_2$) are available and more convenient as hydrogen-donors in the reactions with organic compounds.

Unhindered alkenes are the best reagent for hydroboration. Cyclic compounds containing double bonds also react with hydroboranes. The products of these reactions are cyclic alkylboranes, which are not desirable final products. The alkylboranes must be converted to alkanes via protonolysis. All alkylboranes undergo protonolysis by carobxylic acis such as propanoic or ethanoic acids.[12]

How do hydroboranes react with coal? Modern data allows us to conclude that the structure of coal contains different types of aromatic fragments, some types of sulfur containing fragments, and a number of aliphatic fragments. All these types of structural fragments might be reactive to boron hydrides.

Aromatic fragments could be reactive as a result of double bonds that could be localized by the influence of substitutions. Aliphatic fragments can also contain double bonds in the form of alkenes or dienes. For molecular fragments containing sulfur groups and carbon-carbon double bonds, such a reaction scheme (hydroboration - protonolysis) might provide an alternative to catalytic hydrogenation.[12] The products of these reactions could include primarily cyclic aliphatic molecules, which can be reduced by heat to simple alkanes. In summary, the use of hydroboration - protonolysis reactions seems to be a promising and attractive way of coal hydrogenation upgrading.

Plasma Hydrogenation

Plasma hydrogenation, a second modern method of coal hydrogenation that seems to be even more interesting, uses high-frequency energy. This approach has already been used for coal oxidation. This method uses a very low temperature (< 200°C), which helps to remove organic matter of coal without changing the mineral matter structure.

Application of high-energy electromagnetic fields in coal investigation is based on the formation of a plasma a mixture of neutral, ionized, and excited species, such as atoms, positive and negative ions, radicals. Gas (e.g., oxygen or hydrogen) is transformed into plasma by a high-energy electromagnetic field. The benefits include the atomic and ionic species, which are very reactive, and the low temperature of the plasma.

Hydrogen, which is very reactive, is a preferable reagent in the hydrogenation process. Usual methods of hydrogenation use chemical reactions for generation of atomic hydrogen, such as reactions with solvents. The use of high-frequency energy for generation of atomic hydrogen seems to be more successful, because it does not require an external source of heat, additional reagents (e.g., solvents or catalysts), or high pressure and temperature.

Conversely, plasma hydrogenation cannot be accompanied by pyrolysis because of the low temperature of the process. Low temperature of plasma is related to non-isothermal behavior of this system, indicating that the average velocities of particles in the plasma are different and the electronic temperature (Te) differs from the overall temperature (Tg) of the gas. The difference between Te and Tg allows us to reach a high reactivity of compounds at relatively low temperature. The mechanism of plasma hydrogenation is completely different from the mechanism of catalytic hydrogenation. High-frequency energy influences not only the gas phase of the process, but also the solid and liquid phases. High-frequency energy accelerates a number of organic reactions; however, the mechanism of high-frequency energy influence on reagents is not yet understood. Hence, high-frequency energy not only produces a plasma, but also stimulates the reactivity of organic reagents like coal.

Plasma hydrogenation mechanisms may be comparable to magnetic catalysis. In summary, high frequency energy stimulates the formation of radical pairs in the organic reagents. Radical pairs preferentially form in the points of the coal structure where heteroatoms are located. Electromagnetic energy might conceivably attack these bond types first: C-S, C-0, and C-N. As a result, the radical pairs will be generated and than stabilized by hydrogen atoms from plasma.

In general, low-rank coals, like lignite, contain a large number of heteroatoms. Therefore high-frequency energy will dissipate at these points of the structure, destroying the bonds near the surface. The structure of high-rank coals is more ordered, and also is more aromatic. Therefore, this type of structure contains significant free electrons that characterize aromatic and conjugated systems. In this case, the points of dissipation may be mobile fragments of coal structure.

Another coal structure double bonds in aliphatic and aromatic fragments of structure likely cannot be activated by high-frequency energy because of the homogeneity of electronic density of these bonds. On the other hand, active species of hydrogen plasma easily react with double bonds in the hydrogen abstraction reactions. In summary, plasma hydrogenation might occur in two principal ways: direct hydrogenation of aliphatics and aromatics by active hydrogen, and the destruction of the coal structure by high frequency electromagnetic energy with the formation of new radicals that will be stabilized by active hydrogen. The benefits of this new method of hydrogenation are clear the very low temperature of the process (< 200°C), the use of a vacuum instead of high pressure, and the absence of catalysts and solvents.

Conclusions

Hydrogenation of coal at mild conditions is usually carried out at a temperature in the range of 200°-350°C and under a pressure of 1000 psi in the presence of catalysts and hydrogen-donor solvents. Petrological composition, coal rank, and mineral matter composition must be

taken into account in coal hydrogenation. In particular, the comparison of hydrogenation behavior might be carried out only for coal with similar petrological composition. The most common types of catalysts are the metal precursor catalysts (e.g., Mo, Fe, and Sn) and acid catalysts, such as metal halides.

Computer simulation of coal structure can predict the behavior of coal during conversion and types of expected products. Computer modeling also may help to develop new methods of coal investigation.

New methods that can be applied in coal hydrogenation are based on new approaches. The method of hydroboration-protonolysis uses chemical hydrogenation but is based more on transition effects of reagents, rather than catalytic effects. Another method plasma hydrogenation uses a physical approach to the chemical problem. High-frequency energy is used instead of heating and high pressure for chemical bond cleavage and high reactive radical pair formation. This method could allow us to decrease the temperature to below 200°C and replace high pressure with vacuum.

Table 5.18-1. ASTM Rank Classification of Coals

Class	Group	%FC~ mmmfc	%VMb mmmfc	Calorific Value Btu/lb, mmmfd
Anthracitic	Metaanthracite	> 98	< 2	
	Anthracite	92-98	2-8	
	Semianthracite	86-92	8-14	
Bituminous	Low volatile	78-86	14-22	
	Medium volatile	69-78	22-31	
	High volatile A	< 69	> 31	> 14000
	High volatile B			13000-14000
	High volatile C			10500-13000
Subbituminous	Subbituminous A			10500-11500
	Subbituminous B			9500-10500
	Subbituminous C			8300-9500
Lignite	Lignite A			6300-8300
	Lignite B			< 6300

[1] Berchelot, M. *Ann. Chem. Phys.* 1870. 20.

[2] Bergius, F., S. Aronov, and L. Nesterenko. *Chemistry of Solid Fossil Fuels.* Khar'kov, University of Khar'kov. 1960.

[3] Korobetskii, I. A., and M. J. Shpirt. Genesis and Properties of Mineral Matter of Coal, *Science.* Siberian Branch, Novosibirsk. 1988.

[4] Gorbaty, M. L., J. W. Larsen, and I. Wender. *Coal Science.* 1983. 2.

[5] Maldonado-Hodar, et al. *Fuel.* 1995. 74. 818.

[6] Walter, S. and M. G. Pelipetz. *Md. Eng. Chem.* 1951. 43(5).

[7] Larsen, J. and T. L. Sams. *Fuel.* 1981. 60.

[8] Mayo, F.R., J. G. Hungtington, and N. A. Kirshen. *Organic Chemistry of Coal.* 1978.

[9] Meys, J.A., H. I. Waterman, D. W. Van Krevelen. *Van Krevelen, D.W. Coal.* Amsterdam: Elsevier. 1994.

[10] Geerards, J.J., D. W. Van Krevelen, and H. I. Waterman. *Brennstoff-Chem.* 39.

[11] Nakamura, K., S. Murata, and M. Nomura. *Energy and Fuels.* 1993. 7.

[12] Thomas, S.E. *Organic Synthesis: The Role of Boron and Silicon.* Oxford University Press. 1991.

5.19 HYDROBORATION OF COAL AS A NEW METHOD OF COAL HYDROGENATION AND A POSSIBLE METHOD FOR LIQUID PRODUCT UPGRADING

This study is explained in detail in *Advanced Thermally Stable Jet Fuels Technical Progress Report, October — December 1997.*

Introduction

We performed a study of the reaction between two coals Wyodak and Pittsburgh #8 and a borane-tetrahydrofuran complex. The ability of hydroborane to react with organic compounds containing double and triple bonds and heteroatoms (e.g., oxygen and nitrogen) could make hydroboration a promising method of coal hydrogenation. Recently published results on hydroboration of olefins and other organic compounds containing double bonds,[1, 2, 3, 4, 5, 6] and the results obtained in our laboratory, offer substantiation that hydroboration may be a viable new method of coal hydrogenation.

Boron hydride has been proven to react with substances containing double bonds with the formation of organoboranes.[7, 8, 9, 10] Organoboranes, formed by this reaction, easily react with oxidative or reductive agents with the formation of corresponding alcohols or alkanes, respectively. In organic synthesis, the hydroboration reaction is widely applicable. As has been shown by Brown,[11] a wide variety of organic compounds, including alkenes containing two, three, or four alkyl substituents on the double bond, cyclic and bicyclic olefins, aryl groups on the double bond, and even a number of steroids with highly hindered double bonds, readily undergo hydroboration.

Based on current models of coal structure, the hydroboration reaction may also be applicable as a method of mild hydrogenation of coal.[1213] According to these models, organic matter of coal includes a large number of double-bond-containing fragments that may undergo hydroboration. A successful process involving hydroboration and protonolysis of double bonds in the coal structure may significantly increase the aliphatic fraction of the structure. Such pre-treatment of coal may affect processing results, increasing quality or yield of coal processing products.

Experimental

This study consisted of five major parts:

1. Hydroboration of Pittsburgh #8 coal
2. Hydroboration-liquefication of Pittsburgh #8 coal
3. Hydroboration of Pittsburgh #8 sample pre-treated in hydrogen plasma
4. Hydroboration of Wyodak
5. Hydroboration-liquefaction of Wyodak

The procedures and results are discussed at length in the corresponding Technical Progress Report.[14]

Conclusions

Our research led to the following deductions:

- Aliphatic fraction of structure increases after hydroboration
- Aromatic fraction decreases after hydroboration
- The degree of substitution in aromatic fraction changes
- Hydroboration affects coal liquefaction
- Aromatic fraction is lower for a hydroborated-liquefied (Hp-L) sample than for liquefied sample
- Aromatic fraction is much higher for a liquefied-hydroborated (L-Hp) sample than for a liquefied and Hp-L sample
- Aliphatic fraction is lower for a Hp-L sample than for a liquefied sample
- The structure of Hp-L sample is similar to the structure of a liquefied sample, as demonstrated by photoacoustic FT-i.r. spectra
- The structure of the L-Hp sample is very different from that of both Hp-L and liquefied samples.

Consequently, hydroborane definitely reacts with the coal structure, causing several interesting changes. Hydroborane could react with the condensed structure of the liquefaction residue. If we can confirm this hypothesis through further experimentation, hydroboration could be considered a very effective means of coal hydrogenation. Hydroboration could also possibly enable us to hydrogenate condensed aromatic blocks.

At this stage of study, we must investigate the chemistry of the hydroboration process. Based on the complicated structure of coal, we recommend using model compounds representing fragments of coal structure as the next step in understanding the chemistry of the process. Organic compounds, containing two or three aromatic rings, with or without heteroatoms (e.g., anthracene, fluoranthene, dibenzofuran and carbazole), can be chosen as model compounds.

We plan to follow this study with other analytical techniques for investigating the hydroboration effect. For example, electron paramagnetic resonance (EPR) spectroscopy could provide useful information about changes of free radical concentration in coal samples during different types of treatment. Solid state NMR spectroscopy and gas chromatography can also be applied to the solid residue, liquid products, and gas collected during hydroboration.

---

[1] Matsumoto, Y. *Tetrahedron Letters.* 1991. 32(28). 3387.

[2] Hayashi, T. *Tetrahedron Asymmetry.* 1991. 2(7). 601.

[3] Prasad, A. and S. Bhanu. *Tetrahedron.* 1992. 48(22). 4623.

[4] Molander, G.A. *Journal of Organic Chemistry.* 1994. 59(10). 2676.

[5] Caro, B. *Journal of Organometallic Chemistry.* 1996. 525(1/2). 283.

[6] Pickering, M. *Journal of Chemical Education.* 1990. 67(5). 436.

[7] Brown, H. C. and B.C. Subba Rao. *J. Am. Chem. Soc.* 1956. 78. 5694

[8] Brown, H. C. and B.C. Subba Rao. *J. Am. Chem. Soc.* 1959. 81. 6423.

[9] Brown, H. C. and K. Murray. *J. Am. Chem. Soc.* 1959. 81. 4108.

[10] Brown, H. C. and C.H. Snyder. *J. Am. Chem. Soc.* 1961. 83. 1001

[11] Brown, H. C. *Hydroboration*. New York: W.A. Benjamin, Inc. 1962.

[12] Solomon, P.R. *ACS Symposium Series No. 169.* Washington, DC: Am. Chem. Soc. 1981.

[13] Shinn, J.H. *Fuel*. 1984. 63.

[14] Schobert, H. H., C. Song, and A. Boehman. Advanced Thermally Stable Jet Fuels, Technical Progress Report, October — December 1997.The Pennsylvania State University. #92PC92104-TPR-22. 1998.

5.20 SHAPE-SELECTIVE ISOPROPYLATION OF NAPHTHALENE OVER ZEOLITE CATALYSTS

This study is explained in detail in *Advanced Thermally Stable Jet Fuels Technical Progress Report, October—December 1993.*

Introduction

The economic feasibility of coal liquefaction can be enhanced by selective alkylation of 2-ring aromatic products, producing value-added aromatic chemicals. Conversion of even a small fraction of the 2-ring aromatics can significantly increase the value of the total product slate, while the majority of the liquefaction product is converted to jet fuel. Thus, an opportunity exists for enhancing the net economic feasibility of a coal-to-jet fuel process, via significantly enhanced by-product credits.

Isopropylation of 2-ring aromatics is a viable process for producing dialkyl aromatics. Of particular interest are 2,6-dialkylnaphthalenes and 4,4'-dialkylbiphenyls, which, when oxidized to the corresponding diacids, can be polymerized to produce high value engineered plastics.[1] While alkylation of aromatics is a facile process, regioselective alkylation requires a shape-selective catalyst.

Mordenite zeolite is a high surface area crystalline material with one-dimensional channels formed from 8-atom rings. With an average channel diameter of 6.7 x 7.0 , mordenite affords regioselective alkylation of naphthalene at positions β to the fused-ring carbons, and 1,1'-biphenyl at the 4- and 4'-positions. Regioselectivity is sensitive to catalyst pretreatment and reaction parameters.

Summary

Selective alkylation of naphthalene (NAP) by 2-propene (P) has been studied over native and chemically modified commercial H-mordenites (HM). Experiments were performed in batch mode using a 30 mL tubing bomb reactor. This report summarizes experimental procedures and results for the systematic evaluation of the following reaction parameters.

Temperature: 200°, 250°, or 300¡C

Time: 3.5˚hour standard run, or a *short run* where the reaction was stopped when the total pressure ceased to decrease over a 15 minute interval (0.5-1.5˚hours)

NAP/P ratio: typically 0.5 (molar basis), but 1.0 also used

Solvent: cyclohexane, decahydronaphthalene (decalin), or 1,3,5-trimethylbenzene (mesitylene); solvent volume: 0, 1, 6 or 15˚mL.

The reaction products were primarily mono (MIPN), di (DIPN), tri (TRIPN), and tetra (TEIPN) isopropyl-substituted naphthalenes (IPNs). When no solvent was used, nearly all of the side products were alkylated naphthalenes other than *solely* isopropyl-substituted naphthalenes (RNAPs). Other minor products were propylene oligomers, tetralin and alkylated tetralin (RTET), phenanthrene, anthracene, and binaphthyl (POLY). Generally, products derived from coupling and cracking of naphthalene were only observed at 300¡C. The use of reaction solvents invariably led to other side-reaction products.

Saturated hydrocarbon solvents added to NAP, accounted for 8—20% of the product at 200¡C. With cyclohexane, dimethyldecalins were produced, especially at 250 and 300¡C, probably by Diels-Alder condensation of partially dehydrogenated cyclohexane and propylene dimer. RTET products were observed in significant amounts with decalin solvent at 200¡C, and became significant with cyclohexane solvent at 250¡C. Although mesitylnaphthalene products were not observed, isopropyltrimethylnapthalene compounds were produced in significant amount. Also, compared to the neat reaction, use of mesitylene solvent approximately doubled the fraction of RNAP products, apparently as a result of transalkylation/disproportionation reactions. Side reactions were minimized and selectivity for β-substitution was optimized by using only 1˚mL reaction solvent. Yet, the highest 2,6/2,7 DIPN isomer ratios were obtained with 6˚mL reaction solvent.

Use of a solvent diminished the catalyst activity NAP conversion and the extent of polyalkylation both decreased. However, there are benefits of solvent use. Presence of a solvent in the reactor led to an increase in product recovery according to mass balance calculations. At 200¡C reaction temperature, all solvents increased both the percentage of 2,6-isomer in DIPNs and the 2,6/2,7 isomer ratio. At 250¡C, mesitylene produced the same trend; cyclohexane did not. Decalin was only tested at 200¡C.

A reaction temperature of 200¡C was found to be optimum as neither NAP conversion nor the percentage of alkylation at the β-positions of NAP increased at higher temperatures. At or above 250¡C, the percentage of isopropylnaphthalenes in the product also decreased, while RNAPs became more prevalent, presumably as a result of thermal cracking, isomerization, and transalkylation reactions. Alkylation by solvent (cyclohexane and decalin) and of solvent (mesitylene) also increased markedly at 250¡C.

Effects of varying the reaction time were complex. The most significant conclusions are that both β-selectivity and ββ-selectivity increase with time, while optimization of 2,6-DIPN selectivity requires limiting the reaction time.

HM30 demonstrated the highest activity. Small amounts of K_2O or ZnO were deposited on the surface of HM30 to modify its surface acidity. Modified HM30 catalysts showed small decreases in activity and reactions leading to RNAP products, but native HM30 showed superior shape selectivity. HM20 showed the lowest activity of all the catalysts tested. The one experiment performed with HM20 indicated that a higher percentage of β-alkylation is obtainable with HM30, but more data are required for proper comparison. Similarly, HM30 and modified HM30 catalysts produce significantly higher 2,6/2,7 DIPN isomer ratios than HM20.

Experimental

Catalyst preparation, catalyst testing, and product analysis were discussed at length in the original account of this study.[2] For brevity they have been omitted here.

Conclusions

This report summarizes some collateral efforts toward enhancing coal liquefaction economic feasibility through naphthalene isopropylation to product value-added chemicals, as well as some information obtained from the literature. Several parameters concerning the alkylation process have been investigated, and our conclusions are summarized below.

Preferential substitution at the β-positions of NAP was accomplished in the channels of mordenite. Optimizing 2,6-DIPN in the ββ-DIPN product required kinetic control of the second propylene substitution. External surface acid sites were responsible for isomerization reactions, non-selective substitution, and polysubstitution of NAP (TRIPN and TEIPN). Dealumination of mordenite with reagents (e.g., mineral acids) that are capable of internal surface diffusion has been an effective means for enhancing shape selectivity. However, this procedure results in a gross depletion of acid sites and a decline in activity. Additionally, complete inactivation of external surface sites may require further processing.

Deactivation or inactivation of external surface sites can occur by selective blockage or removal. This and other studies have suggested that this procedure used alone, or in conjunction with mild dealumination, may lead to a superior catalyst.[3]

Cycloparaffin reaction solvents are not suitable for use with strongly acidic mordenites at 200 ¡C or above, as a result of the side-reactions of the solvents. Their use may be possible at lower temperatures or with less acidic catalysts. At 200¡C, all solvents enhanced selectivity for 2,6-DIPN. The mechanism is thought to involve solvent adsorption and/or coke formation. Mesitylene affords the greatest increase in 2,6-DIPN and contributes only mildly to the byproducts.

---

[1] Song, C. and H. H. Schobert. *Fuel Proc. Technol.* 1993**.** 34. 157.

[2] Schobert, H. H. et al. Advanced Thermally Stable Jet Fuels, Technical Progress Report, October — December 1993. The Pennsylvania State University. 1993.

[3] Fellmann, J. D. et al. U. S. Patent No. 5,026,942. June 25, 1991.

5.21 SHAPE-SELECTIVE NAPHTHALENE HYDROGENATION FOR PRODUCTION OF THERMALLY STABLE JET FUELS

a. Converting Naphthalene to *Trans-decalin* using Four Different Zeolites

This study is explained in detail in *Advanced Thermally Stable Jet Fuels Technical Progress Report, July 1994 — September 1994.*

Purpose: Our previous work has shown that for jet fuels, cyclic alkanes have higher thermal stability than normal alkanes. Cycloalkane conformation also affects high temperature (e.g., 450°C) stability. For example *trans*-decalin (t-DeHN) is more stable than *cis*-decalin (c-DeHN). Furthermore, the carbon-forming propensity of jet fuel can be reduced by limiting its aromatic content, as in the complete hydrogenation of naphthalene (Nap). Tests on the thermal stressing of petroleum-derived fuels and model compounds have shown that addition of t-DeHN can significantly retard the rate of carbon deposition. The challenge is to selectively hydrogenate Nap to produce t-DeHN.

Shape-selective hydrogenation of naphthalene to t-DeHN can be accomplished over metal-loaded zeolite molecular sieves. Zeolites are high surface area crystalline aluminosilicates, having regular channel structures of narrow size distribution. They can mediate the course of reaction by controlling diffusion, and the shape and size of products within their channels.

We examined two types of zeolites mordenite and zeolite Y. Mordenite has a two-dimensional channel structure, with elliptically shaped channels of diameter 6.7 x 7.0 . The molecular diameter of the Nap is very close to the dimensions of the channel, which limits the types of reactions that Nap can undergo, and governs regioselectivity in the products. Conversely, zeolite Y has a cage structure with large cavities in the interior and narrow channel openings. A reactant that has entered the channel structure may reorient itself freely and react at catalyst sites on the walls of the cavity. However, because of restricted diffusion at channel openings, only molecules of appropriate diameter can exit the catalyst s interior.

Zeolite supports may also increase catalyst longevity. Zeolites have very high thermal stability, so they can be subjected to oxidative regeneration procedures without undergoing sintering. The high area and acidity of the zeolite surfaces are also believed to prevent or retard catalyst deactivation caused by sulfur poisoning.

Experimental: We prepared and tested eight catalysts in this preliminary effort to selectively convert Nap to t-DeHN using four different commercial zeolites: HY and three hydrogen mordenites with differing silica/alumina ratios. To each zeolite we added an approximate 6 wt% loading of platinum or palladium by impregnation of a corresponding metal chloride salt. Following drying and calcination, the catalysts were tested in batch tubing-bomb reactors at 200°C for 0.25 to 1.0 hours. Reduction of the metal occurred in situ under the hydrogen pressure used for reaction.

Catalysts based on HM38 gave the highest t-DeHN selectivity, and catalysts with palladium gave higher selectivity than those with platinum. Under the chosen test conditions all of the Nap was converted in all cases, almost exclusively to a mixture of *cis*- and *trans*-decalins. As a result, we cannot rank catalyst activity at this point.

X-ray powder diffraction (XRD) was used to examine the state of the metal on the zeolite after the catalysts were recovered from the reactors. Line broadening was used to measure average metal particle sizes, resulting in striking differences in metal particle sizes among the samples.

Findings: A full presentation of the experimental conditions and results are presented in the original Technical Progress Report.[1] For the sake of brevity, only the conclusions drawn from these results are presented here.

Catalysts based on dealuminated mordenite (HM38) provided the highest trans-decalin (t-DeHN) selectivity. Palladium t-DeHN selectivity was higher than that of platinum on the same zeolite. Palladium also isomerized c-DeHN to t-DeHN at a higher rate than platinum. Metal crystallite sizes are highly dependent on the zeolite. Palladium generally had a higher dispersion than did platinum on a given zeolite. A loose correlation exists between decreasing particle size and increasing t-DeHN selectivity. Continued use of XRD line-broadening and transmission electron microscopy will allow us to further investigate this correlation and engineer better catalysts.

A high metal dispersion indicates a proportionately high number of active metal sites; therefore, we will likely also observe improved sulfur tolerance for small metal crystallines. Complete conversion of Nap occurs within the first 0.25 hours in tests with Pt/HM38 and Pd/HM38.

In future work, we will decrease the metal loading on the zeolite to 2 wt% and decrease the catalyst charge in the reactor to moderate Nap conversion. We can then establish an activity scale for the catalysts and possibly observe better t-DeHN selectivity. Our ultimate objective is to develop a catalyst with high sulfur tolerance that may require metal loading greater than 2%. Thiophene added as reactor charge will allow us to investigate sulfur tolerance. Our previous work with mordenites taught us that regioselectivity for reactions involving naphthalene can be enhanced by moredenite dealumination. This technology can someday be applied to engineer better molecular sieve supports.

b. Pursuing Reproducibility of Results and Investigation of Initial Selectivity of Catalysts

This study is explained in detail in *Advanced Thermally Stable Jet Fuels Technical Progress Report, October 1994 — December 1994.*

Purpose: Further our understanding of the parameters that affect reproducibility of the results demonstrated in our previous work (a.) and of the initial selectivity of some catalysts.

Experimental: One important variable is the catalyst s moisture content, which can be determined by thermal gravimetric analysis (TGA). The performance of two catalysts were compared after the following catalyst treatments: storage in a desiccator for an extended period, freshly calcined, and freshly calcined with added water. To determine whether naphthalene could react in hydrogen pressure reactors, even at room temperature, we allowed two loaded reactors to stand at room temperature for 12 hours before the contents were removed and analyzed. Additional studies were performed to probe the kinetics and the thermodynamics of *cis*- to *trans*-decalin isomerization.

As previously reported,[2] naphthalene conversion of 100% was achieved in all catalysts tests, including 15-minute tests of Pt/HM38 and Pd/HM38. In this study we examined the conversion and product distribution of HY-supported catalysts in even shorter runs, because of their interesting product distributions Pt/HY produces a high concentration of c- DeHN, while Pd/HY is more selective for t-DeHN.

Experimental: Details of our experimentation with preparations of 6% Pt/HM38 (AS) and 6% Pd/HM38 (AS), including thermogravimetric analysis (TGA) and reactor tests, were provided in the corresponding Technical Progress Report.[3]

Findings:

Equilibrium Decalin Isomer Distribution. Pd/HM38 afforded the highest t-DeHN selectivity in earlier tests, but was in short supply. Therefore, we chose to use catalyst Pd/HM21 for these experiments, because it exhibited the second highest t-DeHN selectivity. An approximately constant *trans*/*cis*-DeHN ratio of 13.6 was obtained within 6 hours of reaction time; this is likely the practical limit, given that some decalin may reside in the portion of the reactor that extends above the sand level in the fluidized bath (cold zone) and may not react. Based on our calcualtions, if as little as 5% of the decalin doesn t react to form an equilibrium amount of t-DeHN, the equilibrium ratio falls to 13.0.

Product Distribution as a Function of Reaction Time. Based on our earlier findings that Pt/HY produces a high concentration of c-DeHN, while Pd/HY is more selective for t-DeHN, we set out to determine whether higher c-DeHN selectivity could be obtained with Pt/HY in short runs, using Pd/HY runs for comparison. The trend for Pd/HY is similar to that observed for HM38-supported catalysts; initial selectivity for t-DeHN is moderately low, but decreases with time as c-DeHN is isomerized to t-DeHN. For Pt/HY, the initial selectivity for t-DeHN is very low and remains approximately unchanged with time. For some reason, Pt/HY does not promote the thermodynamically favored isomerization.

When tested over a progression of reaction times, the metal-loaded HM38 (AS) catalysts both resulted in complete Nap conversion, with little or no TeHN, even in very short runs. Our tests resulted in significant differences in t-DeHN concentrations compared to those observed by Schmitz and Bowers.[2] We suspect that the difference is caused by the higher metal dispersions likely to occur in the AS catalysts.

Room Temperature Reactions. Naphthalene reacts in hydrogen-pressure reactors, even at room temperature, to produce mainly TeHN. The rate of Nap hydrogenation to TeHn is approximately 21 times faster than that for TeHN hydrogenation. Palladium supported on strongly acidic supports is electron deficient. Electron-rich species, such as Nap, may adsorb very strongly, slowing the hydrogenation reaction. This could explain why Nap conversion is much higher over Pt/HM17.

Influence of Catalyst Moisture Content. For Pt/HM21, neither re-calcination nor added water changes the amount of TeHN produced or the Nap conversion to coincide with G. Bowers data. For both Pd/HM21, calcination increases the trans/cis-DeHN ratio; whereas added water brings the *trans*/*cis*-DEHN ratio into the range cited by Schmitz and Bowers[2], but does not affect conversion or TeHN yield.

Findings: A significant portion of the Nap reacted when the pressurized reactors remained at ambient temperature. This room temperature reaction may explain some discrepancies in data for repeated catalyst tests. Pt/HM17 had higher activity than Pd/HM17 at 25°C. At 200°C, given our reactor loading, we could not rank catalyst activity due to complete conversion of Nap, even in very short runs. Related research will involve reductions of the metal loading on the zeolite and decreased catalyst charge in the reactor. This will enable us to compare catalyst activities at 200°C and evaluate sulfur tolerance.

Catalyst moisture content affects the decalin product distribution. Freshly calcined catalysts give the best t-DeHN selectivity. Addition of water to a reactor with freshly calcined catalyst does not result in a measurable change in activity, but does seem to poison c-DeHN isomerization active sites.

The newly prepared catalysts used in these tests Pt/HM38 (AS) and Pd/HM38 (AS) have very high activity. A near equilibrium trans/cis-DeHN ratio is obtained within 1 hour of reaction time. We deduced that the careful impregnation procedures used for these catalysts led to higher metal dispersions than were achieved in earlier preparation.

Generally, in Nap hydrogenation experiments, c-DeHN is rapidly formed and isomerizes to t-DeHN. In this study, we identified a unique catalyst, Pt/HY, which produces c-DeHN with high selectivity and does not promote the isomerization.

c. Comparison of *Cis*- and *Trans*-Decalin Formation

This study is explained in detail in *Advanced Thermally Stable Jet Fuels Technical Progress Report, January 1995 — March 1995.*

Purpose: Determine whether cis-decalin (c-DeHN) and trans-decalin (t-DeHN) are formed in parallel or t-DeHN is formed primarily by isomerization of c-DeHN on metal-loaded zeolites. We chose to test the previously reported metal-loaded zeolite catalysts[4, 5] under conditions that disfavor c-DeHN isomerization and examine the difference in the decalin product distribution.

Experimental: First, we performed a series of tests that involved decreasing the catalyst charge in the reactor from 0.40 to 0.10 g. In the second series of tests, we again used 0.10 g catalyst, but lowered the temperature from 200° to 100°C. The methods used in these studies were similar to those used in (a). Reactions were run in tubing-bomb reactors charged with 0.10 g catalyst (rather than 0.40 g), 1.0 g Nap, 4.0 *n*-tridecane reaction solvent, and 0.35 g *n*-nonane internal standard. Reaction temperatures were 100° and 200°C. We re-examined four catalysts under the new decreased charge, decreased temperature conditions: Pd/HY (GB), Pt/HY (GB), Pd/HM38 (AS) and Pt/HM38 (AS). (GB refers to the HM-38-supported catalysts prepared by G. Bowers; AS refers to those prepared by A. Schmidt.)

Findings: These studies, using adjusted reaction conditions, confirmed that both decalin isomers can be produced in parallel during Nap hydrogenation over metal-loaded zeolites. t-DeHN selectivity is constant within parallel tests for M/HY. For Pd/HY at 200°C, isomerization of c-DeHN occurs slowly, although complete Nap saturation occurs at an early stage. Isomerization is insignificant, yet the DeHN trans/cis ratio is direct evidence of the parallel formation of the two DeHN isomers. In addition, on Pt/HY, the t-DeHN selectivity is constant at 200°C and c-DeHN isomerization is insignificant.

We researched reaction kinetics for Nap hydrogenation over Pt/Al_2O_3, paying particular attention to the effects of temperature on the relative magnitudes of the rate constants. Consistent with earlier reports, we demonstrated that hydrogenation of $\Delta^{9,10}$-octalin and $\Delta^{1,9}$-octalin may play an important role in determining the DeHN *cis*/*trans* configuration. We proposed that Pt on acidic zeolites is electron deficient, and that strong bonding between the octalins and electron deficient Pt retards the rate of the alkene desorption step necessary for production of t-DeHN. We suggested alternative explanations for the uniquely high c-DeHN selectivity of Pt/HY, such as a bidisperse metal phase or a special shape selectivity that arises from partial channel blockage by large Pt particles.

---

[1] Schobert, H. H. et al. *Advanced Thermally Stable Jet Fuels, Technical Progress Report, July 1994 — September 1994.* The Pennsylvania State University. 1994.

[2] Schmitz, A. D., G. Bowers, and C. Song. *Advanced Thermally Stable Jet Fuels, Technical Progress Report, July 1994 — September 1994.* 92PC92104-TPR-9. 1994. 37.

[3] Schobert, H. H. et al. *Advanced Thermally Stable Jet Fuels, Technical Progress Report, October 1994 — December 1994.* The Pennsylvania State University. 1995.

[4] Schmitz, A. D. and C. Song. Advanced Thermally Stable Jet Fuels, Technical Progress Report, October 1994 — December 1994. 92PC92104-TPR-10. 1995. 66.

[5] Collman, J. P. et al. *Principles and Applications of Organotransition Metal Chemistry.* Mill Valley, CA: University Science Books. 1987.

5.22 NOBLE METAL CATALYSTS FOR LOW-TEMPERATURE NAPHTHALENE HYDROGENATION IN THE PRESENCE OF BENZOTHIOPHENE

This study is explained in detail in *Advanced Thermally Stable Jet Fuels Technical Progress Report, July — September 1995.*

Abstract

This work deals with low-temperature catalytic naphthalene hydrogenation as a model reaction for low-temperature hydrotreating of coal-derived liquids to produce thermally stable jet fuels. Pt/Al_2O_3, Pd/Al_2O_3, and Pd/TiO_2 catalysts were compared to a commercial hydrotreating catalyst, $NiMo/Al_2O_3$, for naphthalene hydrogenation inside tubing bombs at 553 K with a cold feed (at room temperature) of 6.99 MPa H_2 and tridecane as the solvent. The noble metal catalysts were found to be significantly more active than $NiMo/Al_2O_3$. A further study at a reaction temperature of 473K showed that naphthalene hydrogenation over these noble metal catalysts can proceed even in the presence of benzothiophene at a concentration of 4200 ppm. Sulfur addition does decrease the activity of all the noble metal catalysts. However, Pd catalysts appear to have higher sulfur resistance than the Pt catalyst; the Pd/TiO_2 catalyst was found to be the most active and the least affected by benzothiophene among the three noble metal catalysts studied.

Introduction

In our ongoing program to develop advanced thermally stable jet fuels from coal-derived liquids and petroleum, both complete and partial hydrogenation reactions of naphthalene-type compounds play important roles. Complete saturation of naphthalene gives decalins that offer much higher thermal stability than long-chain alkanes, while partial saturation produces tetralin, which can substantially inhibit the thermal degradation and solid-forming tendency of long-chain alkanes in jet fuels at high temperature.[1, 2, 3]

The hydrogenation of aromatic and polycyclic aromatic compounds is typically exothermic; therefore, a lower reaction temperature is thermodynamically favorable. However, in hydrotreating fuels and heavy liquids where polycyclic aromatic compounds are present, a reaction temperature above 623 K is typical in conventional processes, which consequently requires a high concentration of hydrogen to offset the limitation of thermodynamic equilibrium conversion. Noble metal catalysts are active for the hydrogenation of aromatics even at temperatures below 473K,[4, 5, 6] but their cost and their susceptibility to the poisoning by sulfur-containing compounds precluded them from being used for hydrogenation. However, recent studies showed that some noble metal catalysts may not be as sensitive to sulfur as had been generally recognized.[7, 8, 9, 10, 11]

This study examined the potential of using noble metal catalysts for low-temperature hydrotreating reaction in the presence of sulfur-containing compounds. We also explored the value as a model reaction of naphthalene hydrogenation conducted in the absence and presence of benzothiophene.

Experimental

Pt/Al_2O_3, Pd/Al_2O_3, and Pd/TiO_2 catalysts were all prepared by the incipient wetness method using H_2PtCl_6 and $PdCl_2$ as the precursors. The pore volume and surface area of the support are 0.8 cc/g and 200 m^2/g for γ-Al_2O_3 and 0.5 cc/g and 50 m^2/g for TiO_2, respectively. The supports were calcined at 773 K under dry air flow for 2 hours before use. A nominal loading of 2 wt% metal was used for all three catalysts. A commercial hydrotreating catalyst $NiMo/Al_2O_3$ was used as the reference without further pretreatment. The pretreatment conditions for the noble metal catalysts were H_2 reduction at 723 K for Pt/Al_2O_3, 20% O_2 calcination at 673 K for Pd/Al_2O_3, and H_2 reduction at 473 K for Pd/TiO_2; these conditions were found to give relatively higher activities for naphthalene hydrogenation at 553 K with these three noble metal catalysts.[12]

Further experimental detail regarding hydrogenation and product analysis was presented in the corresponding Technical Progress Report.[13]

Results and Discussion

Hydrogenation at 553K. Naphthalene conversions over Pt/Al_2O_3, Pd/Al_2O_3, and Pd/TiO_2 were all above 70% in the one-hour run, compared to a 17% conversion over $NiMo/Al_2O_3$ at a 50% higher catalyst loading. Clearly the three noble metal catalysts are much more active than the $NiMo/Al_2O_3$ hydrotreating catalyst at this reaction condition. The hydrogenation results of TiO_2 and HCl-treated Al_2O_3 indicate that the high activities of these three noble metal catalysts cannot be attributed to the support or the Cl residue in the catalysts. Besides the higher naphthalene conversions with the three noble metal catalysts, the selectivity to hydrogenated naphthalene products (dihydronaphthalene, tetralin, and decalins) and the molar ratios of hydrogen reacted to naphthalene reacted, $\Delta H/\Delta N$, were also significantly higher than the $NiMo/Al_2O_3$ catalyst. The calculated $\Delta H/\Delta N$ ratio for the three noble metal catalysts roughly corresponded to the amount of hydrogen added to form the hydrogenated products. This indicated that the hydrogen reacted was almost all used for hydrogenation with the noble metal catalysts; whereas for $NiMo/Al_2O_3$ a portion of the hydrogen consumed was used in other reaction routes such as in the formation of gas products. The low yields of solid and gas products over the noble metal catalysts also indicate that the hydrogenolysis of naphthalene was not significant at this reaction condition. Clearly the noble metal catalysts are more suitable for low-temperature hydrogenation of naphthalene and, potentially, more suitable for the hydrotreating purposes at 553 K or lower.

The main product of the naphthalene hydrogenation at 553 K was tetralin, even when naphthalene conversion exceeded 90%. This trend is similar to that for $CoMo/Al_2O_3$ catalyst at 623 K.[14] Because both naphthalene hydrogenation and tetralin hydrogenation are exothermic reactions, we anticipated a higher equilibrium yield to more hydrogenated products from thermodynamic considerations at a lower reaction temperature. Therefore, we studied naphthalene hydrogenation at 473 K.

Hydrogenation at 473 K. With naphthalene hydrogenation at 473 K, tetralin remained the only hydrogenated product, with the exception of those runs with 100% conversion. Because decalins would be thermodynamically favorable at this low temperature, the formation of decalins must be kinetically less favorable over the catalysts under the conditions used.

However, the hydrogenation abilities of these noble metal catalysts at 473 K were obvious from the high selectivity to hydrogenated products, high $\Delta H/\Delta N$ ratios, and low selectivity to gases and solids. These results indicate that noble metal catalysts can be useful for low-temperature polycyclic aromatic hydrogenation.

An increase in the catalyst loading from about 0.13 to approximately 0.2 g (with naphthalene amounts kept constant) significantly increased the naphthalene conversion with any of the three catalysts, Pt/Al_2O_3, Pd/Al_2O_3, and Pd/TiO_2. At 0.2 g catalyst loading, all three noble metal catalysts promoted naphthalene conversion to approximately 100%. However, their product selectivity patterns were different. The major products with Pd/Al_2O_3 were tetralin, and *cis*- and *trans*-decalin, but only decalins dominated in the products with Pt/Al_2O_3 and Pd/TiO_2. Pt/Al_2O_3 displayed slightly higher selectivity to *cis*-decalin, whereas both Pd catalysts showed higher selectivity to *trans*-decalin. The highest yield of *trans*-decalin was obtained with Pd/TiO_2.

The results of naphthalene hydrogenation in the presence of benzothiophene showed that benzothiophene can significantly hinder the hydrogenation activities of noble metal catalysts. In addition, a higher sulfur content resulted in a lower conversion during the same period of reaction. However, palladium catalysts were less sensitive to benzothiophene than the platinum catalyst, and the TiO_2 support was superior to the Al_2O_3 support with respect to the catalytic hydrogenation activity. Pd/TiO_2 and Pd/Al_2O_3 catalysts have higher sulfur tolerance than Pt/Al_2O_3, and in that context, the Pd/TiO_2 catalyst is more promising than the other two catalysts.

To see whether the sulfur poisioning of the catalysts is a permanent effect, experiments with an extended reaction period (8 hours) were performed. Naphthalene hydrogenation in the presence of benzothiophene can proceed to a conversion as high as 89% and 78%, respectively, for Pd/TiO_2 and Pd/Al_2O_3. Extending the reaction time with the Pd catalysts from 2 to 8 hours resulted in gradual recovery of naphthalene conversion. This indicated that hydrogenation activity of the Pd catalysts can be recovered as a result of concomitant hydrodesulfurization. However, the sulfur poisoning on Pt/Al_2O_3 catalyst seems to be permanent, as no recovery was observed by extending the reaction time. The reason why Pd catalysts showed better sulfur tolerance than the Pt catalyst is not clear at present. The type of the metal and support and also the pretreatment condition employed caused differences. Arcoya et al. proposed that as the electron-donating character of palladium atoms decreases, the metal becomes more sulfur-tolerant.[15] Since the Pd/Al_2O_3 catalyst used in this study was pretreated in 20% O_2, positively charged Pd could exist in this catalyst. However, this would not apply to the Pd/TiO_2 catalyst, because the hydrogen pretreatment at 473 K was sufficient to reduce Pd to its zero-valence state. On the other hand, Chen et al. found that Pt/TiO_2 showed higher resistance to H_2S than Pt/Al_2O_3 and suggested that the labile oxygen in TiO_2 could react with H_2S to form SO_x.[7] This provides insight to how the support may affect the sulfur-resistance of noble metal catalysts, and this effect may account for why extending the reaction time restored the catalyst activity in the presence of H_2S generated from benzothiophene conversion (see below). However, it is difficult to identify what the so-called labile oxygen is and how it could be generated; further study is required.

No benzothiophene was identified in the liquid products from all the runs with the addition of benzothiophene. In the runs with Pt/Al_2O_3, it is likely that benzothiophene was adsorbed strongly on the surface. With Pd/TiO_2 and Pd/Al_2O_3 the hydrogenation reaction

approached completion with extended reaction time, indicating that benzothiophene was gradually converted to other sulfur species that do not deactivate the catalyst as seriously as benzothiophene. The conversion of the benzothiophene over the Pd catalysts likely proceeded via a hydrodesulfurization reaction to form ethylbenzene and hydrogen sulfide with dihydrobenzothiophene as the intermediate. Accordingly, the hydrogen sulfide formed did not deactivate the palladium catalysts as much as benzothiophene does.

Although the presence of benzothiophene in the feed decreased naphthalene conversion, the selectivity to hydrogenated naphthalene products was not significantly affected. Tetralin was the dominant product except in the region where naphthalene conversion approached 100%, regardless of the presence of benzothiophene. This trend in product selectivity coincides with that of naphthalene hydrogenation at 553 K and that reported for $CoMo/Al_2O_3$ at 623 K.[16] This indicates that the effect of benzothiophene is likely site-blocking, rather than electronic interaction, and that naphthalene hydrogenation could occur concurrently with the benzothiophene hydrodesulfurization. These results suggest that some noble metal catalysts can be useful for low-temperature hydrotreating purposes even when the feed contains sulfur.

Quantitative Estimation of Sulfur Resistance. In an effort to obtain a quantitative analysis of the effect of benzothiophene on the naphthalene hydrogenation over these noble metal catalysts, we performed a pseudo-first order kinetic analysis, estimated the apparent rate constants and then calculated the effect of benzothiophene on the rate of naphthalene hydrogenation as the ratio of the apparent rate constant in the presence of benzothiophene to that without benzothiophene (ks/k). After correction for the amounts of catalysts used in different runs and the effect of reaction temperature,[6] the $k_s(473K)/k(473K)$ ratios become 0.46, 0.56, and 0.1 respectively for Pd/TiO_2, Pd/Al_2O_3, and Pt/Al_2O_3. This again indicates that the palladium catalysts were less affected by the presence of benzothiophene. Based on the equation reported by Lo[17] and the benzothiophene concentration used in this study, a k_s/k ratio of 0.73 was estimated for $NiMo/Al_2O_3$ at 623 K. The k_s/k ratios of the two palladium catalysts at 473 K were comparable, indicating that the palladium catalysts are comparable to $NiMo/Al_2O_3$ for simultaneous hydrogenation and hydrodesulfurization, even at a lower reaction temperature when the $NiMo/Al_2O_3$ catalyst shows little activity.

TGA Analysis. The results of TGA analysis showed that the sample exposed to the reaction mixture at room temperature for 30 minutes exhibited two weak weight loss features at approximately 443 and 693 K. The former feature is within the region where moisture desorbs, while the latter was likely caused by the naphthalene adsorbed on the catalyst, since no reaction would occur at this condition. This 693 K weight loss feature was also observed for other Pd/Al_2O_3 samples whose reaction conversions were less complete. For the sample tested at 473 K for 2 h, the 693 K feature cannot be identified, likely due to the fact that the conversion level was as high as 100%. For the sample used for the reaction in the presence of benzothiophene, this 693 K feature occurred just above the noise level of the baseline, implying that the surface coverage of naphthalene was low when the benzothiophene was present. This supports our conclusion that benzothiophene may be preferably adsorbed. The new feature appearing at around 473 K with the sample tested with benzothiophene could have resulted from the adsorbed benzothiophene.

For the two used Pt/Al_2O_3 samples, only in the region below 473 K were TGA features observed that rule out unambiguous attribution owing to the possible interference from the

moisture. Pd/TiO_2 was found to contain very little moisture and a small weight gain was observed around 493 K that shifted to higher temperature when benzothiophene was present in the feed. An oxidation of either the reduced Pd or the partially reduced TiO_2 could cause this feature. The oxidation of reduced Pd is considered less likely because it was not observed in Pd/Al_2O_3 samples and because all of the samples used in TGA analysis had been air-exposed. The oxygen adsorption isobar of TiO_2 indicated that oxygen adsorption at around 473 K is possible for activated TiO_2.[18] Therefore, the weight gain feature of Pd/TiO_2 could have been caused by the interaction between O_2 and activated TiO_2 (e.g., partially reduced TiO_2) as a result of either the pretreatment or the reducing environment of the reaction. If this speculation is true, the shift to higher temperature when tested in the presence of benzothiophene indicates that benzothiophene might interact with the partially reduced TiO_2. Finally, TGA results showed that there was no coking problem with these noble metal catalysts under the reaction conditions used. This is another potential advantage of low-temperature catalytic hydrogenation with the noble metal catalysts.

Thermodynamic and Kinetic Considerations

The equilibrium of the naphthalene hydrogenation and its reverse reaction has been studied by Frye [19]and by Frye and Weitkamp.[20] The equilibrium constants were found to be well below 0.1 for naphthalene hydrogenation to either tetralin or decalins at a temperature of 573 K or above. Therefore, this reaction is thermodynamically unfavorable at higher reaction temperatures. Similarly, the hydrogenation of phenanthrene and other polycyclic aromatic compounds is also thermodynamically unfavorable at higher temperature. However, the industrial hydrotreating process for improving hydrogen/carbon ratio of heavy liquids typically uses a temperature above 623 K and a high hydrogen pressure with catalysts such as $NiMo/Al_2O_3$. The heavy liquids, especially those from coal liquefaction, contain a significant amount of aromatics and polycyclic aromatic compounds. Thus, a high hydrogen pressure is necessary if high conversion is desired.

In examining the trends of equilibrium conversions of naphthalene and the selectivity of its hydrogenated products, we determined that the equilibrium conversion decreases with increasing temperature and that tetralin becomes the dominant product at higher temperatures where naphthalene conversion drops below ≈80%. A high reaction pressure obviously shifts these trends to a higher temperature range. The reaction at lower temperature and a lower pressure could have the same thermodynamic equilibrium as the reaction at higher temperature and higher pressure. Thus, a lower temperature hydrotreating process is thermodynamically feasible in addition to offering higher energy efficiency.

Kinetic aspects also determine the feasibility of a lower-temperature hydrotreating process. The conventional hydrotreating catalysts operating at the temperature above 623 K usually have the advantage of being inexpensive and capable of simultaneous hydrodesulfurization, hydrodenitrogenation, and hydrodeoxygenation. However, these catalysts are relatively inactive at a temperature below 573 K; therefore, other types of catalysts must be used when a lower-temperature hydrotreating process is desired. Supported Group VIII catalysts have been used for hydrogenation reactions over a wide temperature range, and have shown significant activities for the hydrogenation of aromatic compounds at temperatures below 473 K[1, 5, 6] and could be candidates for low-temperature hydrotreating catalysts. Although the noble metal catalysts were found to be easily poisoned by sulfur,[21] recent studies have shown that the

sulfur resistance of Pt and Pd catalysts is affected by the valence state of metal, the type of support, the preparation procedure, and the extent of presulfurization.[13] This implies that tailoring the supported noble metal catalysts may improve the sulfur resistance and make useful catalysts for low-temperature hydrotreating purposes.

The three noble metal catalysts studied showed their potentials for applications in the polycyclic aromatic hydrogenation and hydrotreating purposes. The high activities of group VIII metal catalysts (Pt, Pd, Ni) toward hydrogenation of alkylbenzenes and of polycyclic aromatic compounds have been known for some time; their activities toward hydrogenation of polycyclic aromatic compounds can be orders of magnitude higher than the conventional hydrotreating catalysts such as $NiMo/Al_2O_3$.[1] Even the presulfided Pt and Pd catalysts showed significantly higher hydrogenation and C-N hydrogenolysis activities than the sulfided Mo catalyst[22], indicating that sulfur-poisoned noble metal catalysts could exhibit comparable activities to the conventional hydrotreating catalysts. Thus, in terms of higher energy efficiency and higher activity of the catalyst, the use of some noble metal catalysts for low-temperature hydrotreating purposes could become an attractive option in the future. However, more detailed studies will be required before we can effectively implement supported noble metal catalysts for these applications.

Summary

Noble metal catalysts such as Pt and Pd supported on Al_2O_3 and TiO_2 can be used for low-temperature hydrogenation of polyaromatic hydrocarbons, and they display catalytic activity even in the presence of sulfur in the feed ranging from 1800 to 4200 ppm. The Pd catalyst showed higher sulfur resistance than Pt when supported on Al_2O_3, and the sulfur tolerance was even higher when Pd was loaded onto a TiO_2 support. The potential of Pd/TiO_2 as a sulfur-tolerant catalyst for low-temperature hydrotreating warrants further detailed study.

---

[1] Song, C., W.-C. Lai, and H.H. Schobert. *Ind. Eng. Chem. Res.* 1994. 33. 548.

[2] Song, C. et al. *Energy & Fuels.* 1993. 7. 234.

[3] Schmitz, A., G. Bowers, and C. Song. *Am. Chem. Soc. Div. Fuel Chem. Prepr.* 1995. 40. 930.

[4] Stanislaus, A. and B. H. Cooper. *Catal. Rev.- Sci. Eng.* 1994. 36. 75.

[5] Sakanishi, K. et al. *Bull. Chem. Soc. Japan.* 1989. 62. 3994.

[6] Nieuwstad, Th. J., P. Klapwijk, and H. van Bekkum. *J. Catal.* 1973. 29. 404.

[7] Chen, Y. et al. *Appl. Catal.* 1990. 63. 107.

[8] Hayes, L. E., C.E. Snape, and S. Affrossman. *Prepr. Am Chem. Soc. Div. Fuel. Chem.* 1991. 36. 1817.

[9] Berube, M. N., B. Sung, and M.A. Vannice. *Appl. Catal.* 1987. 31. 133.

[10] Koussath, M. et al. *Appl. Catal.* 1991. 77. 283.

[11] Koussathana, M. et al. *Appl. Catal. A.* 1992. 80. 99.

[12] Lin, S. D. Unpublished results.

[13] Schobert, H. H. et al. Advanced Thermally Stable Jet Fuels, Technical Progress Report, July — September 1995. (#92PC92104-TPR-13). 1995.

[14] Korre, S. C., M. T. Klein, and R. J. Quann. Ind. Eng. Chem. Res. 1995. 34. 101.

[15] Arcoya, A. et al. *Appl. Catal.* 1990. 62. 35.

[16] Korre, S. C., M. T. Klein, and R.J. Quann. *Ind. Eng. Chem. Res.* 1995. 34. 101.

[17] Lo, H. S. Ph. D. Dissertation, University of Delaware, Newark, Newark, NJ. 1981

[18] Lin, S. D. Ph. D. Dissertation. The Pennsylvania State University, University Park, PA. 1990.

[19] Frye, C, G. *J. Chem. Eng. Data.* 1962. 7. 592.

[20] Frye, C. G. and A. W. Weitkamp. *J. Chem. Eng. Data.* 1969. 14. 372.

[21] Bartholomew, C. H., P. K. Agrawal and J.R. Katzer. *Advan. Catal.* 1982. 31. 135.

[22] Shabtai, J. et al. *J. Catal.* 1988. 113. 206.

5.23 CONFORMATIONAL ISOMERIZATION OF CIS-DECAHYDRONAPHTHALENE (CIS-DECALIN) OVER ZEOLITE CATALYSTS

This study is explained in detail in *Advanced Thermally Stable Jet Fuels Technical Progress Report, October — December 1995.*

Introduction

Commercial decalin (DeHN) solvents from industrial hydrogenation processes consist of almost equimolar mixtures of *cis- and trans*-DeHN. Although the physical properties of these two isomers are similar, their chemical reactivities differ. One example is their difference in thermal stability at high temperatures. We have previously shown that as jet fuel components, *trans-DeHN* is superior to *cis*-DeHN because the former is much more stable at high temperatures.[1] This is important because decalin could be an endothermic jet fuel capable of serving as the primary heat sink to cool the surfaces and components of future high-mach aircraft. In addition, *trans*-DeHN can inhibit the solid deposit formation from jet fuels and their components at high temperatures.[2] Although *cis*-DeHN also has some potential industrial applications, *cis*-DeHN would be more useful for our purposes if transformed to the more thermally stable *trans*-DeHN.

Considerable research has focused on cracking, hydrocracking and dehydrogenation of decalin at temperatures over 673 K under elevated pressures; however, little information is available on the conformational isomerization of *cis*-DeHN into *trans*-DeHN at lower temperatures. Our earlier exploratory work showed that some zeolites can promote the isomerization of *cis*-DeHN into *trans*-DeHN at 523 K for 2 hours under an N_2 environment.

This study represented a continuation of our exploratory studies on the zeolite-catalyzed conformational isomerization of *cis*-DeHN into *trans*-DeHN. We examined the effects of catalyst type, reaction temperature, noble metals, and gas atmosphere on the catalytic reaction, and attempted to develop an overall kinetic model for the catalytic reaction and empirical equations to predict the product yields.

Experimental

The chemicals *cis*-DeHN, *trans*-DEHN and DeHN (an almost equimolar mixture of cis- and trans-DeHN) were used, as well as six catalysts which promoted isomerization reactions: a hydrogen Y zeolite (HY), a metal ion-exchanged Y zeolite (LaHY), a hydrogen mordenite (HM30A), and three noble metal loaded mordenites (Pt/HM30A, Pd/HM30A, and Pt/HM20A). Catalytic isomerization reactions were carried out in 28 mL stainless steel tubing bomb reactors charged with 1 g of *cis*-DeHN, *trans*-DeHN, or DeHN and 0.2 g of catalyst, at 473-573 K for 0.15 to 8 hours under an initial pressure of 0.79 MPa UHP N_2 or H_2. Further details of the preparation and analysis can be found in the original Technical Progress Report.[3]

Conclusions

Pt- and Pd-loaded mordenites are very effective catalysts under H_2 for the conformational isomerization of *cis*-DeHN to *trans*-DeHN at 473 K. The selectivity towards trans-DeHN with these catalysts is very high (nearly 100%) with a *trans*-DeHN/*cis*-DeHN ratio near 13.

On the other hand, Pt- and Pd-loaded mordenites are less effective under a hydrogen-deficient environment such as N_2. The isomerization of *cis*-DeHN to *trans*-DeHN is thought to involve dehydrogenation and hydrogenation on the metal surface. The effectiveness of Pt/HM30A in an N_2 environment could be improved by pre-reduction in H_2. Pt/HM30A is a better catalyst than Pd/HM30A at 473 K under an N_2 atmosphere, in terms of conversion and *trans*-DeHN selectivity, although they are almost equally effective under H_2.

HY, LaHY, and HM30A are not as effective as Pt- and Pd-loaded mordenites and the three catalysts exhibit nearly uniform activities under N_2 and under H_2. HY performs slightly better than LAHY, and the catalyst with the lowest acidity (IB430A) displayed the lowest activity. The observed activity for *cis*-DeHN conversion was: Pt/HM30A ≈ Pd/HM30A ≈ Pt/HM20A > HY > LaHY > HM30A. Selectivity towards *trans*-DeHN decreased with both increasing temperature and increasing conversion level (under isothermal condition).

We proposed a simple reaction pathways model containing parallel-consecutive kinetic schemes and we developed empirical equations capable of predicting product yields. The following equations may be used to predict reaction conversion and major products:

Rate constant: $$D/D_0 = \exp[-(k_1+k_2)\,t] = \exp[-k\,t] \quad (1)$$

For HY: $$E_a = 49.9 \pm 2.6 \text{ kcal/mol} \text{ and } A = 6.03 \times 10^{20} h^{-1} \quad (2)$$

For LAHY: $$E_a = 54.6 \pm 2.6 \text{ kcal/mol} \text{ and } A = 3.36 \times 10^{22} h^{-1} \quad (3)$$

For HY: $$\text{Selectivity} = 1.938 + 0.779\,X - 0.285\,X^2 - 0.00228\,T - 0.0012\,X\,T \quad (4)$$

For LaHY: $$\text{Selectivity} = 1.534 + 2.745\,X - 0.082\,X^2 - 0.00146\,T - 0.0054\,X\,T \quad (5)$$

The theoretical equilibrium compositions of *trans-DeHN and cis-DeHN* at several temperatures were calculated and compared with experimental data. The experimental results for very effective catalysts such as Pt- and Pd-loaded mordenites corroborated well with theoretical calculations. The calculated equilibrium compositions are useful guidelines for evaluating the effects of catalysts and reaction conditions.

---

[1] Song, C., W.-C. Lai, and H. H. Schobert. *Prepr. - Am. Chem. Soc., Div. Fuel Chem*. 1992. 37. 1655.

[2] Song, C., W.-C. Lai and H. H. Schobert. *Ind. Eng. Chem. Res.* 1994. 33. 548.

[3] Schobert, H. H. et al. Advanced Thermally Stable Jet Fuels, Technical Progress Report, October—December 1995.(#92PC92104-TPR-14). 1996.

5.24 ZEOLITE SUPPORTED PD AND PT CATALYSTS FOR LOW-TEMPERATURE HYDROGENATION OF NAPHTHALENE IN THE ABSENCE AND PRESENCE OF BENZOTHIOPHENE

This study is explained in detail in *Advanced Thermally Stable Jet Fuels Technical Progress Report, April — June 1996.*

Introduction

This work examined low-temperature hydrotreating to reduce aromatics in jet fuels. Hydrogenation of aromatic compounds is typically exothermic and, therefore, is thermodynamically favored at a lower reaction temperature. However, in conventional hydrotreating processes, a reaction temperature above 350¡C is typical, which consequently results in relatively higher contents of aromatics at equilibrium composition. Deep hydrogenation of aromatics requires a higher concentration of hydrogen to offset the limitation of thermodynamic equilibrium conversion at high temperatures. Conventional supported Ni-Mo and Co-Mo sulfided catalysts become active only at relatively high temperatures.

Hydrogenation of the two-ring aromatics in coal-derived liquids can produce thermally stable decalin and methyldecalin components. Increasingly more stringent environmental regulations and fuel specifications have necessitated a deep reduction of aromatics in distillate fuels. Although noble metal catalysts are active for the hydrogenation of aromatics, even below 200¡C, they are not used for hydrotreating because of their higher cost and susceptibility to poisoning by sulfur-containing compounds. However, recent studies have shown that some noble metal catalysts may not be as sensitive to sulfur as previously thought.[1]

This study examined the potential of zeolite-supported Pd and Pt catalysts for low-temperature hydrotreating of distillate fuels in the absence and presence of benzothiophene. Hydrogenation of naphthalene in *n*-tridecane was chosen as a model reaction for fuel hydrotreating. Zeolite supports mordenite and Y were selected because they are distinctly different from conventional supports such as alumina and titania, and may offer several advantages. This work is a part of our ongoing effort to develop advanced thermally stable jet fuels from coal-derived liquids and petroleum. Both complete and partial hydrogenation reactions of naphthalene-type compounds are important. Complete saturation of naphthalene gives decalins with much higher thermal stability than long-chain alkanes[2], while partial saturation produces tetralin, which can substantially inhibit the thermal degradation and solid-forming tendency of long-chain alkanes in jet fuels at high temperature.[3]

Experimental

Catalyst preparation and evaluation is addressed in detail in the corresponding Technical Progress Review.[4]

Conclusions

In noble-metal catalyzed hydrogenation of aromatics in distillate fuels, the activity, selectivity and sulfur-resistance of the catalysts strongly depends on the type of support and metal. For hydrogenation of naphthalene in *n*-tridecane at 200¡C in the absence of added sulfur, Pd/HM38 and Pd/HY catalysts were substantially more active than Pd/Al_2O_3 and Pd/TiO_2

catalysts, even when the former was used with lower catalyst amounts under lower H_2 pressure. Pt/HM38 catalyst showed higher activity than Pt/HY and Pt/Al_2O_3 catalysts.

Mordenite-supported Pd and Pt catalysts were more active than Y zeolite-supported Pd and Pt, respectively. At 100% conversion, Y zeolite-supported catalysts afford a higher yield of *cis*-decalin, while mordenite-supported catalysts give a higher yield of *trans*-decalin.

Addition of sulfur in the form of benzothiophene decreased the activity of all the catalysts tested. However, we observed significant improvements in sulfur tolerance of the noble metals when they were supported on zeolites, rather than Al_2O_3 or TiO_2 supports. The Pd catalysts supported on both Y zeolite and mordenite showed higher sulfur tolerance than all of the other catalysts.

Overall, the Pd/HM38 catalyst showed the best activity for naphthalene hydrogenation and the highest resistance to sulfur poisoning. On the other hand, the Pt catalysts loaded on zeolites or alumina have very low sulfur tolerance. The mordenite-supported Pd catalyst is promising for practical application and, therefore, warrants further study.

---

[1] Stanislaus, A. and B. H. Cooper. *Catal. Rev. - Sci. Eng.* 1994. 36. 75.

[2] Song, C. et al. *Energy & Fuels.* 1993. 7. 234.

[3] Song, C., W.-C. Lai, and H. H. Schobert. *Ind. Eng. Chem. Res.* 1994. 33. 548.

[4] Schobert, H. H. et al. *Advanced Thermally Stable Jet Fuels, Technical Progress Report, April — June 1996.* The Pennsylvania State University. 92PC92104-TPR-16. 12.

5.25 A STRUCTURAL STUDY OF BLIND CANYON COALS USING SOLID STATE ^{13}C NMR SPECTROSCOPY

This study is explained in detail in *Advanced Thermally Stable Jet Fuels Technical Progress Report, November 1992 — January 1993.*

Introduction

Coals rich in resinite are potential feed stocks for jet fuels, because resins consist predominantly of two-ring cycloparaffin structures. These cycloparaffins are linked to the side chains of these coal networks and can be cleaved in liquefaction processes. To optimize the liquefaction process, we need to better understand the structures of potential coal feed stocks. In this study, we examined two coal samples DECS-6 and DECS-16, experimenting with cross-polarization and magic-angle spinning (CPMAS), Bloch decay, dipolar dephasing, and varied relaxation time experiments. We used the NMR parameters obtained from these experiments to structurally characterize the two potential coal feed stocks.

Experimental

To ensure that NMR data from CPMAS experiments were quantitative, we obtained a variety of relaxation data to confirm that our experiments met the two necessary conditions:

1. Contact time must be greater than the time required for polarization transfer between the carbons and hydrogens (T^{CH}), and it must be much smaller than the spin-lattice relaxation time of protons in a rotating coordinate system (TH^{1p}).
2. The spin-lattice relaxation times of the protons (T^{1H}) must be at least five times shorter than the delay between the pulses.

Results

From both a qualitative and quantitative standpoint, DECS-6 and DECS-16 were found to have similar chemical characteristics.[1] Their similarities and differences are summarized as:

	DECS-6	DECS-16
Aromatics (%)	≈70%	≈70%
Aliphatic carbons (%)	≈30%	≈30%
Distribution of oxygen-containing functional groups	7% phenolic carbons 3% carboxyl carbons 2% carbonyl carbons 3% oxygenated aliphatic carbons	10% phenolic carbons 1% carboxyl carbons 2% carbonyl carbons 2% oxygenated aliphatic carbons
Hydrogen distributions	79%	83%
No. of protonated carbons per aromatic ring	1.8	1.4
No. of aliphatic carbons	Half that of DECS-16	Twice that of DECS-6

The difference in hydrogen distributions is logical, based on the fact that DECS-16 has a slightly higher resinite content and resinite is rich in aliphatic hydrogen.

The quantitative data obtained in this study of Blind Canyon coals will serve as the foundation for three-dimensional coal molecular models. Succeeding studies performed computer modeling of the coals.

[1] Song, C. et al. *Advanced Thermally Stable Coal-Derived Jet Fuels, Technical Progress Report, July 1991 — November 1991*. 1991.

5.26 THE THERMAL DECOMPOSITION OF ^{13}C-LABELED BIBENZYL IN THE PRESENCE OF ADDITIVE-FREE JET A-1

This study is explained in detail in *Advanced Thermally Stable Jet Fuels Technical Progress Report, October 1993 — December 1993.*

Introduction

Liquid fuels and the materials derived from them have been analyzed considerably by ^{13}C NMR in recent years as instrumentation and analytical techniques have improved. While high resolution ^{13}C NMR has been used to characterize liquid fuels, only McKinney et al. has utilized the technique of ^{13}C labeling along with ^{13}C NMR to examine complex reactions that liquid fuels undergo when subjected to thermal stress.[1] ^{13}C-labeling has been used to examine the reactivity of specific labeled molecules in complex organic systems.

From our studies involving the examination of a potential ^{13}C-labeled antioxidant C-1 ^{13}C-labeled benzyl alcohol and studies examining the reactivity of pollutants, we have gained a great deal of expertise in the use of ^{13}C-labeled compounds to examine the reactivity of specific compounds in complex mixtures.[1, 2] Reactions involving the ^{13}C-labeled carbon led to significant changes in the chemical shift of this carbon in ^{13}C NMR spectra. By enriching a reactive compound with 100% ^{13}C at one reactive site, a significant enhancement in the ^{13}C NMR sensitivity was realized for the labeled carbon. Other unlabeled carbons in the reactive molecule and the reacting substrate were reduced to near background levels in the spectra. Thus, reactions at or near the labeled site can be clearly differentiated from reactions of the unlabeled carbons.

This report and a previous study[2] demonstrate the applicability of ^{13}C NMR labeling in combination with standard ^{13}C NMR experiments to examine thermally induced changes in a complex fossil fuel system, jet fuel. This study examined the reactivity of bibenzyl in the presence of a jet fuel under thermally stressed conditions. Using experimental conditions similar to those employed by McKinney et al,[2] we examined the fate of bibenzyl labeled with 100% ^{13}C at the two benzylic carbons, expecting that any reactions involving these highly reactive labeled carbons could be clearly differentiated with ^{13}C NMR.

Experimental

NMR Analysis. The ^{13}C NMR spectra were obtained on a Bruker WM 360 NMR spectrometer with a resonance frequency of 90.56 MHz. An inverse-gated pulse sequence with a 10-second delay between pulses, and a 45° pulse angle was used to ensure the acquisition of quantitative spectral data. The spectral width used was approximately 21 kHz, and 96 scans were collected for each experiment. The spectra were transformed using 1 Hz line broadening and the intense peaks in the spectra that resulted from the ^{13}C labeled carbons were identified using standard chemical shift tables.[3] The relative amount of each product present in the reaction mixture was obtained from the peak height of the ^{13}C labeled carbon.

Synthesis of Bibenzyl. Samples were prepared from an essentially additive free Jet A-1 fuel. α, α-^{13}C-bibenzyl was synthesized, as shown in Scheme I.[4] Titanium(III) chloride (2.3 g, 15.0 mmol) was weighed under N_2 in a glove bag and placed in a two-necked flask, equipped with a magnetic stir bar and 70 mL of dry dimethoxyethane under dry N_2. Quickly, $LiAlH_4$ (190

mg, 5.0 mmol) was added to the stirred solution and restirred. 100% α-^{13}C-benzyl alcohol (0.52 mL, 5.0 mmol) in a few mL of dry dimethoxyethane was added to the solution and refluxed for 16 hours. After cooling, the reaction mixture was quenched with dilute HCl followed by dilution with H_2O. The mixture was extracted with ether, and the ether extracts combined. The ether solution was washed with brine, dried ($MgSO_4$), filtered, and concentrated at the rotary evaporator. The resulting product, α, α-^{13}C-bibenzyl, was recrystallized, 78% yield, mp 52°C.

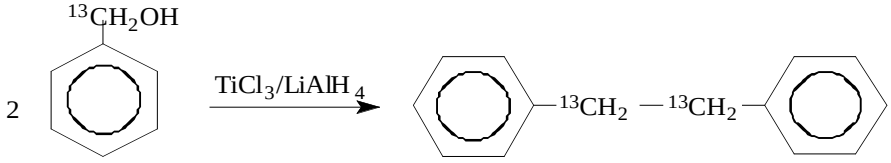

Scheme I

Thermal Stressing Experiments. The thermal stressing and sample preparations were carried out as described by McKinney et al[2] with the following exception: 0.37 g of α, α-^{13}C-bibenzyl was added to 10 mL of jet fuel sample. The bibenzyl still contained a small amount of unreacted benzyl alcohol. After each stressing period (10 min., 1 hr., 3 hrs., 6 hrs., 12 hrs., 24 hrs.), a 0.5 mL aliquot was removed and placed in an NMR tube with 0.5 mL of deuterated chloroform and sealed. The reactor was resealed, repressurized, and heated until the next allotted time. This sampling process enabled us to conserve the expensive ^{13}C-labeled material. If we had been attempting to mimic a real aircraft system, the reaction would have been performed differently; our purpose was merely to show the usefulness of the ^{13}C labeling approach.

Results and Discussion

Examining the ^{13}C NMR spectra for the jet fuel sample laced with α, α-^{13}C-bibenzyl, we determined that prior to stressing, the most significant signals pertained to the ^{13}C-labeled carbons of bibenzyl and benzyl alcohol, located at approximately 38.2 ppm and 65.45 ppm, respectively. As the duration of the thermal stressing increased, three important trends were observed:

1. The concentration of benzyl alcohol decreases, as predicted by earlier work.[2]
2. The concentration of bibenzyl also decreases.
3. The concentration of toluene (21.4 ppm) in the reaction mixture increases.

The graph of relative area versus heating time (425^o C) for these three reactants, shown in **Figure 5.26-1**, clearly displays the visible trends in the ^{13}C NMR spectra. **Table 5.26-1** contains the relative area of benzyl alcohol, bibenzyl, and toluene normalized to the area of one of the aliphatic signals resulting from jet fuel. By normalizing the data in this manner, inconsistencies in sampling are corrected and the resulting areas can be compared from sample to sample.

Conclusions

From the results of the ^{13}C NMR experiments, we were able to follow the decomposition of bibenzyl and benzyl alcohol and the formation of toluene during thermal decomposition reactions. Throughout the course of the 24-hour experiment, we did not detect the formation of

any other ^{13}C-labeled reaction products. We were particularly interested in the formation of high molecular weight aromatic compounds that could form from the decomposition of the ^{13}C-labeled bibenzyl; such an occurrence could have implicated the reactive benzylic radical as a precursor to the formation of carbonaceous solid deposits. However, no intense peaks were observed in the aromatic region of the spectra; therefore, we surmised that the benzylic radicals acted as hydrogen scavengers and were capped to form toluene as the only significant product in the thermal stressing experiments.

Table 5.26-1. Relative Areas of the Reactants and Products of the Thermal Stressing of ^{13}C-labeled Bibenzyl and Benzyl Alcohol in the Presence of Additive-Free Jet A-1 Fuel.

Time (hours)	Relative area* of benzyl alcohol	Relative area* of bibenzyl	Relative area* of toluene
0.000	1.208	10.472	0.328
0.166	0.762	8.339	0.438
1.000	0.425	8.214	0.973
3.000	0.146	7.090	1.760
6.000	0.000	4.551	4.108
12.000	0.000	2.632	6.055
24.000	0.000	1.318	8.595

* area normalized to the area of a signal at 14 ppm

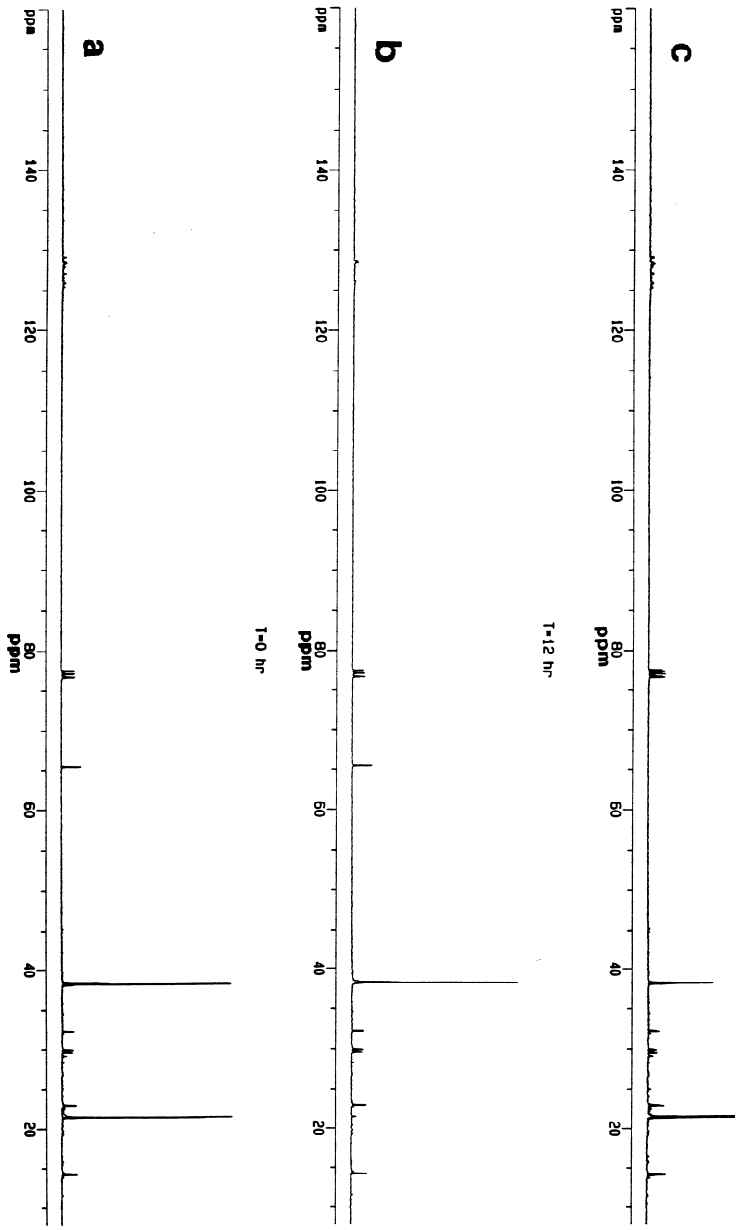

Figure 5.26-1. ^{13}C Inverse-Gated NMR Spectra Sampled of the Thermally Stressed Jet A-1 Fuel Mixture Containing Added ^{13}C-Labeled Bibenzyl and Benzyl Alcohol, (a) 0 hours, (b) 12 hours, and (c) 24 hours.

---

[1] McInnes, A. G. et al. ^{13}C NMR Biosynthetic Studies. *Topics in Carbon-13 NMR Spectroscopy* New York: John Wiley & Sons, 1976. 2. 125-179.

[2] McKinney, D. E., J. M. Bortiatynski, and P. G. Hatcher. *Energy Fuels.* 1993. 7. 578-581.

[3] Breitmaier, E. and W. Voelter. *Carbon-13 NMR Spectroscopy: High Resolution Methods and Applications in Organic Chemistry and Biochemistry.* New York: VCH Publishers. 1987.

[4] McMurry, J. E. and M. Silvestri. *J. Org. Chem.* 1975. 40. 2687.

5.27 A STRUCTURAL STUDY OF THE BLIND CANYON COALS USING SOLID STATE ^{13}C NMR SPECTROSCOPY

This study is explained in detail in *Advanced Thermally Stable Jet Fuels Technical Progress Report, January—March 1994.*

Introduction

The focus of the structural studies of Blind Canyon coal has been to obtain as much information as possible concerning the chemical structure of the potential coal feed stocks for jet fuel production. The experimental approach of the structural studies is to characterize the coal macerals and then utilize computer modeling to generate a three-dimensional model of the whole coal. The macerals are chemically unique, suggesting that the reaction chemistry of whole coal reflects distinctly different components. By examining each maceral component separately, we can obtain a more accurate representation of the whole coal and can predict chemical reactions to generate useful coal liquefaction products. Physical methods are often used to separate coal macerals, but these procedures are extremely time consuming and tedious. Whenever possible, we choose to obtain samples containing virtually pure coal macerals. This study focuses on a pure vitrinite sample obtained from the Deer Creek Mine of the Blind Canyon Seam.

Experimental

The percentage C, H, N, and O (by difference) for the vitrinite sample were obtained on a Leco Model CHN-600 elemental analyzer. The solid state ^{13}C NMR data was obtained on a Chemagnetics M100 NMR spectrometer with a ^{13}C resonance frequency of 25.035 MHz. Both cross polarization magic angle spinning (CPMAS) and dipolar dephasing magic angle spinning experiments were carried out with a pulse width of 14,084 Hz (562.59 ppm), a contact time of 1 millisecond, and a pulse delay of 1 second.

Discussion

Elemental Analysis. The results of the ultimate analysis of the pure vitrinite sample are shown below. This coal is high volatile bituminous by rank and contains carbon, hydrogen and oxygen content typical of this rank of coal.

Rank	%C	%H	%N	%O
HVB	80.36	5.28	0.00	14.36

^{13}C NMR Analysis. The ^{13}C CPMAS and dipolar dephasing spectra of the vitrinite sample were used to determine the aromaticity of the sample and the fraction of carboxyl and carbonyl carbons, in addition to several other structural characteristics, based on the definitions introduced by Solum et al.[1]

Conclusions

We drew several important conclusions concerning the structure of the carbon species in the pure vitrinite sample based on the elemental and solid-state ^{13}C NMR data. The average carbon structure in coal consists of approximately four aromatic rings per cluster with a crosslink density of five attachments per cluster. Aliphatic side chains with terminal methyl groups are the

primary functional groups forming these attachments. The low aliphatic ether and carboxyl and carbonyl fractions suggest that the majority of the oxygen in the vitrinite is found in phenolic or phenolic ether functional groups. The NMR data also predicted that there are approximately 2 protonated carbons, 2 bridgehead carbons, 1.3 substituted carbons, and 0.7 phenolic carbons per cluster. This information can be used with pyrolysis gas chromatography/mass spectrometry and liquefaction data to generate a three dimensional model of the pure vitrinite maceral.

[1] Solum, M.S.; R. J. Pugmire, and D. M. Grant. *Energy and Fuels.* 1989. 3. 187.

5.28 TEMPERATURE-PROGRAMMED LIQUEFACTION OF COALS USING BIMETALLIC DISPERSED CATALYSTS FROM ORGANOMETALLIC COMPLEXES

This study is explained in detail in *Advanced Thermally Stable Jet Fuels Technical Progress Report, August 1992 — October 1992.*

Introduction

Dispersed catalysts are superior to supported catalysts for primary coal liquefaction. Some organometallic compounds, including metal carbonyls and naphthenates, have been tested as catalyst precursors, often requiring the addition of sulfur components. Organometallics offer some unique advantages as catalyst presursors, namely:

1. Most organometallic compounds are soluble in hydrocarbon solvents and may be used as oil-soluble precursors.
2. Some organometallic compounds can be easily decomposed to metal sulfides at low temperatures.

Little research has addressed bimetallic dispersed catalysts for coal liquefaction, although general observations from previous investigations indicate that a synergistic relationship could exist between different metals, and an organometallic precursor may be superior to an inorganic one. Our interest in the heteronuclear organometallic compounds was stimulated by a book on metal clusters.[1] We surmised that highly active catalysts could possibly be prepared from some clusters containing metal-metal bonds, especially the thiocubane clusters containing two metals, such as Fe or Co and Mo in a single molecule.

Two metals bound in a single compound should have a more systematic spatial arrangement in the resulting catalytic phase upon thermal decomposition, than two separate compounds used to introduce the two different metals into the catalytic system. This study explored bimetallic dispersed metal sulfide catalysts for coal liquefaction, including the synthesis of the organometallic thiocubane clusters (that contain Mo and Co and sulfur in a single molecule). It also examined liquefaction of coal impregnated with the precursors under non-programmed and temperature-programmed (TPL) conditions, where the programmed heat-up contributes to both catalyst activation and coal pretreatment or conversion.

Experimental

The experimental conditions and procedures are addressed in the original report.[2]

Conclusion

We synthesized ant tested several heterometallic complexes consisting of two transition metals (i.e., Co and Mo) and sulfur as precursors of bimetallic dispersed catalysts for liquefaction of a subbituminous and a bituminous coal. Both the ligands to the metal species and the type of bonding between the two metals affect the activity of the resulting catalyst significantly. Among the M-M type precursors tested, Mo-Co thiocubane cluster $Mo_2Co_2S_4(Cp)_2(CO)_2$ [MoCo-TC2] produced the best catalyst. Loading of MoCo-TC2 at the level of 0.5 wt%, Mo can increase the conversion of the subbituminous coal from 32 to as much as 80 wt%. The performance of the Mo-Co bimetallic catalyst was further enhanced by using

temperature programmed heat-up (TPL) conditions. For a final temperature of 425°C, using the programmed conditions with MoCo-TC2 significantly increased the conversions by 12-13 wt% for both coals, as compared to the non-programmed runs.

---

[1] Mingos, D. M. P., and D. J. Wales. *Introduction to Cluster Chemistry.* Englewood Cliffs, NJ: Prentice Hall. 1990.

[2] Schobert, H. H. et al. *Advanced Thermally Stable Jet Fuels Technical Progress Report, August 1992 — October 1992*. 1992. 70-72.

5.29 BIMETALLIC DISPERSED SULFIDE CATALYSTS FROM ORGANOMETALLIC CLUSTERS FOR COAL LIQUEFACTION

This study is explained in detail in *Advanced Thermally Stable Jet Fuels Technical Progress Report, November 1992 — January 1993.*

Introduction

Our previous work demonstrated that, in the pyrolytic regime, the gross hydrocarbon makeup of jet fuels plays a key role in determining fuel degradation, and coal-derived fuels are rich in cycloalkanes and are, therefore, inherently more stable and superior for high-temperature applications.[1]

Dispersed catalysts are superior to supported catalysts for primary hydroliquefaction of coal. Because most active catalysts of interest (e.g., MoS2) are insoluble in common solvents, we must use a soluble precursor that can be dispersed onto coal surface from its solution to achieve better dispersion leads. Although the precursor may not be inherently active, it will transform at elevated temperatures into an active catalyst. Both inorganic salts of transition metals[2 3] and organometallic compounds such as metal carbonyls have been tested as precursors for dispersed catalysts.[4] Research on multicomponent catalysts has involved the mixture of two or more inorganic salts,[5] however, little work has focused on bimetallic dispersed sulfide catalysts for coal liquefaction.

The work concerned organometallic precursors that can directly produce bimetallic sulfides upon thermal decomposition. Two important observations from previous investigations could relate to this work:

1. Synergistic effects could exist between two different transition metal compounds
2. For a given metal, an organometallic precursor may be better than an inorganic one for coal liquefaction

We surmised that highly active bimetallic catalysts could potentially be prepared from the thiocubane clusters containing two transition metals, such as Co and Mo, in a single molecule. Two different metals bound together in a single cluster should have a more systematic spatial arrangement in the resulting catalytic phase upon thermal decomposition than if two separate compounds were used to introduce the two different metals to a catalytic system. In the early 1990s, Chianelli et al.[6] and Halbert et al.[7] used the unsupported sulfides from bimetallic complexes to study the promotional effects of Co on MoS2 for hydrodesulfurization (HDS). They showed that the CoMo sulfide catalysts from some organometallic precursors exhibit greatly improved activity for HDS.

This study addressed a potential bimetallic dispersed catalyst system for coal liquefaction from a thiocubane cluster.

Experimental

Catalyst Precursors and Coal Samples. Reagent-grade $Mo(CO)_6$ and $Co_2(CO)_8$ were used as the primary starting materials. We synthesized three Mo-Co bimetallic thiocubane clusters, including $Mo_2Co_2S_4(S_2CNEt_2)_2(CH_3CN)_2(CO)_2$, $Mo_2Co_2S_4Cp_2(CO)_2$, and

$Mo_2Co_2S_4(Cp)_2(CO)_2$, in which Et, Cp and Cp represent ethyl group, cyclopentadiene, and pentamethylcyclopentadiene, respectively. For convenience, we refer to these three clusters as MoCo-TC1, MoCo-TC2, and MoCo-TC3, respectively. The method of Halbert et al. [17] was used to synthesize MoCo-TC1, and that of Brunner and Watcher [18] for MoCo-TC3. We prepared MoCo-TC2 using the same procedure for MoCo-TC3 but with a modification of the starting material for the ligand. For comparative examination, a trianionic compound $(PPh_4)_3Co(MoS_4)_2$, designated as MoCo-S, was also synthesized as a bimetallic sulfide complex based on the procedure of Pan et al. [19].

For catalytic activity tests, we used a Montana subbituminous coal, DECS-9,with the following composition: 76.1% carbon, 5.1% hydrogen, 0.9% nitrogen, 0.3% organic sulfur, and 17.5% oxygen on a dry and mineral matter free (dmmf) basis. The catalyst precursors were dispersed onto the coal (predried at 100¡C in vacuum) by the incipient wetness impregnation method using organic solvents, followed by vacuum drying at 100¡C for over 2 h to remove the impregnating solvent. The loading for the bimetallic thiocubanes was 0.5 wt% of Mo on dmmf coal. When the metal carbonyls $Mo(CO)_6$ and $CO_2(CO)_8$ were used, the loading was 0.5 wt% for Mo and 0.3 wt% for Co metal based on dmmf coal.

The coal liquefaction was carried out in 25 mL microautoclaves in a fluidized sandbath at 400 or 425¡C for 30 minutes under an initial (cold) H2 pressure of 7 MPa (1000 psi). Each reaction used approximately 3 g dried coal and 3 g of 1-methylnapthalene as the reaction solvent. After the reaction, the gaseous product was vented, and the liquid and solid products were separated by sequential Soxhlet extraction into oil (hexane soluble), asphaltene (toluene soluble but hexane insoluble), preasphaltene (THF soluble but toluene insoluble) and residue.

Conclusion

Table 5.29-1 shows the results of liquefaction of the Montana subbituminous coal at 400°C for 30 minutes.

Our results indicated that both the ligands to the metal species and the type of bonding between the two metals affect the activity of the resulting bimetallic MoCo sulfide catalyst significantly. For a given precursor, the solvent used for catalyst impregnation also affected coal conversion, although the impregnating solvent was removed before reaction by evaporation and vacuum drying. Among the M-M type precursors tested, Mo-Co thiocubane* impregnated onto coal from toluene generated in-situ the best catalyst (MoCo-TC2) for coal liquefaction. The performance of the MoCo-TC2 catalyst was further enhanced by using an in-situ thermal pretreatment.

The bimetallic catalysts reported in this work would be rather expensive for use in an industrial process. However, the knowledge derived from this work regarding the dependence of catalyst activity on the structure of the bimetallic precursor and fundamental chemistry are very important for the development of novel catalysts and advanced catalytic processes. Another potential application of the precursors reported here is the preparation of supported Co-Mo catalysts, which are usually prepared from inorganic salts.[8] Some of the bimetallic precursors

* $Mo_2Co_2S_4(Cp)_2(CO)_2$ [Cp = cyclopentadiene]

will be used to prepare supported hydrotreating catalysts for more efficient upgrading of coal liquids and residual oils to high quality gasoline, jet fuels, and diesel fuels.

Table 5.29-1. Catalytic Liquefaction of DECS-9 Subbituminous Coal

Catalyst precursor	Solvent for catalyst loading[a]	In-situ pretreat at LT[b]	Reaction temp ¡C	Oil + Gas dmmf wt%	Asphaltene dmmf wt%	Preasph dmmf wt%	Conversion dmmf wt%
None	None	No	400	**16.0**	**9.4**	**6.8**	**32.2**
MoCo-TC1	CH_3CN	No	400	**22.8**	**4.8**	**5.2**	**32.8**
MoCo-TC1	THF	No	400	**18.7**	**12.8**	**14.8**	**46.3**
MoCo-TC2	Toluene	No	400	**32.4**	**18.0**	**24.2**	**74.6**
MoCo-TC2	THF	No	400	**25.8**	**17.9**	**23.7**	**67.4**
MoCo-TC3	Toluene	Yes	400	**33.8**	**17.8**	**19.9**	**71.5**
MoCo-S[c]	$CHCl_3$	No	400	**21.3**	**12.6**	**16.0**	**49.8**
MoCo-S[d]	CH_2Cl_2	No	400	**25.2**	**16.0**	**27.1**	**68.3**
$Mo(CO)_6$	1-MN	No	400	**25.2**	**10.6**	**16.5**	**52.3**
$Co_2(CO)_8$	1-MN	No	400	**23.7**	**12.6**	**15.0**	**51.3**
$Mo(CO)_6$ + $Co_2(CO)_8$	1-MN	No	400	**23.9**	**18.9**	**17.8**	**60.6**
None	None	Yes	400	**18.9**	**8.2**	**7.0**	**34.1**
MoCo-TC2	Toluene	Yes	400	**37.0**	**19.8**	**22.0**	**78.7**
MoCo-TC2	Toluene	Yes	425	**46.7**	**19.5**	**15.0**	**81.1**
MoCo-TC3	Toluene	Yes	425	**46.3**	**17.5**	**12.9**	**76.6**
$Mo(CO)_6$	1-MN	Yes	400	**24.2**	**11.8**	**16.4**	**52.4**
$Co_2(CO)_8$	1-MN	Yes	400	**23.6**	**12.4**	**14.2**	**50.2**

a. The impregnating solvent was removed by evaporation in vacuum before the reaction solvent 1-MN was added.

b. In-situ low-temperature pretreatment at 200¡C for 15 minutes followed by heat-up to reaction temperature.

c. Used shortly after synthesis without further purification. Decomposition during storage was noticed.

d. Used after further purification immediately before use. The purified MoCo-S was impregnated onto coal using excess amounts of CH_2Cl_2 solution.

[1] Song, C. et al. Pyrolytic degradation Studies of a Coal-Derived and a Petroleum-Derived Aviation Jet Fuel. *Energy and Fuels.* 1993.

Song, C., W. C. Lai, and H. H. Schobert. Hydrogen-Transferring Pyrolysis of Cyclic and Straight-Chain Hydrocarbons. *Enhancing High Temperature Thermal Stability of Aviation Jet Fuels by H-donors*. *Am. Chem. Soc. Div. Fuel Chem. Prepr.* 1992. 37(4). 1655-1663.

Lai, W. C., et al. Pyrolytic Degradation of Coal- and Petroleum-Derived Aviation Jet Fuels and Middle Distillates. *Am. Chem. Soc. Div. Fuel Chem. Prepr.* 1992. 37(4). 1671-1680.

Coleman, M. M., C. Song, and H. H. Schobert. Toward a New Generation of Thermally Stable Jet Fuels. *Chemistry in Britain.* The Royal Chemical Society.

[2] Derbyshire, F.J. Energy & Fuels. 1989. 3. 273-277 (and references cited therein)

Bockrath, B., E. Illig, , and M. Hough. *Am. Chem. Soc. Div. Fuel Chem. Prepr.* 1990. 35 (1). 232-240.

[3] Swanson, A. *Am. Chem. Soc. Div. Fuel. Chem. Prepr.* 1992. 37(1). 149-155.

[4] Yamada, O. et al. *Fuel Processing Technology.* 1985. 11. 297-311.

Suzuki, T., T. Ando, Y. Watanabe. *Energy & Fuels.* 1987. 1. 299-300.

Herrick, D. E. et al. *Energy & Fuels.* 1990. 4. 231-236.

Artok, L. et al. *Energy & Fuels.* 1993. 7. 67-77.

[5] Garg, D. and E. N. Givens. *Fuel Processing Technology.* 1984. 8. 123-134.

Nomura, M. et al. *Fuel.* 1982. 61. 18-20.

Song, C., M. Nomura, and M. Miyake. Fuel. 1986. 65. 922-926.

Song, C. et al. *Chem. Soc. Japan.* 1989. 62. 630-632.

Song,C., M. Nomura, and T. Ono. *Am. Chem. Soc. Div. Fuel. Chem. Prepr.* 1991. 36(2). 586-596.

Sommerfeld, D.A. et al. *Am. Chem. Soc. Div. Fuel Chem. Prepr.* 1992. 37(2). 749-755.

[6] Chianelli, R. R. et al. *Am. Chem. Soc. Div. Petrol. Chem. Prepr.* 1990. 35(2). 227-231.

[7] Halbert, T. R. et al. *J. Catal.* 1991. 130. 116-119.

[8] Song, C., T. Nihonmatsu, and M. Nomura. *Ind. Chem. Res.* 1991. 30. 1726-1734.

Song, C., K. Hanaoka, and M. Nomura. *Energy and Fuels.* 1992. 6. 619-628.

5.30 NOVEL BIMETALLIC DISPERSED CATALYSTS FROM HETERONUCLEAR ORGANOMETALLIC CLUSTERS FOR PROMOTING COAL LIQUEFACTION

This study is explained in detail in *Advanced Thermally Stable Jet Fuels Technical Progress Report, November 1992 — January 1993.*

Introduction

The desirable roles of a catalyst in coal liquefaction are the prompt hydrogenation of the coal-derived reactive fragments (radicals) in the initial stage, and hydroprocessing of unsaturated compounds in the later stage. Dispersed catalysts are superior to supported catalysts for primary hydroliquefaction of coal. Their advantage relates largely to their intimate contact with the surface of coal particles, which facilitates the activation and transfer of hydrogen to the coal-derived fragments and reactive sites.

This work dealt with organometallic precursors that can directly produce dispersed bimetallic sulfides upon thermal decomposition on coal surface. Two important observations from previous investigations could relate to this work:

1. Synergistic effects could exist between two different transition metal compounds
2. For a given metal, an organometallic precursor may be better than an inorganic one for coal liquefaction.

We believed that highly active bimetallic catalysts could be prepared from the thiocubane [1] clusters containing two different transition metals and sulfur in a single molecule. Two different metals bound together in a single cluster should have a more systematic spatial arrangement in the resulting catalytic phase upon thermal decomposition than if two separate compounds were used to introduce the two different metals to a catalytic system. We realize that the bimetallic catalysts involved in this work would be rather expensive for use in an industrial process. However, knowledge of the dependence of catalyst activity on the structure and fundamental chemistry of the bimetallic precursors is important for the development of novel catalysts and advanced catalytic processes. Another potential application of new bimetallic precursors is the preparation of Co-Mo catalysts, which are usually prepared from inorganic salts.[2 3] The bimetallic precursors that are active for coal liquefaction may also be used for preparing hydrotreating catalysts for more efficient upgrading of coal liquids and residual oils to high quality gasoline, jet fuels and diesel fuels. In this paper we will report on a potential MoCo bimetallic sulfide dispersed catalyst system derived from a thiocubane cluster for promoting direct coal liquefaction.

Experimental

We synthesized three Mo-Co bimetallic thiocubane clusters as catalyst precursors, including $Mo_2Co_2S_4(S_2CNEt_2)_2(CH_3CN)_2(CO)_2$, $Mo_2Co_2S_4Cp_2(CO)_2$, and $Mo_2Co_2S_4(Cp)_2(CO)_2$, in which Et, Cp and Cp represent ethyl, cyclopentadiene, and pentamethylcyclopentadiene, respectively. For convenience, we will refer to these three clusters as MoCo-TC1, MoCo-TC2, and MoCo-TC3, respectively.

We obtained a Montana subbituminous coal (DECS-9) with the following composition: 76.1% C, 5.1% H, 0.9% N, 0.3% organic S, and 17.5% O on a dmmf basis. The loading for the

bimetallic thiocubanes was 0.5 wt% Mo on dmmf coal. When $Mo(CO)_6$ and $Co_2(CO)_8$ were used, the loading was 0.5 wt% for Mo and 0.3 wt% for Co metal based on dmmf coal. Temperature-programmed liquefaction (TPL) and non-programmed liquefaction were carried out in 25 mL microautoclaves at a final temperature of 400 ¡C for 30 minutes under an initial (cold) H2 pressure of 7 MPa (1000 psi). Each reaction used 3 g dried coal (< 60 mesh) and 3 g of 1-methylnapthalene (1-MN) as the solvent. The experimental details were more fully described elsewhere.[4] In general, the experimental errors were within – 2 wt% for conversion, and the average data from two or three runs are reported here.

Results

The methodology and results are described in detail in the original Technical Progress Report.[5]

Conclusion

Our results indicated that the structure of the precursors, in particular the type of ligands bound to the metal species, affect the activity of the resulting bimetallic MoCo sulfide catalyst significantly. For a given precursor, the solvents and methods used for catalyst impregnation also affect coal conversion. Among the M-M type precursors tested, $Mo_2Co_2S_4(Cp)_2(CO)_2$ (i.e., MoCo-TC2) impregnated onto coal from toluene-THF, generated in-situ the best catalyst for coal liquefaction. The thiocubane cluster MoCo-TC2 is a promising precursor to the bimetallic sulfide catalyst.

---

[1] Mingos, D.M.P. and D. J. Wales. Introduction to Cluster Chemistry. Englewood Cliffs, New Jersey: Prentice Hall. 1990.

[2] Chianelli, R.R. et al. *Am. Chem. Soc. Div. Petrol. Chem. Prepr.* 1990. 35(2). 227-231.

[3] Song, C., T. Nihonmatsu, M. Nomura. *Ind. Eng. Chem. Res.* 1991. 30. 1726-1734.

[4] Song, C., D. S. Parfitt, and H. H. Schobert. *Am. Chem. Soc. Div. Fuel. Chem. Prepr.* 1993. 38(2). 546-553.

Song, C., H. H. Schobert, and P. G. Hatcher. Energy & Fuels. 1992. 6. 326-328.

[5] Schobert, H. H. et al. *Advanced Thermally Stable Jet Fuels, Technical Progress Report, February 1993 — March 1993.* 1993. 63-65.

5.31 EXPLORATORY STUDIES OF COAL LIQUID UPGRADING USING MESOPOROUS MOLECULAR SIEVE CATALYSTS

Introduction

Upgrading coal liquids to produce useful products like jet fuels involves catalytic hydroprocessing to achieve molecular weight reduction, hydrogenation, and the removal of heteroatoms. Hydroprocessing is usually performed over supported catalysts. Commercial hydroprocessing catalysts consist of a combination of metals distributed over porous, high surface area supports of γ-alumina or silica stabilized γ-alumina.

The conventional hydroprocessing catalysts were designed for refining distillate feeds and have been successfully used in petroleum hydroprocessing for several decades. However, these catalysts cannot contend with the stringent demands of hydroprocessing high-boiling and nondistillable coal liquids or similar feedstocks. Their principal deficiency is their susceptibility to deactivation by reactions that cause the deposition of carbon and metals. There are two approaches to resolving this problem. The first involves control of primary coal dissolution by dispersed catalysts to generate products that can be upgraded by conventional supported catalysts. The second approach which we chose to investigate involves the development of improved or novel supported catalysts for hydroprocess of coal liquids.

Catalyst performance is strongly affected by the pore structure of the support materials. Pore size distribution should be adapted to the type of feed being processed to ensure access of the reactant molecules and minimize processes that cause deactivation. Small pore catalysts provide high surface and activity but are most susceptible to pore-mouth blockage. Larger pore catalysts possess surface areas that are too low for high activity; however, their wider pore mouths allow the more slowly diffusing metal-precursor compounds to penetrate into the catalyst before metals are deposited. The shape and size of the catalyst particles can also influence catalyst life. Increasing the catalyst pore size and reducing the particle size can improve coal and asphaltene conversion.

Zeolite molecular sieves are widely used in the petroleum and petrochemical industries because they offer high crystallinity with uniform pore size, controlled acidity, high thermal stability, and good surface area. Their use is limited to small molecules conversion, because they are restricted to a maximum pore size of 1.4 nm. However, the pore dimensions of mesopolar molecular sieves, such as MCM-41, can be tailored (from 1.5 to 10 nm), through the choice of surfactant and auxiliary chemicals and templates and synthesis conditions. The BET surface area of this material is more than 1000 m^2/g with high sorption capacities (≥ 0.7 cc/g).

This study explored the possibility of using mesoporous molecular sieves to upgrade the coal-derived oils to produce stable jet fuels. Our tasks were divided as follows:

a) Synthesis of mesoporous molecular sieves

b) Characterization of polycyclic aromatic compounds (as model compounds) and of coal-derived oils

c) Catalytic evaluation of polycyclic aromatic compounds (as model compounds) and of coal-derived oils

a. Synthesis of Mesoporous Molecular Sieves

This study is explained in detail in *Advanced Thermally Stable Jet Fuels Technical Progress Report, October 1994 — December 1994.*

Experimental: Three series of samples using three different aluminum sources aluminum isopropoxide, alumina (Catapal B) and aluminum sulfate, with Si/Al ratios 50, 25, 12.5 and 0 were synthesized using two procedures. The resulting peak intensities show that almost all of the samples were well crystallized and phase pure, with a very strong peak and three weak peaks. Some peaks of the non-calcined samples showed extra peaks upon calcination possibly due to the presence of large amounts of surfactants. Calcination seems to lead to a contraction of unit cell, accompanied by a loss in silanol density via condensation of Si-OH groups.

Within each set of samples, a decrease in Si/Al ratio hinders the crystallization process. In all high silical molecular sieves, the more aluminum in the gel, the more difficult crystallization becomes as a result of stability issues. However, the level of crystallinity decreases with increases in the aluminum content the degree to which depends on the type of aluminum source. This could explain the tendency of aluminum sources under hydrolysis to react with silica source and form a gel of a certain nature. The nature of the resulting gel influences the crystallinity and amount of aluminum incorporated in the framework. The aluminum sulfate was easily hydrolized; it may, therefore have reacted with the silica and formed a gel of low pH. This would account for the lower crystallinity of the samples prepared with aluminum sulfate. Samples prepared with Catapal B had high crystallinity similar to those prepared without aluminum indicating that all of the alumina did not react to form gel, but remained as alumina.

There was little change in XRD characteristics that could be attributed to the change in synthesis procedures for samples prepared using Catapal B. However, the samples prepared with aluminum sulfate and aluminum isopropoxide have varied with the different procedures. Our preliminary data did not permit us to conclude the reasons for this variation.

Based on the Si/Al ratio versus d spacing for the three series of samples, we concluded that an increase in aluminum content in the gel increased the unit cell parameter. This is a common observation for all aluminosilicate molecular sieves a result of the incorporation of large aluminum ions as compared to silicon in the framework, which leads to an expansion of unit cell parameter. We also observed that the expansion is linearly proportional to the aluminum incorporation in the framework. The order of expansion of unit cell with increasing aluminum content using three different sources is: aluminum sulfate > aluminum isopropoxide > Catapal B alumina. This phenomena can also be explained by the nature of gel obtained with different aluminum sources.

Findings: These preliminary studies enabled us to synthesize phase pure mesoporous aluminosilicate molecular sieves, A1-MCM-41, with varying Si/Al ratios and different aluminum sources. Aluminum sulfate seems to be a better resource for incorporating more aluminum in the framework; however, poor crystallization results probably as a result of the lower pH of the gel. Hence, aluminum isopropoxide could be a better source for mesoporous aluminosilicate molecular sieves. However, these results depend on future determination of variables such as

surface area, temperature programmed desorption of ammonia, and solid state NMR before their catalytic evaluation.

b. Characterization of Polycyclic Aromatic Compounds (as Model Compounds) and of Coal-Derived Oils

This study is explained in detail in *Advanced Thermally Stable Jet Fuels Technical Progress Report, January 1995 — March 1995.*

Purpose: In (a) we reported the successful synthesis of phase-pure mesoporous sieves, Al-MCM-41, with varying Si/Al ratios and using different aluminum sources.[1] The type of aluminum source and Si/Al ratio has a significant influence on the synthesis and the physico-chemical characteristics of the mesoporous molecular sieves. Aluminum isopropoxide and aluminum sulfate were better sources for complete aluminum incorporation in the framework, compared to the Catapal B alumina source. The higher the Si/Al ratio, the better the crystallinity of the solid obtained.

The purpose of this study was to confirm these early results by examining the results of characterization by chemical analysis, surface area measurement, thermal analysis, and solid state NMR spectroscopy techniques.

Experimental: Collection and analysis techniques were fully addressed in the original Technical Progress Report.[2]

Results: Input ratios were higher than output ratios a common observation in the synthesis of high-silica molecular sieves. This can be attributed to the fact that zeolites normally incorporate all of the aluminum present in the reaction mixture, leaving varying amounts of silica or silicate in the solution, depending on factors such as hydroxide concentration and the presence of various inorganic and organic cations in the reaction mixture.[3] An exception involved the samples prepared with aluminum sulfate, which produced molecular sieves with high SiO_2/Al_2O_3 ratios for no known reason.

All of the calcinated MCM-41 samples, regardless of the source of aluminum, showed similar isotherms. These isotherms were characteristic of mesoporous materials with uniform pore size, with an inflection characteristic of capillary condensation within the pores. The relative pressure at which the inflection occurs increases with the diameter of the pores.

BET surface areas clearly confirmed our earlier results of crystallinity comparison. The MCM-41 sample prepared with Catapal B had a high BET surface area, indicating high crystallinity, and the sample prepared with aluminum sulfate showed just the opposite, conforming poor crystallinity.

Examining the TGA curves, we determined that most of the *n*-butylamine is desorbing below 473 K. From the weight loses resulting from *n*-butylamine desorption, we learned that MCM-41 samples prepared with aluminum isopropoxide and aluminum sulfate adsorbed more n^{-0}butylamine (about 18 wt%), whereas the sample prepared with Catapal B alumina source adsorbed less *n*-butylamine (about 10 wt%). This indicates that the first two samples are more acidic and offer superior aluminum incorporation than the Catapal B.

The ^{29}Si and ^{27}Al MAS NMR spectra showed that all of the Al atoms in the as-synthesized MCM-41 materials are present in a tetrahedral environment.[4] They also indicated that Catapal B is not a good source to incorporate the Al in the framework, confirming that aluminum sulfate and aluminum isopropoxide are better sources for maximum incorporation of aluminum in the framework. The ^{29}Si MAS NMR of the samples prepared the with three different sources closely resemble the spectra of amorphous silica,[5] suggesting a broad range of Si-O-Si bond angles in these materials.

Catalytic test results for the reactions of hydrogenation of naphthalene and phenanthrene and propylation of naphthalene reveal that all are active in the reactions with good conversion. However, reactions went non-selectively, as expected, based on the non-shape-selective nature of mesoporous materials with wide pores.

In the case of hydrogenation of naphthalene, conversion was almost 100% with all of the catalysts. MCM-41 catalysts prepared with Catapal B alumina resulted in large amounts of uncovered tetralin, whereas the other MCM-41 catalysts showed almost complete conversion of tetralin to decalin. MCM-41 catalysts were shown to be less acidic than other zeolites, particularly the MCM-41 catalyst prepared with Catapal B alumina.

All of the results confirmed our earlier findings regarding mesoporous molecular sieves (MCM-41) synthesis and their physico-chemical properties, namely:

- Al-MCM-41 mesoporous molecular sieves can be synthesized using different aluminum sources
- Of the three sources aluminum isopropoxide, aluminum sulfate, and Catapal B the first two provide better aluminum inacorporation and result in superior acidity

These results were confirmed by XRD, NMR, TGA of *n*-butylamine desorption, and catalytic tests.

c. Catalytic Evaluation of Polycyclic Aromatic Compounds (as Model Compounds) and of Coal-Derived Oils

This study is explained in detail in *Advanced Thermally Stable Jet Fuels Technical Progress Report, April 1995 — June 1995.*

In the process of examining the mesoporous molecular sieve catalysts for upgrading coal-derived liquids to jet fuels, we have examined the successful synthesis of phase pure mesoporous molecular sieves, Al-MCM-41, with varying Si/Al ratios, using three different aluminum sources (aluminum isopropoxide, Catapal B alumina, and aluminum sulfate). All of our previous results indicated that the source of aluminum used in the synthesis of Al-MCM-41 samples has a significant influence on their physico-chemical properties including their acid catalytic and supporting properties. This study addresses:

- The synthesis of the same material with another aluminum source (sodium aluminate) and comparison of its acidity with earlier samples by temperature- programmed desorption of *n*-butylamine on TGA and DSC
- Studies on crystallite size of Pt in the Pt-supported Al-MCM-41 samples

- Catalytic test results of these new materials with another model reaction of 1,3,5-tri-isopropylbenzene hydrocracking.

Experimental: Al-MCM-41 with varying Si/Al ratio, using sodium the aluminate as aluminum source, was synthesized similar to the procedure reported in Scheme I of our earlier report.[6] However, to keep the chemical composition of synthesis gel the same, the amounts of sodium silicate and fumed silica were varied. The Al-MCM-41 samples synthesized using sodium aluminate were also calcined at similar conditions.[6] All physico-chemical characterization (chemical analysis, XRD, acidity measurements and solid state NMR) was performed consistent with that of earlier samples.[2, 6, 7] However, the acidity was also measured by DSC, independent of TGA.

The hydrocracking of 1,3,5-tri-isopropylbenzene was performed in a batch reactor and product analyses were performed as reported earlier.[2, 7, 8] All of the reactions were carried out in horizontal tubing-bomb reactors (with vertical shaking, 200 cycles per minute) with 0. 1 g of catalyst and 1.0 g of reactant at 350°C for 2 hours under 1500 psi hydrogen pressure.

Findings: XRD patterns of the samples prepared with sodium aluminate with varying SiO_2/Al_2O_3 molar ratios clearly showed that they are pure MCM-41 type molecular sieves with good crystallinity. As with earlier Al-MCM-41 samples prepared with other sources, the crystallinity of the samples with sodium aluminate also decreased as the SiO_2/Al_2O_3 molar ratio was reduced. The d-spacing values of the major XRD peak indicated that aluminum incorporation in the framework was as good as with aluminum isopropoxide source, perhaps slightly better than with all other sources studied.

The initial SiO_2/Al_2O_3 molar ratios of calcined MCM-41 samples prepared using sodium aluminate were compared to those ratios obtained from the crystalline solid products (output). The output ratios were smaller than the input ratios. Similar results were obtained with samples prepared using Catapal alumina and aluminum isopropoxide. This was attributed to the fact that zeolites normally incorporate all of the aluminum present in the reaction mixture, leaving varying amounts of silica or silicate in solution, depending on such factors as the hydroxide concentration and the presence of various inorganic and organic cations in the reaction mixture.[9]

Thermal analyses of n-butylamine pre-adsorbed MCM-41 samples prepared with sodium aluminate with two different SiO_2/Al_2O_3 molar ratios produced TGA curves which indicated that most of *n*-butylamine desorbs below 473 K, as with all earlier samples prepared with different aluminum sources. The samples with different SiO_2/Al_2O_3 molar ratios (50 and 25) had different levels of *n*-butylamine desorption (22 and 26 wt%), which reinforces our assumption that the different levels of acidity can be attributed to different amounts of aluminum incorporation.

The weight losses caused by the n-butylamine desorption indicated that MCM-41 samples prepared with different aluminum sources adsorbed different levels of *n*-butylamine. The sample prepared with sodium aluminate showed significantly more weight loss, indicating that it was more acidic compared to the samples prepared with other sources. This could be attributed to the improved aluminum incorporation in the framework, thereby confirming the d-spacing values.

In examining the DSC curves, we noted that peak intensities for the sample of SiO_2/Al_2O_3 molar ratio 25 were high, indicating the increased number of acid sites. This, too, confirmed that the increased acidity is attributable to the increased amount of aluminum incorporation in the framework upon decreasing the SiO_2/Al_2O_3 ratio.

The fact that the ^{27}Al MAS NMR spectra showed no peak at 0 ppm corresponding to octahedral Al species in these samples confirmed that all of the Al atoms in the as-synthesized MCM-41 materials are present in a tetrahedral environment.[4] Decreasing the SiO_2/Al_2O_3 molar ratio from 50 to 25 did not change the Al symmetry, indicating that most of the aluminum can be incorporated without increasing Al content.

The preliminary catalytic and non catalytic test results for the reaction of 1,3,5-triisopropylbenzene hydrocracking on Al-MCM-41 sample MRK9b, which was prepared using aluminum isopropoxide, demonstrated that both catalysts (with and without Pt loading) were active (100 and 68% conversion) and almost no conversion (1%) occurred without catalyst at similar conditions. However, reactions went non-selectively, as expected, because of the no shape-selective nature of mesoporous materials with wide pores. The main products for the catalyst without Pt were diisopropyl and isopropylbenzenes, whereas the Pt-loaded catalyst further improved the hydrocracking activity and the products were primarily benzene and other lighter hydrocarbons.

In conclusion, our results indicated:

1. Sodium aluminate is a good source of aluminum to synthesize the mesoporous aluminosilicate molecular sieves with improved acidity
2. DSC can be used to determine the relative acidity of molecular sieves
3. Pt loading on Al-MCM-41 samples by wet impregnation yielded large crystallites with good uniformity
4. These mesoporous molecular sieves are capable of converting large molecules like 1,3,5-triisopropyl benzene.

These results establish the basis for future studies involving broader investigation of Al-MCM-41 molecular sieve catalysts with model reactions and, ultimately, coal liquids.

d. Comparison of the Catalytic Activities of Mesoporous Molecular Sieve Catalysts

Detailed synthesis, characterization, and preliminary catalytic activity screening of mesoporous molecular sieves (MCM-41 aluminosilicates) were reported in our earlier reports [see (a), (b), and (c) in this section]. We found that the source of aluminum used in the synthesis of these materials had a significant influence on their physico-chemical properties. The acid strength of these materials was lower than that of the microporous molecular sieves; how their catalytic activities compare with microporous molecular sieves is not clearly known.

Purpose: Compare the catalytic activities of mesoporous molecular sieve catalysts for upgrading coal-derived liquids to jet fuels. We examined sieves prepared with four different aluminum sources, microporous molecular sieves (mordenite and Y), and alumina for the model reaction of 1,3,5-triisopropylbenzene (TIPB) hydrocracking.

Experimental: A total of seven catalysts were screened: four were mesoporous molecular sieves (MCM-41 aluminosilicates) synthesized using aluminum isopropoxide (AI2), Catapal B alumina (PB2), aluminum sulfate (AS2), and sodium aluminate (SA2) with input SiO_2/Al_2O_3 ratio of 25. The microporous zeolites mordenite (CBV-20A) and Y (LZ-Y62) had SiO_2/Al_2O_3 ratios of 21 and 5, respectively. Prior to the catalytic runs, all of the catalysts were converted to protonic forms by calcining the ammonium forms at 460°C for 4 hours in an air flow of 200 ml/min.

The hydrocracking of 1,3,5-triisopropylbenzene (TIPB) was carried out in a batch reactor; all reactions were carried out in horizontal tubing bomb reactors with 0.1 g of catalyst and 1.0 g of reactant at 300°C for 30 minutes under 1000 psi hydrogen pressure. After the catalytic runs, the recovered catalysts were analyzed by thermal analysis (TGA) in order to estimate the coke formation. The conditions were similar with the earlier work starting from 30° C to 700° C at rate of 10°C/min. in an air flow of 200 ml/min.

Findings: The results of the reaction of 1,3,5-triisopropylbenzene (TIPB) hydrocracking over mesoporous (AI2, PB2, AS2, and SA2), microporous (mordenite and Y) molecular sieves and alumina revealed that propane and propylene were the major gas products common to all the catalysts and benzene, cumene, 1,3-diisopropylbenzene (1,3-DIPB), 1,4-diisopropylbenzene (1,4-DIPB), unreacted TIPB, and some unidentified di- and tri-alkyl benzenes were the major liquid products. The conversion of TIPB over alumina (S-2) is very small (5.4%) compared to those with all other catalysts. Among all the mesoporous molecular sieve catalysts, the catalyst prepared using sodium aluminate (SA2) showed high conversion (47.7%), whereas the one prepared using Catapal B alumina (PB2) showed low conversion (8.9%). The other two mesoporous molecular sieve catalysts (AI2 and AS2), prepared with aluminum isopropoxide and aluminum sulfate, respectively, showed slightly lower conversion (44.4 and 40.5%) compared to the catalyst SA2 (47.7%). The microporous (mordenite and Y) molecular sieve catalysts were also active for this reaction; however, the conversion with zeolite Y is higher (47.5%) than that with mordenite (28.9%).

In molecular sieve catalysis, the hydrocracking activity usually depends on the acidity of the catalyst. In fact, hydrocracking of a model compound over molecular sieve catalysts is one of the ways to characterize their acidity. Among all of the catalysts tested in this study only the alumina catalyst was amorphous and less acidic, resulting in very poor conversion compared to the other catalysts. Although mesoporous molecular sieve catalysts were found to be active for this reaction, the catalyst prepared with Catapal B alumina showed poor activity. The order of catalytic activity among mesoporous molecular sieves is SA2>AI2>AS2>PB2, which is a good correlation with their acidity order, which was observed from TPD of *n*-butylamine and reported earlier.[7, 10, 11, 12] This acidity difference, and the resulting difference in catalytic activity, can be attributed to the difference in the level of aluminum incorporation when different aluminum sources are used in the synthesis.

In the reaction of TIPB hydrocracking, both microporous molecular sieve catalysts (mordenite and Y) showed good activity, but the zeolite Y was more active than mordenite, again following the trend of their acidity. However, the hydrocracking of TIPB over microporous molecular sieves must occur mainly on the surface acid sites of the catalyst until the dealkylation of one or two isopropyl groups takes place, because the TIPB cannot diffuse as such into the pores of microporous molecular sieves.

The hydrocracking of TIPB depends not only on the acidity of the catalyst but also on the porosity of the catalyst. The overall order of catalytic activity (SA2>HY> AI2>AS2> HM>PB2>alumina) is not the order of acidity for the catalysts tested. From an acidity point of view, both HY and HM should have been much more active compared to all other catalysts. This does not hold true because TIPB and their cracked products diffuse easily in mesoporous molecular sieves. As a result, the mesoporous molecular sieve catalysts with better aluminum incorporation and crystallinity have shown better performance in this reaction compared to zeolite Y and mordenite.

Another important factor to be considered is the catalyst stability. In order to understand the catalyst stability in this reaction of TIPB hydrocracking, the coke formation over three catalysts (AI2, HM and HY)was studied by thermal analysis. This study indicated that almost no coke formed with mesoporous catalysts; however, coke formation was observed with microporous molecular sieves. This can be explained by the low acidity and high diffusivity within the mesopores. These two factors in mesoporous molecular sieve catalysts might not favor the formation of coke precursors.

In conclusion, our results indicate that mesoporous molecular sieves are active for the hydrocracking of bulky hydrocarbons; however, acidity is a key factor which depends on aluminum incorporation. Mesoporous molecular sieve catalysts also seem to be more stable for the conversion of bulky hydrocarbons as compared to microporous molecular sieve catalysts, in terms of less coke formation.

e. Low-Temperature Hydrogenation of Aromatics over Mesoporous Zeolite-Supported Noble Metal Catalysts.

This study is explained in detail in *Advanced Thermally Stable Jet Fuels Technical Progress Report, January — March 1996* (#92PC92104-TPR-15).

A primary concern in developing advanced thermally stable jet fuels is our ability to minimize aromatics in the fuel. A high aromatic content results in poor quality jet fuel with low thermal stability and environmentally harmful emissions. Saturation of naphthalene and its derivatives reduces aromatic content and generates decalins, which provide much higher thermal stability than long-chain alkanes in jet fuels at high temperature.[13]

Deep hydrogenation is necessary to reduce the aromatic content of fuels to meet increasingly more stringent regulations. Typically, conventional hydrotreating technology has been adapted for aromatics saturation. Conventional catalysts for fuel hydroprocessing were sulfided Co-Mo and Ni-Mo supported on alumina. Studies have shown that complete hydrogenation of aromatics is not possible under these circumstances, however, as a result of equilibrium limitations and because existing middle distillate hydrotreaters designed to reduce sulfur and nitrogen levels lower the diesel aromatics only marginally.[14, 15] In addition, such catalysts are active only at relatively high temperatures (300°C). Because hydrogenation is exothermic, deep hydrogenation is favored at lower temperature. Potential candidate catalysts for low-temperature hydrotreating include noble metals. One way to improve the hydrogenation activities of noble metal-supported catalysts is to choose the proper support. Zeolites Y and mordenite are good Pt and Pd catalyst supports for hydrogenating the naphthalene more selectively to the thermally stable t-decalin. Zeolites Y and mordenite are microporous,

preventing hydrogenation of the unwanted polyaromatic hydrocarbons. Novel zeolite MCM-41, a mesoporous zeolite with very high surface area and mild acidity, could be a good support.

Purpose: To explore the potential of mesoporous zeolite to serve as a support of noble metal catalysts for deep hydrogenation of aromatics in jet fuel.

Experimental: The mesoporous zeolite with an MCM-41 type structure was synthesized using aluminum isopropoxide as the Al source.[16] We prepared supported catalysts containing 2 wt% Pt or 2 wt% Pd using proton-form MCM-41 (synthesized using Al isopropoxide) and Al_2O_3 and TiO_2 as the support materials. The catalyst precursors were dried at 60°C overnight, and then calcined at 450°C for 4 hours. The nominal metal concentration was kept at 2 wt% for both Pt and Pd catalysts.

All of the catalysts were tested at 200 °C for a given residence time in 25-mL stainless steel microautoclaves. The reactor was charged with 1.0 g naphthalene, 4.0 g *n*-tridecane solvent, and 0.1 g catalyst; flushed with H_2; then pressurized to 1000 psig (cold) to begin the test. The reactor was immersed in a fluidized sand bath preheated to 200°C and shaken vertically at 240 cycles/min. The reactor was then quenched in cold water to room temperature.

Solution products were analyzed by GC-MS and GC-FID. GC and GC-MS indicated that cracking or isomerization of *n*-tidecane, if any, was negligible. The yields of products were determined by quantitative GC analysis using *n*-nonane and the conversion was determined by the amount of naphthalene recovered after the reaction. Selected tests were conducted to examine the effect of pre-reduction.[17]

Findings: Our results clearly indicated that both Pd and Pt catalysts supported on the mesoporous MCM-41 are superior to those supported on Al_2O_3 and TiO_2.

The main products from naphthalene hydrogenation over Pd and Pt catalysts at 200°C for 60 minutes were tetrahydronaphthalene (tetralin or THN), and *cis*- and *trans*decahydronaphthalene (decalin or DEHN). Δ9,10-octalin, which is an intermediate from tetralin to decalin, was also detected as a minor product. The selectivity to tetralin + decalin + octalin approached unity in all of the runs, indicating that there were essentially no side reactions, such as ring-opening cracking and ring-contraction isomerization under the conditions.

The results we observed indicated that MCM-41-supported Pt and Pd catalysts are more active than titania- and alumina-supported catalysts. The higher activity of the mesoporous zeolite-supported Pt and Pd may result from the improved dispersion of the noble metals on MCM-41, which has a much larger surface than that of Al_2O_3 and TiO_2 supports. The mild acidity of MCM-41 may also be a contributing factor, since it contributes to the electron deficiency of the metal on zeolite surface.

The noble metal, partcularly Pt, supported on acidic sites, showed an unusually high tolerance for sulfur poisoning. This unusual behavior is related to the electron deficiency of the noble metal during ion-exchange or impregnation, the metal attaches to acidic sites and reduction leads to the small clusters of metal. The small clusters of metal atoms close to the acid sites are electron deficient and responsible for the superior properties.

The selectivity to decalin isomers depends on the support and metal type. Compared to Pd/Al_2O_3 and Pd/TiO_2 catalysts, the Pd/MCM-41 catalyst afforded a higher *trans/cis* ratio, indicating a higher selectivity to trans-decalin. There appears to be one major difference between Pt and Pd catalysts in selectivity: Pd shows higher selectivity to *trans*-decalin. Therefore, among the three supports, MCM-41 corresponds to higher *trans/cis* ratios. Among the two metals, Pd catalysts always afford higher *trans/cis* ratios. Overall, MCM-41 supported Pd catalysts display the highest selectivity to *trans*-decalin.

Complete naphthalene conversion was reached in 1 hour, so we reduced the residence time and conducted 30-minute runs at 200°C. Although unreduced catalysts were used, nearly complete naphthalene conversion was achieved in all the runs within 30 minutes. However, the product distribution changed with residence time. Yields of tetralin increased and decalin yields decreased with decreasing residence time. It is also clear that the absolute yields of tetralin and decalins strongly depended on the type of support and metal.

Even with reduced residence time, the MCM-41 supported Pt and Pd catalysts were substantially more active than the corresponding catalysts supported on alumina and titania. In general, the activity of both Pt and Pd catalysts for complete hydrogenation of naphthalene to decalin decreased in the following order with respect to the support type: MCM-41 > TiO_2 > Al_2O_3.

Analysis of the tetralin and decalin yields at 30 and 60 minutes indicated that *cis*-decalin isomerizes into *trans*-decalin during the hydrogenation reaction over MCM-41 supported catalysts. This finding is consistent with our previous research.[18, 19] TPD of *n*-butylamine indicates that hydrogen MCM-41 is acidic, but its acidity is lower than that of hydrogen Y zeolite. The presence of Pd metal and acid sites seems to facilitate both tetralin hydrogenation and *cis*-decalin isomerization into *trans*-decalin.

---

[1] Schobert, H. H. et al. *Advanced Thermally Stable Jet Fuels, Technical Progress Report, October 1994 — December 1994.* The Pennsylvania State University. 1995.

[2] Schobert, H. H. et al. *Advanced Thermally Stable Jet Fuels, Technical Progress Report, January 1995 — March 1995.* The Pennsylvania State University. 1995.

[3] Jacobs, P. A. and J. A. Martens. *Synthesis of High Silica Aluminosilicate Zeolites.* Elsevier. 1987.

[4] Chen, C. Y. , H. X. Li, and M. Davis. *Microporous Material.* 1993. 2. 27.

[5] Maciel, G. Ge. And D. W. Sindorf. *J. Am. Chem. Soc.* 1980. 102. 7606.

[6] H. H. Schobert et al. *Advanced Thermally Stable Jet Fuels, Technical Progress Report, October 1994 — December 1994.* The Pennsylvania State University. 1995. 90.

[7] Reddy, K. M. and C. Song. *Catalysis Letters.* 1995.

[8] Reddy, K. M. and C. Song. *Preprints of ACS Symposium.* Chicago. 1995.

[9] Jacobs, P. A. and J. A. Martens. *Synthesis of High Silica Aluminosilicate Zeolites.* Elsevier. 1987.

[10] Schobert, H. H. et al. *Advanced Thermally Stable Jet Fuels, Technical Progress Report, January— March 1995.* The Pennsylvania State University. 1995.

[11] Schobert, H. H. et al. *Advanced Thermally Stable Jet Fuels, Technical Progress Report, April— June 1995.* The Pennsylvania State University. 1995.

[12] Reddy, K. M. and C. Song. *Am. Chem. Soc. Div. Fuel Prpr.* 1995. 40(4) 1003.

[13] Song, C., S. Eser, and P. G. Hatcher. *Energy & Fuels.* 1993. 7. 234.

[14] Stanislaus, A. and B. H. Cooper. *Catal. Rev. — SciEng* 1994. 36. 75.

[15] Copper, B. H., and B. L. B. Donis. *Appl. Catal. A: General.* 1996. 137. 203.

[16] Reddy, K. M. and C. Song. *Catalysis Letters.* 1996. 36. 103.

[17] Schobert, H. H. et al. *Advanced Thermally Stable Jet Fuels, Technical Progress Report, January— March 1996.* The Pennsylvania State University. 1996.

[18] Reddy, K. M. and C. Song. *Catalysis Today.* 1996.

[19] Schmitz, A., G. Bowers, and C. Song. *Catalysis Today.* 1996.

5.32 CONFORMATIONAL ISOMERIZATION OF CYCLOALKANES

This study is explained in detail in *Advanced Thermally Stable Jet Fuels Technical Progress Report, January — March 1998.*

We have previously shown that as jet fuel components, *trans*-DeHN is superior to *cis*-DeHN because the former is much more stable at high temperatures a desirable attribute for use as future high Mach aircraft jet fuel. Cycloalkane is considered a potential endothermic jet fuels that could also serve as the primary heat sink to cool the hot surfaces and system components of aircraft.[1, 2, 3] In addition, *trans*-DeHN has the desirable ability to inhibit solid deposit formation from jet fuels and their components at high temperatures.[4] For example, adding 50 vol% *trans*-DeHN to a JP-8P fuel, *n*-tetradecane, and *n*-butylbenzene thermally stressed at 723 K for 4 hours significantly reduced the deposit formation from 3.1 to 0.1 wt%, 3.0 to 0.1 wt%, and 5.6 to 0 wt%, respectively. Although *cis*-DeHN also has some industrial applications, it is desirable to convert *cis*-DeHN to *trans*-DeHN for enhancing fuel stability at high temperatures.

We performed conformation isomerization of decalin-type components in naphthenic jet fuels using zeolite-supported metal catalysts. Our early results revealed that zeolite-supported metal catalysts are effective for conformational isomerization and amolecular H_2-promotes isomerization reaction.

---

[1] Song, C. et al. *Energy & Fuels.* 1993. 7. 234.

[2] Donath, E. E. and M. Hess. *Chemical Engineering Progress.* 1960. 56. 68.

[3] Lander, H. R. and A. C. Nixon. *Prepr.- Am. Chem. Soc., Div. Pet. Chem*. 1987. 32. 504.

[4] Taylor, P. H. and W. A. Rubey. *Prepr.- Am. Chem. Soc., Div. Pet. Chem*. 1987. 32. 521.

5.33 CARBON SKELETAL ISOMERIZATION

This study is explained in detail in *Advanced Thermally Stable Jet Fuels Technical Progress Report, January — March 1998.*

Introduction

Coal-derived jet fuels are rich in alkylcyclohexanes, decalins and tetralins, and are more thermally stable than petroleum-based jet fuels at temperatures above 400¡C.[1] Some early work suggested that a 5-membered-ring structure may be more stable than the 6-membered-ring structure at high temperatures.[2] Our recent work[1] also indicated that alkylcyclopentane isomers offer higher thermal stability than the corresponding alkylcyclohexanes with the same carbon number. Therefore, these isomers may be superior components of future jet fuels. Further exploration of the conversion of the cyclohexane ring to the cyclopentane ring in monocyclic and bicyclic alkanes will be required in order to achieve more stable fuels.

The next challenge is determining how to produce jet fuels that are rich in cyclopentane-type components with high activity and good selectivity. To address this issue, we explored catalytic isomerization from cyclohexane-type to cyclopentane-type compounds. In our preliminary investigation, we prepared four bifunctional zeolite-supported metal catalysts that were then used to isomerize cyclohexane to methylcyclopentane.

In this report, we present the preliminary experimental results in terms of reaction temperature, initial pressure and residence time on the isomerization of cyclohexane to methylcyclopentane under different reaction conditions.

Experimental

Four catalysts 0.5%Pt-HY, 0.5%Pt-HM, 0.5%Pd-HY and 0.5%Pd-HM were prepared by the incipient wetness impregnation method using tetraammineplatinum (II) chloride hydrate and tetraamminepalladium (II) monohydrate. The Y-zeolite (LZ-Y62 with $SiO_2/Al_2O_3 = 5$) and ammonium mordenite (CBV30A with $SiO_2/Al_2O_3 = 38$) were also used. After incipient wetness impregnation, the obtained catalyst precursors were dried at 120°C for 8 hours and then calcined at 450°C for 4 hours.

Reagent-grade cyclohexane was employed in the isomerization experiments. The reduction of Pt (or Pd) oxide Y-zeolite (or mordenite) was done in situ. In a typical run, 3.2 g cyclohexane and about 0.15 g catalyst precursor (or 2.14 g cyclohexane and about 0.10 g catalyst precursor) were charged into a batch reactor with a total volume of approximately 25 ml. The sealed reactor was subsequently purged 6 times with 1000 psig UHP hydrogen and finally pressurized with the experimental value. It was then placed in a fluidized sand bath operating at experimental temperature. After a period of time (20, 40 or 60 min), the reactor was quenched by immersing in a cold water bath and then air dried. The products were carefully separated from the solid catalyst by filtration. After collection, the liquid was immediately stored in a refrigerator. The liquid products were analyzed on a GC with a FID detector operated in the split/splitless injection mode. The temperature of the column was programmed from 40 to 100°C at a rate of 4°C/minute after a 5 minute isothermal period. Because cyclohexane and

methylcyclopentane have the same weight response factor, the quantification was carried out on the basis that area percent equals weight percent in a GC analysis.

Test Conditions

	Initial Pressure	Reaction Temp.	Reaction Time
Test 1	300 psig	300°C	20 min.
Test 2	650 psig	300°C	20 min.
Test 3	500 psig	330°C	60 min.
Test 4	500 psig	300°C	60 min.
Test 5	1020 psig	300°C	60 min.
Test 6	1020 psig	370°C	60 min.
Test 7	1020 psig	330°C	40 min.

Results and Discussion

According to the experimental results, we observed the following trends:

1. The two mordenite-supported catalysts are effective for cyclohexane isomerization into methylcyclopentane at 300°-330°C. Between 0.5% Pt-HM and 0.5% Pd-HM, the difference in conversion is small and selectivities are almost 100% in the transformation of cyclohexane to methylcyclopentane, with the exception of a single test.
2. Pt- and Pd-loaded zeolite Y are not effective in the isomerization of cyclohexane; the conversions with 0.5% Pt-HY and 0.5% Pd-HY were very low at 300°-330°C. However, the very low or negligible conversions prevent a meaningful discussion of the selectivities of these two loaded zeolite Ys.
3. The results from Test 1 and Test 2 with different pressures (300 psig and 650 psig) revealed slightly higher conversions at 300 psig than at 650 psig for noble metal loaded mordenite catalysts.
4. Between Test 3 and Test 4, conversions are relatively higher at 330°C for all four catalysts. On the other hand, selectivities of 0.5% Pt-HM and 0.5% Pd-HM were much lower at 330°C than at 300°C.
5. When reaction temperature was 370°C and initial pressure was 1020 psig, conversion rates for 0.5% Pt-HM and 0.5% Pd-HM were higher and selectivities were lower in Test 6 than those from the other six tests. However, the conversion rates increased with almost the same selectivities for the two metal-supported Y catalysts.
6. Experimental results from Test 5 and Test 7 showed some interesting aspects pertaining to the influence of loading ratio and reaction time. These aspects warrant further investigation.

---

[1] Lai, W. and C. Song. Pyrolysis of Alkylcyclohexanes In or Near the Supercritical Phase: Product Distribution and Reaction Pathways, *Fuel Processing Technology.* 1996. 48. 1-27.

[2] Harrison, W. E., III. U.S. Air Force, Wright Laboratory. February 14, 1996.

5.34 HYDRODEOXYGENATION UNDER COAL LIQUEFACTION CONDITIONS USING NOVEL ORGANOMETALLIC CATALYST PRECURSORS

This study is explained in detail in *Advanced Thermally Stable Jet Fuels Technical Progress Report, October — December 1997.*

Introduction

The goal of this study was to prove that bimetallic organometallic catalyst precursors produce improved coal liquefaction products compared to those produced by conventional liquefaction systems. When we undertook this study, conventional wisdom held that direct coal liquefaction was a catalytic process. High conversions (> 88%) had been achieved using conventional catalysts of iron and molybdenum.[1] Because conventional catalysts already achieved good conversions, the primary reason for considering unconventional catalysts was to improve the product quality. One of the major concerns with liquefaction product is its abundant oxygen content. Phenols can comprise as much as 40% (for low-rank coals) of the liquefaction distillates.

Oxygen functional groups are undesirable in coal liquefaction distillates, because they have been connected to the instability of these distillates.[2, 3, 4] Ether linkages, connecting structural units within the coal matrix, have been proposed as sites for the depolymerization of the coal, and together with carboxyls and phenolics, have been implicated in facilitating retrogressive, crosslinking, repolymerization reactions.[5, 6]

Conventionally, compounds containing these carboxyls and phonolics are removed downstream in a catalytic hydrodeoxygenation step. Supported CoMo and NiMo catalysts facilitate oxygen removal in these processes.[1, 4, 7] The use of these catalysts increases the complexity and cost of the process. An alternative is to extract the phenols from the distillates, but this essentially discards 40% of the potential product.[2] Therefore, the utilization of either a CoMo or NiMo catalyst in a liquefaction stage has the potential to increase the product quality of liquefaction distillates by combining hydrodeoxygenation and liquefaction in a single stage.

Results

We recommend the following experimentation to ascertain the presence of the relative oxygen functional groups in the coals to be studied. First analyze a range of three subject coals: DECS 26 Wyodak (a subbituminous coal), DECS 24 Illinois #6 (an hvC bituminous), and DECS 23 Pittsburgh (an hvA bituminous). Use CPMAS ^{13}C NMR and FT-IR analysis to ascertain the presence of the relative oxygen functional groups in the coal.

Perform blank experiments without a catalyst and control experiments with ATTM. All reactions should be single-stage liquefactions (SSL) performed at 400°C for 30 minutes with 2:1 solvent (1-methylnaphthalene) at 6.9 MPa hydrogen pressure (cold) and catalyst precursors (when used) at concentrations of 1 wt% Mo. Although these are not optimum conditions for either oxygen removal or liquefaction conversion to desired products, they are comparable to the conditions used by other researchers in the field of coal liquefaction[8, 9] and could complement the body of data from which the impact of these catalyst precursors on the liquefaction product quality could be evaluated.

The liquid products of liquefaction should be analyzed by GC and GC-MS, and the gases by GC. The presence of oxygen functional groups in the residue can be determined using ^{13}C NMR and FTIR.

Comparison of the oxygen functional groups present in the coal and the liquefation residue could provide information on those functionalities that have reacted completely during liquefaction. The oxygen content of the various liquefaction products (especially the oils) for each of the experimental conditions (i.e., non-catalytic, ATTM, CoMo-T2 and NiMo) could provide information on the product quality achieved under liquefaction conditions using the different precursors. Thus, the liquefaction and HDO ability of the precursors could be evaluated. Comparison of the yields of the different product fractions (i.e., preasphaltenes, asphaltenes, and oils) could provide additional information on the liquefaction ability of the precursors.

A selection of two other coals can then be made. Their rank, or more accurately their oxygen content, should be selected based on the results obtained from the previous three coals. Predictions of the behavior of these coals can be made and later compared to the results of the liquefaction experiments performed on the coals under the SSL conditions stated above.

To attain the optimum conditions for a desirable product distribution, a balance has to be achieved with a temperature low enough to favor hydrogenation and keep radical production at a reasonable rate, yet high enough to facilitate hydrocracking. Long reaction times favor extensive conversion to radical species. If the rate of radical production is slow, a radical can be easily capped before recombination can occur. However, long reaction times allow the system to approach equilibrium, again favoring dehydrogenation at the temperatures used in liquefaction.

Optimum conditions for the conversion of coal to desirable products appeared to be lower temperatures for longer reaction times. A system similar to that suggested for temperature-programmed liquefaction seemed appropriate.[10, 11] Temperature programmed liquefaction involves rapid heat-up to a relatively low temperature (200°C) at which the coal catalyst-solvent mixture is soaked for an extended period of time (15 minutes). The mixture is then heated to the conventional liquefaction temperature (400°C) at a steady rate (5°C/minute). This higher temperature is held for approximately 30 minutes. This temperature strategy should be tested as a means to achieve optimum conversion to desirable products. The results of these experiments can then be evaluated in the same way as the SSL results.

Conclusion

A combination of either a CoMo or NiMo catalyst and a liquefaction stage could increase the product quality of liquefaction distillates. The use of organometallic precursors to disperse these catalysts may lead to a greater product quality directly from the liquefaction stage.

A range of coals with varying rank and oxygen content can provide a suitable platform to evaluate these precursors. The results obtained should permit predictions as to the product distribution from the liquefaction of other coals.

If the catalyst precursors are comparable (e.g., have similar surface area, dispersion, active forms and conversion to those active forms) and the organometallic precursors markedly improve the product quality of the coal liquefaction reactions compared to non-catalytic and

ATTM experiments (e.g., greater removal of oxygen from the products), then the hypothesis of this research will have been proved. However, large differences in the characteristics of the catalyst precursors, or no significant improvement of the product quality, will show the hypothesis to be untrue. If the product quality of liquefaction processes can be improved by the utilization of organometallic precursors to disperse bimetallic catalysts, then the optimum conditions under which these precursors operate can be investigated.

---

[1] Watanabe, Y., et al. *Fuel.* 1984. 63. 752.

[2] Burgess,C. *PhD Thesis*, Pennsylvania State University, University Park, PA. 1994.

[3] Pauls, R. E. et al. *Energy & Fuels.* 1990. 4. 236-242.

[4] Song, C., H. H. Schobert, and P. G. Hatcher. *Energy & Fuels.* 1992. 6. 326-328.

[5] Serio, M. A. et al. The Dual Role of Oxygen Functions in Coal Pretreatment and Liquefaction: Crosslinking and Cleavage Reactions *Proceedings of Contractors Review Conference: Coal Liquefaction and Gas Conversion.* Pittsburgh, PA. 15-44.

[6] Weigold, H. *Fuel.* 1992. 61. 1021-1025.

[7] Gevert, S. B., et al. *AppliedCatalysis A*. 1994. 117. 151-162.

[8] Hirschon, A. S. et al. Dispersed Catalysts for Coal Liquefaction. *Coal Science.* Eds.: H. H. Schobert, K. D. Bartle, and L. L. Lynch, ACS Symposium Series 1991. 461.

[9] Song, C. and H. H. Schobert. *Am. Chem. Soc., Div. Fuel Chem. Prepr.* 1992. 37. 42.

[10] Solum, J. M., R. J. Pugmire, and D. M. Grant. *Energy & Fuels.* 1989. 3. 187-193.

[11] Senfle, J. T., et al. *Fuel.* 1984. 63. 245.

5.35 HYDRODEOXYGENATION IN COAL LIQUEFACTION SYSTEMS USING NOVEL ORGANOMETALLIC PRECURSORS

This study is explained in detail in *Advanced Thermally Stable Jet Fuels Technical Progress Report, January — March 1998.*

The objective of these experiments was to convert coal to a hexane soluble (oil) fraction with a low phenolic content. Phenols are detrimental to the thermal stability of the resultant liquid product and are sites for the recombination of radical intermediates in the liquefaction system, forming refractory products.

In previous experiments, a catalyst precursor containing both cobalt and molybdenum (CoMo-T2) in an organometallic, thiocubane structure was compared to ammonium tetrathiomolybdate (ATTM) under coal liquefaction conditions of 400¡C and 1000 psi H_2 for 30 minutes, with methyl naphthalene present as a solvent. ATTM is a commonly used catalyst precursor in the coal liquefaction community and decomposes to MoS_2 at 350¡C in a hydrogen atmosphere.

Results were obtained with three coals: Wyodak, a subbituminous B coal; Illinois #6, a hvC bituminous coal; and Pittsburgh #8, a hvA bituminous coal. The oxygen content of these coals decreased in the order in which they are listed.

CoMo-T2 gave higher yields of oil and desirable products (phenol-free hexane solubles) with both the Illinois #6 and Pittsburgh #8 coals. However, with the Wyodak coal, ATTM gave much higher yields of oil and desirable products. One possible explanation for this result was the low sulfur content of the Wyodak coal compared to the two higher ranked coals. This allows for the possibility that insufficient sulfur was present in the liquefaction system to permit a stoicheometric mixture for the formation of the active form of CoMo-T2.

This conclusion led us to repeat the liquefaction reactions with the addition of H_2S (5% by volume) to the reaction atmosphere. Solvent was excluded to allow for easier analysis of the hexane solubles.

Addition of a sulfur source increased the total conversion and oil yield of the Wyodak coal in the presence of CoMo-T2. ATTM with H_2S reduced the oil yield from liquefaction by increasing gas and asphaltene yields. For reactions without H_2S, solvent was included in the hexane soluble fraction. Allowing for this additional product, all yields increased with the addition of a sulfur source.

Future work will focus on product quality,and will include the quantitative and qualitative analysis of the hexane soluble fractions by GC and GC-MS, respectively.

5.36 NOVEL APPROACHES TO LOW-SEVERITY COAL LIQUEFACTION AND COAL RESID CO-PROCESSING USING WATER AND DISPERSED CATALYSTS

a. Addition of Water in Presence of Dispersed Molybdenum Sulfide Catalyst: Wyodak Subbituminous Coal

This study is explained in detail in *Advanced Thermally Stable Jet Fuels Technical Progress Report, October 1994 — December 1994.*

Purpose: The cost of coal-derived syncrudes by conventional processes ($30-$35 per barrel in 1994) is competitive with petroleum prices. Significant cost reduction of syncrudes could be achieved through the development of a more efficient liquefaction processes.

Conventional opinion has maintained that water is detrimental to catalyst activity during catalytic coal hydroliquefaction.[1, 2, 3] Contrary to conventional wisdom, our work in this area has demonstrated a remarkable synergistic enhancement in the conversion of Wyodak subbituminous coal through the co-use of a dispersed Molybdenum (Mo) catalyst and water under low-severity conditions (325°-375°C for 30 minutes). The effective temperature range was much lower than those employed in current liquefaction technologies (400°-470°C).

An example of this synergistic enhancement is shown in **Figure 5.36-1**. The catalyst precursor was the water soluble inorganic salt ammonium terathiomolybdate (ATTM) at a loading of 1 wt% Mo to dmmf coal. Catalyst impregnation was achieved by incipient wetness. The water/dmmf coal weight ratio was 0.46. As shown in Figure 5.36-1, in comparison to the non-catalytic run of the dried coal, the addition of water alone improved coal conversion from 14.5 to 22.5 wt% (dmmf). The use of ATTM alone increased conversion from 14.5 to 29.8 wt%. When a small amount of water was added to the catalytic reaction at 350°C, however, coal conversion increased dramatically to 66.5 wt%. This represents a 359% increase from the non-catalytic run without water, and a 123% increase from the catalytic run without water.

Conversely, our preliminary work revealed that at higher reaction temperatures (400°-450°C) water addition has a detrimental impact on catalyst activity and coal conversion. The influence of reaction temperature on overall conversion for the Wyodak coal/ATTM/water system results in a volcano-shaped curve over time, indicating a maximum conversion for Wyodak coal of almost 80 wt% at 375°C.

These findings launched efforts to develop an efficient, low-severity liquefaction process for high conversion of coal into solvent-soluble materials amenable to subsequent facile upgrading to produce thermally stable jet fuels. This study was undertaken to clarify the origin of the promotional effects of water on low-severity catalytic coal liquefaction using dispersed catalysts and to explore the potential of H_20-promoted catalytic reactions for application in coal liquefaction and co-processing of coal with petroleum resids.

Experimental: This study was twofold, consisting of:

1. Model compound studies on the effects of water on bond cleavage and cross-linking reactions of various coal-related structures containing etheric C-O, methylenic C-C

linkages, and other O-containing functionalities, such as phenolic OH and carbonyl C=O groups in the presence of dispersed Mo catalyst

2. Catalytic liquefaction of coals and their co-processing with petroleum resid under low- and high-severity conditions.

Results: The first technical approach was intended to yield fundamental information regarding the physical/chemical role of water on the thermal reaction pathways of various coal structures in the presence of dispersed catalyst and molecular hydrogen. The second approach was intended to identify relevant catalyst/coal reaction systems and process conditions for optimum catalyst-water synergistic effects for promoting low severity coal conversion. The distinction between the liquefaction and co-processing experiments lies in the use of a petroleum residuum as a process solvent in the latter runs. The inherent advantages of co-processing include the simultaneous coal conversion and upgrading of heavy petroleum resids, a reduction in the need for solvent recycle, and an increase in the petroleum-like character of transportation fuels. Additional benefits include synergistic effects in hydrogen transfer and the adsorption of metal species in the resids by coal, which reduces deactivation of supported catalysts in downstream processing.

The following reaction variables will be examined:

- Choice of dispersed catalyst, including both water-soluble and oil-soluble precursors
- Effect of catalyst loading level
- Influence of coal rank
- Effect of reaction temperature in the range of 325°-425°C
- Effects of reaction vehicles including pure solvents and process solvents
- Effect of H_2 partial pressure

These approaches will provide valuable mechanistic information concerning the chemical influence of water/dispersed catalyst systems on coal depolymerization reactions, and may contribute to the development of novel low-severity catalytic coal liquefaction processes.

b. Addition of Water in Presence of Dispersed Molybdenum Sulfide Catalyst: Pittsburgh #8

This study is explained in detail in *Advanced Thermally Stable Jet Fuels Technical Progress Report, January 1995 — March 1995.*

Purpose: Replicate the study cited in (a), using both Pittsburgh #8 high-volatile bituminous coal and Wyodak subbituminous coal, to determine whether the addition of water in the presence of dispersed Mo sulfide catalyst is observable with other coals, particularly those of differing rank. Reactions were performed at two temperatures 350° and 400°C.

Findings: A strong synergistic relationship exists between water and a dispersed molybdenum sulfide catalyst for promoting the low temperature (350°C) liquefaction of both Wyodak subbituminous and Pittsburgh #8 bituminous coals. Compared to the catalytic runs of the dried

coals, the co-use of catalyst and water can double the coal conversion at 350°C for 30 minutes, from 29.8 to 66.5 wt% for Wyodak coal and from 24.7 to 51.0 wt% for Pittsburgh #8.

At a higher temperature (400°C), the promotional effects of adding water were lost. In the case of Wyodak coal, the addition actually inhibited catalyst activity, resulting in a reduction in conversion. For Pittsburgh #8, the addition of water at the higher temperature resulted in a conversion similar to that observed when the catalyst is used alone. There was, however, a slight improvement in product quality with the water-added reaction.

Only two temperatures and a single water/dmmf ratio (0.46) were used in these studies. Additional studies could identify the optimum temperature window and water/dmmf ratio under which the water-dispersed catalyst synergistic interaction is maximized for conversion of Pittsburgh #8 coal.

c. Novel Approaches to Low-Severity Coal Liquefaction and Coal Resid Co-processing Using Water and Dispersed Catalysts

This study is explained in detail in *Advanced Thermally Stable Jet Fuels Technical Progress Report, April 1995 — June 1995.*

Previous work demonstrated synergism between water and a dispersed molybdenum sulfide catalyst for promoting liquefaction of Wyodak subbituminous coal at relatively low temperature (350-375°C). Based on these encouraging results with Wyodak coal, we embarked on a more in-depth fundamental and exploratory study on the promotional effects of water on coal hydroliquefaction using dispersed catalysts. Preliminary results from work using Pittsburgh #8 high-volatile bituminous coal indicated a similar marked improvement in coal conversion at 350°C through co-use of water with dispersed molybdenum sulfide catalyst. The overall improvement in conversion observed for the higher-rank coal, however, was somewhat less dramatic than that for Wyodak coal.

Purpose: Conduct a more thorough study of the effects of reaction temperature range (350°-425°C) on the water-promoted catalytic liquefaction of Pittsburgh #8 coal. We constructed a temperature versus conversion profile with the data obtained to date for Pittsburgh #8 coal runs with ammonium tetrathiomolybdate (ATTM) and ATTM + water, previously done by Song and Saini for Wyodak coal runs.[4,5]

Experimental: Experimental details can be found in corresponding Technical Progress Report.[6]

Findings: Strong synergistic effects exist between water and dispersed molybdenum sulfide catalyst (1 wt% Mo on dmmf coal basis) for promoting the low temperature (≤375°C) liquefaction of both Wyodak subbituminous and Pittsburgh #8 bituminous coals. We constructed temperature versus conversion profiles for both the water-promoted catalytic and catalyst-only runs of Pittsburgh #8 coal, similar to those previously constructed for Wyodak coal. Comparison of these profiles for the two coals of different rank reveals certain distinct similarities. Water addition to the catalytic runs of both coals has a promotional effect on conversion at low temperature (≤375°C). The promoting effects of water are more pronounced for the lower-rank subbituminous coal (Wyodak) than for the high-volatile bituminous coal (Pittsburgh #8). Both coals display a maximum conversion at 375°C in the catalyst + water runs. At higher temperatures (≥400°C), water had a negative impact on the catalytic liquefaction of

both coals. The inhibiting effect of water at higher temperatures is more dramatic for Wyodak subbituminous coal than for Pittsburgh #8 high volatile bituminous coal. Based on these findings, 375°C appears to be the optimum temperature at which water-dispersed catalyst synergistic interaction is maximized for conversion of both coals.

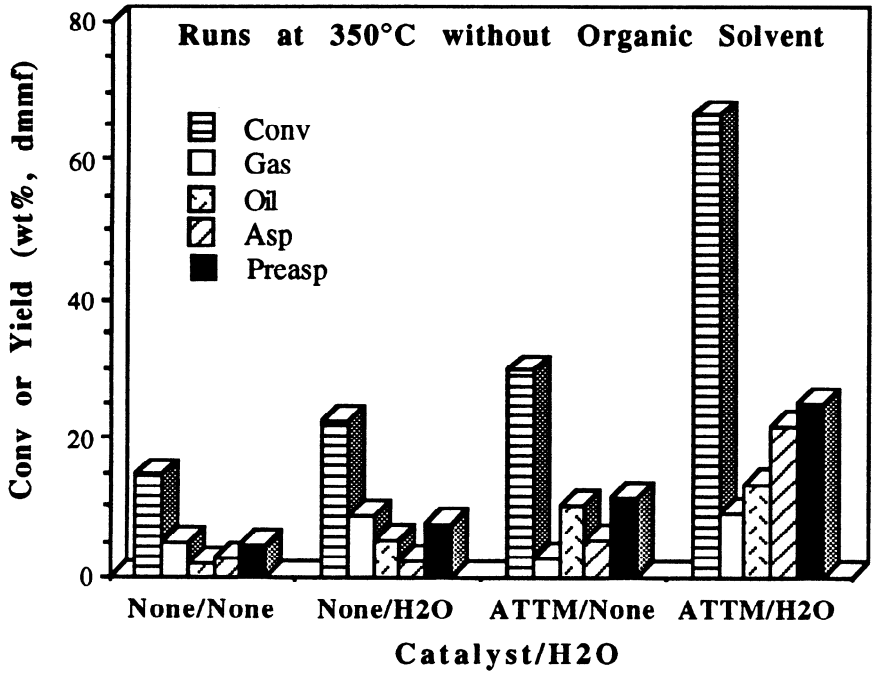

5.36-1. Effect of Temperature on Liquefaction of Wyodak Coal and Dispersed Mo Catalyst and Water

---

[1] Bockrath, B. C., D. H. Finseth, and E. G. Illig. *Fuel Processing Technology*. 1986. 12. 175.

[2] Ruether, J. A., et al. *Energy & Fuels.* 1987. 1. 198.

[3] Kamiya, Y., T. Nobusawa, and S. Futamura. *Fuel Processing Technology.* 1988. 18. 1.

[4] Song, C., A. K. Saini, and H. H. Schobert. *Energy & Fuels.* 1994. 8. 301.

[5] Durand, B. and C. Nicaise. Kerogen, Insoluble Organic Matter from Sedimentary Rocks. *Editions Technip.* Paris. Ed. B. Durand. 1980. 35.

[6] Schobert, H. H. et al. *Advanced Thermally Stable Jet Fuels, Technical Progress Report, April 1995 — June 1995.* The Pennsylvania State University. 1995.

5.37 DEVELOPMENT OF COAL-BASED JET FUELS VIA COPROCESSING OF COAL AND RESID

Delayed coking is a universal conversion process that uses long reaction times to produce gases, distillates, and coke from relatively low value feedstocks such as vacuum resid.[1, 2] It does not suffer from many of the inherent disadvantages associated with direct liquefaction, such as high pressure operation in hydrogen atmospheres, and, therefore, is an attractive alternative to conventional coprocessing methods.

In practice, the feed is rapidly heated to approximately 500°C in the coke drum. The vapor products (gases, naphtha, and gas oil) are stripped off and sent to a fractionator tower while the coke remains in the drum, reacting to produce a high quality coke. The distillates can then be catalytically upgraded to produce synthetic fuels.

One further advantage is that the associated condensation reactions produce a highly aromatic coke enriched in S, N and metals relative to the feed. Typical product distributions from industrial coking operations are: 10-15% gas, 50-60% liquids, and 30-35% coke.[1, 2, 3]

Optimum coal/resid coprocessing conditions are governed by many factors including feed characteristics and reaction conditions. Wallace and co-workers reported an improved interaction between coal and petroleum residua with resid C_{ar} values >40%.[4] Curtis and Hwang observed a decreased oil yield and increased asphaltene, preasphaltene, and residue concentrations commensurate with the addition of 30 wt% coal to residuum.[5]

a. A Qualitative Analysis of the Liquid Products

This study is explained in detail in *Advanced Thermally Stable Jet Fuels Technical Progress Report, July — September 1996.*

Purpose: This work continued previous studies primarily concerned with evaluating retrogressive studies during coal/oil coprocessing.[6, 7] Rather than focusing on the relative yields of soluble and insoluble product, this work incorporated qualitative analysis of the liquid products.

Experimental: Three petroleum vacuum residua were used in the duration of this work VR1, Hondo, and Blend. Elemental and NMR analyses are presented in **Table 5.37-1**. Six coal samples were also used: Upper Sunnyside, Dietz, Pittsburgh #8Upper Banner, Illinois #6, and Wyodak. Samples were ground to -60 mesh and dried under vacuum at 110^{O}C for 2 hours prior to use.

The reactions were carried out in vertical 25 ml microautoclave reactors with an 8 g feed (resid:coal ratio of 2:1 w/w) at 450°C for 60 and 120 minutes. Tests were conducted under 3.5 MPa and atmospheric N_2 environments, respectively.

A detailed explanation of the collection and analysis of products was presented in the original Technical Progress Report.[8]

The experiments conducted at 60 and 120 minutes demonstrated that concentrations of TBF-insoluble material were comparable for the two sets of feed. At 450°C, coking the coals and resid together for 60 minutes under 3.5 MPa N_2 produced more solids than the sum expected

from the independent reactions. Obviously, coal retrogressive reactions dominate at this higher temperature. However, these resids coke more readily in the presence of coal, as suggested by the lower THFI concentrations from similar reactions with a more aromatic resid.[9]

There are many possible reaction mechanisms in coprocessing, because each feedstock can lead to a variety of products. Therefore, separation of coprocessing products into insoluble and soluble material does not discriminate between the amount of insoluble matter originating from the independent reactions of the coal or residuum or, indeed, any resultant interactions. The overall negative conversions measured at 450°C may have resulted from coking reactions of each feedstock independently or the product of interactions between the two components.

The presence of coal in the coking medium presented no significant deterioration in product distribution, with the bituminous coals displaying similar conversion data, especially asphaltene and preasphaltene concentrations. However, there appeared to be a rank effect on the enhancement of coke formation. An important criterion of behavior in coprocessing systems is that the interactions leading to retrogressive reactions are influenced by the thermoplastic properties of the feedstock. Indeed, retrogressive reactions only arise when both the coal and the residuum are undergoing active thermal decomposition. The bituminous coal was chosen, in part, based on its fluidity profiles. The existence of a fluid-like state enhances mixing with the resid and enables hydrogen transfer reactions. This is illustrated by the improved liquid product distribution in reactions of Pittsburgh #8, Upper Banner, and Illinois #6 with VRl all have maximum fluidity in the temperature range of 410-447°C. Conversely, Wyodak coal, a low-rank subbituminous sample, demonstrates no plastic behavior, as reflected by the smaller THF-insoluble residue concentration, and subbituminous coals offer restricted mobility and contact in comparison to their higher rank counterparts.

Preliminary analysis of the *n*-hexane soluble fraction (oils) has shown significant differences in composition between samples from the latter reactions. VRI oils are characterized by mainly small chain paraffins and 1-2 ring hydroaromatic structures. However, upon reaction in the presence of coal (irrespective of rank) heavier hydroaromatics were identified; in each case, selected 4-ring structures such as benzo(a)pyrene were observed.

Findings: Microautoclave reactions conducted with a range of coals and commercial residua demonstrated that at 450°C and reaction times of 60 and 120 minutes, vacuum residua coke more readily in the presence of coals. Continued characterization of both the soluble and insoluble products by standard analyses such as HPLC, NMR, FTIR, and optical microscopy, will determine the contribution of the coal and resid to the overall reaction mechanism. Finally, the solvating capacity of petroleum feedstocks can be enhanced by the addition of an aromatic species, such as anthracene oil.[10] Further work should, therefore, include reactions with ternary systems (e.g., the addition of decant oil to resid/coal mixtures).

Table 5.37-1. Properties of Petroleum Residua

Resid	Hydrogen Distribution				Elemental Composition (%w/w)				
	Har	Hα	Hβ	Hγ	C	H	N	S	H/C
VR1	6.44	12.58	62.88	18.11	85.9	10.82	0.43	1.53	1.51
Hondo	10.7	7.9	52.7	26.5	79.1	10.50	0.80	5.45	1.58
Blend	10.5	12.7	60.7	16.2	84.8	9.9	0.61	4.74	1.39

b. Determination of Whether Rank and Plastic Properties Impact the Reaction Mechanisms of Feedstocks During Coal Resid Co-Processing

This study is explained in detail in *Advanced Thermally Stable Jet Fuels Technical Progress Report, January — March 1997.*

Purpose: The work presented here concerned both evaluation of retrogressive reactions during coal-resid co-processing and qualitative analysis of the liquid products. These phenomena were explored in the belief that rank and plastic properties will play a defining role in the reaction mechanisms of such feedstocks.

Experimental: One petroleum vacuum residuum and four coal samples were used in this study Upper Banner, Pittsburgh #8, Illinois #6, and Wyodak. The reactions were carried out in vertical 25 ml microautoclave reactors with 8g feed (resid:coal ratio of 2:1 w/w) at 450°C for 120 minutes. Tests were conducted under an atmospheric N_2 environment. Product collection and analysis are explained in detail in the corresponding Technical Progress Report.[11]

Findings: An important criterion in behavior in coprocessing systems is that the interactions leading to retrogressive reactions are influenced by the thermoplastic properties of the feedstock. Indeed, reactions only arise when both the coal and the residuum are undergoing active thermal decomposition. The existence of a fluid-like state enhances mixing with the resid and enables hydrogen transfer reactions. The bituminous coals were chosen, in part, for their fluidity profiles.

Examining the product distribution from the reaction matrix tested, we found that within experimental error, the presence of coal in the coking medium generated no significant deterioration in product distribution. As defined in terms of enhanced soluble product formation, Upper Banner and Illinois #6 would at first appear to be the most suitable candidates for co-processing under such conditions; Pittsburgh #8 was the least effective. Furthermore, the results for Wyodak are somewhat surprising given that subbituminous coals offer restricted mobility and contact in comparison to their higher rank counterparts, resulting in limited surface interactions with the residuum components. Moreover, there appeared to be little rank effect on the enhancement of coke formation.

Analysis of the *n*-hexane soluble fraction (oils) demonstrated negligible differences in composition between samples from this series of reactions. VR1 oils were characterized by substituted (predominantly methyl) and unsubstituted 3- and 4-ring hydro- and aromatic structures, the heaviest polycyclic identified was benzo(a)pyrene. The presence of coal, irrespective of rank, imparted no qualitative alteration on oil composition (with the exception of

Upper Banner); the presence of coal-derived 2- and 3-ring aromatics (naphthalene, anthracene, and phenanthrene) were identified in the initial region of the chromatogam.

Optical examination of the TBF-insoluble residues similarly dispelled the hypothesis that plasticity, and consequently rank, was a definitive criterion for optimum reaction conditions. VR1 displayed typical anisotropic flow domains associated with coke formation. Similarly, the systems with Upper Sunnyside, Illinois #6, and Wyodak coal, while not displaying a profound degree of coking, indicated mosaic type textures around the edges of the insoluble particles, indicative of intimate contact during coking. However, the one anomaly was Pittsburgh #8, where no anisotropy was observed.

To summarize, a series of coals and petroleum resid were co-processed under simulated delayed coking conditions to investigate retrogressive reactions and soluble product composition. Exploratory tests identified a system with the propensity to produce 2- and 3-ring aromatics in the liquid products. However, little or no correlation existed between coal behavior and common parameters such as rank or plasticity. Indeed, Pittsburgh #8, characterized by high rank and maximum fluidity in the experimental temperature region, displayed curious behavior in comparison to Upper Banner.

c. Simulated Delayed Coking Experiments

This study is explained in detail in *Advanced Thermally Stable Jet Fuels Technical Progress Report, April — June 1997.*

Purpose: The application of a delayed coking type process to generate coal derived liquids is not new. Speight reports on a such a modified process termed *extractive coking*.[1] Coal and an appropriate H-donor solvent are coked in a two stage process at 400° and 450°C, with continual removal of lighter overhead products (typically fractionated into recycle solvent, gases, light oil, and middle distillates). Similarly, the Exxon Donor Solvent process uses a secondary coking step to produce addition liquids from the vacuum bottom s slurry.[12] Using this two-stage method increases liquid yields by 10 wt%.

Our work has comprised simulated delayed coking experiments with an expanded experimental matrix. In addition to those employed previously[12], feedstocks examined include a commercial coker feed and an additional coal sample. This study addressed three areas of concern: the quantitative aspect of incorporation of coal into this process on the yield of light ends, the qualitative aspect of soluble products, and the physical and optical properties of the resultant coke.

Experimental: The five coal samples used were: Upper Banner, Pittsburgh #8, Blind Canyon, Illinois #6, and Wyodak. Procedural and analysis information can be obtained from the corresponding Technical Progress Report.[13]

Findings: As anticipated, for the reaction conducted at the moderately higher temperature of 500°C with the coker feed, coke concentration is moderately higher in the presence of coals; this increase amounts to 4 g 30-45 wt% of the product distribution. Feed has been listed in order of decreasing rank; DECS 29, 12, 6, 24 and 8. Concentrations of asphaltenes and preasphaltenes were negligible (<0.05 wt%). For these reactions, product distribution did not deviate significantly from the commercial yields discussed above.[1, 14, 15]

In general, coke concentration increased commensurate with the addition of coal. This was most apparent for the higher rank coals examined, particularly Upper Banner. Pittsburgh #8, Blind Canyon, and Illinois #6 demonstrated comparable coke concentrations and Wyodak appeared to be the poorest. However, the light product yield decreased parallel with the increase in coke yield. To this end, the run with Upper Banner would initially appear to be the worst case scenario and Wyodak the best, when considering liquid yield. The other coals, within experimental error, were the same.

Examining the qualitative aspects of simulated delayed coking of coals and resid using gas composition, we identified three main components which were all C_1-C_3 hydrocarbons, as anticipated. Only the run with CF produced appreciable quantities of distillate, which was characterized by 2-, 3-, and 4-ring polyaromatics as the heaviest species (e.g., naphthalene, anthracene/phenanthrene and pyrene, and their alkylated derivatives).

The oils from the suite of feedstocks considered here all displayed similar compositions as that for CF, with the exception of the feed comprising CF and DECS 29. CF oils appear to have a similar composition to that of the distillate with the notable exception that the oils contain smaller alkylated monocyclic species, such as ethyl and dimethyl benzene.

In conclusion, the delayed coking route for advanced aviation feedstock production may yet prove to be viable. Indeed, the fact that product distributions do not vary significantly from industry values is favorable. However, work must continue to enhance the selectivity of the pyrolysis reactions to favor the desired coal-derived aromatics.

---

[1] Speight, J. G. *The Chemistry and Technology of Petroleum: Second Edition.* New York: Marcel Dekker, Inc. 1991.

[2] Gray, M. R. *Upgrading of Petroleum Residues and Heavy Oils.* New York: Marcel Dekker, Inc. 1994.

[3] Rodriguez, J., J. W. Tierney, and I. Wender. *Fuel.* 1994. 73. 1863.

[4] Wallace, S. et al. *Fuel*. 1989. 68. 961.

[5] Curtis, C.W. and J. Hwang. *Fuel Processing Technology.* 1992. 32. 47.

[6] Tomic, J. *Ph.D. Thesis Dissertation.* The Pennsylvania State University, University Park, PA. 1993.

[7] Tomic, J., and H. H. Schobert. *Energy and Fuels.* 1997.

[8] Schobert, H. H. et al. *Advanced Thermally Stable Jet Fuels, Technical Progress Report, July — September 1996.* The Pennsylvania State University. 92PC92104-TPR-17. 1996.

[9] Tomic, J. and H. H. Schobert. *Energy and Fuels.* 1997.

[10] Rincom, J.M., J. Ramirez, and S. Cruz. *Fuel.* 1990. 69. 1052.

[11] Schobert, H. H. et al. *Advanced Thermally Stable Jet Fuels, Technical Progress Report, January — March 1997.* The Pennsylvania State University. 92PC92104-TPR-19. 1997.

[12] Martin, S.C. and H. H. Schobert. *Advanced Thermally Stable Jet Fuel, Technical Progress Report, July – September 1996.* The Pennsylvania State University. 972PC92104-TPR-17. 1996.

[13] Schobert, H. H. et al. *Advanced Thermally Stable Jet Fuels, Technical Progress Report, April — June 1997.* The Pennsylvania State University. 92PC92104-TPR-20. 1997.

[14] Gray, M. R. *Upgrading of Petroleum Residues and Heavy Oils.* New York: Marcel Dekker, Inc. 1994.

[15] Mochida, I. *Chemistry in the Production and Utilization of Needle Coke Chemistry and Physics of Carbon 24.* 1992. l24-130.

5.38 COAL/RESID COPROCESSING

This study is explained in detail in *Advanced Thermally Stable Jet Fuels Technical Progress Report, January — March 1998.*

Introduction

The objective of this task was to explore effective ways to produce liquids through coprocessing of coal and petroleum resids. The preferred products from the coprocessing are the oils that can be upgraded into cycloalkane-rich jet fuels in subsequent upgrading by catalytic hydroprocessing.

Our recent work demonstrated a strong synergetic effect between water and ammonium tetrathiomolybdate (ATTM) catalyst on coal liquefaction at relatively low temperatures (350°-375¡C).[1, 2] Further study on model compound reactions revealed the same trend.[3] With respect to reaction conditions, temperature-programmed liquefaction (TPL) was found to achieve better conversion on coal liquefaction compared with single stage liquefaction (SSL).[4, 5] Also a fundamental study on heavy petroleum resid upgrading under different catalysts, including ATTM, was carried out.

This work, which is based on the previous findings, explores effective coal/resid coprocessing systems, focusing on the effect of water with ATTM catalyst on coal conversion under different temperature programs.

Experimental

The two coals used were DECS-8 (Wyodak subbituminous coal) and DECS-12 (Pittsburgh #8 bituminous coal). In addition to ATTM, two resids were used an atmospheric resid (AR) and a vacuum resid (VR2). The coprocessing reactions were carried out in micro-autoclaves(tubing bomb reactors) charged with 3 g of coal (dmmf base) and 3 g resid for each run. The catalyst loading was 1 wt % of metal not the compound itself based on dmmf coal. The ATTM was loaded onto the coal using incipient wetness impregnation (IWI) followed by drying in vacuum oven at 110¡C for 2 hours. When water was added, the ratio of water to dmmf coal was 0.56. The original hydrogen pressure was 6.9 MPa (cold).

Three temperature programs were used. For temperature-programmed liquefaction (TPL), the reactor was held at a lower temperature for 30 minutes, then heated to a higher reaction temperature in 25 minutes and held at that point for 30 minutes. For single stage liquefaction (SSL), the reaction time was 60 minutes (in order to match the TPL reaction time). For the temperature-staged liquefaction (TSL), or two-step liquefaction, the procedure was the same as TPL, except that the reactor was vented during the inter-stage, in order to remove the water. The reactor was then recharged with hydrogen to a pressure of 6.9 MPa prior to the second stage reaction.

Product work up. The gas yield was obtained by weighing the reactor before and after gas venting. The gas sample was analyzed by GC with FID for hydrocarbons and with TCD for CO, CO_2 and H_2. The liquid and solid products were separated by a sequential Soxhlet extraction by hexane, toluene and tetrahydrofuran (THF). The conversion of coal (on the dmmf base of the

coal) was calculated from the weight of THF-insoluble materials after sequential extraction. The product distribution was based on whole dmmf product, including gas, oil, asphaltene, preasphaltene and residue (THF-insoluble organic materials). The oil samples from selected runs were analyzed by high temperature simulated distillation GC (HT-SimDis) for their boiling point distribution.

Conclusion

We have explored temperature-programmed catalytic coprocessing of two coals and two petroleum resids and examined the effects of ATTM as a catalyst precursor and the influence of water addition in this preliminary study. We concluded that water can aid the conversion of coal/resid coprocessing with an ATTM catalyst at 375¡C and suppress the conversion at 425¡C. Water removal before the second stage reaction at 425¡C can significantly improve the coal conversion. Further increasing either the first stage temperature from 375¡C or the second stage temperature from 425¡C can be detrimental to the conversion in coal/resid coprocessing under the conditions used.

---

[1] Song, C. and A. K. Saini. *Energy and Fuels.* 1995. 9. 188-189.

[2] Song, C., A. K. Saini, and McConnie. *Proc. 8th Int. Conf. Coal Sci.* 1995. 1391-1394.

[3] Song, C., et al. *Proc. 90th Int. Conf.Coal Sci.* 1997. 1413-1416.

[4] Huang, L., C. Song, and H. H. Schobert. *Am. Chem. Soc. Fuel Chem. Prepr*. 1992. 37(1). 223-227.

[5] Song, C., S. D. Parfitt, and H. H. Schobert. *Am. Chem. Soc., Fuel Chem. Prepr*. 1993. 38(2). 546-553.

5.39 COPROCESSING OF COAL/PETROLEUM

This study is explained in detail in *Advanced Thermally Stable Jet Fuels Technical Progress Report, January — March 1998.*

Introduction

In studying more effective ways to produce liquids by coprocessing coal and petroleum resids, we concluded that water could decrease coal conversion in an ATTM catalytic reaction under TPL and SSL conditions, provided that a system temperature of 425¡C was used. In addition, coal conversion could be significantly improved if the water was removed before the second stage reaction at 425¡C in a TPL run.[1]

This study presents the results of coal liquefaction with the non-hydrogen donor solvent, tetradecane, using ATTM with or without adding water. The same TPL conditions were employed as were used in the experiment cited earlier in this report. Our goals in undertaking these experiments were to

- Further understand the role of water with an ATTM catalyst precursor in coal/resid coprocessing and coal liquefaction with a organic solvent
- Compare the coal/solvent liquefaction system with the coal/petroleum resid coprocessing system in which the resid might be considered partly as a solvent.

Conclusion

Proper addition and removal of water can lead to significant improvements in coal/resids coprocessing. Water can aggressively promote the retrogressive reaction in coal liquefaction during the second stage at 425¡C. Tetradecane plays a role similar to resid as a solvent in coal liquefaction. A modified experimental procedure for coal/resid coprocessing system is needed to achieve a better water removal effect, which will likely improve coal conversion.

---

[1] Wei, B. and C. Song. Water Effect on Coprocessing of Coal/Petroleum Resid Using ATTM Catalyst Precursor. *Monthly Report to USAF/WL.* March 1998.

5.40 CO-COKING OF PETROLEUM RESIDUA AND COALS

This study is explained in detail in *Advanced Thermally Stable Jet Fuels Technical Progress Report, January — March 1998.*

Introduction

In the initial batch microautoclave reactions (500°C, 2 hours, 2:1 w/w resid:coal, N_2 atmosphere), coke concentration increased commensurate with the addition of coal. This was most apparent for the higher rank coals examined, particularly Upper Banner. Pittsburgh #8, Blind Canyon, and Illinois #6 demonstrated comparable coke concentrations (≈40-45 wt%) with Wyodak appearing to be the poorest (≈30 wt%). In addition, the light product yield decreased parallel with the increase in coke yield.

Based on these findings, the run with Upper Banner appeared to be the worst case scenario and Wyodak the preferred, considering that their liquid yields were 55 and 65 wt% respectively. The concentrations of asphaltenes and preasphaltenes were negligible in all cases (≤ 0.05 wt%). This work was concerned not only with the quantitative aspects of simulated delayed coking of coals and resid, but also with the qualitative aspect of the products.

We investigated the possibility of placing coal directly into a delayed coker with petroleum residua to obtain a desirable increase in the concentration of 2- and 3-ring aromatics in the process stream without adversely effecting coke quality. Our previous work focused on evaluating a rank suite of coals (subbit C through hvAb) with a commercial petroleum resid feed in simulated delayed coker experiments. Microautoclave tests at 450°C and 500°C, for 2 hr under a N_2 atmosphere and the associated product analyses (both distillates and coke) showed that the Upper Banner seam (the highest rank hvAb coal studied) performed well. It generated more 2- and 3-ring aromatic compounds, more hexane-soluble fraction and more semicoke than the other, lower rank coals studied at 450°C.[1], [2] In general, coals of this rank also possess the greatest thermoplastic properties and the ability to generate relatively strong anisotropic properties necessary to maintain the quality of the resulting coke products.

There may be an economic advantage in identifying coals that are either naturally suited to accomplish these goals or can be upgraded with marginal cost and effort; therefore, we surveyed hvAb-mvb rank coals to identify specific coals that are available in the market place. In particular, we sought coals possessing exceptionally high fluid properties, relatively low ash yield, and inertinite content were sought. Coals of this type would be more likely to blend with the petroleum resid and would be less obtrusive in the resulting coke structure. Once located, these and a number of the coals used in earlier studies were employed in experiments to establish the influence petroleum resid/coal blending might have on thermoplastic properties.

Experimental

Details pertaining to the coal survey and evaluation are provided in the pertinent Technical Progress Report.[3]

Conclusions and Future Plans

Two premium grade hvAb metallurgical coals of exceptionally high fluidity were located and used in this work Powellton and Eagle seam coals. The thermoplastic properties of four coals (Powellton, Upper Banner, Pittsburgh, and Illinois #6) and coal/resid blends were evaluated under standard conditions of heating rate and maximum temperature employed by the Gieseler plastometer. Results showed that at relatively low concentrations of resid (<25%), the thermoplastic properties of the blends are enhanced. With increasing concentration of resid, the fluid temperature range and the duration at maximum fluidity are expanded for hvAb coals. The fluidity profiles suggest that a sympathetic relationship may exist with regard to the devolatilization of the coal and resid components of the blend, particularly for the higher rank hvAb coals, such as the Upper Banner and Powellton coals tested.

To gain a better understanding of the devolatilization range of coal and resid under both plastometer and delayed coker conditions, we later performed thermogravimetric analyses. Thermal conditions of the plastometer (heating rate and final soak temperature) were changed to better approximate those of the delayed coker. Microautoclave tests with the new high fluidity coals were performed, matching those conditions used in our earlier investigation. Solid residues from the experiments were inspected under the optical microscope to establish the degree of homogenization of the coal and resid semicoke components. These results are presented in subsequent sections of this report.

---

[1] Martin, S. C. Exploratory Studies on the Direct Conversion of Coal to High-Quality Jet Fuels. Advanced Thermally Stable Jet Fuels, Technical Progress Report, January — March 1997. Ed.: H. HSchobert et al. The Pennsylania State University. 92PC92104-TPR-19. 1997. 19-22.

[2] Martin, S. C. Exploratory Studies on the Direct Conversion of Coal to High-Quality Jet Fuels. Advanced Thermally Stable Jet Fuels, Technical Progress Report, April — June 1997. Ed.: H. H. Schobert et al. The Pennsylania State University. 92PC92104-TPR-20. 1997. 33-41.

[3] Schobert, H. H. et al. Advanced Thermally Stable Jet Fuels, Technical Progress Report, January — March 1998. The Pennsylania State University. 92PC92104-TPR-23. 1998.